Functional Characterisation of the Host Sterol Metabolic Network in the Interferon Antiviral Response

Wei Yuan Hsieh

THE UNIVERSITY
of EDINBURGH

A Thesis presented for the degree of
Doctor of Philosophy,
The University of Edinburgh

October 2014

Division of Infection and Pathway Medicine

College of Medicine and Veterinary Medicine

I hereby declare that this thesis and the work presented in it are my own.

I confirm that:

• This work was done wholly or mainly while in candidature for a research degree at this University.

• Where any part of this thesis has previously been submitted for a degree or any other qualification at this University or any other institution, this has been clearly stated.

• Where I have consulted the published work of others, this is always clearly attributed.

• Where I have quoted from the work of others, the source is always given. With the exception of such quotations, this thesis is entirely my own work.

• I have acknowledged all main sources of help.

• Where the thesis is based on work done by myself jointly with others, I have made clear exactly what was done by others and what I have contributed myself.

……

Wei Yuan Hsieh

University of Edinburgh

Acknowledgements

This thesis would not have been possible without the support, encouragement and inspiration of many individuals. First and foremost, I would like to thank my parents, Ruecy-Ching Wang and Chir-Lih Shieh, for their unconditional love and support in providing me opportunities to excel in my academics and travel to many places.

My deepest gratitude goes to my supervisor, Professor Peter Ghazal, who supported me throughout the entire thesis project. We spent countless hours discussing the science of cholesterol over expensive high fat meals. We also spent many hours talking about cooking, his dog, and his love for sailing. Without his intellect and challenges, I would not have developed many skills that I have acquired during my stay in Edinburgh. I often tell him that the Wednesday meetings are more difficult than meeting my fiancée's parents. One of the most important lessons that I learned from Peter is the art of science – how to write a good story, how to present a story, and how to sell a story.

I would like to thank my other two supervisors, Professor Mike Shipston and Professor Margarete Heck, for their support of my thesis topic and ongoing commitment of my study. Special thanks to Dr. Kevin Robertson for providing financial support and hands-on knowledge of conducting experiments properly. Importantly, he told me that there is life outside of the lab, and that a 32" LCD television is not too small. Alan Ross, thank you for conducing tedious lab work for me. Also, it is good to know that someone else in this department has a PS3. I would like to thank Dr. Douglas Roy for his time spent editing the thesis and offering his suggestions. Thanks to Marilyn Horne for taking the time to help me with various administrative tasks. Also, thank you, Marilyn, for putting the parking pass under the keyboard for Rui and Gandi.

I would like to send my appreciation to Dr. Mathieu Blanc and Dr. Kai Kropp for having me involved in their projects. It was always "fun" working on weekends and nights for the both of you. Publications would not have been successful without the collaboration with Prof. Timothy Osborne and Prof. Christopher K. Glass.

I would like to extend my appreciation to my grade 8 teacher, Yu Chen Yen. Among all of the teachers that I met during my life, she was the only one who believed in my potential and ability to be successful in my educational career. She inspired me to pursue my goal and to never give up despite harsh criticism from other people. She is a model teacher who taught me to think outside of the box, which is a very important attribute in science.

To Dan "Lord" Voicu, we would not have met if it had not been raining. Thank you for being a good friend since 2007. This thesis could not have been completed without all of those papers that you emailed from the University of Toronto.

Thank you Dr. Shahida Syed, for being my awesome friend. You taught me that little details matter regardless of whether you are making dinner or a cake or writing a thesis. Thanks to Rui Chen for being my Italian-Chinese friend who is also a Bambi. To Dr. Fairus Hassim, thank you for being a badminton partner, as well as a good

friend with “standards”. I would like to thank the Bachmann group (aka the Batman group) for providing me with their German-made pipettes, RNase Zap, and Bunsen burner for my research.

There were a few individuals who helped me with improving my English language in the last 15 years. Dana Komer was a very kind English teacher who helped me successfully pass high school English, and to be fair, to this date I have only read two novels. I appreciate the help from Jordon Cook with improving my English writing. You are a great teacher. I learned how to be articulate with my words from Mary McPherson. Thank you for letting me crash at your house with your three cats. Thank you, Chao Yang, for helping me in high school and introducing me to Canadian culture. She supported me through many hardships, personally and academically, in the last 15 years. If it weren’t for Chao, I would not have met my fiancée, Elizabeth.

I would also like to thank my sister, Yi-Lun Hsieh, for being very nice to me. Thank you for reading my first draft of my layman abstract, and telling me that it’s not sexy (and it sucked).

There is no better friend than Dr. Senthil Kumar Gandi. I enjoy working with Gandi, and I have learned a lot about the beauty of design. I am glad that he enjoys my cooking and has not suffered from extreme food poisoning yet. I can say that Gandi’s advice has contributed to many of my successes in poster and speech competitions. He is a friend that every person should have in his/her life.

I want to send a shout out to Thomas and Mao Vang, Bai, Lee Pao, Rosie, Jimmy, Xue, Choua, Barbara, Paul, Andrew, Vue, Seng and all of the kids. Thank you for making me feel like family each time that I see you all in Canada.

Elizabeth Vang, thank you for being a part of my life. You witnessed the start and the end of my entire PhD career. Without you, I would not be able to find my passion for life and science. Thank you for taking care of me for the past five years. Thank you for your patience and understanding, and believing in my ability to achieve my goal. We always have fun together regardless of place and time, though sometimes, I get food poisoning for having too much fun. You are very special to me (in a non-retarded way). Thank you for always thinking of me over five time zones and 5574 kilometers. I always miss PdB. I look forward to spending every day with you in 2015.

At the end of everything, we will find a new beginning.

When you do things right, people won't be sure you've done anything at all. -Futurama, Season 3 Episode 20

Table of Contents

LIST OF FIGURES X

LIST OF TABLES XII

LIST OF COMMON ABBREVIATIONS XIII

ABSTRACT 1

LAYMAN ABSTRACT 4

CHAPTER 1

INTRODUCTION

1.1 Historical perspective of sterol metabolism and immunity 6

1.2 Description of the sterol metabolic network 7

1.3 Regulation of the sterol pathway by Sterol Regulatory Element-Binding Proteins (SREBP) 12

1.4 The importance of sterol metabolism in the development of innate and adaptive immunity 16

1.4.1 Classification of immune cell types 17

1.4.2 Regulation of hematopoietic stem cells by sterol 18

1.4.3 Regulation of APCs by sterol 20

1.4.4 Sterol mediated APC inflammatory responses 22

1.4.5 Regulation of T cells by sterol 23

1.4.6 Regulation of B cells by sterol 29

1.5 Cytomegalovirus as a viral model system 32

1.7 Interactions between CMV and the sterol biosynthesis pathway 38

1.8 Concluding remarks and overall hypothesis 40

1.9 References 43

CHAPTER 2

INVESTIGATION OF THE ROLE OF THE MEVALONATE-ISOPRENOID ARM IN MCMV REPLICATION

2.1 Introduction 52

2.2 Results 57

2.2.1 siRNA knock-down of the mevalonate-isoprenoid branch of the sterol biosynthesis pathway is antiviral 57

2.2.2 Inhibition of sterol biosynthesis by statin has antiviral effects against CMV 60

2.2.3 Analysis of the effects of statin on cellular apoptosis 64

2.2.4 The antiviral effect of statin can be metabolically rescued with specific sterol biosynthesis secondary metabolites 65

2.2.5 Statin pre-treatment does not inhibit viral entry but reduces intra and extracellular viral titre and viral plaque formation 67

2.2.6 Pre-treatment of statin inhibits viral immediately early promoter activity 68

2.2.7 Statin alters protein prenylation in fibroblasts and macrophages 70

2.3 Discussion 72

2.3.1 The importance of mevalonate-isoprenoid arm on MCMV replication 72

2.3.2 Inhibition of MCMV replication by statins 73

2.3.3 Lipophilicity of statins 75

2.3.4 Cellular response to fatostatin mediated sterol metabolism inhibition 77

2.4 References 79

Publications associated with Chapter 2 82

CHAPTER 3

INVESTIGATION OF THE ROLE OF 25-HYDROXYCHOLESTEROL IN THE INTERFERON MEDIATED STEROL-IMMUNE ANTIVIRAL RESPONSE

3.1 Introduction 83

3.2 Results 89

3.2.1 Transcription of cholesterol 25-hydroxylase is activated upon interferon, CMV and TLR stimulations 89

3.2.2 Exogenous treatment of 25-HC has broad antiviral potency and is lipid condition dependent 91

3.2.3 The antiviral effect of 25-HC is LXR independent 94

3.2.4 25-HC antiviral action blocks post entry viral growth and is independent of cellular apoptosis 96

3.2.5 The antiviral effect of 25-HC partially involves the mevalonate-isoprenoid pathway 99

3.2.6 Time dependent pre-treatment of 25-HC leads to MCMV immediate early gene suppression 101

3.2 Discussion 103

3.3.1 Relationships between 25-HC and the SREBP2 pathway 103

3.3.2 Physiological roles of 25-HC in in vivo 104

3.3.3 Potential binding targets of 25-HC 105

3.3.4 Potential 25-HC antiviral mechanisms 106

3.3.5 Pro- and anti-inflammatory effects of 25-HC 108

3.4 References 111

3.5 Supporting information 116

Publication associated with Chapter 3 119

CHAPTER 4

INVESTIGATION OF REDUNDANT ANTIVIRAL PATHWAYS IN MCMV REPLICATION

4.1 Introduction 120

4.2 Results 127

4.2.1 Viral replication is affected by changes in lipid conditions 127

4.2.2 Treatments of sterol intermediates stimulate MCMV replication but have no effects on cellular growth 129

4.2.3 Identification of SREBP2 dependent genes and cellular response to changes in lipid condition 131

4.2.4 Differential feedback response to sterol biosynthesis inhibition by 25-HC and statin in BMDM 136

4.2.5 Analysis of drug combination reveals common and facilitated antiviral modes of action and potential interaction profiles 138

4.2.6 Non-redundant siRNA knockdown of the sterol biosynthesis pathway under lipidated and delipidated conditions reveals additional antiviral targets of interest 143

4.3 Discussion 146

4.3.1 Sterol dependent and independent effects on viral replication 146

4.3.2 Combinatorial effects of statin, 25-HC, IFN, and ganciclovir and their respective antiviral modes of action 148

4.3.3 Potential importance of the Bloch-Kandutsch pathways in MCMV replication 152

4.4 References 155

4.5 Supporting information 158

Publications associated with Chapter 4 171

CHAPTER 5

INVESTIGATION OF THE DEPENDENCY OF MCMV REPLICATION ON THE PRENYLATION BRANCH OF THE MEVALONATE PATHWAY

5.1 Introduction 172

5.2 Results 181

5.2.1 Inhibition of GGTase2 by psoromic acid is antiviral against MCMV 181

5.2.2 Bioinformatics prediction of prenyltransferases targets 182

5.2.3 Systematic unbiased loss-of-function screening of GGT2 targets on MCMV replication 183

5.2.4 Effects of siRNA knockdown of selected RabGTPase effectors on MCMV replication 187

5.3 Discussion 190

5.3.1 Identification of prenylation targets 190

5.3.2 siRNA knockdown of RabGTPases 191

5.3.3 Integrating the role of RabGTPases with the assembly and egress of HCMV and MCMV 198

5.4 References 204

5.5 Supporting information 210

CHAPTER 6

CONCLUSION: CONVERGING INNATE-IMMUNE PATHWAYS WITH CMV REPLICATION AND STEROL METABOLISM 220

References 226

CHAPTER 7

EXPERIMENTAL PROCEDURES

7.1 Cell propagation and culture 227

7.2 Chemical reagents 229

7.2.1 Sterol metabolites 229

7.2.2 Statins 229

7.2.3 Oxysterols and LXR ligands 230

7.2.4 Prenylation inhibitors 230
7.2.5 Cytokine and TLR ligands 230
7.3 Virology techniques 231
7.3.1 Reporter Viruses 231
7.3.2 Determination of viral titre by plaque assay 232
7.3.3 Determination of intracellular and extracellular viral titre using single hit-kinetics 233
7.3.4 Reporter virus screening 233
7.3.5 Transfection and siRNA knock-down assays 234
7.3.6 Plaque reduction assay for statin and 25-HC 235
7.3.7 Isolation and quantification of viral genome copy number using qPCR 236
7.3.8 Comparison of methods for removing cell surface viral particles 237
7.4 Molecular biology techniques 238
7.4.1 Gluc reporter assay 238
7.4.2 Cell viability and apoptosis assay 238
7.4.3 Duo luciferase reporter assay for the activation of LXR 239
7.4.4 Testing the effects of solvents on viral replication and cell viability 240
7.4.5 Statistical analysis and generating viral inhibition dose curves 242
7.5 Proteomic techniques 243
7.5.1 Western blotting 243
7.5.2 Extraction and measurement of intracellular cholesterol 245
7.6 Genomics techniques 247
7.6.1 Quantitative RT-PCR and probe efficiency testing 247
7.7 References 253
CONFERENCE POSTERS 254

List of Figures

CHAPTER 1

Figure 1.2 Schematic representation of the sterol biosynthesis network. 9
Figure 1.3 Sterol mediated activation and inhibition of SREBP2. 15
Figure 1.4 Role of the sterol biosynthesis pathway in the development and function of innate/adaptive immunity. 19
Figure 1.5 The cytomegalovirus replication cycle. 34
Figure 1.1 Illustration of the sterol biosynthesis pathway using the systems biology graphical notation. 41

CHAPTER 2

Figure 2.1 The activation SREBP2 pathway leads to the activation of sterol biosynthesis and is inhibited by statin. 55
Figure 2.2 siRNA knock-down of mevalonate-isoprenoid branch of the sterol biosynthesis pathway is antiviral. 58
Figure 2.3 Statins are effective at lowering intracellular cholesterol. 60
Figure 2.4 Statins elicit antiviral effects against both MCMV and HCMV. 62
Figure 2.5 Statins are effective at inducing apoptosis. 64
Figure 2.6 Statins antiviral effect can be reversed with cholesterol secondary metabolites. 65
Figure 2.7 Statin does not affect viral entry but leads to decrease in both intra and extracellular viral titre reduction. 66
Figure 2.8 Statin inhibits MCMV viral plaque formation. 67
Figure 2.9 Not all statins inhibit MCMV MIE expression in fibroblasts. 68
Figure 2.10 Statin treatment leads to accumulation of unprenylated proteins in fibroblasts and macrophages. 70

CHAPTER 3

Figure 3.1 Cholesterol and oxysterol mediated proteolytic control of the SREBP2 pathway. 86
Figure 3.2 Enzymatic transformation of cholesterol into oxysterols. 87
Figure 3.3 Expression of *Ch25h* is induced upon interferon, CMV, or TLR stimulations. 90
Figure 3.4 25-HC is antiviral at sub-micromolar concentrations without affecting cell viability. 93
Figure 3.5 25-HC antiviral efficacy is lipid condition dependent. 94
Figure 3.6 25-HC antiviral actions are LXR independent. 95
Figure 3.7 25-HC inhibits post-entry viral growth and does not induce cellular apoptosis. 97
Figure 3.8 25-HC retards viral plaque formation. 98
Figure 3.9 25-HC antiviral action partially involves the mevalonate branch. 100
Figure 3.10 25-HC inhibits MCMV MIE expression and is treatment timing dependent but LXR independent. 102
Figure 3.11 25-HC inhibits MCMV ie1 expression in macrophages and fibroblasts. 102
Figure S3.1 Constitutive MCMV ie1 gene expression is suppressed in 25-HC treated BAM25. 116
Figure S3.2 Antiviral effect of oxysterols and LXR ligands in HCMV. 117
Figure S3.3 *Ch25h*$^{-/-}$ BMDM fails to achieve MIEP suppression with exogenous 25-HC. 118

CHAPTER 4

Figure 4.1 Potential non-SREBP2 mediated feedback regulation of the sterol biosynthesis pathway. 126
Figure 4.2 Changes in media serum condition affects MCMV replication. 128
Figure 4.3 The effects of sterol metabolites on MCMV replication and cell growth in different serum conditions. 130
Figure 4.4 The effects of *Srebf2* knockdown and 25-HC treatments on sterol biosynthesis gene expressions. 133
Figure 4.5 Effects of changing serum conditions on sterol biosynthesis gene expressions. 135
Figure 4.6 Effects of 25-HC and mevastatin on sterol biosynthesis gene expressions in BMDM. 137
Figure 4.7 Synergistic antiviral effects of 25-HC and ganciclovir. 139
Figure 4.8 The combination of 25-HC and IFN has an additive effect on viral growth. 141

Figure 4.9 The combination of mevastatin and 25-HC/IFN has mild synergistic antiviral effects. 142
Figure 4.10 Non-redundant siRNA knockdown of sterol biosynthesis pathway on MCMV replication under different serum condition. 144
Figure 4.11 Pathway inference on the possible antiviral mode of action between IFN, 25-HC, mevastatin, and ganciclovir. 150
Figure S4.1 Changes in media serum condition affects MCMV replication. 158
Figure S4.2 The effects of mevalonate on MCMV replication and cell growth in different serum conditions. 160
Figure S4.3 The effects of squalene on MCMV replication in different serum conditions. 162
Figure S4.4 The effects of farnesol on MCMV replication in full serum conditions. 164
Figure S4.5 The effects of farnesol on MCMV replication in delipidised serum conditions. 166
Figure S4.6 The effects of geranylgeraniol on MCMV replication in different serum conditions. 168
Figure S4.7 Effects of mevastatin on sterol biosynthesis gene expressions in NIH-3T3 fibroblasts. 169
Figure S4.8 siRNA knockdown of selective fatty acid and cholesterol biosynthesis regulatory genes on MCMV replication under different serum conditions. 170

CHAPTER 5

Figure 5.1 Overview of the protein prenylation pathway. 174
Figure 5.2 Overview of the RabGTPase cycle and vesicular transport. 176
Figure 5.3 The intracellular localization of Rabs. 178
Figure 5.4 Inhibition of geranylgeranyl transferase type 2 (RabGGTase) by psoromic acid is antiviral. 182
Figure 5.5 Distribution of predicted prenylation targets among the three prenyltransferases. 183
Figure 5.6 Small interfering RNA screen identifies the dependency of MCMV on RabGTPases. 187
Figure 5.7 Validation of deconvolution siRNA on MCMV replication. 187
Figure 5.8 Validation of deconvolution siRNA on MCMV replication. 189
Figure S5.1 Effects on siRNA knockdown of selected RAB adaptor proteins and the ESCRT complex on MCMV replication under different serum conditions. 218
Figure S5.2 Restriction validation of RabGTPase expression vectors. 219

CHAPTER 6

Figure 6.1 Summary of the main findings of the current study. 222
Figure 6.2 Converging innate-immune pathways with CMV replication and sterol metabolism. 225

List of Tables

CHAPTER 1

Table 1.1 Interaction table on the sequential synthesis of cholesterol from acetyl-CoA. 42

CHAPTER 5

Table S5.1 Bioinformatics prediction of all prenylation targets in human identified in Maurer-Stroh et al., 2007 210

Table S5.2 Bioinformatics prediction of all GGT2 targets in mouse identified in Maurer-Stroh et al., 2007 216

List of Common Abbreviations

Abbreviation (listed in alphabetical order)	Full name
20α-HC	20α-hydroxycholesterol
22(R)-HC	22(R)-hydroxycholesterol
25-HC	25-hydroxycholesterol
7-KC	7-ketocholesterol
7α,25-HC	7α-25-dihydroxycholesterol
ABCA1	ATP-binding cassette transporter A1
ABCG1	ATP-binding cassette sub-family G member 1
APC	Antigen presenting cell
ApoE	Apolipoprotein E
BCR	B cell receptor
BHK-21	Baby Hamster Kidney fibroblasts
BMDM	Bone marrow derived macrophage
Ch25h	Cholesterol 25-hydroxylase
CLP	Common lymphoid progenitor
CMP	Common myeloid progenitor
CTL	Cytotoxic T lymphocyte
DC	Dendritic cell
EAE	Experimental autoimmune encephalomyelitis
EBI2	Epstein-Barr virus-induced G protein-coupled receptor 2
EBV	Epstein-Barr virus
FH	Familial hypercholesterolemia
FOH	Farnesol
gB	Glycoprotein B
GGOH	Geranylgeraniol
GGTase1	Geranylgeranyltransferase type I
GGTase2	Geranylgeranyltransferase type II
GMPs	Granulocyte-monocyte progenitors
HCMV	Human cytomegalovirus
HFF	Human foreskin fibroblasts
HMG-CoA	3-hydroxy-3-methylglutaryl-coenzyme A
HMGCR	HMG-CoA reductase
HPβCD	Hydroxypropyl-β-cyclodextrin
HSC	Hematopoietic stem cell
HSV	herpes simplex virus
IE	Immediate early
IFN	Interferon
INSIG1	Insulin-induced gene 1
INSIG2	Insulin-induced gene 2
ISG	Interferon stimulated gene

KHSV	Kaposi's sarcoma-associated herpesvirus
LDLR	LDL receptor
LXR	Liver X receptor
MCMV	Murine cytomegalovirus
Mev	Mevalonate
MHC	Major histocompatibility complex
MHV-68	Murid herpesvirus 68
MIE	Major immediate-early enhancer
MRC-5	Human lung fibroblast
NK	Natural Killer
PFU	Plaque forming unit
Pmef	Primary mouse embryonic fibroblast
PRR	Pattern recognition receptor
SCAP	SREBP cleavage-activating protein
Sqle	Squalene
SRE	Sterol regulatory element
SREBP	Sterol regulatory element binding protein
Tc	Cytotoxic T cell
TCR	T cell receptor
Th	T helper
TLR	Toll-like receptor
VZV	Varicella zoster virus

Abstract

Sterols play many important roles in physiology, including maintaining cell membrane integrity, and producing vitamin D and steroid hormones. Recent studies implicate sterol metabolism in the host innate immune response. Previous work, based on transcriptional profiling studies of mouse cytomegalovirus (MCMV) infection of primary bone-marrow-derived macrophages (BMDM, MΦ), uncovered a previously uncharacterized role of interferon in regulating the cholesterol pathway. Notably, Toll-like receptor (TLR) induced interferon modulates the suppression of SREBP2 (Sterol Regulatory Element-Binding Protein 2) activation, the master transcription factor for sterol biosynthesis. This finding resulted in the downregulation of the sterol biosynthesis pathway. However, how interferon is molecularly linked to sterol metabolism, and what part of the pathway mediates the antiviral effect remains unknown. **The central hypothesis of the thesis is that the antiviral effect of interferon is in part mediated by secondary sterol metabolites and the dependency of viral replication on the host mevalonate branch of the sterol biosynthesis pathway.** To test this hypothesis, my studies have examined the components of the host sterol pathway and their respective roles in influencing viral replication. Paradigmatically, I used MCMV and BMDM to explore the host-metabolic-virus interactions. Specifically, my findings address the question of how MCMV replication depends on the sterol biosynthesis pathway, and how the pathway is modulated by interferon as an antiviral response.

In Chapter 2, the importance of the sterol biosynthesis pathway for viral replication was investigated using a combination of gene silencing and pharmacological inhibitors. These studies demonstrated that resistance to viral infection through suppressing the cholesterol pathway is not due to a requirement of the virus for cholesterol itself, but instead involves the mevalonate-isoprenoid arm of the pathway. This branch of the pathway chemically links lipids to specific host

proteins (protein prenylation). These results suggest a new role for the mevalonate arm during viral infection.

In Chapter 3, I examined what part of the sterol pathway mediates the antiviral effects. Oxysterols are natural modulators of sterol biosynthesis, and are produced by the oxidation of cholesterol by the enzyme cholesterol hydroxylase. Oxysterol suppression of SREBP2 activation leads to transcriptional repression of the sterol biosynthesis pathway. Additionally, oxysterols also modulate cholesterol homeostasis through cholesterol efflux. My studies led to identifing cholesterol-25-hydroxylase (Ch25h) as an interferon-stimulated gene (ISG). CH25H oxidizes cholesterol to produce a soluble oxysterol metabolite, 25-hydroxycholesterol (25-HC). Treatment of cells with 25-HC resulted in antiviral effects against MCMV and MHV-68. 25-HC was found to have no effects on MCMV entry into the host cell, but rather mediated inhibition of viral gene transcription. In addition, 25-HC-specific antiviral effect partially involved the suppression of the isoprenoid pathway, rather than cholesterol efflux. This work uncovered a physiological role for 25-HC as a sterol-lipid effector of an innate immune pathway.

The antiviral activity of 25-HC in a lipid replete condition was found to occur at a concentration higher than the concentration required to inhibit SREBP2 activation. This implies that the antiviral effects of 25-HC is independent of SREBP2 in sterol replete conditions. Conversely, the antiviral action of 25-HC was significantly enhanced in cells under sterol-depleted conditions, suggesting that the antiviral effect of 25-HC is likely mediated through multiple processes involving SREBP2 dependent and independent mechanisms. These sterol dependent and independent mechanisms are examined in Chapter 4, using pathway expression profiling and pharmacological synergy studies. These studies showed that 25-HC suppression of the isoprenoid synthetic pathway is crucial in controlling infection, but also highlighted that other 25-HC dependent antiviral mechanisms are likely to exist.

The inhibition of the mevalonate-isoprenoid arm by statins and 25-HC clearly demonstrated that MCMV replication dependents on protein prenylation. Chapter 5

investigation showed that either chemical inhibition of geranylgeranylation of host proteins or limiting mevalonate production led to restriction of MCMV replication. Importantly, through a series of systematic loss of function siRNA screenings demonstrated that specific host RabGTPases mediating vesicular transport pathways play vital roles in the replication and the assembly of the virus. This finding provides new mechanistic insights in to the dependency of cytomegalovirus replication on the host cell trafficking pathways and lays the groundwork for further definition of this important aspect of host-viral interactions. In summary, the overall findings of this research support the original hypothesis, by highlighting the importance of the host mevalonate-isoprenoid pathway, and provide further definition of the mechanisms and components linking sterol metabolism with interferon mediated antiviral effect.

Layman abstract

Controlling cholesterol in the body is key for strong immunity.

Cholesterol performs essential roles in the body, such as producing sex and stress hormones and maintaining brain functions. However, high cholesterol is often associated with increased risk of cardiovascular diseases. Maintaining a healthy cholesterol level can not only reduce adverse health conditions, but also help the body fight against viral infections.

Pathogens such as viruses are known to manipulate the production of cholesterol, leading to the progression of an infection.

The research presented in this thesis investigates how viruses depend on cholesterol synthesis to multiply, and what arm of the immune system can utilize cholesterol as a weapon to fight against infection.

Initial investigation showed that using drugs like statins to fine-tune cholesterol synthesis can protect cells against viral infection. Upon further examination, it was discovered that viral replication does not solely depend on cholesterol, but rather it depends on the production of cholesterol precursors. These precursors are critical for helping viruses to escape and to spread between cells.

Remarkably, further research also revealed that the body's immune cells can modify cholesterol to fight against infection. When immune cells detect the presence of a virus, these cells will secrete several immune hormones, known as interferons, to interfere with the replication of the virus. Interferons directly trigger the conversion of cholesterol into oxygenated cholesterol, known as 25-hydroxycholesterol (25-HC). This phenomenon can occur within six hours of infection. Studies by others have shown that this process can occur in the human body.

25-HC is potent at blocking the production of cholesterol and its precursors. As a result, it is very effective against deadly pathogens, including herpes and flu, because it not only inhibits viral replication, but also stops the virus from exiting infected cells.

Surprisingly, it was shown that 25-HC can work in conjunction with statins to provide enhanced antiviral therapeutic effects. This suggests that 25-HC plays an important role in protecting the host from infection.

The findings of this thesis have uncovered a direct link between the workings of our immune system and cholesterol metabolism, in particular, demonstrating that balancing cholesterol synthesis is the key to preventing harmful infection.

This research paves the way for designing novel antiviral therapeutic strategies through controlling the body's metabolism.

Chapter 1

Introduction

1.1 Historical perspective of sterol metabolism and immunity

Progress in medicine and public health depends on understanding the causes of disease. Infectious agents interact with the host to produce clinical symptoms, while the host counters pathogens by triggering an immune response. One of the hallmarks of the immune response is the perturbation of the host sterol metabolism. Early clinical observations made by Kipp showed a notable decrease in blood cholesterol levels in patients during the acute phase of lobar pneumonia (Kipp, 1920). Likewise, similar findings were reported by Wacker and Hueck in patients suffering from cavernous phthisis (productive tuberculosis) and ulcerating tumours (Kipp, 1920). *In vivo* experiments conducted by Shope using pigs and hog cholera (classical swine fever) also demonstrated a drop in serum cholesterol during the incubation period of the disease (Shope, 1930). Perhaps one of the most important pieces of evidence in supporting these early observations was a clinical study conducted by the U.S. Army in the early 1970s (Lees et al., 1972). During the 17-day trial, a group of healthy young males between the ages of 20–24 were placed in a controlled environment and on a liquid-diet. On the 7th day of the trial, volunteers were infected with sandfly fever virus. Their cholesterol, phospholipids, triglycerides, free fatty acid levels, and other metabolic parameters were monitored for the next 10 days. Significant decline in serum cholesterol levels occurred within 2 days post infection, with gradual recovery over time. This response was uniformly consistent across all infected subjects, while lipid metabolism in healthy controls remained unchanged.

All of the above clinical investigations suggested that the early phase of infection is coupled with the reduction in serum cholesterol (hypocholesterolemia). This drop is followed by a period of hypercholesterolemia, which coincides with the onset of clinical manifestations and lasts throughout the convalescence period. A return to the normal cholesterol content is associated with the elimination of the pathogen.

With the implementation of vaccines and interferon therapies, the effects of immune responses on lipid metabolism were soon recognised. Initial observations made by Ferry and Mathews noticed a decrease in serum HDL-cholesterol levels following influenza virus subunit vaccination (Mathews and Feery, 1978). Similar results were obtained in children receiving attenuated measles vaccines (Rimevax), showing hypocholesterolemia between 1-7 days post vaccination, followed by a short period of hypercholesterolemia (Viikari et al., 1979). Importantly, direct injection of either interferon-α, or -β in healthy volunteers led to fluctuations in cholesterol levels reminiscent of virus-infected or vaccinated subjects (Rosenzweig et al., 1987; Schectman et al., 1992). Even though the molecular biochemical explanation was not provided in these clinical studies, it became clear that alteration in cholesterol metabolism is part of the host immune response against natural virus infection or viral antigens.

1.2 Description of the sterol metabolic network

The concept of sterols and other lipids regulating cellular activation and proliferation is well established. Early studies indicated that proliferation of PHA (phytohemagglutinin) inducted T lymphocytes can be inhibited when cultured in human low density lipoprotein (LDL) serum (Curtiss and Edgington, 1976; Cuthbert and Lipsky, 1984). Conversely, exposure of myeloid progenitors in a sterol deprivation environment impedes the growth and subsequent maturation of neutrophils (Subramanian et al., 2012). Thus, cholesterol and other sterol intermediates are strongly implicated in having critical roles influencing the metabolic events associated with the induction of immune response, and the development of both innate and adaptive immunity. The core sterol metabolic pathway presented in this thesis consists

of 76 nodes, of which 25 are proteins and 51 enzymes (Figure 1.1). A total of 52 enzymatic reactions are described in the pathway map, with the catalysis inputs and outputs listed in the subsequent table (Table 1.1). For simplicity, a condensed and segmented version of the sterol pathway map is also provided in Figure 1.2 and described below.

The mevalonate arm starts with the substrate acetyl-CoA entering the pathway and ends with the production of squalene (Figure 1.2). During this process, acetyl-CoA is first converted into 3-hydroxy-3-methylglutaryl-coenzyme A (HMG-CoA) by the enzyme HMGCS1. HMG-CoA is then converted into mevalonate by the HMG-CoA reductase (HMGCR), the rate-limiting step in cholesterol biosynthesis (Knight et al., 1983). The activity of HMGCR can be inhibited using a class of compounds, known as statins. Mevalonate (C5) is subsequently converted into isopentenyl pyrophosphate (IPP, C5), then dimethylallyl pyrophosphate (DMAPP, C5) in the next 4 steps. Combining DMAPP with an additional IPP by the enzyme FDPS yields geranyl pyrophosphate (GPP, C10), an intermediate for the production of isoprenoids including farnesyl pyrophosphate (FPP, C15), and geranylgeranyl pyrophosphate (GGPP, C20). These isoprenoid moieties can subsequently be attached to specific protein targets, a process known as protein prenylation. The attachment of a hydrophobic 15-carbon (farnesyl) or a 20-carbon (geranylgeranyl) isoprenoid moiety is carried out by different prenyltransferases. Protein farnesylation is carried out by a single enzyme, farnesyltransferase (FTase), whereas geranylgeranylation is carried out by the protein geranylgeranyltransferase type I (GGTase1) and by geranylgeranyltransferase type II (GGTase2, also known as RabGGTase) for the Rab proteins.

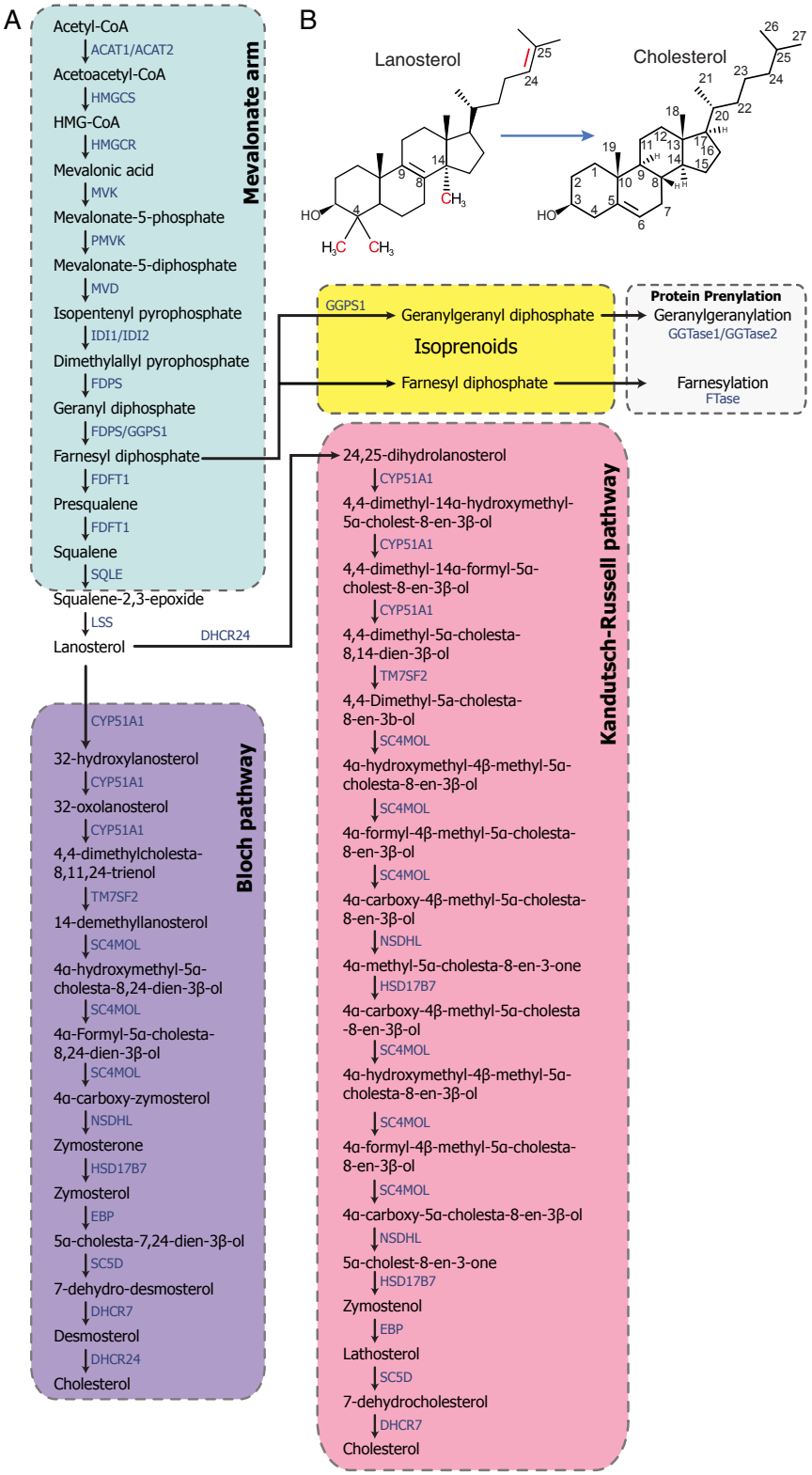

Figure 1.2 Schematic representation of the sterol biosynthesis network.
(A) A linear non-redundant illustration of the sterol biosynthesis pathway. The pathway is segregated into the mevalonate arm, where the production of isoprenoids and lanosterol take place. The Bloch pathway, or the Kandutsch-Russell converts lanosterol into cholesterol. (B) Comparison between the structure of lanosterol and cholesterol. Numbering represents the position of the carbon atom on the molecule. Condensed structure of lanosterol with the 3 extra CH_3 groups and the C=C bonds are highlighted in red.

In the second segment of the sterol biosynthesis pathway, squalene is first converted into lanosterol, which feeds into either the Bloch pathway or the Kandutsch-Russell pathway for the production of cholesterol (Figure 1.2A). The synthesis of squalene from isoprenoids was first described in the work of Langdon and Bloch, where squalene could be chemically synthesized by condensing geranylacetone (Langdon and Bloch, 1953). Feeding rats with radiolabeled squalene over time yielded radiolabeled cholesterol, indicating that squalene was one of the precursors of cholesterol. Subsequent biochemical work, utilizing rat liver homogenates and structural analysis, revealed that squalene (C30) was first converted to lanosterol (C30, Figure 1.2B), prior to the production of cholesterol (C27, Figure 1.2B) (Tchen and Bloch, 1957). However, lanosterol contains three more methyl groups (CH_3) than cholesterol, and also has different C=C bond orientations (Figure 1.2B). It was soon proposed that a 27-carbon sterol intermediate might be present. Johnston and Bloch later showed that this intermediate was zymosterol (5α-Cholesta-8,24-dien-3β-ol, the substrate of EBP), which can be further converted into cholesterol in yeast under aerobic conditions (Johnston and Bloch, 1957).

Concurrently, the work from Stokes and Fish isolated two companion sterols (apart from cholesterol) in 14-day chicken embryos, one of them being desmosterol (also known as 24-dehydrocholesterol, the substrate of DHCR24) (Stokes et al., 1956). Further investigation revealed that desmosterol can be converted into cholesterol in rat liver homogenates and *in vivo* (Stokes et al., 1958). Kinetic profiling (via acetate-1-^{14}C injection) of sterol metabolism in neonate rat brains demonstrated a cascade conversion of lanosterol → zymosterol → cholesterol (now known as the Bloch pathway) (Holstein et al., 1966).

Adjoining the work of Bloch and Fish, sterol profiling of mouse preputial gland tumours by Kandutsch and Russell (Kandutsch and Russell, 1959) identified the presence of lanosterol, 24,25-dihydrolanosterol (the product of DHCR24), Δ7-cholestenol (the product of EBP), 7-dehydrocholesterol (the product of SC5D), cholesterol (the product of DHCR7 and DHCR24), and an unknown sterol B2 (now known as 4α-methyl-Δ8-cholesten-3β-ol, the product of SC4MOL

(Kandutsch and Russell, 1960a)). Their subsequent sodium acetate-1-^{14}C labelling experiment (combined with sterol chromatography), revealed that conversion of lanosterol to cholesterol follows the sequential steps of lanosterol → 24,25-dihydrolanostero → 4α-methyl-Δ8-cholesten-3β-ol → Δ7-cholestenol → 7-dehydrocholesterol →cholesterol (Kandutsch and Russell, 1960b). The activity of this pathway was higher in preputial gland tumours, skin, and intestine than in the liver. In addition, several other sterol intermediates, including 14-norlansterol (a possible precursor to the 32-hydroxylanosterol, substrate of CYP51A1), zymosterol, and desmosterol were found not to be part of this metabolic sequence. Collectively, this evidence strongly argued the existence of an alternative sterol biosynthesis pathway (now known as the Kandutsch-Russell pathway). It was generally agreed at the time of discovery that the two pathways split from lanosterol and end with the conversion of the immediate precursor 7-dehydrocholesterol to cholesterol (Bloch, 1965). The two pathways were later refined with the discovery of DWF1 in Arabidopsis thaliana (later identified in humans, known as DHCR24) (Takahashi et al., 1995; Zerenturk et al., 2013). In the Kandutsch–Russell pathway, the C=C bond on the side chain (between C24 and C25. Figure 1.2) is reduced (C=C → C-C) early in the pathway, whereas the side-chain is reduced as the final step in the Bloch pathway (Ačimovič and Rozman, 2013).

1.3 Regulation of the sterol pathway by Sterol Regulatory Element-Binding Proteins (SREBP)

One of the earliest approaches to understand the regulation of sterol metabolism was by observing patients suffering from diseases associated with hypercholesterolaemia (high levels of cholesterol in blood). One of these diseases, hypercholesterolemic xanthomatosis, was marked by deposits of cholesterol in the skin, tendons and blood vessels (Roper, 1964). This disease was soon linked with an abnormal increase in total serum-lipid content in patients (Ahrens and Kunkel, 1949). Case studies have shown that the hypercholesterolemic disease phenotype can be reverted in some patients, but not all, by placing them on fat-restricted diets (Borrie, 1957; Roper, 1964). The use of 2-phenylethyl acetate, which evidently forms a stable complex with acetyl-CoA (the source of cholesterol biosynthesis) can also provide partial relief to xanthoma and atheroma (accumulation of macrophages in the artery walls) (Borrie, 1957). Furthermore, metabolic flux analysis using [^{14}C]acetate (which is converted into cholesterol) demonstrated that not all hypercholesterolaemia patients exhibit significant increases in cholesterol biosynthesis and turnover rate (Gee et al., 1959; Nestel et al., 1969). These early clinical investigations clearly illustrated the complexity of cholesterol metabolism and the potential genetic and environmental factors associated with the regulation of the pathway.

The successful isolation of low-density lipoprotein (LDL) (Briner et al., 1959; Scanu et al., 1968) provided mechanistic insights into the regulation of cholesterol synthesis. By measuring the rate of conversion of 3-^{14}C hydroxyethylglutaryl-CoA to 3-^{14}C mevalonate in fibroblasts, a process mediated by the enzyme HMGCR (Figure 1.2), Brown and Goldstein first showed that the HMGCR activity was enhanced in a sterol-depleted environment. This activation can subsequently be inhibited with the addition of fetal calf serum or cholesterol (Brown et al., 1973). This finding suggests that the regulation of intracellular cholesterol synthesis is influenced by the presence of extracellular sterol. Using fibroblast cells isolated from a familial hypercholesterolemia (FH) patient (named J.D.), Brown and Goldstein showed that the

defects in J.D. fibroblasts exhibited a significant decrease in LDL binding affinity and degradation capabilities (Brown and Goldstein, 1974). Further investigation led to the identification of LDL receptor (LDLR), and the mutation defects in the internalization of LDLR (Brown and Goldstein, 1976).

Through a series of mutagenesis experiments, the promoter sequence responsible for the transcriptional activation of *Hmgcr* and *Ldlr* have been uncovered (Dawson et al., 1988; Osborne et al., 1988; Smith et al., 1988). Sterol regulatory elements, or SRE, represented by the octamer sequence 5'-CACC(C/G)CAC-3', have been mapped out on the 5' promoter region of Hmgcr, and Ldlr. Mutations in the SRE sequence abolish sterol-dependent regulations of these genes. Using plasmid constructs overexpressing multiple SREs, investigations led by Goldstein and Brown's group identified two DNA-binding proteins, known as sterol regulatory element binding proteins 1 (SREBP1) and 2 (SREBP2) (Wangs et al., 1993). In mammals, three SREBP isoforms, denoted as SREBP1a , SREBP1c (DeBose-Boyd et al., 2001), and SREBP2 (Inoue et al., 1996), have been identified. SREBP1 is primarily responsible for fatty acid metabolism, while SREBP2 preferentially activates genes for cholesterol synthesis (Amemiya-Kudo et al., 2002; Sundqvist and Ericsson, 2003). SREBP2 regulates cholesterol biosynthesis through a feedback loop. The SREBP2 precursor is synthesized as an endoplasmic reticulum (ER) protein (Figure 1.3A1). When cells are depleted of cholesterol, the SREBP2 precursor is transported from the ER to the Golgi apparatus by the transporter SCAP (SREBP cleavage-activating protein) (Matsuda et al., 2001), where two proteases (S1P and S2P) act sequentially to release the active SREBP2 bHLH-ZIP domain from the membrane (DeBose-Boyd et al., 1999; Rawson et al., 1997) (Figure 1.3A2). The bHLH-ZIP domain enters the nucleus and binds to SREs in the promoter region of cholesterol biosynthesis genes,activating their transcription (Dobrosotskaya et al., 2003; Janowski, 2002; Yang et al., 2002) (Figure 1.3A3-4). In addition to activating cholesterol biosynthesis, SREBP2 also promotes cholesterol intake through increasing expression of *Ldlr*. Binding of cholesterol-rich LDL particles to the LDL receptor triggers the internalization of the LDLR complex (Wangs et al., 1993), leading to a decrease of serum cholesterol levels.

These two mechanisms effectively increase intracellular cholesterol levels. Excess cholesterol later binds directly to SCAP, preventing SREBP2 translocation (Figure 1.3B).

While SREBP2 regulates the synthesis and uptake of cholesterol, the liver X receptor (LXR) transcription factor family provides alternative signals for the export and removal of excess cholesterol (Chawla et al., 2001). Nuclear receptors LXRα and LXRβ have important roles in regulating cholesterol homeostasis by positively regulating the expression of genes encoding lipid-transports, such as *ABCA1* (ATP-binding cassette transporter A1), *ABCG1* (ATP-binding cassette sub-family G member 1), and ApoE (Apolipoprotein E) (Gelissen et al., 2006; Wójcicka et al., 2007). ABCA1 facilitates the transport of cholesterol (and also sphingomyelin, and phosphatidylcholine) to either cell surface-bound or internalized apolipoproteins such as apoA to I (Li et al., 2013a). While the exact function of ABCG1 remains unclear, it was proposed that ABCG1 mediates cholesterol efflux by regulating protein trafficking (Li et al., 2013a). Mutations in ABC transporters are associated with several human diseases, including Tangier disease (accumulation of cellular and tissue cholesterol due to mutations in Abca1 (Wang et al., 2001)), and familial hypoalphalipoproteinemia (low HDL-cholesterol, (Rader and deGoma, 2012)) (Singaraja et al., 2006). In addition, activation of LXRs also induce the expression of SREBP1c, which promotes fatty acid synthesis (which consumes acetyl-CoA) (Kamei et al., 2008). The transcription activity of LXRs are regulated by desmosterol, and oxidized cholesterols known as oxysterols (Figure 1.3C) (Spann et al., 2012).

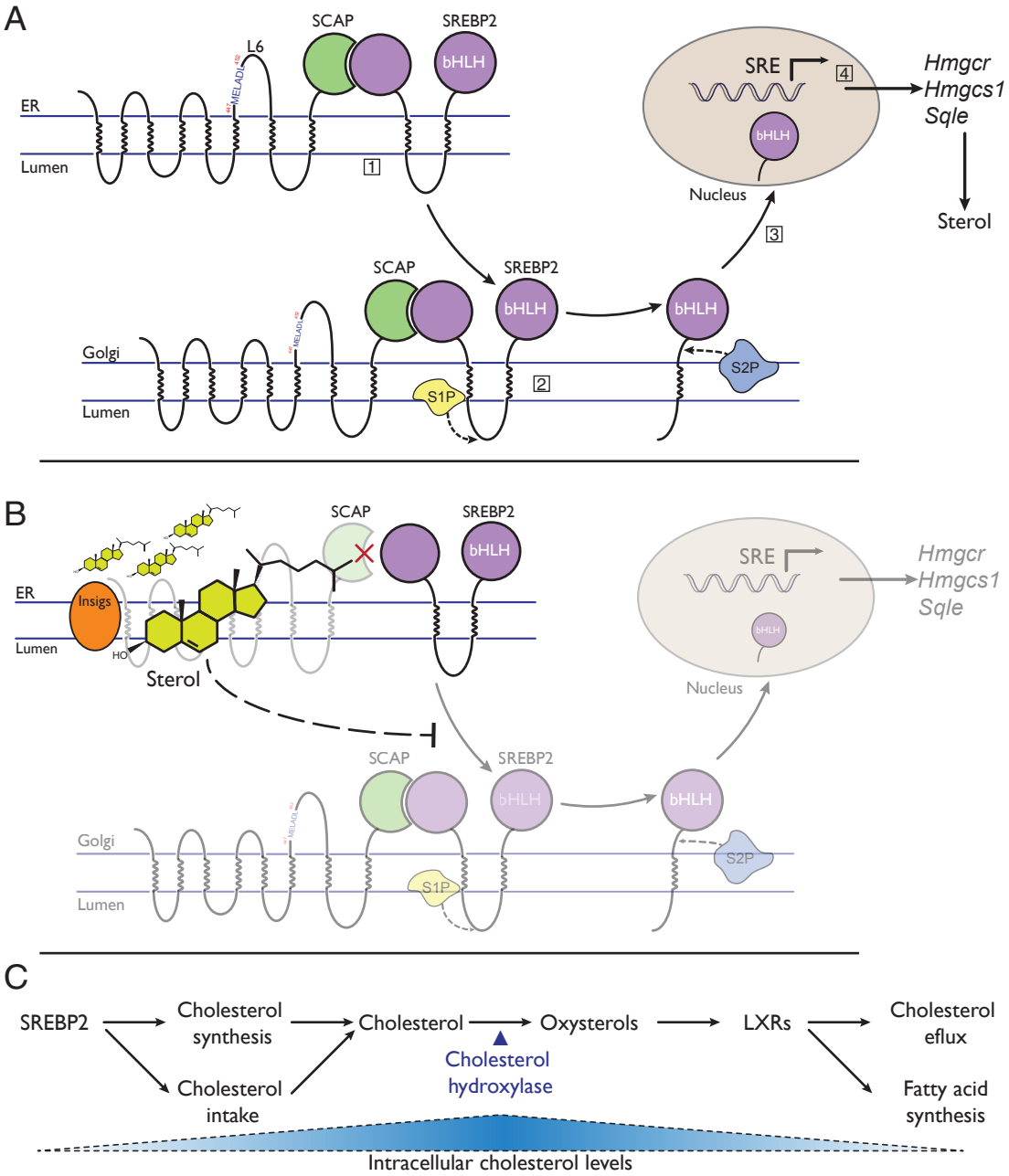

Figure 1.3 Sterol mediated activation and inhibition of SREBP2.
(A) SREBP2 is synthesized as an ER membrane bound precursor. When the cells are depleted in cholesterol, SREBP cleavage-activating protein (SCAP) binds and escorts SREBP2 from the ER to the Golgi apparatus. This translocation is mediated by the MELADL sequence (aa 447-452) on loop 6 of SCAP. The release of SREBP2 is initiated through two sequential cleavages by Site-1 Protease (S1P) and Site-2 Protease (S2P). After the second cleavage, the active SREBP2-bHLH domain leaves the membrane. The cleaved SREBP2 nuclear fraction enters the nucleus, where it binds to the sterol response element (SRE) and activates genes controlling cholesterol synthesis and uptake. (B) When the cholesterol level is above a certain threshold, sterol binds directly to SCAP, triggering SCAP to bind to INSIGs [insulin induced gene 1 (Insig1) and insulin induced gene 2 (Insig2)], preventing the translation and subsequent activation of SREBP2. (C) Linear non-redundant illustration of the regulation of cholesterol biosynthesis. SREBP2 activates cholesterol synthesis and influx, while excess cholesterol is converted to oxysterol by the hydroxylase. The activation of LXRs by oxysterols trigger cholesterol efflux and fatty acid synthesis, thus lowering intracellular cholesterol levels.

1.4 The importance of sterol metabolism in the development of innate and adaptive immunity

The immune system consists of many different cell types that play discrete and interlocking roles in innate and adaptive immunity. At first glance, the development of these cells appears distinctive. However, studies have suggested that common regulatory mechanisms exist in controlling the development and proliferation of these immune cells. These mechanisms are involved in the control of metabolisms of carbohydrates and lipids (Everts and Pearce, 2014; Maceyka and Spiegel, 2014). An earlier study by Curtiss and Edgington, 1976, demonstrated that cholesterol removal inhibits normal proliferation of T lymphocytes. Likewise, the work of Shine et al., 1980 showed that the addition of sterol in lipoprotein-deficient media cultured splenic cells promotes the formation of sheep red blood cell responsive plaque-forming T lymphocytes. These studies indicated that cholesterol and various sterol metabolites, in particular, play pivotal roles in providing “checkpoints” to the developmental process of immunity. Here, I first present a brief overview of the classification of the immune cells using Kuby immunology as the primary reference (Kindt, Thomas J, Richard A. Goldsby, Barbara A. Osborne, 2007). Based on this classification, I then summarise recent progress concerning the roles of the sterol metabolic pathway in modulating various aspects of immune cell development and activation. Figure 1.4 provides a graphical summary of all the findings discussed in this section.

1.4.1 Classification of immune cell types

The development of immune cells generally begins with the self-renewal hematopoietic stem cells (HSCs) inside the bone marrow. In the process known as hematopoiesis, HSCs are differentiated into one of the two linages: the myeloid progenitors or the lymphoid progenitors. The myeloid progenitors are the antigen presenting cells (APCs), which include monocytes, dendritic cells (DCs) and macrophages. These APCs are critical for providing the necessary signals for the activation of naïve T and B cells through the major histocompatibility complex 2 (MHC II), and the co-stimulatory B7 family proteins.

The lymphoid progenitors can be broadly subdivided into four populations: T cells, B cells, regulatory T cells, and natural killer cells. During the formation of naïve T cells, the T cell receptors (TCRs) are first rearranged to produce TCRs with an α and β chain, or with a γ and δ chain. The αβ naïve T cells are subsequently divided into either $CD4^+$ or $CD8^+$ naïve T cells. The $CD4^+$ T cells generally function as MHC II restricted T helper (Th) cells, while the $CD8^+$ T cells generally function as MHC I restricted T cytotoxic (Tc) cells. During the process of activating naïve $CD4^+$ T cells, the initial signal (signal 1) is generated by interaction of an antigenic peptide from the MHC II on the APC with the TCR complex. A second signal (signal 2) is provided by the interaction between CD28 on the T cell and the B7 family proteins on the APC. The activated $CD4^+$ cells can be further induced by cytokines, leading to either Th1 or Th2 responses. The Th1 involves the secretion of proinflammatory cytokines, including IL-2, IFNγ, and TNF-α, while the Th2 response activates B cells through the secretion of IL-4, IL-5, IL-6, and IL-10. The cytotoxic T cells are activated by the interaction of MHC I molecules on the surface of an infected cell. This causes the activation of Tc cells into an effector cell known as cytotoxic T lymphocytes (CTLs), which are involved in the direct killing of the target.

The formation of B cells begins in the bone marrow when lymphoid progenitors differentiate into progenitor B cells (pro-B cells). Through a multi-stage process, these pro-B cells are further differentiated into IgM and IgD expressing naïve B cells (mature B cells), and migrate to the cortex of the lymph node through the afferent lymphatics. Upon a primary innate response, the naïve B cells migrate from the cortex to the paracortex, where the B cells interact and are activated by the T helper cells. The activated B cells enter the secondary follicles and form the germinal centre. During the first stage of germinal-centre formation, activated B cells undergo intense proliferation. These proliferating B cells (centroblasts) are localized to a compartment inside the germinal centre, known as the dark zone. Centroblasts eventually give rise to centrocytes, which are nondividing B cells that express membrane immunoglobulin. The centrocytes move from the dark zone into a region containing follicular dendritic cells called the light zone, where the final affinity maturation process takes place.

1.4.2 Regulation of hematopoietic stem cells by sterol

The process of HSC proliferation was shown to be regulated by cholesterol efflux (Yvan-Charvet et al., 2010). It was found that *Abca1*$^{-/-}$ *Abcg1*$^{-/-}$ mice that are unable to promote cholesterol efflux had a significant increase in Lin^{-} Sca^{+} cKit^{+} (LSK) expressing HSCs in the bone marrow. These HSCs were mainly comprised of granulocyte-monocyte progenitors (GMPs) and common myeloid progenitors (CMPs), while the population of common lymphoid progenitors (CLPs) was unchanged. Importantly, it was shown that the proliferation of myeloid progenitors in the wild type bone marrow can be inhibited through the activation of the LXR-ABCA1-ABCG1 pathway. This was in contrast to the myeloid progenitors in *Abca1*$^{-/-}$ *Abcg1*$^{-/-}$ bone marrow where the suppression of proliferation can only be achieved through direct removal of cholesterol, or by inhibiting the RasGTPase mediated cell cycle. Together, these results indicated that the proliferation of HSCs is regulated by cholesterol efflux mechanisms involving LXRs, ABCA1, ABCG1, and sterol.

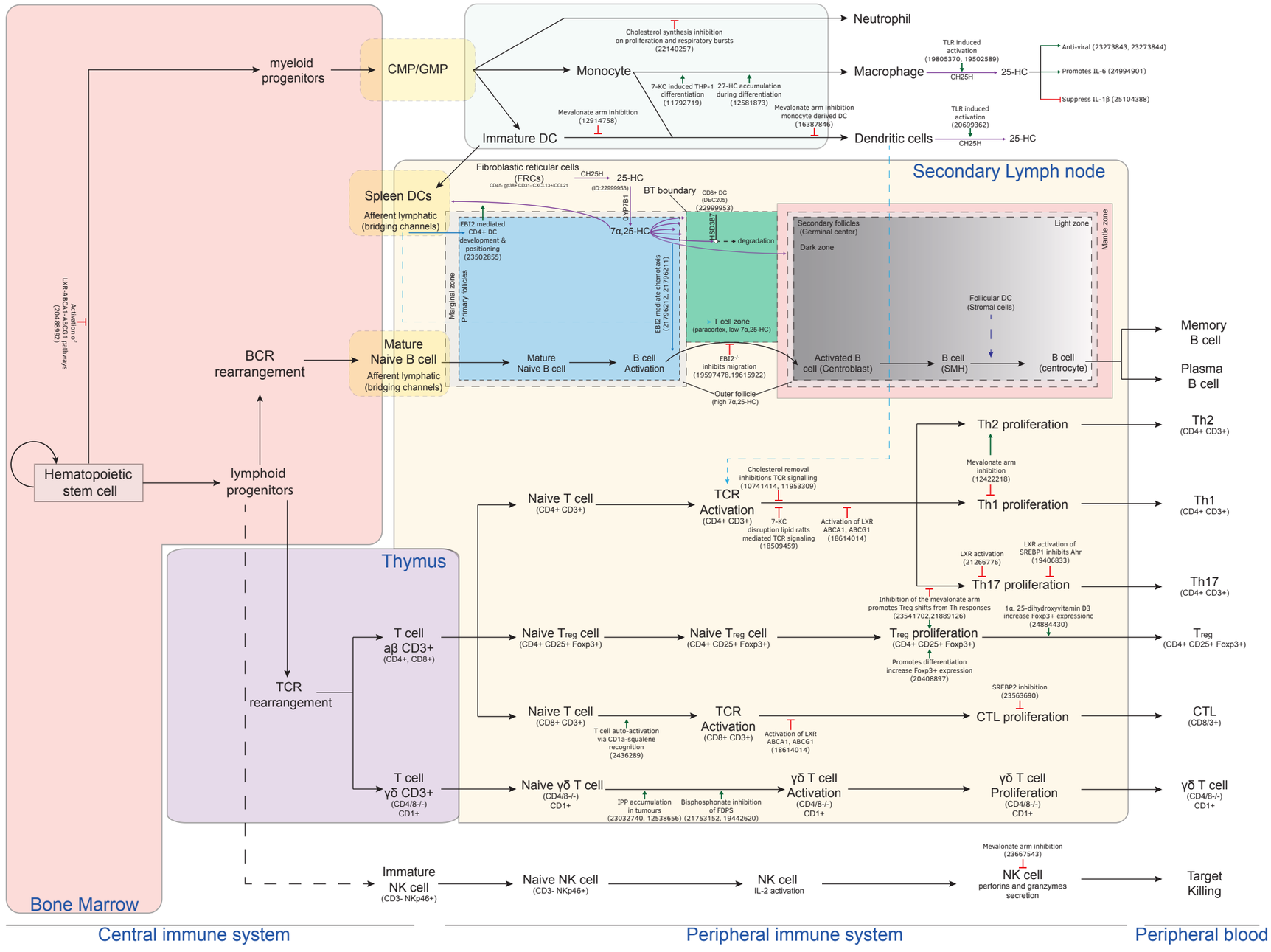

Figure 1.4 Role of the sterol biosynthesis pathway in the development and function of innate/adaptive immunity.
The immune system is generally divided into three segments: the central immune system, the peripheral immune system, and the peripheral blood. This figure is presented from the left to right, with all the immune cells originated from the bone marrow via the hematopoietic stem cells (HSCs). The HSCs are differentiated into two progenitor types: the myeloids and the lymphoids. Myeloid progenitors give raise to neutrophils, macrophages, and dendritic cells. DCs provide the "signal 1" for activating naive T cells (represented by the blue dash lines). DCs can also migrate to the spleen to form the speen DCs. They are responsible for capcturing blood antigens for activating T cells inside the lymph nodes. Lymphoid porgenetors give raise to NK, Treg, T cells, and B cells. The development of NK cells can occurr in other organs, such as the liver and the lung, while T cells are matured in the thymus. B cells are matured in the bone marrow, and subsequently migrate to the lymph node to be activated by the T cells. The roles of the sterol biosynthesis pathway are labelled as shown (either activation or inhibition), with the Pubmed ID shown in brackets. SREBPs play important roles in the expansion of T cells, while oxysterols are important for the positioning of B cells. Both macrophages and DCs can synthesize 25-HC, and can elicit strong antiviral effects. The activation of CH25H is mediated through a TLR-IFN-STAT1 pathway.

The dependency of myeloid linage cells on sterol was further shown in the study of neutrophils. Using EML (erythroid, myeloid, and lymphoid) derived promyelocytes (EPROs) as a model system, Subramanian et al., 2012 showed that treatment with lipoprotein-deficient media or lovastatin significantly inhibits the growth rate of EPROs, and their subsequent respiratory burst in response to antigen challenges. The reduction in cell growth and respiratory bursts was associated with the thinning of the plasma membrane. Collectively, these results were consistent with earlier studies showing that cholesterol levels are important in the proliferation of myeloid progenitors (Fernández et al., 2005; Ferruelo et al., 2001). The increasing demand on cholesterol is likely to be required for functional responses in terminally differentiated cells.

1.4.3 Regulation of APCs by sterol

During the development of macrophages, several lines of evidence have suggested that oxysterols play important roles in promoting macrophage differentiations. Hayden et al., 2002 reported that 7-ketocholesterol (7-KC) promotes the differentiation of THP-1 monocytes into macrophages. Treatment of THP-1 with 7-KC led to an increase in cell adherence, and the expression of mature macrophage markers CD68, CD36, and CD11b. Furthermore, 7-KC induced THP-1 macrophages showed phenotypic resemblance to foam cells, indicating that oxysterols may also play a role in the development of atherosclerosis (Hayden et al., 2002). Likewise, it has been shown that mature macrophages encode the enzyme 27-hydroxylase, which catalyses the conversion of cholesterol into 27-hydroxycholesterol and 3β-hydroxy-5-cholestenoic acid (Babiker et al., 1997; Björkhem et al., 1994). These oxygenated cholesterols are subsequently secreted and utilized for the synthesis of bile acids. The expression of 27-hydroxylase is elevated during differentiation of monocytes into macrophages as part of reprogramming of the cell (Hansson et al., 2003). The author proposed that the hydroxylation of cholesterol is likely one of the important secretory mechanisms in which macrophages can rapidly eliminate the accumulation of intracellular cholesterol.

In addition to the role of promoting cholesterol efflux, oxysterol has also been implicated as a chemoattractant for monocytes. *In vitro* studies by Eibinger et al., 2013 showed that the secretion of 25-hydroxycholesterol (25-HC) by human U87MG and

GM133 glioblastoma cell lines constitutes a driving force for the migration of THP-1 cells and primary human monocytes. siRNA knockdown of Epstein-Barr virus-induced G protein-coupled receptor 2 (EBI2; also termed GPR183), a receptor for oxysterols including 25-hydroxycholesterol (25-HC) and 7α-25-dihydroxycholesterol (7α,25-HC) can partially reduce the migration effects (Hannedouche et al., 2011). From these experiments, the authors posited that 25-HC might contribute to monocyte attraction in tumour environment. The increase in monocyte-derived macrophage trafficking to the tumour site would likely increase the invasiveness of glioblastoma (Ye et al., 2012), resulting in the further progression of gliomagenesis.

The importance of the sterol biosynthesis pathway has been shown in the activation of dendritic cells. Treatment of bone marrow-derived dendritic cells with lovastatin inhibits MHC II and CD40 expression (Sun, 2003). As a result, T cell stimulatory activity of DC is inhibited. Similar findings were also reported by Yilmaz et al., 2006 showing that the inhibition of the mevalonate pathway in monocyte-derived DCs perturbs their ability to induce T cell proliferation, as well as the secretion of IFNγ and IL-2 from T cells. More recently, it was shown that 7α,25-HC and its receptor EBI2 play a role in the positioning of dendritic cells in the spleen (localized to the bridging channels of the afferent lymphatic). In particular, *Ebi2*$^{-/-}$ mouse spleens were shown to contain a lower abundance of $CD4^+$ DCs, (Gatto et al., 2013). As a result, DC mediated activation of $CD4^+$ T cells was impaired. However, it was also shown that EBI2 deficiency had no effects on $CD8^+$ DCs, nor on their ability to activate $CD4^+$ T cells. This suggests that oxysterol could have preferential biological effects that are cell type and subset specific.

1.4.4 Sterol mediated APC inflammatory responses

Responses to infection and bacterial endotoxin are mediated by the innate immune system. These responses involve the activation of TLR, which lead to the transcription of cytokines such as interferons, which amplify the inflammatory response. The work of Bauman et al., 2009 indicated that oxysterol 25-hydroxycholesterol (25-HC) is secreted by macrophages in response to TLR activation via LPS. 25-HC negatively regulates the secretion of IgA by B cells, indicating a role for oxysterol in the immune system. Likewise, Diczfalusy et al., 2009 showed that direct injection of LPS into healthy volunteers raises the serum concentration of 25-HC. Inhibition of TLR4 signalling prevents the synthesis of 25-HC by macrophages. These results provided the evidence that 25-HC synthesis is dependent on TLR activation and can occur *in vivo*. Further investigation showed that in addition to macrophages, bone marrow derived DCs could also synthesize 25-HC upon stimulation (Park and Scott, 2010). The activation of 25-hydroxylase (Ch25h), the enzyme involved in the synthesis of 25-HC, was dependant on signalling through the IFNαR and STAT1. More recently, my work, Blanc and Hsieh et al., 2013 (see Chapter 3) and Liu et al., 2013, demonstrated that secretion of 25-HC by macrophages plays a potent antiviral role in protecting the host from viral infection. This work provides a direct link between the workings of innate immunity and cholesterol metabolism. Subsequent studies by Gold et al., 2014 and Reboldi et al., 2014 (discussed in Chapter 3) showed that 25-HC acts as an inflammatory signalling amplifier in the secretion of IL-6, or alternatively, an anti-inflammatory molecule to regulate the secretion of IL-1β.

1.4.5 Regulation of T cells by sterol

In T lymphocytes, engagement of the T cell receptors (TCRs) with the MHC ligand triggers intracellular signalling cascades that are required for T cell development and functions (Kindt, Thomas J, Richard A. Goldsby, Barbara A. Osborne, 2007). The TCR complex is localized to cholesterol-rich lipid rafts on the plasmid membrane of the cell. Disruption of lipid rafts, thus, is likely to have effects on T cell signalling. One of the main components of the TCR signal initiation machinery is the tyrosine kinase LCK. Upon the interaction between peptide-MHC and the TCR, the CD3ζ complex is phosphorylated by LCK, which permits the recruitment of kinase ZAP-70 (Kabouridis et al., 2000). ZAP-70 phosphorylates the tyrosine residues of the transmembrane protein known as Linker-for-Activation of T cells (LAT). LAT subsequently mediates the immediate downstream signalling such as the Ras-ERK pathway and the induction of Ca^{2+} (Kabouridis et al., 2000). In this regard, it was shown that cyclodextrin-mediated cholesterol extraction in Jurkat T cells caused an alteration to the kinase activity of LCK and the inhibition of Ca^{2+} influx in response to TCR-CD3 stimulations (Kabouridis et al., 2000). A similar study was carried out by Drevot et al., 2002 using cholesterol oxidase in 3A9 T cells, showing that removal of cholesterol from lipid rafts severely impaired TCR-CD3 induced phosphorylation of CD3ζ. Collectively, these two studies demonstrated that cholesterol, as part of the membrane rafts, is essential for efficient activation of TCR signalling cascades upon receptor engagement. Indeed, a more recent study by Rentero et al., 2008 found that incorporation of the oxysterol 7-ketocholesterol (7-KC) in the plasma membrane prevents the formation of lipid rafts. 7-KC loaded JCaM2 T cells had reduced CD3 expression and membrane fluidity. Furthermore, 7-KC enriched Jurkat T cells showed compromised TCR-CD3 signalling, and reduced secretion of IL-2. These above studies implicated the importance of cholesterol content in lipid rafts in modulating the effectiveness of TCR signal transduction.

T cells expressing the TCR-γδ chain represents a minor subset of T cells with unusual tissue distribution. These cells are present in primary lymphoid organs and in a large population in the skin and gut associated lymphoid tissues

(Gogoi and Chiplunkar, 2013). Different from the conventional αβ T cells, γδ T cells are $CD3^+$ T cells that do not show specific MHC restriction, but rather depend on other receptors for activation (Dar et al., 2014). In particular, γδ T cells are known to recognise metabolites of the mevalonate pathway for activation. These ubiquitous sterol intermediates are critical for the synthesis of isoprenoids and are essential for cell survival. Earlier studies have shown that Vγ9Vδ2 T cells can be activated in response to exogenous addition of isopentenylpyrophosphate (IPP) and farnesylpyrophosphate (FPP) (Gober et al., 2003; Wang et al., 2011). Alternatively, γδ T cells can also be activated via sterol intermediates originated from microbes, virus infected cells, and even tumours (Jameson et al., 2010; Kistowska et al., 2008). Dysregulation of the mevalonate pathway in certain tumours leads to the production of higher concentrations of IPP, which can trigger Vγ9Vδ2 activation and the killing of tumours (Benzaïd et al., 2012; Gober et al., 2003). Furthermore, treatments of some cancer cell types with bisphosphonate (zoledronate or risedronate), an FDPS inhibitor, were shown to elicit strong γδ T cell activation (Benzaïd et al., 2012; Castella et al., 2011; Roelofs et al., 2009). The combination treatment using Vγ9Vδ2 T cells along with bisphosphonate has demonstrated *in vivo* effectiveness against solid tumours (Goto et al., 2013). Several recent clinical trials showed evidence that the addition of bisphosphonate as an adjuvant provided beneficial outcomes in treating patients with breast cancer (Li and Dong, 2009; van der Vliet and Verheul, 2012); however, the exact anti-cancer mechanism requires further investigation.

One of the cholesterol intermediates that has been long recognised as an adjuvant in promoting robust T cell responses is squalene. The works of Jules T. Freund first described the use of adjuvants by mixing heat-killed Mycobacterium, Corynebacterium and Nocardia with mineral oil to facilitate an immunological response (Freund, 1947). Since then, the use of an oil-based substance and an emulsifying agent to constitute immunological adjuvants has been designated as Freund's adjuvants. The original published formulation of Freund's adjuvant was later modified due to impurity within the mineral oil. By replacing mineral oil with various naturally occurring branched hydrocarbons, including squalene, pristine (bute hydrocarbon), and vitamin K,

Whitehouse et al., 1974 showed that mixing squalene with heat-killed Mycobacterium tuberculosis provided the most significant boosts in eliciting an immune response. However, it was also noted that squalene is capable of eliciting encephalomyelitis (inflammation of the brain and spinal cord) in Lewis rats and guinea pigs when directly injected into the spinal cord. The capacity of squalene to induce T cell inflammatory response was shown using arthritis-prone DA rats. The work of Carlson et al., 2000 showed that squalene injection led to squalene-induced arthritis in the ankles and metatarsal joints of DA rats. Histological staining of the joints revealed upregulation of CD4, CD8, αβ TCR, CD11b/c, and MHC II markers that are associated with T cell activation. Injecting DA rats with established the arthritis with anti-αβ TCR monoclonal antibody abolished the arthritis, indicating the role of T cells in mediating the squalene induced inflammatory response. Squalene has been incorporated into the formulation of MF59, a commercially available adjuvant that is currently under clinical trials in boosting the effects of influenza and CMV vaccines (Allison, 1999; Nolan et al., 2014; Wang et al., 2014).

The mechanism involving the recognition of squalene by T cells was recently uncovered. The CD1 proteins were first shown to mediate T cell autoreactivity through the presentation of lipid antigens (Ly and Moody, 2014). In humans, CD1 proteins can be classified into CD1a, -1b, -1c, 1d, and -1e. However, in mice, only two copies of CD1d are present. CD1d has been well studied for its ability to detect foreign lipid antigens in natural killer and γδ T cells (Uldrich et al., 2013). Conversely, αβ T cells expressing CD1a were shown to recognise self-antigens. Using a the CD1a-TCR reporter assay, de Jong et al., 2014 first showed that the autoreactivity of T cells is strictly dependent on the expression of CD1a. Isolation of lipids that are bound to CD1a-TCR complex in auto-activated T cells revealed that triacylglyceride, an apolar lipid, was one of the ligands for CD1a. Given that CD1a-expressing Langerhans cells (skin DCs) and CD1a-autoreactive T cells constitute part of the skin mediated immunity, subsequent screening of apolar lipids extracted from donor skin and sebaceous glands showed that squalene, wax esters and triacylglycerides were potent activators of CD1a mediated T cell activation. These studies implied that alterations in

sterol metabolism might influence disease, in particular, by promoting the activation of T cells through the CD1a receptor.

The importance of SREBP in controlling the clonal expansion of T cells was recently demonstrated. After the activation of naïve T cells, T lymphocytes activate glycolysis and lipid metabolic pathways in response to increasing demand for organelle biogenesis and cellular replication. Kidani et al., 2013 first showed that SREBP1 and -2 mediated lipid biosynthesis pathways are rapidly induced within 6 hr of T cell activation. This activation is coupled with an increase in the rate of mitochondria respiration for the production of ATP. Using *Scap*$^{fl/fl}$ mice, the author further demonstrates that perturbation of SREBP signalling in SCAP knockouts significantly inhibited the proliferation and growth of CD8^{+} cytotoxic T cells. This deficiency can be subsequently rescued with the addition of cholesterol but not isoprenoids, suggesting that cholesterol itself is the limiting factor for clonal expansion. Interestingly, it was also revealed that SREBP activity was not required for the homeostatic proliferation of CD8^{+} T cells. This indicates that in certain cell types under inactive conditions, the activity of the SREBP pathway can be low. In addition, it was also noted that the disruption of SREBP did not affect the proliferation of CD4^{+} T cells. Collectively, the author concluded that SREBPs are essential in controlling antigen-driven clonal expansion of CTL, and that the degree of dependency of the sterol biosynthesis pathway could be one of the key differences between memory cells and effector cells during expansion.

The effects of inhibiting the mevalonate pathway on the function of cytotoxic lymphocytes was further studied in Natural Killer (NK) cells. NK cells are involved in the killing of virally infected cells and tumours through the secretion of perforins and granzymes (Podack and Lowrey, 1988). Perforins induce pore formations on the cell membrane, while granzymes are serine proteases that mark the target cell for immune elimination (Thiery and Lieberman, 2014). A study by Poggi et al., 2013 reported that fluvastatin inhibits the activity and the localisation of the small GTPase RhoA in NK cells (CD3^{-} NKp46^{+}, (Walzer et al., 2007)). As a result, granule polarization and calcium accumulation processes that are required for the contact and delivery of cytotoxic

granules are also inhibited. The inhibitory effect of fluvastatin on NK cell polarization could be completely reversed with the addition of mevalonate, demonstrating that fluvastatin is specifically targeting the mevalonate arm for its effect. Furthermore, it was also shown that fluvastatin did not compromise FasL(CD95L)/Fas–mediated killing of tumour cells nor the release of TNF-α. Collectively, these results demonstrate that modulating the mevalonate pathway in NK cells can selectively interfere with some molecular mechanisms responsible for the killing of target cells.

While SREBPs mediated lipid biogenesis is specifically involved in the blasting of $CD8^+$ T cells, it has been shown that the LXR-mediated cholesterol efflux pathway plays a role in regulating the overall T cell proliferation and acquired immune responses. The work of Bensinger et al., 2008 showed that during the process of T cell proliferation, the expression of LXR target genes involved in cholesterol transport was suppressed, while the SREBP2 pathway responsible for cholesterol synthesis was actively induced. Activation of LXR signalling by agonists GW3965 or 22(*R*)-hydroxycholesterol markedly reduced the proliferative capacity of cultured T cells. Conversely, loss of LXR expression promotes the proliferative capacity of both $CD4^+$ and $CD8^+$ T cells, resulting in enhanced antigen-responses. Importantly, it was shown that oxysterol-metabolizing enzyme SULT2B1 was rapidly induced in response to T cell activation. SULT2B1 has been previously described in modifying oxysterols through sulfation to reduce their LXR activating capacity (Javitt et al., 2001). This work provides an example of how T cells can proliferate through the activation of the SREBP pathway while converting oxysterols to reduce its effects on cholesterol efflux.

The $CD4^+$ T cells can be divided into several subsets. The Th17 cells are characterized by their secretions of cytokines IL-17A, IL-17F, and IL-22 (Xu et al., 2009). Th17 cells have been suggested to play a role in autoimmune diseases, including encephalomyelitis (EAE), an animal model of multiple sclerosis. It has been shown that the activation of LXR via LXR agonist T0901317 inhibits the production of IL-17A in splenocytes derived from Vα2.3/Vβ8.2 TCR transgenic mice. This effect was caused by the reduction in the number of $Th17^+$ T cells. Direct injection of T0901317 into mouse

spinal cords reduced MOG-peptide induced encephalomyelitis and the reduction in the expression of IL-17A, IFNγ, and IL-23R, indicating that the suppression of Th17 cells can be achieved through the activation of LXR. Subsequent mechanistic study by Cui et al., 2011 showed that LXR activation triggers the synthesis of SREBP1, which acts as an antagonist to the aryl hydrocarbon receptor (AHR). Interactions between the N-terminal acidic region of SREBP1 and Ahr impede the ability of Ahr to bind to the Il-17 promoter, thus preventing the formation of Th17 cells. In this regard, these two studies demonstrated that contrary to the positive roles of SREBP in promoting the proliferation of various immune cells. LXR-SREBP signalling can also act as a negative regulator in suppressing Th17 T cell development through transcriptional inhibition.

During the development of $CD4^+$ Th1 and Th2 T cells, inhibition of the mevalonate pathway by atorvastatin was shown to promote Th2 responses in mice. It was shown that administration of atorvastatin reduced the expression of MHC II on microglia (macrophages of the central nervous system (CNS)), an APC responsible for activating T cells in the CNS (Youssef et al., 2002). Furthermore, *in vivo* atorvastatin treatment showed suppressed secretion of IL-2, IL-12, IFNγ and TNF-α when mice were immunized with encephalitogenic peptides, whereas the secretion of IL-4, IL-5, IL-10 and TGF-β was increased. This result was consistent with in vitro experiments showing that atorvastatin preferentially promotes the development of Th0 cells into Th2 cells. It was also noted that the Th2 bias can be reversed with the addition of mevalonate, demonstrating that regulation of the mevalonate pathway is important in controlling Th1/2 responses. Mechanistically, it was shown that treatment with atorvastatin *in vivo* led to an increase in the phosphorylation of STAT6 and the decrease of STAT4 phosphorylation. STAT4 plays a key role in Th1 lineage commitment, while STAT6 is required for Th2 lineage commitment. These findings suggest that in addition to modulating the differentiation of T helper responses, manipulation of the mevalonate arm could also alter inflammatory signalling in T cells.

1.4.6 Regulation of B cells by sterol

During antibody responses, the newly activated B cells migrate from the primary follicles to the germinal centre inside the spleen, where the process of B cell clonal expansion, somatic hyper mutation (SHM) and self-selection take place (Victora et al., 2012). These events promote B cell receptors in recognizing various foreign antigens for the synthesis of antibodies. Considerable work has focused on identifying factors that influence the transition of B cells from the dark zone to the light zone. Relatively little is known about the driving force behind the migration of B cells from the primary follicle across the T cell zone to the secondary follicle. Epstein–Barr virus-induced gene 2 (EBI2, also known as GPR183) is a G-protein-coupled receptor that was first discovered to be significantly elevated in Epstein-Barr virus infected Blurkitt's lymphoma (B lymphocyte cancer) (Birkenbach et al., 1993). At the time of discovery, the natural ligand of EBI2 was unknown. Initial work by Pereira et al., 2009 using *Ebi2*$^{GFP/+}$ mice showed that EBI2 is unregulated during the initial development of B cells in the bone marrow, and is expressed throughout the maturation process. Upon BCR stimulation, EBI2 was detectable on B cells localized within the vicinity of outer follicles and the T cell zone, while it was undetectable once the B cells centralized to the germinal centre. In *EBI2*$^{-/-}$ mice, EBI2 deficient B cells showed no defects in their ability to be activated by T cells. However, the trafficking of activated B cells from the inner follicle to the outer follicle is impaired. This prevents the activated B cells from migrating toward the germinal centre to participate in the subsequent affinity maturation process. Similar findings were reported by Gatto et al., 2009, showing that differential expression of EBI2 during the development of B cells is critical for positioning B cells for T cell activation and effective antibody genesis.

The relationship between B cell migration and the sterol biosynthesis pathway was recently established during the search for the natural ligand of EBI2. By testing the ability of sheep liver extracts (obtained from a sheep suffering from peritonitis sepsis, inflammation of the abdominal organs) to activate an EBI2 reporter cell line, Hannedouche et al., 2011 revealed that oxysterol 7α,25-dihydroxycholesterol (7α,25-HC) was the ligand for activating EBI2 in a

dose dependent manner. 7α,25-dihydroxycholesterol can be synthesized through the rapid metabolism of 25-hydroxycholesterol by enzymes CYP7A1 and CYP7B1 (Honda et al., 2011; Li-Hawkins et al., 2000; Norlin et al., 2000). Through retrograde synthesis, Hannedouche et al., 2011 was able to demonstrate the production of 7α,25-HC and its strong binding affinity towards EBI2. In addition, it was shown that 7α,25-HC was capable of attracting the migration of EBV-infected B cells and Burkitt's lymphoma (RS11846) in a EBI2 dependent manner. The binding and the chemoattractant ability of 7α,25-HC was also reported by another study (Liu et al., 2011). Importantly, in *Ch25h*$^{-/-}$ mice that are unable to synthesize 25-HC, it was shown that the activated B cells failed to localize to the germinal centre but instead remained near the B-T cell boundary: a phenotype reminiscent to the EBI2 knockouts. This work provides the first evidence that oxysterols, as derivatives of cholesterol, can function as chemoattractants in the immune system.

The above studies have shown that 7α,25-HC is synthesized through the hydroxylation of cholesterol by CH25H at the 25 position, followed by CYP7B1 mediated hydroxylation of 25-HC at the 7α position (see Figure 1.2 for the numbering of the cholesterol molecule). The conversion process between 25-HC and 7α,25-HC in lymphoid organs was further investigated *in vivo* using *Cyp7b1*$^{-/-}$ mice. Extracts from *Cyp7b1*$^{-/-}$ spleen and lymph nodes failed to elicit EBI2 ligand activity, while the wild type extracts were sufficient at triggering an EBI2 response (Yi et al., 2012). Similarly, activated B cells in *Cyp7b1*$^{-/-}$ mice failed to localize to the germinal centre, indicating that the activity CYP7B1 is required for migration of B cell across the B-T boundary. To identify cells that are responsible for the production of 7α,25-HC, Yi et al., 2012 further analysed various cell types that constitute the lymphoid follicle. It was shown that CD45^{-} stromal cells, in particular, the gp39^{+}CD31^{-} fibroblastic reticular cells, were the main contributors to EBI2 ligand production.

The lack of EBI2 expression in the germinal centre indicated that 7α,25-HC is not required for B cell affinity maturation, and thus can be metabolized and removed by other enzymes. HSD3B7 (hydroxy-delta-5-steroid dehydrogenase) has been shown to metabolize 7α,25-HC in the synthesis of bile acids (Yi et al., 2012). In the same study

by Yi et al., 2012, the authors showed that HSD3B7 expressed by follicular dendritic cells around the T cell zone is required for the effective positioning of activated B cells. The differential expression of CH25H, CYP7B1, and HSD3B7 within the lymphoid organs permits the formation of an oxysterol gradient. 7α,25-HC is concentrated around the perimeter of outer follicles, while the level of 7α,25-HC inside the T cell zone is low. This work provides an effective transit mechanism for B cells and promotes efficient interactions between B and T cells at the B-T boundary. Collectively, these studies demonstrate how cholesterol derived oxysterols can act in a gradient fashion in modulating B cell responses.

In summary, the above sections have examined the importance of the sterol metabolic pathway in the development, function, and modulation of various immune cells. In particular, these studies reveal differential dependencies of immune cells on the SREBP signalling during different stages of proliferation. Perturbation of the mevalonate arm can lead to immune cell activation, or alternatively, prevent the proliferation of certain immune cell types. Likewise, the cholesterol-derivative oxysterols can act as chemoattractants, or as inhibitors to the formation of lipid rafts. These examples highlight that effective innate and adaptive immunity involves a highly coordinated and regulated sterol biosynthesis pathway. All of these add up a flexible and rapid defence in response to pathogen challenges.

1.5 Cytomegalovirus as a viral model system

The herpesviridaeare is a large family of enveloped DNA virues that can establish primary and persistent infection in the host. They are characterized by a double-stranded linear DNA genome contained within an icosahedral capsid. The capsid is surrounded by a layer of tegument proteins, followed by an envelope that contains multiple viral glycoproteins. The three subfamilies of herpesviruses, alphaherpesviruses (including herpes simplex virus (HSV) and varicella zoster virus (VZV)), betaherpesviruses (including human cytomegalovirus (HCMV)) and gammaherpesviruses (including Epstein-Barr virus (EBV), Kaposi's sarcoma-associated herpesvirus (KHSV), and Murid herpesvirus 68 (MHV-68)) are differentiated by their biological properties, such as the duration of the replication cycle, cell type specificity, and the structure of the viral genome (McGeoch et al., 1995) Human cytomegalovirus (HCMV), a member of the β-herpesvirus family, establishes persistent infection in all infected individuals. Symptomatic CMV infection predominantly occurs in newborns and immune-compromised individuals (including individuals with HIV and recipients of organ transplants), and can result in serious neurological and life- threatening diseases (Bhaijee et al., 2011).

Primary infection with cytomegalovirus normally begins with entry into epithelial cells, followed by spread to numerous cells types, including endothelial cells, neuronal cells, hepatocytes, monocytes and macrophages (Ibanez et al., 1991; Myerson et al., 1984; Sinzger et al., 2000). Macrophages have been shown to be involved in CMV propagation and latency (Frascaroli et al., 2009; Popkin and Virgin, 2003; Zhang et al., 2005). Additionally, macrophages play important roles in both lipid metabolism and immunity, in part, by mediating the secretion of type one interferon (IFN-α/β) (Alsharifi et al., 2008; Ren et al., 2008; Thompson et al., 2010).

Viral entry into host cells involves the binding of viral proteins, including glycoprotein B (gB), gH, gM, and gL (Compton and Feire, 2007), to cell surface molecules such as the cell-surface heparin sulfate proteoglycans (HSPG) and integrin (Compton et al., 1993; Feire et al., 2004) leading to fusion between the viral envelope and the cellular membrane (Figure 1.5A). This fusion delivers the viral nucleocapsid into the cytoplasm, which is then subsequently transported to the nuclear envelope, possibly via the microtubule network (Figure 1.5B) (Ogawa-Goto et al., 2003). Viral DNA is then injected into the nucleoplasm, which can be immediately transcribed. The newly transcribed immediate early (*Ie*) mRNAs are translated to viral proteins IE1 and IE2 (or IE3 for MCMV) that promote further transcription and replication of the viral DNA (Figure 1.5C) (Greaves and Mocarski, 1998; Iskenderian et al., 1996; Meier and Pruessner, 2000). In addition, these immediate early (IE1-72 and IE2-86) proteins induce cell cycle arrest (Castillo et al., 2000) and inhibit apoptosis (Bresnahan et al., 1996; Chen et al., 2001) to prolong survival of infected cells and enhance disease progression. During productive infection, viral DNAs are replicated in the nucleus through the actions of viral polymerase (UL54, M54 in MCMV) and other viral proteins, such as UL44 (Komazin-Meredith et al., 2008; Loregian et al., 2003). Newly synthesized viral DNA is used as the template for all viral gene transcripts, and late viral mRNAs produce viral structural proteins. The production of infectious cytomegalovirus occurs during the late phase of infection through the assembly of procapsids, followed by the packaging of viral DNA and maturation (Figure 1.5D).

The assembled cytomegalovirus nucleocapsids are exported from the nuclear compartment. The first step in nuclear egress is primary envelopment, in which the capsids from the inner nuclear membrane (INM) enter the perinuclear space through the dissolution and reassembly of the nuclear lamina (IMN) (Komazin-Meredith et al., 2008; Mettenleiter et al., 2009) (Figure 1.5E). The disruption of the nuclear lamina is thought to be mediated by the conserved herpesviral protein kinases (CHPKs) (Hamirally et al., 2009). The CHPK (pUS3) of HSV-1 phosphorylates lamins, leading to the redistribution of the nuclear lamina (Mou et al., 2007). In HCMV, CHPK (pUL97) recruits host factors (such as peptidylprolyl cis-trans isomerase PIM1) to further alter the lamina structure (Marschall et al., 2005; Milbradt et al., 2010).

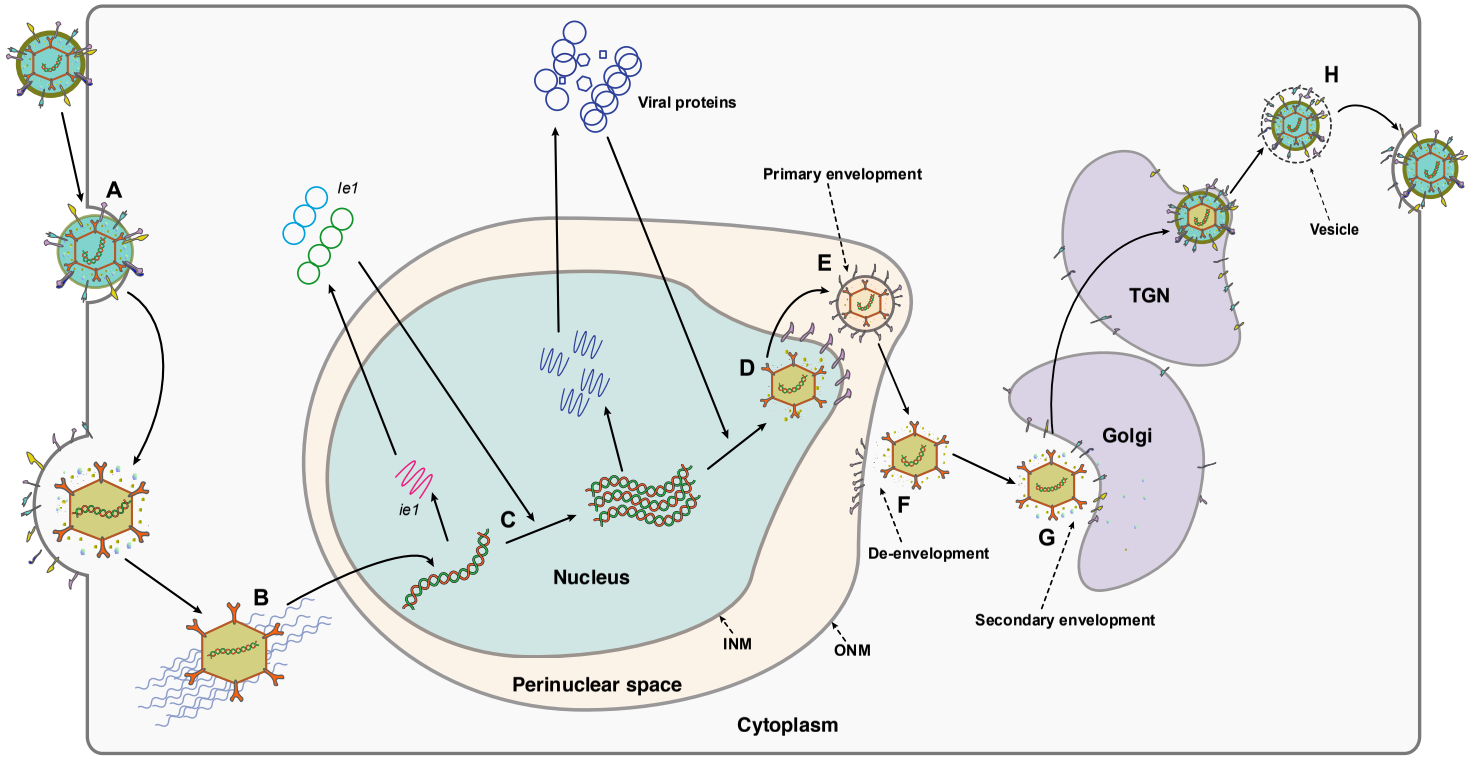

Figure 1.5 The cytomegalovirus replication cycle.
Cytomegalovirus initiates cell entry by integrating virions with the cell-surface heparin sulfate proteoglycan (HSPGs). The viral glycoprotein gB protein also interacts with epidermal growth factor receptor (EGFR) and/or integrins for docking, however; not all CMV permissive cell types express EGFR. The docking results in the fusion between the virion envelope and the cellular membrane, delivering the viral nucleocapsid into the cytoplasm. Through the microtubule network, the capsid is transported to the nuclear envelope, where they bind to the nuclear pore and inject the viral DNA into the nucleoplasm. The 235kb HCMV genome (230 for MCMV) can be immediately transcribed to produce early mRNAs (e.g. IE1 and 2 for HCMV, IE1 and 3 for MCMV). The IE products promote further transcription and replication of the viral DNA. The IE products also induce cell cycle arrest and apoptosis inhibition. During the productive infection, the viral DNA is replicated in the nucleus by the viral polymerases and other viral replicative machinery. Newly synthesized viral DNAs are used as templates for early and late gene transcription, and late mRNAs produce viral structural proteins. During the late stage of infection, replicated DNAs are packaged into capsids in the nucleoplasm. After capsids are formed in the nucleus, they bud into the inner nuclear membrane (INM), forming an enveloped particle in the perinuclear space. This is known as primary envelopment. These particles subsequently fuse with the outer nuclear membrane (ONM) (de-envelopment) and are released into the cytoplasm, leaving the primary envelope in the ONM. In the cytosol, the capsids are coated with a layer of proteins that form the tegument that fills the space between the capsid and the virion envelope. The capsids then bud into the cytoplasmic membrane (secondary envelopment). Several glycoprotein complexes (gc I, II, and III) are assembled and attached to the envelope. The enveloped virion is then transported through the trans-Golgi network (TGN), and subsequently secreted from the cell through the secretory pathway (release).

In the second stage of nuclear egress, enveloped particles in the perinuclear space fuse with the outer nuclear membrane (ONM), delivering unenveloped capsids into the cytoplasm (Figure 1.5F). This process is known as de-envelopment. During the egress of the virus, the tegument proteins are added to the virion in several subcellular locations. Cytomegalovirus capsids acquire several tegument proteins in the nucleus, including pp65, ppUL69 and pp150 (Sanchez et al., 1998, 2000a). Additional quantities of pp65 and pp150 are added to the virion within the cytoplasm (AuCoin et al., 2006; Sanchez et al., 2007).

Other tegument proteins, including pp28, pp71, are found exclusively in the cytoplasm, and incorporated into the virion (Marshall et al., 2002; Sanchez et al., 2000b). The second envelopment (re-envelopment) of cytomegalovirus begins with the budding of tegument–coated capsids in the cytoplasm into the cytoplasmic membrane (that includes cis-Golgi, the medial Golgi, the TGN and endosomes) (Das et al., 2007; Sanchez et al., 2000a) (Figure 1.5G). During the egress pathway, three glycoprotein complexes (designated gc I, II, and III), located on the cytoplasmic membrane, are attached to the envelope, producing the infectious CMV virions (Britt, 1984; Huber and Compton, 1997; Kari et al., 1990). These glycoprotein complexes are trafficked to the specific cytoplasmic locations. (Das et al., 2007). The budding of viral capsids, from the cytoplasm into the cytoplasmic membrane, invert the orientation of the glycoprotein complexes, causing the receptor portion of the complexes to face outward (Das et al., 2007).

During the last stage of viral egress, cytoplasmic vesicles carrying enveloped virions are transported to the cell surface, where they fuse with the plasma membrane to release the virions (Figure 1.5H). It is thought that the packaging, transport and the fusion of viral nucleocapsids are mediated by cellular exocytic fusion machinery (the exocytic pathway) rather than by viral fusion proteins. However, the precise role of both viral and host proteins participating in viral egress remain undetermined.

1.6 Immune detection of CMV

Viral particles, the entry process, and replication are detected by host sensors (also known as pattern recognition receptors, PRRs), leading to the activation of innate immune signalling. Previous works have shown that CMV are recognised by several host toll-like receptors (TLRs). HCMV gB, and gH proteins have been shown to directly interact with TLR2 (a cell surface receptor, detects lipoproteins) (Boehme et al., 2006), while, TLR4 (a cell surface receptor, detects lipopolysaccharides) (Yew et al., 2012), TLR3 (detects dsRNA) and TLR9 (detects CpG oligodeoxynucleotide) (endosome/lysosommal comparment receptors) (Nahum et al., 2012; Tabeta et al., 2004) have also been shown to play important roles at modulating host immunity against CMV infection. In addition to TLRs, recent studies have also identified several cytosolic DNA sensors that are capable of detecting foreign DNA. Currently, DNA sensors, including DAI (DNA-dependent activator of interferon regulatory factor) (Takaoka et al., 2007), IFI16 (Gamma-interferon-inducible protein 16) (Unterholzner et al., 2010), and cGAS (Cyclic GMP-AMP synthase) (Sun et al., 2013), have been found to detect herpes simplex virus 1 (HSV-1) and other retroviruses, such as HIV (Gao et al., 2013; Kerur et al., 2011; Li et al., 2013b; Pham et al., 2013). However, whether these DNA sensors can detect CMV DNA is yet to be confirmed.

The detection of CMV by TLR3, or TLR4 triggers the recruitment of the adaptor protein TRIF (Yamamoto, 2004) (TLR4 requires an additional protein TRAM), leading to activation of transcription factors NF-kB, AP-1, and kinases TBK-1 through a series of protein phosphprylations (the TRAF3 pathway) (Kawai and Akira, 2008; Oliveira-Nascimento et al., 2012). Similarily, detection of viral DNA by DAI, IFI16, or cGAS triggers the recruitment of adaptor STING, which also leads to the activation of NF-κB and TBK-1 (Pham et al., 2013; Wu et al., 2013). In both cases, activation of TBK-1 is followed by the phosphorylation of IRF3 (interferon regulatory factor 3), a member of the interferon regulatory transcription factor (IRF) family, in the cytosol. Phosphorylated IRF3 forms a complex with CREBBP, and translocated to the nucleus to activate the transcription of type one interferon (IFN-α/β) (Bauernfeind and Hornung, 2009; Korherr et al., 2006). In addition, activation of NF-kB from TLRs (2,3,4, and 9) provides the signal for the transcription of other pro-inflammatory cytokines, such as TNF-α (Kawai and Akira, 2008).

1.7 Interactions between CMV and the sterol biosynthesis pathway

Lipid rafts are cholesterol microdomains within the plasma membrane that serve as platforms for molecules involved in cell signalling, endocytic trafficking, and cell adhesion (Diaz-Rohrer et al., 2014). It is becoming evident that many viruses use lipid rafts as mechanisms for viral entry (Bender et al., 2003; Choi et al., 2005; Diaz-Rohrer et al., 2014). In HCMV, it has been shown that destabilization of lipid rafts via cholesterol removal significantly inhibits viral entry (Juckem et al., 2008). Furthermore, the work of Machesky et al., 2008 showed that upon infection, HCMV triggers the de novo lipid synthesis of sphingolipids via inducing the expression of sphingosine kinase (SphK). Along similar lines, Sanchez and Dong, 2010 found that HCMV-Towne infection in human foreskin fibroblasts (HFF) led to significant upregulation of genes including Neimann–Pick disease, type C1- like protein (NPC1L1), leptin, cholesterol ester transfer protein (CETP), cholesterol ester lipase (CEL), and apolipoprotein A1 (apoA1) that are involved in cholesterol influx. Conversely, ABCA1, which is involved in cholesterol efflux, was downregulated and further suppressed 6 hr post infection. These studies suggest that the manipulation of cellular cholesterol levels is essential to the viral life cycle of HCMV. A recent study by Gudleski-O'Regan et al., 2012 showed that in response to HCMV infection, infected cells elevate low density lipoprotein -related receptor 1 (LRP1), a plasma membrane receptor, to counter virus-induced accumulation of cholesterol. siRNA knockdown of LRP1 caused the accumulation of intracellular cholesterol, resulting in the production of cholesterol enriched viral particles. Consequently, the increase in virion-associated cholesterol promotes the fusion between the viral envelope and the plasma membrane, thus enhancing viral entry and infectivity.

In addition to modulating intracellular lipid content through influx, HCMV also promotes lipid synthesis through the induction of SREBP. Supplementary data from Sanchez and Dong, 2010 showed that the expression of *SREBF1* and *-2* is upregulated (~1.5 fold increase) at 6 hpi, while the repressors for SREBP, *INSIG1* and *-2*, are downregulated. The upregulation of SREBF2 was accompanied by the transcriptional activation of sterol biosynthesis genes including HMGCR, IDI1, and MVK (~1.04–4 fold increase). These results were further supported by the work of Spencer et al., 2011, showing that HCMV induces proteolytic processing of SREBP2. The increasing SREBP2 activation was consistent with the transcriptional activation of the sterol biosynthesis pathway, as well as the expression of acetyl-CoA carboxylase (ACC1), which serves as the first enzyme leading to fatty acid biosynthesis. Indeed, a subsequent study by Yu et al., 2012 revealed that HCMV infection also triggers the proteolytic processing of SREBP1a in human foreskin fibroblasts. However, different from SREBP2, the activation of SREBP1a by HCMV was independent of sterol sensing, but rather involved the ER stress dependent downregulation of INSIG1 (Yu et al., 2013). Collectively, these studies argue that HCMV is capable of exploiting cholesterol and fatty acid biosynthesis pathways through independent mechanisms to facilitate replication.

1.8 Concluding remarks and overall hypothesis

This chapter provides an overview of the role of the sterol metabolic pathway in host immunity. Early clinical observations have suggested that immunological responses could lead to fluctuations in cholesterol metabolism. More recent studies have identified that the cholesterol pathway participates in the development of innate and adaptive immunity. Products of the sterol biosynthesis pathway, in particular, isoprenoids, cholesterol, and oxysterols, can modulate various aspects of immune cell physiology. Likewise viruses, such as CMV, have been shown to manipulate host lipid synthesis through the upregulation of SREBPs. In this regard, previous work, based on transcriptional profiling studies of mouse cytomegalovirus (MCMV) infection of primary bone-marrow-derived macrophages (BMDM, MΦ), uncovered a previously uncharacterized role of interferon in regulating the cholesterol pathway. Notably, TLR induced interferon modulates the suppression of SREBP2, resulting in the downregulation of the sterol biosynthesis pathway. However, how interferon is molecularly linked to sterol metabolism and what part of the pathway mediates the antiviral effect remains unknown. The central hypothesis of the thesis is that the antiviral effect of interferon is in part mediated by secondary sterol metabolites and the dependency of viral replication on the host mevalonate branch of the sterol biosynthesis pathway. This thesis examines the components of the host sterol pathway and their respective roles in influencing viral replication. The findings presented in the next four results chapters specifically address the question of how MCMV replication depends on the sterol biosynthesis pathway, and how the pathway is modulated by interferon as an antiviral response.

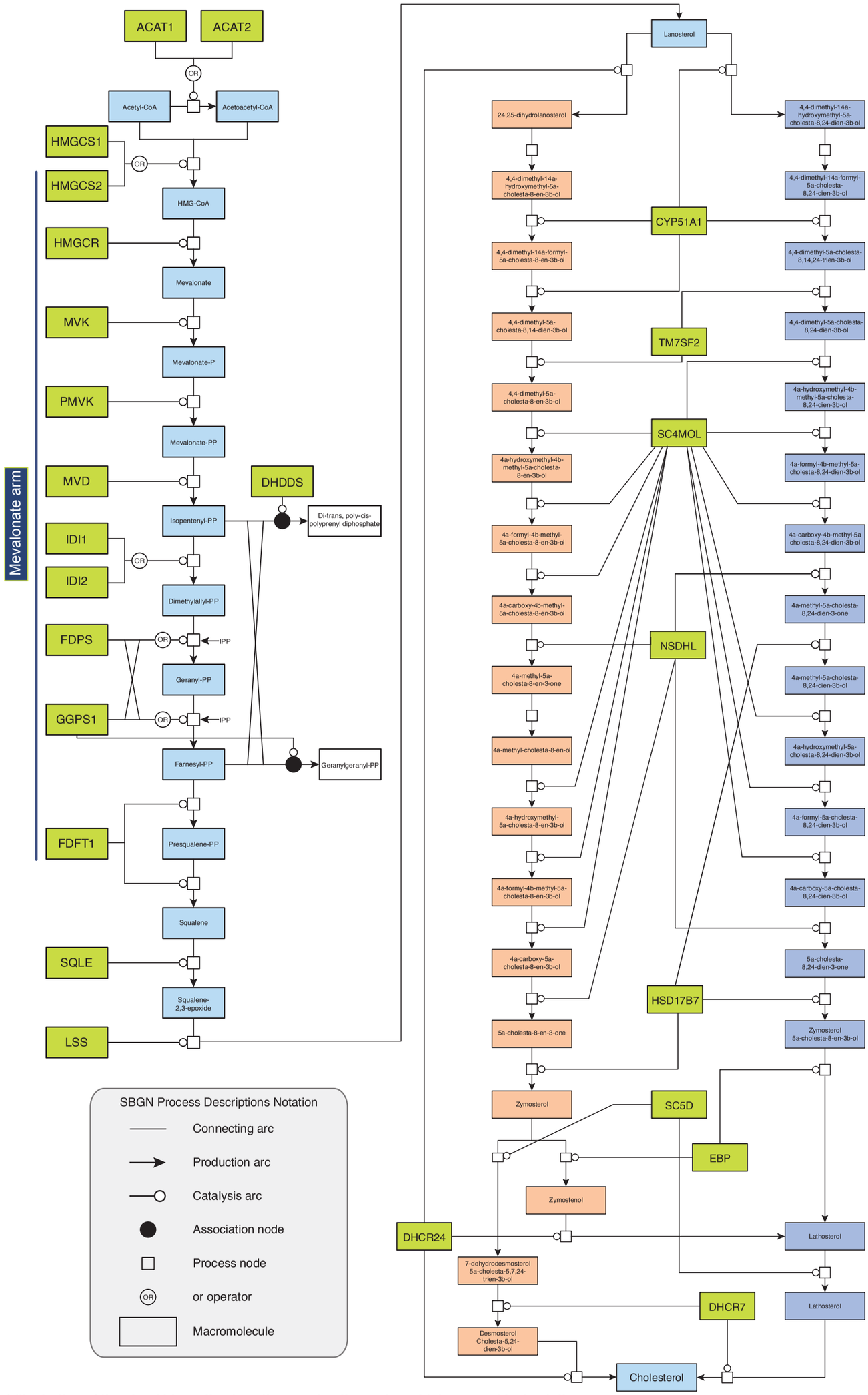

Figure 1.1 Illustration of the sterol biosynthesis pathway using the systems biology graphical notation.
This map details the synthesis of cholesterol from acetyl-CoA with corresponding notations shown on the bottom left. All the nodes are drawn using the systems biology graphical notation (Process Descriptions). The mevalonate isoprenoid arm is labelled as shown. Synthesis of cholesterol from lanosterol is divided into two pathways (Bloch pathway or the Kandutsch-Russell pathway). Details of each gene are listed in Table 1.1 (see next page). A total of 52 enzymatic reactions are described in the pathway map.

Table 1.1 Interaction table of the sequential synthesis of cholesterol from acetyl-CoA .

INTERACTANT 1 GENE SYMBOL	INTERACTANT 1 GENE NAME	HUMAN INTERACTANT 1 ENTREZ GENE ID (MOUSE)	AA SEQUENCE IDENTITY (HUMAN:MOUSE)	HUMAN CHROMOSOMAL LOCATION (MOUSE)	CATALYSIS INPUTS	CATALYSIS OUTPUTS
ACAT1	acetyl-CoA acetyltransferase 1	38 (110446)	84.07%	11q22.3 (9 29.12 cM)	acetyl-CoA (*2)	acetoacetyl-CoA
ACAT2	acetyl-CoA acetyltransferase 2	39 (110460)	87.66%	6q25.3 (17 8.73 cM)	acetyl-CoA (*2)	acetoacetyl-CoA
HMGCL	3-hydroxymethyl-3-methylglutaryl-CoA lyase	3155 (15356)	88.00%	1p36.1-p35 (4 68.14 cM)	HMG-CoA	acetoacetate
HMGCS1	3-hydroxymethyl-3-methylglutaryl-CoA synthase 1	3157 (208715)	94.62%	5p14-p13 (13)	acetyl-CoA + acetoacetyl-CoA	HMG-CoA
HMGCS2	3-hydroxymethyl-3-methylglutaryl-CoA synthase 2	3158 (15360)	81.69%	1p13-p12 (3 42.74 cM)	acetyl-CoA + acetoacetyl-CoA	HMG-CoA
HMGCR	3-hydroxymethyl-3-methylglutaryl-CoA reductase	3156 (15357)	93.47%	5q13.3-q14 (13 50.65 cM)	HMG-CoA	mevalonate
MVK	mevalonate kinase	4598 (17855)	80.81%	12q24 (5 55.99 cM)	mevalonate	mevalonate-5-phosphate
PMVK	phosphomevalonate kinase	10654 (68603)	83.33%	1q22 (3)	mevalonate-5-phosphate	mevalonate-5-diphosphate
MVD	diphosphomevalonate decarboxylase	4597 (192156)	83.79%	16q24.3 (8)	mevalonate-5-diphosphate	isopentenyl-5-diphosphate
IDI1	isopentenyl-diphosphate delta isomerase 1	3422 (319554)	79.23%	10p15.3 (13)	isopentenyl-5-diphosphate	dimethylallyl diphosphate
IDI2	isopentenyl-diphosphate delta isomerase 2	91734 (320581)	65.64%	10p15.3 (13)	isopentenyl-5-diphosphate	dimethylallyl diphosphate
FDPS	farnesyl diphosphate synthase	2224 (110196)	83.57%	1q22 (3 39.01 cM)	dimethylallyl diphosphate OR geranyl diphosphate	geranyl diphosphate OR farnesyl diphosphate
FDFT1	farnesyl diphosphate farnesyltransferase 1	2222 (14137)	88.25%	8p23.1-p22 (14 33.24 cM)	farnesyl diphosphate (*2)	squalene
GGPS1	geranylgeranyl diphosphate synthase 1	9453 (14593)	93.67%	1q43 (13 5.29 cM)	farnesyl diphosphate	geranylgeranyl diphosphate
DHDDS	dehydrodolichyl diphosphate synthase	79947 (67422)	82.58%	1p36.11 (4)	farnesyl diphosphate + isopentenyl diphosphate	polyprenyl diphosphate
SQLE	squalene epoxidase	6713 (20775)	84.15%	8q24.1 (15)	squalene	2,3-oxidosqualene
LSS	lanosterol synthase	4047 (16987)	85.68%	21q22.3 (10 39.1 cM)	2,3-oxidosqualene	lanosterol
DHCR7	7-dehydrocholesterol reductase	1717 (13360)	88.00%	11q13.4 (7 F5)	7-dehydrocholesterol	cholesterol
CYP51A1	cytochrome P450, family 51, subfamily A, polypeptide 1	1595 (13121)	90.18%	7q21.2 (5 2.3 cM)	lanosterol	cholesterol
TM7SF2	transmembrane 7 superfamily member 2	7108 (73166)	79.95%	11q13 (19)	14-demethyllanosterol	4,4-dimethyl-5α-cholesta-8,14,24-trien-3β-ol
MSMO1 (Sc4mol)	methylsterol monooxygenase 1 (sterol-c4-methyl oxidase-like)	6307 (66234)	49.49%	4q32-q34 (8)	4,4-dimethyl-5α-cholest-7-en-3β-ol	3β-hydroxy-4β-methyl-5α-cholest-7-ene-4α-carboxylate
NSDHL	NAD(P) dependent steroid dehydrogenase-like	50814 (18194)	82.62%	Xq28 (X 37.29 cM)	3β-hydroxy-4β-methyl-5α-cholest-7-ene-4α-carboxylate	4α-methyl-5α-cholest-7-en-3-one
HSD17B7	hydroxysteroid (17-beta) dehydrogenase 7	51478 (15490)	76.83%	1q23 (1)	4α-methyl-5α-cholest-7-en-3β-ol	4α-methyl-5α-cholest-7-en-3-one
EBP	emopamil binding protein (sterol isomerase)	10682 (13595)	77.83%	Xp11.23-p11.22 (X 3.7 cM)	lathosterol OR zymosterol	cholestenol OR 5α-cholesta-7,24-dien-3β-ol
SC5D	sterol-C5-desaturase	6309 (235293)	83.61%	11q23.3 (9 B)	lathosterol	7-dehydrocholesterol
DHCR24	24-dehydroxycholesterol reductase	1718 (74754)	96.90%	1p32.3 (4)	desmosterol OR lanosterol	cholesterol OR 24,25-dihydrolanosterol

This table details the synthesis of cholesterol from acetyl-CoA by the sterol biosyntehsis enzyme. The table is presented in a chronological order. Columns 1 and 2 are the names of the enzymes. Column 3 is the Entrez gene ID for the enzyme with the mouse ID included in brackets. Column 3 is the amino acid sequence identity represented in % between human and mouse. Column 5 is the chromosome location of the gene. The catalysis inputs enter the pathway and are catalyzed by the enzyme listed in column 1 to produce the catalysis outputs. For example, 2 acetyl-CoA molecules are consumed by the enzyme ACAT1 to produce a molecule of acetoacetyl-CoA.

1.9 References

Ačimovič, J., and Rozman, D. (2013). Steroidal triterpenes of cholesterol synthesis. Molecules 18, 4002–4017.

Ahrens, E.H., and Kunkel, H.G. (1949). The relationship between serum lipids and skin xanthomata in 18 patients with primary biliary cirrhosis. J. Clin. Invest. 28, 1565–1574.

Allison, a C. (1999). Squalene and squalane emulsions as adjuvants. Methods 19, 87–93.

Alsharifi, M., Mullbacher, A., and Regner, M. (2008). Interferon type I responses in primary and secondary infections. Immunol Cell Biol 86, 239–245.

Amemiya-Kudo, M., Shimano, H., Hasty, A.H., Yahagi, N., Yoshikawa, T., Matsuzaka, T., Okazaki, H., Tamura, Y., Iizuka, Y., Ohashi, K., et al. (2002). Transcriptional activities of nuclear SREBP-1a, -1c, and -2 to different target promoters of lipogenic and cholesterogenic genes. J Lipid Res 43, 1220–1235.

AuCoin, D.P., Smith, G.B., Meiering, C.D., and Mocarski, E.S. (2006). Betaherpesvirus-conserved cytomegalovirus tegument protein ppUL32 (pp150) controls cytoplasmic events during virion maturation. J. Virol. 80, 8199–8210.

Babiker, a., Andersson, O., Lund, E., Xiu, R.-J., Deeb, S., Reshef, a., Leitersdorf, E., Diczfalusy, U., and Bjorkhem, I. (1997). Elimination of Cholesterol in Macrophages and Endothelial Cells by the Sterol 27-Hydroxylase Mechanism: COMPARISON WITH HIGH DENSITY LIPOPROTEIN-MEDIATED REVERSE CHOLESTEROL TRANSPORT. J. Biol. Chem. 272, 26253–26261.

Bauernfeind, F., and Hornung, V. (2009). TLR2 joins the interferon gang. Nat. Immunol. 10, 1139–1141.

Bauman, D.R., Bitmansour, A.D., McDonald, J.G., Thompson, B.M., Liang, G., and Russell, D.W. (2009). 25-Hydroxycholesterol secreted by macrophages in response to Toll-like receptor activation suppresses immunoglobulin A production. Proc. Natl. Acad. Sci. U. S. A. 106, 16764–16769.

Bender, F.C., Whitbeck, J.C., Ponce de Leon, M., Lou, H., Eisenberg, R.J., and Cohen, G.H. (2003). Specific Association of Glycoprotein B with Lipid Rafts during Herpes Simplex Virus Entry. J. Virol. 77, 9542–9552.

Bensinger, S.J., Bradley, M.N., Joseph, S.B., Zelcer, N., Janssen, E.M., Hausner, M.A., Shih, R., Parks, J.S., Edwards, P. a, Jamieson, B.D., et al. (2008). LXR signaling couples sterol metabolism to proliferation in the acquired immune response. Cell 134, 97–111.

Benzaïd, I., Mönkkönen, H., Bonnelye, E., Mönkkönen, J., and Clézardin, P. (2012). In vivo phosphoantigen levels in bisphosphonate-treated human breast tumors trigger Vγ9Vδ2 T-cell antitumor cytotoxicity through ICAM-1 engagement. Clin. Cancer Res. 18, 6249–6259.

Bhaijee, F., Subramony, C., Tang, S.J., and Pepper, D.J. (2011). Human immunodeficiency virus-associated gastrointestinal disease: common endoscopic biopsy diagnoses. Patholog. Res. Int. 2011, 247923.

Birkenbach, M., Josefsen, K., Yalamanchili, R., Lenoir, G., and Kieff, E. (1993). Epstein-Barr virus-induced genes: first lymphocyte-specific G protein-coupled peptide receptors. J. Virol. 67, 2209–2220.

Björkhem, I., Andersson, O., Diczfalusy, U., Sevastik, B., Xiu, R.J., Duan, C., and Lund, E. (1994). Atherosclerosis and sterol 27-hydroxylase: evidence for a role of this enzyme in elimination of cholesterol from human macrophages. Proc. Natl. Acad. Sci. U. S. A. 91, 8592–8596.

Blanc, M., Hsieh, W.Y.Y., Robertson, K.A. a, Kropp, K.A. a, Forster, T., Shui, G., Lacaze, P., Watterson, S., Griffiths, S.J.J., Spann, N.J.J., et al. (2013). The transcription factor STAT-1 couples macrophage synthesis of 25-hydroxycholesterol to the interferon antiviral response. Immunity 38, 106–118.

Bloch, K. (1965). The biological synthesis of cholesterol. Science 150, 19–28.

Boehme, K.W., Guerrero, M., and Compton, T. (2006). Human cytomegalovirus envelope glycoproteins B and H are necessary for TLR2 activation in permissive cells. J. Immunol. 177, 7094–7102.

Borrie, P. (1957). Essential hyperlipaemia and idiopathic hypercholesterolaemic xanthomatosis. Br. Med. J. 2, 911–915.

Bresnahan, W.A., Boldogh, I., Thompson, E.A., and Albrecht, T. (1996). Human cytomegalovirus inhibits cellular DNA synthesis and arrests productively infected cells in late G1. Virology 224, 150–160.

Briner, W.W., Riddle, J.W., and Cornwell, D.G. (1959). Studies on the immunochemistry of human low density lipoproteins utilizing an hemagglutination technique. J. Exp. Med. 110, 113–122.

Britt, W.J. (1984). Neutralizing antibodies detect a disulfide-linked glycoprotein complex within the envelope of human cytomegalovirus. Virology 135, 369–378.

Brown, M.S., and Goldstein, J.L. (1974). Familial hypercholesterolemia: defective binding of lipoproteins to cultured fibroblasts associated with impaired regulation of 3-hydroxy-3-methylglutaryl coenzyme A reductase activity. Proc. Natl. Acad. Sci. U. S. A. 71, 788–792.

Brown, M.S., and Goldstein, J.L. (1976). Analysis of a mutant strain of human fibroblasts with a defect in the internalization of receptor-bound low density lipoprotein. Cell 9, 663–674.

Brown, M.S., Dana, S.E., and Goldstein, J.L. (1973). Regulation of 3-hydroxy-3-methylglutaryl coenzyme A reductase activity in human fibroblasts by lipoproteins. Proc. Natl. Acad. Sci. U. S. A. 70, 2162–2166.

Carlson, B.C., Jansson, a M., Larsson, a, Bucht, a, and Lorentzen, J.C. (2000). The endogenous adjuvant squalene can induce a chronic T-cell-mediated arthritis in rats. Am. J. Pathol. 156, 2057–2065.

Castella, B., Riganti, C., Fiore, F., Pantaleoni, F., Canepari, M.E., Peola, S., Foglietta, M., Palumbo, A., Bosia, A., Coscia, M., et al. (2011). Immune modulation by zoledronic acid in human myeloma: an advantageous cross-talk between Vγ9Vδ2 T cells, αβ CD8+ T cells, regulatory T cells, and dendritic cells. J. Immunol. 187, 1578–1590.

Castillo, J.P., Yurochko, A.D., and Kowalik, T.F. (2000). Role of human cytomegalovirus immediate-early proteins in cell growth control. J. Virol. 74, 8028–8037.

Chawla, a, Boisvert, W. a, Lee, C.H., Laffitte, B. a, Barak, Y., Joseph, S.B., Liao, D., Nagy, L., Edwards, P. a, Curtiss, L.K., et al. (2001). A PPAR gamma-LXR-ABCA1 pathway in macrophages is involved in cholesterol efflux and atherogenesis. Mol. Cell 7, 161–171.

Chen, Z., Knutson, E., Kurosky, A., and Albrecht, T. (2001). Degradation of p21cip1 in cells productively infected with human cytomegalovirus. J. Virol. 75, 3613–3625.

Choi, K.S., Aizaki, H., and Lai, M.M.C. (2005). Murine coronavirus requires lipid rafts for virus entry and cell-cell fusion but not for virus release. J. Virol. 79, 9862–9871.

Compton, T., and Feire, A. (2007). Early events in human cytomegalovirus infection. In Human Herpesviruses: Biology, Therapy, and Immunoprophylaxis, A. Arvin, G. Campadelli-Fiume, E. Mocarski, P.S. Moore, B. Roizman, R. Whitley, and K. Yamanishi, eds. (Cambridge),.

Compton, T., Nowlin, D.M., and Cooper, N.R. (1993). Initiation of human cytomegalovirus infection requires initial interaction with cell surface heparan sulfate. Virology 193, 834–841.

Cui, G., Qin, X., Wu, L., and Zhang, Y. (2011). Liver X receptor (LXR) mediates negative regulation of mouse and human Th17 differentiation. J. Clin. … 121.

Curtiss, L.K., and Edgington, T.S. (1976). Regulatory serum lipoproteins: regulation of lymphocyte stimulation by a species of low density lipoprotein. J. Immunol. 116, 1452–1458.

Cuthbert, J.A., and Lipsky, P.E. (1984). Immunoregulation by low density lipoproteins in man. Inhibition of mitogen-induced T lymphocyte proliferation by interference with transferrin metabolism. J. Clin. Invest. 73, 992–1003.

Dar, A.A., Patil, R.S., and Chiplunkar, S.V. (2014). Insights into the Relationship between Toll Like Receptors and Gamma Delta T Cell Responses. Front. Immunol. 5, 366.

Das, S., Vasanji, A., and Pellett, P.E. (2007). Three-dimensional structure of the human cytomegalovirus cytoplasmic virion assembly complex includes a reoriented secretory apparatus. J. Virol. 81, 11861–11869.

Dawson, P. a, Hofmann, S.L., van der Westhuyzen, D.R., Südhof, T.C., Brown, M.S., and Goldstein, J.L. (1988). Sterol-dependent repression of low density lipoprotein receptor promoter mediated by 16-base pair sequence adjacent to binding site for transcription factor Sp1. J. Biol. Chem. 263, 3372–3379.

DeBose-Boyd, R., Brown, M., and Li, W. (1999). Transport-dependent proteolysis of SREBP: relocation of site-1 protease from Golgi to ER obviates the need for SREBP transport to Golgi. Cell 99, 703–712.

DeBose-Boyd, R. a, Ou, J., Goldstein, J.L., and Brown, M.S. (2001). Expression of sterol regulatory element-binding protein 1c (SREBP-1c) mRNA in rat hepatoma cells requires endogenous LXR ligands. Proc. Natl. Acad. Sci. U. S. A. 98, 1477–1482.

Diaz-Rohrer, B., Levental, K.R., and Levental, I. (2014). Rafting through traffic: Membrane domains in cellular logistics. Biochim. Biophys. Acta.

Diczfalusy, U., Olofsson, K.E., Carlsson, A.-M., Gong, M., Golenbock, D.T., Rooyackers, O., Fläring, U., and Björkbacka, H. (2009). Marked upregulation of cholesterol 25-hydroxylase expression by lipopolysaccharide. J. Lipid Res. 50, 2258–2264.

Dobrosotskaya, I.Y., Goldstein, J.L., Brown, M.S., and Rawson, R.B. (2003). Reconstitution of sterol-regulated endoplasmic reticulum-to-Golgi transport of SREBP-2 in insect cells by co-expression of mammalian SCAP and Insigs. J Biol Chem 278, 35837–35843.

Drevot, P., Langlet, C., Guo, X.-J., Bernard, A.-M., Colard, O., Chauvin, J.-P., Lasserre, R., and He, H.-T. (2002). TCR signal initiation machinery is pre-assembled and activated in a subset of membrane rafts. EMBO J. 21, 1899–1908.

Eibinger, G., Fauler, G., Bernhart, E., Frank, S., Hammer, A., Wintersperger, A., Eder, H., Heinemann, A., Mischel, P.S., Malle, E., et al. (2013). On the role of 25-hydroxycholesterol synthesis by glioblastoma cell lines. Implications for chemotactic monocyte recruitment. Exp. Cell Res. 319, 1828–1838.

Everts, B., and Pearce, E.J. (2014). Metabolic control of dendritic cell activation and function: recent advances and clinical implications. Front. Immunol. 5, 203.

Feire, A.L., Koss, H., and Compton, T. (2004). Cellular integrins function as entry receptors for human cytomegalovirus via a highly conserved disintegrin-like domain. Proc. Natl. Acad. Sci. U. S. A. 101, 15470–15475.

Fernández, C., Martín, M., Gómez-Coronado, D., and Lasunción, M. a (2005). Effects of distal cholesterol biosynthesis inhibitors on cell proliferation and cell cycle progression. J. Lipid Res. 46, 920–929.

Ferruelo, A.J., Sua, Y., Ferna, C., and Mart, J. (2001). Dose-dependent e ¡ ects of lovastatin on cell cycle progression . Distinct requirement of cholesterol and non-sterol mevalonate derivatives. 1532, 185–194.

Frascaroli, G., Varani, S., Blankenhorn, N., Pretsch, R., Bacher, M., Leng, L., Bucala, R., Landini, M.P., and Mertens, T. (2009). Human cytomegalovirus paralyzes macrophage motility through down-regulation of chemokine receptors, reorganization of the cytoskeleton, and release of macrophage migration inhibitory factor. J Immunol 182, 477–488.

Freund, J. (1947). Some Aspects of Active Immunization. Annu. Rev. Microbiol. 1, 291–308.

Gao, D., Wu, J., Wu, Y.-T., Du, F., Aroh, C., Yan, N., Sun, L., and Chen, Z.J. (2013). Cyclic GMP-AMP synthase is an innate immune sensor of HIV and other retroviruses. Science 341, 903–906.

Gatto, D., Paus, D., Basten, A., Mackay, C.R., and Brink, R. (2009). Guidance of B cells by the orphan G protein-coupled receptor EBI2 shapes humoral immune responses. Immunity 31, 259–269.

Gatto, D., Wood, K., Caminschi, I., Murphy-Durland, D., Schofield, P., Christ, D., Karupiah, G., and Brink, R. (2013). The chemotactic receptor EBI2 regulates the homeostasis, localization and immunological function of splenic dendritic cells. Nat. Immunol. 14, 446–453.

Gee, D., Goldstein, J., Gray, C., and Fowler, J. (1959). Biosynthesis of cholesterol in familial hypercholesterolaemic xanthomatosis. Br. Med. J. 2, 341–344.

Gelissen, I.C., Harris, M., Rye, K.-A., Quinn, C., Brown, A.J., Kockx, M., Cartland, S., Packianathan, M., Kritharides, L., and Jessup, W. (2006). ABCA1 and ABCG1 synergize to mediate cholesterol export to apoA-I. Arterioscler. Thromb. Vasc. Biol. 26, 534–540.

Gober, H.-J., Kistowska, M., Angman, L., Jeno, P., Mori, L., and De Libero, G. (2003). Human T Cell Receptor Cells Recognize Endogenous Mevalonate Metabolites in Tumor Cells. J. Exp. Med. 197, 163–168.

Gogoi, D., and Chiplunkar, S. V (2013). Targeting gamma delta T cells for cancer immunotherapy: bench to bedside. Indian J. Med. Res. 138, 755–761.

Gold, E.S., Diercks, A.H., Podolsky, I., Podyminogin, R.L., Askovich, P.S., Treuting, P.M., and Aderem, A. (2014). 25-Hydroxycholesterol acts as an amplifier of inflammatory signaling. Proc. Natl. Acad. Sci. U. S. A.

Goto, H., Matsuda, K., Srikoon, P., Kariya, R., Hattori, S., Taura, M., Katano, H., and Okada, S. (2013). Potent antitumor activity of zoledronic acid-induced Vγ9Vδ2 T cells against primary effusion lymphoma. Cancer Lett. 3.

Greaves, R.F., and Mocarski, E.S. (1998). Defective growth correlates with reduced accumulation of a viral DNA replication protein after low-multiplicity infection by a human cytomegalovirus ie1 mutant. J. Virol. 72, 366–379.

Gudleski-O'Regan, N., Greco, T.M., Cristea, I.M., and Shenk, T. (2012). Increased expression of LDL receptor-related protein 1 during human cytomegalovirus infection reduces virion cholesterol and infectivity. Cell Host Microbe 12, 86–96.

Hamirally, S., Kamil, J.P., Ndassa-Colday, Y.M., Lin, A.J., Jahng, W.J., Baek, M.C., Noton, S., Silva, L.A., Simpson-Holley, M., Knipe, D.M., et al. (2009). Viral mimicry of Cdc2/cyclin-dependent kinase 1 mediates disruption of nuclear lamina during human cytomegalovirus nuclear egress. PLoS Pathog. 5, e1000275.

Hannedouche, S., Zhang, J., Yi, T., Shen, W., Nguyen, D., Pereira, J.P., Guerini, D., Baumgarten, B.U., Roggo, S., Wen, B., et al. (2011). Oxysterols direct immune cell migration via EBI2. Nature 475, 524–527.

Hansson, M., Ellis, E., Hunt, M.C., Schmitz, G., and Babiker, A. (2003). Marked induction of sterol 27-hydroxylase activity and mRNA levels during differentiation of human cultured monocytes into macrophages. Biochim. Biophys. Acta - Mol. Cell Res. 1593, 283–289.

Hayden, J.M., Brachova, L., Higgins, K., Obermiller, L., Sevanian, A., Khandrika, S., and Reaven, P.D. (2002). Induction of monocyte differentiation and foam cell formation in vitro by 7-ketocholesterol. J. Lipid Res. 43, 26–35.

Holstein, T.J., Fish, W. a, and Stokes, W.M. (1966). Pathway of cholesterol biosynthesis in the brain of the neonatal rat. J. Lipid Res. 7, 634–638.

Honda, A., Miyazaki, T., Ikegami, T., Iwamoto, J., Maeda, T., Hirayama, T., Saito, Y., Teramoto, T., and Matsuzaki, Y. (2011). Cholesterol 25-hydroxylation activity of CYP3A. J. Lipid Res. 52, 1509–1516.

Huber, M.T., and Compton, T. (1997). Characterization of a novel third member of the human cytomegalovirus glycoprotein H-glycoprotein L complex. J. Virol. 71, 5391–5398.

Ibanez, C.E., Schrier, R., Ghazal, P., Wiley, C., and Nelson, J.A. (1991). Human cytomegalovirus productively infects primary differentiated macrophages. J. Virol. 65, 6581–6588.

Inoue, J., Sato, R., Kawabe, Y., Kodama, T., Takano, T., and Maeda, M. (1996). Sterol-dependent Transcriptional Regulation of Sterol Regulatory Element-binding Protein-2. J. Biol. Chem. 271, 26461–26464.

Iskenderian, A.C., Huang, L., Reilly, A., Stenberg, R.M., and Anders, D.G. (1996). Four of eleven loci required for transient complementation of human cytomegalovirus DNA replication cooperate to activate expression of replication genes. J. Virol. 70, 383–392.

Jameson, J.M., Cruz, J., Costanzo, A., Terajima, M., and Ennis, F. a (2010). A role for the mevalonate pathway in the induction of subtype cross-reactive immunity to influenza A virus by human gammadelta T lymphocytes. Cell. Immunol. 264, 71–77.

Janowski, B.A. (2002). The hypocholesterolemic agent LY295427 up-regulates INSIG-1, identifying the INSIG-1 protein as a mediator of cholesterol homeostasis through SREBP. Proc Natl Acad Sci U S A 99, 12675–12680.

Javitt, N.B., Lee, Y.C., Shimizu, C., Fuda, H., and Strott, C. a (2001). Cholesterol and hydroxycholesterol sulfotransferases: identification, distinction from dehydroepiandrosterone sulfotransferase, and differential tissue expression. Endocrinology 142, 2978–2984.

Johnston, J.D., and Bloch, K. (1957). In Vitro Conversion of Zymosterol and Dihydrozymosterol to Cholesterol. J. Am. Chem. Soc. 79, 1145–1149.

De Jong, A., Cheng, T.-Y., Huang, S., Gras, S., Birkinshaw, R.W., Kasmar, A.G., Van Rhijn, I., Peña-Cruz, V., Ruan, D.T., Altman, J.D., et al. (2014). CD1a-autoreactive T cells recognize natural skin oils that function as headless antigens. Nat. Immunol. 15, 177–185.

Juckem, L.K., Boehme, K.W., Feire, a. L., and Compton, T. (2008). Differential Initiation of Innate Immune Responses Induced by Human Cytomegalovirus Entry into Fibroblast Cells. J. Immunol. 180, 4965–4977.

Kabouridis, P.S., Janzen, J., Magee, a L., and Ley, S.C. (2000). Cholesterol depletion disrupts lipid rafts and modulates the activity of multiple signaling pathways in T lymphocytes. Eur. J. Immunol. 30, 954–963.

Kamei, Y., Miura, S., Suganami, T., Akaike, F., Kanai, S., Sugita, S., Katsumata, A., Aburatani, H., Unterman, T.G., Ezaki, O., et al. (2008). Regulation of SREBP1c gene expression in skeletal muscle: role of retinoid X receptor/liver X receptor and forkhead-O1 transcription factor. Endocrinology 149, 2293–2305.

Kandutsch, A.A., and Russell, A.E. (1959). Preputial gland tumor sterols. I. The occurrence of 24,25-dihydrolanosterol and a comparison with liver and the normal gland. J. Biol. Chem. 234, 2037–2042.

Kandutsch, A.A., and Russell, A.E. (1960a). Preputial gland tumor sterols. 2. The identification of 4 alpha-methyl-Delta 8-cholesten-3 beta-ol. J. Biol. Chem. 235, 2253–2255.

Kandutsch, A.A., and Russell, A.E. (1960b). Preputial gland tumor sterols. 3. A metabolic pathway from lanosterol to cholesterol. J. Biol. Chem. 235, 2256–2261.

Kari, B., Goertz, R., and Gehrz, R. (1990). Characterization of cytomegalovirus glycoproteins in a family of complexes designated gC-II with murine monoclonal antibodies. Arch. Virol. 112, 55–65.

Kawai, T., and Akira, S. (2008). Toll-like receptor and RIG-I-like receptor signaling. Ann. N. Y. Acad. Sci. 1143, 1–20.

Kerur, N., Veettil, M.V., Sharma-Walia, N., Bottero, V., Sadagopan, S., Otageri, P., and Chandran, B. (2011). IFI16 acts as a nuclear pathogen sensor to induce the inflammasome in response to Kaposi Sarcoma-associated herpesvirus infection. Cell Host Microbe 9, 363–375.

Kidani, Y., Elsaesser, H., Hock, M.B., Vergnes, L., Williams, K.J., Argus, J.P., Marbois, B.N., Komisopoulou, E., Wilson, E.B., Osborne, T.F., et al. (2013). Sterol regulatory element-binding proteins are essential for the metabolic programming of effector T cells and adaptive immunity. Nat. Immunol. 14, 489–499.

Kindt, Thomas J, Richard A. Goldsby, Barbara A. Osborne, and J.K. (2007). Kuby immunology (New York: W.H. Freeman).

Kipp, H.A. (1920). Variation in the cholesterol content of the serum in pneumonia.

Kistowska, M., Rossy, E., Sansano, S., Gober, H.-J., Landmann, R., Mori, L., and De Libero, G. (2008). Dysregulation of the host mevalonate pathway during early bacterial infection activates human TCR gamma delta cells. Eur. J. Immunol. 38, 2200–2209.

Knight, B.L., Patel, D.D., and Soutar, a K. (1983). The regulation of 3-hydroxy-3-methylglutaryl-CoA reductase activity, cholesterol esterification and the expression of low-density lipoprotein receptors in cultured monocyte-derived macrophages. Biochem. J. 210, 523–532.

Komazin-Meredith, G., Petrella, R.J., Santos, W.L., Filman, D.J., Hogle, J.M., Verdine, G.L., Karplus, M., and Coen, D.M. (2008). The human cytomegalovirus UL44 C clamp wraps around DNA. Structure 16, 1214–1225.

Korherr, C., Gille, H., Schäfer, R., Koenig-Hoffmann, K., Dixelius, J., Egland, K. a, Pastan, I., and Brinkmann, U. (2006). Identification of proangiogenic genes and pathways by high-throughput functional genomics: TBK1 and the IRF3 pathway. Proc. Natl. Acad. Sci. U. S. A. 103, 4240–4245.

Langdon, R.G., and Bloch, K. (1953). The utilization of squalene in the biosynthesis of cholesterol. J. Biol. Chem. 200, 135–144.

Lees, R.S., Fiser, R.H., Beisel, W.R., and Bartelloni, P.J. (1972). Effects of an experimental viral infection on plasma lipid and lipoprotein metabolism. Metabolism. 21, 825–833.

Li, L.N., and Dong, P.W. (2009). Endocrine therapy plus zoledronic acid in premenopausal breast cancer. N. Engl. J. Med. 360, 2368; author reply 2369–70.

Li, G., Gu, H.-M., and Zhang, D.-W. (2013a). ATP-binding cassette transporters and cholesterol translocation. IUBMB Life 65, 505–512.

Li, X.-D., Wu, J., Gao, D., Wang, H., Sun, L., and Chen, Z.J. (2013b). Pivotal roles of cGAS-cGAMP signaling in antiviral defense and immune adjuvant effects. Science 341, 1390–1394.

Li-Hawkins, J., Lund, E.G., Turley, S.D., and Russell, D.W. (2000). Disruption of the oxysterol 7alpha-hydroxylase gene in mice. J. Biol. Chem. 275, 16536–16542.

Liu, C., Yang, X. V, Wu, J., Kuei, C., Mani, N.S., Zhang, L., Yu, J., Sutton, S.W., Qin, N., Banie, H., et al. (2011). Oxysterols direct B-cell migration through EBI2. Nature 475, 519–523.

Liu, S.-Y., Aliyari, R., Chikere, K., Li, G., Marsden, M.D.D., Smith, J.K.K., Pernet, O., Guo, H., Nusbaum, R., Zack, J.A. a, et al. (2013). Interferon-inducible cholesterol-25-hydroxylase broadly inhibits viral entry by production of 25-hydroxycholesterol. Immunity 38, 92–105.

Loregian, A., Appleton, B.A., Hogle, J.M., and Coen, D.M. (2003). Residues of Human Cytomegalovirus DNA Polymerase Catalytic Subunit UL54 That Are Necessary and Sufficient for Interaction with the Accessory Protein UL44. J. Virol. 78, 158–167.

Ly, D., and Moody, D.B. (2014). The CD1 size problem: lipid antigens, ligands, and scaffolds. Cell. Mol. Life Sci. 71, 3069–3079.

Maceyka, M., and Spiegel, S. (2014). Sphingolipid metabolites in inflammatory disease. Nature 510, 58–67.

Machesky, N.J., Zhang, G., Raghavan, B., Zimmerman, P., Kelly, S.L., Merrill, A.H., Waldman, W.J., Van Brocklyn, J.R., and Trgovcich, J. (2008). Human cytomegalovirus regulates bioactive sphingolipids. J. Biol. Chem. 283, 26148–26160.

Marschall, M., Marzi, A., aus dem Siepen, P., Jochmann, R., Kalmer, M., Auerochs, S., Lischka, P., Leis, M., and Stamminger, T. (2005). Cellular p32 recruits cytomegalovirus kinase pUL97 to redistribute the nuclear lamina. J. Biol. Chem. 280, 33357–33367.

Marshall, K.R., Rowley, K. V, Rinaldi, A., Nicholson, I.P., Ishov, A.M., Maul, G.G., and Preston, C.M. (2002). Activity and intracellular localization of the human cytomegalovirus protein pp71. J. Gen. Virol. 83, 1601–1612.

Mathews, J.D., and Feery, B.J. (1978). Cholesterol and immune response to influenza antigens. Lancet 2, 1212–1213.

Matsuda, M., Korn, B.S., Hammer, R.E., Moon, Y. a, Komuro, R., Horton, J.D., Goldstein, J.L., Brown, M.S., and Shimomura, I. (2001). SREBP cleavage-activating protein (SCAP) is required for increased lipid synthesis in liver induced by cholesterol deprivation and insulin elevation. Genes Dev. 15, 1206–1216.

McGeoch, D.J., Cook, S., Dolan, A., Jamieson, F.E., and Telford, E.A. (1995). Molecular phylogeny and evolutionary timescale for the family of mammalian herpesviruses. J Mol Biol 247, 443–458.

Meier, J.L., and Pruessner, J.A. (2000). The human cytomegalovirus major immediate-early distal enhancer region is required for efficient viral replication and immediate-early gene expression. J. Virol. 74, 1602–1613.

Mettenleiter, T.C., Klupp, B.G., and Granzow, H. (2009). Herpesvirus assembly: an update. Virus Res. 143, 222–234.

Milbradt, J., Webel, R., Auerochs, S., Sticht, H., and Marschall, M. (2010). Novel mode of phosphorylation-triggered reorganization of the nuclear lamina during nuclear egress of human cytomegalovirus. J. Biol. Chem. 285, 13979–13989.

Mou, F., Forest, T., and Baines, J.D. (2007). US3 of herpes simplex virus type 1 encodes a promiscuous protein kinase that phosphorylates and alters localization of lamin A/C in infected cells. J. Virol. 81, 6459–6470.

Myerson, D., Hackman, R.C., Nelson, J.A., Ward, D.C., and McDougall, J.K. (1984). Widespread presence of histologically occult cytomegalovirus. Hum. Pathol. 15, 430–439.

Nahum, A., Dadi, H., Bates, A., and Roifman, C.M. (2012). The biological significance of TLR3 variant, L412F, in conferring susceptibility to cutaneous candidiasis, CMV and autoimmunity. Autoimmun. Rev. 11, 341–347.

Nestel, P.J., Whyte, H.M., and Goodman, D.S. (1969). Distribution and turnover of cholesterol in humans. J. Clin. Invest. 48, 982–991.

Nolan, T., Bravo, L., Ceballos, A., Mitha, E., Gray, G., Quiambao, B., Patel, S.S., Bizjajeva, S., Bock, H., Nazaire-Bermal, N., et al. (2014). Enhanced and persistent antibody response against homologous and heterologous strains elicited by a MF59®-adjuvanted influenza vaccine in infants and young children. Vaccine 1–11.

Norlin, M., Andersson, U., Björkhem, I., and Wikvall, K. (2000). Oxysterol 7 alpha-hydroxylase activity by cholesterol 7 alpha-hydroxylase (CYP7A). J. Biol. Chem. 275, 34046–34053.

Ogawa-Goto, K., Tanaka, K., Gibson, W., Moriishi, E., Miura, Y., Kurata, T., Irie, S., and Sata, T. (2003). Microtubule Network Facilitates Nuclear Targeting of Human Cytomegalovirus Capsid Microtubule Network Facilitates Nuclear Targeting of. J. Virol. 77, 8541–8547.

Oliveira-Nascimento, L., Massari, P., and Wetzler, L.M. (2012). The Role of TLR2 in Infection and Immunity. Front. Immunol. 3, 79.

Osborne, T.F., Gil, G., Goldstein, J.L., and Brown, M.S. (1988). Operator constitutive mutation of 3-hydroxy-3-methylglutaryl coenzyme A reductase promoter abolishes protein binding to sterol regulatory element. J. Biol. Chem. 263, 3380–3387.

Park, K., and Scott, A.L. (2010). Cholesterol 25-hydroxylase production by dendritic cells and macrophages is regulated by type I interferons. J. Leukoc. Biol. 88, 1081–1087.

Pereira, J.P., Kelly, L.M., Xu, Y., and Cyster, J.G. (2009). EBI2 mediates B cell segregation between the outer and centre follicle. Nature 460, 1122–1126.

Pham, T.H., Kwon, K.M., Kim, Y.-E., Kim, K.K., and Ahn, J.-H. (2013). DNA sensing-independent inhibition of herpes simplex virus 1 replication by DAI/ZBP1. J. Virol. 87, 3076–3086.

Podack, E., and Lowrey, D. (1988). Function of Granule Perform and Esterases in T Cell-Mediated Reactions. Ann. New … 016960.

Poggi, A., Boero, S., Musso, A., and Zocchi, M.R. (2013). Selective role of mevalonate pathway in regulating perforin but not FasL and TNFalpha release in human Natural Killer cells. PLoS One 8, e62932.

Popkin, D.L., and Virgin, H.W. th (2003). Murine cytomegalovirus infection inhibits tumor necrosis factor alpha responses in primary macrophages. J Virol 77, 10125–10130.

Rader, D.J., and deGoma, E.M. (2012). Approach to the patient with extremely low HDL-cholesterol. J. Clin. Endocrinol. Metab. 97, 3399–3407.

Rawson, R.B., Zelenski, N.G., Nijhawan, D., Ye, J., Sakai, J., Hasan, M.T., Chang, T.Y., Brown, M.S., and Goldstein, J.L. (1997). Complementation cloning of S2P, a gene encoding a putative metalloprotease required for intramembrane cleavage of SREBPs. Mol. Cell 1, 47–57.

Reboldi, a., Dang, E. V., McDonald, J.G., Liang, G., Russell, D.W., and Cyster, J.G. (2014). 25-Hydroxycholesterol suppresses interleukin-1-driven inflammation downstream of type I interferon. Science (80-.). 345, 679–684.

Ren, X., Glende, J., Yin, J., Schwegmann-Wessels, C., and Herrler, G. (2008). Importance of cholesterol for infection of cells by transmissible gastroenteritis virus. Virus Res 137, 220–224.

Rentero, C., Zech, T., Quinn, C.M., Engelhardt, K., Williamson, D., Grewal, T., Jessup, W., Harder, T., and Gaus, K. (2008). Functional implications of plasma membrane condensation for T cell activation. PLoS One 3, e2262.

Roelofs, A.J., Jauhiainen, M., Mönkkönen, H., Rogers, M.J., Mönkkönen, J., and Thompson, K. (2009). Peripheral blood monocytes are responsible for gammadelta T cell activation induced by zoledronic acid through accumulation of IPP/DMAPP. Br. J. Haematol. 144, 245–250.

Roper, B. (1964). Essential Hypercholesterolaemic Xanthomatosis. Br. Med. J. 1963–1964.

Rosenzweig, I.B., Wiebe, D. a, Borden, E.C., Storer, B., and Shrago, E.S. (1987). Plasma lipoprotein changes in humans induced by beta-interferon. Atherosclerosis 67, 261–267.

Sanchez, V., and Dong, J.J. (2010). Alteration of lipid metabolism in cells infected with human cytomegalovirus. Virology 404, 71–77.

Sanchez, V., Angeletti, P.C., Engler, J.A., and Britt, W.J. (1998). Localization of human cytomegalovirus structural proteins to the nuclear matrix of infected human fibroblasts. J. Virol. 72, 3321–3329.

Sanchez, V., Greis, K.D., Sztul, E., and Britt, W.J. (2000a). Accumulation of virion tegument and envelope proteins in a stable cytoplasmic compartment during human cytomegalovirus replication: characterization of a potential site of virus assembly. J. Virol. 74, 975–986.

Sanchez, V., Sztul, E., and Britt, W.J. (2000b). Human cytomegalovirus pp28 (UL99) localizes to a cytoplasmic compartment which overlaps the endoplasmic reticulum-golgi-intermediate compartment. J. Virol. 74, 3842–3851.

Sanchez, V., Mahr, J.A., Orazio, N.I., and Spector, D.H. (2007). Nuclear export of the human cytomegalovirus tegument protein pp65 requires cyclin-dependent kinase activity and the Crm1 exporter. J. Virol. 81, 11730–11736.

Scanu, a, Pollard, H., and Reader, W. (1968). Properties of human serum low density lipoproteins after modification by succinic anhydride. J. Lipid Res. 9, 342–349.

Schectman, G., Kaul, S., Mueller, R. a., Borden, E.C., and Kissebah, a. H. (1992). The effect of interferon on the metabolism of LDLs. Arterioscler. Thromb. Vasc. Biol. 12, 1053–1062.

Shine, T.E., Little, J.R., Shore, V., Medoff, G., and Abegg, a (1980). Effect of exogenous lipids and lipoproteins on the primary immune response in vitro. Eur. J. Immunol. 10, 714–718.

Shope, R. (1930). Variations in the plasma cholesterol and cholesterol ester content in hog cholera. J. Exp. Med. 51, 179–187.

Singaraja, R.R., Visscher, H., James, E.R., Chroni, A., Coutinho, J.M., Brunham, L.R., Kang, M.H., Zannis, V.I., Chimini, G., and Hayden, M.R. (2006). Specific mutations in ABCA1 have discrete effects on ABCA1 function and lipid phenotypes both in vivo and in vitro. Circ. Res. 99, 389–397.

Sinzger, C., Kahl, M., Laib, K., Klingel, K., Rieger, P., Plachter, B., and Jahn, G. (2000). Tropism of human cytomegalovirus for endothelial cells is determined by a post-entry step dependent on efficient translocation to the nucleus. J. Gen. Virol. 81, 3021–3035.

Smith, J.R., Osborne, T.F., Brown, M.S., Goldstein, J.L., and Gil, G. (1988). Multiple sterol regulatory elements in promoter for hamster 3-hydroxy-3-methylglutaryl-coenzyme A synthase. J. Biol. Chem. 263, 18480–18487.

Spann, N.J., Garmire, L.X., McDonald, J.G., Myers, D.S., Milne, S.B., Shibata, N., Reichart, D., Fox, J.N., Shaked, I., Heudobler, D., et al. (2012). Regulated accumulation of desmosterol integrates macrophage lipid metabolism and inflammatory responses. Cell 151, 138–152.

Spencer, C.M., Schafer, X.L., Moorman, N.J., and Munger, J. (2011). Human cytomegalovirus induces the activity and expression of acetyl-coenzyme A carboxylase, a fatty acid biosynthetic enzyme whose inhibition attenuates viral replication. J. Virol. 85, 5814–5824.

Stokes, W.M., Fish, W.A., and Hickey, F.C. (1956). Metabolism of cholesterol in the chick embryo. II. Isolation and chemical nature of two companion sterols. J. Biol. Chem. 220, 415–430.

Stokes, W.M., C, H.F., and Fish, W.A. (1958). Sterol metabolism. I. The occurrence of desmosterol (24-dehydrocholesterol) in rat skin and its conversion in vivo to cholesterol. J. Biol. Chem. 232, 347–359.

Subramanian, G., Chaudhury, P., Malu, K., Fowler, S., Manmode, R., Gotur, D., Zwerger, M., Ryan, D., Roberti, R., and Gaines, P. (2012). Lamin B receptor regulates the growth and maturation of myeloid progenitors via its sterol reductase domain: implications for cholesterol biosynthesis in regulating myelopoiesis. J. Immunol. 188, 85–102.

Sun, D. (2003). Lovastatin inhibits bone marrow-derived dendritic cell maturation and upregulates proinflammatory cytokine production. Cell. Immunol. 223, 52–62.

Sun, L., Wu, J., Du, F., Chen, X., and Chen, Z.J. (2013). Cyclic GMP-AMP synthase is a cytosolic DNA sensor that activates the type I interferon pathway. Science 339, 786–791.

Sundqvist, A., and Ericsson, J. (2003). Transcription-dependent degradation controls the stability of the SREBP family of transcription factors. Proc Natl Acad Sci U S A 100, 13833–13838.

Tabeta, K., Georgel, P., Janssen, E., Du, X., Hoebe, K., Crozat, K., Mudd, S., Shamel, L., Sovath, S., Goode, J., et al. (2004). Toll-like receptors 9 and 3 as essential components of innate immune defense against mouse cytomegalovirus infection. Proc. Natl. Acad. Sci. U. S. A. 101, 3516–3521.

Takahashi, T., Gasch, a, Nishizawa, N., and Chua, N.H. (1995). The DIMINUTO gene of Arabidopsis is involved in regulating cell elongation. Genes Dev. 9, 97–107.

Takaoka, A., Wang, Z., Choi, M.K., Yanai, H., Negishi, H., Ban, T., Lu, Y., Miyagishi, M., Kodama, T., Honda, K., et al. (2007). DAI (DLM-1/ZBP1) is a cytosolic DNA sensor and an activator of innate immune response. Nature 448, 501–505.

Tchen, T.T., and Bloch, K. (1957). On the conversion of squalene to lanosterol in vitro. J. Biol. Chem. 226, 921–930.

Thiery, J., and Lieberman, J. (2014). Perforin: a key pore-forming protein for immune control of viruses and cancer. Subcell. Biochem. 80, 197–220.

Thompson, P.A., Gauthier, K.C., Varley, A.W., and Kitchens, R.L. (2010). ABCA1 promotes the efflux of bacterial LPS from macrophages and accelerates recovery from LPS-induced tolerance. J Lipid Res.

Uldrich, A.P., Le Nours, J., Pellicci, D.G., Gherardin, N. a, McPherson, K.G., Lim, R.T., Patel, O., Beddoe, T., Gras, S., Rossjohn, J., et al. (2013). CD1d-lipid antigen recognition by the γδ TCR. Nat. Immunol. 14, 1137–1145.

Unterholzner, L., Keating, S.E., Baran, M., Horan, K. a, Jensen, S.B., Sharma, S., Sirois, C.M., Jin, T., Latz, E., Xiao, T.S., et al. (2010). IFI16 is an innate immune sensor for intracellular DNA. Nat. Immunol. 11, 997–1004.

Victora, G.D., Dominguez-Sola, D., Holmes, A.B., Deroubaix, S., Dalla-Favera, R., and Nussenzweig, M.C. (2012). Identification of human germinal center light and dark zone cells and their relationship to human B-cell lymphomas. Blood 120, 2240–2248.

Viikari, J., Ruuskanen, O., Salmi, T., and Halonen, P. (1979). Effect of measles and measles vaccine on serum-cholesterol. Lancet 1, 326.

Van der Vliet, H.J., and Verheul, H.M.W. (2012). Breast-cancer adjuvant therapy with zoledronic acid. N. Engl. J. Med. 366, 188–9; author reply 189.

Walzer, T., Jaeger, S., Chaix, J., and Vivier, E. (2007). Natural killer cells: from CD3(-)NKp46(+) to post-genomics meta-analyses. Curr. Opin. Immunol. 19, 365–372.

Wang, H., Sarikonda, G., Puan, K.-J., Tanaka, Y., Feng, J., Giner, J.-L., Cao, R., Mönkkönen, J., Oldfield, E., and Morita, C.T. (2011). Indirect stimulation of human Vγ2Vδ2 T cells through alterations in isoprenoid metabolism. J. Immunol. 187, 5099–5113.

Wang, H., Yao, Y., Huang, C., Fu, X., Chen, Q., Zhang, H., Chen, J., Fang, F., Xie, Z., and Chen, Z. (2014). An adjuvanted inactivated murine cytomegalovirus (MCMV) vaccine induces potent and long-term protective immunity against a lethal challenge with virulent MCMV. BMC Infect. Dis. 14, 195.

Wang, N., Silver, D.L., Thiele, C., and Tall, a R. (2001). ATP-binding cassette transporter A1 (ABCA1) functions as a cholesterol efflux regulatory protein. J. Biol. Chem. 276, 23742–23747.

Wangs, X., Briggsq, R., Hua, X., Yokoyama, C., Goldstein, J.L., Briggss, M.R., Wango, X., and Brown, M.S. (1993). Nuclear Protein That Binds Sterol Regulatory Element of Low Density Lipoprotein Receptor Promoter. 268, 14490–14496.

Whitehouse, M.W., Orr, K.J., Beck, F.W., and Pearson, C.M. (1974). Freund's adjuvants: relationship of arthritogenicity and adjuvanticity in rats to vehicle composition. Immunology 27, 311–330.

Wójcicka, G., Jamroz-wiśniewska, A., and Horoszewicz, K. (2007). Liver X receptors (LXRs). Part I : Structure , function , regulation of activity , and role in lipid metabolism Receptory wątrobowe X (LXR). Część I : Budowa , funkcja , regulacja aktywności i znaczenie w metabolizmie lipidów. 736–759.

Wu, J., Sun, L., Chen, X., Du, F., Shi, H., Chen, C., and Chen, Z.J. (2013). Cyclic GMP-AMP is an endogenous second messenger in innate immune signaling by cytosolic DNA. Science 339, 826–830.

Xu, J., Wagoner, G., Douglas, J.C., and Drew, P.D. (2009). Liver X receptor agonist regulation of Th17 lymphocyte function in autoimmunity. J. Leukoc. Biol. 86, 401–409.

Yamamoto, M. (2004). TIR domain-containing adaptors define the specificity of TLR signaling. Mol. Immunol. 40, 861–868.

Yang, T., Espenshade, P.J., Wright, M.E., Yabe, D., Gong, Y., Aebersold, R., Goldstein, J.L., and Brown, M.S. (2002). Crucial step in cholesterol homeostasis: sterols promote binding of SCAP to INSIG-1, a membrane protein that facilitates retention of SREBPs in ER. Cell 110, 489–500.

Ye, X., Xu, S., Xin, Y., Yu, S., Ping, Y., Chen, L., Xiao, H., Wang, B., Yi, L., Wang, Q., et al. (2012). Tumor-associated microglia/macrophages enhance the invasion of glioma stem-like cells via TGF-β1 signaling pathway. J. Immunol. 189, 444–453.

Yew, K.-H., Carpenter, C., Duncan, R.S., and Harrison, C.J. (2012). Human cytomegalovirus induces TLR4 signaling components in monocytes altering TIRAP, TRAM and downstream interferon-beta and TNF-alpha expression. PLoS One 7, e44500.

Yi, T., Wang, X., Kelly, L.M., An, J., Xu, Y., Sailer, A.W., Gustafsson, J.-A., Russell, D.W., and Cyster, J.G. (2012). Oxysterol gradient generation by lymphoid stromal cells guides activated B cell movement during humoral responses. Immunity 37, 535–548.

Yilmaz, A., Reiss, C., Weng, A., Cicha, I., Stumpf, C., Steinkasserer, A., Daniel, W.G., and Garlichs, C.D. (2006). Differential effects of statins on relevant functions of human monocyte-derived dendritic cells. J. Leukoc. Biol. 79, 529–538.

Youssef, S., Stüve, O., Patarroyo, J.C., Ruiz, P.J., Radosevich, J.L., Hur, E.M., Bravo, M., Mitchell, D.J., Sobel, R. a, Steinman, L., et al. (2002). The HMG-CoA reductase inhibitor, atorvastatin, promotes a Th2 bias and reverses paralysis in central nervous system autoimmune disease. Nature 420, 78–84.

Yu, Y., Maguire, T.G., and Alwine, J.C. (2012). Human cytomegalovirus infection induces adipocyte-like lipogenesis through activation of sterol regulatory element binding protein 1. J. Virol. 86, 2942–2949.

Yu, Y., Pierciey, F.J., Maguire, T.G., and Alwine, J.C. (2013). PKR-like endoplasmic reticulum kinase is necessary for lipogenic activation during HCMV infection. PLoS Pathog. 9, e1003266.

Yvan-Charvet, L., Pagler, T., Gautier, E.L., Avagyan, S., Siry, R.L., Han, S., Welch, C.L., Wang, N., Randolph, G.J., Snoeck, H.W., et al. (2010). ATP-binding cassette transporters and HDL suppress hematopoietic stem cell proliferation. Science 328, 1689–1693.

Zerenturk, E.J., Sharpe, L.J., Ikonen, E., and Brown, A.J. (2013). Desmosterol and DHCR24: unexpected new directions for a terminal step in cholesterol synthesis. Prog. Lipid Res. 52, 666–680.

Zhang, M., Xin, H., Duan, Y., and Atherton, S.S. (2005). Ocular reactivation of MCMV after immunosuppression of latently infected BALB/c mice. Invest Ophthalmol Vis Sci 46, 252–258.

Chapter 2

Investigation of the role of the mevalonate-isoprenoid arm in MCMV replication

2.1 Introduction

Host defense against viral infection requires the induction of both innate and adaptive immune responses. The former is mediated partially by complex interactions between interferon, monocytes/macrophages, and natural killer cells. Recently, changes in cholesterol gene expression have been observed during HCV (Park et al., 2009), HIV (Zheng et al., 2003), and West Nile virus (Mackenzie et al., 2007) infections, underlying the importance of cholesterol metabolism in viral replication. In addition, extensive literature review (Chapter 1) has further highlighted the importance of the sterol biosynthesis pathway in the modulation and the development of both innate and adaptive immunity.

Cholesterol plays many important regulatory roles in physiology, including maintaining membrane fluidity and integrity, and acting as a precursor for hormones and signaling molecules. Conversely, focal buildup of cholesterol in arteries produces atherosclerotic plaques, the cause of many cardiovascular conditions such as myocardial infarction and stroke (Wang et al., 2008). Cholesterol homeostasis is maintained at multiple levels, notably through synthesis and transport. Cholesterol and many other steroids are synthesized from acetyl-CoA, a metabolite from the catabolism of carbohydrates, lipids and proteins. Acetyl-CoA is converted to cholesterol through the sterol biosynthesis pathway, which involves at least 23 enzymes (Horton et al., 2002, 2003; Sun et al., 2007) (Figure 1.1). Central to this pathway is a family of membrane-bound transcription factors termed

sterol regulatory element-binding proteins (SREBPs). SREBP2 is the predominant transcription factor that regulates cholesterol biosynthesis. Reduction in intracellular cholesterol by either serum deprivation or cholesterol removal triggers the translocation and activation of SREBP2 (Figure 2.1A). SREBP2 responsive genes in the cholesterol biosynthetic pathway include the enzymes HMG-CoA synthase (*Hmgcs1*) (Moriyama et al., 1998), HMG-CoA reductase (*Hmgcr*) (Sato, Miyamoto et al. 1999), farnesyl diphosphate synthase (*Fdps*) (Ericsson et al., 1996), and squalene epoxidase (*Sqle*) (Guan et al., 1995). Cholesterol acts as an inhibitory signal for the proteolytic activation of SREBP2 (Figure 2.2B), effectively turning off cholesterol biosynthesis gene transcription.

In addition to SREBP2 mediated pathway feedback regulation, cholesterol synthesis can be artificially manipulated by direct inhibition of enzymes within the pathway. Triparanol (MER-29) was one of the first clinically approved compounds for treating hypercholesterolemia with significantly positive outcomes (Hollander et al., 1960; Jepson, 1962; Kandutsch and Russell, 1960). Triparanol works by preventing the reduction of the C24-C25 double bond of lanosterol (see Chapter 1, Figure 1.2B), thus preventing cholesterol synthesis (Steinberg et al., 1961). However, triparanol was later withdrawn due to serious side-effects, including cataracts (clouding of the lens inside the eye) (Kirby, 1967; Modell, 1967; Winkelmann et al., 1963). The work of Brown and Goldstein has shown that the activity of HMGCR is negatively correlated with cholesterol concentrations (Brown et al., 1973), indicating that inhibition of HMG-CoA reductase would be an effective means of lowering plasma cholesterol. Citrinin, from *Pythium ultimum*, was the first antibiotic compound isolated from fungi that was capable of inhibiting cholesterol synthesis from acetate (Endo and Kuroda, 1976). Structural analysis has indicated that citrinin functions by binding to the HMGCR catalytic domain, inhibiting the synthesis of mevalonate (Tanzawa et al., 1977). ML-236B, now known as compactin or mevastatin, was isolated from *Penicillium citrinum* (Pen-51) by Akira Endo, Masao Kuraoda, and Yoshio Tsujita (Endo et al., 1976). Compactin (mevastatin) was also shown as an HMGCR inhibitor and was capable of lowering cholesterol *in vitro* and *in vivo* (Endo et al., 1977, 1979). However, compactin

was never marketed by Sankyo due to the lack of commercial interest (Endo, 2010). A derivative version of compactin called CS-514 (pravastatin) was later launched as a replacement of compactin (Nakaya et al., 1987; Tobert, 1987). Currently, pravastatin, lovastatin (mevinolin, monacolin K, isolated from *Monascus ruber*) (Endo, 1979), and simvastatin (MK-733) (Mol et al., 1986; Walker and Tobert, 1987) make up some of the most widely used cholesterol lowering drugs (see Experimental procedure 7.2.2 for statin structural information).

We previously showed that genes encoding cholesterol biosynthesis enzymes are down-regulated upon infection in bone marrow derived macrophages (BMDM) by type one interferon (IFN-I) as an antiviral response to murine cytomegalovirus (MCMV) (Blanc, Hsieh et al. 2011). Significant reductions in the level of sterol biosynthesis enzymes (*Hmgcr*, *Hmgcs1*, and *Sqle*) and free intracellular cholesterol were also observed 24-hours post MCMV infection or IFN-β treatment. Collectively, these findings imply that cholesterol metabolism is modulated during infection and inflammatory response. However, the molecular connection between interferon response and cholesterol metabolism is not well understood.

Prompted by the evidence that cholesterol metabolism is regulated by interferon as a part of the overall antiviral response, I hypothesize that there is a dependency of MCMV replication on the sterol biosynthesis pathway. Specifically, this chapter aims to identify which parts of the sterol biosynthesis pathway are important for viral replication. In this present study, a series of gene knockdown experiments were first performed, showing that the mevalonate-isoprenoid arm (see Figure 1.1 for reference) of the sterol biosynthesis pathway is important for MCMV replication. Pharmacological inhibition of sterol biosynthesis by statins leads to significant reductions in viral growth and plaque size expansion. Importantly, statin inhibition can be overcome with the addition of mevalonate and/or geranylgeraniol. Together, these results demonstrate the dependency of MCMV replication on the sterol and isoprenoid pathways. The findings are integral to the understanding of the interferon-sterol regulatory mechanism and subsequent chapters will focus on the further development of these mechanisms.

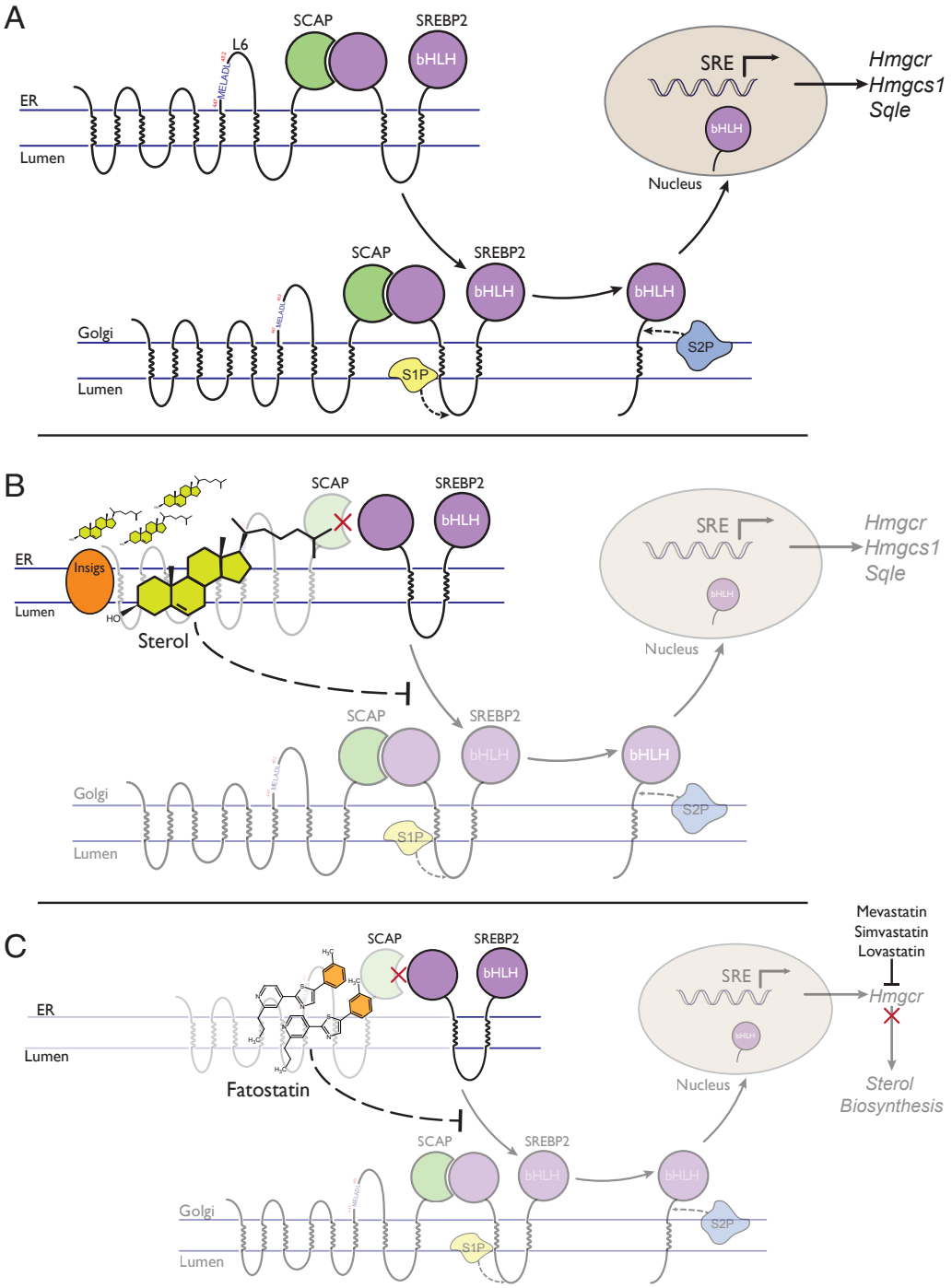

Figure 2.1 The activation SREBP2 pathway leads to the activation of sterol biosynthesis and is inhibited by statin.

(A) SREBP2 is synthesized as an ER membrane bound precursor. When the cells are depleted in cholesterol, SREBP cleavage-activating protein (SCAP) binds and escorts SREBP2 from the ER to the Golgi apparatus. This translocation is mediated by the MELADL sequence (aa 447-452) on loop 6 of SCAP. The release of SREBP2 is initiated through two sequential cleavages by Site-1 Protease (S1P) and Site-2 Protease (S2P). After the second cleavage, the active SREBP2-bHLH domain leaves the membrane. The cleaved SREBP2 nuclear fraction enters the nucleus, where it binds to the sterol response element (SRE) and activates genes controlling cholesterol synthesis and uptake. (B) When the cholesterol level is above a certain threshold, sterol binds directly to SCAP, triggering SCAP to bind to INSIGs [insulin induced gene 1 (*Insig1*) and insulin induced gene 2 (*Insig2*)], preventing the translation and subsequent activation of SREBP2. (C) Fatostatin directly binds to SCAP, thus preventing the translocation of the SCAP-SREBP2 complex and subsequent sterol biosynthesis steps. Mevastatin, simvastatin, lovastatin are HMG-CoA reductase competitive inhibitors. Binding of statin to the reductase inhibits the synthesis of mevalonate intermediate, limiting the production of cholesterol.

2.2 Results

2.2.1 siRNA knock-down of the mevalonate-isoprenoid branch of the sterol biosynthesis pathway is antiviral

As a first step to assess whether the sterol biosynthesis pathway is important in regulating MCMV replication, siRNA knockdown experiments were performed targeting different parts of the cholesterol metabolism enzymes (Figure 2.2). These experiments utilize a GFP reporter virus (MCMV-GFP) that encodes an HCMV promoter-driven GFP gene under the control of the MCMV major immediate-early enhancer (MIE) (see Experiment procedure 7.3.1 for the viral construct (Δie3revgfp) and 7.3.5 for siRNA screening procedure). As the reporter virus replicates, GFP accumulates within the cell culture. The rate of GFP accumulation, determined by changes in fluorescent intensity over time (e.g. slope), reflects the rate of viral replication (Angulo et al., 2000). This technique provides a real-time measurement for monitoring changes in viral replication. Silencing of an anti-viral gene would result in an increase in the rate of viral replication, and a faster rate of GFP accumulation (e.g. a steeper slope). Conversely, silencing of a pro-viral gene would result in a decrease in the rate of viral growth, leading to slower GFP accumulation in the culture (e.g. a shallow slope) (see Experimental procedure 7.3.4 for the illustration). In the siRNA knockdown experiments, NIH-3T3 fibroblasts were transfected with siRNA for 48 hr, followed by MCMV-GFP infection. As a control, *RISC free* siRNA (which cannot be incorporated into the cellular RNA-induced silencing complex (RISC)), was used as a reference control to negate the effects of transfection. Additionally, *M54* siRNA, which specifically targets MCMV ORF (MCMV polymerase) was also used as a control for the expected antiviral knockdown profile. Prior to the infection experiments, the efficiency and specificity of siRNAs at silencing their designated gene targets were first tested. RNA from transfected cells was harvested, and the abundance of gene transcript was assayed by qRT-PCR (see Experimental procedure 7.6.1). Figure 2.2C shows that siRNAs targeting *Hmgcs1*, *Hmgcr*, *Idi1*, *Fdps*, *Ggps1*, *Dhcr7*, and *Sqle* had >70% knockdown efficiency, while *Fdft1*, *RabggtA*, and *RabggtB* had >50% knockdown efficiency. The knockdown efficiencies of *FntA* and *B* were not tested due

to the availability of the probe-primer sets. The knockdown efficiency experiments confirmed that these commercially designed siRNAs are effective at silencing their specific gene targets. To demonstrate that siRNAs themselves do not cause cytotoxicity, cell viability of the transfected cells was measured using CellTiter-Blue prior to infection (48 hr post-transfect) (see Experimental procedure 7.4.2). Apart from *M54* (Figure 2.2B), none of the siRNAs displayed any significant cytotoxic effects.

In the reporter virus experiments, siRNA targeting *Hmgcs1*, *Hmgcr*, and *Fdps* that are upstream of the prenylation branch (Figure 2.2A) (See Figure 1.1 for pathway reference) displayed significant decrease in the rate of viral replication. To further dissect the specific role of other pathway members, additional siRNA knockdown studies were conducted targeting genes distal to the mevalonate-isoprenoid branch of the pathway. The Knockdown of *Fdft1*, *Sqle* (which is immediately downstream of the prenylation branch), and *Dhcr7* led to stimulation of viral replication (Figure 2.2A). To further investigate the specificity of the prenylation branch of the pathway, siRNA knockdown experiments were performed targeting the prenyltransferases (these are farnesyltransferase, geranylgeranyltransferase type I, and geranylgeranyltransferase type II enzymes). Significant viral inhibition was observed with siRNA targeting geranylgeranyltransferase type II enzymes (*Rabggta* & *Rabggtb*), but not *Pggt1b* (geranylgeranyltransferase type I), or *Fntb* (farnesyltransferase) (Figure 2.2A).

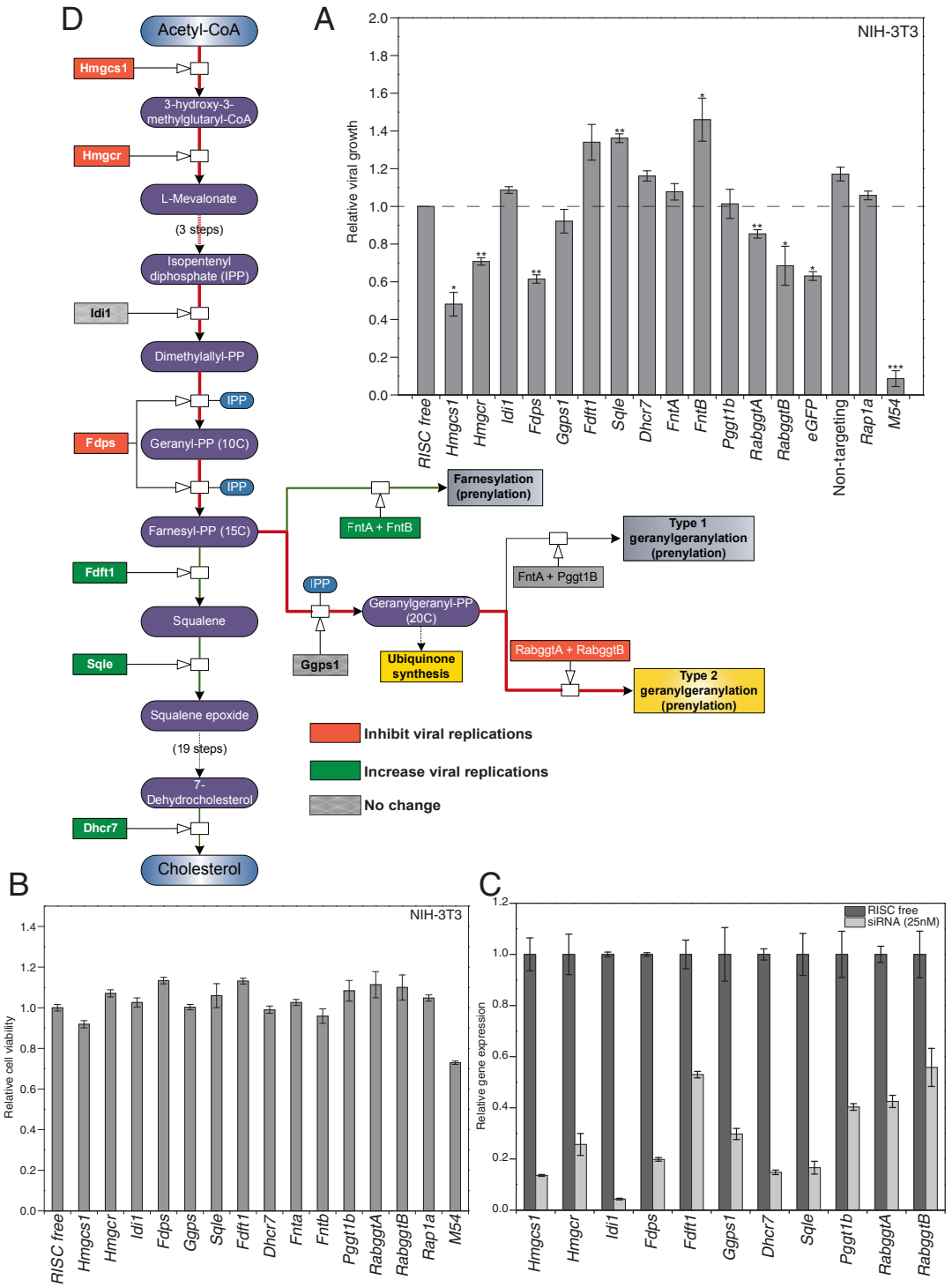

Figure 2.2 siRNA knock-down of mevalonate-isoprenoid branch of the sterol biosynthesis pathway is antiviral.

(A) NIH-3T3 fibroblasts (1.5x10^4 cells/well) were transfected in 96-well plates with On-target plus siRNAs as indicated for 48 hr then infected with MCMV-GFP (MOI = 0.05). *RISC free* was used as a transfection control, while *M54* specifically targets MCMV polymerase. The level of infection was determined by measuring the increase in GFP fluorescence (slope) during the linear-phase of viral growth. The graph represents the relative level of infection compared to *RISC free* transfected and data are the mean of 6 biological replicates ± SEM. *p<0.05, **p<0.01, ***p<0.001 (B) NIH-3T3 fibroblasts (1.5x10^4 cells/well) were transfected with On-target plus siRNAs as indicated in 96-well plates for 48 hr, then the cell viability was measured using CellTiter-Blue as described in Experimental procedure 7.4.2. Relative cell viability was calculated by normalizing to the *RISC free* transfected samples and data are the mean of 6 biological replicates ± SEM. (C) Measuring the efficiency of the transfection knock-down. NIH-3T3 fibroblasts (3.5x10^4 cells/well)

were transfected in 48-well plates with On-target plus siRNAs as indicated for 48 hr then the total cellular RNA was isolated. Relative abundance of the specific siRNA targeted gene transcript with respect to *RISC free* transfected sample was assayed by qRT-PCR using 25ng of RNA. Data are the mean of 3 biological replicates ± SEM. (D) Sterol pathway diagram summarizing the siRNA knockdown findings.

2.2.2 Inhibition of sterol biosynthesis by statin has antiviral effects against CMV

The above siRNA knockdown experiments demonstrated that the mevalonate-isoprenoid branch of the pathway is important for MCMV replication. To complement these findings, I then utilize the use of a class of cholesterol lowering pharmacological compounds, known as statins. Among the 5 statins examined in this chapter, mevastatin, simvastatin, lovastatin, and pravastatin are potent and selective inhibitors of HMGCR (Figure 2.1C) (Gazzerro et al., 2012). Inhibition of HMGCR results in a reduction of mevalonate and an accompanying drop in intracellular cholesterol (Gazzerro et al., 2012). Fatostatin, however, does not inhibit HMGCR. The binding of fatostatin to SCAP prevents the translocation of SREBP1 and 2 and the transcription of sterol biosynthesis enzymes (Figure 2.1C), resulting in an eventual decrease in cholesterol (Kamisuki et al., 2009).

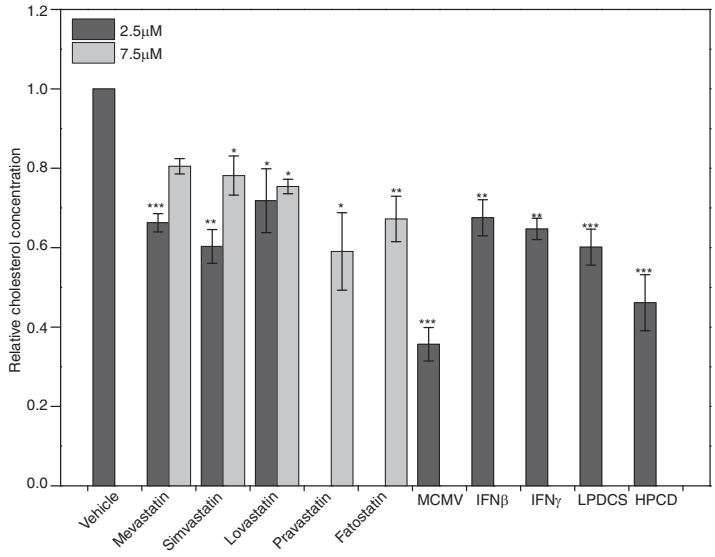

Figure 2.3 Statins are effective at lowering intracellular cholesterol.
Relative intracellular cholesterol concentrations in NIH-3T3 fibroblasts ($8x10^5$ cells/well in 6-well) following 2 x 24 hr incubation of mevastatin, simvastatin, lovastatin, pravastatin, fatostatin, IFNβ (100U/ml), IFNγ (100U/ml), or infected with MCMV (MOI = 1), or 50 min incubation with 0.1% w/v HPCD compared to vehicle treated samples. Cholesterol was extracted from lysates of each sample, and the cholesterol level was measured using the Amplex Red Cholesterol assay kit as described in Experimental procedure 7.5.2. Protein concentration in each sample relative to the corresponding vehicle was calculated using a standard BCA assay. Calculated cholesterol concentrations were divided by relative protein concentrations to better represent the cholesterol produced by equivalent cell numbers receiving each treatment. Data represent the means ± SEM from seven independent experiments (2 for HPCD). *p<0.05, **p<0.01, ***p<0.001

As statins are capable of lowering cholesterol, control experiments were first conducted to address whether these statins are biologically active. In these experiments, NIH-3T3 fibroblasts were treated with statins, interferon, or infected with MCMV for 48 hr, and the intracellular cholesterol levels were measured (see Experimental procedure 7.5.2). As positive controls, additional cells were also incubated in either delipidised media (see Experimental procedure 7.1 for formulation) or media supplemented with hydroxypropyl-β-cyclodextrin (HPβCD). Due to the lack of lipids in the delipidised media, cells grown under this condition consume intracellular cholesterol over time, leading to cholesterol reduction. Furthermore, cyclodextrin, such as HPCD, can rapidly solubilize and remove intracellular cholesterol, which leads to cholesterol deprivation. Figure 2.3 shows that all 5 statins can significantly reduce intracellular cholesterol (~30% reduction) when compared to vehicle treated samples. Similarly, treatment with interferon (β/γ) and CMV infection also significantly reduce intracellular cholesterol, an agreement with our previous observations in BMDM (Blanc, Hsieh et al., 2011).

To determine whether statins are antiviral, NIH-3T3 fibroblasts were pretreated with statins for 24 hr, followed by MCMV infection. The amounts of infectious particles were measured four days post-infection via plaque assay (see Experimental procedure 7.3.2). Treatments with mevastatin, simvastatin, and lovastatin resulted in a significant inhibition of MCMV plaque formation (Figure 2.4A), while pravastatin and fatostatin failed to elicit any antiviral effects. To clarify whether the antiviral effect of the above statins is restricted to murine CMV, similar experiments were conducted using human lung fibroblasts (MRC-5) and a more clinically relevant virus, human CMV. In these experiments, MRC-5 was pre-treated with statins, followed by HCMV-GFP reporter virus infection. Treatments with mevastatin, simvastatin, and lovastatin also showed a dose-dependent inhibition of HCMV replication with a 50% inhibitory concentration (IC_{50}, see Experimental procedure 7.4.5 for the calculation) of 1.2, 0.7 and 0.8μM respectively (Figure 2.4C). Notably, the antiviral effect of these statins occurred below the concentration of observable cell toxicity (>15μM) (Figure 2.4B and D). Similar to the results obtained with the MCMV,

both pravastatin and fatostatin failed to show any inhibitory effects against HCMV. Collectively, these results showed that although all the statins tested in the above experiment can lower intracellular cholesterol in NIH-3T3 fibroblasts, only mevastatin, simvastatin, and lovastatin showed antiviral effect. This indicates that inhibition of cholesterol synthesis by statin does not contribute to the inhibition of the virus, but rather it involves the disruption of other parts of the sterol biosynthesis pathway.

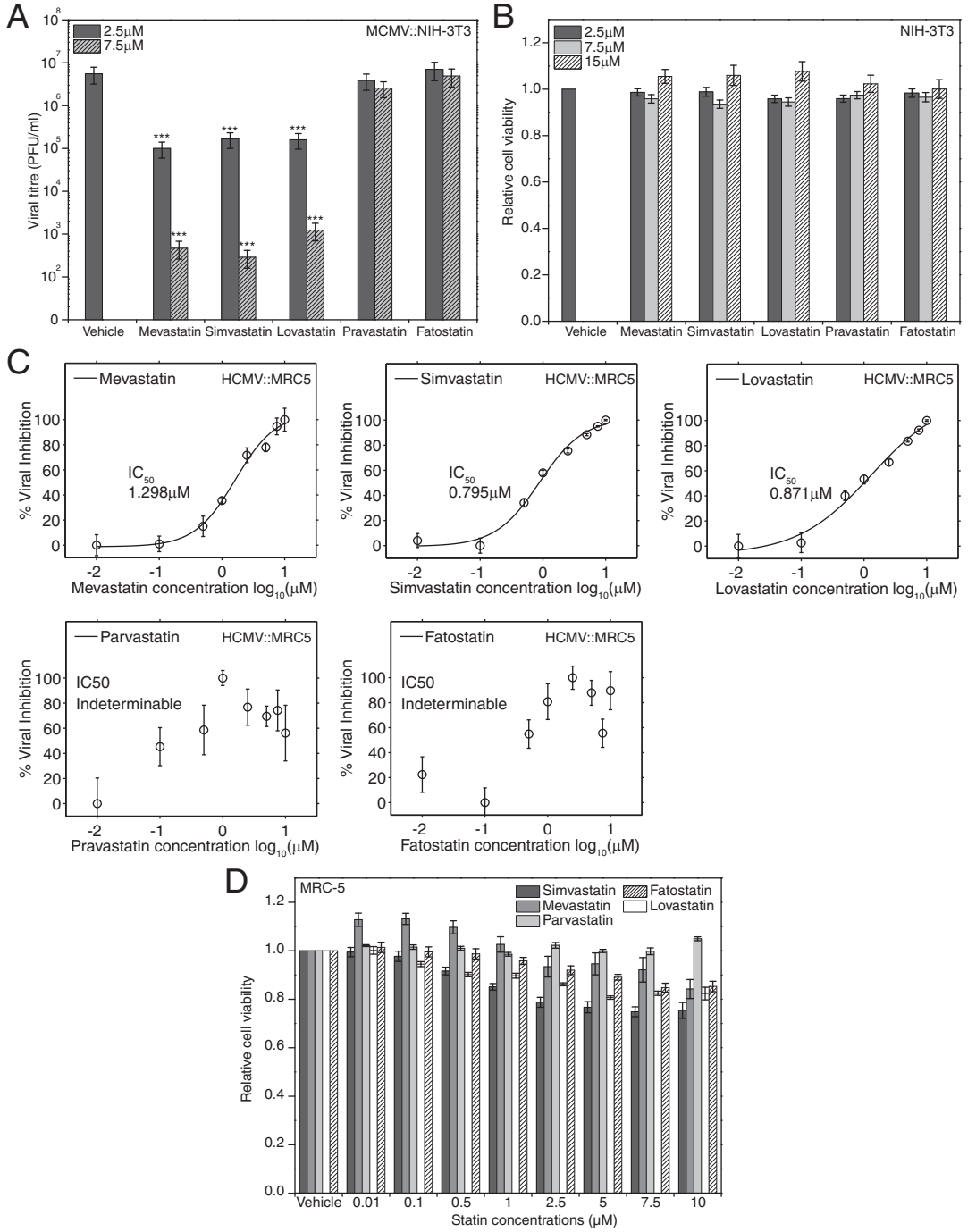

Figure 2.4 Statins elicit antiviral effects against both MCMV and HCMV.
(A) NIH-3T3 fibroblasts were seeded in 6-well plate at $8x10^5$ cells/well. The next day, cells were treated with five different statins at 2 different concentrations (2.5 or 7.5μM) for 24 hr then infected with MCMV (MOI = 0.05). At 4 dpi, 200μl of viral supernatant was taken and the viral titre was determined by plaque assay as described in Experimental procedure 6.3.2. n = 8, with mean ± SEM. ***p<0.001 (B) NIH-3T3 fibroblasts ($3x10^4$ cells/well in 96-wells) were treated with statins (2.5, 7.5, or 15μM) 24 hr then re-fed with statins for another 48 hr. Cell viability was measured 96 hr post treatment using CellTiter-Blue as described in Experimental procedure 7.4.2. Relative cell viability was calculated by normalizing to vehicle treated samples and data are the mean of 12 biological replicates ± SEM. (C) MRC-5 ($3x10^4$ cells/well in 96-wells) were treated with statins at an increasing dosage 24 hr prior to and after infection with HCMV-AD169-GFP (MOI = 0.25). The level of infection was determined by measuring the increase in GFP fluorescence (slope) during the linear-phase of viral growth. Data represents mean ± SEM for two experiments (8 replicates per experiment). (D) MRC-5 ($3x10^4$ cells/well in 96-wells) were treated with statins at an increasing dosage 24 hr re-fed with statins for another 48 hr. Cell viability was measured 96 hr post treatment using CellTiter-Blue. Relative cell viability was calculated by normalizing to vehicle treated samples, and data are the mean of 12 biological replicates ± SEM.

2.2.3 Analysis of the effects of statin on cellular apoptosis

To explore the potential antiviral mechanisms of statins, the first step was to examine the known biological effects of statins and their relevant contributions to the antiviral affects. Statins have been shown to exert anti-inflammatory and anti-proliferative functions (Cafforio et al., 2005), while inducing apoptosis in human T (Denoyelle et al., 2001), B (Yavasoglu et al., 2013) and myeloma tumour (Qi et al., 2013) cells. Statin induced apoptosis is characterized by the induction of cysteine-dependent aspartate-directed protease 3 (caspase 3) (Föcking et al., 2004; Werner et al., 2004) and 7 (caspase 7) (van der Meulen et al., 2006). Activation of caspase 3 and 7 (also known as the effector caspase) by the initiator caspases (caspase 2, 8, 9 and 10) leads to the subsequent cleavage of other protein substrates, triggering the apoptosis signalling cascade (Zmasek et al., 2007). To investigate whether apoptosis induced by statin leads to an antiviral state, NIH-3T3 fibroblasts were treated with statins at three different dosages (2.5, 7.5, and 15μM) for 48 hr, and the level of caspase 3/7 was assayed as an indicator of apoptosis (see Experimental procedure 7.4.2). Staurosporine, a known inducer for cellular apoptosis, was used as a control (24 hr treatment only) (Belmokhtar et al., 2001). Treatments of mevastatin, simvastatin, lovastatin, and fatostatin, but not pravastatin led to a dose-dependent increase in caspase 3/7 activities (Figure 2.5A) (1.2, 1.7, 3 fold increase respectively). In comparison, staurosporine elicited a stronger induction in caspase activities (~4.5 fold).

The plaque assay and apoptosis results indicated that although statins can induce cellular apoptosis, the magnitude of induction is insufficient to achieve a decrease of more than 2 logs in viral titre. Furthermore, fatostatin, which also induces apoptosis, failed to elicit any antiviral effect. Overall, these findings show that inhibition of viral growth is not due to cholesterol deprivation or apoptosis, but rather a part of the pathway involving a proximal mevalonate-prenylation step.

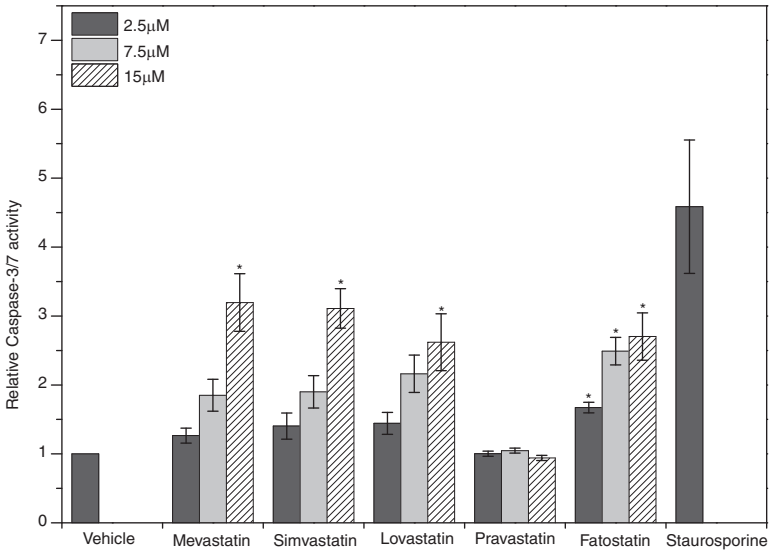

Figure 2.5 Statins are effective at inducing apoptosis.
NIH-3T3 fibroblasts were seeded in 96 well plates at $3x10^4$ cells/well. The next day, cells were treated with statins (2.5, 7.5, or 15μM) for 48 hr or 0.1μM staurosporine for 24 hr and the level of apoptosis was assessed using the Caspase-Glo 3/7 assay as described in Experimental procedure 6.4.2. n = 3, mean ± SEM. *$p<0.05$

2.2.4 The antiviral effect of statin can be metabolically rescued with specific sterol biosynthesis secondary metabolites

The cumulative data above suggest that blocking of HMG-CoA reductase by statin is linked to the inhibition of viral replication. Pharmacological reagents such as statins often have non-specific off-target effects. To demonstrate that statin inhibition is specific to the cholesterol biosynthesis pathway, metabolic rescue experiments were performed. In these experiments, NIH-3T3 fibroblasts were first infected with MCMV-GFP, then treated with vehicle or mevastatin supplemented with or without specific sterol secondary metabolites. Figure 2.6A shows that the addition of farnesol or squalene did not rescue the inhibitory activity of statin, whilst the addition of mevalonate or mevalonolactone, or geranylgeraniol fully rescued the antiviral activity. This observation was subsequently validated via viral growth curve analysis (Figure 2.6B). Interestingly, in the viral GFP assay, cells treated with geranylgeraniol alone showed strong induction (~3.5 fold) in viral replication (Figure 2.6A). However, this induction did not lead to a significant increase in viral particle formation as measured by plaque assay (Figure 2.6B). Thus, it was possible that this enhancement was due to the unspecific effects of geranylgeraniol.

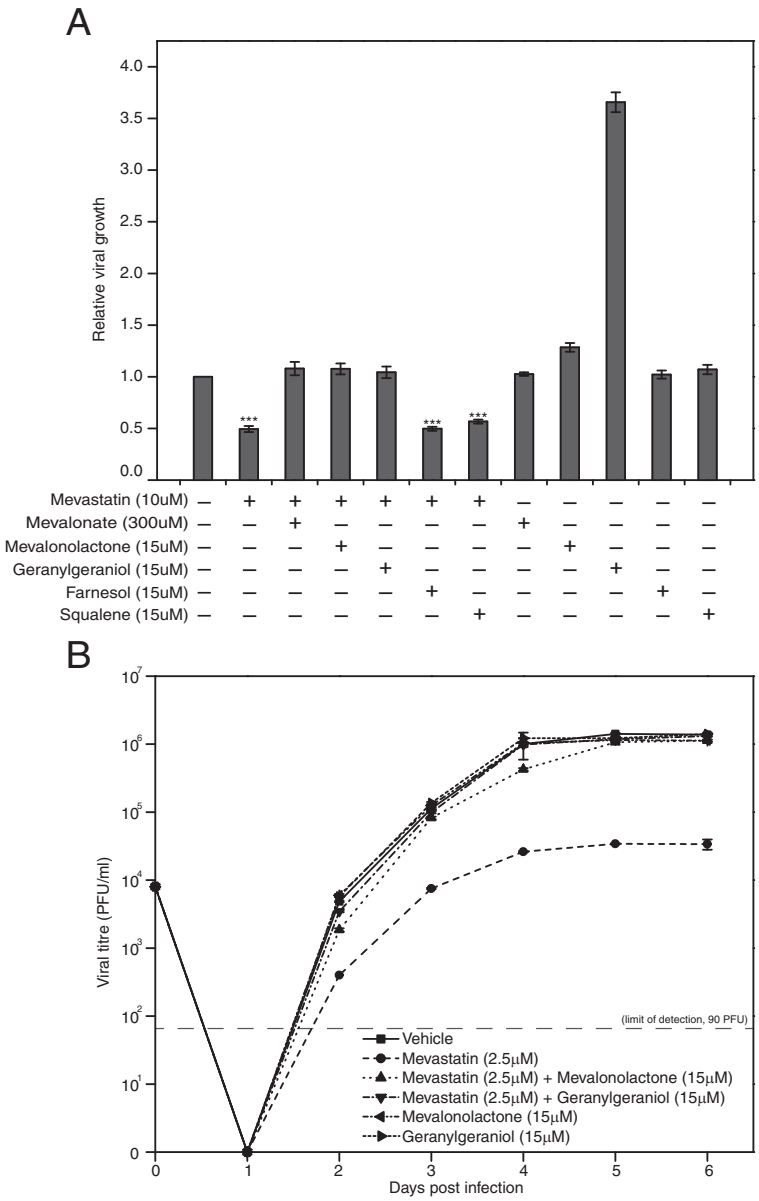

Figure 2.6 Statins antiviral effect can be reversed with cholesterol secondary metabolites.
(A) NIH-3T3 fibroblasts were seeded at a seeding density of $3x10^4$ cells/well in 96-well plates. The next day, cells were infected with MCMV-GFP (MOI = 0.05) for 1 hr and subsequently incubated with media supplemented with either vehicle, mevastatin ± sterol metabolites as indicated in the figure. The level of infection was determined by measuring the increase in GFP fluorescence (slope) during the linear-phase of viral growth. Data are normalized to vehicle treated wells. Data represents mean ± SEM for four experiments (8 replicates per experiment). ***$p<0.001$ (B) NIH-3T3 fibroblasts were seeded at a seeding density of $8x10^5$ cells/well in 6-well plates. The next day, cells were infected with MCMV-C3X (MOI = 0.01) for 1 hr, followed by 5 washes with blank media. After washing, cells were incubated with vehicle, mevastatin ± mevalonolactone or geranylgeraniol as indicated in the figure. 200μl supernatants were collected every day, while cells were refed with the same treatment (200μl/well) and viral titre was quantitated by plaque assay. Data are the mean of 6 biological replicates ± SEM.

2.2.5 Statin pre-treatment does not inhibit viral entry but reduces intra and extracellular viral titre and viral plaque formation

Previous studies with HIV (Gigue`re, 2004) and Andes virus (Petersen et al., 2014) have shown that statin treatment inhibits viral entry. To determine whether statin treatment affects MCMV entry, NIH-3T3 fibroblasts were pre-treated with mevastatin (10μM) for 24 hr, followed by MCMV-C3X infection. The number of MCMV genomes entering the cells, represented by the copy number of MCMV *M115* late gene, was quantified by PCR (see Experimental procedure 7.3.7). Treatment with statin did not alter the number of viral genome copies in the infected cell (Figure 2.7A), indicating that inhibition of MCMV entry is not part of the statin-mediated antiviral mechanisms.

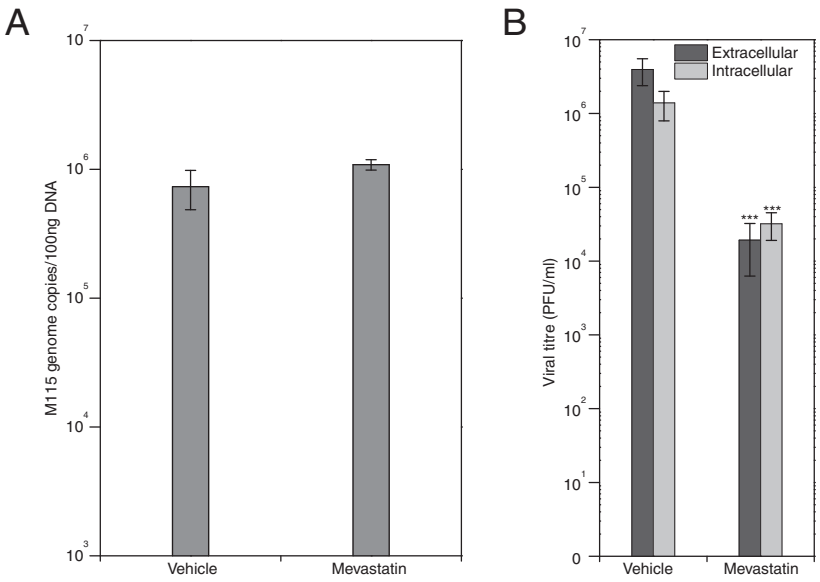

Figure 2.7 Statin does not affect viral entry but leads to decrease in both intra and extracellular viral titre reduction.

(A) NIH-3T3 fibroblasts (1x10^5 cells/well, 24-well plates) were pre-treated with vehicle, or mevastatin (10μM) for 24 hr. Cells were then infected with MCMV-C3X (MOI = 1) for 1 hr. After adsorption, cells were washed 3 times with media and incubated in fresh media for another 2 hr. Cells were harvested through trypsinization, and the viral DNA was extracted using the QIAamp DNA extraction kit as described in Experimental procedure 7.3.7. The number of copies of MCMV-M115 was assayed as described in Experimental procedure 6.3.7. (B) NIH-3T3 fibroblasts (8x10^5 cells/well, 6-well plate) were pre-treated with either vehicle or mevastatin (10μM) for 24 hr. Cells were then infected with MCMV (MOI = 2.5) for 1 hr and washed with blank media 5 times. Cells were then incubated in media containing vehicle or mevastatin (10μM). Two dpi supernatants (extracellular virus) and intracellular viral titre were quantitated by plaque assay as described in Experimental procedure 6.3.3. n = 6, mean ± SEM. ***$p \leq 0.001$.

To further elucidate the antiviral mechanism of statin, I then explored intra and extracellular viral particle formation using single-step growth analysis. In these experiments, NIH-3T3 fibroblasts were pre-treated with mevastatin (10μM) for 24 hr, followed by MCMV-C3X infection at a high viral titre (MOI = 2.5). Intracellular

(retained) and extracellular (secreted) viral titres were then assayed by plaque assay (see Experimental procedure 7.3.3). Significant reductions in both secreted and retained MCMV particles were observed in mevastatin treated cells (Figure 2.6B), indicating that mevastatin attenuates MCMV infection progression in fibroblasts. To visually observe the effects of statin on MCMV plaque formation, a plaque reduction assay was performed (see Experimental procedure 7.3.6). NIH-3T3 fibroblasts were first infected with MCMV-GFP (MOI = 0.002), then overlaid in agarose containing mevastatin (1μM). Agarose permits cell-to-cell viral spread and limits long distance transmission. The number of infected foci (e.g. GFP positive cells) were counted 24 hr post infection, and the diameter of the plaques were subsequently measured on 3 dpi. A significant difference in the diameter of viral plaques was observed between vehicle or mevastatin treated cells (Figure 2.8B). Taken together, the above results show that statin inhibits MCMV post entry replication, thus preventing viral plaque expansion and viral secretion.

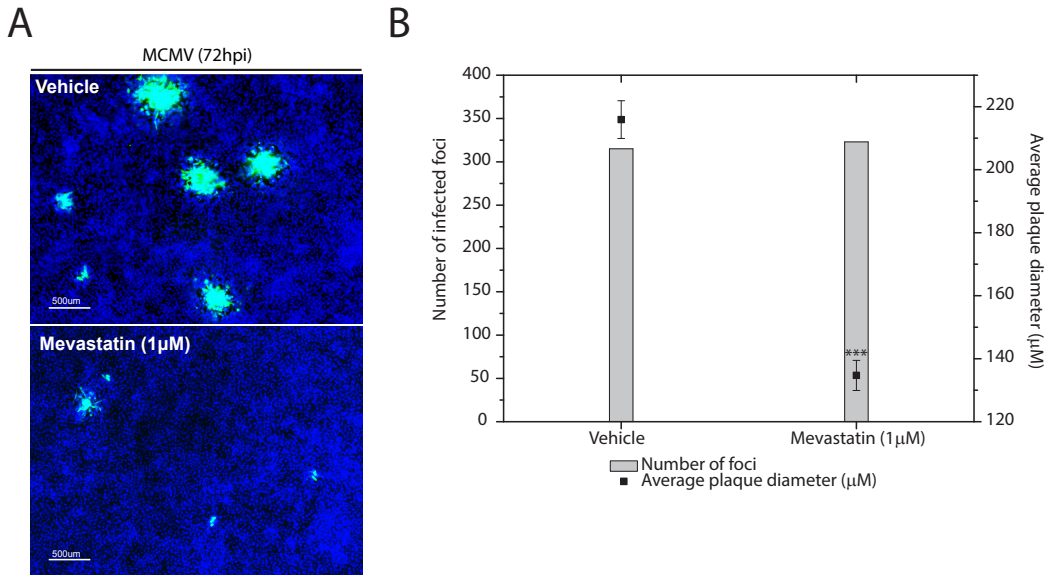

Figure 2.8 Statin inhibits MCMV viral plaque formation.
(A) NIH-3T3 fibroblasts ($8x10^5$ cells/well, 6-well plates) were infected with MCMV-GFP (MOI = 0.002) and overlaid in media containing 2.5% (w/v) and vehicle or 1μM mevastatin. (B) Plaque diameter was measured 3 dpi. Plaque diameters are mean of 302 and 316 plaque counted ± SEM (6 biological replicates). ***p<0.001

2.2.6 Pre-treatment of statin inhibits viral immediately early promoter activity

A previous study by Murayama et al., 2011 indicated that statin inhibits HCMV immediate early gene transcription (*Ie1*). To determine whether statin can also inhibit MCMV immediate early gene transcription, a reporter virus

(MCMV-ΔIE2GFP-Gluc) that encodes a secreted form of Gaussia luciferase enzyme (Gluc) was used to measure the activity of immediate early enhancer-promoter (MIE) (see Experimental procedure 7.3.1 for the viral construct (Δie2gfpGluc)). The transcription of Gluc is under the control of MIE and is opposite to the transcription direction of *Ie1* (e.g. bi-directional). The transcription rate of Gluc thus corresponds to the rate of *Ie1* synthesis (Kropp et al., 2011). Translated Gluc is secreted into supernatant and the activity of the enzyme can be measured using the substrate coelenterazine. Catalysis of coelenterazine by Gluc emits light, which can be detected using a luminescence reader. The intensity of the light corresponds to the activity of the enzyme. A higher Gluc activity indicates stronger MIE activation, whereas, a lower Gluc activity indicates the suppression of MIE. In these experiments, primary fibroblasts (pMEF, see Experimental procedure 7.1 for generating pMEFs) were pre-treated with statins (2.5 or 7.5μM) for 24 hr. Cells were then infected with MCMV-ΔIE2GFP-Gluc. The level of Gaussia luciferase activity was assayed at 4 and 24 hpi. Figure 2.9A shows that pre-treatment of mevastatin, simvastatin, lovastatin, fatostatin, but not pravastatin led to the suppression of MIE at 2 hr post infection. This suppression persisted when measured at 24 hr post infection (Figure 2.9B). Based on the results, it was concluded that treatments of lipophilic statins are capable of inhibiting MCMV MIE.

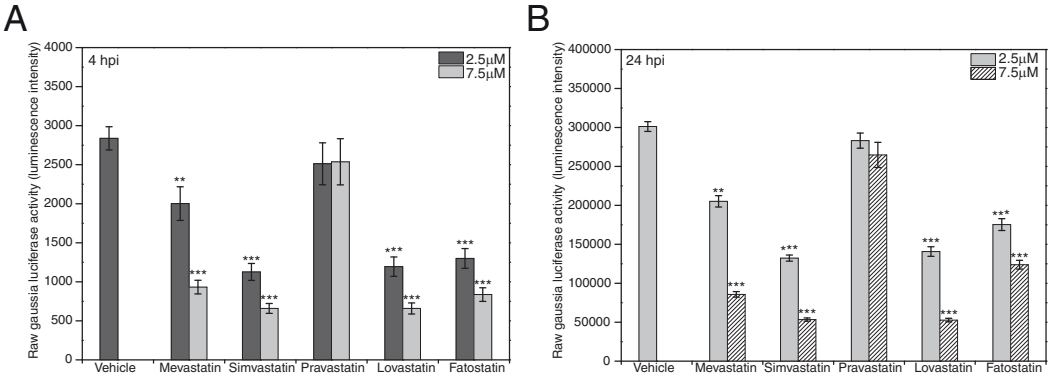

Figure 2.9 Not all statins inhibit MCMV MIE expression in fibroblasts.
pMEFs ($3x10^4$ cells/well, 96-well plate) were pre-treated with vehicle, or statins (2.5 or 7.5μM) as indicated for 24 hr. Cells were then infected with Gluc-MCMV (MOI = 0.15) for 1 hr. After adsorption, cells were washed once with medium. After wash, 120μl of fresh medium containing vehicle of statins were added. Supernatant was collected at (A) 4 hpi, and cells were re-fed with fresh media containing the same treatment, and the supernatant was harvested again at (B) 24 hpi. Gluc activity was measured using the native form of the Gluc substrate coelenterazine as described in Experimental procedure 7.4.1. Raw Gluc activity (represented by the luminescence intensity) was plotted. Data represents mean ± SEM for 3 experiments (8 replicates per experiment).**p<0.01, ***p<0.001

2.2.7 Statin alters protein prenylation in fibroblasts and macrophages

One of the secondary metabolites of the cholesterol pathway are the isoprenoids, which are consumed in a post-translation process known as prenylation. This process is carried out by enzymes known as prenyltransferases. Currently, there are limited techniques for detecting geranylgeranylation of specific proteins, with most of them requiring the use of [^{3}H]mevalonate (that is incorporated into GGPP) or LC/MS (liquid chromatography–mass spectrometry) to detect changes in a specific protein molecular weight (Berndt and Sebti, 2011). Alternatively, a simpler method is to generate antibodies that recognize specific unprenylated protein targets as a surrogate marker for levels of protein geranylgeranylation in the cell culture. However, this method depends exclusively on the availability of antibodies. The siRNA experiment indicated that silencing GGTase2 has an inhibitory effect on MCMV replication (Figure 2.2), while statin inhibition of the virus can be rescued with GGOH (Figure 2.6). Collectively, these results indicate that the utilization of geranylgeranyl by the host or the virus is important for MCMV propagation. To determine whether treatment of statin alters protein prenylation, NIH-3T3 fibroblasts and bone-derived macrophages (BMDM, see Experimental procedure 7.1 for generating BMDM) were treated with a vehicle, or mevastatin (2.5μM) w/o geranylgeraniol (GGOH, 15μM) for 24 hr. Equal amounts (25μg) of protein were separated on SDS-PAGE and probed with antibodies that specifically detect the unprenylated form of the small GTPase RAP1A or total RAP1 (see Experimental procedure 7.5.1 for western blotting) (Das et al., 2014; Guenther et al., 2010; Wasko et al., 2011). Unprenylated RAP1A accumulates within both cell types following uptake of mevastatin, while the total pool or RAP1 remains unchanged (Figure 2.10). Furthermore, the accumulation of unprenylated RAP1A can be reversed with the co-treatment of GGOH. This finding was in contrast with reports showing that a non-toxic concentration of pravastatin is incapable of inhibiting protein prenylation in various cell types (Mohamed et al., 2012; Takaguri et al., 2008).

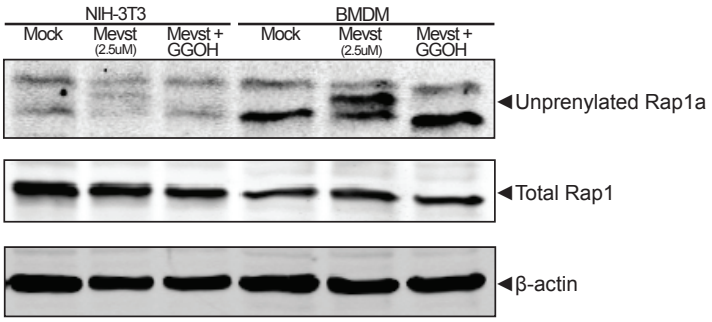

Figure 2.10 Statin treatment leads to accumulation of unprenylated proteins in fibroblasts and macrophages.

NIH-3T3 fibroblasts and BMDM ($8x10^5$ cells/well, 6-well plates) were treated with mevastatin (2.5μM) ± geranylgeraniol (15μM) for 24 hr. The next day, cells were washed once with ice cold PBS, and the total protein was extracted as described in Experimental procedure 7.5.1. 20μg of total cell lysate was separated on 12.5% SDS-PAGE and probed with antibodies that detect specifically unprenylated RAP1A or total RAP1. β-actin antibody was used as loading controls. Results represent three independent experiments.

2.3 Discussion

The aim of this chapter is to identify parts of the host sterol pathway that are important for viral replication. Utilizing strategies combining siRNA screening, biochemical, and proteomic approaches, I showed that the mevalonate-isoprenoid arm plays a pivotal role in pro-viral functions. Mechanistic studies indicate that parts of the antiviral capabilities of statins rely on the inhibition of MCMV MIE activity, as well as on the blocking of protein prenylation. Aspects of these findings are discussed here and explored in later chapters.

2.3.1 The importance of the mevalonate-isoprenoid arm on MCMV replication

The mevalonate-isoprenoid arm of the sterol pathway is responsible for the production of the isoprenoids (farnesyl-PP, geranylgeranyl-PP), and squalene. These intermediates are subsequently utilized in the process of protein prenylation and sterol production. The siRNA knockdown experiments showed that silencing genes within the isoprenoid branch generated antiviral effects. Notably, significant inhibition of viral replication is observed for the knockdown of *Fdps*, an enzyme essential for isoprenoid biosynthesis. In the pharmacological experiments, the antiviral activity of mevastatin was completely reversed by the addition of mevalonate to cells in culture. This shows that the antiviral mechanism was due to the inhibition of HMGCR and not the off-target effects of statin. While this result agrees with the siRNA screen, it also implicates that inhibition of cholesterol synthesis is responsible for the antiviral activity. However, feeding statin-treated fibroblasts with squalene failed to reverse the inhibitory activity, indicating that the antiviral effect is unlikely to be cholesterol mediated. A recognized outcome of using statins to reduce cholesterol levels is the suppression of the proximal mevalonate arm. This repression also perturbs the synthesis of branch derivatives, such as geranylgeraniol and farnesol involved in the protein geranylgeranylation and farnesylation pathways. This was demonstrated by the accumulation of unprenylated RAP1A, which was reversed with the addition of geranylgeraniol. The addition of farnesol also did not rescue the inhibitory effect of mevastatin, whereas, the addition of geranylgeraniol fully rescued viral replication. In the case of the downstream

prenyltransferases, reduced viral replication was only observed with siRNA targeting GGTase2. Silencing FTase or GGTase1 had no effects on viral replication. Collectively, these experiments show the specific metabolic requirements for the antiviral activity and highlight a possible role for the mevalonate-isoprenoid arm of the sterol pathway in protection against MCMV infection. A later chapter will focus on identifying protein targets that are substrates of GGTase2 and determine whether these targets are involved in MCMV replication.

2.3.2 Inhibition of MCMV replication by statins

Another mechanism associated with inhibition of MCMV replication by statins is the suppression of the MIE. The activity of the enhancer is measured using a reporter virus that encodes a Gaussia luciferase. Gaussia luciferase activity in the supernatant thus reflects the activity of the MIE. This method provides an indirect measurement of MIE in MCMV-infected cell culture. In an agreement with the work of Murayama et al., 2011 in HCMV, treatments of mevastatin, simvastatin, and lovastatin inhibited MCMV MIE, while pravastatin did not. Interestingly, Murayama et al. 2011 proposed that the antiviral mechanism of statin was due to cell cycle arrest. Indeed, qPCR analysis from their study demonstrated that the expression of *Cdk-2* and *Arf-1* that are involved in cell-cycle regulation were repressed by the three statins. CDK-2 is a member of the Ser/Thr protein kinase families that is essential for cell cycle G1/S phase transition (Hydbring and Larsson, 2010). ARF-1, a member of the RAS superfamily, is involved in the growth and migration of the MDA-MB-231 breast cancer cell line (Boulay et al., 2008). Inhibition of both CDK2 and ARF-1 would theoretically inhibit DNA synthesis and cell growth, which, in turn, restricts CMV replication. However, Murayama et al., 2011 did not indicate in their work whether pravastatin would inhibit CDK2 and ARF-1. An earlier report by Tanaka et al., 1998 indicated that pravastatin is capable of inhibiting CDK2 and DNA synthesis in rat astrocytes at concentrations above 18mM (7.6mg). While this concentration is still below the clinically prescribed dosage of pravastatin (40mg/day), the concentration of 18mM would be expected to cause various non-specific effects in tissue culture (Björkhem-Bergman et al., 2011). Thus, it is unlikely that pravastatin would inhibit

CDK2 and ARF-1.

In addition to the mechanism proposed above, it was noted that the inhibition of HCMV *Ie1* and IE1 by statins shown in Murayama et al., 2011 was only assayed at 24 hpi, whereas the Gluc experiments were conducted within the immediate early period of infection (4 hpi). This indicates that apart from DNA synthesis inhibition, statins could also inhibit transcriptional activation of MIE. The anti-inflammatory effects of statins were well documented *in vitro* and *in vivo* (Dichtl, 2002). One of the mechanisms by which statin suppresses the inflammatory response is by inhibiting the activation of transcription factors, including NF-κB and AP-1. NF-κB in its inactive state forms a complex with its inhibitors, the IκBs, in the cytosol. Upon signal activation, the IκB kinase (IKK complex) phosphorylates IκBs, and targets IκBs for polyubiquitination and degradation by the 26S proteosome complex. NF-κB enters the nucleus and transactivates NF-κB responsive genes (Demeritt et al., 2004). AP-1 activation by phosphorylation also leads to the production of proinflammatory cytokines (Newton and Dixit, 2012). Several studies have demonstrated that treatments with statins not only inhibit basal levels of NF-κB and AP-1, but also their activation (Dichtl, 2002; Khattri and Zandman-Goddard, 2013; Lenglet et al., 2014). Promoter analysis of CMV MIE reveals multiple binding sites for both NF-κB and AP-1, while NF-κB is essential for the efficient transactivation of the major immediate early promoter (DeMeritt et al., 2006; Demeritt et al., 2004; Isern et al., 2011). It is possible that the suppression of MIE by statins is achieved through the downregulation of NF-κB. This hypothesis is supported by the work of Ahn et al., 2008, which showsS that the TNF-α stimulated NF-κB activation in KBM-5 cells can be inhibited by mevastatin, simvastatin, and lovastatin, but not pravastatin. Further experimentation is required to confirm this hypothesis. Nevertheless, results from the metabolic rescue and MIE experiments have demonstrated statin's multilayer inhibition of MCMV replication.

2.3.3 Lipophilicity of statins

Among the four HMGCR inhibitors examined in this chapter, only pravastatin showed no antiviral response. However, treatments of fibroblasts with pravastatin showed a reduction in intracellular cholesterol levels, implicating that the drug is functional. When comparing the structure of mevastatin, simvastatin, lovastatin, and pravastatin (see Experimental procedure 7.2.2 for structural reference), pravastatin has a hydrophilic tail and no β-hydroxy-δ-lactone moiety that the other three statins commonly include in their chemical structures. This difference leads to different pharmacokinetic and pharmacodynamic properties. Early reports indicated that pravastatin is hydrophilic (with the lowest $P_{o/w}$ compared with other statins) and is not significantly metabolized by cytochrome P450 enzymes (Schachter, 2005; Serajuddin et al., 1991). Further *in vitro work* with rat hepatocytes showed that pravastatin has greater hepatoselectivity the other lipophilic agents, while having significantly reduced potential for uptake by peripheral cells (McTaggart et al., 2001). Indeed, multiple studies have shown the lack of influence of pravastatin on lymphoblasts and myeloma cells apoptosis (Cafforio et al., 2005), brain cholesterol levels (Thelen et al., 2006), and NK cell cytotoxicity (Tanaka et al., 2007) are likely due to the low penetration of the drugs. A recent study by Menter et al., 2011 indicated that pravastatin is selectively taken up by a sodium-independent organic anion transporter protein-1B1 (OATP1B1) exclusively expressed in the liver, while hydrophobic statins enter the cell via other mechanisms. It is possible that pravastatin could achieve an antiviral effect when used at a significantly higher dosage, as demonstrated in the work of Tanaka et al., 1998.

Another possible explanation why pravastatin was ineffective in inhibiting CMV replication is its inability to block protein prenylation. siRNA knockdown and metabolic rescue experiments have demonstrated that the prenylation branch of the sterol biosynthesis pathway is critical for MCMV replication. In particular, western blotting of macrophages and fibroblasts treated with mevastatin showed accumulation of unprenylated RAP1A (Figure 2.10). Thus, mevastatin is effective in inhibition prenylation, a finding consistent with previous reports (Das et al., 2014;

van de Donk et al., 2003; Kaur et al., 2013; Maalouf et al., 2007). Conversely, other studies have also demonstrated that pravastatin fails to inhibit protein prenylation (Mohamed et al., 2012; Takaguri et al., 2008). Although one study by Flint et al., 1997 showed that pravastatin at a concentration of 400μM> could cause changes in the mobility of small molecular proteins (<21-26kDa), the author did not specify the identity of these proteins. Similarly, Tanaka et al., 2000 showed that pravastatin at a concentration of 300μM> could affect the translocation of the small GTPase RhoA. However, these experiments did not explain whether the translocation inhibition of RhoA by pravastatin was due to the inhibition of protein prenylation. Collectively, these studies showed although that pravastatin is biologically active in lowering intracellular cholesterol levels, it has minimal effects on protein prenylation, hence the lack of antiviral effects. Additional experiments will be performed to determine whether pravastatin can elicit an antiviral effect when used in conjunction with other sterol metabolism inhibitors.

2.3.4 Cellular response to fatostatin mediated sterol metabolism inhibition

The only non-HMGCR inhibitor used in the pharmacological screening was fatostatin. Similar to the results with pravastatin, treatments of fatostatin had no effects on viral replication. Yet, fibroblasts treated with fatostatin had an increase in cellular apoptosis and reduced intracellular cholesterol, suggesting that fatostatin is effective at eliciting a cellular response. This observation supports the notion that cholesterol deprivation is not part of statins' antiviral response. However, the findings also argue that the replication of MCMV in these experimental settings does not require the activation of the SREBP2 pathway. This result is an apparent contradiction to previous studies (reviewed in Chapter 1), showing that HCMV promotes the activation of SREBP1 and -2 during the replication of the virus (Spencer et al., 2011). Currently, there is limited information regarding the pharmacokinetics and dynamics of fatostatin. Therefore, the following discussion heavily relies on the current understanding of this compound.

Fatostatin functions as a SREBP2 inhibitor through the direct binding to SCAP and prevents the translocation of SREBP2. However, this interaction is reversible, as fatostatin does not covalently bind to SCAP without UV cross-linking (Kamisuki et al., 2009). Thus, the effects of fatostatin depended heavily on the concentration of the drug, as well as the amount of SCAP present within the cell. Indeed, western blotting results indicated that >20μM of fatostatin is required to inhibit the proteolytic cleavage of SREBP2 in CHO-K1 (CHO-K1 is a model cell line for cholesterol manipulation work) (Kamisuki et al., 2009). Furthermore, mutagenesis and pull-down assays revealed that fatostatin does not affect the binding of SREBP2 to SCAP, nor does it recruit SREBP2's native inhibitor INSIG-1. The lack of INSIG-1 recruitment also increases the chance of SREBP2 translocation. Therefore, fatostatin at a concentration ≤10μM (the highest concentration used in this chapter) would provide only very limited effects on SREBP2 processing and overall cholesterol biosynthesis.

Another possible explanation for the fatostatin results would be the presence of lipids in the culture condition. The work of Goldstein and Brown using CHO-K1 cells demonstrated that the activation of SREBP-2 was maximized when culturing cells in lipoprotein-deficient serum (LPDCS), with >2μM of compactin for a minimum of 16 hr (Sakai et al., 1998). Supplementing CHO-K1 with either mevalonate or calf serum diminishes SREBP2 proteolytic cleavage (Radhakrishnan et al., 2008). In the fatostatin experiment, fibroblasts were grown in media containing 10% (v/v) lipidated calf serum, which provides a sufficient lipid source for inhibiting the SREBP2 pathway (through LDLR uptake). Indeed, the study published by Spencer et al., 2011 showed that the accumulation of SREBP2 during HCMV infection was only observed in serum-starved MRC-5 cells. Thus, in lipidated media, SREBP2 mediated pathway activity is likely to be low in NIH-3T3 fibroblasts and MRC-5. As the result, fatostatin is unlikely to have any additional effect on inhibiting the SREBP2 pathway, mainly because the pathway is simply inactive. Based on this reasoning, treatment of cells with fatostatin in delipidated medium would be likely to have an antiviral effect. Preliminary results obtained through student projects have shown that fatostatin is antiviral when cells are cultured in delipidated media. This hypothesis will be examined in future studies.

In summary, results presented in this chapter support the hypothesis that viral replication depends on the host lipid metabolism, in particular the mevalonate-isoprenoid arm. Subsequent chapters will explore these non-cholesterol mediated antiviral effects and integrate these findings with the understanding of sterol metabolism and immunity.

2.4 References

Ahn, K., Sethi, G., and Aggarwal, B. (2008). Reversal of chemoresistance and enhancement of apoptosis by statins through down-regulation of the NF-κB pathway. Biochem. Pharmacol. 75, 907–913.

Angulo, a, Ghazal, P., and Messerle, M. (2000). The major immediate-early gene ie3 of mouse cytomegalovirus is essential for viral growth. J. Virol. 74, 11129–11136.

Belmokhtar, C. a, Hillion, J., and Ségal-Bendirdjian, E. (2001). Staurosporine induces apoptosis through both caspase-dependent and caspase-independent mechanisms. Oncogene 20, 3354–3362.

Berndt, N., and Sebti, S.M. (2011). Measurement of protein farnesylation and geranylgeranylation in vitro, in cultured cells and in biopsies, and the effects of prenyl transferase inhibitors. Nat. Protoc. 6, 1775–1791.

Björkhem-Bergman, L., Lindh, J.D., and Bergman, P. (2011). What is a relevant statin concentration in cell experiments claiming pleiotropic effects? Br. J. Clin. Pharmacol. 72, 164–165.

Blanc, M., Hsieh, W.Y., Robertson, K.A., Watterson, S., Shui, G., Lacaze, P., Khondoker, M., Dickinson, P., Sing, G., Rodriguez-Martin, S., et al. (2011). Host defense against viral infection involves interferon mediated down-regulation of sterol biosynthesis. PLoS Biol 9, e1000598.

Boulay, P.-L., Cotton, M., Melançon, P., and Claing, A. (2008). ADP-ribosylation factor 1 controls the activation of the phosphatidylinositol 3-kinase pathway to regulate epidermal growth factor-dependent growth and migration of breast cancer cells. J. Biol. Chem. 283, 36425–36434.

Brown, M.S., Dana, S.E., and Goldstein, J.L. (1973). Regulation of 3-hydroxy-3-methylglutaryl coenzyme A reductase activity in human fibroblasts by lipoproteins. Proc. Natl. Acad. Sci. U. S. A. 70, 2162–2166.

Cafforio, P., Dammacco, F., Gernone, A., and Silvestris, F. (2005). Statins activate the mitochondrial pathway of apoptosis in human lymphoblasts and myeloma cells. Carcinogenesis 26, 883–891.

Das, S., Edwards, P. a, Crockett, J.C., and Rogers, M.J. (2014). Upregulation of endogenous farnesyl diphosphate synthase overcomes the inhibitory effect of bisphosphonate on protein prenylation in Hela cells. Biochim. Biophys. Acta 1841, 569–573.

DeMeritt, I., Podduturi, J., and Tilley, A. (2006). Prolonged activation of NF-κB by human cytomegalovirus promotes efficient viral replication and late gene expression. Virology 346, 15–31.

Demeritt, I.B., Milford, L.E., and Yurochko, A.D. (2004). Activation of the NF- B Pathway in Human Cytomegalovirus-Infected Cells Is Necessary for Efficient Transactivation of the Major Immediate-Early Promoter. 78, 4498–4507.

Denoyelle, C., Vasse, M., Körner, M., Mishal, Z., Ganné, F., Vannier, J.P., Soria, J., and Soria, C. (2001). Cerivastatin, an inhibitor of HMG-CoA reductase, inhibits the signaling pathways involved in the invasiveness and metastatic properties of highly invasive breast cancer cell lines: an in vitro study. Carcinogenesis 22, 1139–1148.

Dichtl, W. (2002). HMG-CoA Reductase Inhibitors Regulate Inflammatory Transcription Factors in Human Endothelial and Vascular Smooth Muscle Cells. Arterioscler. Thromb. Vasc. Biol. 23, 58–63.

Van de Donk, N.W.C.J., Kamphuis, M.M.J., van Kessel, B., Lokhorst, H.M., and Bloem, A.C. (2003). Inhibition of protein geranylgeranylation induces apoptosis in myeloma plasma cells by reducing Mcl-1 protein levels. Blood 102, 3354–3362.

Endo, A. (1979). Monacolin K, a new hypocholesterolemic agent produced by a Monascus species. J. Antibiot. (Tokyo). 32, 852–854.

Endo, A. (2010). A historical perspective on the discovery of statins. Proc. Japan Acad. Ser. B 86, 484–493.

Endo, A., and Kuroda, M. (1976). Citrinin, an inhibitor of cholesterol synthesis. J. Antibiot. (Tokyo). 29, 841–843.

Endo, A., Kuroda, M., and Tsujita, Y. (1976). ML-236A, ML-236B, and ML-236C, new inhibitors of cholesterogenesis produced by Penicillium citrinium. J. Antibiot. (Tokyo). 29, 1346–1348.

Endo, A., Tsujita, Y., Kuroda, M., and Tanzawa, K. (1977). by ML-236A and ML-236B , Competitive Inhibitors of 3-Hydroxy-3-methylglutaryl-Coenzyme A Reductase. 36, 31–36.

Endo, A., Tsujita, Y., Kuroda, M., and Tanzawa, K. (1979). Effects of ML-236B on cholesterol metabolism in mice and rats: lack of hypocholesterolemic activity in normal animals. Biochim. Biophys. Acta 575, 266–276.

Ericsson, J., Jackson, S.M., and Edwards, P.A. (1996). Synergistic binding of sterol regulatory element-binding protein and NF-Y to the farnesyl diphosphate synthase promoter is critical for sterol-regulated expression of the gene. J Biol Chem 271, 24359–24364.

Flint, O.P., Masters, B. a, Gregg, R.E., and Durham, S.K. (1997). HMG CoA reductase inhibitor-induced myotoxicity: pravastatin and lovastatin inhibit the geranylgeranylation of low-molecular-weight proteins in neonatal rat muscle cell culture. Toxicol. Appl. Pharmacol. 145, 99–110.

Föcking, M., Besselmann, M., and Trapp, T. (2004). Statins potentiate caspase-3 activity in immortalized murine neurons. Neurosci. Lett. 355, 41–44.

Gazzerro, P., Proto, M.C., Gangemi, G., Malfitano, A.M., Ciaglia, E., Pisanti, S., Santoro, A., Laezza, C., and Bifulco, M. (2012). Pharmacological actions of statins: a critical appraisal in the management of cancer. Pharmacol. Rev. 64, 102–146.

Gigue`re, J.-F. (2004). Statin Compounds Reduce Human Immunodeficiency Virus Type 1 Replication by Preventing the Interaction between Virion-Associated Host Intercellular Adhesion Molecule 1 and Its Natural Cell. 78, 12062–12065.

Guan, G., Jiang, G., Koch, R.L., and Shechter, I. (1995). Molecular cloning and functional analysis of the promoter of the human squalene synthase gene. J Biol Chem 270, 21958–21965.

Guenther, A., Gordon, S., Tiemann, M., Burger, R., Bakker, F., Green, J.R., Baum, W., Roelofs, A.J., Rogers, M.J., and Gramatzki, M. (2010). The bisphosphonate zoledronic acid has antimyeloma activity in vivo by inhibition of protein prenylation. Int. J. Cancer 126, 239–246.

Hollander, W., Chobanian, A., and Wilkins, R. (1960). The effects of triparanol (MER-29) in subjects with and without coronary artery disease. JAMA 174, 5–12.

Horton, J.D., Goldstein, J.L., and Brown, M.S. (2002). SREBPs: activators of the complete program of cholesterol and fatty acid synthesis in the liver. J Clin Invest 109, 1125–1131.

Horton, J.D., Shah, N.A., Warrington, J.A., Anderson, N.N., Park, S.W., Brown, M.S., and Goldstein, J.L. (2003). Combined analysis of oligonucleotide microarray data from transgenic and knockout mice identifies direct SREBP target genes. Proc Natl Acad Sci U S A 100, 12027–12032.

Hydbring, P., and Larsson, L.-G. (2010). Cdk2: a key regulator of the senescence control function of Myc. Aging (Albany. NY). 2, 244–250.

Isern, E., Gustems, M., Messerle, M., Borst, E., Ghazal, P., and Angulo, A. (2011). The activator protein 1 binding motifs within the human cytomegalovirus major immediate-early enhancer are functionally redundant and act in a cooperative manner with the NF-{kappa}B sites during acute infection. J. Virol. 85, 1732–1746.

Jepson, E.M. (1962). MER-29 (triparanol) in the control of hypercholesterolaemia. Proc. R. Soc. Med. 55, 480–484.

Kamisuki, S., Mao, Q., Abu-Elheiga, L., Gu, Z., Kugimiya, A., Kwon, Y., Shinohara, T., Kawazoe, Y., Sato, S., Asakura, K., et al. (2009). A small molecule that blocks fat synthesis by inhibiting the activation of SREBP. Chem. Biol. 16, 882–892.

Kandutsch, A.A., and Russell, A.E. (1960). Preputial gland tumor sterols. 3. A metabolic pathway from lanosterol to cholesterol. J. Biol. Chem. 235, 2256–2261.

Kaur, J., Dutta, S., Chang, K.-P., and Singh, N. (2013). A member of the Ras oncogene family, RAP1A, mediates antileishmanial activity of monastrol. J. Antimicrob. Chemother. 1–10.

Khattri, S., and Zandman-Goddard, G. (2013). Statins and autoimmunity. Immunol. Res. 56, 348–357.

Kirby, T.J. (1967). Cataracts produced by triparanol. (MER-29). Trans. Am. Ophthalmol. Soc. 65, 494–543.

Kropp, K. a, Robertson, K. a, Sing, G., Rodriguez-Martin, S., Blanc, M., Lacaze, P., Hassim, M.F.B.N., Khondoker, M.R., Busche, A., Dickinson, P., et al. (2011). Reversible inhibition of murine cytomegalovirus replication by gamma interferon (IFN-γ) in primary macrophages involves a primed type I IFN-signaling subnetwork for full establishment of an immediate-early antiviral state. J. Virol. 85, 10286–10299.

Lenglet, S., Quercioli, A., Fabre, M., Galan, K., Pelli, G., Nencioni, A., Bauer, I., Pende, A., Python, M., Bertolotto, M., et al. (2014). Statin treatment is associated with reduction in serum levels of receptor activator of NF-κB ligand and neutrophil activation in patients with severe carotid stenosis. Mediators Inflamm. 2014, 720987.

Maalouf, M. a, Wiemer, A.J., Kuder, C.H., Hohl, R.J., and Wiemer, D.F. (2007). Synthesis of fluorescently tagged isoprenoid bisphosphonates that inhibit protein geranylgeranylation. Bioorg. Med. Chem. 15, 1959–1966.

Mackenzie, J.M., Khromykh, A. a, and Parton, R.G. (2007). Cholesterol manipulation by West Nile virus perturbs the cellular immune response. Cell Host Microbe 2, 229–239.

McTaggart, F., Buckett, L., Davidson, R., Holdgate, G., McCormick, A., Schneck, D., Smith, G., and Warwick, M. (2001). Preclinical and clinical pharmacology of Rosuvastatin, a new 3-hydroxy-3-methylglutaryl coenzyme A reductase inhibitor. Am. J. Cardiol. 87, 28B–32B.

Menter, D.G., Ramsauer, V.P., Harirforoosh, S., Chakraborty, K., Yang, P., Hsi, L., Newman, R. a, and Krishnan, K. (2011). Differential effects of pravastatin and simvastatin on the growth of tumor cells from different organ sites. PLoS One 6, e28813.

Van der Meulen, K., Garré, B., Croubels, S., and Nauwynck, H. (2006). In vitro comparison of antiviral drugs against feline herpesvirus 1. BMC Vet. Res. 2, 13.

Modell, W. (1967). Mass drug catastrophes and the roles of science and technology. Science 156, 346–351.

Mohamed, A., Saavedra, L., Di Pardo, A., Sipione, S., and Posse de Chaves, E. (2012). β-amyloid inhibits protein prenylation and induces cholesterol sequestration by impairing SREBP-2 cleavage. J. Neurosci. 32, 6490–6500.

Mol, M.J., Erkelens, D.W., Leuven, J.A., Schouten, J.A., and Stalenhoef, A.F. (1986). Effects of synvinolin (MK-733) on plasma lipids in familial hypercholesterolaemia. Lancet 2, 936–939.

Moriyama, T., Sather, S.K., McGee, T.P., and Simoni, R.D. (1998). Degradation of HMG-CoA reductase in vitro. Cleavage in the membrane domain by a membrane-bound cysteine protease. J Biol Chem 273, 22037–22043.

Murayama, T., Bi, C., Li, Y., Ishigaki, Y., Takano, F., Takegami, T., Ohta, T., Sumino, H., Ubukata, K., and Takahashi, T. (2011). Inhibitory Effects of Statins on Cytomegalovirus Production in Human Cells: Comprehensive Analysis of Gene Expression Profiles. J. Exp. Clin. Med. 3, 40–45.

Nakaya, N., Homma, Y., Tamachi, H., Shigematsu, H., Hata, Y., and Goto, Y. (1987). The effect of CS-514 on serum lipids and apolipoproteins in hypercholesterolemic subjects. JAMA 257, 3088–3093.

Newton, K., and Dixit, V.M. (2012). Signaling in innate immunity and inflammation. Cold Spring Harb. Perspect. Biol. 4.

Park, C.-Y.Y., Jun, H.-J.J., Wakita, T., Cheong, J.H., and Hwang, S.B. (2009). Hepatitis C virus nonstructural 4B protein modulates sterol regulatory element-binding protein signaling via the AKT pathway. J Biol Chem 284, 9237–9246.

Petersen, J., Drake, M.J., Bruce, E. a., Riblett, A.M., Didigu, C. a., Wilen, C.B., Malani, N., Male, F., Lee, F.-H., Bushman, F.D., et al. (2014). The Major Cellular Sterol Regulatory Pathway Is Required for Andes Virus Infection. PLoS Pathog. 10, e1003911.

Qi, X.-F., Zheng, L., Lee, K.-J., Kim, D.-H., Kim, C.-S., Cai, D.-Q., Wu, Z., Qin, J.-W., Yu, Y.-H., and Kim, S.-K. (2013). HMG-CoA reductase inhibitors induce apoptosis of lymphoma cells by promoting ROS generation and regulating Akt, Erk and p38 signals via suppression of mevalonate pathway. Cell Death Dis. 4, e518.

Radhakrishnan, A., Goldstein, J.L., McDonald, J.G., and Brown, M.S. (2008). Switch-like control of SREBP-2 transport triggered by small changes in ER cholesterol: a delicate balance. Cell Metab. 8, 512–521.

Rodríguez-Martín, S., Kropp, K.A., Wilhelmi, V., Lisnic, V.J., Hsieh, W.Y., Blanc, M., Livingston, A., Busche, A., Tekotte, H., Messerle, M., et al. (2012). Ablation of the regulatory IE1 protein of murine cytomegalovirus alters in vivo pro-inflammatory TNF-alpha production during acute infection. PLoS Pathog. 8, e1002901.

Sakai, J., Rawson, R.B., Espenshade, P.J., Cheng, D., Seegmiller, a C., Goldstein, J.L., and Brown, M.S. (1998). Molecular identification of the sterol-regulated luminal protease that cleaves SREBPs and controls lipid composition of animal cells. Mol. Cell 2, 505–514.

Schachter, M. (2005). Chemical, pharmacokinetic and pharmacodynamic properties of statins: an update. Fundam. Clin. Pharmacol. 19, 117–125.

Serajuddin, A.T., Ranadive, S.A., and Mahoney, E.M. (1991). Relative lipophilicities, solubilities, and structure-pharmacological considerations of 3-hydroxy-3-methylglutaryl-coenzyme A (HMG-CoA) reductase inhibitors pravastatin, lovastatin, mevastatin, and simvastatin. J. Pharm. Sci. 80, 830–834.

Spencer, C.M., Schafer, X.L., Moorman, N.J., and Munger, J. (2011). Human cytomegalovirus induces the activity and expression of acetyl-coenzyme A carboxylase, a fatty acid biosynthetic enzyme whose inhibition attenuates viral replication. J. Virol. 85, 5814–5824.

Steinberg, D., Avigan, J., and Feigelson, E.B. (1961). EFFECTS OF TRIPARANOL (MER-29) ON CHOLESTEROL BIOSYNTHESIS AND ON BLOOD STEROL LEVELS IN MAN. J. Clin. Invest. 40, 884–893.

Sun, L.P., Seemann, J., Goldstein, J.L., and Brown, M.S. (2007). Sterol-regulated transport of SREBPs from endoplasmic reticulum to Golgi: Insig renders sorting signal in Scap inaccessible to COPII proteins. Proc Natl Acad Sci U S A 104, 6519–6526.

Takaguri, A., Satoh, K., Itagaki, M., Tokumitsu, Y., and Ichihara, K. (2008). Full Paper Effects of Atorvastatin and Pravastatin on Signal Transduction Related to Glucose Uptake in 3T3L1 Adipocytes. 89, 80–89.

Tanaka, T., Tatsuno, I., Noguchi, Y., Uchida, D., Oeda, T., Narumiya, S., Yasuda, T., Higashi, H., Kitagawa, M., Nakayama, K., et al. (1998). Cyclin-dependent Kinase 2 (Cdk2) in Growth-stimulated Rat Astrocytes GERANYLGERANYLATED Rho SMALL GTPase (s) ARE ESSENTIAL FOR THE INDUCTION. J. Biol. … 273, 26772–26778.

Tanaka, T., Tatsuno, I., Uchida, D., Moroo, I., Morio, H., Nakamura, S., Noguchi, Y., Yasuda, T., Kitagawa, M., Saito, Y., et al. (2000). Geranylgeranyl-Pyrophosphate , an Isoprenoid of Mevalonate Cascade , Is a Critical Compound for Rat Primary Cultured Cortical Neurons to Protect the Cell Death Induced by 3-Hydroxy-3- Methylglutaryl-CoA Reductase Inhibition. 20, 2852–2859.

Tanaka, T., Porter, C.M., Horvath-Arcidiacono, J. a, and Bloom, E.T. (2007). Lipophilic statins suppress cytotoxicity by freshly isolated natural killer cells through modulation of granule exocytosis. Int. Immunol. 19, 163–173.

Tanzawa, K., Kuroda, M., and Endo, a (1977). Time-dependent, irreversible inhibition of 3-hydroxy-3-methylglutaryl-coenzyme A reductase by the antibiotic citrinin. Biochim. Biophys. Acta 488, 97–101.

Thelen, K.M., Rentsch, K.M., Gutteck, U., Heverin, M., Olin, M., Andersson, U., Eckardstein, A. Von, Bjo, I., and Lu, D. (2006). Brain Cholesterol Synthesis in Mice Is Affected by High Dose of Simvastatin but Not of Pravastatin. 316, 1146–1152.

Tobert, J. a. (1987). New developments in lipid-lowering therapy: the role of inhibitors of hydroxymethylglutaryl-coenzyme A reductase. Circulation 76, 534–538.

Walker, J.F., and Tobert, J. a (1987). The clinical efficacy and safety of lovastatin and MK-733--an overview. Eur. Heart J. 8 Suppl E, 93–96.

Wang, H.-W.W., Liu, P.-Y.Y., Oyama, N., Rikitake, Y., Kitamoto, S., Gitlin, J., Liao, J.K., and Boisvert, W. a (2008). Deficiency of ROCK1 in bone marrow-derived cells protects against atherosclerosis in LDLR-/- mice. FASEB J 22, 3561–3570.

Wasko, B.M., Dudakovic, A., and Hohl, R.J. (2011). Bisphosphonates Induce Autophagy by Depleting Geranylgeranyl Diphosphate. 337, 540–546.

Werner, M., Sacher, J., and Hohenegger, M. (2004). Mutual amplification of apoptosis by statin-induced mitochondrial stress and doxorubicin toxicity in human rhabdomyosarcoma cells. Br. J. Pharmacol. 143, 715–724.

Winkelmann, R.K., Perry, H.O., Achor, R.W., and Kirby, T.J. (1963). Cutaneous syndromes produced as side effects of triparanol therapy. Arch. Dermatol. 87, 372–377.

Yavasoglu, I., Sargin, G., Kadikoylu, G., Karul, A., and Bolaman, Z. (2013). The activity of atorvastatin and rosiglitazone on CD38, ZAP70 and apoptosis in lymphocytes of B-cell chronic lymphocytic leukemia in vitro. Med. Oncol. 30, 603.

Zheng, Y.-H.H., Plemenitas, A., Fielding, C.J., and Peterlin, B.M. (2003). Nef increases the synthesis of and transports cholesterol to lipid rafts and HIV-1 progeny virions. Proc Natl Acad Sci U S A 100, 8460–8465.

Zmasek, C.M., Zhang, Q., Ye, Y., and Godzik, A. (2007). Surprising complexity of the ancestral apoptosis network. Genome Biol. 8, R226.

Publications associated with Chapter 2

Blanc M, **Hsieh WY**, Robertson KA, Watterson S, Shui G, Lacaze P, Khondoker M, Dickinson P, Sing G, Rodríguez-Martín S, Phelan P, Forster T, Strobl B, Müller M, Riemersma R, Osborne T, Wenk MR, Angulo A, Ghazal P. Host defense against viral infection involves interferon mediated down-regulation of sterol biosynthesis. PLoS Biol. 2011 Mar;9(3):e1000598.

Mazein A, Watterson S, **Hsieh WY**, Griffiths WJ, Ghazal P. A comprehensive machine-readable view of the mammalian cholesterol biosynthesis pathway. Biochem Pharmacol. 2013 Jul 1;86(1):56-66.

OPEN ACCESS Freely available online

PLOS BIOLOGY

Host Defense against Viral Infection Involves Interferon Mediated Down-Regulation of Sterol Biosynthesis

Mathieu Blanc[1], Wei Yuan Hsieh[1], Kevin A. Robertson[1,2], Steven Watterson[1,2], Guanghou Shui[3], Paul Lacaze[1], Mizanur Khondoker[1], Paul Dickinson[1,2], Garwin Sing[1], Sara Rodríguez-Martín[1], Peter Phelan[5], Thorsten Forster[1,2], Birgit Strobl[6], Matthias Müller[6], Rudolph Riemersma[7], Timothy Osborne[5], Markus R. Wenk[3], Ana Angulo[4], Peter Ghazal[1,2]*

1 Division of Pathway Medicine and Centre for Infectious Diseases, University of Edinburgh, Edinburgh, United Kingdom, **2** Centre for Systems Biology at Edinburgh, The King's Buildings, Edinburgh, United Kingdom, **3** Department of Biochemistry and Department of Biological Sciences, National University of Singapore, Singapore, **4** Institut d'Investigacions Biomediques August Pi i Sunyer, Barcelona, Spain, **5** Metabolic Signaling Diseases Program, Sanford-Burnham Medical Research Institute, Orlando, Florida, United States of America, **6** Institute of Animal Breeding and Genetics, Veterinary University of Vienna, Vienna, Austria, **7** Centre for Cardiovascular Disease, University of Edinburgh, Edinburgh, United Kingdom

Abstract

Little is known about the protective role of inflammatory processes in modulating lipid metabolism in infection. Here we report an intimate link between the innate immune response to infection and regulation of the sterol metabolic network characterized by down-regulation of sterol biosynthesis by an interferon regulatory loop mechanism. In time-series experiments profiling genome-wide lipid-associated gene expression of macrophages, we show a selective and coordinated negative regulation of the complete sterol pathway upon viral infection or cytokine treatment with IFNγ or β but not TNF, IL1β, or IL6. Quantitative analysis at the protein level of selected sterol metabolic enzymes upon infection shows a similar level of suppression. Experimental testing of sterol metabolite levels using lipidomic-based measurements shows a reduction in metabolic output. On the basis of pharmacologic and RNAi inhibition of the sterol pathway we show augmented protection against viral infection, and in combination with metabolite rescue experiments, we identify the requirement of the mevalonate-isoprenoid branch of the sterol metabolic network in the protective response upon statin or IFNβ treatment. Conditioned media experiments from infected cells support an involvement of secreted type 1 interferon(s) to be sufficient for reducing the sterol pathway upon infection. Moreover, we show that infection of primary macrophages containing a genetic knockout of the major type I interferon, IFNβ, leads to only a partial suppression of the sterol pathway, while genetic knockout of the receptor for all type I interferon family members, *ifnar1*, or associated signaling component, *tyk2*, completely abolishes the reduction of the sterol biosynthetic activity upon infection. Levels of the proteolytically cleaved nuclear forms of SREBP2, a key transcriptional regulator of sterol biosynthesis, are reduced upon infection and IFNβ treatment at both the protein and de novo transcription level. The reduction in *srebf2* gene transcription upon infection and IFN treatment is also found to be strictly dependent on *ifnar1*. Altogether these results show that type 1 IFN signaling is both necessary and sufficient for reducing the sterol metabolic network activity upon infection, thereby linking the regulation of the sterol pathway with interferon anti-viral defense responses. These findings bring a new link between sterol metabolism and interferon antiviral response and support the idea of using host metabolic modifiers of innate immunity as a potential antiviral strategy.

Citation: Blanc M, Hsieh WY, Robertson KA, Watterson S, Shui G, et al. (2011) Host Defense against Viral Infection Involves Interferon Mediated Down-Regulation of Sterol Biosynthesis. PLoS Biol 9(3): e1000598. doi:10.1371/journal.pbio.1000598

Academic Editor: Skip W. Virgin, Washington University School of Medicine, United States of America

Received August 4, 2010; **Accepted** January 26, 2011; **Published** March 8, 2011

Copyright: © 2011 Blanc et al. This is an open-access article distributed under the terms of the Creative Commons Attribution License, which permits unrestricted use, distribution, and reproduction in any medium, provided the original author and source are credited.

Funding: This work was supported by the Wellcome Trust (WT066784/Z/02/Z) and by the BBSRC/EPSRC and reagent support by the RNAi Global Initiative to PG. MB was supported by a studentship from the British Heart Foundation reference FS/05/022 and University of Edinburgh Alumni Fund. SRM was supported by a BBSRC studentship and Principal's Fellowship. PL is supported by BBSRC studentship. The Centre for Systems Biology at Edinburgh is a Centre for Integrative Systems Biology (CISB) supported by the BBSRC and EPSRC, reference BB/D019621/1. BS and MM are supported by the Austrian Science Fund FWF SFB F28 and Austrian Federal Ministry of Science and Research GEN-AU III Austromouse. MRW is supported by the Singapore National Research Foundation under CRP Award No. 2007-04, the Biomedical Research Counncil of Singapore (R-183-000-211-305) and the National Medicial Research Council (R-183-000-224-213. AA is supported by funding from the Ministerio de Educación y Ciencia (SAF2008-00382). The funders had no role in study design, data collection and analysis, decision to publish or preparation of the manuscript.

Competing Interests: The authors have declared that no competing interests exist.

Abbreviations: CMV, cytomegalovirus; Fdps, farnesyl diphosphate synthase; HCV, Hepatitis C virus; hpi, hours post-infection; HSV1, herpes simplex virus 1; IFN, interferon; IFNAR1, IFN-α/β receptor; JAK, Janus kinase; LAG, Lipid Associated Gene; mCMV, murine cytomegalovirus; MRM, multiple reaction monitoring; PRR, host recognition receptor; SREBP2, sterol regulatory binding protein 2; STAT, signal transducer and activator of transcription; Tyk 2, tyrosine kinase 2

* E-mail: p.ghazal@ed.ac.uk

Introduction

Sterols and fatty acids are common intermediary metabolites that play key roles in many biological pathways involved in inflammatory diseases such as atherosclerosis and chronic heart disease [1–4]. Significantly, mounting evidence shows a connection between innate immune signaling processes and the regulation of sterol and fatty acid metabolism [5–8]. Specifically,

Author Summary

Currently, little is known about the crosstalk between the body's immune and metabolic systems that occurs after viral infection. This work uncovers a previously unappreciated physiological role for the cholesterol-metabolic pathway in protecting against infection that involves a molecular link with the protein interferon, which is made by immune cells and known to "interfere" with viral replication. We used a clinically relevant model based on mouse cytomegalovirus (CMV) infection of bone-marrow-derived cells. Upon infection these cells produce high levels of interferon as part of the innate-immune response, which we show in turn signals through the interferon receptor resulting in lowering enzyme levels on the cholesterol pathway. We observed this effect with a range of other viruses, and in each case it leads to a notable drop in the metabolites involved in the cholesterol pathway. We found that the control mechanism involves regulation by interferon of an essential transcription factor, named SREBP-2, which coordinates the gene activity of the cholesterol pathway. This mechanism may explain clinical observations of reduced cholesterol levels in patients receiving interferon treatment. Our initial investigation into how lowered cholesterol might protect against viral infection reveals that the protection is not due to a requirement of the virus for cholesterol itself but instead involves a particular side-branch of the pathway that chemically links lipids to proteins. Drugs such as statins and small interfering RNAs that block this part of the pathway are also shown to protect against CMV infection of cells in culture and in mice. This provides the first example of targeting a host metabolic pathway in order to protect against an acute infection.

cholesterol and its metabolites have been shown to alter inflammatory mediator behavior [9–11], and conversely, innate immune signaling has been shown to modulate the dynamics of cholesterol transport, storage, and excretion [12–15]. Recent studies have also begun to show that the perturbation of lipid metabolism in a range of virally infected cells is a hallmark of cellular changes associated with infection. For instance, studies analyzing the consequences of human cytomegalovirus (CMV) infection have shown that increases in the flux of the fatty acid biosynthesis pathway are essential for optimal viral growth in fibroblasts [16]. Further, Hepatitis C virus (HCV) has been shown to co-opt the prenylation pathway to promote the efficient replication of its genome [17–19]. More generally, a number of other viruses, notably Measles, HIV, West Nile virus, and Dengue virus, also have the ability to change cholesterol pathway gene expression in a variety of cellular systems [20–24]. Whether the effects of virus infection on the cholesterol pathway are directly mediated by the pathogen or indirectly host-mediated mechanisms is not known. From a therapeutic perspective, studies have also shown that the pharmacological disruption of the cholesterol metabolism by statins and other metabolic modifiers can result in the inhibition of viral replication [25–32].

It is well documented that the cross-talk between immune programs of macrophage activation and lipid homeostasis plays a central part in chronic inflammatory diseases [33,34]. In particular an anti-atherosclerosis transcriptional axis of PPARγ regulating a pathway of cholesterol efflux by inducing ABCA1 expression and cholesterol removal from macrophages, via a transcriptional cascade mediated by activated LXRα, has been reported [35]. Significantly, cellular metabolic, signaling, and regulatory pathways also play a critical "collaborative" role in modulating immune responses to infection [36]. In this context, Toll-like pathogen recognition receptors, crucial to the initiation of innate immune signaling, have recently been shown to regulate the expression of key lipid-associated genes following bacterial infection. This occurs due to microbial ligand activation of the IRF3 pathway, which blocks the induction of LXR target genes such as ABCA1 and inhibits cholesterol efflux from macrophages in an interferon independent manner [5]. In this context, LXRα−/− mice are more susceptible to bacterial infection [37], further emphasizing the importance of this pathway in the innate immune response. From a viral perspective, an interferon-inducible protein "viperin" is known to inhibit influenza A virus and HCV by disrupting the formation of cholesterol-enriched lipid rafts, which act as attachment sites for viral production [38,39]. Significantly, despite increasing numbers of studies in this area, the question remains as to whether the immune regulation of lipid pathways can also serve a role as part of a protective anti-viral response. Indeed, in the context of host protection pathways, it is not known whether a central immune regulatory mechanism involving interferon response is directly or indirectly required in modulating lipid metabolism in infection.

We are interested in elucidating the relationship between transcriptional networks and immune regulatory pathways and host-cell dependency mechanisms of pathogens, especially viruses, as identifying host dependency mechanisms at the pathway level provides a new molecular systems-level approach for understanding viral pathogenesis, which can be harnessed as an anti-infective strategy [40–42]. For many years, studies of virus-host interactions, in particular for large DNA viruses, have proven invaluable in the characterization of host cell molecular pathways and their connectivity to the inflammatory response. Murine cytomegalovirus (mCMV), which has a large double-stranded DNA genome, represents one of the few model organisms studied in its natural host and has both biological and clinical relevance to human CMV disease [43]. In this study, we have sought to apply a systems-level approach, bringing together functional genomics, lipidomics, and biochemical experimentation, to understand the interplay between sterol pathway down-regulation and the innate immune response to mCMV infection. Our investigations reveal a previously undisclosed dependency role for down-regulation of the sterol metabolic network, which is integral to the protective immune response requiring a type 1 interferon receptor regulatory loop mechanism.

Results

Sterol Biosynthesis Pathway–Associated Genes Are Coordinately Down-Regulated by IFNγ Treatment and mCMV Infection in Primary Bone-Marrow–Derived Macrophages

As a first step, an integrative approach combining bioinformatics tools and a time-series analysis of gene expression changes was applied to mCMV-infected or interferon (IFN) γ-activated primary bone-marrow-derived macrophages (BMDM). These primary BMDM cultures represent a physiologically relevant cell system for the combined analysis of infection, inflammation, and lipogenesis [44–46]. In the following experiments, infected or IFNγ-treated BMDM RNA was harvested every 30 min up to 12 h post-challenge for microarray gene expression profiling. In this study, analysis of expression data was exclusively restricted to lipogenic-associated genes. For this purpose, a combination of literature and data-mining identified over one thousand genes with published direct or indirect functions relating to cellular lipid metabolism, regulation, and synthesis (Text S1). When this resource was used to interrogate a subset of our time-series data

which passed a stringent filtering threshold ($p<10^{-6}$), 89% of lipogenic-associated genes were detected, of which 12% were significantly regulated (113/958) upon IFNγ treatment and 23% were significantly altered in their expression (195/958) after mCMV infection. This represented a significant and highly selective lipogenic response (Figure S1) with altered genes showing a high degree of overlap between infection and IFNγ activation (Table S1). Notably, clear differences in the specific class of lipogenic genes in up- and down-regulated groups were observed. Of the IFNγ down-regulated transcripts, a significant proportion (14/35, 40%) were related to the sterol pathway, while fatty acid pathways were pre-eminent (6/35, 17%) in the up-regulated gene group (Figure S1C). A statistical evaluation investigating pathway over-representation indicated a highly pathway-specific response including previously known pathways for inositol (Table S2E–F) [47] perturbed by mCMV infection. Significantly, however, the most pronounced pathway changes in the down-regulated genes common to both stimuli were associated with sterol lipid metabolism (Table S2E and Figure 1A), which exhibited a gradual, temporal decline in expression from 6 h post-infection (hpi) onwards (Figure 1B). Additional microarray experiments to further explore this observation revealed a further reduction in sterol pathway gene expression observed at 24 hpi (unpublished data). It is worth noting, however, that the observed level of reduction in expression for any particular transcript was relatively modest (ranging from 1.3- to 5-fold for infection and 1.3- to 3-fold for IFNγ treatment over a 24 h time frame).

To independently validate the microarray data described above, Q-RT-PCR analyses of five independent experiments were performed for both infection and IFNγ treatment. In agreement, we find that Q-RT-PCR analysis of selected members of the pathway—*Hmgcs1*, *Hmgcr*, *Idi1*, and *Sqle*—shows a statistically significant but quantitatively modest reduction in expression (Figure 1C and 1D). Notably, a similar quantitative decrease is also exhibited at the protein level for HMGCS1, HMGCR, and SQLE (Figure 2A).

Down-Regulation of the Sterol Biosynthesis Pathway Is Specific to IFNγ and IFNβ Treatment

Since the alterations in expression of the cholesterol-related genes were consistent but of relatively small magnitude, we considered whether these perturbations represented either non-specific "noise" generated during the pro-inflammatory stimulation of a macrophage or a more specific response to a particular challenge. To test whether alternative pro-inflammatory mediators could also lead to the modulation of the sterol pathway genes, macrophage cultures were treated with a range of doses of the following inflammatory cytokines: IL1β, TNF, IL6, and IFNβ. *Hmgcs1*, *Hmgcr*, *Idi1*, and *Sqle* gene expression changes were then analyzed by Q-RT-PCR (Figure 1E–H). Of the cytokines tested, only IFNβ elicited the down-regulation of sterol pathway gene expression in primary macrophage cultures (Figure 1E). In summary, these data indicate a highly specific response of macrophages through a coordinated negative regulation of multiple sterol pathway members upon viral infection or treatment with IFNγ or β but not IL1β, TNF, or IL6. Once again, these effects are quantitatively "modest" but statistically significant.

Experimental Testing of Bioinformatic Predictions: Infection Results in a Decrease of Sterol Metabolites in Primary Macrophages and Fibroblasts

We next sought to explore how multiple small reductions in enzyme levels impact upon the biosynthetic activity of the pathway by measuring the steady-state metabolic output of the pathway. For these experiments, free intra-cellular cholesterol level, as a metabolic end product of the sterol pathway, was determined using an enzymatic method on infected macrophages (Figure 2B). We observe a significant decrease in cholesterol metabolite levels 24 hpi. Similar results were also observed with infection of NIH/3T3 cells (Figure 2C), indicating that the effect is not macrophage specific.

It is possible that the experimentally observed drop in sterol lipid levels could be due to a non-specific and generalized response to infection, although from the microarray analysis of the lipidomic associated genes we clearly observe highly specific lipogenic responses rather than a broad response to infection (Figures S1 and S2). To further determine whether the down-regulation of sterol biosynthesis is specific between mCMV infection and select lipogenesis pathways, total cell extracts were analyzed by electrospray ionization as well as atmosphere chemical ionization mass spectrometry (see Materials and Methods). These lipidomic approaches allow quantification of the major membrane lipid classes (such as glycerophospholipids and sterols) as well as individual molecular lipid species at high sensitivity. Overall, we find no coordinated or substantial differences in the overall levels of major glycerophospholipids (phosphatidylcholine, phosphatidylserine, and phosphatidylethanolamine) during infection with CMV, although a small number of the individual species in the phosphatidylcholine and phosphatidylserine group are affected (Figure S3A–C). In marked contrast, levels of free cholesterol, as well as its immediate precursor, zymosterol, 14-demethyl-lanosterol, and 7-dehydrocholesterol, were strongly reduced at 24 hpi (2–3-fold) and 48 hpi (4–6-fold) (Figure S2A–D). These results further support a specific alteration of sterol biosynthesis upon infection. Furthermore, the reduced free cholesterol levels are also developed in a dose-dependent manner by treatment with IFNβ and γ but not IL1β, IL6, or TNF (Figure 2D). Altogether, we conclude that the effect of the coordinated down-regulation is to reduce metabolic output of the sterol pathway.

Pharmacologic Inhibition and siRNA Knock-Down of the Sterol Biosynthesis Pathway Has an Antiviral Effect

To assess whether the sterol biosynthesis pathway plays a pro- or anti-viral role in regulating mCMV replication, we exploited the pharmacologic compound "simvastatin," a potent and selective inhibitor of HMGCR [48]. Inhibition of HMGCR is known to result in a reduction of the metabolic intermediate mevalonate (Figure 3) and an accompanying drop in cholesterol synthesis by the cell [49]. The treatment of cells with simvastatin resulted in a dose-dependent inhibition of mCMV plaque formation (unpublished data) and in live cell replication assays (Figure 4A) with an IC50 of 2 μM that is comparable to the "gold standard" anti-viral Gancyclovir (Figure 4A) in the murine model system. Notably, the observed inhibitory effect of simvastatin occurred below a level at which non-specific toxic effects to cells were observed (15 μM) (Figure S7). These experiments pointed to a potential protective anti-viral role via a targeted disruption of the sterol pathway and raised the question of whether pharmacologic treatment in vivo also develops an inhibitory effect. To investigate whether simvastatin could play an anti-infective role in vivo, mice were administered with an established pre-clinical pharmacologic dose of simvastatin or vehicle alone and infected by intra-peritoneal inoculation with mCMV. Viral titres were then determined in a variety of organs at day 4 post-inoculation. Markedly, viral titres are reduced by over one order of magnitude in multiple organs following treatment with simvastatin (Figure 4B).

To determine the extent of the overlap between the sterol biosynthesis pathway and anti-viral activity, we employed a series of metabolite rescue and interference RNA knock-down experi-

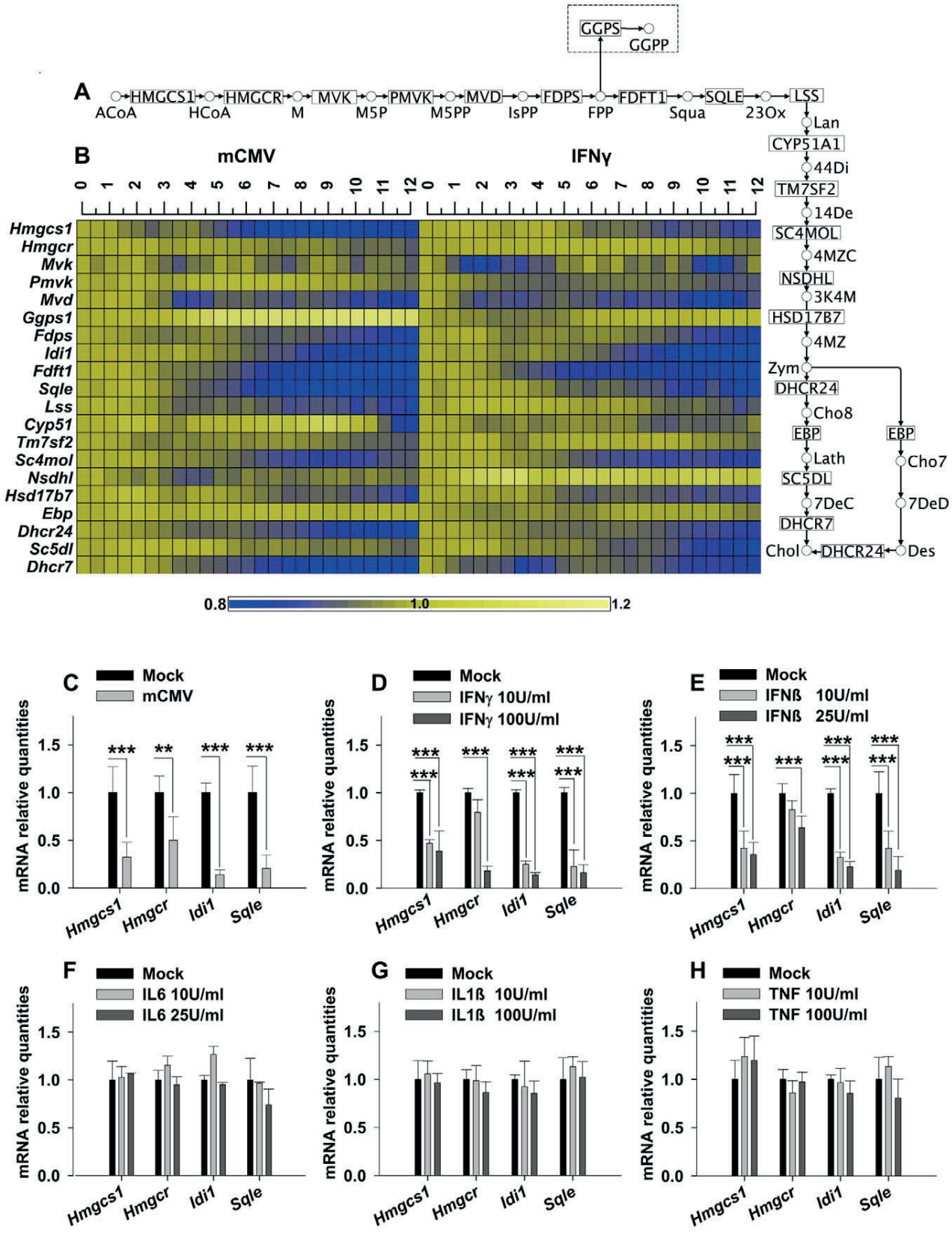
A
GGPS
GGPP
HMGCS1
HMGCR
MVK
PMVK
MVD
FDPS
FDFT1
SQLE
LSS
ACoA
HCoA
M
M5P
M5PP
IsPP
FPP
Squa
23Ox
Lan
CYP51A1
44Di
TM7SF2
14De
SC4MOL
4MZC
NSDHL
3K4M
HSD17B7
4MZ
Zym
DHCR24
Cho8
EBP
Lath
SC5DL
7DeC
DHCR7
Chol
DHCR24
Des
EBP
Cho7
7DeD
B
mCMV
IFNγ
0 1 2 3 4 5 6 7 8 9 10 11 12
Hmgcs1
Hmgcr
Mvk
Pmvk
Mvd
Ggps1
Fdps
Idi1
Fdft1
Sqle
Lss
Cyp51
Tm7sf2
Sc4mol
Nsdhl
Hsd17b7
Ebp
Dhcr24
Sc5dl
Dhcr7
0.8
1.0
1.2
C
Mock
mCMV
D
Mock
IFNγ 10U/ml
IFNγ 100U/ml
E
Mock
IFNß 10U/ml
IFNß 25U/ml
F
Mock
IL6 10U/ml
IL6 25U/ml
G
Mock
IL1ß 10U/ml
IL1ß 100U/ml
H
Mock
TNF 10U/ml
TNF 100U/ml
mRNA relative quantities
0.0
0.5
1.0
1.5
***
**
Hmgcs1
Hmgcr
Idi1
Sqle

Figure 1. Regulation of the cholesterol pathway upon mCMV infection. (A) The Sterol biosynthesis pathway shown in KEGG notation with abbreviated metabolites (abbreviations listed in Text S1). The geranylgeranylation pathway responsible for GGPP synthesis is shown in the dashed box. (B) Heat map of the cholesterol biosynthesis temporal genes' expression during the first 12 h of mCMV infection (left panel) or IFNγ treatment (right panel). Each time point corresponds to one independent biological sample, and columns indicate time in hours. Fold changes of expression levels are represented on a Log2 scale compared to mock-treated cells, ranging from a 0.8× lower expression (dark blue) to a 1.2× higher expression (bright yellow). (C–H) Expression analysis measured by qRT-PCR of *Hmgcs1*, *Hmgcr*, *Idi1*, and *Sqle* genes in BMDM infected with mCMV(24 hpi) (C) or treated for 24 h with IFNγ (10 and 100 U/ml) (D), IFNβ (10 and 25 U/ml) (E), IL6 (10 and 25 U/ml) (F), IL1β (10 and 100 U/ml) (G), or TNF (10 and 100 U/ml) (H). Graphs show levels of mRNA expression of the respective genes either infected or cytokines-treated relative to mock samples. Bars represent the means ± SD of five independent experiments with biological triplicates for each experiment. *$p<0.05$, **$p<0.01$, ***$p<0.001$, determined with an unpaired Student's *t* test.
doi:10.1371/journal.pbio.1000598.g001

ments. In these experiments we observed that simvastatin anti-viral activity could be completely reversed by the addition of mevalonate to cells in culture (Figure 5A). This showed that the anti-viral mechanism was due to an inhibition of HMGCoA reductase. While this result supports the requirement of the mevalonate arm of the sterol pathway, it does not necessarily implicate cholesterol as being responsible for the anti-viral activity. Notably, feeding macrophages with a cell permeable form of cholesterol or squalene failed to reverse the inhibitory activity (Figures 3 and 5A), indicating that the anti-viral effect is unlikely to be cholesterol mediated and thus unrelated to any regulatory sterols or to the structural requirements of virus replication associated with lipid droplets. The addition of cell permeable farnesol also did not rescue the inhibitory activity of simvastatin, while conversely the addition of geranylgeraniol fully rescued the anti-viral activity (Figures 3 and 5A). These experiments show the specificity of the metabolic requirement for anti-viral activity and highlight a possible role for the mevalonate-isoprenoid arm of the sterol pathway in protection against mCMV infection (Figure 3).

While the rescue of statin inhibition of viral growth by mevalonate and geranylgeraniol strongly indicates the involvement of the proximal arm of the sterol pathway, it is still conceivable that other mechanisms of action unrelated to the capacity to inhibit biosynthesis may be responsible for the effect on virus replication. For this reason and to additionally test the specific requirement of members of the sterol biosynthesis pathway for viral growth control, siRNA knock-down experiments were performed. For these experiments, *Hmgcs1* and *Hmgcr* were first targeted in the pathway using low concentrations of siRNA to avoid non-specific interferon responses, including a series of non-targeting siRNA for non-targeting effects. Knock-down of these genes (Figure S5) resulted in a specific and significant decrease in the optimal rate and end-point yield of viral replication (Figures 5B). To further dissect the specific role of pathway members in mediating the anti-viral response, additional siRNA inhibition studies were conducted involving targeted genes distal to the mevalonate-prenylation branch of the sterol biosynthesis pathway. In these experiments, Fdft1, Sqle, and Dhcr7 were targeted. Figure 5B clearly shows that targeting these members of the pathway fails to inhibit and even positively influences viral growth, a result that is consistent with the above described metabolite rescue experiments. To further investigate and to independently assess the specificity of the prenylation branch of the pathway, additional siRNA knock-down experiments were performed targeting farnesyl diphosphate synthase (Fdps), an enzyme essential for isoprenoid biosynthesis, and all three prenyltransferases (these are farnesyltransferase, geranylgeranyltransferase type I, and Rab geranylgeranyltransferase type II enzymes). In these experiments knock-down of Hmgcr and Dhcr7 and viral ORFs (M54 and M86) are used as controls and developed the expected knock-down profile (Figure 5C). Notably, significant inhibition of viral replication is observed for knock-down of Fdps. In the case of the downstream prenyltransferases, reduced viral replication is observed with siRNA targeting Rabggtb specific for geranylgeranyltransferase type II enzyme, but not Pggt1b or Fntb specific for gernylgeranyltransferase type I and farsenyltransferase, respectively (Figure 5C). These experiments indicate specificity of targeting the isoprenoid pathway but will require further functional validation work.

Overall, these findings show that inhibition of viral growth is not due to cholesterol deprivation, but rather a part of the pathway involving a proximal mevalonate-prenylation step. This raises the notion of whether depletion of geranylgeraniol may be one potential mode for interferon to inhibit viral replication. In this scenario we might expect that feeding cells with geranylgeraniol upon interferon treatment would counter, in part, the anti-viral effect. To determine the effect of interferon on viral replication, in the absence and presence of geranylgeraniol, we performed a metabolite rescue experiment in the presence of increasing units of IFNβ. Figure 5D shows that the anti-viral effect of 1 and 5 U/ml of IFNβ is dramatically reduced in the presence of geranylgeraniol (at both 15 and 150 μM), while at a more potent level of IFNβ (at 25 U/ml) approximately 70% and 25% of the anti-viral activity remains with 15 and150 μM GGOH, respectively. Taken together, these results support a role of the mevalonate-isoprenoid arm of the sterol pathway for optimal mCMV replication and highlight the potential role for down-regulating this pathway in protecting the host from viral infection. These findings also suggest that sterol biosynthesis regulation acts as a marker for antiviral activity.

An Interferon Regulatory Loop Is Responsible for the Transcriptional Down-Regulation of the Sterol Biosynthesis Pathway in Response to Infection

We next sought to investigate whether specific viral or cellular modes of action might be responsible for the reduction in sterol biosynthesis upon infection. First, it is possible that the effects monitored in our experimental system are specific to mCMV. To test whether the down-regulation of sterol pathway gene expression is a more general effect rather than specific to mCMV, primary macrophages (BMDM) were infected with a number of different viruses and harvested for gene expression analysis. Figure 6A shows the expression profile of the sterol pathway and other pathways for infection (innate immune activation pathways) by an enveloped DNA virus, herpes simplex (HSV1); an RNA virus, semliki forest virus (SFV); cytoplasmic DNA virus, vaccinia virus (VV); and non-enveloped nuclear DNA virus, adenovirus. All the viruses tested show a specific and coordinate decrease in gene expression for members of the sterol biosynthesis pathway.

In the case of mCMV, it is worth noting that the reduction in gene expression occurs approximately 6 hpi (e.g., see Figure 1). Consequently, it is possible that a viral early or late gene product may be required for the effect. To test this possibility, we used a replication and early/late gene defective mCMV virus (mCMVdie3 in [50]). The mCMVdie3 strain is capable of infecting cells at levels equivalent to wild-type virus but is incapable of expressing its genome downstream of a rather

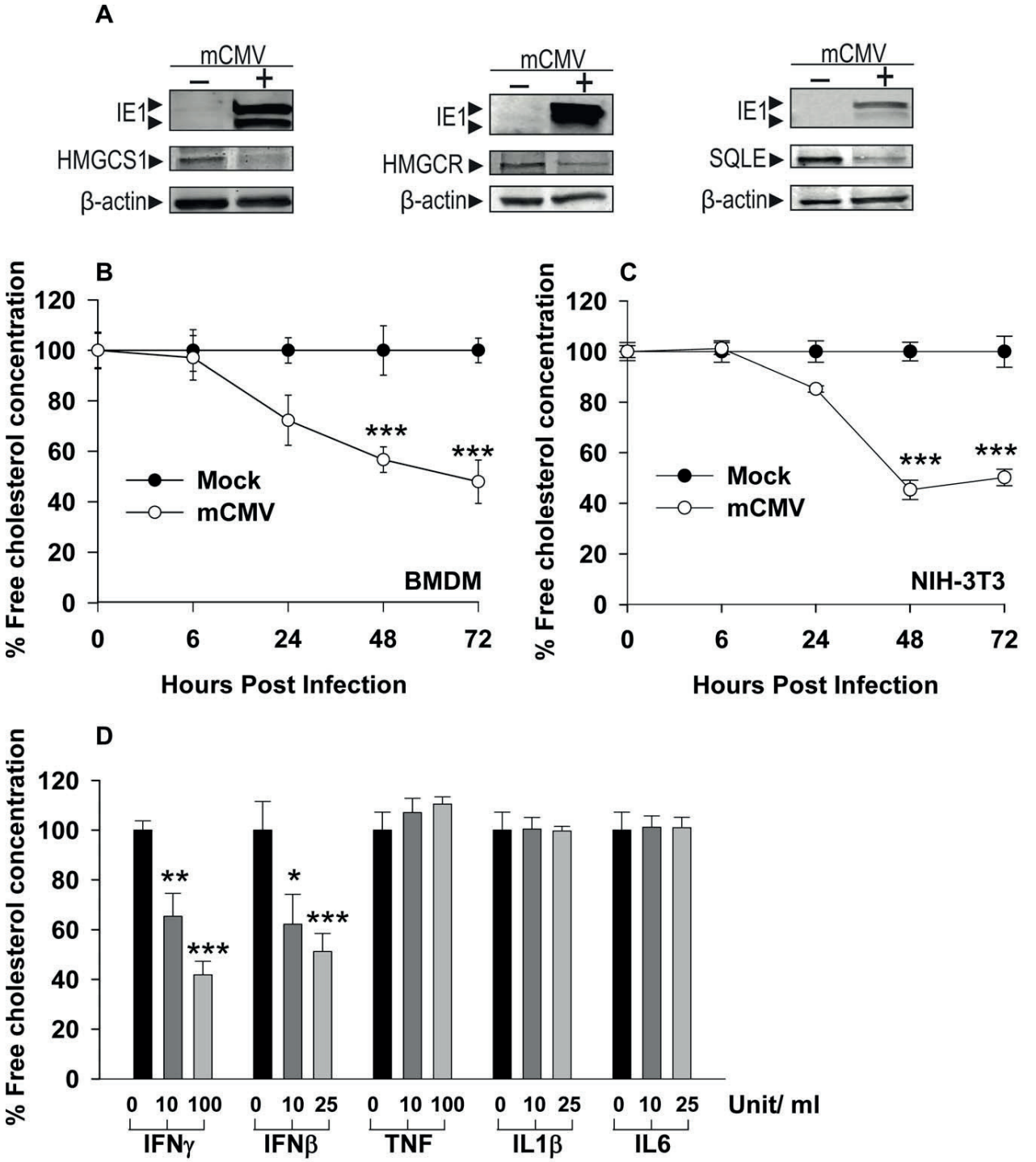

Figure 2. Effect of a coordinated reduction in multiple enzymes on sterol biosynthesis. (A) Comparison by Western blot analysis of HMGCS1, HMGCR, and SQLE protein levels in mCMV infected (24 hpi) or mock-treated BMDM. Infection was measured by detection of the IE1 mCMV antigen. Intensity values relative to β-actin calculated by densitometry show a decrease of the total amount of protein in the mCMV-infected BMDM compared to the mock-treated samples of 64% for HMGCS1, 50% for HMGCR, and 85% for SQLE. Graphs are representative of two independent experiments with biological duplicates and triplicates, respectively. (B–C) Free cholesterol concentration was determined experimentally by enzymatic assay (Materials and Methods) at 0, 6, 24, 48, and 72 hpi in BMDM (B) and NIH/3T3 cells (C). Cholesterol content is presented as the percentage of free intracellular cholesterol concentration from infected cells compared to mock treatment. Graphs represent the means ± SD of three independent experiments with biological quadruplicates for each experiment. (D) Free cholesterol concentration in BMDM cultures treated with varying concentrations of IFNγ, IFNβ, TNF, IL1β, or IL6. The cholesterol concentration was measured as mentioned above after 48 h post-cytokine treatment. Bars represent means ± SD of two independent experiments with biological quadruplicates for each experiment. *$p<0.05$, **$p<0.01$, ***$p<0.001$, determined with an unpaired Student's *t* test.
doi:10.1371/journal.pbio.1000598.g002

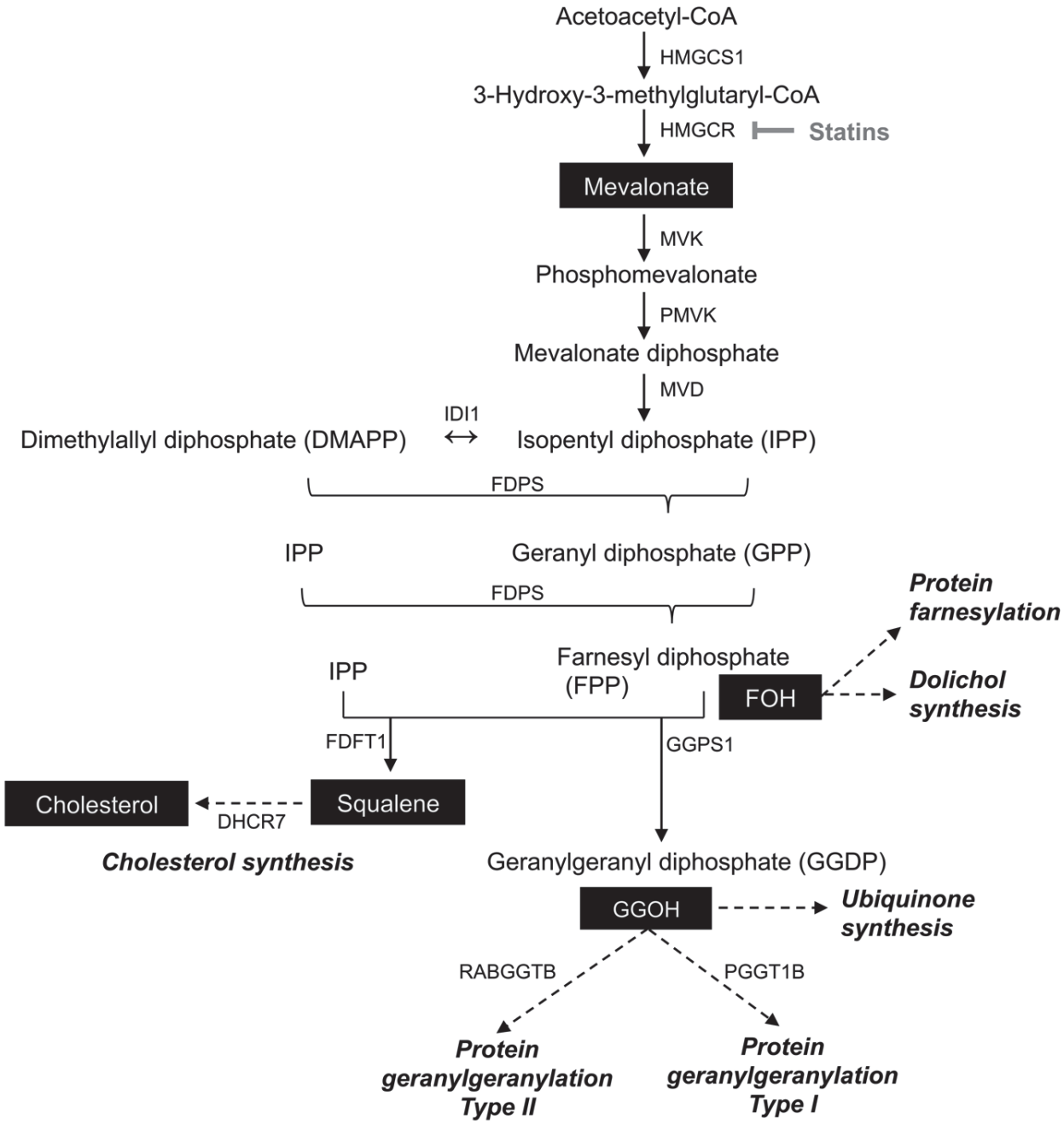

Figure 3. Schematic of the mevalonate-isoprenylation branch point of the sterol biosynthesis pathway. Metabolites (shown in inverse print) and inhibitor (Simvastatin) (shown in grey) used to dissect the pathway are indicated: Simvastatin inhibits HMGCR and prevents the synthesis of mevalonate and downstream lipids.
doi:10.1371/journal.pbio.1000598.g003

restricted immediate-early phase. The results of these experiments are shown in Figure 6B, in which mCMVdie3 potently develops an equivalent level of down-regulation of sterol genes as the parental wild-type and revertant viruses, respectively.

It is well established for many viruses, including mCMV, that infection leads to the induced expression of type 1 interferon and pro-inflammatory cytokines. Two signaling cascades—a virus-induced interferon-producing signal and an interferon receptor-mediated secondary signal—regulate the interferon system. The first is initiated by the detection of viral components by host recognition receptors (PRRs) and leads to the activation of transcription factors—NFkB, ATF2/c-Jun, IRF3, and IRF7—that activate IFNα and β genes. The expressed interferons then transmit a secondary autocrine or paracrine signal through interactions with type I receptors that activate the JAK-STAT pathway. In this context, the above studies with the combined observation that interferon treatment and the cell response to infection are equally capable of causing a down-regulation of the sterol metabolic pathway raise the question of whether infection-mediated regulation might result from an interferon regulated loop. In support of this notion we find that

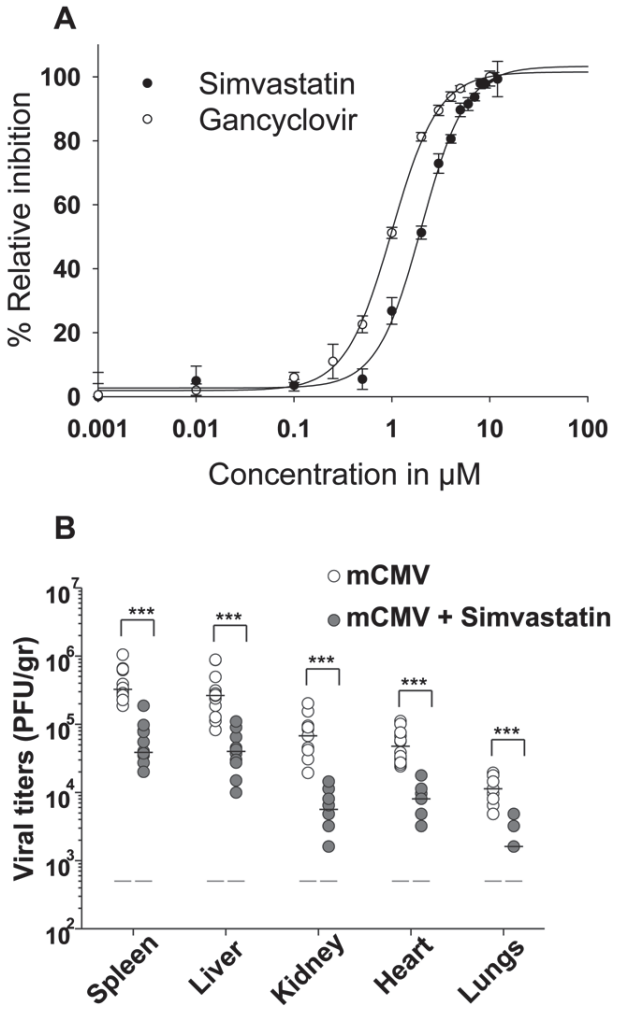

Figure 4. Effect of statins on mCMV growth in vitro and in vivo. (A) NIH/3T3 cells were infected with mCMV-GFP (MOI of 0.2) and subsequently treated with varying concentrations of Simvastatin or Gancyclovir immediately after infection. GFP expression was measured to monitor the level of infection (Materials and Methods). Graph represents the percentage of viral inhibition as a function of drug treatment. Data points represent mean ± SD of two independent experiments with six biological replicates for each experiment. (B) Mice were fed with simvastatin (50 mg/kg/mice) daily for 5 d by gavages and at day 1 post-treatment, were challenged with 2×10^6 PFU of mCMV by intraperitoneal injection, and sacrificed; at 4 dpi, viral titers in different organs were measured by plaque assay and are expressed per gram of tissue. Data points represent mean ± SD of two independent experiments with five mice per group for each experiment. *$p<0.05$, **$p<0.01$, ***$p<0.001$, determined with a Mann-Whitney U test.
doi:10.1371/journal.pbio.1000598.g004

low multiplicities of infection still exhibit a significantly reduced level of free cholesterol (Figure S6) and that conditioned media from infected macrophages 8 hpi (prior to release of any new viral particles) are sufficient to down-regulate the sterol biosynthesis pathway genes in uninfected control cultures (Figure 6C).

On the basis of temporal expression, causal inference of candidate effectors can be tested. A search of cytokine profiles suggested a strong correlation following IFNβ synthesis, further raising the hypothesis for a potential interferon regulatory loop mechanism that is responsible for modulating sterol biosynthesis. First, we investigated directly whether IFNβ is responsible by infecting BMDM from ifnβ−/− mice and examining gene expression for representative members of the sterol pathway. Figure 7A shows that following the genetic ablation of IFNβ, there is still statistically significant sterol gene expression reduction but that there is a partial loss in the degree of reduction indicating that IFNβ is not absolutely necessary. It is possible that other type I IFN members may compensate for the lack of IFNβ. The redundancy among the various type I interferons can be directly evaluated through genetic knockout of their shared receptor, IFNAR1.

For this reason we next investigated whether the sterol response to infection is dependent on the type I interferon receptor. To this end, primary macrophages derived from IFNAR1−/− mice were challenged with mCMV or IFNβ, and the sterol biosynthesis gene expression and free cholesterol levels were analyzed. As shown in Figure 7B–D, the lack of interferon type I receptor abolished the ability of macrophages to reduce both sterol biosynthesis gene expression and cholesterol yield upon either infection with mCMV or treatment with IFNβ. We conclude from these experiments that a type I interferon-dependent innate immune response stringently regulates the metabolic alteration of the sterol biosynthesis network observed upon infection.

Type 1 interferon has an important role in the control of mCMV replication, and the tyrosine kinase 2 (Tyk 2) signaling component is absolutely essential for the type I defense against mCMV infection. Notably, the lack of Tyk2 is known to selectively impair the transcription of only a subset of virally induced IFNAR1 responsive genes [51]. Since this occurs at the promoter-transcriptional level, we first asked whether the down-regulation of the sterol pathway in response to infection also occurs at the level of gene transcription. For this purpose and to directly measure the level of de novo transcription of members of the sterol pathway, we exploited a recently established labeling protocol for the isolation and analysis of newly transcribed RNA [52]. In these experiments, macrophages were infected with mCMV in the presence of 4-thiouridine, for 30 min at 6 hpi, allowing efficient labeling of nascent RNA for isolation and interrogation by microarray analysis. Figure 8A shows that infection by mCMV results in the anticipated reduced level of newly transcribed RNA of the sterol biosynthetic pathway genes. Next we sought to test whether the Tyk2 receptor-signaling component is required for the type I interferon-dependent down-regulation of the sterol pathway. For these experiments we used tyk2−/− macrophages and observe an almost complete abrogation of the transcriptional down-regulation by mCMV infection (Figure 8B). These results demonstrate a requirement for Tyk2 in the mCMV-mediated gene down-regulation of the sterol biosynthesis pathway and suggest a novel role of interferon type I receptor signaling as a transcriptional modifier of the host's metabolic response to infection.

SREBP2 Is Down-Regulated upon Infection and IFN Treatment by a Type I Interferon-Dependent Mechanism

The above studies strongly point to a transcriptional mechanism in down-regulating the sterol pathway upon infection. The sterol regulatory binding protein 2 (SREBP2) is the principal transcription factor involved in coordinating the regulation of the sterol biosynthesis pathway [53]. SREBP2 is synthesized as a precursor and anchored in the endoplasmic reticulum membrane and through limited proteolysis is activated to generate mature forms that can enter the nucleus and interact with multiple sterol pathway genes to coordinate their expression. Hence, in order to gain further insight into the potential mechanism for participating in the transcriptional down-regulation of the sterol pathway, we investigated in the first instance the protein levels of activated cleaved forms of SREBP2

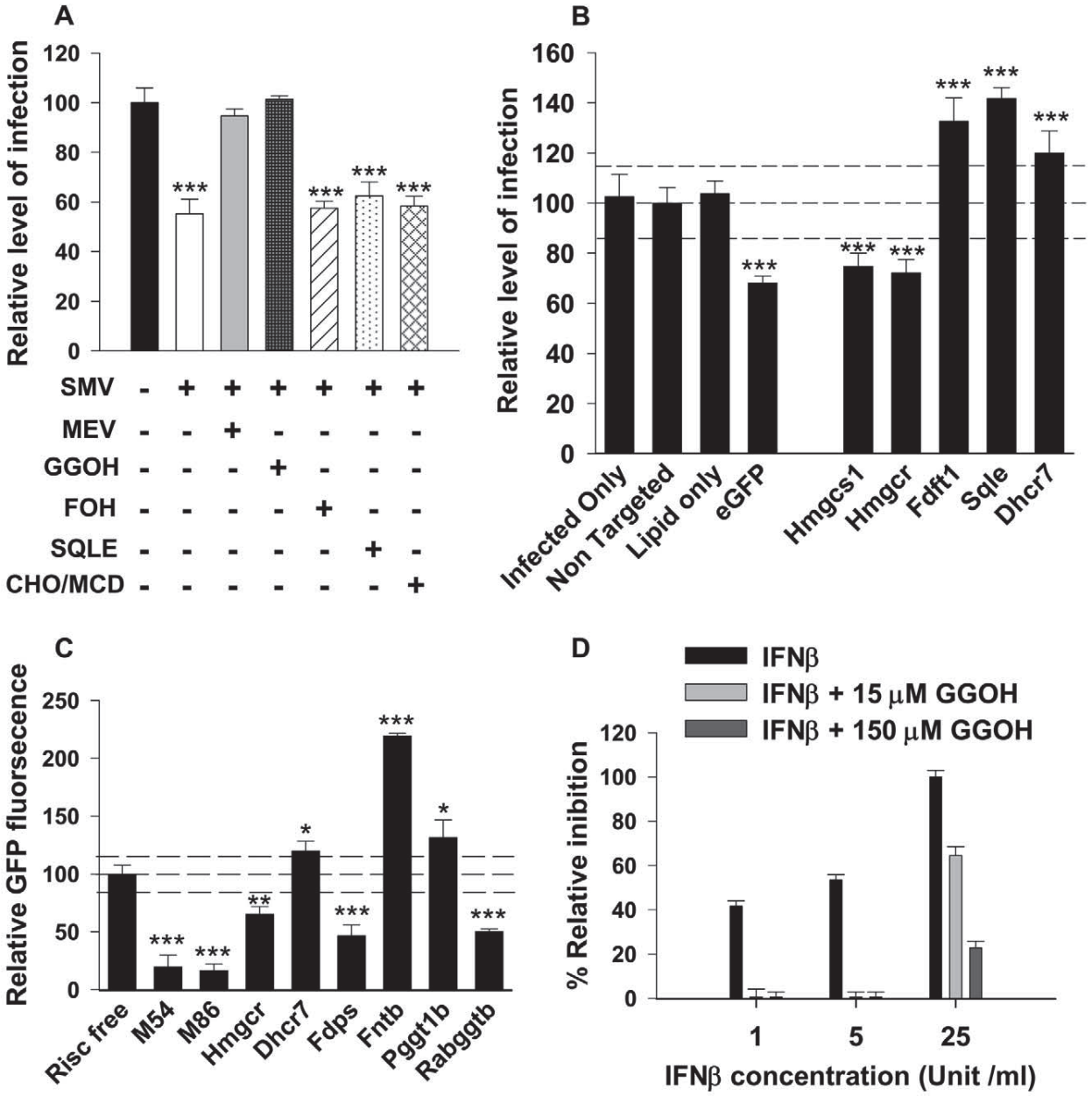

Figure 5. Metabolic investigation of the sterol pathway in infection. (A) NIH/3T3 cells were infected with mCMV-GFP (MOI of 0.2) and subsequently treated with Simvastatin (SMV) (2.5 μM) and mevalonate (MEV) (300 μM) or geranylgeraniol (GGOH) (15 μM) or farnesol (FOH) (15 μM) or squalene (SQE) (15 μM) or of water soluble cholesterol (complexes of cholesterol with methyl-β-cyclodextrin, CHO/MCD) (5 μg/ml) for 72 h. The level of infection was determined by measuring GFP fluorescence at 76 hpi (Material and Methods). Graph represents the relative level of infection compared to the untreated cells, and bars represent mean values ± SD of three independent experiments with five biological replicates for each experiment. (B) NIH/3T3 cells were transfected for 48 h with either non-targeted, eGFP, Hmgcs1, Hmgcr, Sqle, Fdft1, or Dhcr7 On-target plus siRNA smart pool and then infected with mCMV-GFP (MOI of 0.2). (C) NIH/3T3 cells were transfected for 48 h with either Risc Free, M54, and M86 (knocking down mCMV viral genes), Hmgcr, Dhcr7, Fdps, Fntb, Pggt1b, or Rabggtb On-target plus siRNA smart pool, and then infected with mCMV-GFP (MOI of 0.2). The level of non-targeted siRNA (B) and Risc Free (C) treated cells was used as a baseline estimate for the cutoff point (two standard deviations and a p value <0.001 (determined with an unpaired Student's t test) as significant). Bars represent means ± SD of two independent experiments with three biological replicates for each experiment. (D) NIH/3T3 cells were incubated with various doses of IFNβ for 18 h in the presence or absence of 15 and 150 μM GGOH. The graph represents the inhibition of viral replication (in percentages) as a function of drug concentration. Bars represent mean ± SD of biological triplicates for each experiment. *$p<0.05$, **$p<0.01$, ***$p<0.001$, determined with an unpaired Student's t test.
doi:10.1371/journal.pbio.1000598.g005

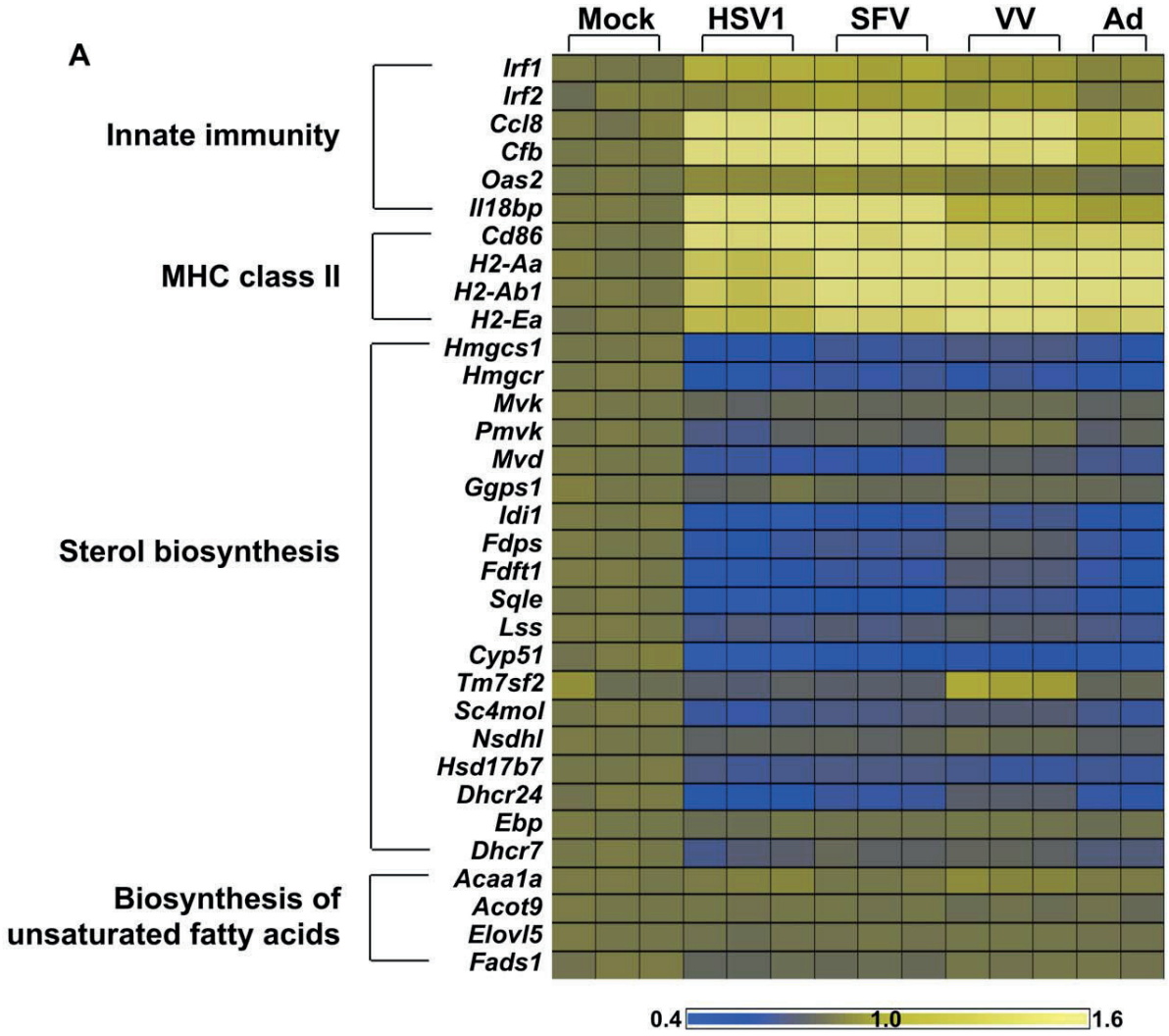
A
Mock
HSV1
SFV
VV
Ad
Innate immunity
Irf1
Irf2
Ccl8
Cfb
Oas2
Il18bp
MHC class II
Cd86
H2-Aa
H2-Ab1
H2-Ea
Sterol biosynthesis
Hmgcs1
Hmgcr
Mvk
Pmvk
Mvd
Ggps1
Idi1
Fdps
Fdft1
Sqle
Lss
Cyp51
Tm7sf2
Sc4mol
Nsdhl
Hsd17b7
Dhcr24
Ebp
Dhcr7
Biosynthesis of unsaturated fatty acids
Acaa1a
Acot9
Elovl5
Fads1
0.4
1.0
1.6

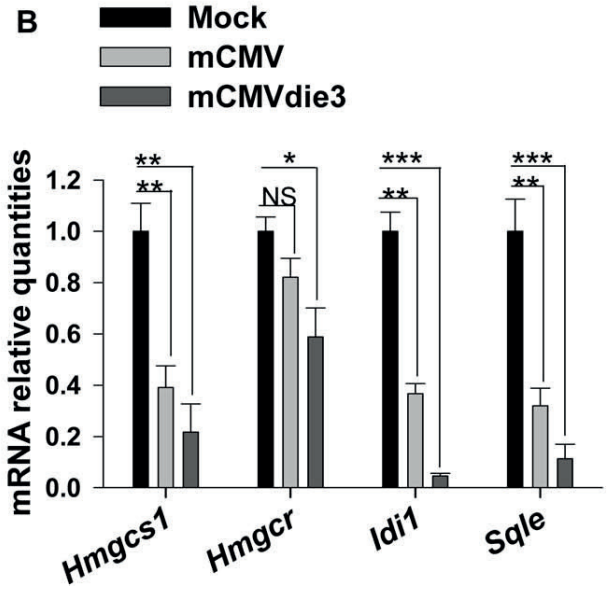
B
Mock
mCMV
mCMVdie3
mRNA relative quantities
0.0
0.2
0.4
0.6
0.8
1.0
1.2
**
**
*
NS
***
**
***
**
Hmgcs1
Hmgcr
Idi1
Sqle

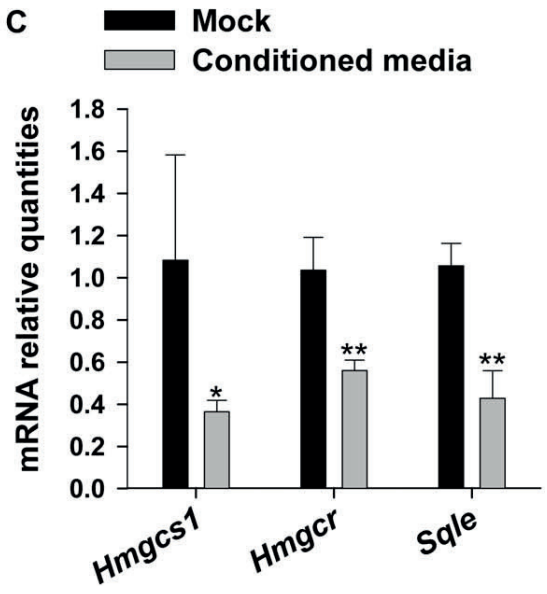
C
Mock
Conditioned media
mRNA relative quantities
0.0
0.2
0.4
0.6
0.8
1.0
1.2
1.4
1.6
1.8
*
**
**
Hmgcs1
Hmgcr
Sqle

Figure 6. Alteration of gene expression upon HSV1, SFV, VV, adenovirus, and non-infectious mCMV in primary macrophages. (A) Heat map of expression levels of a set of genes after 24 h mock treatment, infection with Herpes simplex virus 1 (HSV1), Semliki forest virus (SFV), Vaccinia virus (VV), or Adenovirus (Ad) in BMDM (Text S1). Genes represent the innate immunity activation, the MHC class II antigen presentation, and the cholesterol and unsaturated fatty acids biosynthesis. Each square represents a single biological replicate. Fold changes of expression levels are represented on a Log2 scale compared to mock-treated cells, ranging from a 0.4× lower expression (dark blue) to a 1.6× higher expression (bright yellow). (B) Expression analysis measured by qRT-PCR of *Hmgcs1*, *Hmgcr*, *Idi1*, and *Sqle* genes in BMDM after 24 h mock treatment, mCMV, or mCMVdie3 infection, respectively. Graphs show the level of expression of the indicated genes relative to mock-treated samples and bars represent mean ± SD of two independent experiments with triplicate biological measurements for each experiment. (C) BMDM were infected with mCMV or mock treated, and supernatant was collected after 8 h and directly added to fresh BMDM. After 24 h, RNA from these cultures was collected and *Hmgcs1*, *Hmgcr*, and *Sqle* expression were measured by qRT-PCR. To test for the presence of any detectable virus, an aliquot of the supernatant was used to perform a standard plaque assay (no infectious virus detected, unpublished data). Graphs show the level of expression of the indicated genes relative to mock-treated samples and bars represent means ± SD of three independent experiments with triplicate biological measurements for each experiment. *$p<0.05$, **$p<0.01$, ***$p<0.001$, determined with an unpaired Student's *t* test.
doi:10.1371/journal.pbio.1000598.g006

upon infection and interferon treatment. Accordingly, we next performed Western blot experiments to determine levels of mature form of SREBP2. In these experiments, infection of macrophages with mCMV at 24 hpi developed a significant decrease in the nuclear form (Figure 9A). Furthermore, treatment of macrophages with either IFNβ or IFNγ clearly exhibits a decrease in SREBP2 levels (Figure 9A). We next sought to examine whether this is also seen at the level of transcription. In experiments measuring de novo RNA synthesis, we observed a specific transcriptional reduction from the *Srebf2* gene upon infection while increased levels of transcription are seen for interferon-associated transcription factor Stat1 (Figure 9B), indicating a selective transcriptional basis for the reduced levels of expression. Markedly, the reduction in RNA levels upon infection was completely reversed upon genetic ablation of the *ifnar1* gene (Figure 9C). Altogether these results demonstrate a coordinate reduction in SREBP2 at both the protein and RNA expression level upon infection, which is tightly dependent on activation of the type 1 interferon receptor.

Discussion

Through the application of a pathway biology strategy integrating genomic, lipidomic, and biochemical approaches with bioinformatics, we show, for the first time, the coupling of the type I interferon response upon viral infection to the sterol pathway and identify the mevalonate-isoprenoid arm as playing a pivotal role in antiviral functions. A definitive link to sterol metabolism that is independent of cholesterol is established by the observation that the anti-viral effect of down-regulating the sterol pathway upon infection is completely blocked if cells are provided with an excess of mevalonate but not cholesterol. Furthermore, the anti-viral potency of type 1 interferon is severely diminished in the presence of excess geranylgeraniol metabolite, highlighting a requirement of the mevalonate-isoprenoid branch as part of an interferon mechanism for protecting against infection. Further on the basis of genetic elimination studies we unequivocally document a molecular dependency between sterol biosynthesis and interferon signaling upon infection, leading to a modest but highly significant coordinate decrease in gene expression, which subsequently causes a marked alteration in the metabolic activity of the sterol pathway.

A Two-Step Immune-Signaling Cascade Involved in Regulating Sterol Biosynthesis upon Infection

Our results are consistent with a model involving a two-step interferon response for modulating endogenous sterol pathway activity upon infection. Figure 10 illustrates the two signaling cascades, a virus-induced interferon-producing signal and an interferon receptor-mediated secondary signal. The first is initiated by the detection of virion proteins and nucleic acids by host recognition receptors with the result of the infected cell producing type I interferon. As part of the second step all type I interferons bind to one common receptor (IFNAR1). The IFN-α/β receptor (IFNAR1) signals through the JAK/STAT pathway by phosphorylation of the Janus kinase (JAK)1, tyrosine kinase (Tyk)2, and signal transducer and activator of transcription (STAT)1 and STAT2, which subsequently modulates a diverse array of genes. In the case of mCMV the first step has been extensively investigated and shown to involve TLR2, TLR3, and TLR9 recognition receptors [54,55], whose activation leads to the induction of transcription factors, NFkB, ATF2/c-Jun, and IRF3 that directly activate IFNα and β genes. Interestingly, previous studies [5,37] have shown that microbial activation of TLR3 or TLR4 inhibits by an as-yet unknown mechanism LXR target genes such as ABCA1, resulting in the inhibition of cholesterol efflux from macrophages. This is reported to occur in a type I interferon-independent manner [5]. Similar to microbial-mediated TLR activation of IRF3, many viruses including mCMV potently induce IRF3 and may also have the potential to inhibit LXR functions. Despite recent progress in the definition of links between intracellular cholesterol homeostasis and innate immunity, little is known regarding the influence of interferon-regulated signaling on this phenomenon.

In the present study, we demonstrate that transcriptional regulation of the cellular sterol biosynthesis pathway upon infection has an impact on viral replication and depends on an interferon-regulated loop involving type 1 interferon signaling. Specifically, we show that infection of cells by a wide range of viruses or direct interferon stimulation is accompanied by the down-regulation of sterol biosynthesis as a result of reducing the rate of sterol gene transcription. In the context of ligand-activation of the type I receptor, we also demonstrate that this requires the Tyk2 signaling component (Figure 10).

In the context of type I interferon genes induced upon infection, it is worth noting that viperin, a type I interferon-regulated gene, is involved in cellular defense against a number of viruses and functions to disrupt cholesterol-rich lipid rafts that are used as viral production sites in the cell [34,38,56]. In addition, an intracellular interaction of viperin with Fdps, an enzyme essential for isoprenoid biosynthesis (Figure 3), has been reported to lower, by a small extent, the activity of the enzyme [38]. It is not known whether targeting Fdps enzyme activity alone is an effective anti-viral mechanism, although the RNAi targeting results of Figure 5 (panel C) suggest that this may be a plausible mechanism (Figure 5C). However, it is more likely that a combination of interferon-mediated transcriptional down-regulation of the sterol biosynthesis genes and the potential enzymatic protein modification at the isoprenoid branch point represents a concerted anti-viral host defense mechanism.

Coordinate Transcriptional Regulation of Sterol Pathway Members

From a transcriptional perspective, the sterol biosynthesis pathway genes are co-ordinately controlled by the sterol regulatory

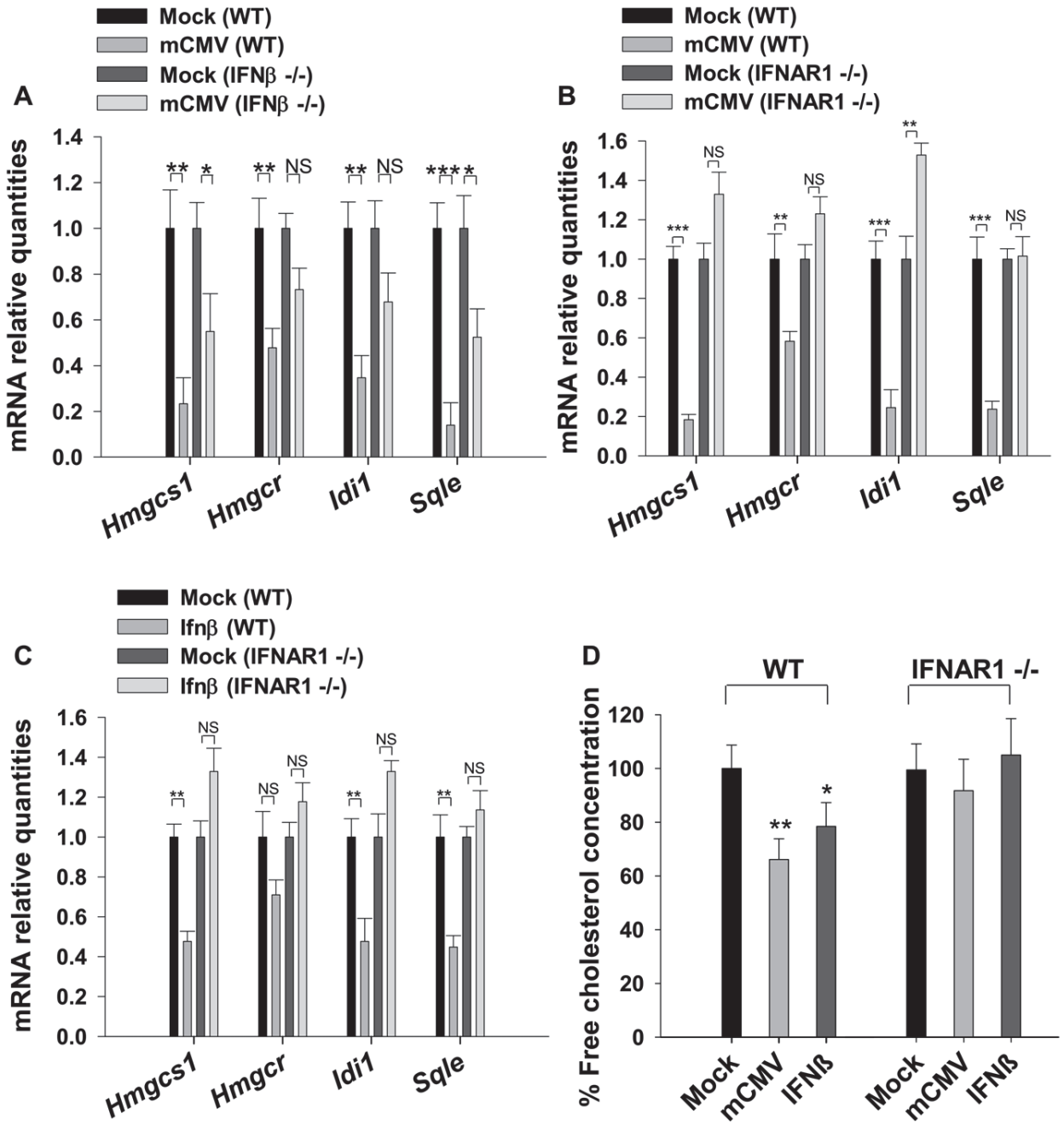

Figure 7. Contribution of type I interferon response in the regulation of sterol biosynthesis genes upon infection. (A–C) Wild type BMDM or BMDM from IFNβ−/− knockout mice or from IFNAR1−/− knockout mice were mock treated, infected with mCMV, or treated with IFNβ (10 U/ml) for 24 h. RNA was collected and the gene expression of *Hmgcs1*, *Hmgcr*, *Idi1*, and *Sqle* was measured by qRT-PCR. Graphs show the level of expression of the indicated genes relative to mock-treated samples. Bars represent the mean ± SD of biological quadruplicates. (D) Wild type BMDM or BMDM from IFNAR1−/− knockout mice were infected with mCMV or treated with IFNβ (10 U/ml). After 48 h, free cholesterol concentration was measured by enzymatic assay (Materials and Methods). Bars represent the mean ± SD of biological quadruplicates. *$p<0.05$, **$p<0.01$, ***$p<0.001$, determined with an unpaired Student's *t* test.
doi:10.1371/journal.pbio.1000598.g007

element binding protein 2 transcription factor (SREBP2). Significantly, we find in our system that the overall abundance of the mature protein (the proteolytically cleaved active form) and the rate of gene transcription of its gene are significantly reduced upon infection or interferon treatment. Significantly, both are strictly dependent on the presence and activation of the type 1 interferon receptor *Ifnar1*. These findings suggest that a possible mechanism for the coordinate down-regulation of sterol biosynthesis is by interferon regulation of *Srebf2*. Interestingly and consistent with the possibility of interferon regulating *Srebf2*, chemical inhibition of SREBP2 has been shown to inhibit HCV replicon activity [32]. This would also support the view of

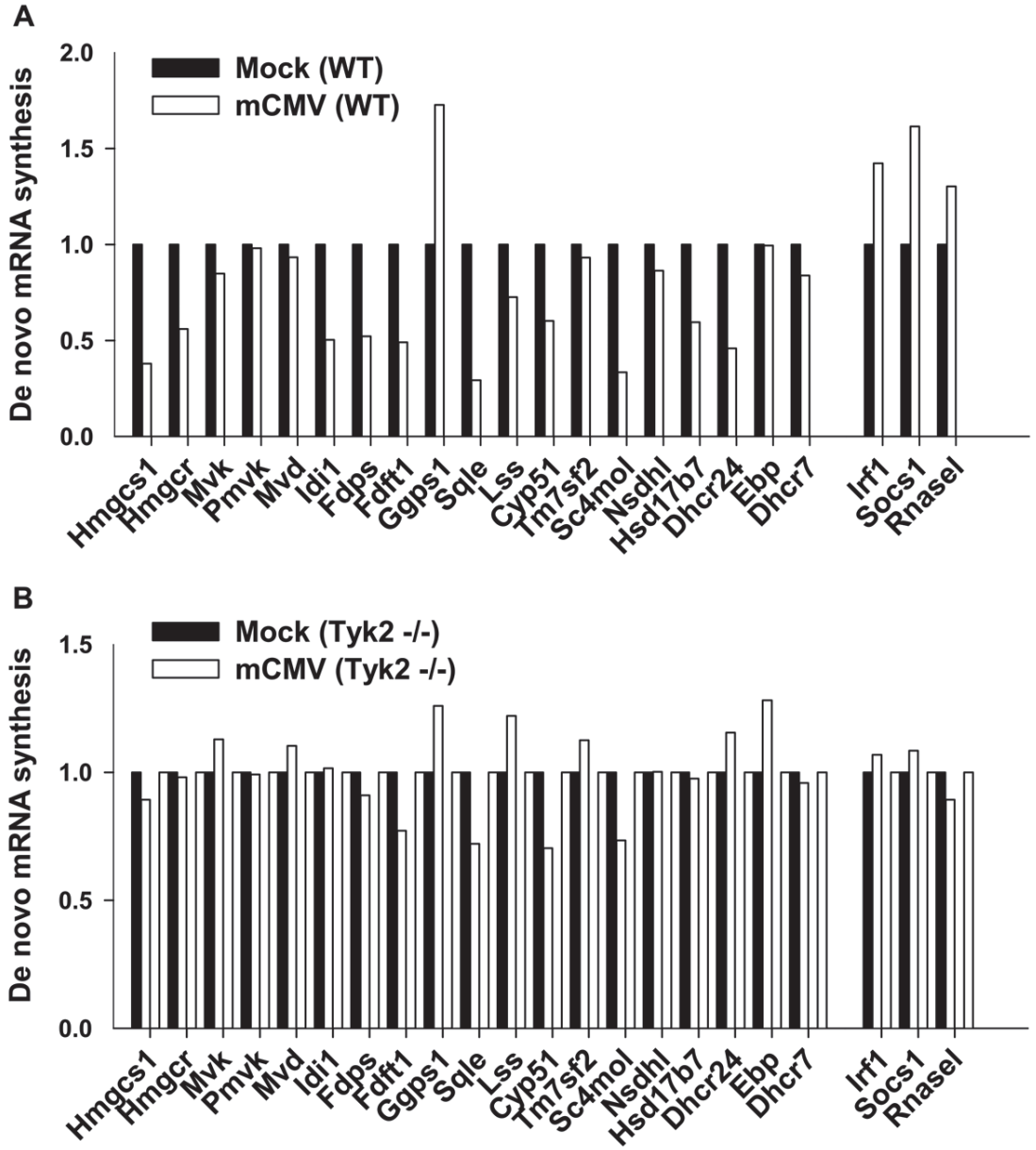

Figure 8. Measurement of de novo mRNA synthesis of sterol biosynthesis genes upon viral infection. Wild Type or Tyk2$^{-/-}$ BMDM were infected with mCMV at an MOI of 1 for 1 h. De novo RNA was labeled between 360 and 390 min post-infection, isolated, and hybridized to Affymetrix Gene 1.0 ST microarrays (Materials and Methods). After scanning and data capture, gene expression in mock-infected or infected cells was analyzed, and for the purposes of presentation, gene expression values from control (mock infected) BMDM (black) were adjusted to a value of 1. Values for expression in infected cells (white) were then expressed as a number relative to the control.
doi:10.1371/journal.pbio.1000598.g008

implicating negative feedback on SREBP-2 via oxysterol metabolites. Further studies are required to elucidate more precisely the mechanism or mechanisms by which interferon mediates down-regulation of the sterol biosynthesis pathway. Whatever the mechanism, the IFN-dependent coupling of the mevalonate-sterol metabolic network and anti-viral activity represents a previously unrecognized mechanism in the regulation of protective immunity.

From an immune response and metabolic/pharmacological perspective, modulating cholesterol biosynthesis via small, coordinate transcriptional changes offers advantages and disadvantages over single enzyme control. At the homeostatic level, coordinate control of a metabolic pathway could potentially increase the robustness of modulation; the redundant rate-limiting interactions, downstream of the true rate-limiting interaction, can protect the pathway from surges in the levels of downstream metabolites. Coordinate control also increases the specificity of the pathway modulation as a small reduction of the enzyme level in an interaction ensures that the level of the interacting metabolite need not drop as far to affect a reduction in flux. This has the advantage of potentially lessening the impact on other branched or cross-linked pathways that use the same metabolites and thus provides a high degree of pathway specificity.

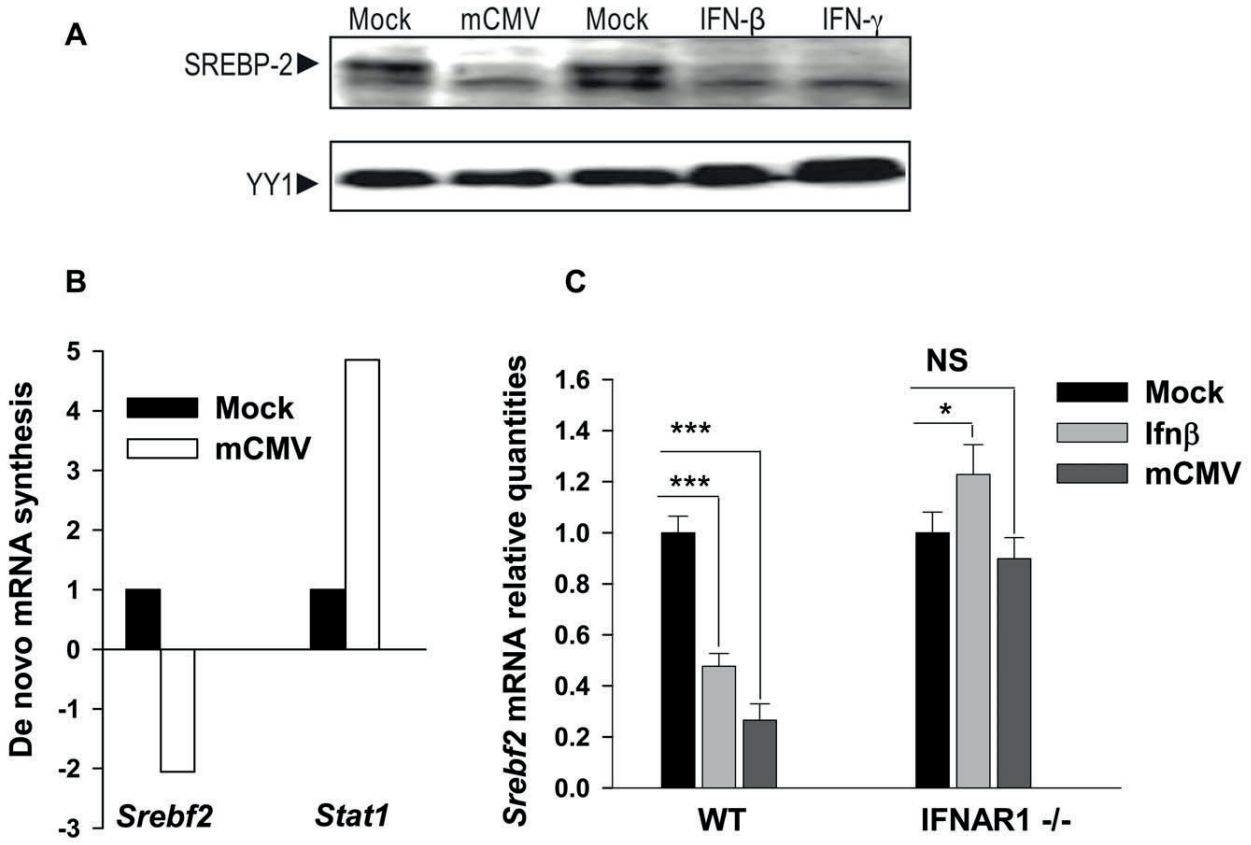

Figure 9. Regulation of SREBP2 by mCMV infection and IFNβ treatment. (A) Comparison of cleaved SREBP2 protein in mock-infected (lane 1), mCMV-infected (MOI of 1) (lane 2), mock-treated (lane 3), IFNβ- (50 U/ml) (lane 4), or IFNγ- (50 U/ml) treated (lane 5) BMDM for 24 h by Western blot analysis using YY1 as a loading control. Arrow indicates SREBP2 cleaved form that is induced upon lovastatin and ezetimibe treatment from liver extracts of cholesterol-fed mice (see Figure S8). The blot is representative of two independent experiments with biological triplicates for each experiment. (B) Wild type BMDM were infected with mCMV for 1 h. De novo RNA was labeled between 360 and 390 min post-infection, isolated, and hybridized to Affymetrix Gene 1.0 ST microarrays (Materials and Methods). After scanning and data capture, gene expression in mock-infected or infected cells was analyzed, and for the purposes of presentation, *Srebf2* gene expression values from control (mock-infected) BMDM (black) were adjusted to a value of 1. Values for expression in infected cells (white) were then expressed as a number relative to the control. (C) BMDM from wild type or IFNAR1−/− knockout mice were treated with 10 U/ml of IFNβ or infected with mCMV. After 24 h, RNA was collected and the gene expression of *Srebf2* was measured by qRT-PCR. Results show the level of gene expression of the treated or infected samples relative to the mock-treated samples. Bars represent the mean ± SD of biological quadruplicates. *$p<0.05$, **$p<0.01$, ***$p<0.001$, determined with an unpaired Student's *t* test.
doi:10.1371/journal.pbio.1000598.g009

Therapeutic Perspective

Several viruses including human CMV have been reported to be sensitive to statin administration [25,26,28–31]. Although the mechanism of action of most is not known, it has in some cases been correlated with a lower abundance of cholesterol in lipid rafts of cell membranes. A recognized potential complicating factor of using statins to specifically reduce cholesterol levels is that suppression of the proximal mevalonate arm also perturbs the synthesis of branch derivatives such as geranylgeraniol and farnesol involved in the protein farnesylation and prenylation pathways. In the case of HCV, the mechanisms of the inhibitory effects of the statins have been examined extensively and have been shown to relate to the prenylation of a host protein (FLB2) essential for viral replication [18,57]. Recently a combination chemical screening study has been conducted to explore how the sterol and protein prenylation pathways work together to affect HCV in a replicon assay [32]. In agreement with those studies we also find reduced mCMV growth in siRNA knock-down experiments targeting enzymes in the isoprenod biosynthesis pathway. These studies indicate the importance of the geranylgeranylation to viral replication. Although, it is worth noting that the isoprenoid biosynthesis pathway is highly complicated with multiple branch points involving redundant enzymatic steps, sharing of subunits, and competing reactions. In our current study, we uncoupled the cholesterol synthesis pathway from non-steroidal modifications through targeted metabolic rescue and siRNA knock-down studies of mCMV and reveal an absolute requirement for the prenylation branch of the sterol pathway for mediating anti-viral effects. As further indicated from computational modeling work (unpublished data), targeting HMGCR is likely to have a broad range of non-specific effects on various efferent branch points of the pathway and thus may well not be ideal for anti-infective therapy. In addition, statins are also known to have a range of immune-modulatory activities by mechanisms yet to be fully characterized. In this context, it is worth noting that the activity of the type I interferons, especially IFNβ, have considerable overlap with many of the immune-related activities of statins [58]. Moreover, it is especially noteworthy that IFNβ treatment in patients has also been reported to have decreased plasma cholesterol levels [59,60]. Since our studies uncover a

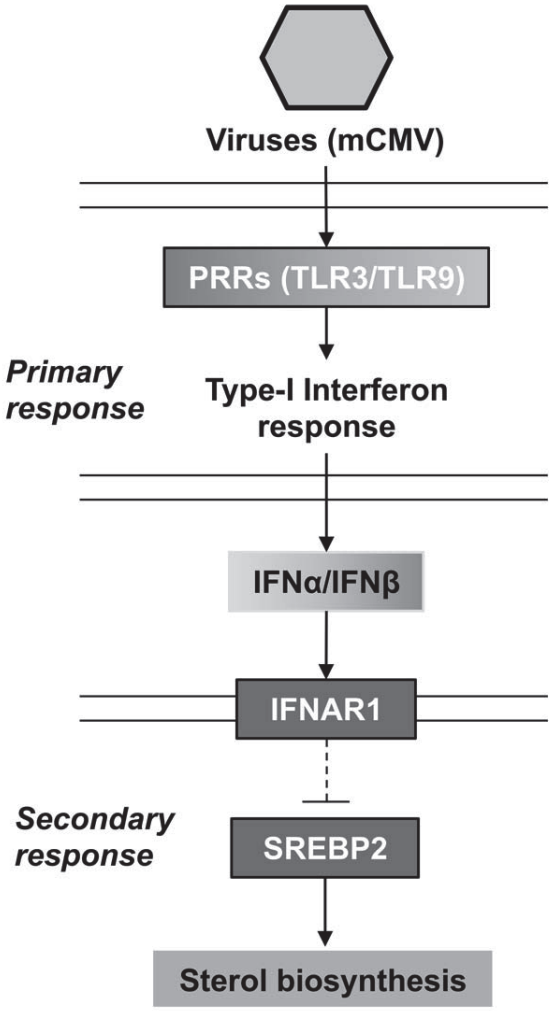

Figure 10. Proposed model for down-regulation of the sterol synthesis by type I interferon response to viral infection.
doi:10.1371/journal.pbio.1000598.g010

molecular dependency of type 1 signaling, including a Tyk2 signaling component, this may provide an entirely new therapeutic pathway for lowering cholesterol. Moreover, our findings may have important implications for the development of broadly active new adjuvant strategies (e.g., the use of inhibitors of SREBP2 activity) to existing anti-infective therapies (e.g., antiviral drugs such as ganciclovir). On this basis we posit the principal of using metabolic modifiers, i.e. drugs that target metabolic pathways, of protective innate immunity as holding future promise for developing host-directed anti-viral therapies. Overall, this study supports the original concept [40,41] of selectively targeting host pathways as an efficacious anti-infective strategy.

Materials and Methods

Microarray Experiment, Bioinformatic Analysis

Microarray analysis of the time course experiments of infected and interferon treated macrophages were conducted using Agilent microarray platform and a detailed description of the experimental set up; statistical and bioinformatics analysis is in the Supporting Information section. All other microarray studies were conducted using Affymetrix (Mouse Genome 430) microarray platform. Data from hybridized Affymetrix microarrays were acquired using proprietary Affymetrix platform scanners and GCOS software (Affymetrix). Processed CEL files were imported into Partek Genomics SuiteTM (MO, USA), then background corrected, quantile normalized, and probe-set summarized using the RMA algorithm [61,62]. A non-specific filter was applied to remove genes that were not expressed on any of the samples across the experiment. Microarray signals were then per-gene normalized to the average of the three mock samples (which was set to a value of 1) for visualization purposes in the heat map for Figure 6. In the case of de novo RNA expression, analysis was performed using the Affymetrix Mouse Gene 1.0 ST arrays, consisting of a total of eight chips and three experiment factors: time (60–90 min, 360–390 min), genetic background (Tyk2KO, WT), and treatment (mock, mCMV). Data from hybridized chips were acquired using GCOS software (Affymetrix). Prior to further processing and analysis with the R statistical programming environment, Affymetrix Power Tools (APT, Affymetrix) were used to summaries and annotate chip data to gene level. After initial quality control assessment, data were background-corrected, quantile normalized, and probe-set summarized using the RMA algorithm.

Mice BMDM Cultures

Wild type C57BL/6 and BALBc were from the Biomedical Research Resources, Little France, University of Edinburgh. IFNβ−/− and Tyk2−/− mice were from the Institute of Animal Breeding and Genetics Veterinary University of Vienna. BMDM were derived from monocytes obtained from femurs of male mice aged 10 to 12 wk. Cells were grown in DMEM-F12 media supplemented with 10% L929 cell-conditioned medium as a source of macrophage colony-stimulating factor (M-CSF) for 7 d as described [63]. Characterization of BMDM was performed by standard flow cytometry, evaluating the presence of the F4/80 marker and CD11b surface protein. In average of all experiments more than 93% of cells possessed both proteins.

Viruses

The mouse CMV C3X strain, generated from the recombinant C3X bacterial artificial chromosome clone and originally derived for the Smith strain of mCMV [64], was propagated in NIH 3T3 cells, and titers were determined by standard plaque assay on MEFp53−/−. For live cell assay, NIH/3T3s were infected with a recombinant mCMV expressing the green fluorescent protein (GFP) marker inserted in front of the ie2 gene (pSM3fr-rev, called mCMV-GFP in this study [65]). Viral growth curves comparing wild type and GFP virus were assessed by standard plaque assay, and the results showed no differences between the growth curve of the two viruses (unpublished data). To establish the role of viral gene expression in the regulation of sterol genes, the mCMVdie3 strain was used [50]. For the microarray experiment, Semliki Forest Virus (SFV, MOI of 10), Herpes simplex virus type 1 (HSV1, MOI of 1), Vaccinia virus (VV, MOI of 1), and Adenovirus (Ad, MOI of 100) were used to infect BMDM for 1 h in DMEM:F12 3% FCS, 10% L929, and 100 U of penicillin/streptomycin per ml.

Infection

BMDM and NIH/3T3 were infected with the different viruses at an MOI of 1, unless specified. For BMDM, viral stock was diluted in DMEM:F12 3% FCS, 10% L929, and 100 U of penicillin/streptomycin per ml, and after 1 h adsorption, cells were washed in PBS and incubated in fresh DMEM:F12 10%

FCS, 10% L929, and 100 U of penicillin/streptomycin per ml. For NIH/3T3 viral stock was diluted in DMEM 3% CS and 100 U of penicillin/streptomycin per ml, and after 1 h adsorption, cells were washed in PBS and incubated in fresh DMEM:F12 10% CS and 100 U of penicillin/streptomycin per ml. SFV (MOI of 10), HSV1 (MOI = 1), VV (MOI of 1), and Ad (MOI of 100) were used to infect BMDM for 1 h in DMEM:F12 3% FCS, 10% L929, and 100 U of penicillin/streptomycin per ml.

Cytokines and Pharmacological Treatments

IFNγ (Boehringer Manheim Corp), IFNβ, IL6, TNF, and IL1β (Biosource International, USA) stock were dissolved in PBS supplemented with 0.2% BSA and diluted in fresh media just prior to the experiment. The effect of cytokine treatment on cell viability was tested for each concentration used in the experiment and did not show any alteration of viability. For the pharmacological experiment, 25 mg of simvastatin (Sigma-Aldrich) was activated by hydrolysis of the lactone by adding 1 ml of 0.1 N NaOH, 100% ethanol. After heating at 50°C for 2 h, the solution was neutralized with HCl to a pH of ≈7.2 and sterilized by filtration through a 0.2 μm filter. The stock solution was diluted to the appropriate concentration in sterile PBS and the solution was aliquoted, stored at −20°C, and used within a month of activation. Mevalonate and water soluble cholesterol (Sigma-Aldrich, Germany) was resuspended in media to the appropriate concentration and sterilized by filtration through a 0.2 μm filter. Geranylgeraniol and farnesol squalene (Sigma-Aldrich, Germany) stocks were dissolved in DMSO and sterilized by filtration through a 0.2 μm filter. The stock solutions were dissolved in media at the appropriate concentration just prior to the experiment. The final concentration of DMSO in media did not exceed 0.1%. Effects of sterol intermediates treatment on the cell were tested for each concentration used in the experiment and did not show any alteration of viability. Gancyclovir (Cymevene, Hoffman-La Roche, UK) was resuspended in saline solution and sterilized by filtration through a 0.2 μm filter. Gancyclovir was then diluted in media, to the indicated concentration.

Quantitative RT-PCR

Taqman Primer probe sets were purchased from Applied Biosystems, Warrington, UK (Assay ID: Hmgcs1: Mm00524111-m1; Hmgcr: Mm01282499-m1; Idi1: Mm00836417-g1; Sqle: Mm00436772-A1). For each sample QRT-PCR was performed in 20 μl volumes using MicroAmp Optical 96-well reaction plates and MicroAmp Optical Caps (Applied Biosystems). Two microliters of diluted RNA samples (≈100 ng of RNA) were added to 10 μl of 2× PCR master mix, 1 μl of a Taqman primer/probe set (Applied Biosystems, CA) for the gene of interest at the recommended concentration, 0.25 μl of Superscript III (Applied Biosystems, CA), and 6.25 μl of double-distilled H_20. After an initial incubation at 50°C for 30 s to activate the RNA polymerase, samples were then subject to 40 cycles under Taqman standard conditions (combined annealing and primer extension phase at 60°C for 1 min and a short denaturation at 72°C for 30 s). Stratagene MXPro software was then used to analyze the data. Threshold determinations were automatically performed by the instrument for each reaction. The C_T values were exported into Microsoft Excel and relative quantification of marker gene mRNA expression was calculated with the comparative C_T method [66].

Western Blot Analysis

BMDM cells were washed with PBS and resuspended in whole-cell lysis buffer (50 mM Tris-HCl, pH 7.5, 100 mM NaCl, 1% NP40, protease inhibitors, and phosphatase inhibitors), and cell lysates were centrifuged at 4°C for 10 min and the collected supernatants were stored at −20°C. Protein concentration was measured by Pierce BCA assay (Thermo Scientific). For Western blotting, proteins were separated by SDS-PAGE, transferred to Immobilon-FL membranes (Millipore), and probed with goat anti-HMGCR (Santa Cruz, sc-27578, 1:500), goat anti-SQLE (Santa Cruz, sc-49754, 1:500), anti-HMGCS1 (Santa Cruz, Sc-32422, 1:500), mouse anti-mCMV IE1 (Chroma 101, 1:1000), and rabbit anti-β-actin (Cell Signalling, 4970, 1:2500) diluted in PBST (0.1% Tween20). For secondary anti-goat IR-680 (Invitrogen, A21088, 1:10,000), IR-800 anti-mouse (Thermo Fisher Scientific, 35571, 1:10,000), and IR-800 anti-rabbit (Cell Signalling, 5151, 1:10,000), antibodies were diluted in Odyssey blocking buffer (0.1% Tween20, 0.01% SDS). For probing, visualization, and quantification, the Odyssey protocol (LI-COR) was followed. The fluorescence was quantified by Odyssey system (Li-COR). For details of anti-mouse SREBP-2 polyclonal antibody (custom antibody raised against mature SREBP-2 form [67]) and immunoblot procedures, see Text S1.

Measurement of Free Cholesterol Concentration by Enzymatic Assay

Intracellular cholesterol concentration was determined enzymatically using the Amplex-Red cholesterol Assay Kit (Molecular Probes) according to manufacturer recommendations. Briefly, cells were washed with 1 ml ice-cold PBS and then lysed in 200 μl cold Lipid buffer containing 0.5 M of potassium phosphate, pH 7.4, 0.25 mM cholic acid, and 0.5% triton X-100. Cell lysates were sonicated on ice with three 10-s pulses at high intensity. 20 μl were then used to determine protein concentration using a standard BCA assay to normalize the protein concentration. For cholesterol measurement, 20 μl of each sample were added to the 80 μl assay solution, which contained 300 μM Amplex Red reagent, 2 U per ml HRP and 2 U per ml cholesterol oxidase, 0.1 M of potassium phosphate, pH 7.4, 0.05 mM cholic acid, and 0.1% triton X-100. After preincubation for 30 min at 37°C under light exclusion conditions, fluorescence was measured using excitation at 530±2.5 nm and fluorescence detection at 590±2.5 nm with a Polarstar Optima Multifunciton Microplate Reader (BMG Labtech, UK). The values were corrected from the background. The relative amount of free cholesterol to the mock-treated samples was calculated using the manufacturer's supplied standard curve.

Analysis of Lipids Using High-Performance Liquid Chromatography/Mass Spectrometry and Electrospray Ionization

An Agilent high-performance liquid chromatography (HPLC) system coupled with an Applied Biosystem Triple Quadrupole/Ion Trap mass spectrometer (4000Qtrap) was used for quantification of individual polar lipids (Phospholipids and sphingolipids). Electrospray ionization-based multiple reaction monitoring (MRM) transitions were set up for the quantitative analysis of various polar lipids [68]. HPLC atmosphere chemical ionization/MS were carried out for analysis of sterols [69].

Live Cell Replication Assay

To measure the effect of multiple drugs and siRNA transfection on viral growth, a sensitive live cell infection assay was developed using the properties of the mCMV GFP tagged virus. 1.5×10^4 NIH/3T3 cells were infected for 1 h in black 96-well plates (Costar, UK) at an MOI of 0.2 in 25 μl of fresh DMEM phenol

red-free media, 3% CS, and 100 U of penicillin/streptomycin per ml. After infection, the inoculums were carefully removed by pipetting and replaced by 150 µl of DMEM phenol red-free media with 10% FCS. Viral growth was measured by recording the GFP signal over time using an OPTIMA Polarstar plate reader (excitation wave length of 485 nm and emission of 520 nm). As an optimization step we checked the correlation between GFP levels and MOIs. Results showed a good correlation between multiplicity of infection and growth kinetics (Figure S4). Comparing the GFP value and number of viral particles per ml using plaque assay checked levels of GFP signal corresponding to different levels of virus. Results (unpublished data) showed a strong correlation between differences in levels of GFP expression and differences in number of viral particles assessed by plaque assay: a drop of 20% of GFP signals corresponding to a log difference in the number of viral particles monitored by plaque assay.

Transfection and siRNA Knock-Down Assays

For transfection, siRNA (SMARTpools-ON-TARGETplus modification) from Thermo Fisher Inc. were purchased. The samples were supplied at a concentration of 5 mM and diluted and aliquoted in 2 µM amounts. To transfect at a final concentration of 20 nM per well, 1 µl of siRNA SMARTpool was used with 9 µl of Optimem (Invitrogen, CA, USA) solution while 0.4 µl of Dharmafect 1 (Dharmacon, Perbio Science, Bonn, Germany) was mixed with 9.6 µl Optimem. Following incubation for 5 min, the siRNA mix was added to the Dharmafect 1 (0.4%) mix and incubated for a further 30 min, after which 1.5×10^4 NIH3T3 cells in 80 µl of DMEM 10% CS medium lacking antibiotics was added to the siRNA:Dharmafect 1 complexes. Growth medium was removed and cells were washed 1× in PBS before 100 µl of the siRNA: Dharmafect 1 liposomes were added. Transfection conditions were optimized by using siGLO RED from Thermo Fisher Scientific (Dharmacon) as an indicator of transfection efficiency and cell viability was assessed as described before. For every gene targeted, the knock-down efficiency was checked by QPCR after 48 h incubation. Each of the three genes targeted (*Hmgcs1*, *Hgmcr*, and *Idi1*) were knocked down by more than 70%, 48 h after transfection (Figure S5). Knock-down efficiency and cell viability were also checked at 5 d post-infection for the mCMV-GFP assay, and showed no alteration of the viability and a knock-down efficiency ≥50% (unpublished data).

Nascent RNA Expression Profiling of TYK2−/− mCMV Infected Macrophages Experiment

BMDM were isolated and grown in the presence of Csf1 derived from L929 cells as described [63] except cells were cultivated in 15 cm diameter tissue culture plates for 7 d before treatment. Incorporation of 4-thiouridine (Sigma) into nascent RNA was undertaken as described [52]. In brief, at 360 min post-infection, 10 ml medium was aspirated from all plates, added to 80 µl 4-Thiouridine, mixed, and immediately returned to the culture dish. After 30 min, to end the RNA labeling period, terminate transcription, and lyse the cells, medium was aspirated from the labeled BMDM and replaced with 4 ml of RLT lysis buffer (Qiagen). Total RNA was isolated using an RNeasy Midi kit (Qiagen) according to the manufacturer's instructions, quantitated using a Nanodrop (Thermo Scientific), and integrity was confirmed using an Agilent Bioanalyser (Agilent UK). Newly transcribed RNA (ntRNA) was then isolated as described in [52] and again quantitated using a Nanodrop.

Processing of ntRNA samples (94 ng) for hybridization to Affymetrix Mouse Gene 1.0 ST arrays was undertaken according to the manufacturer's instructions (Affymetrix). Hybridisation, washing, staining, and scanning of the arrays were also undertaken following standard Affymetrix protocols. For the purposes of presentation, gene expression values for the specific genes of interest from control (mock-infected) BMDM were adjusted to a value of 1. Values for expression in infected cells (white) were then expressed as a number relative to the control.

In Vivo Studies

All animal experiments had approval by the local animal ethics committee (University of Edinburgh, Edinburgh, UK) in accordance with recommendations of the Federation of European Animal Science Association and European legislation. Twelve mice (C57/BL6, Charles River, 12 wk of age) were randomized into two groups of six animals each in two separate experiments. Simvastatin was prepared as described above. The dosages of statins used in the present investigation were chosen according to the literature [30]. At day 1, mice were inoculated i.p. with 2×10^6 PFU per mouse. Animals were sacrificed 4 d post-infection. Spleen, liver, kidney, heart, and lung were harvested and sonicated as a 10% (wt/vol) tissue homogenate, and titers were determined by standard plaque assays, including centrifugal enhancement of infectivity on MEFp53−/−. The dashed line indicates the limit of detection (5×10^2 PFU/g). Horizontal bars indicate the median values.

Statistical Analysis

Normalization, filtering, statistical hypothesis testing for microarray data was carried out within the R Language and Environment for Statistical Computing (www.r-project.org), using packages provided through the Bioconductor repository (www.bioconductor.org). The majority of explorative analyses and visualizations were conducted with Partek (Partek Incorporated, USA) and GeneSpring GX (Agilent). Statistical analyses on other data sources were performed in Microsoft Excel software. For real-time PCR and replication assay, all graphs represent the mean ± SD. An unpaired Student's t test was used for evaluation of statistical significance of real-time PCR. For in vivo experiment a Mann-Whitney U test was used. See Text S1 for statistical analysis of microarray experiments. Statistical significance: $*p<0.05$, $**p<0.01$, $***p<0.001$.

Supporting Information

Figure S1 Pie chart representing the percentage of lipid class present in (A): 62 down-regulated and 133 up-regulated Lipid Associated Genes (LAGs) upon mCMV infection, (B) 51 down-regulated and 65 up-regulated LAGs after IFNγ treatment, and (C) 35 down-regulated and 47 up-regulated LAGs by mCMV infection and IFNγ treatment.
Found at: doi:10.1371/journal.pbio.1000598.s001 (3.83 MB TIF)

Figure S2 Concentrations of four cholesterol synthesis-related metabolites following mCMV infection. (A–D) Concentrations of Zymosterol, 14-demethyl-lanosterol, 7-dehydro-cholesterol, and free cholesterol are measured from lipid extract by MRM analysis (Materials and Methods) from BMDM following mCMV infection (MOI of 1 at 24 and 48 hpi). Bars represent means ± SD of triplicates biological measurements.
Found at: doi:10.1371/journal.pbio.1000598.s002 (0.31 MB TIF)

Figure S3 Lipidomic analysis using high performance liquid chromatography/mass spectrometry and electroscopy ionization of mCMV infected BMDM. Lipid analysis of total glycerophospholipids (phosphatidylcholine, phosphatidylserine, phosphatidylethanolamine; A) and individual species of phosphatidylcholine (B)

and phosphatidylserine (C) (Materials and Methods). Bars represent means ± SD of triplicates biological measurements.
Found at: doi:10.1371/journal.pbio.1000598.s003 (6.02 MB TIF)

Figure S4 Live cell mCMV-GFP growth curve. NIH3T3 were infected at an MOI of 0.01, 0.1, and 1 with mCMV-GFP for 1 h, and viral inoculums were replaced by fresh media. GFP signal was measured at a different time post-infection (Materials and Methods).
Found at: doi:10.1371/journal.pbio.1000598.s004 (0.09 MB TIF)

Figure S5 Knock-down efficiency. NIH3T3 cells were transfected with 0.4% Dharmafect 1 and 25 nm of Hmgcs1, Hmgcr, or Idi1 SiRNA smart pool (Dharmacon). After 48 h, RNA was collected and QPCR was performed to check gene expression for Hmgcs1, Hmgcr, and idi1. Gapdh was used for normalization. Hmgcs1 shows an 81% decrease in expression following transfection, Hmgcr a 70% decrease, and Idi1 an 82% decrease. Bars represent means ± SD of triplicate biological measurements.
Found at: doi:10.1371/journal.pbio.1000598.s005 (1.23 MB TIF)

Figure S6 mCMV infection reduced free intra-cellular cholesterol in a dose-dependent manner in BMDM at 48 hpi. BMDM were infected at different MOI (0, 0.1, 0.2, 0.5, and 1) with mCMV virus. Data are represented as the percentage of free intracellular cholesterol concentration from infected cells in comparison to mock treatment. Results represent means ± SD from two independent experiments with triplicate biological measurements for each experiment.
Found at: doi:10.1371/journal.pbio.1000598.s006 (1.32 MB TIF)

Figure S7 Effects of various concentrations of Simvastatin on NIH-3T3 fibroblasts cell viability. NIH-3T3 fibroblasts were treated with various concentrations of Simvastatin or with vehicle for 72 h. Cell viability was determined using the Cell titre blue assay as described in Methods. Cell viability is expressed as the percentage of fluorescence signal from treated cells compared to untreated cells. Graphs represent the average values (±SD) of two independent experiments with triplicate biological measurements for each experiment.
Found at: doi:10.1371/journal.pbio.1000598.s007 (0.04 MB TIF)

Figure S8
Found at: doi:10.1371/journal.pbio.1000598.s008 Specificity of the SREBP2 antibody. Lane 1 and 2: Nuclear extract protein prepared from livers of mice fed chow supplemented with either a 2% cholesterol diet (CHOL) or a mixture of lovastatin and ezetimibe were loaded as controls. Arrow indicates the specific SREBP2 cleaved form. As a comparison, lanes 3 and 4 show nuclear protein extracts prepared from macrophages cultured from mock or mCMV infected. YY1 protein was used as a loading control. (1.36 MB TIF)

Table S1 List of lipogenic associated genes (LAGs) down- (A) or up- (B) regulated by mCMV infection or down- (C) and up- (D) regulated by IFNγ treatment.
Found at: doi:10.1371/journal.pbio.1000598.s009 (0.09 MB XLS)

Table S2 Canonical pathway analysis. Analysis was performed using IPA from Ingenuity (www.ingenuity.com): (A) 62 down-regulated LAGs in response to mCMV infection, (B) 133 up-regulated LAGs in response to mCMV infection, (C) 51 down-regulated LAGs in response to IFNγ treatment, (D) 65 up-regulated LAGs in response to IFNγ treatment, (E) 35 down-regulated LAGS in response to mCMV infection and IFNγ treatment, and (F) 47 up-regulated LAGs in response to mCMV infection and IFNγ treatment. For each table, the top 5 most significant pathways are represented.
Found at: doi:10.1371/journal.pbio.1000598.s010 (0.02 MB XLS)

Text S1 Supporting methods. This file gives an overview of the methods used in this article.
Found at: doi:10.1371/journal.pbio.1000598.s011 (0.13 MB DOC)

Acknowledgments

We would like to thank Daniel M. Wall and Maire C. O'Sullivan for experimental help, Dr. John McLauchlan and Dr. Amy Buck for advice and helpful comments, and Marie Craigon and Andrew Livingston for technical support.

Author Contributions

The author(s) have made the following declarations about their contributions: Conceived and designed the experiments: MB PG. Performed the experiments: MB WYH KAR GS SRM TO. Analyzed the data: MB WYH KAR SW GS PL MK PD GS TF RR MRW AA PG. Contributed reagents/materials/analysis tools: PP BS MM. Wrote the paper: MB PG.

References

1. Makowski L, Hotamisligil GS (2005) The role of fatty acid binding proteins in metabolic syndrome and atherosclerosis. Curr Opin Lipidol 16: 543–548.
2. Lusis AJ (2000) Atherosclerosis. Nature 407: 233–241.
3. Wood DA, Butler S, Riemersma RA, Thomson M, Oliver MF, et al. (1984) Adipose tissue and platelet fatty acids and coronary heart disease in Scottish men. Lancet 2: 117–121.
4. Riemersma RA, Perkins D, Brown AJ, Brown J (1994) Linoleic acid and coronary artery disease. Am J Clin Nutr 59: 949–950.
5. Castrillo A, Joseph SB, Vaidya SA, Haberland M, Fogelman AM, et al. (2003) Crosstalk between LXR and toll-like receptor signaling mediates bacterial and viral antagonism of cholesterol metabolism. Mol Cell 12: 805–816.
6. Zelcer N, Tontonoz P (2006) Liver X receptors as integrators of metabolic and inflammatory signaling. J Clin Invest 116: 607–614.
7. Ogawa S, Lozach J, Benner C, Pascual G, Tangirala RK, et al. (2005) Molecular determinants of crosstalk between nuclear receptors and toll-like receptors. Cell 122: 707–721.
8. Wang S, Wu D, Lamon-Fava S, Matthan NR, Honda KL, et al. (2009) In vitro fatty acid enrichment of macrophages alters inflammatory response and net cholesterol accumulation. Br J Nutr 102: 497–501.
9. Yvan-Charvet L, Wang N, Tall AR (2010) Role of HDL, ABCA1, and ABCG1 transporters in cholesterol efflux and immune responses. Arterioscler Thromb Vasc Biol 30: 139–143.
10. Bauman DR, Bitmansour AD, McDonald JG, Thompson BM, Liang G, et al. (2009) 25-Hydroxycholesterol secreted by macrophages in response to Toll-like receptor activation suppresses immunoglobulin A production. Proc Natl Acad Sci U S A 106: 16764–16769.
11. Zhu X, Lee JY, Timmins JM, Brown JM, Boudyguina E, et al. (2008) Increased cellular free cholesterol in macrophage-specific Abca1 knock-out mice enhances pro-inflammatory response of macrophages. J Biol Chem 283: 22930–22941.
12. Haas MJ, Mooradian AD (2010) Regulation of high-density lipoprotein by inflammatory cytokines: establishing links between immune dysfunction and cardiovascular disease. Diabetes Metab Res Rev.
13. Maitra U, Parks JS, Li L (2009) An innate immunity signaling process suppresses macrophage ABCA1 expression through IRAK-1-mediated downregulation of retinoic acid receptor alpha and NFATc2. Mol Cell Biol 29: 5989–5997.
14. Gerbod-Giannone MC, Li Y, Holleboom A, Han S, Hsu LC, et al. (2006) TNFalpha induces ABCA1 through NF-kappaB in macrophages and in phagocytes ingesting apoptotic cells. Proc Natl Acad Sci U S A 103: 3112–3117.
15. Eguchi J, Yan QW, Schones DE, Kamal M, Hsu CH, et al. (2008) Interferon regulatory factors are transcriptional regulators of adipogenesis. Cell Metab 7: 86–94.
16. Munger J, Bennett BD, Parikh A, Feng XJ, McArdle J, et al. (2008) Systems-level metabolic flux profiling identifies fatty acid synthesis as a target for antiviral therapy. Nat Biotechnol 26: 1179–1186.
17. Kapadia SB, Barth H, Baumert T, McKeating JA, Chisari FV (2007) Initiation of hepatitis C virus infection is dependent on cholesterol and cooperativity between CD81 and scavenger receptor B type I. J Virol 81: 374–383.

18. Wang C, Gale M, Jr., Keller BC, Huang H, Brown MS, et al. (2005) Identification of FBL2 as a geranylgeranylated cellular protein required for hepatitis C virus RNA replication. Mol Cell 18: 425–434.
19. Ye J, Wang C, Sumpter R, Jr., Brown MS, Goldstein JL, et al. (2003) Disruption of hepatitis C virus RNA replication through inhibition of host protein geranylgeranylation. Proc Natl Acad Sci U S A 100: 15865–15870.
20. Park CY, Jun HJ, Wakita T, Cheong JH, Hwang SB (2009) Hepatitis C virus nonstructural 4B protein modulates sterol regulatory element-binding protein signaling via the AKT pathway. J Biol Chem 284: 9237–9246.
21. Robinzon S, Dafa-Berger A, Dyer MD, Paeper B, Proll SC, et al. (2009) Impaired cholesterol biosynthesis in a neuronal cell line persistently infected with measles virus. J Virol 83: 5495–5504.
22. Zheng YH, Plemenitas A, Fielding CJ, Peterlin BM (2003) Nef increases the synthesis of and transports cholesterol to lipid rafts and HIV-1 progeny virions. Proc Natl Acad Sci U S A 100: 8460–8465.
23. Mackenzie JM, Khromykh AA, Parton RG (2007) Cholesterol manipulation by West Nile virus perturbs the cellular immune response. Cell Host Microbe 2: 229–239.
24. Rothwell C, Lebreton A, Young Ng C, Lim JY, Liu W, et al. (2009) Cholesterol biosynthesis modulation regulates dengue viral replication. Virology 389: 8–19.
25. Mohan KV, Muller J, Atreya CD (2008) Defective rotavirus particle assembly in lovastatin-treated MA104 cells. Arch Virol 153: 2283–2290.
26. Bader T, Fazili J, Madhoun M, Aston C, Hughes D, et al. (2008) Fluvastatin inhibits hepatitis C replication in humans. Am J Gastroenterol 103: 1383–1389.
27. Liu S, Rodriguez AV, Tosteson MT (2006) Role of simvastatin and methyl-beta-cyclodextrin [corrected] on inhibition of poliovirus infection. Biochem Biophys Res Commun 347: 51–59.
28. Cohen JI (2005) HMG CoA reductase inhibitors (statins) to treat Epstein-Barr virus-driven lymphoma. Br J Cancer 92: 1593–1598.
29. del Real G, Jimenez-Baranda S, Mira E, Lacalle RA, Lucas P, et al. (2004) Statins inhibit HIV-1 infection by down-regulating Rho activity. J Exp Med 200: 541–547.
30. Gower TL, Graham BS (2001) Antiviral activity of lovastatin against respiratory syncytial virus in vivo and in vitro. Antimicrob Agents Chemother 45: 1231–1237.
31. Potena L, Frascaroli G, Grigioni F, Lazzarotto T, Magnani G, et al. (2004) Hydroxymethyl-glutaryl coenzyme a reductase inhibition limits cytomegalovirus infection in human endothelial cells. Circulation 109: 532–536.
32. Owens CM, Mawhinney C, Grenier JM, Altmeyer R, Lee MS, et al. Chemical combinations elucidate pathway interactions and regulation relevant to Hepatitis C replication. Mol Syst Biol 6: 375.
33. Hong C, Tontonoz P (2008) Coordination of inflammation and metabolism by PPAR and LXR nuclear receptors. Curr Opin Genet Dev 18: 461–467.
34. Hansson GK (2005) Inflammation, atherosclerosis, and coronary artery disease. N Engl J Med 352: 1685–1695.
35. Chawla A, Boisvert WA, Lee CH, Laffitte BA, Barak Y, et al. (2001) A PPAR gamma-LXR-ABCA1 pathway in macrophages is involved in cholesterol efflux and atherogenesis. Mol Cell 7: 161–171.
36. Diamond DL, Syder AJ, Jacobs JM, Sorensen CM, Walters KA, et al. Temporal proteome and lipidome profiles reveal hepatitis C virus-associated reprogramming of hepatocellular metabolism and bioenergetics. PLoS Pathog 6: e1000719. doi:10.1371/journal.ppat.1000719.
37. Joseph SB, Bradley MN, Castrillo A, Bruhn KW, Mak PA, et al. (2004) LXR-dependent gene expression is important for macrophage survival and the innate immune response. Cell 119: 299–309.
38. Wang X, Hinson ER, Cresswell P (2007) The interferon-inducible protein viperin inhibits influenza virus release by perturbing lipid rafts. Cell Host Microbe 2: 96–105.
39. Hinson ER, Cresswell P (2009) The antiviral protein, viperin, localizes to lipid droplets via its N-terminal amphipathic alpha-helix. Proc Natl Acad Sci U S A 106: 20452–20457.
40. Ghazal P, Gonzalez Armas JC, Garcia-Ramirez JJ, Kurz S, Angulo A (2000) Viruses: hostages to the cell. Virology 275: 233–237.
41. Fruh K, Simmen K, Luukkonen BG, Bell YC, Ghazal P (2001) Virogenomics: a novel approach to antiviral drug discovery. Drug Discov Today 6: 621–627.
42. Wenk MR (2006) Lipidomics of host-pathogen interactions. FEBS Lett 580: 5541–5551.
43. Reddehase MJ, Podlech J, Grzimek NK (2002) Mouse models of cytomegalovirus latency: overview. J Clin Virol 25(Suppl 2): S23–S36.
44. Brautigam AR, Dutko FJ, Olding LB, Oldstone MB (1979) Pathogenesis of murine cytomegalovirus infection: the macrophage as a permissive cell for cytomegalovirus infection, replication and latency. J Gen Virol 44: 349–359.
45. Selgrade MK, Osborn JE (1974) Role of macrophages in resistance to murine cytomegalovirus. Infect Immun 10: 1383–1390.
46. Davies P (1976) Essential role of macrophages in chronic inflammatory processes. Schweiz Med Wochenschr 106: 1351–1354.
47. Valyi-Nagy T, Bandi Z, Boldogh I, Albrecht T (1988) Hydrolysis of inositol lipids: an early signal of human cytomegalovirus infection. Arch Virol 101: 199–207.
48. Ishida F, Sato A, Iizuka Y, Kamei T (1989) Inhibition of acyl coenzyme A: cholesterol acyltransferase by 3-hydroxy-3-methylglutaryl coenzyme A reductase inhibitors. Chem Pharm Bull (Tokyo) 37: 1635–1636.
49. Goldstein JL, Brown MS (1990) Regulation of the mevalonate pathway. Nature 343: 425–430.
50. Ghazal P, Messerle M, Osborn K, Angulo A (2003) An essential role of the enhancer for murine cytomegalovirus in vivo growth and pathogenesis. J Virol 77: 3217–3228.
51. Strobl B, Bubic I, Bruns U, Steinborn R, Lajko R, et al. (2005) Novel functions of tyrosine kinase 2 in the antiviral defense against murine cytomegalovirus. J Immunol 175: 4000–4008.
52. Dolken L, Ruzsics Z, Radle B, Friedel CC, Zimmer R, et al. (2008) High-resolution gene expression profiling for simultaneous kinetic parameter analysis of RNA synthesis and decay. RNA 14: 1959–1972.
53. Brown MS, Goldstein JL (1997) The SREBP pathway: regulation of cholesterol metabolism by proteolysis of a membrane-bound transcription factor. Cell 89: 331–340.
54. Tabeta K, Georgel P, Janssen E, Du X, Hoebe K, et al. (2004) Toll-like receptors 9 and 3 as essential components of innate immune defense against mouse cytomegalovirus infection. Proc Natl Acad Sci U S A 101: 3516–3521.
55. Compton T, Kurt-Jones EA, Boehme KW, Belko J, Latz E, et al. (2003) Human cytomegalovirus activates inflammatory cytokine responses via CD14 and Toll-like receptor 2. J Virol 77: 4588–4596.
56. Jiang D, Weidner JM, Qing M, Pan XB, Guo H, et al. Identification of five interferon-induced cellular proteins that inhibit west nile virus and dengue virus infections. J Virol 84: 8332–8341.
57. Kapadia SB, Chisari FV (2005) Hepatitis C virus RNA replication is regulated by host geranylgeranylation and fatty acids. Proc Natl Acad Sci U S A 102: 2561–2566.
58. Neuhaus O, Stuve O, Archelos JJ, Hartung HP (2005) Putative mechanisms of action of statins in multiple sclerosis–comparison to interferon-beta and glatiramer acetate. J Neurol Sci 233: 173–177.
59. Dixon RM, Borden EC, Keim NL, Anderson S, Spennetta TL, et al. (1984) Decreases in serum high-density-lipoprotein cholesterol and total cholesterol resulting from naturally produced and recombinant DNA-derived leukocyte interferons. Metabolism 33: 400–404.
60. Morra VB, Coppola G, Orefice G, De Michele G, Vacca G, et al. (2004) Interferon-beta treatment decreases cholesterol plasma levels in multiple sclerosis patients. Neurology 62: 829–830.
61. Irizarry RA, Hobbs B, Collin F, Beazer-Barclay YD, Antonellis KJ, et al. (2003) Exploration, normalization, and summaries of high density oligonucleotide array probe level data. Biostatistics 4: 249–264.
62. Irizarry RA, Bolstad BM, Collin F, Cope LM, Hobbs B, et al. (2003) Summaries of Affymetrix GeneChip probe level data. Nucleic Acids Res 31: e15.
63. Martinat C, Mena I, Brahic M (2002) Theiler's virus infection of primary cultures of bone marrow-derived monocytes/macrophages. J Virol 76: 12823–12833.
64. Wagner M, Jonjic S, Koszinowski UH, Messerle M (1999) Systematic excision of vector sequences from the BAC-cloned herpes virus genome during virus reconstitution. J Virol 73: 7056–7060.
65. Ghazal P, Visser AE, Gustems M, Garcia R, Borst EM, et al. (2005) Elimination of ie1 significantly attenuates murine cytomegalovirus virulence but does not alter replicative capacity in cell culture. J Virol 79: 7182–7194.
66. Livak KJ, Schmittgen TD (2001) Analysis of relative gene expression data using real-time quantitative PCR and the 2(-Delta Delta C(T)) method. Methods 25: 402–408.
67. Jeon TI, Zhu B, Larson JL, Osborne TF (2008) SREBP-2 regulates gut peptide secretion through intestinal bitter taste receptor signaling in mice. J Clin Invest 118: 3693–3700.
68. Fei W, Shui G, Gaeta B, Du X, Kuerschner L, et al. (2008) Fld1p, a functional homologue of human seipin, regulates the size of lipid droplets in yeast. J Cell Biol 180: 473–482.
69. Huang Q, Shen HM, Shui G, Wenk MR, Ong CN (2006) Emodin inhibits tumor cell adhesion through disruption of the membrane lipid Raft-associated integrin signaling pathway. Cancer Res 66: 5807–5815.

Biochemical Pharmacology 86 (2013) 56–66

Contents lists available at SciVerse ScienceDirect

Biochemical Pharmacology

journal homepage: www.elsevier.com/locate/biochempharm

A comprehensive machine-readable view of the mammalian cholesterol biosynthesis pathway

Alexander Mazein [a,b,**,1], Steven Watterson [a,b,1], Wei-Yuan Hsieh [a], William J. Griffiths [c], Peter Ghazal [a,b,*]

[a] Division of Pathway Medicine, University of Edinburgh, Chancellor's Building, Little France Crescent, Edinburgh EH16 4SB, Scotland, UK
[b] Centre for Synthetic and Systems Biology, University of Edinburgh, CH Waddington Building, The King's Buildings, Mayfield Road, Edinburgh EH9 3JD, Scotland, UK
[c] Institute of Mass Spectrometry, College of Medicine, Grove Building, Swansea University, Singleton Park, Swansea SA2 8PP, Wales, UK

ARTICLE INFO

Article history:
Received 29 January 2013
Accepted 26 March 2013
Available online 10 April 2013

Keywords:
Cholesterol
Sterol
SBGN
Metabolic network
Pathway map

ABSTRACT

Cholesterol biosynthesis serves as a central metabolic hub for numerous biological processes in health and disease. A detailed, integrative single-view description of how the cholesterol pathway is structured and how it interacts with other pathway systems is lacking in the existing literature. Here we provide a systematic review of the existing literature and present a detailed pathway diagram that describes the cholesterol biosynthesis pathway (the mevalonate, the Kandutch-Russell and the Bloch pathway) and shunt pathway that leads to 24(S),25-epoxycholesterol synthesis. The diagram has been produced using the Systems Biology Graphical Notation (SBGN) and is available in the SBGN-ML format, a human readable and machine semantically parsable open community file format.

© 2013 Elsevier Inc. All rights reserved.

1. Introduction

Cholesterol is an intensively studied, multi-functional lipid that is key to many aspects of immunological, neuronal, viral and hepatocyte biology. It is an essential component of cellular membranes and is a precursor to steroids, bile acids and oxysterols whilst its own precursors contribute to prenylation and dolichylation and the formation of vitamin D_3. One of the oxysterols known to be involved in linking sterol metabolism to innate immunity [1,2] is 25-hydroxycholesterol. However its place in the sterol metabolism has not yet been well established.

Despite the importance of the cholesterol synthesis pathway to cellular function and its value in pharmaceutical therapies, an integrative picture of how the pathway is structured has not been well described in the literature, impeding the development of a more rigorous understanding of the role of the cholesterol metabolism in cellular processes. Publications typically focus on segments of the cholesterol biosynthesis pathway showing variable level of details. Kovacs and co-authors focus on the mevalonate section of the pathway and on the subcellular location of the enzymes involved [3]. Wang and co-authors concentrate on the steps leading to 24(S),25-epoxycholesterol synthesis and their similarity to steps in the cholesterol biosynthesis pathway [4]. Previous work studying the role of the cholesterol biosynthesis pathway has shown a modest level of detail on the sterol arms of the pathway [5–7] in innate immunity. The LIPID MAPS consortium offers the most detailed descriptions of the Bloch and Kandutsch-Russell branches of cholesterol biosynthesis, but these lack cell compartment information and lack integration with the 24(S),25-epoxycholesterol shunt arm and other branching pathways [8].

Here we present a comprehensive literature review of the cholesterol synthesis pathway and we implement this as a detailed pathway that captures enzymatic activity and compartmental localization and summarizes all intermediate metabolic forms. Our review also clearly indicates what information is missing and where additional research is required.

2. Materials and methods

The model of the cholesterol biosynthesis pathway presented in this work has been assembled using a variety of publicly available resources including the research findings of the LipidMaps

* Corresponding author at: Division of Pathway Medicine, University of Edinburgh, Chancellor's Building, Little France Crescent, Edinburgh EH16 4SB, Scotland, UK. Tel.: +44 131 242 6288; fax: +44 131 242 6244.
** Corresponding author. Current address: Biological Systems Unit, Okinawa Institute of Science and Technology, 1919-1 Tancha, Onna-son, Kunigami-gun, Okinawa 904-0495, Japan.
E-mail addresses: a.mazein@oist.jp (A. Mazein), p.ghazal@ed.ac.uk (P. Ghazal).
[1] Joint first authors.

0006-2952/$ – see front matter © 2013 Elsevier Inc. All rights reserved.
http://dx.doi.org/10.1016/j.bcp.2013.03.021

consortium [8] and results obtained from thorough searches of the published literature that have been manually curated and validated by domain experts.

In cases where there were conflicting reports, preference was given to the more recent papers and to the works in which more reliable and advanced methods were used. The suggested order of events is supported by a number of independently obtained research results. The principles of the Evidence Ontology (ECO) [9], the Gene Ontology Evidence Codes [10] and the Evidence Code Decision Tree [11] were considered during the pathway reconstruction.

A brief summary is provided for each enzyme and the corresponding metabolic reactions involved in the pathway. For each enzyme we endeavored to capture the following information where available: corresponding gene name approved by HUGO Gene Nomenclature Committee [12], alternative names, enzymological activities according to the Enzyme Nomenclature Committee of the IUBMB [13], enzyme function description, subunit structure, subcellular location and related disorders.

We have included a list of UniProt IDs for the proteins captured in the model (Table 1) and a list of metabolite names (common and systematic) as used in the LipidMaps database [8] (Table 2). Common names are used on the map where available.

The pathway that we present here is described using the Systems Biology Graphical Notation (SBGN) [14], a community driven consensus graphical schema for capturing the molecular details of pathway systems. In particular, we use the SBGN Process Description language [15]. A machine-readable model is available as part of the supplementary material in SBGN-ML format [16] and we present it graphically in Figs. 1–3, in an enhanced form. The SBGN-ML format files can be read using a variety of software packages.

In particular, the supplementary files provide a description of the pathway that can be edited and modified in accordance with the SBGN standard in order to be of future use to the research community. The SBGN-ML file format encodes the biological meaning associated with each component of the model. This allows the model to be parsed by software (i) to ensure that modification is biologically valid and (ii) to facilitate automatic generation of mathematical descriptions of the pathway biology. It should be possible to open these files in any software designed to comply with the SBGN-ML standard, including but not limited to VANTED and Cytoscape [17,18]. For the purpose of this review, we compiled and tested the files using the VANTED software tool [17]. Here we shall outline how the files can be opened and accessed using the VANTED and CYTOSCAPE [18] software tools.

2.1. Accessing supplementary SBGN-ML files using the VANTED software tool

2.1.1 Download the files with '.sbgn' file extension from the supplementary material.
2.1.2 Download and install VANTED from http://vanted.ipk-gatersleben.de/.
2.1.3 Open VANTED and you will be greeted by a screen divided into two regions: an empty area on the left for diagrams and a column on the right containing settings under various tabs.
2.1.4 Using the automated installer to obtain the SBGN-ML add-on.
2.1.4.1 In the right hand column select the 'Help' tab and then the 'Settings' tab beneath and click on the 'Install/Configure Add-ons' button. This will open the Add-on Manager.
2.1.4.2 Click on the 'Find Add-ons/Updates' button on the bottom of the Add-on Manager window. This, in turn, opens the 'Direct Add-on Download' window.
2.1.4.3 At the top right of the Add-ons window, left and right arrows allow the user to move through a list of the available Add-ons. Find the Add-on entitled, 'SBGN-ED' and click the corresponding 'Install Add-on' button. VANTED will now automatically download the SBGN extension.
2.1.4.4 Click 'OK' and you will return to the 'Add-on Manager' where 'SBGN-ED' will now be listed as an Add-on. Ensure that the Active button is ticked beside the SBGN-ED entry to the list.
2.1.4.5 Click 'OK' on the 'Add-on Manager'. The software is now installed.
2.1.4.6 From the menus at on the top of the VANTED window, select File>Open and choose your downloaded file with the '.sbgn' file extension, in the usual way.
2.1.5 Manual installing the SBGN-ML add-on
2.1.5.1 *From* http://vanted.ipk-gatersleben.de/ Select Add-ons and then 'SBGN-ED – Editing, Translating and Validating of SBGN Maps'.
2.1.5.2 Select 'Download & Installation' and then 'SBGN-ED' under downloads. A file called sbgn-ed.jar should start to download.
2.1.5.3 Return to Vanted and in the right hand column select the 'Help' tab and then the 'Settings' tab beneath. Click on the 'Install/Configure Add-ons' button. This will open the Add-on Manager.
2.1.5.4 Click the 'Install Add-on' button and select the sbgn-ed.jar file downloaded previously. Click the 'Install' button. This will return you to the 'Add-on Manager'.
2.1.5.5 A message will appear the top of the Add-on Manager window stating that 'Add-on ''sbgn-ed.jar'' will be updated when application is restarted'. Select OK and quit the program, before relaunching it.
2.1.5.6 From the menus at on the top of the VANTED window, select File>Open and choose your downloaded file with the '.sbgn' file extension, in the usual way.

2.2. Accessing supplementary SBGN-ML files using the Cytoscape software tool

2.2.1 Download and install Cytoscape from http://www.cytoscape.org/.
2.2.2 Open Cytoscape and select the Plugins menu followed by 'Manage Plugins'.
2.2.3 In the search bar, type sbgn and hit return. Folders will appear in the window and under 'Available for install' will appear a Utility folder.
2.2.4 Open the utility folder and select the latest version of CySBGN before hitting the install button. The CySBGN plugin will then be downloaded and installed. Once it is installed, close the 'Manage Plugins' window.
2.2.5 From the File menu select import followed by 'Network (Multiple File Types)'. In the window that opens, make sure that the 'Local' option is chosen and high the 'Select' button to bring up a file selector. Choose the downloaded file with the 'sbgn' file extension in the usual way.

3. Results and discussion

3.1. Pathway maps

Fig. 1 shows the mevalonate arm of the cholesterol biosynthesis pathway and includes enzymatic activity in the mitochondria, peroxisome, cytoplasm and endoplasmic reticulum. The arm starts with the consumption of acetyl-CoA, which occurs in parallel in three cell compartments (the mitochondria, cytoplasm and peroxisome) and terminates with the production of squalene in

Table 1
Uniprot IDs for the enzymes in the pathways shown in Figs. 1 and 2.

Uniprot ID	Link	EC	Order	Gene name	Protein name	Related disease	Reference
P24752	http://www.uniprot.org/uniprot/P24752	2.3.1.9	1	ACAT1	Acetyl-CoA acetyltransferase, mitochondrial; THIL	Alpha-methylacetoacetic aciduria	OMIM #203750
Q9BWD1	http://www.uniprot.org/uniprot/Q9BWD1	2.3.1.9	1	ACAT2	Acetyl-CoA acetyltransferase, cytosolic	ACAT2 deficiency	OMIM #614055
Q01581	http://www.uniprot.org/uniprot/Q01581	2.3.3.10	2	HMGCS1	Hydroxymethylglutaryl-CoA synthase, cytoplasmic	Not found	OMIM #142940
P54868	http://www.uniprot.org/uniprot/P54868	2.3.3.10	2	HMGCS2	Hydroxymethylglutaryl-CoA synthase, mitochondrial	HMG-CoA synthase deficiency	OMIM #605911; PMID 16601895
P35914	http://www.uniprot.org/uniprot/P35914	4.1.3.4	3	HMGCL	Hydroxymethylglutaryl-CoA lyase, mitochondrial	HMG-CoA lyase deficiency	OMIM #246450; PMID 17692550
P04035	http://www.uniprot.org/uniprot/P04035	1.1.1.34	4	HMGCR	3-Hydroxy-3-methylglutaryl-coenzyme A reductase	Not found	OMIM #142910
Q03426	http://www.uniprot.org/uniprot/Q03426	2.7.1.36	5	MVK	Mevalonate kinase	Mevalonic aciduria	OMIM #610377; PMID 16722536
Q15126	http://www.uniprot.org/uniprot/Q15126	2.7.4.2	6	PMVK	Phosphomevalonate kinase	Not found	OMIM #607622
P53602	http://www.uniprot.org/uniprot/P53602	4.1.1.33	7	MVD	Mevalonate diphosphate decarboxylase	Not found	OMIM #603236
Q13907	http://www.uniprot.org/uniprot/Q13907	5.3.3.2	8	IDI1	Isopentenyl-diphosphate delta-isomerase 1	Not found	OMIM #604055
Q9BXS1	http://www.uniprot.org/uniprot/Q9BXS1	5.3.3.2	8	IDI2	Isopentenyl-diphosphate delta-isomerase 2	Not found	Not found
P14324	http://www.uniprot.org/uniprot/P14324	2.5.1.10; 2.5.1.1	9	FDPS	Farnesyl diphosphate synthase; dimethylallyltranstransferase	Not found	Not found
O95749	http://www.uniprot.org/uniprot/O95749	2.5.1.29; 2.5.1.10; 2.5.1.1	10	GGPS1	Geranylgeranyl pyrophosphate synthase; farnesyl diphosphate synthase; dimethylallyltranstransferase	Not found	Not found
P37268	http://www.uniprot.org/uniprot/P37268	2.5.1.21	11	FDFT1	Farnesyl-diphosphate farnesyltransferase 1; squalene synthase	Not found	OMIM #184420
Q14534	http://www.uniprot.org/uniprot/Q14534	1.14.13.132	12	SQLE	Squalene monooxygenase; squalene epoxidase	Not found	OMIM #602019
P48449	http://www.uniprot.org/uniprot/P48449	5.4.99.7	13	LSS	Lanosterol synthase	Not found	OMIM #600909
Q15392	http://www.uniprot.org/uniprot/Q15392	1.3.1.72	14	DHCR24	Delta(24)-sterol reductase; 24-dehydrocholesterol reductase	Desmosterolosis	OMIM #602398; PMID 21559050
Q16850	http://www.uniprot.org/uniprot/Q16850	1.14.13.70	15	CYP51A1	Lanosterol 14-alpha demethylase; cytochrome P450, family 51, subfamily A, polypeptide 1	Not found	OMIM #601637
O76062	http://www.uniprot.org/uniprot/O76062	1.3.1.70	16	TM7SF2	Delta(14)-sterol reductase; transmembrane 7 superfamily member 2	Not found	OMIM #603414
Q15800	http://www.uniprot.org/uniprot/Q15800	1.14.13.72	17	MSMO1; SC4MOL	Methylsterol monooxygenase 1	Psoriasiform dermatitis; microcephaly; developmental delay	PMID 21285510
Q15738	http://www.uniprot.org/uniprot/Q15738	1.1.1.170	18	NSDHL	Sterol-4-alpha-carboxylate 3-dehydrogenase, decarboxylating; NAD(P) dependent steroid dehydrogenase-like	CK syndrome; CHILD syndrome	OMIM #300831; PMID 21129721; OMIM #308050
P56937	http://www.uniprot.org/uniprot/P56937	1.1.1.270	19	HSD17B7	3-Keto-steroid reductase; 17-beta-hydroxysteroid dehydrogenase 7	Not found	OMIM #606756
Q15125	http://www.uniprot.org/uniprot/Q15125	5.3.3.5	20	EBP	3-Beta-hydroxysteroid-delta(8), Delta(7)-isomerase; emopamil-binding protein	Conradi-Hünermann-Happle syndrome	OMIM #302960; PMID 21163155; PMID 22229330
O75845	http://www.uniprot.org/uniprot/O75845	1.14.21.6	21	SC5DL	Lathosterol oxidase; sterol-C5-desaturase (ERG3 delta-5-desaturase homolog, S. cerevisiae)-like	Lathosterolosis	OMIM #607330; PMID 12189593
Q9UBM7	http://www.uniprot.org/uniprot/Q9UBM7	1.3.1.21	22	DHCR7	7-Dehydrocholesterol reductase	Smith-Lemli-Opitz syndrome (SLOS)	OMIM #270400; PMID 23059950; PMID 23042628
P08684	http://www.uniprot.org/uniprot/P08684	1.14.13.97	23	CYP3A4	Cytochrome P450 3A4	Not found	OMIM #124010
O95992	http://www.uniprot.org/uniprot/O95992	1.14.99.38	24	CH25H	Cholesterol 25-hydroxylase	Alzheimer's disease	OMIM #604551; PMID 20580938; PMID 16909003
P22680	http://www.uniprot.org/uniprot/P22680	1.14.13.17	25	CYP7A1	Cholesterol 7-alpha-monooxygenase	Not found	OMIM #118455
Q02318	http://www.uniprot.org/uniprot/Q02318	1.14.13.15	26	CYP27A1	Sterol 26-hydroxylase, mitochondrial	Cerebrotendinous xanthomatosis	OMIM #606530; PMID 2019602; PMID 8514861
Q9Y6A2	http://www.uniprot.org/uniprot/Q9Y6A2	1.14.13.98	27	CYP46A1	Cholesterol 24-hydroxylase	Alzheimer's disease	OMIM #604087; PMID 12533085; PMID 12533083

Table 2
Systematics names, common names (where available) and LipidMaps IDs for the metabolites shown in Figs. 1 and 2.

Pathway	LM_ID	Common Name	Systematic Name
Lanosterol biosynthesis	LMFA07050029	Acetyl-CoA	Acetyl-CoA
Lanosterol biosynthesis	LMFA07050030	Acetoacetyl-CoA	Acetoacetyl-CoA
Lanosterol biosynthesis	LMFA07050028	HMG-CoA	3S-Hydroxy-3-methyl-glutaryl CoA
Lanosterol biosynthesis	LMFA01050352	Mevalonic acid	3R-Methyl-3,5-dihydroxy-pentanoic acid
Lanosterol biosynthesis	LMFA01050415	Mevalonate-P	3R-Methyl-3-hydroxypentanoic acid 5-phosphate
Lanosterol biosynthesis	LMFA01050416	Mevalonate-PP	3R-Methyl-3-hydroxypentanoic acid 5-diphosphate
Lanosterol biosynthesis	LMPR01010008	Isopentenyl-diphosphate	3-Methylbut-3-enyl pyrophosphate
Lanosterol biosynthesis	LMPR01010001	Dimethylallyl-diphosphate	3-Methylbut-2-enyl pyrophosphate (dimethylallyl-diphosphate)
Lanosterol biosynthesis	LMPR0102010001	Geranyl diphosphate	Geranyl pyrophosphate
Lanosterol biosynthesis	LMPR0103010002	Farnesyl diphosphate	Farnesyl pyrophosphate
Lanosterol biosynthesis	LMPR0106010003	Presqualene diphosphate	Presqualene diphosphate
Lanosterol biosynthesis	LMPR0106010002	Squalene	Squalene
Lanosterol biosynthesis	LMPR0106010010	3S-Squalene-2,3-epoxide	2,3S-Epoxy-2,6,10,15,19,23-hexamethyltetracosa-6E,10E,14E,18E,22-pentaene
Lanosterol biosynthesis	LMST01010017	Lanosterol	Lanosta-8,24-dien-3β-ol
Cholesterol biosynthesis (Bloch)	LMST01010124	32-Hydroxylanosterol	4,4-Dimethyl-14α-hydroxymethyl-5α-cholesta-8,24-dien-3β-ol
Cholesterol biosynthesis (Bloch)	LMST01010222	32-oxolanosterol	4,4-Dimethyl-14α-formyl-5α-cholesta-8,24-dien-3β-ol
Cholesterol biosynthesis (Bloch)	LMST01010149	4,4-dimethylcholesta-8,11,24-trienol	4,4-Dimethyl-5α-cholesta-8,14,24-trien-3β-ol
Cholesterol biosynthesis (Bloch)	LMST01010176	14-demethyllanosterol	4,4-Dimethyl-5α-cholesta-8,24-dien-3β-ol
Cholesterol biosynthesis (Bloch)	LMST01010232	not available	4α-Hydroxymethyl-4β-methyl-5α-cholesta-8,24-dien-3β-ol
Cholesterol biosynthesis (Bloch)	LMST01010229	not available	4α-Formyl-4β-methyl-5α-cholesta-8,24-dien-3β-ol
Cholesterol biosynthesis (Bloch)	LMST01010150	4α-carboxy-4β-methyl-zymosterol	4α-Carboxy-4β-methyl-cholesta-8,24-dien-3β-ol
Cholesterol biosynthesis (Bloch)	LMST01010237	3-Keto-4α-methyl-zymosterol	4α-Methyl-5α-cholesta-8,24-dien-3-one
Cholesterol biosynthesis (Bloch)	LMST01010151	4α-Methyl-zymosterol	4α-Methyl-5α-cholesta-8,24-dien-3β-ol
Cholesterol biosynthesis (Bloch)	LMST01010234	Not available	4α-Hydroxymethyl-5α-cholesta-8,24-dien-3β-ol
Cholesterol biosynthesis (Bloch)	LMST01010226	Not available	4α-Formyl-5α-cholesta-8,24-dien-3β-ol
Cholesterol biosynthesis (Bloch)	LMST01010152	4α-Carboxy-zymosterol	4α-Carboxy-5α-cholesta-8,24-dien-3β-ol
Cholesterol biosynthesis (Bloch)	LMST01010168	Zymosterone	5α-Cholesta-8,24-dien-3-one
Cholesterol biosynthesis (Bloch)	LMST01010066	Zymosterol	5α-Cholesta-8,24-dien-3β-ol
Cholesterol biosynthesis (Bloch)	LMST01010206	5α-Cholesta-7,24-dien-3β-ol	5α-Cholesta-7,24-dien-3β-ol
Cholesterol biosynthesis (Bloch)	LMST01010121	7-Dehydro-desmosterol	Cholest-5,7,24-trien-3β-ol
Cholesterol biosynthesis (Bloch)	LMST01010016	Desmosterol	Cholest-5,24-dien-3β-ol
Cholesterol biosynthesis (Kandustch-Russell)	LMST01010087	24,25-Dihydrolanosterol	5α-Lanost-8-en-3β-ol
Cholesterol biosynthesis (Kandustch-Russell)	LMST01010224	Not available	4,4-Dimethyl-14α-hydroxymethyl-5α-cholest-8-en-3β-ol
Cholesterol biosynthesis (Kandustch-Russell)	LMST01010223	Not available	4,4-Dimethyl-14α-formyl-5α-cholest-8-en-3β-ol
Cholesterol biosynthesis (Kandustch-Russell)	LMST01010277	Not available	4,4-Dimethyl-5α-cholesta-8,14-dien-3β-ol
Cholesterol biosynthesis (Kandustch-Russell)	LMST01010225	Not available	4,4-Dimethyl-5α-cholest-8-en-3β-ol
Cholesterol biosynthesis (Kandustch-Russell)	LMST01010233	Not available	4α-Hydroxymethyl-4β-methyl-5α-cholest-8-en-3β-ol
Cholesterol biosynthesis (Kandustch-Russell)	LMST01010230	Not available	4α-Formyl-4β-methyl-5α-cholest-8-en-3β-ol
Cholesterol biosynthesis (Kandustch-Russell)	LMST01010227	Not available	4α-Carboxy-4β-methyl-5α-cholest-8-en-3β-ol
Cholesterol biosynthesis (Kandustch-Russell)	LMST01010236	Not available	4α-Methyl-5α-cholest-8-en-3-one
Cholesterol biosynthesis (Kandustch-Russell)	LMST01010197	4α-Methylcholest-8-en-3β-ol	4α-Methyl-5α-cholest-8-en-3β-ol
Cholesterol biosynthesis (Kandustch-Russell)	LMST01010235	Not available	4α-Hydroxymethyl-5α-cholest-8-en-3β-ol
Cholesterol biosynthesis (Kandustch-Russell)	LMST01010231	Not available	4α-Formyl-5α-cholest-8-en-3β-ol
Cholesterol biosynthesis (Kandustch-Russell)	LMST01010228	Not available	4α-Carboxy-5α-cholest-8-en-3β-ol
Cholesterol biosynthesis (Kandustch-Russell)	LMST01010239	Not available	5α-Cholest-8-en-3-one
Cholesterol biosynthesis (Kandustch-Russell)	LMST01010096	Zymostenol	5α-Cholest-8-en-3β-ol
Cholesterol biosynthesis (Kandustch-Russell)	LMST01010089	Lathosterol	Cholest-7-en-3β-ol
Cholesterol biosynthesis (Kandustch-Russell)	LMST01010069	7-Dehydrocholesterol	Cholesta-5,7-dien-3β-ol
Cholesterol biosynthesis (Kandustch-Russell)	LMST01010001	Cholesterol	Cholest-5-en-3β-ol
Cholesterol biosynthesis (Kandustch-Russell/Bloch)	LMST01010018	25-Hydroxy-cholesterol	Cholest-5-en-3β,25-diol
Cholesterol biosynthesis (Kandustch-Russell/Bloch)	LMST01010014	4β-Hydroxy-cholesterol	Cholest-5-en-3β,4β-diol
Cholesterol biosynthesis (Kandustch-Russell/Bloch)	LMST01010013	7α-Hydroxy-cholesterol	Cholest-5-en-3β,7α-diol
Cholesterol biosynthesis (Kandustch-Russell/Bloch)	LMST01010057	27-Hydroxy-cholesterol	Cholest-5-en-3β,26-diol
Cholesterol biosynthesis (Kandustch-Russell/Bloch)	LMST01010164	24-Hydroxy-cholesterol	Cholest-5-en-3β,24-diol

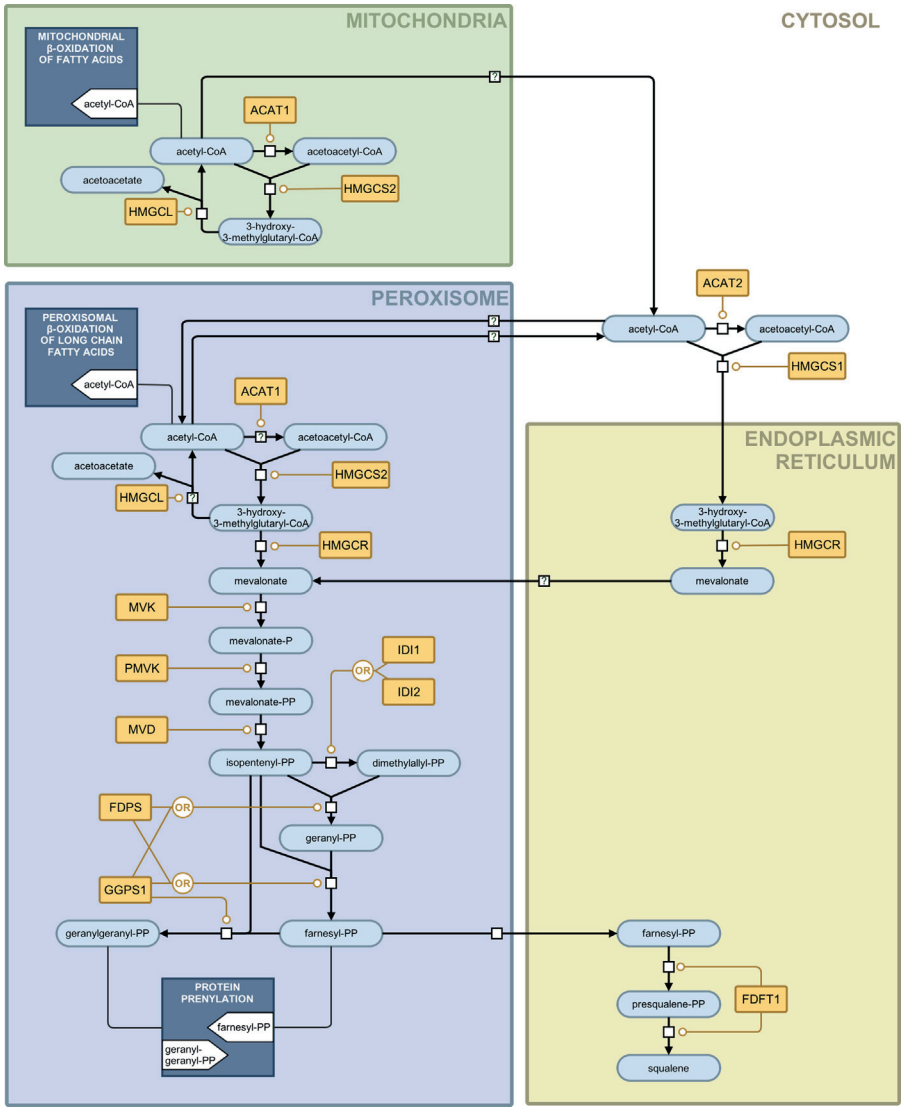

Fig. 1. The mevalonate arm of the cholesterol biosynthesis pathway presented in SBGN notation. An interactive, parsable version of this figure, encoded using the SBGN-ML file format, is available in the supplementary material. The various glyph are explained in the legend in Fig. 3.

the endoplasmic reticulum. Fig. 2 shows the sterol arms of the cholesterol biosynthesis pathway and this includes the Bloch pathway, the Kandutsch-Russell pathway and the shunt pathway. This arm starts with Squalene and terminates with cholesterol production on the Bloch and Kandutsch-Russell pathways and with 24(S),25-epoxycholesterol on the shunt pathway. Fig. 3 provides a legend for the SBGN schema, explaining the various nodes and edges.

3.2. Mevalonate arm of the cholesterol biosynthesis pathway

3.2.1. Acetyl-CoA acetyltransferase (ACAT1; ACAT2; Acetoacetyl-CoA thiolase; EC 2.3.1.9) is an enzyme that catalyzes the reversible condensation of two molecules of acetyl-CoA and forms acetoacetyl-CoA. This reaction is an important step in ketone body formation. Both mitochondrial ACAT1 and cytosolic ACAT2 enzymes are homotetramers [19,20]. Kovacs et al. suggest a possibility of distribution of ACAT1 between peroxisomes and mitochondria as experimental evidence supports the formation of acetoacetyl-CoA in peroxisomes [3]. The proposed step in peroxisomes is shown in Fig. 1 by a reaction glyph with a question mark. Mutations of the ACAT1 gene cause alpha-methylacetoacetic aciduria, an autosomal recessive disorder [21].

3.2.2. Hydroxymethylglutaryl-CoA synthase (HMGCS1; HMGCS2; EC 2.3.3.10) forms HMG-CoA from acetyl-CoA and acetoacetyl-CoA. The two proteins with this enzymological activity are HMGCS1 and HMGCS2 (Table 1). HMGCS1 is a cytoplasmic enzyme and HMGCS2 is localized to mitochondria and peroxisome [3]. Ortiz and co-authors provide evidence for the involvement of HMGCS2 in producing cholesterol-convertible HMG-CoA [22]. Peroxisomal localization of this enzyme was subsequently confirmed and the significance of the peroxisomal pathway in cholesterol production was demonstrated [39,40]. The schema proposed by Kovacs and co-authors implies that the mitochondrial component of HMG-CoA is being converted into acetyl-CoA and acetoacetate by HMGCL (see 3.2.3) and is not likely to be involved in further steps contributing to cholesterol formation [3]. The possibility of HMG-CoA transport from the mitochondria to the endoplasmic reticulum or peroxisome requires further study.

3.2.3. Hydroxymethylglutaryl-CoA lyase, mitochondrial (HMGCL; EC 4.1.3.4) is a key enzyme in the ketone body formation pathway that provides fuel to extrahepatic tissues [23]. It

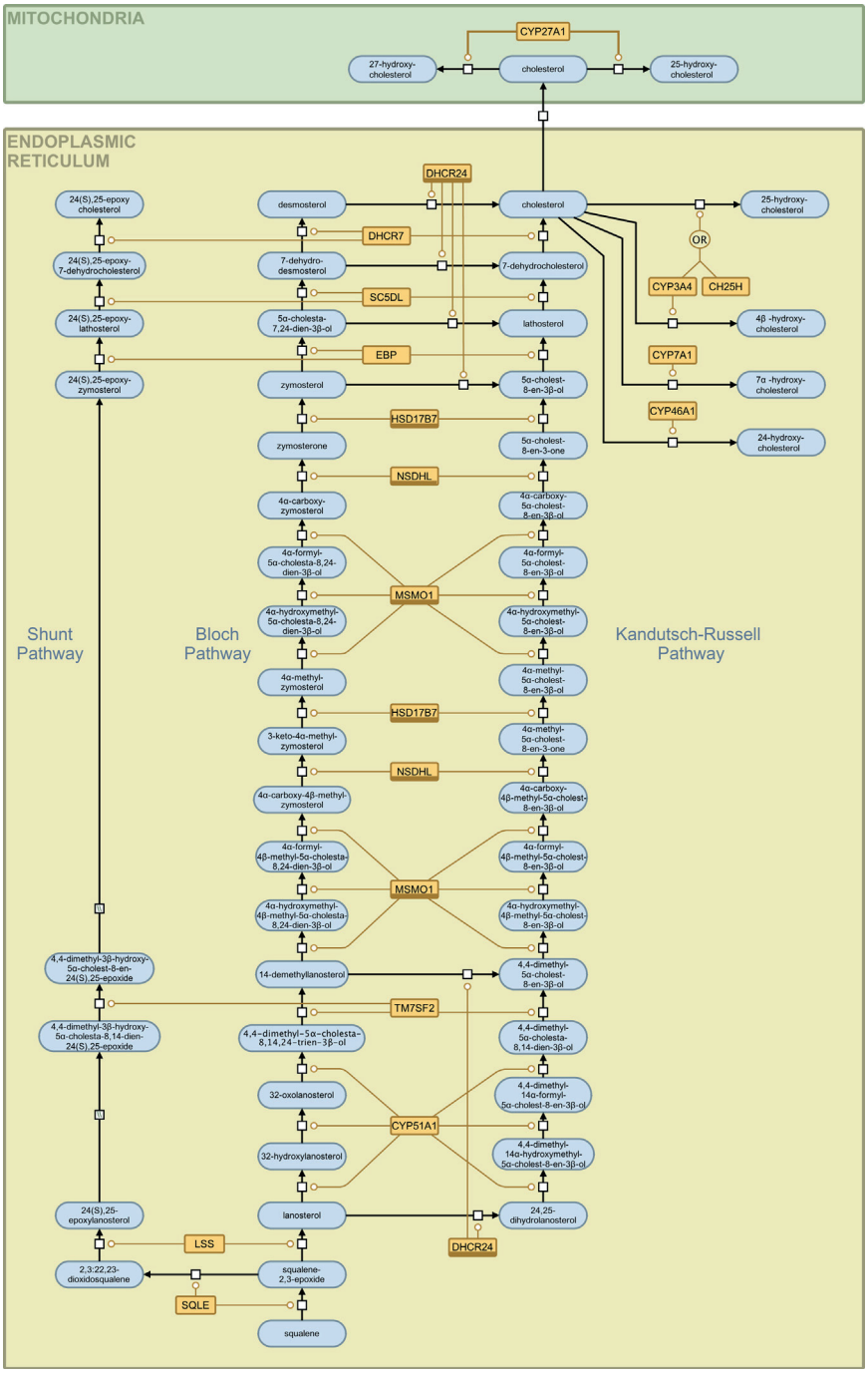

Fig. 2. The sterol arms of the cholesterol biosynthesis pathway (shunt, Bloch and Kandutsch-Russell) presented in SBGN notation. An interactive, parsable version of this figure, encoded using the SBGN-ML file format, is available in the supplementary material. The various glyph are explained in the legend in Fig. 3.

transforms HMG-CoA into acetyl-CoA and acetoacetate. HMGCL is a mitochondrial enzyme and Kovacs et al. suggest peroxisomal localization in addition to mitochondrial [3]. Since the peroxisomal localization is not confirmed yet, we show this step with a question mark on the diagram (Fig. 1). The enzyme deficiency (HMGCLD) or hydroxymethylglutaric aciduria may be due to a variety of mutations and can be fatal [24].

3.2.4. 3-Hydroxy-3-methylglutaryl-coenzyme A reductase (HMGCR; EC 1.1.1.34) catalyzes the conversion of 3-hydroxy-3-methylglutaryl-CoA into mevalonic acid. The enzyme is highly regulated by relevant signaling pathways that include the SREBP pathway [25]. Kovacs et al. confirm endoplasmic reticulum localization of HMGCR and provide evidence that suggests peroxisomal localization [3]. In our model both locations for this enzyme are included. This enzyme is conventionally regarded as being rate limiting in the pathway and its interactions are targeted by the statin class of drug.

3.2.5. Mevalonate kinase (MVK; ATP:mevalonate 5-phosphotransferase; EC 2.7.1.36) catalyzes conversion of mevalonate into phosphomevalonate. According to Hogenboom and co-authors [26–29] mevalonate kinase (MVK), phosphomevalonate kinase (PMK) and mevalonate pyrophosphate decarboxylase (MVD) are cytosolic enzymes. This contradicts studies of Kovacs and co-authors that confirm their previous findings of peroxisomal localization of the three enzymes [30] using stable isotopic techniques and human cells [3]. MVK is regulated by intermediates

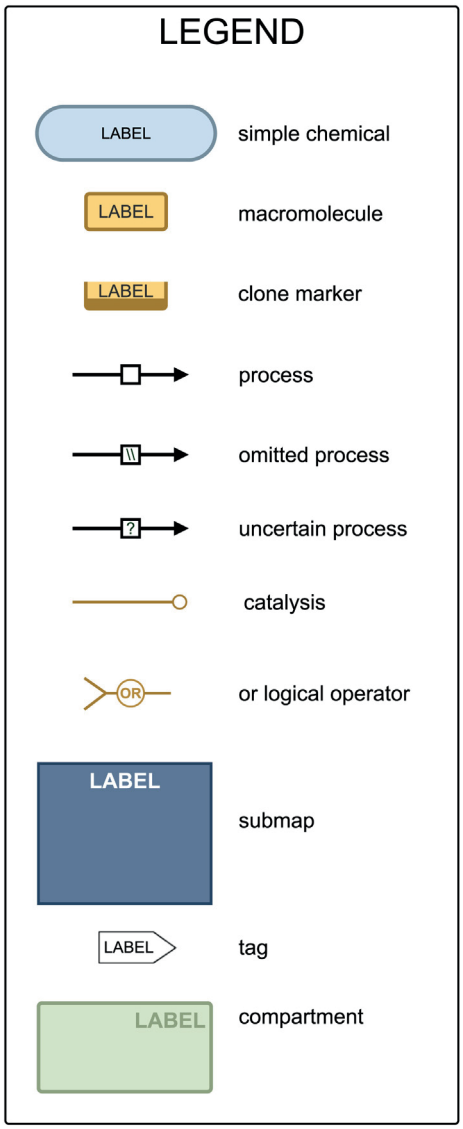

Fig. 3. The legend explaining the SBGN glyphs used in Figs. 2 and 3.

of the cholesterol metabolism pathway [31]. MVK can be competitively inhibited by farnesyl- and geranyl-pyrophosphates [32]. Mutation of the MVK gene causes mevalonate kinase deficiency [33], a disorder that leads to the lower activity of the enzyme and the accumulation of mevalonic acid, resulting in mevalonic aciduria [34] and hyperimmunoglobulinemia D syndrome [35].

3.2.6. Phosphomevalonate kinase (PMVK; EC 2.7.4.2) catalyzes formation of mevalonate 5-diphosphate from mevalonate 5-phosphate, an essential step in the mevalonate pathway. It is a reversible reaction and kinetic constants have been determined for human enzymes, both for forward and reverse reactions [36,37]. Expression of this enzyme is regulated in response to dietary sterol levels and this regulation is coordinated with HMGCR [38]. Peroxisomal localization of the enzyme has been confirmed [3,30,38–40].

3.2.7. Diphosphomevalonate decarboxylase (MVD; mevalonate (diphospho) decarboxylase; EC 4.1.1.33 is an enzyme that decarboxylates mevalonate 5-diphosphate forming isopentenyl diphosphate while hydrolyzing ATP. This enzyme is considered to be a useful target for lowering serum cholesterol levels [41] and is active as a homodimer [41]. Information on peroxisomal localization of diphosphomevalonate decarboxylase is provided in the section on mevalonate kinase (3.2.5).

3.2.8. Isopentenyl-diphosphate delta-isomerases (IDI1; IDI2; EC 5.3.3.2) perform isomerization of isopentenyl diphosphate into dimethylallyl diphosphate. These metabolites serve as fundamental building blocks of isoprenoids. This is an essential rate-limiting regulatory step for isoprenoid biosynthesis [42]. There are two types of isopentenyl-diphosphate delta-isomerase, IDI1 and IDI2. They differ in their structure and activity [43]. Both enzymes act via a proton addition/elimination mechanism [44]. IDI2 requires the presence of a reduced flavin mononucleotide cofactor [43] and both enzymes are localized to the peroxisome [45].

3.2.9. Farnesyl diphosphate synthase (FDPS; EC 2.5.1.10; EC 2.5.1.1; Dimethylallyltranstransferase) catalyzes two reactions that lead to farnesyl diphosphate formation. In the first (EC 2.5.1.1 activity) isopentenyl diphosphate and dimethylallyl diphosphate are transformed into geranyl diphosphate. Next, geranyl diphosphate and isopentenyl diphosphate are transformed into farnesyl diphosphate (EC 2.5.1.10 activity). The enzyme is a homodimer [46]. It is reported to be localized in peroxisomes [47]. FDPS supplies precursors for synthesis of steroids, dolichols and ubiquinones, protein fanesylation and geranylation. This enzyme has been suggested as an important target for drug development [48].

3.2.10. Geranylgeranyl pyrophosphate synthase (GGPS1; EC 2.5.1.29; EC 2.5.1.10; farnesyl diphosphate synthase; EC 2.5.1.1; dimethylallyltranstransferase) is able to catalyze the two reactions of farnesyl diphosphate formation. In addition, the enzyme catalyzes the addition of three molecules of isopentenyl diphosphate to dimethylallyl diphosphate and forms geranylgeranyl diphosphate, an important precursor of geranylated proteins [49] (EC 2.5.1.29 activity). The active enzyme is homohexamer [49] and is assumed to be localized to the endoplasmic reticulum.

3.2.11. Farnesyl-diphosphate farnesyltransferase 1 (FDFT1; EC 2.5.1.21; Squalene synthase) catalyzes a two-step reductive dimerization of two farnesyl diphosphate molecules and synthesizes squalene [50–52]. The FDFT1 expression level is regulated by cholesterol status: the human FDFT1 gene has a complex promoter with multiple binding sites for SREBP-1a and SREBP-2 [53].

3.3. Sterol arms of the sterol biosynthesis pathway

3.3.1. Squalene epoxidase (SQLE; EC 1.14.13.132; squalene monooxygenase) catalyzes the conversion of squalene into squalene-2,3-epoxide and the conversion of squalene-2,3-epoxide (2,3-oxidosqualene) into 2,3:22,23-diepoxysqualene (2,3:22,23-dioxidosqualene). The first reaction is the first oxygenation step in the cholesterol biosynthesis pathway and the second reaction is the first step in 24(S),25-epoxycholesterol formation from squalene-2,3-epoxide [4,54]. The steps are localized to the endoplasmic reticulum membrane [55] and it has been suggested that this is one of the rate-liming steps in the pathway [56].

3.3.2. Lanosterol synthase (LSS; OLC; OSC; 2,3-oxidosqualene:lanosterol cyclase; EC 5.4.99.7) catalyzes cyclization of squalene-2,3-epoxide to lanosterol and 2,3:22,23-diepoxysqualene to 24(S),25-epoxylanosterol [4,54]. The active monomeric enzyme is localized to the endoplasmic reticulum membrane [57]. Together with FDFT1 and SQLE, LSS has been considered as prospective target for antihypercholesterolemia drugs as an alternative to statin-based therapies [58,59].

3.3.3. Delta(24)-sterol reductase (DHCR24; 24-dehydrocholesterol reductase; EC 1.3.1.72) is a special enzyme in cholesterol biosynthesis pathway due to its broad substrate specificity. It catalyzes the reduction of the delta-24 double bond of intermediate metabolites. In particular, DHCR24 converts lanosterol into 24,25-dihydrolanostrol, the initial metabolite of

the Kandutsch-Russell pathway, and also provides the last step of Bloch pathway converting desmosterol into cholesterol. Intermediates of the Bloch pathway are converted by DHCR24 into intermediates of Kandutsch-Russell pathway [4]. Endoplasmic reticulum membrane localization has been confirmed for the enzyme [60]. Recent studies investigating the regulation of the DHCR24 promoter present evidence of binding sites for SREBP-2 [61,62]. DHCR24 participates in the inflammatory response and induces heme oxigenase-1, a potentially cardioprotective enzyme [63]. Mutations in the DHCR24 gene causes desmosterolosis [64], a rare autosomal disorder that is characterized by elevated level of desmosterol in tissues [65].

3.3.4. Lanosterol 14-alpha demethylase (CYP51A1; cytochrome P450, family 51, subfamily A, polypeptide 1; EC 1.14.13.70) converts lanosterol into 4,4-dimethyl-5α-cholesta-8,14,24-trien-3β-ol and 24,25-dihydrolanosterol into 4,4-dimethyl-5α-cholesta-8,14-dien-3β-ol in three steps [8].

3.3.5. Delta(14)-sterol reductase (TM7SF2; transmembrane 7 superfamily member 2; EC 1.3.1.70) catalyzes reactions on the three branches of the cholesterol and 24(S),25-epoxycholesterol pathways [4,8]. This enzyme is localized to the endoplasmic reticulum membrane [66].

3.3.6. Methylsterol monooxygenase 1 (MSMO1; SC4MOL; C-4 methylsterol oxidase; EC 1.14.13.72) catalyzes demethylation of C4-methylsterols [8]. This protein is localized to the endoplasmic reticulum membrane [67]. Mutations in the MSMO1 gene cause psoriasiform dermatitis, microcephaly and developmental delay [68].

3.3.7. Sterol-4-alpha-carboxylate 3-dehydrogenase, decarboxylating (NSDHL; NAD(P) dependent steroid dehydrogenase-like; EC 1.1.1.170) participates in several steps of post-squalene cholesterol and 24(S),25-epoxycholesterol synthesis [4,8]. Defects in the NSDHL gene cause CK syndrome [69], recessive mental retardation syndrome [70] and CHILD syndrome [71], congenital hemidysplasia with ichythyosiform erythrodema and limb defects [72].

3.3.8. 3-keto-steroid reductase (HSD17B7; 17-beta-hydroxysteroid dehydrogenase 7; EC 1.1.1.270) was the last unknown enzyme of mammalian cholesterol biosynthesis [73]. It was previously reported in the regulation of the activity of sex steroids [4,8,73,74]. It converts zymosterone into zymosterol in the Bloch pathway.

3.3.9. 3-Beta-hydroxysteroid-delta(8),delta(7)-isomerase (EBP; emopamil-binding protein; EC 5.3.3.5) catalyzes the conversion of delta(8)-sterols into delta(7)-sterols. Mutations in the EBP gene cause Conradi-Hunermann-Happle syndrome [75] characterized by punctiform calcification in the bones [76,77]. It is an endoplasmic reticulum membrane localized protein [78].

3.3.10. Lathosterol oxidase (SC5DL; Sterol-C5-desaturase (ERG3 delta-5-desaturase homolog, S. cerevisiae)-like; EC 1.14.21.6) catalyzes the production of 7-dehydrocholesterol, 7-dehydrodesmosterol and 24(S),25-epoxy-7-dehydrocholesterol [5]. Endoplasmic reticulum membrane localization has been suggested [79]. Lanosterol side chain amines were reported to be selective inhibitors for lathosterol oxidase [80] and together with other inhibitors for the post-squalene enzymes of the cholesterol biosynthesis pathway were suggested as potential targets for therapies to reduce the risk of cardiovascular disease [81]. Defects in the enzyme are the cause of lathosterolosis [82], an autosomal recessive disorder that is characterized by multiple congenital anomalies and liver disease [83].

3.3.11. 7-Dehydrocholesterol reductase (DHCR7; EC 1.3.1.21) catalyses reduction of the C7–C8 double bond of 7-dehydrocholesterol and formation of cholesterol. It also produces desmosterol from 7-dehydrodesmosterol [8] and 24(S),25-epoxycholesterol from 24(S),25-epoxy-7-dehydrocholesterol [4]. Mutations in the gene that encodes DHCR7 causes Smith-Lemli-Opitz syndrome, a recessively inherited autosomal disease [84].

3.3.12. Cytochrome P450, family 3, subfamily A, polypeptide 4 (CYP3A4; 1,8-cineole 2-exo-monooxygenase; taurochenodeoxycholate 6α-hydroxylase; EC 1.14.13.97) catalyses the hydroxylation of cholesterol leading to 25-hydroxycholesterol [85] and 4β-hydroxycholesterol [86,87]. It is localized to the endoplasmic reticulum [88].

3.3.13. Cholesterol 25-hydroxylase (CH25H; Cholesterol 25-monooxygenase; EC 1.14.99.38) uses di-iron cofactors to catalyze the hydroxylation of cholesterol [89–91] to produce 25-hydroxycholesterol. Has the capacity to catalyze the transition of 24-hydroxycholesterol to 24,25-dihydroxycholesterol. It is an endoplasmic reticulum localized enzyme [89] and has been shown to have a role in innate immunity [1,2]. Mutations have been associated with Alzheimer's disease [92,93].

3.3.14. Cytochrome P450, family 7, subfamily A, polypeptide 1 (CYP7A1; cholesterol 7-alpha-hydroxylase; EC 1.14.13.17) responsible for introducing a hydrophilic moiety at position 7 of cholesterol to form 7α-hydroxycholesterol [94]. It is localized to the endoplasmic reticulum [95].

3.3.15. Cytochrome P450, family 27, subfamily A, polypeptide 1 (CYP27A1; Sterol 27-hydroxylase; EC 1.14.13.15) was the first hydroxylase to be isolated [96]. It catalyses the transition of mitochondrial cholesterol to 27-hydroxycholesterol [97] and 25-hydroxycholesterol [98,99]. It is localized to the mitochondria [97] and mutations are associated with the recessive autosome disorder Cerebrotendinous Xanthomatosis [100].

3.3.16. Cytochrome P450 46A1 (CYP46A1, cholesterol 24-hydroxylase, EC 1.14.13.98) catalyses transformation of cholesterol into 24(S)-hydroxycholesterol. Localized to endoplasmic reticulum membrane [101], the enzyme is mainly expressed in brain tissue and is considered to be an important biomarker for neurodegenerative disorders [102–105].

3.4. Oxysterol 24(S),25-epoxycholesterol synthesis from squalene

24(S),25-Epoxycholesterol is produced in a shunt pathway that is parallel to the two branches of the cholesterol synthesis pathway [4,106–108]. The same set of enzymes is involved in the formation of cholesterol from 24,25-dihydrolanosterol in the Kandutsch-Russell pathway, desmosterol from lanosterol in the Bloch pathway and 24(S),25-epoxycholesterol from 24(S),25-epoxylanosterol in a shunt pathway [4]. Due to its importance in regulatory processes 24(S),25-epoxycholesterol is in the focus of several recent publications [107,109–112]. However, further research is necessary to confirm each step of the shunt pathway and the corresponding intermediate metabolites. In our representation, the known intermediates of the shunt pathway are shown and likely missing information is noted with the appropriate SBGN glyph.

3.5. Transport of the intermediate metabolites between different cellular compartments

Little is known about transporting of the intermediate metabolites of the cholesterol biosynthesis pathway between different cellular compartments. It is not known whether metabolites in the mitochondria participate in cholesterol biosynthesis and, in a number of cases, it is unclear whether metabolites move between compartments through diffusion or transportation. This is something that should be addressed in the future. It has been suggested that limitations in subcellular fractionation methods are a significant factor in our poor understanding of the subcellular localization of these enzymes [3].

4. Concluding remarks

The diagrams presented here show a comprehensive view of the mevalonate, Kandutsch-Russell, Bloch and shunt pathways. The diagrams are described using the SBGN schema, an open and community developed graphical language for unambiguously capturing pathway structure. Missing/uncertain information is clearly marked on the pathway diagrams and shows the areas that need to be further explored. Models of these diagrams are available as supplementary material in the SBGN-ML and SBML/CellDesigner [113] file formats for future development and refinement.

We hope that by elucidating and integrating the detailed structure of this pathway, we will contribute to a finer level of understanding of cholesterol metabolism and its function and that this will serve as a useful resource for future studies of the cholesterol biosynthesis pathway.

Acknowledgements

SynthSys Edinburgh is a Center for Integrative Systems Biology funded by BBSRC and EPSRC award no. D019621. This work was supported by the Wellcome Trust programme grant no. WT066784 (to P.G.) WJG is supported by BBSRC (BB/I001735/1).

Appendix A. Supplementary data

Supplementary data associated with this article can be found, in the online version, at http://dx.doi.org/10.1016/j.bcp.2013.03.021.

References

[1] Blanc M, Hsieh W, Robertson KA, Kropp KA, Forster T, Shui G, et al. The transcription factor STAT-1 couples macrophage synthesis of 25-hydroxycholesterol to the interferon antiviral response. Immunity 2012. http://dx.doi.org/10.1016/j.immuni.2012.11.004 (in press).
[2] Liu SY, Aliyari R, Chikere K, Li G, Marsden MD, Smith JK, et al. Interferon-inducible cholesterol-25-hydroxylase broadly inhibits viral entry by production of 25-hydroxycholesterol. Immunity 2012. http://dx.doi.org/10.1016/j.immuni.2012.11.005 (in press).
[3] Kovacs WJ, Tape KN, Shackelford JE, Duan X, Kasumov T, Kelleher JK, et al. Localization of the pre-squalene segment of the isoprenoid biosynthetic pathway in mammalian peroxisomes. Histochem Cell Biol 2007;127(3):273–90.
[4] Wang Y, Sousa KM, Bodin K, Theofilopoulos S, Sacchetti P, Hornshaw M, et al. Targeted lipidomic analysis of oxysterols in the embryonic central nervous system. Mol Biosyst 2009;5(5):529–41.
[5] Blanc M, Hsieh W, Robertson KA, Watterson S, Shui G, Lacaze P, et al. Host defense against viral infection involves interferon mediated down-regulation of sterol biosynthesis. PLoS Biol 2011;9(3). e1000598.
[6] Watterson S, Guerriero ML, Blanc M, Mazein A, Loewe L, Robertson KA, et al. A model of flux regulation in the cholesterol biosynthesis pathway: immune mediated graduated flux reduction versus statin-like led stepped flux reduction. Biochimie 2012. http://dx.doi.org/10.1016/j.biochi.2012.05.024 (in press).
[7] Owens CM, Mawhinney C, Grenier JM, Altmeyer R, Lee MS, Borisy AA, et al. Chemical combinations elucidate pathway interactions and regulation relevant to hepatitis C replication. Mol Syst Biol 2010;6:375.
[8] Lipid Maps Pathways, http://www.lipidmaps.org/pathways/.
[9] The Evidence Ontology, http://www.evidenceontology.org/.
[10] Guide to GO Evidence Codes, http://www.geneontology.org/GO.evidence.shtml.
[11] GO Evidence Code Decision Tree, http://www.geneontology.org/GO.evidence.tree.shtml.
[12] HUGO Gene Nomenclature Committee, http://www.genenames.org/.
[13] Enzyme Nomenclature, http://www.chem.qmul.ac.uk/iubmb/enzyme/.
[14] Le Novère N, Hucka M, Mi H, Moodie S, Schreiber F, Sorokin A, et al. The systems biology graphical notation. Nat Biotechnol 2009;27(8):735–41.
[15] The Systems Biology Graphical Notation, http://www.sbgn.org/.
[16] Czauderna T, Klukas C, Schreiber F. Editing, validating and translating of SBGN maps. Bioinformatics 2010;26(18):2340–1.
[17] Klukas C, Schreiber F. Integration of -omics data and networks for biomedical research with VANTED. J Integr Bioinformatics 2010;7(2):112. http://vanted.ipk-gatersleben.de/.
[18] Shannon P, Markiel A, Ozier O, Baliga NS, Wang JT, Ramage D, et al. Cytoscape: a software environment for integrated models of biomolecular interaction networks. Genome Res 2003;13(11):2498–504.
[19] Haapalainen AM, Meriläinen G, Pirilä PL, Kondo N, Fukao T, Wierenga RK. Crystallographic and kinetic studies of human mitochondrial acetoacetyl-CoA thiolase: the importance of potassium and chloride ions for its structure and function. Biochemistry 2007;46(14):4305–21.
[20] Kursula P, Sikkilä H, Fukao T, Kondo N, Wierenga RK. High resolution crystal structures of human cytosolic thiolase (CT): a comparison of the active sites of human CT, bacterial thiolase, and bacterial KAS I. J Mol Biol 2005;347(1):189–201.
[21] OMIM Entry – #203750 – Alpha-Methylacetoacetic Aciduria, http://www.omim.org/entry/203750 [Accessed 01.01.13].
[22] Ortiz JA, Gil-Gómez G, Casaroli-Marano RP, Vilaró S, Hegardt FG, Haro D. Transfection of the ketogenic mitochondrial 3-hydroxy-3-methylglutaryl-coenzyme A synthase cDNA into Mev-1 cells corrects their auxotrophy for mevalonate. J Biol Chem 1994;269:28523–26.
[23] Holmes HC, Burns SP, Chalmers RA, Bain MS, Iles RA. Ketogenic flux from lipids and leucine, assessment in 3-hydroxy-3-methylglutaryl CoA lyase deficiency. Biochem Soc Trans 1995;23(3):489S.
[24] Pié P, López-Viñas E, Puisac B, Menao S, Pié A, Casale C, et al. Molecular genetics of HMG-CoA lyase deficiency. Mol Genet Metab 2007;92(3):198–209.
[25] Mazein A, Watterson S, Gibbs HC, Hsieh W, Ba Abdullah M, Blanc M, et al. Regulation and feedback of cholesterol metabolism. Nature Precedings 2011. http://dx.doi.org/10.1038/npre.2011.6315.1.
[26] Hogenboom S, Tuyp JJM, Espeel M, Koster J, Wanders RJA, Waterham HR. Phosphomevalonate kinase is a cytosolic protein in humans. J Lipid Res 2004;45(4):697–705.
[27] Hogenboom S, Wanders RJA, Waterham HR. Cholesterol biosynthesis is not defective in peroxisome biogenesis defective fibroblasts. Mol Genet Metab 2003;80(3):290–5.
[28] Hogenboom S, Tuyp JJM, Espeel M, Koster J, Wanders RJA, Waterham HR. Human mevalonate pyrophosphate decarboxylase is localized in the cytosol. Mol Genet Metab 2004;81(3):216–24.
[29] Hogenboom S, Tuyp JJM, Espeel M, Koster J, Wanders RJA, Waterham HR. Mevalonate kinase is a cytosolic enzyme in humans. J Cell Sci 2004;117(4):631–9.
[30] Kovacs WJ, Olivier LM, Krisans SK. Central role of peroxisomes in isoprenoid biosynthesis. Prog Lipid Res 2002;41(5):369–91.
[31] Hinson DD, Chambliss KL, Toth MJ, Tanaka RD, Gibson KM. Post-translational regulation of mevalonate kinase by intermediates of the cholesterol and nonsterol isoprene biosynthetic pathways. J Lipid Res 1997;38(11):2216–23.
[32] Mevalonate kinase – Homo sapiens (Human), http://www.uniprot.org/uniprot/Q03426 [Accessed 31.12.12].
[33] Vuch J, Marcuzzi A, Bianco AM, Tommasini A, Zanin V, Crovella S. Evolutionary hypothesis of the mevalonate kinase deficiency. Med Hypotheses 2012. http://dx.doi.org/10.1016/j.mehy.2012.10.016 (in press).
[34] OMIM Entry – #610377 – Mevalonic Aciduria; MEVA, http://www.omim.org/entry/610377 [Accessed 31.12.12].
[35] Haas D, Hoffmann GF. Mevalonate kinase deficiencies: from mevalonic aciduria to hyperimmunoglobulinemia D syndrome. Orphanet J Rare Dis 2006;1:13.
[36] Pilloff D, Dabovic K, Romanowski MJ, Bonanno JB, Doherty M, Burley SK, et al. The kinetic mechanism of phosphomevalonate kinase. J Biol Chem 2003;278(7):4510–5.
[37] Herdendorf TJ, Miziorko HM. Phosphomevalonate kinase: functional investigation of the recombinant human enzyme. Biochemistry 2006;45(10):3235–42.
[38] Olivier LM, Chambliss KL, Gibson KM, Krisans SK. Characterization of phosphomevalonate kinase: chromosomal localization, regulation, and subcellular targeting. J Lipid Res 1999;40(4):672–9.
[39] Olivier LM, Krisans SK. Peroxisomal protein targeting and identification of peroxisomal targeting signals in cholesterol biosynthetic enzymes. Biochim Biophys Acta 2000;1529(1–3):89–102.
[40] Olivier LM, Kovacs W, Masuda K, Keller GA, Krisans SK. Identification of peroxisomal targeting signals in cholesterol biosynthetic enzymes. AA-CoA thiolase, HMG-CoA synthase, MPPD, and FPP synthase. J Lipid Res 2000;41(12):1921–35.
[41] Toth MJ, Huwyler L. Molecular cloning and expression of the cDNAs encoding human and yeast mevalonate pyrophosphate decarboxylase. J Biol Chem 1996;271(14):7895–8.
[42] Berthelot K, Estevez Y, Deffieux A, Peruch F. Isopentenyl diphosphate isomerase: a checkpoint to isoprenoid biosynthesis. Biochimie 2012;94(8):1621–34.
[43] Rothman SC, Johnston JB, Lee S, Walker JR, Poulter CD. Type II, isopentenyl diphosphate isomerase: irreversible inactivation by covalent modification of flavin. J Am Chem Soc 2008;130(14):4906–13.
[44] Heaps NA, Poulter CD. Type-2 isopentenyl diphosphate isomerase: evidence for a stepwise mechanism. J Am Chem Soc 2011;133(47):19017–19.
[45] Clizbe DB, Owens ML, Masuda KR, Shackelford JE, Krisans SK. IDI2, a second isopentenyl diphosphate isomerase in mammals. J Biol Chem 2007;282(9):6668–76.
[46] Szkopińska A, Płochocka D. Farnesyl diphosphate synthase; regulation of product specificity. Acta Biochim Pol 2005;52(1):45–55.

[47] Krisans SK, Ericsson J, Edwards PA, Keller GA. Farnesyl-diphosphate synthase is localized in peroxisomes. J Biol Chem 1994;269(19):14165–69.
[48] Dhar MK, Koul A, Kaul S. Farnesyl pyrophosphate synthase: a key enzyme in isoprenoid biosynthetic pathway and potential molecular target for drug development. N Biotechnol 2012;30(2):114–23.
[49] Kavanagh KL, Dunford JE, Bunkoczi G, Russell RGG, Oppermann U. The crystal structure of human geranylgeranyl pyrophosphate synthase reveals a novel hexameric arrangement and inhibitory product binding. J Biol Chem 2006;281(31):22004–12.
[50] Do R, Kiss RS, Gaudet D, Engert JC. Squalene synthase: a critical enzyme in the cholesterol biosynthesis pathway. Clin Genet 2009;75(1):19–29.
[51] Radisky ES, Poulter CD. Squalene synthase: steady-state, pre-steady-state, and isotope-trapping studies. Biochemistry 2000;39(7):1748–60.
[52] Pandit J, Danley DE, Schulte GK, Mazzalupo S, Pauly TA, Hayward CM, et al. Crystal structure of human squalene synthase. A key enzyme in cholesterol biosynthesis. J Biol Chem 2000;275(39):30610–17.
[53] Tansey TR, Shechter I. Squalene synthase: structure and regulation. Prog Nucleic Acid Res Mol Biol 2001;65:157–95.
[54] Trapani L, Segatto M, Pallottini V. Regulation and deregulation of cholesterol homeostasis: the liver as a metabolic 'power station'. World J Hepatol 2012;4(6):184–90.
[55] Squalene Monooxygenase – Homo sapiens (Human), http://www.uniprot.org/uniprot/Q14534, [Accessed 02.01.13].
[56] Nagai M, Sakakibara J, Wakui K, Fukushima Y, Igarashi S, Tsuji S, et al. Localization of the squalene epoxidase gene (SQLE) to human chromosome region 8q24.1. Genomics 1997;44(1):141–3.
[57] Ruf A, Müller F, D'Arcy B, Stihle M, Kusznir E, Handschin C, et al. The monotopic membrane protein human oxidosqualene cyclase is active as monomer. Biochem Biophys Res Commun 2004;315(2):247–54.
[58] Huff MW, Telford DE. Lord of the rings – the mechanism for oxidosqualene:lanosterol cyclase becomes crystal clear. Trends Pharmacol Sci 2005;26(7):335–40.
[59] Trapani L, Segatto M, Ascenzi P, Pallottini V. Potential role of nonstatin cholesterol lowering agents. IUBMB Life 2011;63(11):964–71.
[60] Lu X, Li Y, Liu J, Cao X, Wang X, Wang D, et al. The membrane topological analysis of 3β-hydroxysteroid-delta24 reductase (DHCR24) on endoplasmic reticulum. J Mol Endocrinol 2012;48(1):1–9.
[61] Daimiel LA, Fernández-Suárez ME, Rodríguez-Acebes S, Crespo L, Lasuncion MA, Gomez-Coronado D, et al. Promoter analysis of the 3β-hydroxysterol Δ24-reductase (DHCR24) gene: characterization of sterol regulatory element-binding protein (SREBP)-mediated activation. Biosci Rep 2013;33(1):e00006.
[62] Zerenturk EJ, Sharpe LJ, Brown AJ. Sterols regulate 3β-hydroxysterol Δ24-reductase (DHCR24) via dual sterol regulatory elements: cooperative induction of key enzymes in lipid synthesis by sterol regulatory element binding proteins. Biochim Biophys Acta 2012;1821(10):1350–60.
[63] Wu BJ, Chen K, Shrestha S, Ong KL, Barter PJ, Rye KA. High density lipoproteins inhibit vascular endothelial inflammation by increasing 3β-hydroxysteroid-{delta}24 reductase expression and inducing heme oxygenase-1. Circ Res 2013;112:278–88.
[64] OMIM Entry – # 602398 – Desmosterolosis, http://www.omim.org/entry/602398 [Accessed 02.01.13].
[65] Zolotushko J, Flusser H, Markus B, Shelef I, Langer Y, Heverin M, et al. The desmosterolosis phenotype: spasticity, microcephaly and micrognathia with agenesis of corpus callosum and loss of white matter. Eur J Hum Genet 2011;19(9):942–6.
[66] Holmer L, Pezhman A, Worman HJ. The human lamin B receptor/sterol reductase multigene family. Genomics 1998;54(3):469–76.
[67] MSMO1 Methylsterol Monooxygenase 1 [Homo sapiens] – Gene – NCBI, http://www.ncbi.nlm.nih.gov/gene/6307 [Accessed 31.12.12].
[68] He M, Kratz LE, Michel JJ, Vallejo AN, Ferris L, Kelley RI, et al. Mutations in the human SC4MOL gene encoding a methyl sterol oxidase cause psoriasiform dermatitis, microcephaly, and developmental delay. J Clin Invest 2011;121(3):976–84.
[69] OMIM Entry – #300831 – CK Syndrome, http://www.omim.org/entry/300831 [Accessed 02.01.13].
[70] McLarren KW, Severson TM, du Souich C, Stockton DW, Kratz LE, Cunningham D. Hypomorphic temperature-sensitive alleles of NSDHL cause CK syndrome. Am J Hum Genet 2010;87(6):905–14.
[71] OMIM Entry – #308050 – Congenital Hemidysplasia with Ichthyosiform Erythroderma and Limb Defects. http://www.omim.org/entry/308050 [Accessed 02.01.13].
[72] OMIM Entry – #300275 – NAD(P)H Steroid Dehydrogenase-Like Protein; NSDHL. http://www.omim.org/entry/300275 [Accessed 02.01.13].
[73] Marijanovic Z, Laubner D, Moller G, Gege C, Husen B, Adamski J, et al. Closing the gap: identification of human 3-ketosteroid reductase, the last unknown enzyme of mammalian cholesterol biosynthesis. Mol Endocrinol 2003;17(9):1715–25.
[74] Törn S, Nokelainen P, Kurkela R, Pulkka A, Menjivar M, Ghosh S, et al. Production, purification, and functional analysis of recombinant human and mouse 17beta-hydroxysteroid dehydrogenase type 7. Biochem Biophys Res Commun 2003;305(1):37–45.
[75] OMIM Entry – #302960 – Chondrodysplasia Punctata 2, X-Linked Dominant; CDPX2. http://www.omim.org/entry/302960 [Accessed 02.01.13].
[76] Braverman N, Lin P, Moebius FF, Obie C, Moser A, Glossmann H, et al. Mutations in the gene encoding 3 beta-hydroxysteroid-delta 8, delta 7-isomerase cause X-linked dominant Conradi-Hünermann syndrome. Nat Genet 1999;22(3):291–4.
[77] Becker K, Csikós M, Horváth A, Kárpáti S. Identification of a novel mutation in 3beta-hydroxysteroid-delta8-delta7-isomerase in a case of Conradi-Hünermann-Happle syndrome. Exp Dermatol 2001;10(4):286–9.
[78] Dussossoy D, Carayon P, Belugou S, Feraut D, Bord A, Goubet C, et al. Colocalization of sterol isomerase and sigma(1) receptor at endoplasmic reticulum and nuclear envelope level. Eur J Biochem 1999;263(2):377–86.
[79] Lathosterol Oxidase – Homo Sapiens (Human), http://www.uniprot.org/uniprot/O75845#ref6, [Accessed 02.01.13].
[80] Giera M, Renard D, Plössl F, Bracher F. Lathosterol side chain amides: a new class of human lathosterol oxidase inhibitors. Steroids 2008;73(3):299–308.
[81] Giera M, Plössl F, Bracher F. Fast and easy in vitro screening assay for cholesterol biosynthesis inhibitors in the post-squalene pathway. Steroids 2008;72(8):633–42.
[82] OMIM Entry – #607330 – Lathosterolosis. http://www.omim.org/entry/607330 [Accessed 02.01.13].
[83] Brunetti-Pierri N, Corso G, Rossi M, Ferrari P, Balli F, Rivasi F, et al. Lathosterolosis, a novel multiple-malformation/mental retardation syndrome due to deficiency of 3beta-hydroxysteroid-delta5-desaturase. Am J Hum Genet 2002;71(4):952–8.
[84] OMIM Entry – #270400 – Smith-Lemli-Opitz Syndrome; SLOS, http://www.omim.org/entry/270400 [Accessed 31.12.12].
[85] Honda A, Miyazaki T, Ikegami T, Iwamoto J, Maeda T, Hirayama T, et al. Cholesterol 25-hydroxylation activity of CYP3A4. J Lipid Res 2011;52:1509–16.
[86] Diczfalusy U, Nylén H, Elander P, Bertilsson L. 4β-hydroxycholesterol, an endogenous marker of CYP3A4/5 activity in humans. Br J Clin Pharmacol 2011;71(2):183–9.
[87] Bodin K, Andersson U, Rystedt E, Ellis E, Norlin M, Pikuleva I, et al. Metabolism of 4β-hydroxycholesterol in humans. J Biol Chem 2002;277(35):31534–40.
[88] Wang Y, Guan S, Acharya P, Liu Y, Thirumaran RK, Brandman R, et al. Multisite phosphorylation of human liver cytochrome P450 3A4 enhances its gp78- and CHIP-mediated ubiquitination: a pivotal role of its Ser-478 residue in the gp78-catalyzed reaction. Mol Cell Proteomic 2012;11(2). M111, 010132.
[89] Lund EG, Kerr TA, Sakai J, Li WP, Russell DW. cDNA cloning of mouse and human cholesterol 25-hydroxylases, polytopic membrane proteins that synthesize a potent oxysterol regulator of lipid metabolism. J Biol Chem 1998;273:34316–27.
[90] Fox BG, Shanklin J, Ai J, Loehr TM, Sanders-Loehr J. Resonance Raman evidence for an Fe–O–Fe center in stearoyl-ACP desaturase. Primary sequence identity with other diiron-oxo proteins. Biochemistry 1994;33:12776–86.
[91] Russell DW. The enzymes, regulation, and genetics of bile acid synthesis. Annu Rev Biochem 2003;72:137–74.
[92] Wollmer MA. Cholesterol-related genes in Alzheimer's disease. Biochim Biophys Acta 2010;1801(8):762–73.
[93] Papassotiropoulos A, Lambert JC, Wavrant-De Vrièze F, Wollmer MA, von der Kammer H, Streffer JR, et al. Cholesterol 25-hydroxylase on chromosome 10q is a susceptibility gene for sporadic Alzheimer's disease. Neurodegener Dis 2005;2(5):233–41.
[94] Norlin M, Wikvall K. Enzymes in the conversion of cholesterol into bile acids. Curr Mol Med 2007;7(2):199–218.
[95] Hubbard PA, Shen AL, Paschke R, Kasper CB, Kim JJ. NADPH-cytochrome P450 oxidoreductase. Structural basis for hydride and electron transfer. J Biol Chem 2001;276(31):29163–70.
[96] Wikvall K. Hydroxylations in biosynthesis of bile acids. Isolation of a cytochrome P-450 from rabbit liver mitochondria catalyzing 26-hydroxylation of C27-steroids. J Biol Chem 1984;259:3800–4.
[97] Russell DW. Oxysterol biosynthetic enzymes. Biochim Biophys Acta 2000;1529(1–3):126–35.
[98] Honda A, Yamashita K, Hara T, Ikegami T, Miyazaki T, Shirai M, et al. Highly sensitive quantification of key regulatory oxysterols in biological samples by LC-ESI-MS/MS. J Lipid Res 2009;50(2):350–7.
[99] Diczfalusy U, On the formation and possible biological role of 25-hydroxycholesterol, Biochimie (in press) doi: 10.1016/j.biochi.2012.06.016.
[100] Gallus GN, Dotti MT, Federico A. Clinical and molecular diagnosis of cerebrotendinous xanthomatosis with a review of the mutations in the CYP27A1 gene. Neurol Sci 2006;27(2):143–9.
[101] Mast N, Liao WL, Pikuleva IA, Turko IV. Combined use of mass spectrometry and heterologous expression for identification of membrane-interacting peptides in cytochrome P450 46A1 and NADPH-cytochrome P450 oxidoreductase. Arch Biochem Biophys 2009;83:81–9.
[102] Hughes TM, Kuller LH, Lopez OL, Becker JT, Evans RW, Sutton-Tyrrell K, et al. Markers of cholesterol metabolism in the brain show stronger associations with cerebrovascular disease than Alzheimer's disease. J Alzheimers Dis 2012;30:53–61.
[103] Jeitner TM, Voloshyna I, Reiss AB. Oxysterol derivatives of cholesterol in neurodegenerative disorders. Curr Med Chem 2011;18:1515–25.
[104] Leoni V, Caccia C. Oxysterols as biomarkers in neurodegenerative diseases. Chem Phys Lipids 2011;164:515–24.
[105] Leoni V, Caccia C. 24S-hydroxycholesterol in plasma: a marker of cholesterol turnover in neurodegenerative diseases. Biochimie 2013;95:595–612.
[106] Wong J, Quinn CM, Brown AJ. Synthesis of the oxysterol, 24(S), 25-epoxycholesterol, parallels cholesterol production and may protect against cellular accumulation of newly-synthesized cholesterol. Lipids Health Dis 2007;6(10.).

[107] Brown AJ. 24 (S) 25-epoxycholesterol: a messenger for cholesterol homeostasis. Int J Biochem Cell Biol 2009;41(4):744–7.
[108] Rowe AH, Argmann CA, Edwards JY, Sawyez CG, Morand OH, Hegele RA, et al. Enhanced synthesis of the oxysterol 24(S), 25-epoxycholesterol in macrophages by inhibitors of 2,3-oxidosqualene:lanosterol cyclase: a novel mechanism for the attenuation of foam cell formation. Circ Res 2003;93(8):717–25.
[109] Beyea MM, Reaume S, Sawyez CG, Edwards JY, O'Neil C, Hegele RA, et al. The oxysterol 24(s), 25-epoxycholesterol attenuates human smooth muscle-derived foam cell formation via reduced low-density lipoprotein uptake and enhanced cholesterol efflux. J Am Heart Assoc 2012;1(3):e000810.
[110] Zerenturk EJ, Kristiana I, Gill S, Brown AJ. The endogenous regulator 24(S), 25-epoxycholesterol inhibits cholesterol synthesis at DHCR24 (Seladin-1). Biochim Biophys Acta 2012;1821(9):1269–77.
[111] Fukunaga M, Nunomura S, Nishida S, Endo K, Gon Y, Hashimoto S, et al. Mast cell death induced by 24(S), 25-epoxycholesterol. Exp Cell Res 2010;316(19):3272–81.
[112] Theofilopoulos S, Wang Y, Kitambi SS, Sacchetti P, Sousa KM, Bodin K, et al. Brain endogenous liver X receptor ligands selectively promote midbrain neurogenesis. Nat Chem Biol 2012. http://dx.doi.org/10.1038/nchembio.1156 (in press).
[113] Funahashi A, Tanimura N, Morohashi M, Kitano H. CellDesigner: a process diagram editor for gene-regulatory and biochemical networks. BIOSILICO 2003;1:159–62.

Chapter 3

Investigation of the role of 25-Hydroxycholesterol in the interferon mediated sterol-immune antiviral response

3.1 Introduction

There is increasing evidence indicating that the regulation of the sterol metabolic network is an integral part of the host immune response (Im et al., 2011). Central to sterol metabolism is a family of transcription factors, known as sterol regulatory element-binding proteins (SREBPs), that is essential for the synthesis of sterols and fatty acids (Horton et al., 2002). SREBP and liver x receptor (LXR) signalling play essential roles in the development of host immunity, including the proliferation of $CD8^+$ effector T cells (Bensinger et al., 2008; Kidani et al., 2013), enhancing macrophage activation (Spann et al., 2012) and increasing protection of macrophages from bacterial toxins (Im and Osborne, 2012). Nearly all enzymes of the sterol biosynthesis pathway are transcriptionally regulated by SREBP2, suggesting that the regulation of SREBP2 is an important step at tuning sterol biosynthesis (Inoue, 1996; Radhakrishnan et al., 2008). The proteolytic activation of SREBP2 is regulated through multiple mechanisms: the binding of cholesterol to SCAP (sterol regulatory element-binding protein) prevents the translocation of SREBP2 to the nucleus (Figure 3.1A, B) (Brown and Goldstein, 1999), and the binding of oxysterols (oxidized cholesterol) to INSIG-1 (Gong et al., 2006; Yabe et al., 2002), which subsequently inhibit SREBP2 proteolytic cleavage and activation (Radhakrishnan et al., 2008).

Oxysterols are side-chain oxidized cholesterols (Figure 3.2 for structural reference) that are involved in many physiological roles, such as brain and neuron development (Meljon et al., 2012). Importantly, oxysterols have been shown to regulate cholesterol metabolism through the activation of LXR (Brown and Goldstein, 2013; Chuu and Lin, 2010). Oxysterol (or oxycholesterol by its original name) was an accidental discovery by Lifschütz and the Rosenheim family (Sigmund Otto and Mary) (Rosenheim, 1914b) when they tried to profile cholesterol and cholesterol-ester from ox and human brains. Using the Adolf Windaus method, the quantity of cholesterol and cholesterol-ester can be estimated by precipitating chemically dissolved tissues with digitonin. The quantity of cholesterol in the tissue extract corresponds to the amount of digitonin used (Rosenheim, 1914b, 1906). Brain extracts from adult brains did not contain any cholesterol ester, while a powdery like substance was recovered. This substance turns bright emerald green when it interacts with ferric chloride in acetic acid (Rosenheim, 1914a). Subsequent spectroscopic examination indicated that this powdery compound, now known as oxycholesterol, has a distinctive absorbance (λ630 and λ650, green colour) from cholesterol (Rosenheim, 1916).

7β-hydroxycholesterol (7β-HC) was the first oxysterol to be structurally identified, and synthesized through the oxidation of cholesteryl-hydrogen-phthalate using potassium permanganate (Barr et al., 1936). 7α-hydroxycholesterol (7α-HC), a biological oxysterol, was later isolated from ox livers (Haslewood, 1939). 25-hydroxycholesterol (cholest-5-en-3β,25-diol, 25-HC), and 26-hydroxycholesterol (cholest-5-ene-3β,26-diol, 26-HC) were both synthesized from cholesterol-4-C^{14} in mouse liver mitochondria extracts (Fredrickson and Ono, 1956). *In vivo* experiments showed that 25-HC was not metabolized into cholic acid (bile acid), but instead forms steroid acid derivatives (now known as 7α-25-HC, the product of CYP7B1 (Toll et al., 1994)). This provides the first evidence that oxysterols might have other biological functions rather than being merely hormone intermediates.

The earliest studies that showed oxysterol is capable of regulating sterol metabolism came from the work of Hall and Koritz, 1964, on thebovine adrenal cortex. Conversion of [7α-^{3}H]cholesterol to [^{3}H]pregnenolone was significantly reduced in the presence of 20α-hydroxycholesterol (20α-HC). Further experimentation showed that 20α-HC and cholesterol were competing substrates for the enzyme CYP11A1 (Shikita and Hall, 1974). The work of Kandutsch and Chen showed that rates of cholesterol synthesis from [1-C^{14}]acetate in primary mouse liver cell cultures were repressed in the presence of 7α-HC, 7β-HC, and 7α-ketocholesterol (7α-KC) (Kandutsch and Chen, 1973). 25-HC, when compared with other oxysterols (7α-HC, 7α-KC, and 20α-HC), had even stronger inhibitory effects on L-cell (subcutaneous connective tissue fibroblast) growth (1μg/ml or 2.5μM for 90% inhibition) (Chen et al., 1974). Importantly, metabolic rescue experiments using 20α-HC (10μg/ml or 25μM) showed that the suppression of oxysterol on L-cell growth could only be reversed by the addition of mevalonate salt (1μg/ml or 5.9mM), desmosterol (50μg/ml or 130μM), or cholesterol (50μg/ml or 130μM), but not acetate, HMG-CoA, or 5α-cholestane-3-one (Chen et al., 1974). This experiment clearly demonstrated that the suppression of sterol biosynthesis by oxysterol occurred at the level downstream of the HMGCR.

Mechanistic studies showed that 25-HC is potent at suppressing cholesterol biosynthesis through the binding to INSIG-1 or -2, but not to SCAP, as 25-HC fails to cross-link with SCAP (Adams et al., 2004). The binding of 25-HC to INSIG-1 or -2 prevents the necessary SCAP conformational changes, thus inhibits the translocation or activation of SREBP2 (Figure 3.1C).

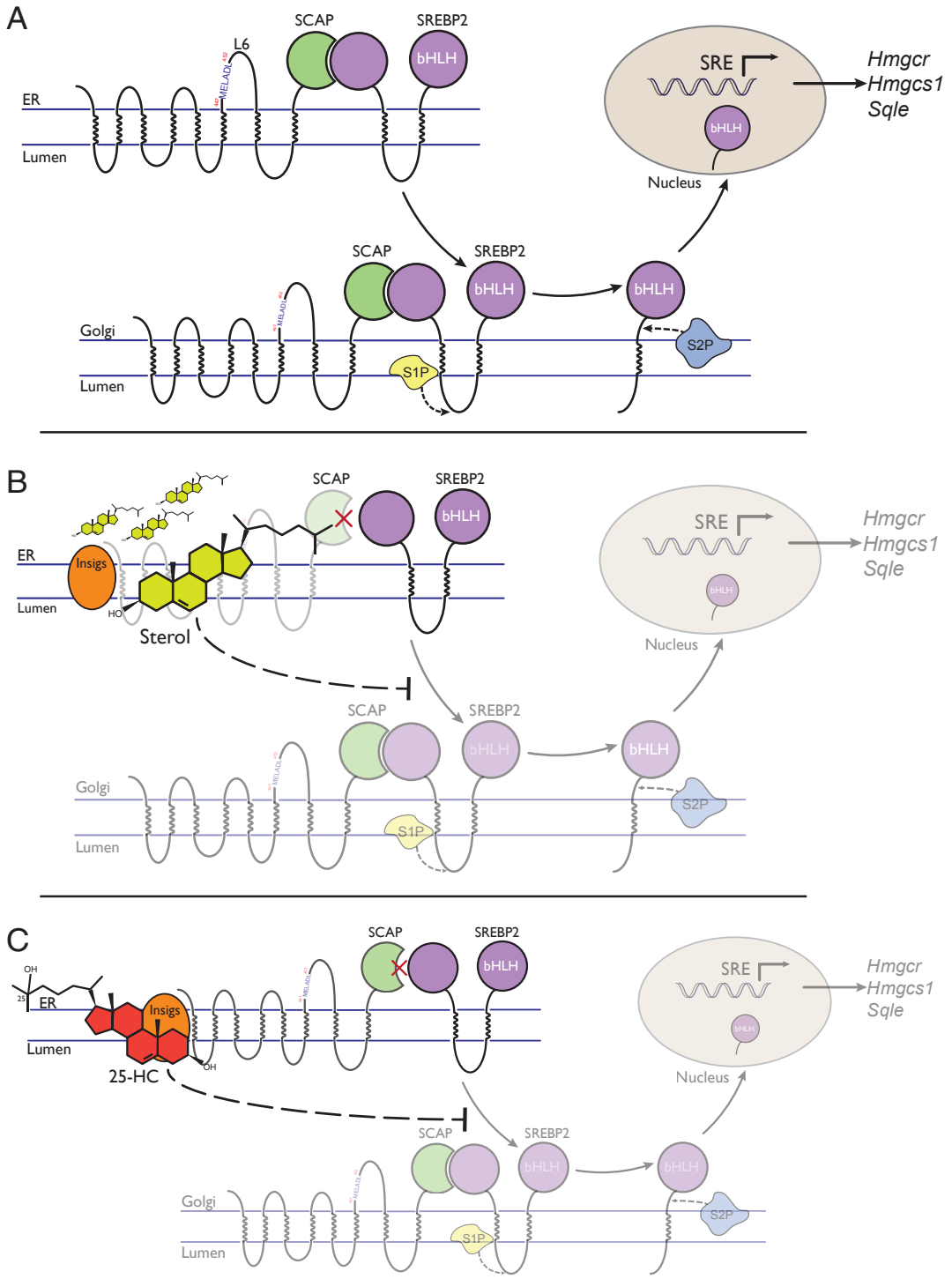

Figure 3.1 Cholesterol and oxysterol mediated proteolytic control of the SREBP2 pathway.
(A) SREBP2 is synthesized as an ER membrane bound precursor. When the cells are depleted in cholesterol, SREBP cleavage-activating protein (SCAP) binds and escorts SREBP2 from the ER to the Golgi apparatus. This translocation is mediated by the MELADL sequence (aa 447-452) on loop 6 of SCAP. The release of SREBP2 is initiated through two sequential cleavages by Site-1 Protease (S1P) and Site-2 Protease (S2P). After the second cleavage, the active SREBP2-bHLH domain leaves the membrane. The cleaved SREBP2 nuclear fraction enters the nucleus, where it binds to the sterol response element (SRE) and activates genes controlling cholesterol synthesis and uptake. (B) When the cholesterol level is high, sterol binds directly to SCAP, triggering SCAP to bind to INSIGs [insulin induced gene 1 (Insig1) and insulin induced gene 2 (Insig2)], preventing the translation and subsequent activation of SREBP2. (C) Oxysterols, such as 25-HC, bind directly to INSIG-1, preventing the translocation of SREBP2.

In the mevalonate-isoprenoid arm of the sterol biosynthesis pathway, 25-HC has been shown to induce proteasome degradation of HMG-CoA reductase (HMGCR), a key enzyme of sterol biosynthesis, through the recruitment of Insig1 (Sever et al., 2003). A subsequent study revealed that INSIG-1 acts as a bridge for the recruitment of two ubiquitin ligases, gp78 and Trc8, to the reductase (Jo et al., 2011). The resultant ubiquitination of the reductase is then delivered for proteasome degradation. In addition, 25-HC may also regulate sterol biosynthesis through its ability to activate LXRs and other isoprenoids and sterol-metabolic intermediates that lead to negative feedback on sterol biosynthesis (Espenshade and Hughes, 2007; Ma et al., 2008; Song et al., 2005).

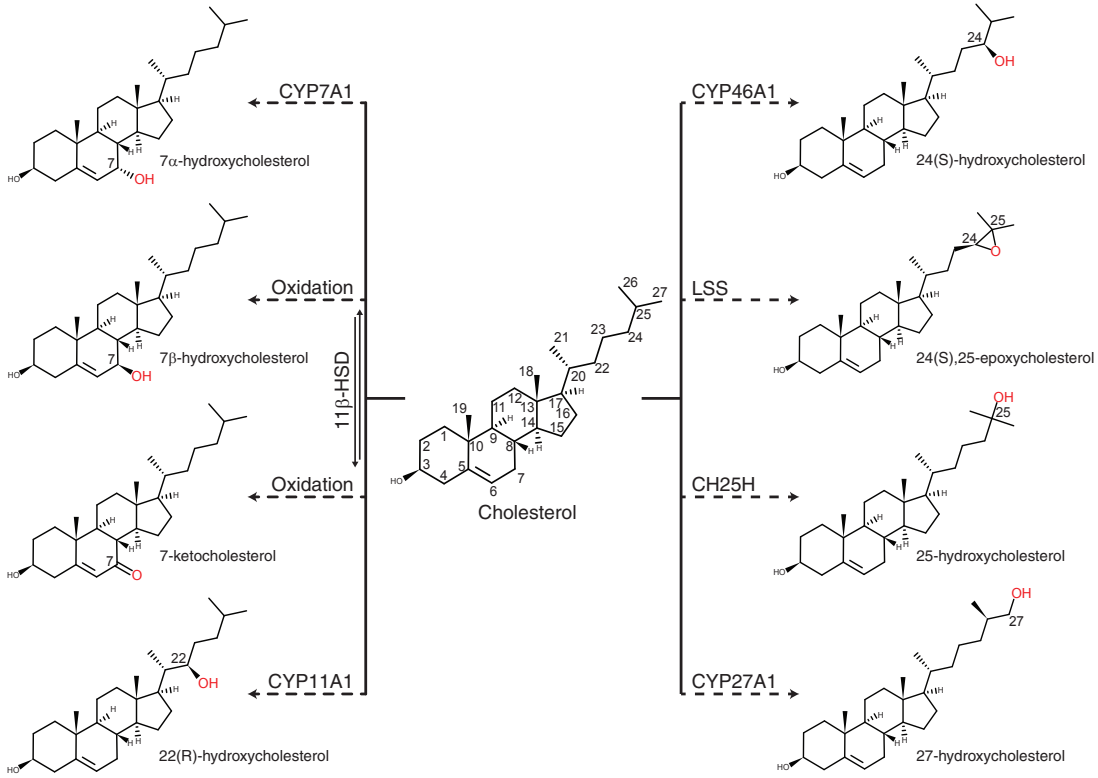

Figure 3.2 Enzymatic transformation of cholesterol into oxysterols.
The structure of the cholesterol molecule with carbon positions labelled. Oxysterols are shown with the oxygen group highlighted and with oxidized carbon position numbered. CYP7A1: cholesterol-7α-hydroxylase, CYP11A1: cytochrome P450 11A1, CYP46A1: cholesterol-24-hydroxylase, LSS: lanosterol synthase, CH25H: cholesterol-25-hydroxylase, CYP27A1: sterol-27-hydroxylase. The interconversion of 7β-hydroxycholesterol and 7-ketocholesterol done by the enzyme 11β-hydroxysteroid dehydrogenase (11β-HSD).

Viruses and other pathogens are known to alter host lipid metabolism and the immune response to facilitate their own replication (Aizaki et al., 2008; Carere et al., 2013; Hanley et al., 2010; Sen et al., 2011) (Reviewed in Chapter 1). Our previous work indicated that sterol metabolism is downregulated in macrophages (BMDM, MΦ) as an interferon mediated antiviral response. SREBP2, the key sterol biosynthesis transcription factor, was also suppressed by interferon (Blanc, Hsieh et al., 2011). In the previous chapter (Chapter 2), it was shown that chemical and pharmacological inhibitions of sterol biosynthesis have detrimental effects on viral infection. Collectively, these data signify the importance of the mevalonate pathway in the viral replication cycle. Oxysterols are involved in many aspects of sterol regulation, implicating their potential importance in immunity. This connection is strengthened by studies showing that cholesterol hydroxylase, in particular, cholesterol 25-hydroxylase (*Ch25h*), is induced in macrophages, dendritic cells, and monocytes in response to toll-like receptors (TLRs) and interferon stimulation (Bauman et al., 2009; Eibinger et al., 2013; Holmes et al., 2011; Park and Scott, 2010). Importantly, however, the precise role of *Ch25h* and its product 25-HC, as a part of interferon regulation on the sterol metabolic network, remains unclear.

In this chapter, I have undertaken a mechanistic investigation of the biological role of 25-HC as a part of the host innate response against viral infection. The aim of the experiments focused on understanding what triggers the transcription activation of *Ch25h*, the potential antiviral capacity of 25-HC, how 25-HC modulates viral replication, and potential antiviral mechanisms. Results demonstrated that 25-HC elicits broad antiviral effects through multiple mechanisms, highlighting the direct coupling of the 25-hydroxycholesterol sterol metabolic network to the interferon antiviral response.

3.2 Results

3.2.1 Transcription of cholesterol 25-hydroxylase is activated upon interferon, CMV and TLR stimulations

To investigate whether cholesterol 25-hydroxylase in MΦ can be induced upon immune stimulation, BMDM were first stimulated with various TLR-ligands [LPS::TLR4 (Lu et al., 2008), Poly I:C::TLR3 (Bogunovic et al., 2011), Pam3CSK4::TLR1/2 (Cardoso et al., 2013), R848::TLR7/8 (Grela et al., 2011), and ODN1668::TLR9 (Xu et al., 2012)] for 4 hr, followed by qRT-PCR gene expression analysis (see Experimental procedure 7.5). Expression of *Ch25h* was induced upon all TLR-ligand stimulations (Figure 3.3A), with Poly I:C providing the strongest induction (7 fold). To confirm that the TLR-ligands are effective at stimulating inflammatory genes, expressions of *Ifnβ1*, *Il-6*, and *Tnf-α* were also examined (Figure 3.3C, D, E). The activation of TLR3 by Poly(I:C) is known to strongly elicit the production of interferon (Figure 3.3C) (Li et al., 2012), thus, I next examined whether treatments of interferon can directly induce *Ch25h* expression. Figure 3.3B shows that *Ch25h* is strongly induced in the presence of IFNγ or MCMV-C3X (14, 5 fold induction respectively) in wild type BMDM, whereas *Ch25h*$^{-/-}$ BMDM failed to elicit any responses.

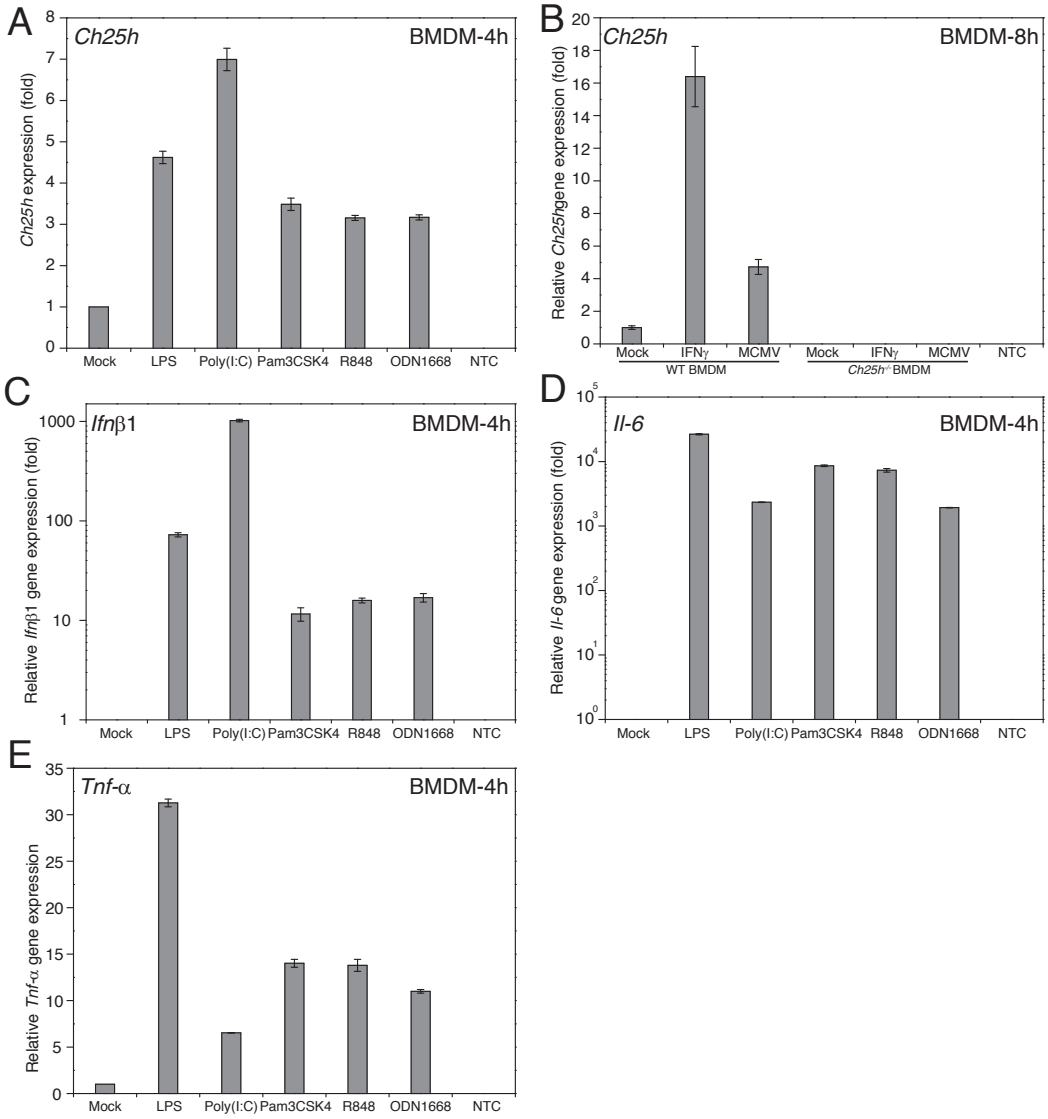

Figure 3.3 Expression of Ch25h is induced upon interferon, CMV, or TLR stimulations.
(A, C, D, and E) BMDM were seeded at a seeding density of $2.5x10^5$ in 24 well plates. The next day, cells were treated with PBS (vehicle), LPS (TLR4, 5ng/µl), Poly(I:C) (TLR3, 10µg/ml), Pam3CSk4 (TLR1/2, 100nM), R848 (TLR7/8, 100nM), or ODN1668 (TLR9, 100nM) for 4 hr. Relative abundance of *Ch25h*, *Ifnβ1*, *Il-6*, and *Tnf-α* were assayed by qPT-PCR using 30ng of RNA. n = 4; mean ± SEM. (B) Wild type or *Ch25h*$^{-/-}$ BMDM were seeded at a seeding density of $2x10^5$ cells/well in 24 well plates. The next day, cells were treated or infected with IFNγ (100 U/ml) or MCMV-C3X (MOI = 0.5) for 8 hr. Relative abundance of *Ch25h* was assayed by qRT-PCR using 30ng of RNA. n = 3; mean ± SEM.

3.2.2 Exogenous treatment of 25-HC has broad antiviral potency and is lipid condition dependent

As *Ch25h* is induced by interferon and CMV infection, it is possible that 25-HC might function as an antiviral mediator in the interferon regulated sterol metabolic network. To test this idea, I addressed whether physiologically relevant concentrations of 25-HC are capable of establishing an antiviral state (The human serum concentration of 25-HC was approximately ~12-15ng/ml (30-37nM) when volunteers were injected with LPS for 4 hr (Diczfalusy et al., 2009)). To determine the inhibitory concentrations (IC) of 25-HC, fibroblasts (NIH-3T3, pMEFs) and BHK-21 were first infected with MCMV-GFP or MHV-68-GFP, followed by administration of 25-HC in a dose-response manner. Figure 3.4(A and C) show that under the normal serum condition (lipid saturated), where the SREBP2 cycle is not involved, 25-HC has an IC_{50} of 1.83μM against MCMV and 0.32μM against MHV-68. Because the inhibitory effect is greater than the known level of 25-HC that is required to inhibit SREBP2 processing (100% SREBP2 inhibition is achieved in CHO using 2.5μM 25-HC (Radhakrishnan et al., 2008)), the antiviral effect of 25-HC is unlikely to involve the SREBP pathway.

Because cells grown under lipid-deficient conditions have an increased dependency on sterol biosynthesis (Sakai et al., 1998), it is likely that 25-HC may elicit a different response under delipidised media. As shown in Figure 3.4A, there is an increase in sensitivity of MCMV inhibition by 25-HC. Little IC_{50} changes were observed in MHV-68 infected BHK-21 (0.47μM VS. 0.32μM), highlighting the sensitivity differences between cell types to 25-HC. This sensitivity is reflected by the cell viability data, as oxysterols are known inducers of apoptosis (Perales et al., 2009; Spyridopoulos et al., 2001). BHK-21 is found to be more sensitive than pMEFs and NIH-3T3 fibroblasts to 25-HC (Figure 3.4B, D, F), resulting in a decrease in cell viability. Additional observations (on-going investigation) made in other cell types indicated that the threshold of cytotoxicity of 25-HC occurs at ≤3μM in BMDM (normal serum), ≤10μM (normal serum, ≤5μM delipidised) in MRC5 (see Figure S3.2). In this regard, the antiviral concentration of 25-HC is still below the toxic concentration (<70% cell viability).

To determine whether the results seen from the viral reporter assay are reflected on viral particle formation, pMEFs were infected with MCMV-C3X (MOI = 0.1) and treated with 25-HC. Supernatant from each day of the infection was collected and the viral titre was determined by plaque assay. Cells treated with increasing concentrations of 25-HC showed incremental decreases in viral titre (Figure 3.5A). In the delipidised condition, a pronounced inhibitory effect was observed between high (≥2.5μM) and low (<2.5μM) concentrations of 25-HC (Figure 3.5B). In addition, at 2.5μM of 25-HC, the inhibitory effect of 25-HC on the GFP reporter is (Figure 3.4A, ≈15% reduction), consistent with the slight reduction in viral particle formation (Vehicle: $7.9x10^6$ PFU/ml, 25-HC: $6.57x10^6$ PFU/ml, ≈16% reduction). Thus, these experiments show interesting evidence that the antiviral effect of 25-HC is depended on the lipid content of the culture media.

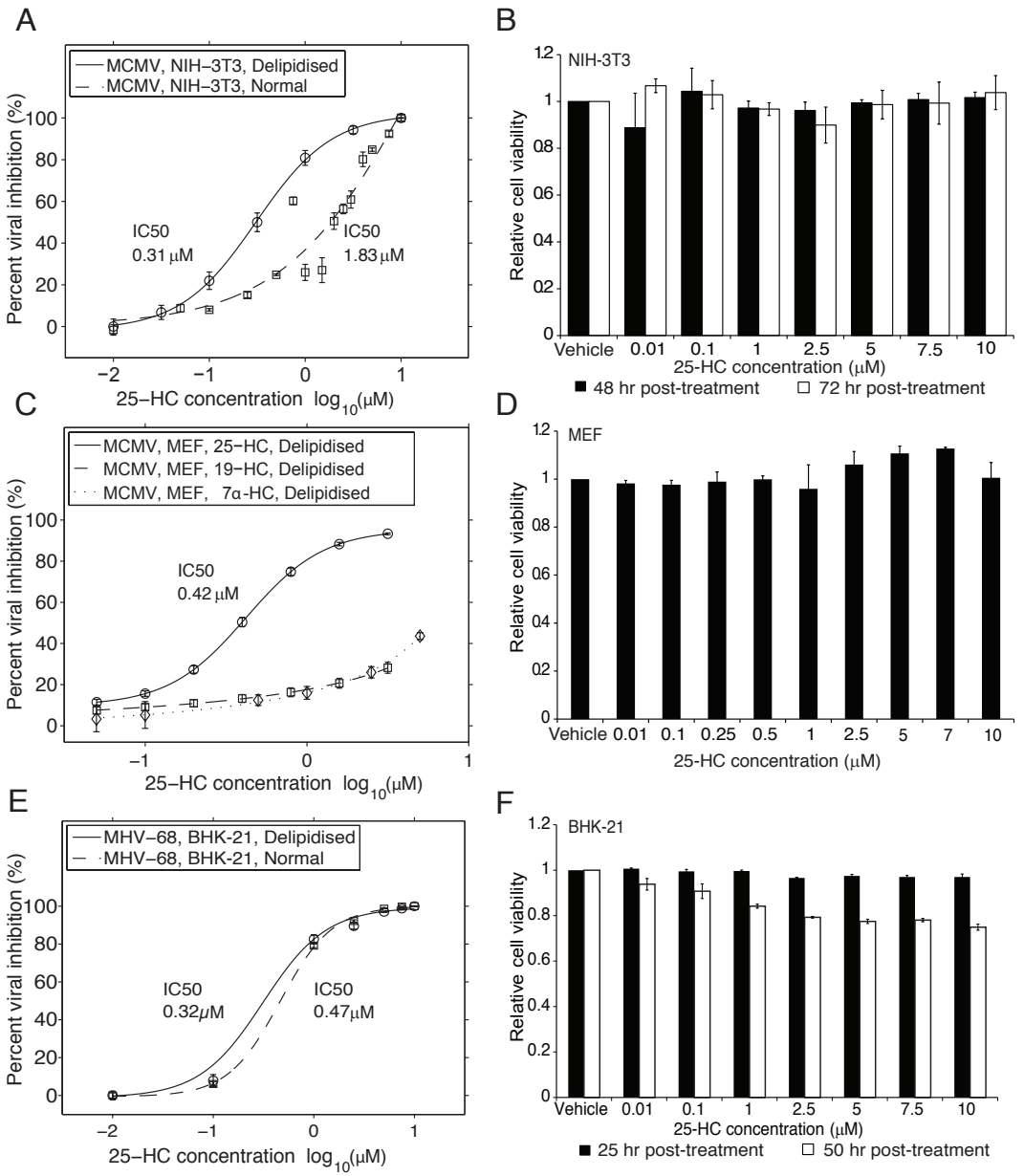

Figure 3.4 25-HC is antiviral at sub-micromolar concentrations without affecting cell viability. Virus replication was monitored (A, C, and E) as a function of kinetic GFP fluorescence. Description of the experimental parameters are detailed in Experimental procedure 7.3.4. Briefly, cells were seeded at a seeding density of $3x10^4$ cells/well in black 96 well plates. The next day, cells were infected with MCMV-GFP (MOI = 0.05). After adsorption, infection inoculum was remove and cells were cultured in normal or delipidised serum supplemented with media containing vehicle or 25-HC at increasing concentrations. Replication slopes over the linear phase were calculated and normalized to vehicle treated cells, and the mean replication slope from independent experiments calculated. Analysis of 25-HC effects on cell viability (B, D, and F). Cells were treated with 25-HC as indicated and viability analysed using the CellTiter-Blue assay as described in Experimental procedure 7.4.2. Data are: NIH-3T3 fibroblasts mean ± SEM for two experiments (8 replicates per experiment), pMEF mean ± SEM for 2 experiments (8 replicates per experiment), and BHK-21 mean ± SEM for two experiments (8 replicates per experiment).

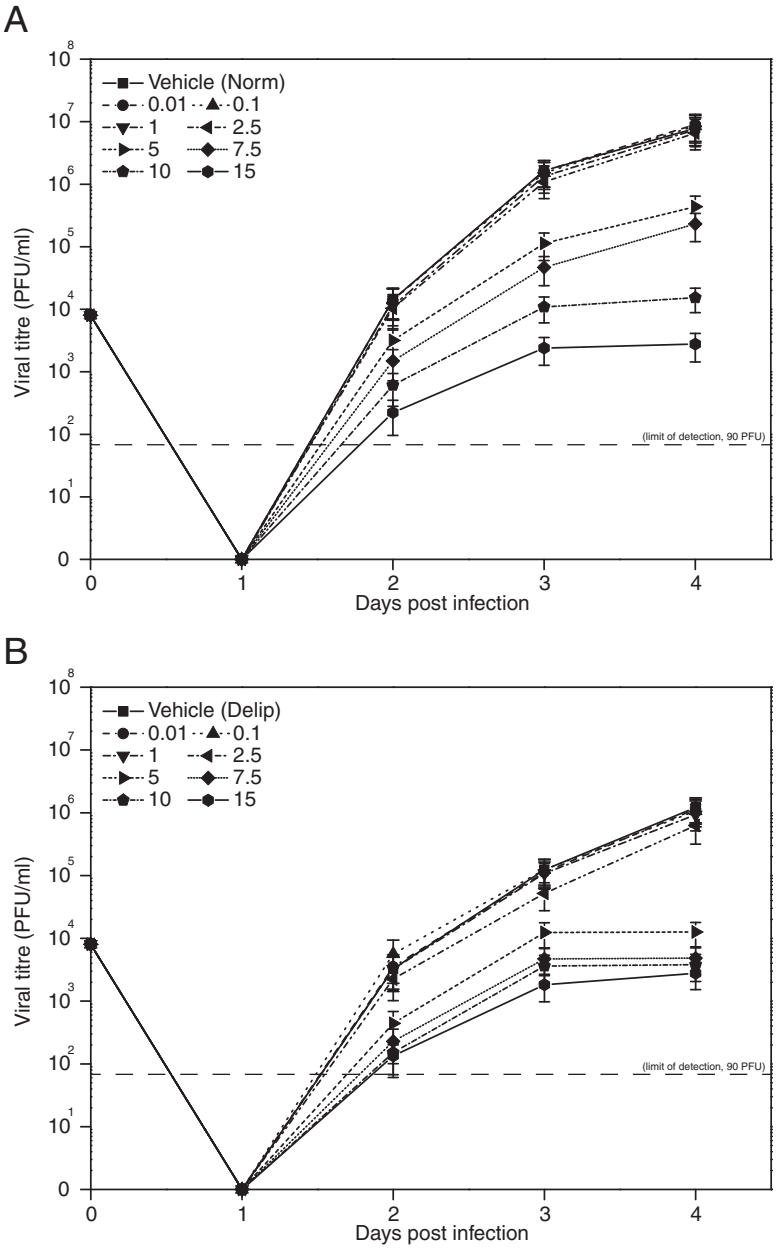

Figure 3.5 25-HC antiviral efficacy is lipid condition dependent.
pMEFs were seeded at a seeding density of $8x10^5$ cells/well in 6 well plates. The next day, cells were infected with MCMV-C3X (MOI = 0.1). After adsorption, cells were washed 5 times with blank medium (DMEM only). After washing, cells were cultured in (A) normal or (B) delipidised media containing vehicle or 25-HC at increasing concentrations (0.01, 0.1, 1, 2.5, 5, 7.5, 10, and 15μM). Supernatants were collected every day, and virus titre was quantitated by plaque assay. Data are the mean of 3 biological replicates ± SEM.

3.2.3 The antiviral effect of 25-HC is LXR independent

Supplementary studies (Blanc et al., 2013 and unpublished data) indicated that some oxysterols, such as 22(*R*)-hydroxycholesterol and 7α-hydroxycholesterol (Figure 3.4C), can elicit antiviral effects at high concentrations (5μM≥). This raises the possibility that activation of LXR by oxysterols contributes to the antiviral

effect of 25-HC. Activation of LXR by LXR agonists should confer similar antiviral effects of oxysterols. Prior studies have indicated that compounds GW3965 (EC_{50} = 125nM, (Repa, 2000a)) and T09011317 (EC_{50} = 50nM, (Leik et al., 2007)) are potent and selective agonists for both LXRα and LXRβ. To validate the potency of these two compounds at activating LXR, pMEFs were transfected with a LXR reporter system, followed by GW3965 or T0901317 stimulation. Figure 3.6A show that at 1μM, both GW3965 and T0901317 are sufficient at activating the LXR reporter system (≈3 fold induction). To directly test whether LXR activation is sufficient to develop an antiviral state, pMEFs were first infected with MCMV-C3X, followed by treatments with vehicle or the two potent synthetic ligands (1 and10μM). Extracellular viral titre was determined by plaque assay. Although the ligands are active in the reporter assay, they failed to elicit an antiviral effect (Figure 3.6B). It was, therefore, concluded that LXR activation does not contribute to 25-HC mediated antiviral effect in either normal or delipidised conditions.

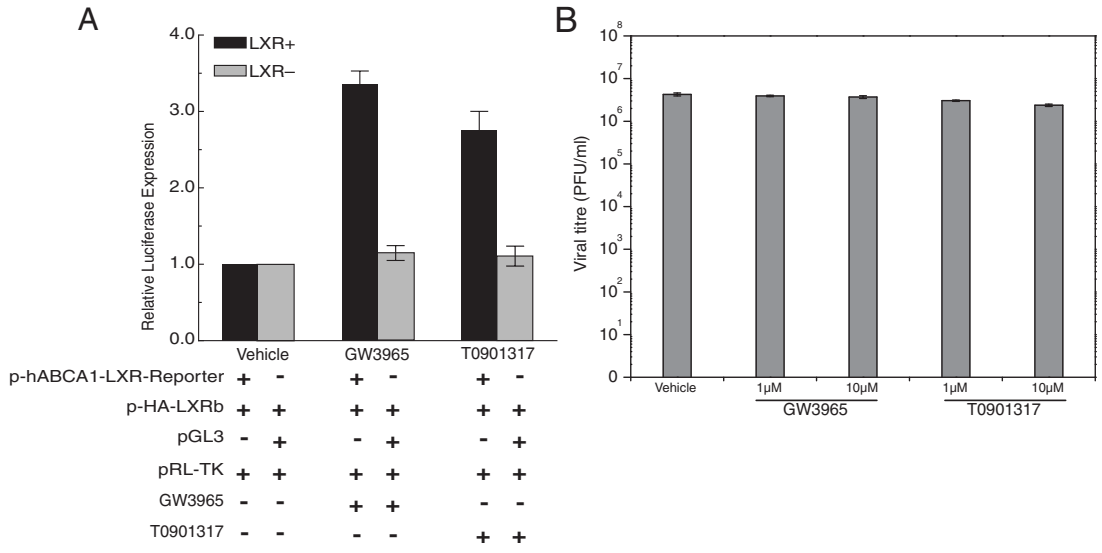

Figure 3.6 25-HC antiviral actions are LXR independent.
(A) pMEFs were seeded in 96 well plates at 1x10^4 cells/well. Next day, cells were transfected with 25ng of p-HA-LXRβ, 15ng of pRL-TK (Promega), 50ng of phABCA1-LXR-Reporter or pGL3 empty vector using jetPRIME transfection reagent (Polyplus, 114) according to manufacturer's protocol. 4 hr post transfection, transfection medium was replaced with fresh media. The next day, cells were stimulated with either vehicle or GW3965 (1μM) or T0901317 (1μM) for 18 hr. Cells were then lysed and Firefly reporter activity was assayed using the Luciferase Assay System (Promega, E1501) as described in Experimental procedure 7.4.3. For the transfection control, the Renilla reporter activity was assayed using coelenterazine as described in Experimental procedure 7.4.2. Data are normalized to negative control wells treated with vehicle alone and are the mean of three independent experiments ± SEM (6 replicates per experiment). (B) pMEFs were seeded in 6 well plates at 8x10^5 cells/well. The next day, cells were infected with MCMV-C3X (MOI = 0.1). After adsorption, cells were washed 5 times with normal medium. After washing, cells were cultured in normal medium containing vehicle or GW3965 (1/10μM) or T0901317 (1/10μM) as indicated. Four dpi supernatants were collected and virus titre was quantitated by plaque assay as described in Experimental procedure 7.3.2. Data are the mean of 2 biological replicates ± SEM.

3.2.4 25-HC antiviral action blocks post entry viral growth and is independent of cellular apoptosis

The dynamics of the lipid raft is an important determinant for the successful entry of many pathogens. Disruption of the cell membrane by removing intracellular cholesterol (using cyclodextrin including hydroxypropyl-β-cyclodextrin (HPβCD) or methyl-beta-cyclodextrin (MBCD)) has been shown to inhibit entry of *Mycobacterium tuberculosis* (Gatfield, 2000; Muñoz et al., 2009), hepatitis B virus (Bremer et al., 2009; Xie et al., 2012), and members of the *Leishmania* genus (De Cicco et al., 2012; Yao et al., 2013). Lipid mediators, such as oxysterols, can potentially alter membrane physiology through regulating sterol biosynthesis, blocking viral entry. To investigate at what stage in infection 25-HC blocks MCMV growth, NIH-3T3 fibroblasts were pretreated with two doses (0.5 and 10μM) of 25-HC for 24 hr, followed by MCMV-C3X infection. Results shown in Figure 3.7A indicate that the internalized MCMV genome (represented by MCMV late M115 gene) is unaffected by treatments of 25-HC. Furthermore, in the plaque reduction assay, the number of primary infectious foci (Figure 3.8B, quantified at 18 hpi) is equivalent in the presence or absence of 25-HC. These findings argue against viral entry as a primary mode of MCMV growth inhibition.

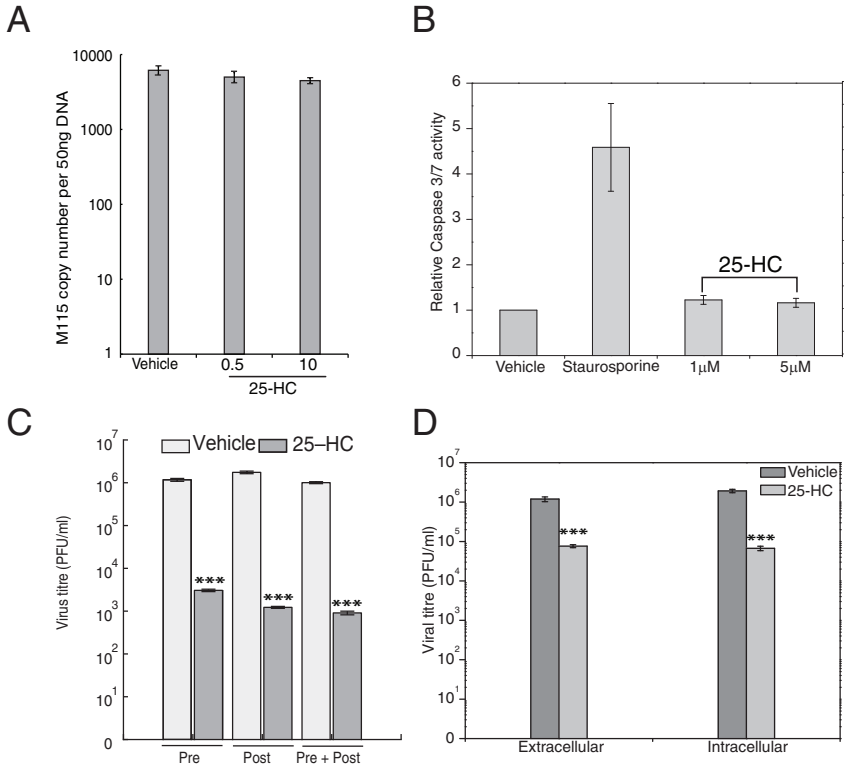

Figure 3.7 25-HC inhibits post-entry viral growth and does not induce cellular apoptosis.
(A) NIH-3T3 fibroblasts were seeded in 24 well plates at $1x10^5$ cells/well. The next day, cells were treated with 25-HC (0, 0.5 or 10μM) for 24 hr then infected with MCMV-C3X (MOI = 2). At 3 hpi, M115 copy number were determined by q-PCR. (B) NIH-3T3 fibroblasts were seeded in 96 well plates at $3x10^4$ cells/well. The next day, cells were treated with 25-HC (1 or 5μM) for 48 hr or 0.1μM staurosporine for 24 hr in normal media and the level of apoptosis was assessed. (C) pMEFs ($8x10^5$ cells/well in 6 wells) were treated with 25-HC (5μM) 24 hr prior to and/or after infection with MCMV-C3X (MOI = 2.5) in delipidised media as described in Experimental procedure. Extracellular viral titre were determined by plaque assay at 4 dpi. n = 4, with mean ± SEM. ***$p \leq 0.001$. (D) NIH-3T3 fibroblasts ($8x10^5$ cells/well, 6 well plate) were pre-treated with either vehicle or 25-HC (5μM) for 24 hr. Cells were then infected with MCMV (MOI = 2.5) for 1 hr and washed with blank media 5 times. Cells were then incubated in delipidised medium containing vehicle or 25-HC (5μM). Two dpi supernatants (extracellular virus) and intracellular virus were quantitated by plaque assay. n = 4, mean ± SEM. ***$p \leq 0.001$

Initial cell viability data (Figure 3.4B, D, F) indicates that some cell lines are more sensitive to 25-HC. 25-HC has been shown to promote apoptosis in macrophage-like cell-lines through the induction of cysteine-dependent aspartate-directed protease 3 (caspase 3) (Rusiñol et al., 2004). Activation of caspase 3 and 7 (also known as the effector caspase) by the initiator caspases (caspase 2, 8, 9 and 10) leads to the subsequent cleavage of other protein substrates, triggering apoptosis signalling cascade (Zmasek et al., 2007). Since the cell viability is a measurement of the oxidation state in mitochondria in a cell population (e.g. a single well), it does not specifically detect minor cell apoptosis. To directly test whether 25-HC induces apoptosis, NIH-3T3 fibroblasts were incubated with different doses of 25-HC, and the level of secreted caspase 3/7 (as indicators of apoptosis) were measured. Treatments of

25-HC at a high concentration (Figure 3.7B, 5μM, 48 hr) failed to significantly induce apoptosis in comparison with the positive control staurosporine (0.1μM, 24 hr). These results indicate that 25-HC induced apoptosis does not contribute to the inhibition of MCMV growth in NIH-3T3 fibroblasts. However, this data does not exclude the role of apoptosis in other cell-virus systems, especially in the case of macrophages and HFFs that are hypersensitive to oxysterols.

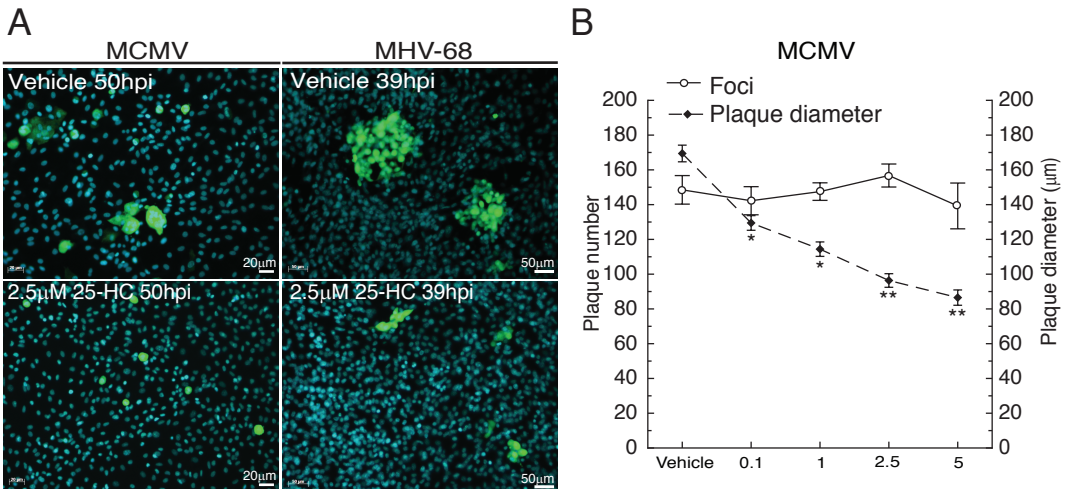

Figure 3.8 25-HC retards viral plaque formation.
(A) NIH-3T3 fibroblasts ($8x10^5$ cells/well, 6 well plate) were treated with and without 25-HC (2.5μM) and infected with MCMV-GFP (MOI = 0.01) or MHV-68 (MOI = 0.01). (B) $p53^{-/-}$ MEFs ($8x10^5$ cells/well, 6 well plate) were infected with MCMV-GFP (MOI = 0.001) and overlaid in normal medium containing 2.5% (w/v) agarose and 0.1, 1, 2.5, or 5μM 25-HC. Plaque diameter was measured at 3 dpi. Data are mean 170 and 220 plaques counted ± SEM (three biological replicates). *$p \leq 0.05$, **$p \leq 0.01$.

To further elucidate the antiviral effect of 25-HC, I then explored the association between treatment timing and viral replication using single-step growth analysis. Single-step growth analysis infects the cells with a high viral load (MOI = 2.5) to ensure comprehensive and syncretize infection. Figure 3.7C shows that 25-HC is able to achieve significant viral titre reduction when administered prior or post infection. Furthermore, intra and extracellular plaque forming unit (PFU) quantitation showed significant decrease in both intracellular (retained) and extracellular (secreted) viral titres (Figure 3.7D). In the plaque reduction assay, a significant dose-dependent difference in the diameter of the viral plaque was observed (Figure 3.8B). This finding is supported by fluorescent microscopy images showing the inhibition of MCMV and MHV-68 viral spread by 25-HC (Figure 3.8A). The above results further indicate multiple levels of antiviral mechanisms exerted by 25-HC.

3.2.5 The antiviral effect of 25-HC partially involves the mevalonate-isoprenoid pathway

As mentioned previously, the mevalonate branch of the sterol biosynthesis pathway leads to the production of several metabolites, notably, coenzyme Q, dolichols, squalene, and isoprenoids (farnesyl and geranylgeranyl). The isoprenoids are subsequently utilized in the process of protein prenylation. In the previous chapter, inhibition of HMG-CoA reductase by statin leads to the reduction of cholesterol intermediates, resulting in the accumulation of unprenylated RAP1A. Targeting the mevalonate-isoprenoid branch using gene specific siRNA showed an antiviral effect, indicating the importance of the mevalonate branch. 25-HC is known to downregulate cholesterol biosynthesis through the degradation of HMG-CoA reductase and to inhibit the activation of SREBP2 (Brown and Goldstein, 2009). To address whether 25-HC directly targets and suppresses the mevalonate pathway as its antiviral mechanism, MCMV-C3X infected pMEFs were treated with 25-HC in the presence or absence of four different sterol metabolites: mevalonolactone, geranylgeraniol, farnesyl and squalene. Supernatant was collected at 4 dpi and the viral titre was quantified by plaque assay. In these metabolic rescue experiments, only mevalonolactone and geranylgeraniol (Figure 3.9A) but not farnesol and squalene (Figure 3.9B) were able to reverse the effects of 25-HC. Notably, however, in the presence of saturating inhibitory concentrations of 25-HC (≥5μM), none of the metabolites could recover the effects of 25-HC.

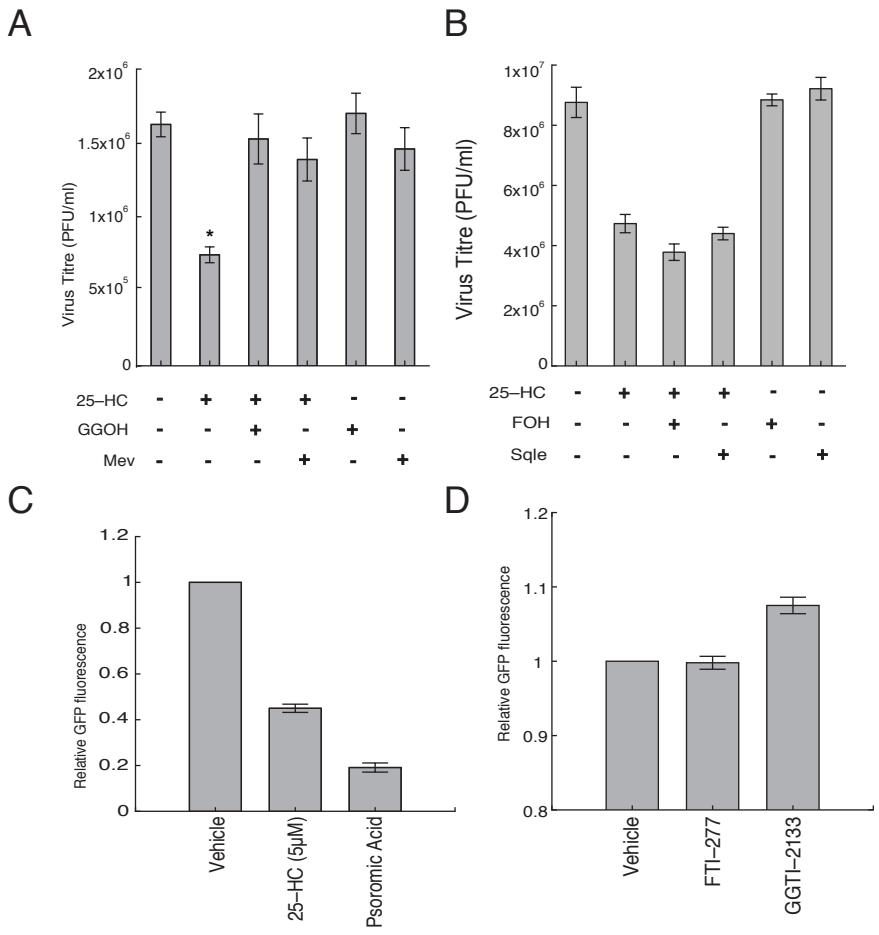

Figure 3.9 25-HC antiviral action partially involves the mevalonate branch.
pMEFs were seeded in 6 well plates at $8x10^5$ cells/well. The next day, cells were infected with MCMV (MOI = 0.1) for 1 hr, followed by 5 washes with blank media. After washing, cells were incubated with (A) 25-HC (1μM) and/or GGOH (20μM) or MEV (20μM) or (B) vehicle, 25-HC – (1μM), and/ or Farnesol (FOH – 20μM) or Squalene (Sqle – 20μM). MCMV titres (at 4 dpi) were determined by plaque assay. Data are mean of three independent experiments ± SEM. *$p \leq 0.05$. (C) pMEF ($3x10^4$ cells/well, 96 well plate) were pretreated with 25-HC (5μM) or psoromic acid (20μM) for 24 hr, infected with MCMV-GFP (MOI = 0.05), and then incubated with EMEM with the same concentrations of 25-HC or psoromic acid. Data are normalized to vehicle treated wells and are the mean of two independent experiments. (D) pMEFs ($3x10^4$ cells/well, 96 well plate) were pre-treated with vehicle, FTI-277 (10μM), or GGTI-2133 (10μM) for 24 hr, infected with MCMV-GFP (MOI = 0.05), and incubated with the same concentrations of FTI-277 or GGTI-2133 as prior to infection. Data are normalized to vehicle treated wells and are the mean of two independent experiments with three biological replicates (error bars represent range).

Data presented in Chapter 2 suggested that prenyltransferases involved in protein prenylation are important for viral replication. In particular, siRNA targeting type II prenyltranferase significantly inhibits MCMV growth. To further validate this finding, pMEFs were pre-treated with prenyltransferase inhibitors then infected with MCMV. As expected, inhibitors of GGTase I (GGTT-2133) or farnesyltransferases (FTI-277) failed to inhibit MCMV (Figure 3.9D), whereas psoromic acid (an inhibitor of GGTase II) (Deraeve et al., 2012) reduced viral growth (Figure 3.9C).

Altogether, these findings support that the blocking of the mevalonate-isoprenoid arm of the pathway by 25-HC partially contributes to MCMV growth inhibition.

3.2.6 Time dependent pre-treatment of 25-HC leads to MCMV immediate early gene suppression

The replication of MCMV is initiated through the transcription of immediate early gene products: *ie1* and *ie3* (*Ie1* and *Ie2* in HCMV). Deletion of MCMV *ie1* (Busche et al., 2009) or *ie3* (Angulo et al., 2000) leads to the attenuation or complete inhibition of viral growth, respectively. The above results show post-entry viral inhibition by 25-HC, implicating the possibility of viral gene transcription inhibition. Using a reporter virus (MCMV-ΔIE2GFP-Gluc), Figure 3.10A shows that cells pre-treated with 25-HC leads to a downregulation of the major immediate early promoter (MIEP) activity. The suppression of MIEP persists throughout the replication cycle of MCMV (4 hpi and 24 hpi). As expected, activation of LXR via LXR ligands failed to induce any inhibitory effects on the MIEP, reinforcing that 25-HC acts through a LXR independent mechanism. Furthermore, the inhibition of MIEP by 25-HC follows a dose dependent manner in both pMEFs (Figure 3.10B) and MΦ (Figure 3.10C), with greater sensitivity observed in macrophages (pMEF EC_{50}: 1.8μM, MΦ EC_{50}: 0.6μM). Surprisingly, *Ch25h*$^{-/-}$ macrophages fail to elicit significant inhibition of MIEP when pre-treated with the maximum tolerable doses of 25-HC (3μM, Figure S3.3). To determine the treatment time for 25-HC to exert inhibitory effects on the MIEP, MΦ were pre-treated with 25-HC (3μM) for various durations (2 hr – 24 hr), followed by MCMV infection. The half-maximum (50%) effective pretreatment time (ET_{50}) (Kropp et al., 2011) of 25-HC in MΦ is approximately 6 hr (Figure 3.10D).

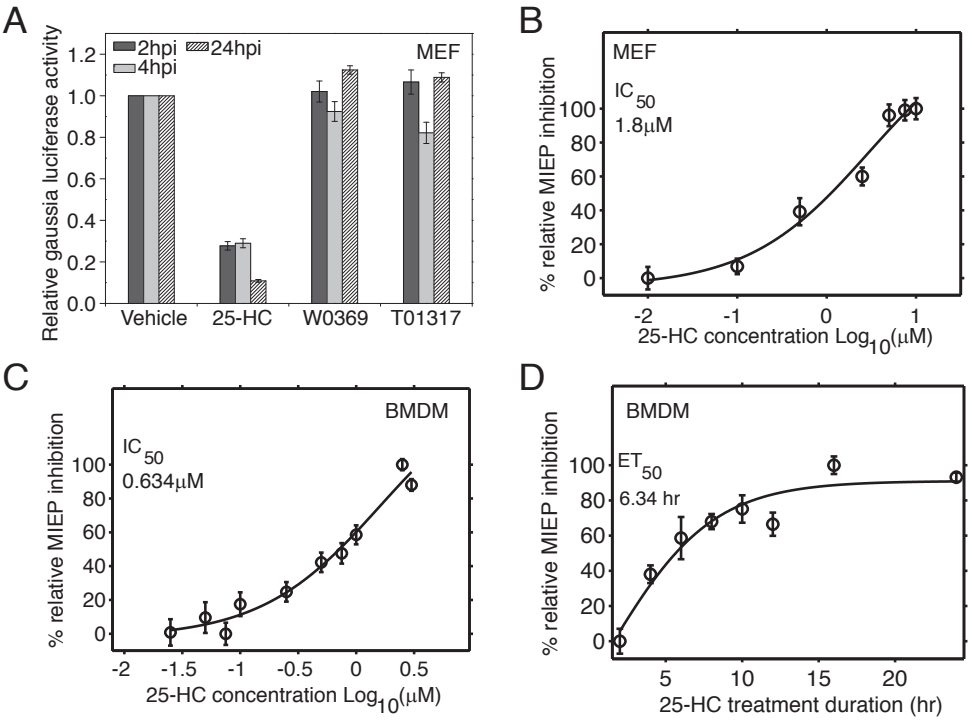

Figure 3.10 25-HC inhibits MCMV MIE expression and is treatment timing dependent but LXR independent.

(A) pMEFs (3x10^4 cells/well, 96 well plate) were pre-treated with vehicle, 25-HC (5μM), or LXR agonists (1μM) for 24 hr. Cells were then infected with Gluc-MCMV (MOI = 0.1) for 1 hr. After adsorption, cells were washed once with normal medium. After wash, 120μl of fresh medium containing GW3965 (1μM), T0901317 (1μM), or 25-HC (5μM) were added. Supernatant was collected at 2, 4, and 24 hpi. (B) pMEFs (3x10^4 cells/well, 96 well plate) or (C) BMDM (3x10^4 cells/well, 96 well plate) were pre-treated with vehicle or 25-HC at various concentrations for 24 hr. Cells were then infected with Gluc-MCMV (MOI = 0.1) for 1 hr. After adsorption, cells were washed once with normal medium. After wash, 120μl of fresh medium containing vehicle or 25-HC were added. Supernatant was collected at 4 hpi. (D) BMDM (3x10^4 cells/well, 96 well plate) were pre-treated with vehicle or 25-HC (3μM) for various durations. Cells were then infected with Gluc-MCMV (MOI = 0.1) for 1 hr. After adsorption, cells were washed once with normal medium. After wash, 120μl of fresh medium containing vehicle or 25-HC were added. Supernatant was collected at 4 hpi. Gluc activity was measured using the native form of the Gluc substrate coelenterazine as described in Experimental procedure 7.4.1. Data are normalized to negative control wells treated with vehicle alone. Data are the mean of three independent experiments ± SEM (8 replicates per experiment).

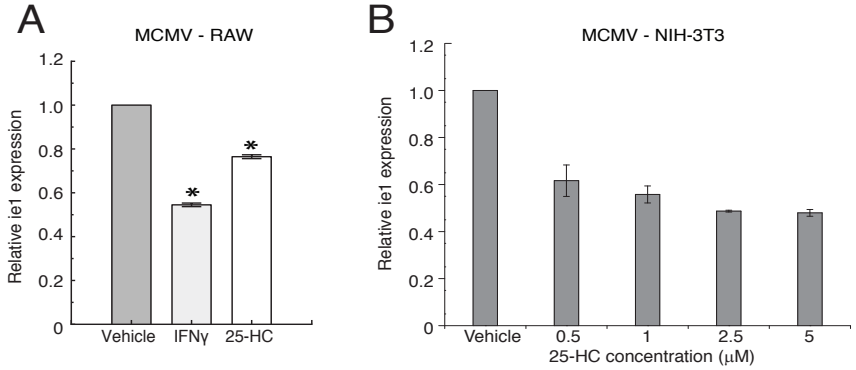

Figure 3.11 25-HC inhibits MCMV ie1 expression in macrophages and fibroblasts.

(A) RAW264.7 macrophages (2x10^5 cells/well, 24 well plate) were pre-treated with IFNγ (10 U/ml) or 25-HC (2μM) for 24 hr. Cells were then infected with MCMV-C3X (MOI = 2) for 1 hr. After adsorption, cells were washed once with medium and incubated in normal medium containing vehicle, IFNγ (10 U/ml) or 25-HC (2μM) for 24 hr. Relative abundance of the MCMV *ie1* assayed by qRT-PCR. n = 3; mean ± SEM. *p≤0.05. (B) NIH-3T3 fibroblasts (1x10^5 cells/well, 24 well plate) were pre-treated with vehicle or 25-HC for 24 hr. Cells were then infected with MCMV-C3X (MOI = 0.1) for 1 hr. After adsorption, cells were incubated in normal medium containing vehicle or 25-HC for 4 hr. Relative abundance of the MCMV *ie1* was assayed by qRT-PCR. n = 3; mean ± SEM.

3.2 Discussion

The data presented in this chapter provided functional characterizations of an interferon inducible oxysterol, known as 25-hydroxycholesterol. 25-HC has been demonstrated as a negative feedback mediator of the cholesterol biosynthesis pathway. The results presented in this chapter provide further evidence that it can mediate antiviral functions through multiple mechanisms. In addition to MCMV and MHV-68, 25-HC has been shown to inhibit HSV, VSV, influenza A (Blanc, Hsieh et al., 2013), HIV, Nipah virus (Liu et al., 2013), and HCV (Pezacki et al., 2009). Collectively, these studies bridge an emergent relationship between innate immunity and sterol metabolism.

3.3.1 Relationships between 25-HC and the SREBP2 pathway

The antiviral effect of 25-HC is shown to be media lipid condition dependent, linking the potential involvement of the SREBP2 processing pathway. In lipid replete conditions, where cells directly acquire cholesterol through uptake, the SREBP pathway activity is minimal. This is consistent with the finding that in NIH-3T3 fibroblasts, minimal cleavage of SREBP2 is observed when treated with 1% cyclodextrin (which rapidly removes intracellular cholesterol) in normal serum for 50 minutes (any prolonged incubation (≥50 min) leads to cell detachment and death). Thus, antiviral effects elicited by 25-HC in the normal serum conditions are likely to be SREBP2 independent. Conversely, the antiviral potency of 25-HC is increased under lipid-depleted conditions that favour SREBP2 processing. Under these conditions, cleavage of SREBP2 can be observed and subsequently inhibited with the addition of 25-HC (Radhakrishnan et al., 2008). Thus, the antiviral effects of 25-HC observed in the delipidised media are the summation of both SREBP dependent and independent mechanisms. This is evident in the viral growth curves showing a step wise dose response in the normal media (decrease in viral replication as the concentration of 25-HC increases), whereas an all-or-none response (non-significant to significant viral reduction) was observed in lipid-free conditions. Future study will be required to distinguish the contribution of the SREBP2 dependent

and independent pathways to 25-HC induced antiviral activity.

3.3.2 Physiological roles of 25-HC in in vivo

In addition to mechanistic studies described in this chapter, other studies have also been carried out using *Ch25h*$^{-/-}$ mice. My preliminary results indicated that *Ch25h*$^{-/-}$ BMDM produce a higher viral titre than the wild-type BMDM (MOI = 2). Furthermore, fluorescent imaging showed a higher percentage of *Ch25h*$^{-/-}$ BMDM expressing MCMV IE1 than the wild-type (26.32%±1.8 vs. 12.43%±1.74, 72 hpi, n = 5410) (manuscript under preparation). Additional observations made by collaborators showed that infection in *Ch25h*$^{-/-}$ mice with MHV-68 leads to significant increase in viral replication (Liu et al., 2013). These findings indicate that *Ch25h*$^{-/-}$ mice are more susceptible to viral infection.

Interestingly, the work by Mcdonald and Russell, 2010 revealed that *Ch25h* genetic knockout (*Ch25h*$^{-/-}$) mice showed no marked differences in fatty acid and cholesterol metabolism, suggesting 25-HC might play a minor role in *in vivo* cholesterol homeostasis. Apart from SREBP2, cholesterol homeostasis is also maintained through LXR. LXRα and -β are ligand activated transcription factors that can increase SREBP1c levels for fatty acid synthesis and cholesterol storage through cholesterol esterification (Repa, 2000b). However, 25-HC has been shown as a relatively weak LXR activator (Janowski et al., 1996) in comparison with other oxysterols, such as 22(*R*)-hydroxycholesterol, 24(*S*)-hydroxycholesterol, and 24(*S*),25-epoxycholesterol (Janowski et al., 1999). In the LXR experiments, LXR agonists showed no effect on viral replication. Collectively, the antiviral effect of 25-HC is LXR independent.

3.3.3 Potential binding targets of 25-HC

One of previously described binding targets of 25-HC is INSIG-1 (see 3.1 Introduction) (Adams et al., 2004). Binding of 25-HC to INSIG-1 inhibits the translocation of SCAP-SREBP2 complex, resulting in the transcriptional silencing of the sterol biosynthesis pathway and a decrease in the production of cholesterol and isoprenoids. Furthermore, 25-HC also mediates the degradation of HMGCR through INSIG-1 (Sever et al., 2003). This will further reduce the activity of the pathway. The pathway response to 25-HC will be further examined in the next chapter.

Another potential binding targets of 25-HC are the oxysterol binding proteins (OSBPs). OSBPs have been shown as intracellular receptors for cholesterol and oxysterols (Kandutsch and Elaine, 1981). Binding of sterols to OSBPs lead to alterations in lipid metabolism, regulation of vesicle transport, and cell signalling events. To date, 12 OSBPs have been identified, with different affinities to cholesterol and oxysterols (Kandutsch et al., 1984; Lehto and Olkkonen, 2003). Currently, the association between the effects of 25-HC and OSBPs have yet to be investigated. However, several reports and our oxysterol screening have suggested several possible 25-HC interacting targets:

1. Cells photo-cross-linking with [^{3}H]photo-25-HC or [^{3}H]photo-cholesterol have demonstrated that ORP1, ORP3, ORP5, ORP6, ORP7, ORP8, ORP10 and ORP11 have 25-HC binding capabilities, while ORP1, ORP3, ORP5 and ORP8 can cross-link with photo cholesterol (Suchanek et al., 2007).

2. ORP1 has a very strong affinity to both cholesterol and 25-HC. However, statin metabolic rescue experiments have shown that the addition of cholesterol has no effect on viral replication (Blanc et al., 2011). In addition, treatments with 22(*R*)-HC, which also strongly binds to ORP1, showed no antiviral effects (unpublished results). These results suggest ORP1 is an unlikely target.

3. Among the 8 OSBPs selected, MΦ microarray data show that ORP6 and ORP7 are expressed at very low levels (probe intensity ≤300-400 vs. *Hmgcr* ≥2000), while ORP5 and 10 are not expressed. In addition, ORP6 and ORP7 have been shown to

have relatively weak 25-HC binding affinities. This characteristic effectively removes these OSBPs' associations with macrophage's hypersensitivity to 25-HC.

The remaining 3 OSBPs, -3 (probe intensity: 500-1000), -8 (probe intensity: 4000-6000), and -11 (probe intensity: 2500-4000) have been shown to play roles in cholesterol transport (Yan et al., 2013), cell migration (Lehto et al., 2008), and cell morphology alterations (Zhou et al., 2012). Future characterization of these OSBPs is necessary to determine their roles in 25-HC mediated sterol-immune responses. The importance of these OSBPs will be examined in future studies.

3.3.4 Potential 25-HC antiviral mechanisms

In regards to the antiviral mechanisms, viral transcript analysis revealed that MCMV *ie1* is suppressed in the presence of 25-HC. Similar results were also obtained using a reporter virus (MCMV-Gluc). Likewise, treatments of BAM25 [which constitutively express MCMV ie transcripts (Gober et al., 2003; Wang et al., 2011)] with 25-HC showed a ≈30% reduction in ie1 expression (2.5μM, 72 hr, Figure S3.1). In Chapter 2, it was shown that lipophilic statins could inhibit the activity of MIE (Figure 2.9). Given the role of statin and 25-HC in modulating sterol biosynthesis, these findings argue that 25-HC and statin can impede viral gene transcriptions through a sterol dependent mechanism. This hypothesis is consistent with observations that HCMV promotes the activation of SREBP1 and -2, while delaying the degradation of these two transcription factors (Spencer et al., 2011; Yu et al., 2012). However, the accumulation of SREBP has not been associated with the activation of MIE. It should also be noted that promoter binding site analysis of MCMV MIE identified no SREBP binding sites, indicating that SREBPs could not activate the promoter through direct binding. Thus, it is possible that rather than SREBP, other sterol metabolites might participate in the activation of MIE through direct or indirect interactions.

Alternatively, the inhibition of CMV MIE by 25-HC could also involve a sterol independent mechanism. The ET_{50} of 25-HC (6.3 hr, Figure 3.10D) revealed that a finite pre-treatment time is required for the molecule to inhibit the viral enhancer. This suggests that the anti-CMV MIE effects of 25-HC does not depend on direct

binding-inhibition of the transcription start site (e.g. a repressor), but rather it involves transcriptional activation of antiviral host factors. Although studies have identified host factors, such as Daxx (Benzaïd et al., 2012; Castella et al., 2011; Roelofs et al., 2009) and PML-body (Goto et al., 2013) that can inhibit HCMV *Ie* expressions, little is known for MCMV. Further global transcriptional profiling of cells treated with 25-HC is required to identify these host factors.

The genome copy experiments suggest that the antiviral effects of 25-HC occur predominately post-entry. This result was complemented by the plaque reduction assay (Figure 3.8), showing that the number of initial infected foci remained relatively unchanged regardless of the treatment, while the expansion of the plaque was significantly deterred in 25-HC treated cells. These data suggest that in addition to MIE inhibition, 25-HC could also block viral egress. Though, experiments using VSV and HIV have shown that 25-HC can also affect the fusion process involving the viral and cellular membrane (Li and Dong, 2009; van der Vliet and Verheul, 2012). Additional experiments are needed to address 25-HC mediated viral diffusion and gene transcription inhibitions.

3.3.5 Pro- and anti-inflammatory effects of 25-HC

As demonstrated in this chapter, 25-HC elicits significant inhibition against both MCMV and HCMV. The antiviral effect of 25-HC is partially due to the inhibition of the SREBP2 cycle, leading to the downregulation of the sterol biosynthesis pathway and the synthesis of isoprenoids. Likewise, 25-HC also inhibits CMV immediate early enhancer promoter (MIEP) activity, causing transcription silencing of MCMV immediate early genes. Since the publication of this work, several recent studies have highlighted the additional roles of 25-HC as a key mediator in regulating pro- and anti-inflammatory responses.

The work of Shibata et al., 2013 first showed that treatment with 25-HC alters cholesterol ester and sphingolipid formation in BMDM. Notably, 25-HC elicits significant accumulation of several cholesterol esters, while suppressing cholesterol synthesis. Importantly, gene expression analysis revealed that 25-HC activates integrated stress response (ISR) genes, including *Atf4*, *Chop/Ddit3*, *Chac1*, *Trib3*, and asparagine synthetase (*Asns*). The activation of these ISR signals lead to the phosphorylation of eIF2α via the kinase of GCN2. This causes the attenuation of protein translation. These results suggest that in addition to the antiviral effect, 25-HC also modulates the reprograming of macrophages, through both transcription and translation mechanisms. This concept is illustrated in Figure 6.2**E** as a part of the overall summary figure of this thesis.

A more recent study by Gold et al., 2014 showed that 25-HC can also act as a pro-inflammatory signalling amplifier. Microarray analysis between poly(I:C) stimulated WT and *Ch25h*$^{-/-}$ BMDM revealed that several important inflammatory mediators, including interleukin 6 (*Il6*), colony stimulating factor 1 (*Csf1*), and nitric oxide synthase 2 (*Nos2*), were differentially downregulated in *Ch25h*$^{-/-}$ BMDM. This downregulation can be reversed with the addition of exogenous 25-HC, suggesting that 25-HC is required for the activation of these inflammatory genes. Further CHIP analysis showed that in the WT BMDM, there is an enrichment of members of the AP-1 transcription factor family (FOS and JUN) on the promoter of Csf1 and Il6. However, this enrichment was abolished in the *Ch25h*$^{-/-}$ BMDM. Surprisingly, WT *Ch25h* mice showed increasing

morbidity following Influenza H1N1 and H3N2 challenge in comparison with the knockout mice. This effect was due to significant elevation in pro-inflammatory cytokines (IL-6, MCSF, IFNA14, and TNF), causing pronounced tissue lesions and damage in the lung.

In contrast with the two previous studies, the work of Reboldi et al., 2014 proposed a SREBP2 dependent anti-inflammatory role of 25-HC. Following LPS injection, *Ch25h*$^{-/-}$ mice exhibited an increase in the proportion of IL-17A–producing T cells (TH17), a key mediator in the secretion of pro-inflammatory cytokines, IL-1β, IL-23, and IL-6. Subsequent in vitro studies using LPS stimulated BMDM showed that *Ch25h*$^{-/-}$ macrophages had a significant increase in both synthesis (transcription) and secretion of IL-1β in comparison to the WT. Notably, inflammasome-activated protease Caspase-1 that is responsible for the cleavage of pro–IL-1β into IL-1β was also significantly elevated in the *Ch25h*$^{-/-}$ BMDM. This heightened Caspase1 and IL-1β response can be reversed with the addition of 25-HC, suggesting that the inhibition of SREBP2 by 25-HC dampens the inflammatory response. Likewise, *Ch25h*-deficient mice were more resistant to the bacterium Listeria Monocytogenes infection. The authors attribute this resistance to the ample proliferation of IL-17A^{+} T cells and neutrophils, and the excess secretion of IL-1β. However, it was also shown that *Ch25h*-deficient mice display increasing susceptibility to septic shock, and experimental allergic encephalomyelitis (EAE, a model for brain inflammation). Interestingly, different from Gold et al., 2014, Reboldi et al., 2014 showed that stimulation of *Ch25h*$^{-/-}$ BMDM with LPS did not enhance the expression of Il-6. However, it has been shown that LPS (a TLR4 ligand) stimulation could lead to more robust activation of IRF3 and NF-κB than poly(I:C) (a TLR3 ligand) in human macrophages (Reimer et al., 2008). Thus, it is likely that depending on the immune activation pathway, 25-HC is likely to participate in amplifying or damping certain inflammatory signalling, resulting in differential cytokine responses. Furthermore, in contrast with the antiviral effect of 25-HC, the above two studies also demonstrated that 25-HC can exert other tissue specific effects, resulting in unpredictable responses to pathogen challenges. The dual effects of 25-HC in mediating various pathogen

challenges should be carefully evaluated through future studies.

In summary, results presented in this chapter demonstrate a previously uncharacterized biological role of 25-HC as an interferon induced antiviral lipid mediator. This also highlights potential antiviral roles of other oxysterols and, importantly, the dependency of viral replication on the host sterol metabolic network.

3.4 References

Ačimovič, J., and Rozman, D. (2013). Steroidal triterpenes of cholesterol synthesis. Molecules 18, 4002–4017.

Ahrens, E.H., and Kunkel, H.G. (1949). The relationship between serum lipids and skin xanthomata in 18 patients with primary biliary cirrhosis. J. Clin. Invest. 28, 1565–1574.

Allison, a C. (1999). Squalene and squalane emulsions as adjuvants. Methods 19, 87–93.

Amemiya-Kudo, M., Shimano, H., Hasty, A.H., Yahagi, N., Yoshikawa, T., Matsuzaka, T., Okazaki, H., Tamura, Y., Iizuka, Y., Ohashi, K., et al. (2002). Transcriptional activities of nuclear SREBP-1a, -1c, and -2 to different target promoters of lipogenic and cholesterogenic genes. J Lipid Res 43, 1220–1235.

Benzaïd, I., Mönkkönen, H., Bonnelye, E., Mönkkönen, J., and Clézardin, P. (2012). In vivo phosphoantigen levels in bisphosphonate-treated human breast tumors trigger Vγ9Vδ2 T-cell antitumor cytotoxicity through ICAM-1 engagement. Clin. Cancer Res. 18, 6249–6259.

Bhaijee, F., Subramony, C., Tang, S.J., and Pepper, D.J. (2011). Human immunodeficiency virus-associated gastrointestinal disease: common endoscopic biopsy diagnoses. Patholog. Res. Int. 2011, 247923.

Bloch, K. (1965). The biological synthesis of cholesterol. Science 150, 19–28.

Bordier, B.B., Ohkanda, J., Liu, P., Lee, S., Salazar, F.H., Marion, P.L., Ohashi, K., Meuse, L., Kay, M.A., Casey, J.L., et al. (2003). In vivo antiviral efficacy of prenylation inhibitors. Pharmacia 112, 407–414.

Borrie, P. (1957). Essential hyperlipaemia and idiopathic hypercholesterolaemic xanthomatosis. Br. Med. J. 2, 911–915.

Briner, W.W., Riddle, J.W., and Cornwell, D.G. (1959). Studies on the immunochemistry of human low density lipoproteins utilizing an hemagglutination technique. J. Exp. Med. 110, 113–122.

Brown, M.S., and Goldstein, J.L. (1974). Familial hypercholesterolemia: defective binding of lipoproteins to cultured fibroblasts associated with impaired regulation of 3-hydroxy-3-methylglutaryl coenzyme A reductase activity. Proc. Natl. Acad. Sci. U. S. A. 71, 788–792.

Brown, M.S., and Goldstein, J.L. (1976). Analysis of a mutant strain of human fibroblasts with a defect in the internalization of receptor-bound low density lipoprotein. Cell 9, 663–674.

Brown, M.S., Dana, S.E., and Goldstein, J.L. (1973). Regulation of 3-hydroxy-3-methylglutaryl coenzyme A reductase activity in human fibroblasts by lipoproteins. Proc. Natl. Acad. Sci. U. S. A. 70, 2162–2166.

Carlson, B.C., Jansson, a M., Larsson, a, Bucht, a, and Lorentzen, J.C. (2000). The endogenous adjuvant squalene can induce a chronic T-cell-mediated arthritis in rats. Am. J. Pathol. 156, 2057–2065.

Castella, B., Riganti, C., Fiore, F., Pantaleoni, F., Canepari, M.E., Peola, S., Foglietta, M., Palumbo, A., Bosia, A., Coscia, M., et al. (2011). Immune modulation by zoledronic acid in human myeloma: an advantageous cross-talk between Vγ9Vδ2 T cells, αβ CD8+ T cells, regulatory T cells, and dendritic cells. J. Immunol. 187, 1578–1590.

Chawla, a, Boisvert, W. a, Lee, C.H., Laffitte, B. a, Barak, Y., Joseph, S.B., Liao, D., Nagy, L., Edwards, P. a, Curtiss, L.K., et al. (2001). A PPAR gamma-LXR-ABCA1 pathway in macrophages is involved in cholesterol efflux and atherogenesis. Mol. Cell 7, 161–171.

Curtiss, L.K., and Edgington, T.S. (1976). Regulatory serum lipoproteins: regulation of lymphocyte stimulation by a species of low density lipoprotein. J. Immunol. 116, 1452–1458.

Cuthbert, J.A., and Lipsky, P.E. (1984). Immunoregulation by low density lipoproteins in man. Inhibition of mitogen-induced T lymphocyte proliferation by interference with transferrin metabolism. J. Clin. Invest. 73, 992–1003.

Dar, A.A., Patil, R.S., and Chiplunkar, S.V. (2014). Insights into the Relationship between Toll Like Receptors and Gamma Delta T Cell Responses. Front. Immunol. 5, 366.

Dawson, P. a, Hofmann, S.L., van der Westhuyzen, D.R., Südhof, T.C., Brown, M.S., and Goldstein, J.L. (1988). Sterol-dependent repression of low density lipoprotein receptor promoter mediated by 16-base pair sequence adjacent to binding site for transcription factor Sp1. J. Biol. Chem. 263, 3372–3379.

DeBose-Boyd, R., Brown, M., and Li, W. (1999). Transport-dependent proteolysis of SREBP: relocation of site-1 protease from Golgi to ER obviates the need for SREBP transport to Golgi. Cell 99, 703–712.

DeBose-Boyd, R. a, Ou, J., Goldstein, J.L., and Brown, M.S. (2001). Expression of sterol regulatory element-binding protein 1c (SREBP-1c) mRNA in rat hepatoma cells requires endogenous LXR ligands. Proc. Natl. Acad. Sci. U. S. A. 98, 1477–1482.

Dobrosotskaya, I.Y., Goldstein, J.L., Brown, M.S., and Rawson, R.B. (2003). Reconstitution of sterol-regulated endoplasmic reticulum-to-Golgi transport of SREBP-2 in insect cells by co-expression of mammalian SCAP and Insigs. J Biol Chem 278, 35837–35843.

De Jong, A., Cheng, T.-Y., Huang, S., Gras, S., Birkinshaw, R.W., Kasmar, A.G., Van Rhijn, I., Peña-Cruz, V., Ruan, D.T., Altman, J.D., et al. (2014). CD1a-autoreactive T cells recognize natural skin oils that function as headless antigens. Nat. Immunol. 15, 177–185.

Drevot, P., Langlet, C., Guo, X.-J., Bernard, A.-M., Colard, O., Chauvin, J.-P., Lasserre, R., and He, H.-T. (2002). TCR signal initiation machinery is pre-assembled and activated in a subset of membrane rafts. EMBO J. 21, 1899–1908.

Fernández, C., Martín, M., Gómez-Coronado, D., and Lasunción, M. a (2005). Effects of distal cholesterol biosynthesis inhibitors on cell proliferation and cell cycle progression. J. Lipid Res. 46, 920–929.

Ferruelo, A.J., Sua, Y., Ferna, C., and Mart, J. (2001). Dose-dependent e ¡ ects of lovastatin on cell cycle progression . Distinct requirement of cholesterol and non-sterol mevalonate derivatives. 1532, 185–194.

Gee, D., Goldstein, J., Gray, C., and Fowler, J. (1959). Biosynthesis of cholesterol in familial hypercholesterolaemic xanthomatosis. Br. Med. J. 2, 341–344.

Gelissen, I.C., Harris, M., Rye, K.-A., Quinn, C., Brown, A.J., Kockx, M., Cartland, S., Packianathan, M., Kritharides, L., and Jessup, W. (2006). ABCA1 and ABCG1 synergize to mediate cholesterol export to apoA-I. Arterioscler. Thromb. Vasc. Biol. 26, 534–540.

Gober, H.-J., Kistowska, M., Angman, L., Jenö, P., Mori, L., and De Libero, G. (2003). Human T cell receptor gammadelta cells recognize endogenous mevalonate metabolites in tumor cells. J. Exp. Med. 197, 163–168.

Gogoi, D., and Chiplunkar, S. V (2013). Targeting gamma delta T cells for cancer immunotherapy: bench to bedside. Indian J. Med. Res. 138, 755–761.

Goto, H., Matsuda, K., Srikoon, P., Kariya, R., Hattori, S., Taura, M., Katano, H., and Okada, S. (2013). Potent antitumor activity of zoledronic acid-induced Vγ9Vδ2 T cells against primary effusion lymphoma. Cancer Lett. 3.

Hayden, J.M., Brachova, L., Higgins, K., Obermiller, L., Sevanian, A., Khandrika, S., and Reaven, P.D. (2002). Induction of monocyte differentiation and foam cell formation in vitro by 7-ketocholesterol. J. Lipid Res. 43, 26–35.

Holstein, T.J., Fish, W. a, and Stokes, W.M. (1966). Pathway of cholesterol biosynthesis in the brain of the neonatal rat. J. Lipid Res. 7, 634–638.

Inoue, J., Sato, R., Kawabe, Y., Kodama, T., Takano, T., and Maeda, M. (1996). Sterol-dependent Transcriptional Regulation of Sterol Regulatory Element-binding Protein-2. J. Biol. Chem. 271, 26461–26464.

Janowski, B.A. (2002). The hypocholesterolemic agent LY295427 up-regulates INSIG-1, identifying the INSIG-1 protein as a mediator of cholesterol homeostasis through SREBP. Proc Natl Acad Sci U S A 99, 12675–12680.

Janowski, B. a, Grogan, M.J., Jones, S. a, Wisely, G.B., Kliewer, S. a, Corey, E.J., and Mangelsdorf, D.J. (1999). Structural requirements of ligands for the oxysterol liver X receptors LXRalpha and LXRbeta. Proc. Natl. Acad. Sci. U. S. A. 96, 266–271.

Janowski, B.A., Willy, P.J., Devi, T.R., Falck, J.R., and Mangelsdorf, D.J. (1996). An oxysterol signalling pathway mediated by the nuclear receptor LXR alpha. Nature 383, 728–731.

Johnston, J.D., and Bloch, K. (1957). In Vitro Conversion of Zymosterol and Dihydrozymosterol to Cholesterol. J. Am. Chem. Soc. 79, 1145–1149.

Kabouridis, P.S., Janzen, J., Magee, a L., and Ley, S.C. (2000). Cholesterol depletion disrupts lipid rafts and modulates the activity of multiple signaling pathways in T lymphocytes. Eur. J. Immunol. 30, 954–963.

Kamei, Y., Miura, S., Suganami, T., Akaike, F., Kanai, S., Sugita, S., Katsumata, A., Aburatani, H., Unterman, T.G., Ezaki, O., et al. (2008). Regulation of SREBP1c gene expression in skeletal muscle: role of retinoid X receptor/liver X receptor and forkhead-O1 transcription factor. Endocrinology 149, 2293–2305.

Kandutsch, A.A., and Russell, A.E. (1959). Preputial gland tumor sterols. I. The occurrence of 24,25-dihydrolanosterol and a comparison with liver and the normal gland. J. Biol. Chem. 234, 2037–2042.

Kandutsch, A.A., and Russell, A.E. (1960a). Preputial gland tumor sterols. 2. The identification of 4 alpha-methyl-Delta 8-cholesten-3 beta-ol. J. Biol. Chem. 235, 2253–2255.

Kandutsch, A.A., and Russell, A.E. (1960b). Preputial gland tumor sterols. 3. A metabolic pathway from lanosterol to cholesterol. J. Biol. Chem. 235, 2256–2261.

Kindt, Thomas J, Richard A. Goldsby, Barbara A. Osborne, and J.K. (2007). Kuby immunology (New York: W.H. Freeman).

Kipp, H.A. (1920). Variation in the cholesterol content of the serum in pneumonia.

Knight, B.L., Patel, D.D., and Soutar, a K. (1983). The regulation of 3-hydroxy-3-methylglutaryl-CoA reductase activity, cholesterol esterification and the expression of low-density lipoprotein receptors in cultured monocyte-derived macrophages. Biochem. J. 210, 523–532.

Langdon, R.G., and BLOCH, K. (1953). The utilization of squalene in the biosynthesis of cholesterol. J. Biol. Chem. 200, 135–144.

Lees, R.S., Fiser, R.H., Beisel, W.R., and Bartelloni, P.J. (1972). Effects of an experimental viral infection on plasma lipid and lipoprotein metabolism. Metabolism. 21, 825–833.

Li, L.N., and Dong, P.W. (2009). Endocrine therapy plus zoledronic acid in premenopausal breast cancer. N. Engl. J. Med. 360, 2368; author reply 2369–2370.

Li, G., Gu, H.-M., and Zhang, D.-W. (2013). ATP-binding cassette transporters and cholesterol translocation. IUBMB Life 65, 505–512.

Ly, D., and Moody, D.B. (2014). The CD1 size problem: lipid antigens, ligands, and scaffolds. Cell. Mol. Life Sci. 71, 3069–3079.

Mathews, J.D., and Feery, B.J. (1978). Cholesterol and immune response to influenza antigens. Lancet 2, 1212–1213.

Matsuda, M., Korn, B.S., Hammer, R.E., Moon, Y. a, Komuro, R., Horton, J.D., Goldstein, J.L., Brown, M.S., and Shimomura, I. (2001). SREBP cleavage-activating protein (SCAP) is required for increased lipid synthesis in liver induced by cholesterol deprivation and insulin elevation. Genes Dev. 15, 1206–1216.

Mcdonald, J.G., and Russell, D.W. (2010). life in immunology. 1071–1072.

McGeoch, D.J., Cook, S., Dolan, A., Jamieson, F.E., and Telford, E.A. (1995). Molecular phylogeny and evolutionary timescale for the family of mammalian herpesviruses. J Mol Biol 247, 443–458.

Nestel, P.J., Whyte, H.M., and Goodman, D.S. (1969). Distribution and turnover of cholesterol in humans. J. Clin. Invest. 48, 982–991.

Nolan, T., Bravo, L., Ceballos, A., Mitha, E., Gray, G., Quiambao, B., Patel, S.S., Bizjajeva, S., Bock, H., Nazaire-Bermal, N., et al. (2014). Enhanced and persistent antibody response against homologous and heterologous strains elicited by a MF59®-adjuvanted influenza vaccine in infants and young children. Vaccine 1–11.

Osborne, T.F., Gil, G., Goldstein, J.L., and Brown, M.S. (1988). Operator constitutive mutation of 3-hydroxy-3-methylglutaryl coenzyme A reductase promoter abolishes protein binding to sterol regulatory element. J. Biol. Chem. 263, 3380–3387.

Rader, D.J., and deGoma, E.M. (2012). Approach to the patient with extremely low HDL-cholesterol. J. Clin. Endocrinol. Metab. 97, 3399–3407.

Rawson, R.B., Zelenski, N.G., Nijhawan, D., Ye, J., Sakai, J., Hasan, M.T., Chang, T.Y., Brown, M.S., and Goldstein, J.L. (1997). Complementation cloning of S2P, a gene encoding a putative metalloprotease required for intramembrane cleavage of SREBPs. Mol. Cell 1, 47–57.

Rentero, C., Zech, T., Quinn, C.M., Engelhardt, K., Williamson, D., Grewal, T., Jessup, W., Harder, T., and Gaus, K. (2008). Functional implications of plasma membrane condensation for T cell activation. PLoS One 3, e2262.

Repa, J.J. (2000). Regulation of mouse sterol regulatory element-binding protein-1c gene (SREBP-1c) by oxysterol receptors, LXRalpha and LXRbeta. Genes Dev. 14, 2819–2830.

Roelofs, A.J., Jauhiainen, M., Mönkkönen, H., Rogers, M.J., Mönkkönen, J., and Thompson, K. (2009). Peripheral blood monocytes are responsible for gammadelta T cell activation induced by zoledronic acid through accumulation of IPP/DMAPP. Br. J. Haematol. 144, 245–250.

Roper, B. (1964). Essential Hypercholesterolaemic Xanthomatosis. Br. Med. J. 1963–1964.

Rosenzweig, I.B., Wiebe, D. a, Borden, E.C., Storer, B., and Shrago, E.S. (1987). Plasma lipoprotein changes in humans induced by beta-interferon. Atherosclerosis 67, 261–267.

Scanu, a, Pollard, H., and Reader, W. (1968). Properties of human serum low density lipoproteins after modification by succinic anhydride. J. Lipid Res. 9, 342–349.

Schectman, G., Kaul, S., Mueller, R. a., Borden, E.C., and Kissebah, a. H. (1992). The effect of interferon on the metabolism of LDLs. Arterioscler. Thromb. Vasc. Biol. 12, 1053–1062.

Shine, T.E., Little, J.R., Shore, V., Medoff, G., and Abegg, a (1980). Effect of exogenous lipids and lipoproteins on the primary immune response in vitro. Eur. J. Immunol. 10, 714–718.

Shope, R. (1930). Variations in the plasma cholesterol and cholesterol ester content in hog cholera. J. Exp. Med. 51, 179–187.

Singaraja, R.R., Visscher, H., James, E.R., Chroni, A., Coutinho, J.M., Brunham, L.R., Kang, M.H., Zannis, V.I., Chimini, G., and Hayden, M.R. (2006). Specific mutations in ABCA1 have discrete effects on ABCA1 function and lipid phenotypes both in vivo and in vitro. Circ. Res. 99, 389–397.

Smith, J.R., Osborne, T.F., Brown, M.S., Goldstein, J.L., and Gil, G. (1988). Multiple sterol regulatory elements in promoter for hamster 3-hydroxy-3-methylglutaryl-coenzyme A synthase. J. Biol. Chem. 263, 18480–18487.

Spann, N.J., Garmire, L.X., McDonald, J.G., Myers, D.S., Milne, S.B., Shibata, N., Reichart, D., Fox, J.N., Shaked, I., Heudobler, D., et al. (2012). Regulated accumulation of desmosterol integrates macrophage lipid metabolism and inflammatory responses. Cell 151, 138–152.

Spencer, C.M., Schafer, X.L., Moorman, N.J., and Munger, J. (2011). Human cytomegalovirus induces the activity and expression of acetyl-coenzyme A carboxylase, a fatty acid biosynthetic enzyme whose inhibition attenuates viral replication. J. Virol. 85, 5814–5824.

Stokes, W.M., Fish, W.A., and Hickey, F.C. (1956). Metabolism of cholesterol in the chick embryo. II. Isolation and chemical nature of two companion sterols. J. Biol. Chem. 220, 415–430.

Stokes, W.M., C, H.F., and Fish, W.A. (1958). Sterol metabolism. I. The occurrence of desmosterol (24-dehydrocholesterol) in rat skin and its conversion in vivo to cholesterol. J. Biol. Chem. 232, 347–359.

Subramanian, G., Chaudhury, P., Malu, K., Fowler, S., Manmode, R., Gotur, D., Zwerger, M., Ryan, D., Roberti, R., and Gaines, P. (2012). Lamin B receptor regulates the growth and maturation of myeloid progenitors via its sterol reductase domain: implications for cholesterol biosynthesis in regulating myelopoiesis. J. Immunol. 188, 85–102.

Sun, D., and Fernandes, G. (2003). Lovastatin inhibits bone marrow-derived dendritic cell maturation and upregulates proinflammatory cytokine production. Cell. Immunol. 223, 52–62.

Sundqvist, A., and Ericsson, J. (2003). Transcription-dependent degradation controls the stability of the SREBP family of transcription factors. Proc Natl Acad Sci U S A 100, 13833–13838.

Takahashi, T., Gasch, a, Nishizawa, N., and Chua, N.H. (1995). The DIMINUTO gene of Arabidopsis is involved in regulating cell elongation. Genes Dev. 9, 97–107.

Tchen, T.T., and Bloch, K. (1957). On the conversion of squalene to lanosterol in vitro. J. Biol. Chem. 226, 921–930.

Uldrich, A.P., Le Nours, J., Pellicci, D.G., Gherardin, N. a, McPherson, K.G., Lim, R.T., Patel, O., Beddoe, T., Gras, S., Rossjohn, J., et al. (2013). CD1d-lipid antigen recognition by the γδ TCR. Nat. Immunol. 14, 1137–1145.

Viikari, J., Ruuskanen, O., Salmi, T., and Halonen, P. (1979). Effect of measles and measles vaccine on serum-cholesterol. Lancet 1, 326.

Van der Vliet, H.J., and Verheul, H.M.W. (2012). Breast-cancer adjuvant therapy with zoledronic acid. N. Engl. J. Med. 366, 188–189; author reply 189.

Wang, H., Sarikonda, G., Puan, K.-J., Tanaka, Y., Feng, J., Giner, J.-L., Cao, R., Mönkkönen, J., Oldfield, E., and Morita, C.T. (2011). Indirect stimulation of human Vγ2Vδ2 T cells through alterations in isoprenoid metabolism. J. Immunol. 187, 5099–5113.

Wang, H., Yao, Y., Huang, C., Fu, X., Chen, Q., Zhang, H., Chen, J., Fang, F., Xie, Z., and Chen, Z. (2014). An adjuvanted inactivated murine cytomegalovirus (MCMV) vaccine induces potent and long-term protective immunity against a lethal challenge with virulent MCMV. BMC Infect. Dis. 14, 195.

Wang, N., Silver, D.L., Thiele, C., and Tall, a R. (2001). ATP-binding cassette transporter A1 (ABCA1) functions as a cholesterol efflux regulatory protein. J. Biol. Chem. 276, 23742–23747.

Wangs, X., Briggsq, R., Hua, X., Yokoyama, C., Goldstein, J.L., Briggss, M.R., Wango, X., and Brown, M.S. (1993). Nuclear Protein That Binds Sterol Regulatory Element of Low Density Lipoprotein Receptor Promoter. 268, 14490–14496.

Whitehouse, M.W., Orr, K.J., Beck, F.W., and Pearson, C.M. (1974). Freund's adjuvants: relationship of arthritogenicity and adjuvanticity in rats to vehicle composition. Immunology 27, 311–330.

Wójcicka, G., Jamroz-wiśniewska, A., and Horoszewicz, K. (2007). Liver X receptors (LXRs). Part I : Structure , function , regulation of activity , and role in lipid metabolism Receptory wątrobowe X (LXR). Część I : Budowa , funkcja , regulacja aktywności i znaczenie w metabolizmie lipidów. 736–759.

Yang, T., Espenshade, P.J., Wright, M.E., Yabe, D., Gong, Y., Aebersold, R., Goldstein, J.L., and Brown, M.S. (2002). Crucial step in cholesterol homeostasis: sterols promote binding of SCAP to INSIG-1, a membrane protein that facilitates retention of SREBPs in ER. Cell 110, 489–500.

Ye, X., Xu, S., Xin, Y., Yu, S., Ping, Y., Chen, L., Xiao, H., Wang, B., Yi, L., Wang, Q., et al. (2012). Tumor-associated microglia/macrophages enhance the invasion of glioma stem-like cells via TGF-β1 signaling pathway. J. Immunol. 189, 444–453.

Yilmaz, A., Reiss, C., Weng, A., Cicha, I., Stumpf, C., Steinkasserer, A., Daniel, W.G., and Garlichs, C.D. (2006). Differential effects of statins on relevant functions of human monocyte-derived dendritic cells. J. Leukoc. Biol. 79, 529–538.

Yu, Y., Maguire, T.G., and Alwine, J.C. (2012). Human cytomegalovirus infection induces adipocyte-like lipogenesis through activation of sterol regulatory element binding protein 1. J. Virol. 86, 2942–2949.

Yvan-Charvet, L., Pagler, T., Gautier, E.L., Avagyan, S., Siry, R.L., Han, S., Welch, C.L., Wang, N., Randolph, G.J., Snoeck, H.W., et al. (2010). ATP-binding cassette transporters and HDL suppress hematopoietic stem cell proliferation. Science 328, 1689–1693.

Zerenturk, E.J., Sharpe, L.J., Ikonen, E., and Brown, A.J. (2013). Desmosterol and DHCR24: unexpected new directions for a terminal step in cholesterol synthesis. Prog. Lipid Res. 52, 666–680.

3.5 Supporting information

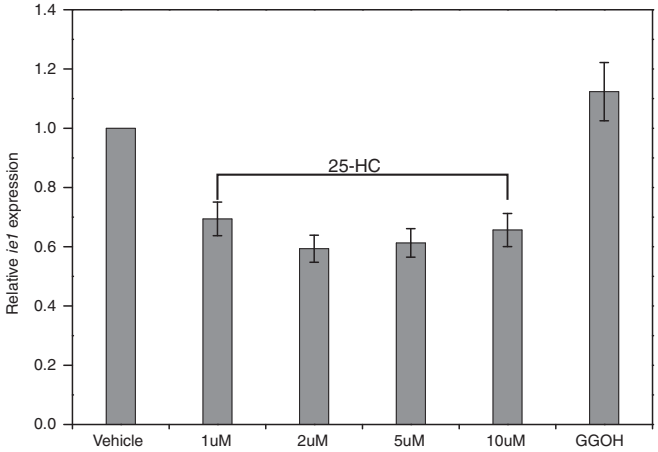

Figure S3.1 Constitutive MCMV ie1 gene expression is suppressed in 25-HC treated BAM25.
BAM25 fibroblasts (8x10^5 cells/well, 6 well plate) were treated with vehicle, 25-HC or GGOH (20μM) for 72 hr. Relative abundance of the MCMV *ie1* was assayed by qRT-PCR using 25ng of RNA. n = 3; mean ± SEM.

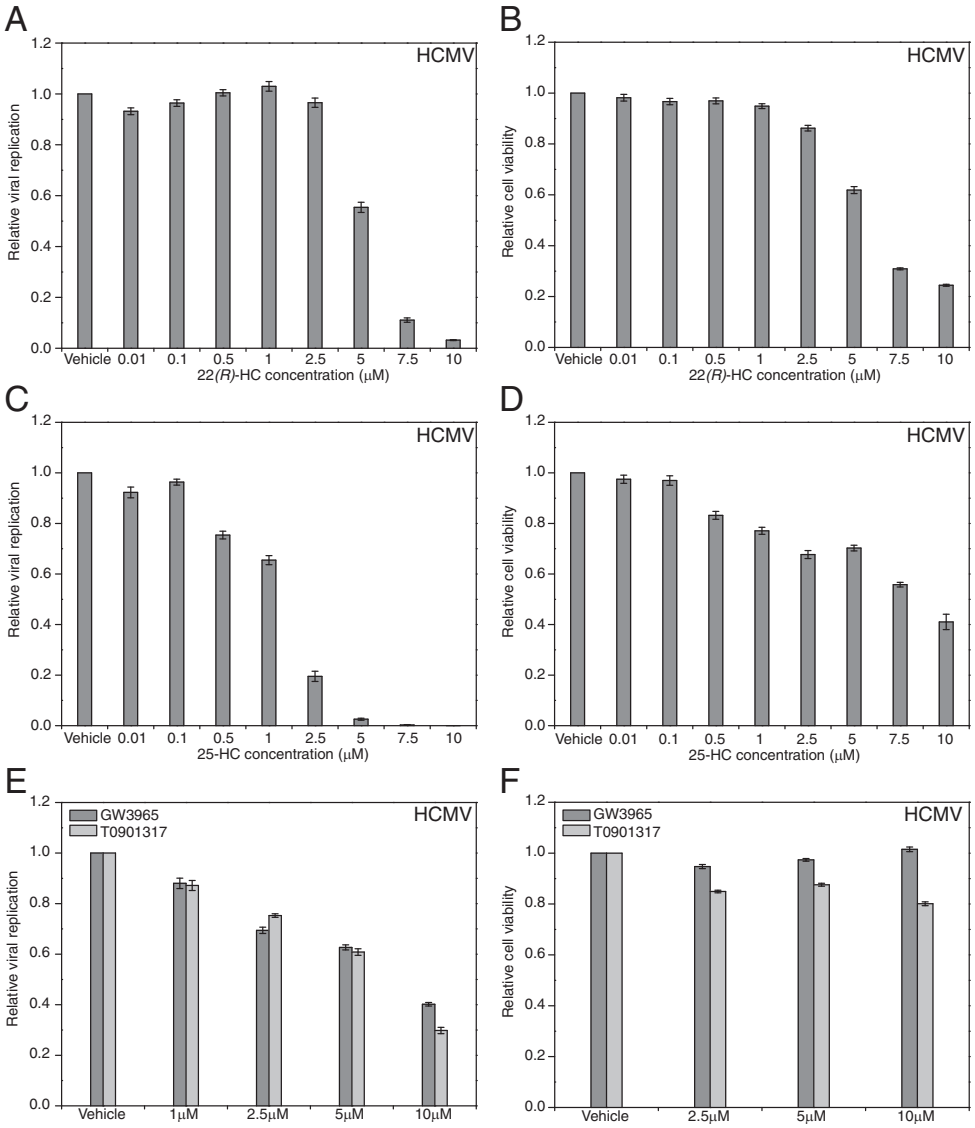

Figure S3.2 Antiviral effect of oxysterols and LXR ligands in HCMV.

HCMV replication was monitored (A, C, and E) as a function of kinetic GFP fluorescence. MRC5 were seeded at a seeding density of $2x10^4$ cells/well in black 96 well plates. The next day, cells were pre-treated with (A) 22(*R*)-HC, (C) 25-HC, or (E) LXR ligands GW3965/T0901317 as indicated for 24 hr. Next day, cells were infected with HCMV-AD169-GFP (MOI = 0.3). After adsorption, infection inoculum was removed and cells were cultured in normal serum supplemented with media containing vehicle or 22(*R*)-HC, 25-HC, or GW3965/T0901317 at increasing concentrations. Replication slopes over the linear phase (63 – 116 hpi) were calculated and normalized to vehicle treated cells, and the mean replication slope from independent experiments calculated. Analysis on the effects of oxysterols and LXR ligands on cell viability (B, D, and F). Cells were treated with 22(*R*)-HC, 25-HC, or GW3965/T0901317 as indicated for 72 hr and viability analysed using the CellTiter-Blue assay as described in Experimental procedure 7.4.2. Data represents mean ± SEM for two experiments (4 replicates per experiment).

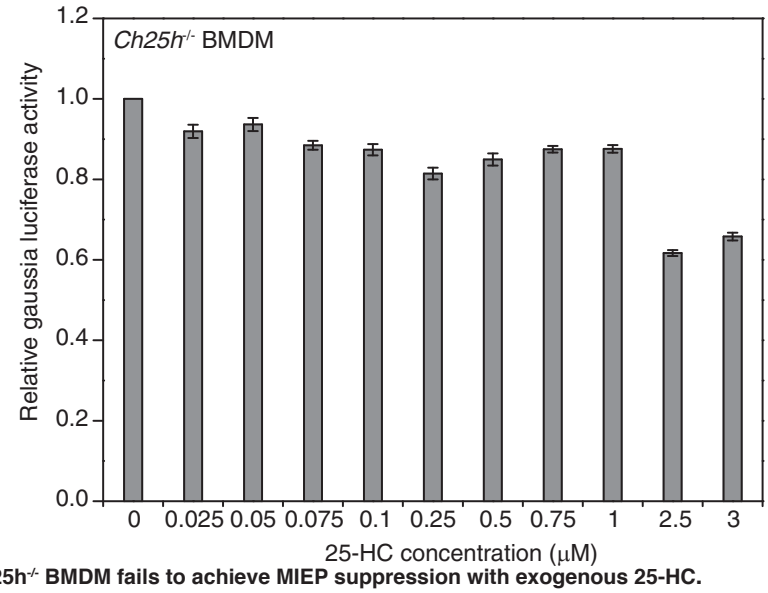

Figure S3.3 Ch25h$^{-/-}$ BMDM fails to achieve MIEP suppression with exogenous 25-HC.
Ch25h$^{-/-}$ BMDM (3x10^4 cells/well, 96 well plate) were pre-treated with vehicle or 25-HC at various concentrations for 24 hr. Cells were then infected with Gluc-MCMV (MOI = 0.1) for 1 hr. After adsorption, cells were washed once with normal medium. After wash, 120µl of fresh medium containing vehicle or 25-HC were added. Supernatant was collected at 4 hpi. Gluc activity was measured using the native form of the Gluc substrate coelenterazine as described in Experimental procedure 7.4.1. Data are normalized to negative control wells treated with vehicle alone. Data represents mean ± SEM for one experiment containing 16 replicates.

Publication associated with Chapter 3

Blanc M, **Hsieh WY***, Robertson KA, Kropp KA, Forster T, Shui G, Lacaze P, Watterson S, Griffiths SJ, Spann NJ, Meljon A, Talbot S, Krishnan K, Covey DF, Wenk MR, Craigon M, Ruzsics Z, Haas J, Angulo A, Griffiths WJ, Glass CK, Wang Y, Ghazal P. The transcription factor STAT-1 couples macrophage synthesis of 25-hydroxycholesterol to the interferon antiviral response. Immunity. 2013 Jan 24;38(1):106-18. (*First co-author)

Immunity
Article

The Transcription Factor STAT-1 Couples Macrophage Synthesis of 25-Hydroxycholesterol to the Interferon Antiviral Response

Mathieu Blanc,[1,9] Wei Yuan Hsieh,[1,9] Kevin A. Robertson,[1,2] Kai A. Kropp,[1] Thorsten Forster,[1] Guanghou Shui,[3] Paul Lacaze,[1] Steven Watterson,[1,2] Samantha J. Griffiths,[1] Nathanael J. Spann,[4] Anna Meljon,[5] Simon Talbot,[1] Kathiresan Krishnan,[6] Douglas F. Covey,[6] Markus R. Wenk,[3] Marie Craigon,[1] Zsolts Ruzsics,[7] Jürgen Haas,[1] Ana Angulo,[8] William J. Griffiths,[5] Christopher K. Glass,[4] Yuqin Wang,[5] and Peter Ghazal[1,2,*]

[1]Division of Pathway Medicine and Edinburgh Infectious Diseases, University of Edinburgh, Edinburgh EH16 4SB, UK
[2]SynthSys (Synthetic and Systems Biology), University of Edinburgh, The King's Buildings, Edinburgh EH9 3JD, UK
[3]Departments of Biochemistry and Biological Sciences, Yong Loo Lin School of Medicine, National University of Singapore, Singapore 117597
[4]Department of Molecular Biology, University of California, San Diego, La Jolla, CA 92093, USA
[5]Institute of Mass Spectrometry, College of Medicine, Grove Building, Swansea University, Singleton Park, Swansea SA2 8PP, UK
[6]Department of Developmental Biology, Washington University School of Medicine, St. Louis, MO 63011, USA
[7]Max von Pettenkofer-Institut, Ludwig-Maximilians-Universität München, Genzentrum, Feodor Lynen Str. 25, 81377 Munich, Germany
[8]Facultad de Medicina, Institut d'Investigacions Biomèdiques August Pi i Sunyer, Rosselló 149-153, Barcelona 08036, Spain
[9]These authors contributed equally to this work
*Correspondence: p.ghazal@ed.ac.uk
http://dx.doi.org/10.1016/j.immuni.2012.11.004
Open access under CC BY license.

SUMMARY

Recent studies suggest that the sterol metabolic network participates in the interferon (IFN) antiviral response. However, the molecular mechanisms linking IFN with the sterol network and the identity of sterol mediators remain unknown. Here we report a cellular antiviral role for macrophage production of 25-hydroxycholesterol (cholest-5-en-3β,25-diol, 25HC) as a component of the sterol metabolic network linked to the IFN response via Stat1. By utilizing quantitative metabolome profiling of all naturally occurring oxysterols upon infection or IFN-stimulation, we reveal 25HC as the only macrophage-synthesized and -secreted oxysterol. We show that 25HC can act at multiple levels as a potent paracrine inhibitor of viral infection for a broad range of viruses. We also demonstrate, using transcriptional regulatory-network analyses, genetic interventions and chromatin immunoprecipitation experiments that Stat1 directly coupled *Ch25h* regulation to IFN in macrophages. Our studies describe a physiological role for 25HC as a sterol-lipid effector of an innate immune pathway.

INTRODUCTION

Metabolism and innate immunity are increasingly viewed as being connected and pathway mechanisms exist for sharing resources and cross-regulation (Im et al., 2011).

Cholesterol is a vital component of cellular membranes and is critical to a broad range of cellular functions. As a result, elaborate homeostatic mechanisms have evolved to control sterol metabolism at multiple levels within and outside the cell (Horton et al., 2002). Importantly, several of these mechanisms involve 25-hydroxycholesterol (25HC). The synthesis of transcripts encoding virtually all enzymes of the sterol biosynthesis pathway is regulated by the transcription factor Srebp2. Moreover, the Srebp2 processing pathway, responsible for endoplasmic reticulum retention of the protein or proteolytic activation and translocation to the nucleus, is subject to inhibition by 25HC (Gong et al., 2006; Radhakrishnan et al., 2007; Yabe et al., 2002). In the mevalonate arm of the pathway, HMGCR serves as a key control point (Rodwell et al., 1976) and is further regulated by oxysterols (in particular 25HC) through proteasomal degradation elicited by INSIG1. In addition, 25HC may also regulate cholesterol homeostasis through its ability to activate liver X receptors (LXR) and a variety of other isoprenoid and sterol metabolic intermediates can negatively feedback on sterol biosynthesis (Espenshade and Hughes, 2007; Song et al., 2005).

Viruses are known to alter cellular lipid metabolism to facilitate their own multiplication and, importantly, inhibition of cholesterol and fatty acid biosynthetic pathways has been shown to curtail virus replication, maturation and secretion (Clark et al., 2012; del Real et al., 2004; Munger et al., 2008; Peña and Harris, 2012; Potena et al., 2004; Spencer et al., 2011; Taylor et al., 2011; Ye et al., 2003; Yu et al., 2012). In this regard, interferon (IFN)-mediated downregulation of the sterol biosynthesis pathway has been shown to be an integral part of Mϕ host defense (Blanc et al., 2011; Watterson et al., 2012). It is well recognized that IFNs, in particular type I, play a pivotal role in inhibiting viral growth through the activation of IFN-stimulated genes (ISGs). However, the specific functions of many ISGs and the mechanisms by which they restrict viral replication are not well defined (O'Neill and Bowie, 2010). The notion that there is an intrinsic connection between the sterol network and IFN is further supported by studies showing IFN modulation of the cholesterol

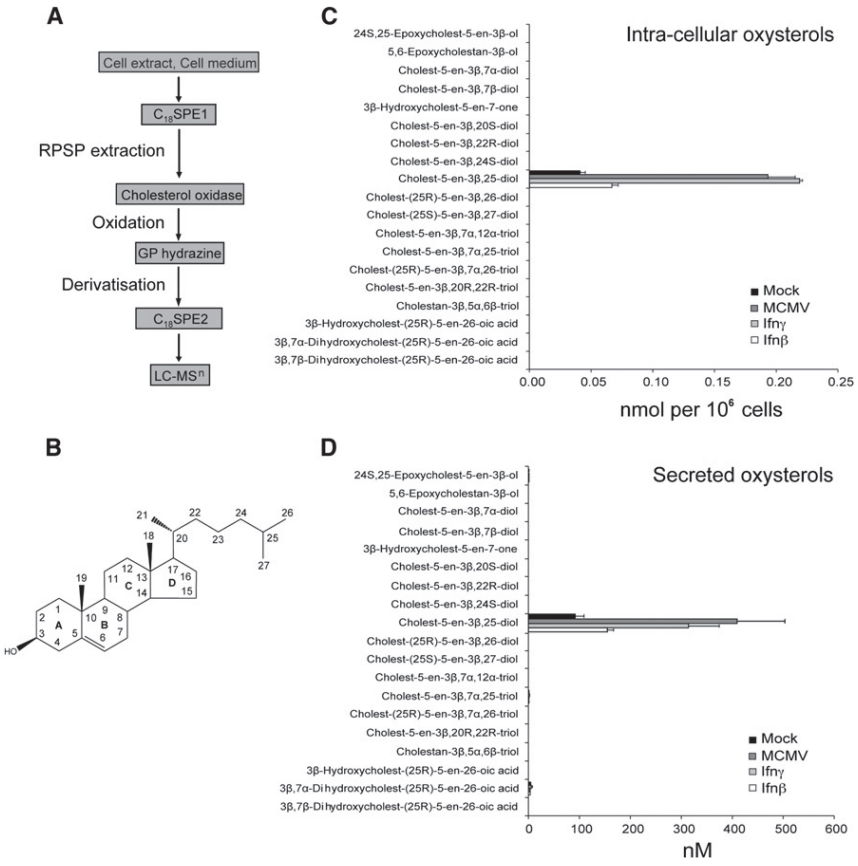

Figure 1. 25HC Synthesis and Secretion by Mϕ after Interferon Treatment or MCMV Infection

(A) Work-flow for the LC-MS(MS^n) analysis of oxysterols. Quantification was performed from reconstructed ion chromatograms by reference to deuterated internal standards.

(B) Structure of cholesterol, the scaffold on which oxysterols are built.

(C) Intracellular levels of oxysterols in BMDM following MCMV infection (MOI = 1), Ifn-γ (25 U/ml) or Ifn-β (25 U/ml) stimulation for 12 hr. A mock sample of BMDM without stimulation or infection was similarly analyzed.

(D) Analysis of oxysterols secreted by cells into medium when treated as in (C). n = 3, data are mean ± SEM.

hydroxylase gene, *Ch25h* (Bauman et al., 2009; Diczfalusy et al., 2009; Park and Scott, 2010). Importantly, however, the precise mechanisms and physiological roles by which IFN regulates the sterol metabolic network remain unclear.

Here, we have undertaken a comprehensive, unbiased investigation of the biological role of oxysterols produced by Mϕ during infection and upon IFN stimulation. We provide evidence for a biological role for 25HC as a lipid effector of the innate immune response, highlighting the targeting of host metabolic regulatory networks during viral infections and, more broadly, inflammation.

RESULTS

Quantitative Oxysterol Profiling of Infected or Interferon-Activated Primary Macrophages

We speculated that the synthesis of oxysterols might have a role in the negative regulation of sterol biosynthesis upon infection (Blanc et al., 2011). Accordingly, we performed a comprehensive quantitative determination of all known naturally occurring side-chain and steroid-ring oxysterol metabolites that are produced and/or secreted by either infected or interferon (β or γ) stimulated primary Mϕ (Figures 1A, 1C, and 1D). Bone-marrow-derived macrophages (BMDMs) were infected (mouse cytomegalovirus, MCMV) or stimulated (Ifn-β or Ifn-γ) for 12 hr and the oxysterol content of cells and medium measured by LC-MS(MS^n) following derivatization (see Figure 1A for workflow schematic). By generating reconstructed ion chromatograms (RICs) for mono- and dihydroxycholesterols, epoxycholesterols, and mono- and dihydroxycholestenoic acids (see Figure 1B for chemical structure), essentially all naturally occurring oxysterols and their immediate downstream metabolites were profiled. Figure 1 shows the list for common oxysterols and those oxysterols not shown were inclusive for 3β-hydroxycholest-5-en-22-one, cholest-5-ene-3β,4β-diol, cholest-4-ene-3β,6α -diol, cholest-4-ene-3β,6β –diol, cholest-5-en-3β, 19-diol, cholest-5-ene-3β,22S-diol, cholest-5-ene-3β,24R-diol, cholest-5-ene-3β,7β,25-triol, cholest-(25R)-5-ene-3β,7β,26-triol, cholest-5-ene-3β,24,25-triol, 3β-hydroxycholest-(25S)-5-en-27-oic acid.

The results of this oxysterol-metabolome and secretome screen are summarized in Figure 1C (intracellular) and 1D (secreted). Interestingly, in this study noticeable amounts of 25HC were found in unstimulated Mϕ but not media—a result that perhaps reflects a pre-existing subprimed activation of Mϕ (Kropp et al., 2011). Strikingly, amounts of only 25HC were markedly increased by infection or treatment with MCMV or Ifn (β or γ), respectively (Figures 1C and 1D). In this study, the only other detectable oxysterols (with systemic names provided in brackets) were 24(S),25-epoxycholesterol (24S,25-epoxycholest-5-en-3β-ol), 3β,7α-dihydroxycholestenoic (3β,7α-dihydroxycholest-[25R]-5-en-26-oic) acid and 7α,25-dihydroxycholesterol (cholesten-5-en-3β,7α,25-diol) but at extremely low levels. Because LC-MS(MS^n) assays are exceptionally sensitive and these products were detected in the media only, it is possible that they were generated by auto-oxidation. Notably, no other oxysterol or downstream 3-oxo-4-ene metabolites of the listed oxysterols were found. Similarly, we found no evidence for oxysterol mono- or disulphates. The sulphation of oxysterols is known to catabolically inactivate oxysterol activity and also generate alternative-biologically active products. However, we find no detectable presence of either the 3- or 25-monosulphate or 3,25-disulphate.

To avoid potential issues relating to serum-derived lipid contamination, we proceeded to investigate the production of 25HC using lipid-depleted media. Time course experiments

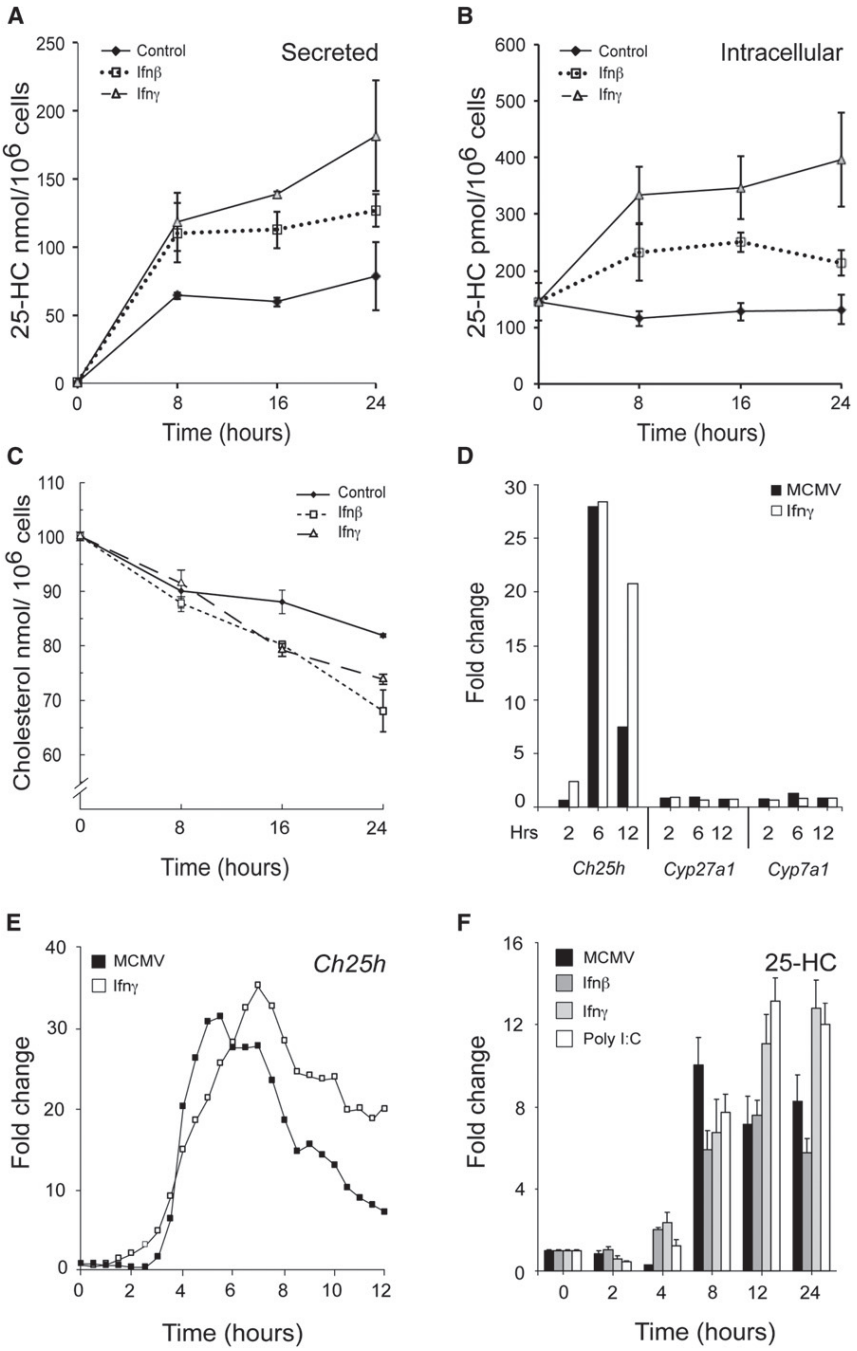

Figure 2. Temporal Analyses of *Ch25h* Synthesis and 25HC Production

(A) Levels of secreted (A) and cellular (B) 25HC and cellular cholesterol (C) with Ifn-β (25 U/ml) or Ifn-γ (25 U/ml) in delipidized media. n = 3, mean ± SEM.

(D) Expression level of *Ch25h*, *Cyp27a1*, and *Cyp7a1* from microarray time course experiment in WT BMDM following MCMV infection (MOI = 1) or Ifn-γ (10 U/ml) stimulation (*Cyp46a* and *Cyp7b1* did not reach the threshold of expression).

(E) *Ch25h* expression BMDM following MCMV infection (MOI = 1) or Ifn-γ (10 U/ml) stimulation.

(F) 25HC level in BMDM 24 hr following MCMV infection, Ifn-β (10 U/ml), Ifn-γ (10 U/ml) or PolyI:C (10 ng/ml) with the mean ± SEM for data obtained from three independent biological replicates.

revealed that the majority of 25HC was secreted during the first 8 hr of incubation, and levels continued to rise more gradually until the 24 hr endpoint (Figures 2A and 2B). As previously reported for cells grown in normal media, a steady and significant fall in free cholesterol, and its direct precursor desmosterol, was observed with time suggesting a reduced biosynthetic output (Figure 2C; data not shown) (Watterson et al., 2012). In summary, the LC-MS(MS^n) experiments revealed 25HC as the only oxysterol notably upregulated following macrophage infection or activation by IFNs. This occurred during the first hours after infection or treatment before overall levels of cholesterol in treated cells fell notably below those of the control. Figures 2D and 2E show data that suggests that the highly-specific increase in 25HC was attributable to upregulated expression of the hydroxylase *Ch25h*; levels of the only other expressed hydroxylases *Cyp27a* and *Cyp7a* that are also implicated in 25HC metabolism were unaltered. When a different perspective on this result was sought and interferon or polyI:C was used to stimulate BMDMs, increased levels of secreted 25HC were clearly detectable 4 hr after treatment. PolyI:C is a potent Tlr3 agonist that stimulates high levels of Ifn-β production (Figure 2F). Notably, in contrast to the observed decline in *Ch25h* transcript expression, levels of secreted 25HC metabolite levels remained relatively high until 24 hr in these experiments. We conclude from the above data that interferon activation or MCMV infection of Mϕ results in a large and highly focused production of intracellular and secreted 25HC.

Exogenous Treatment and Endogenous Secretion of 25HC by BMDM Has Broad Antiviral Potency

It is possible that 25HC might function as an antiviral mediator in the IFN-regulated sterol metabolic network (Blanc et al., 2011). To test this idea, we sought to address whether physiologically relevant concentrations of 25HC, secreted by activated Mϕ, are capable of conferring an antiviral state. We first determined in dose-response experiments the inhibitory concentrations (IC) for viral growth of MCMV in normal serum (i.e., sterol-replete media would favor restricted Srebp2 processing). Figure 3A shows that under these conditions 25HC has an IC_{10} of approximately 0.1 μM and an IC_{50} of 2 μM and did not induce a cytotoxic effect (see Figure S1 available online). Because this level of inhibition is greater than

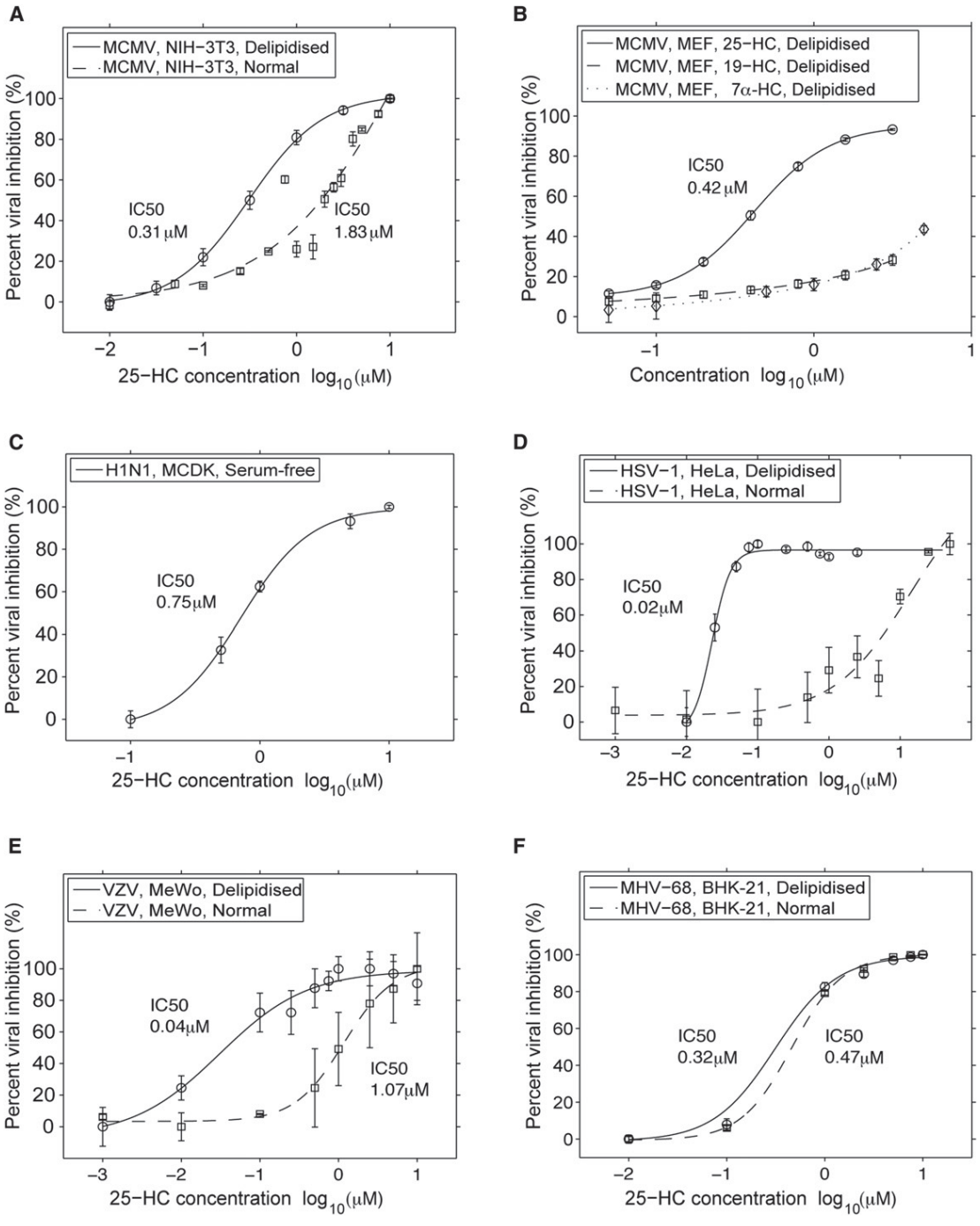

Figure 3. Analysis of 25HC Anti-Viral Effects, See Also Figure S1

Virus replication was monitored (A, B, D, E, and F) as a function of kinetic GFP fluorescence. Replication slopes over the linear phase were calculated and normalized to vehicle treated cells, and the mean replication slope from independent experiments calculated. For (C) Influenza virus, supernatant was collected at 16 hpi for analysis of viral titer by plaque assay. Data are mean ± SEM (three replicates).

the known levels of 25HC that are sufficient to disrupt Srebp processing (Radhakrishnan et al., 2007), we infer from these experiments that in sterol-replete conditions 25HC is unlikely to involve the Srebp processing pathway for maximal antiviral activity (Adams et al., 2004; Yabe et al., 2002).

Because cells grown under lipid-deficient media conditions have an increased dependency on sterol biosynthesis, we also evaluated the antiviral effect of 25HC under lipid-depleted conditions (Sun et al., 2007). As shown in Figures 3A and 3B, there is an increase in sensitivity of MCMV to inhibition by 25HC under

these conditions. This antiviral effect is specific to 25HC because other related enzymatically generated oxysterols, 19-HC and 7α-HC, fail to repress viral infection (Figure 3B). These oxysterols are known not to inhibit the Srebp-pathway (Radhakrishnan et al., 2007). In contrast, other oxysterols known to inhibit the Srebp-pathway through INSIG, such as 27-HC and 24(S), 25 epoxycholesterol, are similarly capable of inhibiting MCMV growth (Figure S1B). These observations point to the possibility that although the Srebp pathway is not absolutely essential for mediating the antiviral effects of 25HC, it might contribute toward enhancing the sensitivity to 25HC inhibition. The physiological relevance for the lipid dependency is presently unclear. The differential sensitivities under sterol-replete and -depleted conditions raise the possibility for multiple levels of control. To determine whether the differential modes of inhibition by 25HC are specific to MCMV or whether it might have a broader antiviral role, we next evaluated, in normal or lipid-depleted conditions, its potency to inhibit a range of other viruses in different cell systems. Figures 3C–3F show the quantitative determination of the dose-dependent potency of 25HC to inhibit Influenza A (H1N1), herpes simplex virus-1 (HSV-1), varicellar zoster virus (VZV) and murine gamma herpes virus 68 (MHV-68) viral infections in MDCK, HeLa, MeWo, and BHK cells, respectively. The results of these titration experiments clearly show a broad and highly potent (IC_{50} values ranging from 20 nM to 750 nM) antiviral role of 25HC (Figures 3D–3F). This effect is selective because Figure S1C shows that under the conditions tested, 25HC does not specifically inhibit Adenovirus 5 or 19a. We conclude that 25HC has a high potency to inhibit a broad spectrum of viruses from high to low physiological concentrations depending on lipid conditions and virus-host cell system.

The pharmacologic agent LY295427 (3α,4α,5α)-4-(2-propenylcholestan-3-ol) is a known antagonist of 25HC, whereas LY306039, the 3β-isomer of LY295427, fails to derepress the effect of 25HC (Janowski et al., 2001). We used these agents to test whether they have any efficacy in interfering with the antiviral activity mediated by 25HC. Figure 4A shows the ability of exogenous 25HC to potently inhibit viral growth and that the observed antiviral effect can be completely blocked in the presence of LY295427 but not LY306039. These results validated our subsequent use of LY295427 in interfering with endogenously secreted 25HC. Accordingly, conditioned media (10 hr post-treatment) from mock-treated, infected, Ifn-β, or Ifnγ-treated Mϕ was incubated with vehicle alone, or with LY295427 or LY306039 and then applied to MCMV-infected NIH 3T3 cells. As expected, mock-conditioned media failed to inhibit viral growth and drug treatment had no effect (Figure 4B). Meanwhile, conditioned media from infected or IFN-treated cells had pronounced antiviral activity. In the presence of LY295427, antiviral activity was partially blocked (Figure 4B). We interpret the results of these experiments to show that endogenously secreted 25HC has a potent antiviral activity and, if we assume, LY295427 is an exclusive inhibitor of 25HC, this accounts for at least 40%–50% of the antiviral secretome activity. It is likely that the secretion of other antiviral cytokines rather than an incomplete blockade provides the remaining antiviral activity. Overall, these experiments demonstrate that Mϕ activated *Ch25h* generates biological antiviral activity through paracrine, and in the case of Mϕ also autocrine effects of 25HC.

25HC Antiviral Actions Are LXR Independent and Enantioselective

The above studies raise the possibility for potentially direct and indirect modes of 25HC action. It is conceivable that inhibitory effects of 25HC above 0.5 μM might involve an indirect membrane-mediated mechanism, whereas those below 0.5 μM may have a direct protein mediated mode of action. It is also plausible that 25HC could be metabolized to a more potent antiviral metabolite. A candidate pathway is the Epstein-Barr virus-induced gene 2 (*EBI2/GPR183*) enzyme system (Hannedouche et al., 2011; Liu et al., 2011). The natural ligand for EBI2 has been identified as 7α,25-diHC. In this pathway, a critical enzyme required for the generation of 7α,25-diHC is CH25H, however, in our mouse experiments *Ebi2* gene expression is downregulated in Mϕ upon productive and nonproductive infection as well as polyI:C treatment, in an IFN-dependent manner (Figure 4C), suggesting that it is unlikely to be involved in the antiviral response. Intriguingly, the coordinated IFN suppression of the *Ebi2* mediated 25HC-catabolic-pathway further underscores the highly focused 25HC Mϕ response and is unlikely to involve an intermediary metabolite mode of action.

To evaluate generalized membrane effects and further test the specificity of 25HC actions, we studied the activity of *ent*-25HC, an enantiomer of 25HC. In these experiments, we assumed the well-known ability of 25HC to interact and change the properties of cellular membranes would be enantiomer insensitive while protein specific inhibitory effects on viral growth would be restricted to 25HC. Figure 4D shows that *ent*-25HC has antiviral activity but only at concentrations exceeding 1 μM, which is below the nonselective effects of oxysterols on viral infection and is an order of magnitude less potent at inhibiting MCMV than 25HC (Figure 4D). These results show that the effect of 25HC on antiviral activity is highly enantio-selective, consistent with the idea that 25HC antiviral functions occurs through a specific protein target(s). Because *ent*-25HC can exert an antiviral effect at high concentrations it is likely that this activity occurs via an indirect mode of action mediated at the membrane level. Notably, the antiviral effect of *ent*-25HC provides evidence for Srebp-independent antiviral pathway that might act as a cofactor for membrane proteins or acting as a determinant for membrane lipid composition or compartmentalization (Contreras et al., 2012).

In the case of lipid-depleted conditions, our data is consistent with a subordinate inhibition of the Srebp pathway by 25HC and by other oxysterols such as 24S, 25-epoxycholesterol or 27-HC. Notably, these oxysterols are also known to activate LXR (Janowski et al., 2001). Thus, we next evaluated the transcriptional responses of LXR and Srebp target genes in Ifnγ-treated or MCMV-infected Mϕ. In these experiments, molecular profiling of Ifnγ and MCMV infected Mϕ every 30 min for 12 hr showed the expected downregulation of Srebp2 target messenger RNAs (mRNAs) including *Insig1* (Figure 4E). However, the temporal dynamic changes were complex. In this analysis, increased expression of *Ch25h* mRNA levels is associated with a subsequent activation of the LXR target genes *Mylip* and *Abcg1*. To directly test whether LXR ligand activation is sufficient to develop an antiviral state, we treated MCMV infected cells with 1 μM of the potent synthetic LXR ligands (GW3965 and T0901317). Although these ligands were active in LXR-dependent reporter assays

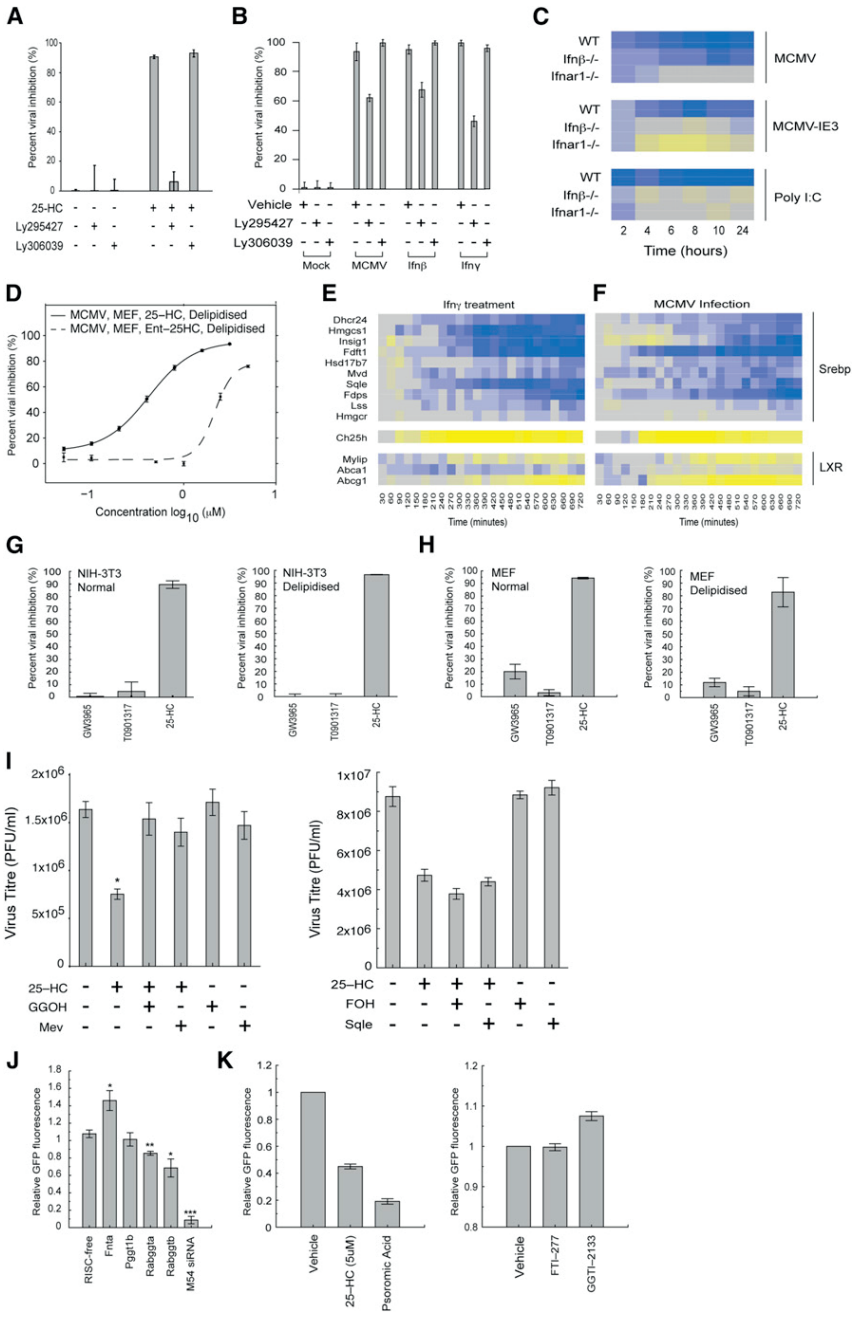

Figure 4. Investigation of Specificity and Selectivity of 25HC Antiviral Activity, See Also Figure S2

(A) NIH 3T3 cells were infected with MCMV-GFP virus (MOI = 0.05) treated with 25HC in the presence or absence of Ly295427 (20 μM) or Ly306039 (20 μM). The level of infection was measured by determining the GFP fluorescence level after 72 hr infection. n = 3, data are mean ± SEM (three replicates per experiment).

(B) NIH 3T3 cells infected with MCMV-GFP virus (MOI = 0.05) received conditioned medium from BMDM infected, or treated with IFN-β (25 U/ml) or IFN-γ (10 U/ml) ± 20 μM Ly295427 or 20 μM Ly306039. n = 3, and data are mean ± SEM (with three biological replicates per experiment).

(C) Expression analysis of *Gpr183* (relative to t = 0) in WT, *Ifnb*$^{-/-}$ or *Ifnar1*$^{-/-}$ BMDM infected with MCMV or MCMVdie3 (MOI = 1) or treated with PolyI:C (10 ng/ml). Each column represents one time point and row represents one gene. Gene expression is shown as a pseudocolor – blue = decrease, yellow = increase. Log fold change values were calculated by subtracting the t = 0 signal value from the signal value at time points after infection or treatment.

(D) MEF were pretreated with 25HC or ent-25HC in delipidized medium for 24 hr and infected with MCMV-GFP (MOI = 1). n = 2, data are mean ± SEM (with three biological replicates per experiment).

(E) BMDM treated with 10 U/ml Ifn-γ or mock-treated (F). Heatmap showing temporal alterations in abundance of sterol-related transcripts in Ifn-γ-treated BMDM (E, relative to t = 0) or MCMV infected BMDM (F, relative to t = 0) as in (C).

(G) NIH 3T3 cells were pretreated with GW3965 (1 μM), T0901317 (1 μM) or 25HC (10 μM) in normal or delipidized medium for 24 hr and then infected with MCMV-GFP. After infection, all wells received fresh medium containing normal or delipidized serum and GW3975, T0901317, or 25HC. Data are normalized to negative controls treated with vehicle alone and are the mean of six independent experiments ± SEM (three biological replicates per experiment).

(H) MEFs were pretreated with GW3965 (1 μM), T0901317 (1 μM) or 25HC (10 μM) in normal or delipidized medium for 24 hr and then infected with MCMV-GFP as described in (G). Data are normalized to negative controls treated with vehicle alone and are the mean of six independent experiments ± SEM (three replicates per experiment).

(I) Left shows MEFs infected with MCMV (MOI = 0.1) incubated with 25HC (1 μM) and/or GGOH (20 μM) or MEV (20 μM) and MCMV titer determined by plaque assay. Data are mean of three independent experiments ± SEM. *p ≤ 0.05. Right shows that MEFs infected with MCMV (MOI = 0.1) were incubated with vehicle, 25HC – (1 μM), and/ or Farnesol (FOH – 20 μM) or Squalene (Sqle – 20 μM) and MCMV titer was determined by plaque assay. Data are the mean of two independent experiments.

(J) RISC-Free, Fnta, Fntb, Pggt1b, Rabggta, Rabggtb, or MCMV M54 siRNA (25nM) were reverse-transfected into NIH/3T3 cells. Forty-eight hr after transfection, cells were infected with MCMV-GFP (MOI = 0.05) and virus replication monitored. Data are normalized to RISC-free wells and are mean of six independent experiments ± SEM.*p < 0.05, **p < 0.01, *** < 0.001.

(K) Left shows that MEF were pretreated with 25HC (5 μM) or psoromic acid (20 μM) for 24 hr, infected with MCMV-GFP (MOI = 0.05), and then incubated with EMEM with the same concentrations of 25HC or psoromic acid. Data are normalized to vehicle treated wells and are mean of two independent experiments. Right shows that MEFs were pretreated with vehicle, FTI-277 (10 μM), or GGTI-2133 (10 μM) for 24 hr, infected with MCMV-GFP (MOI = 0.05), and incubated with the same concentrations of FTI-277 or GGTI-2133 as prior to infection. Data are normalized to vehicle treated wells and are mean of two independent experiments with three biological replicas (error bars represent range).

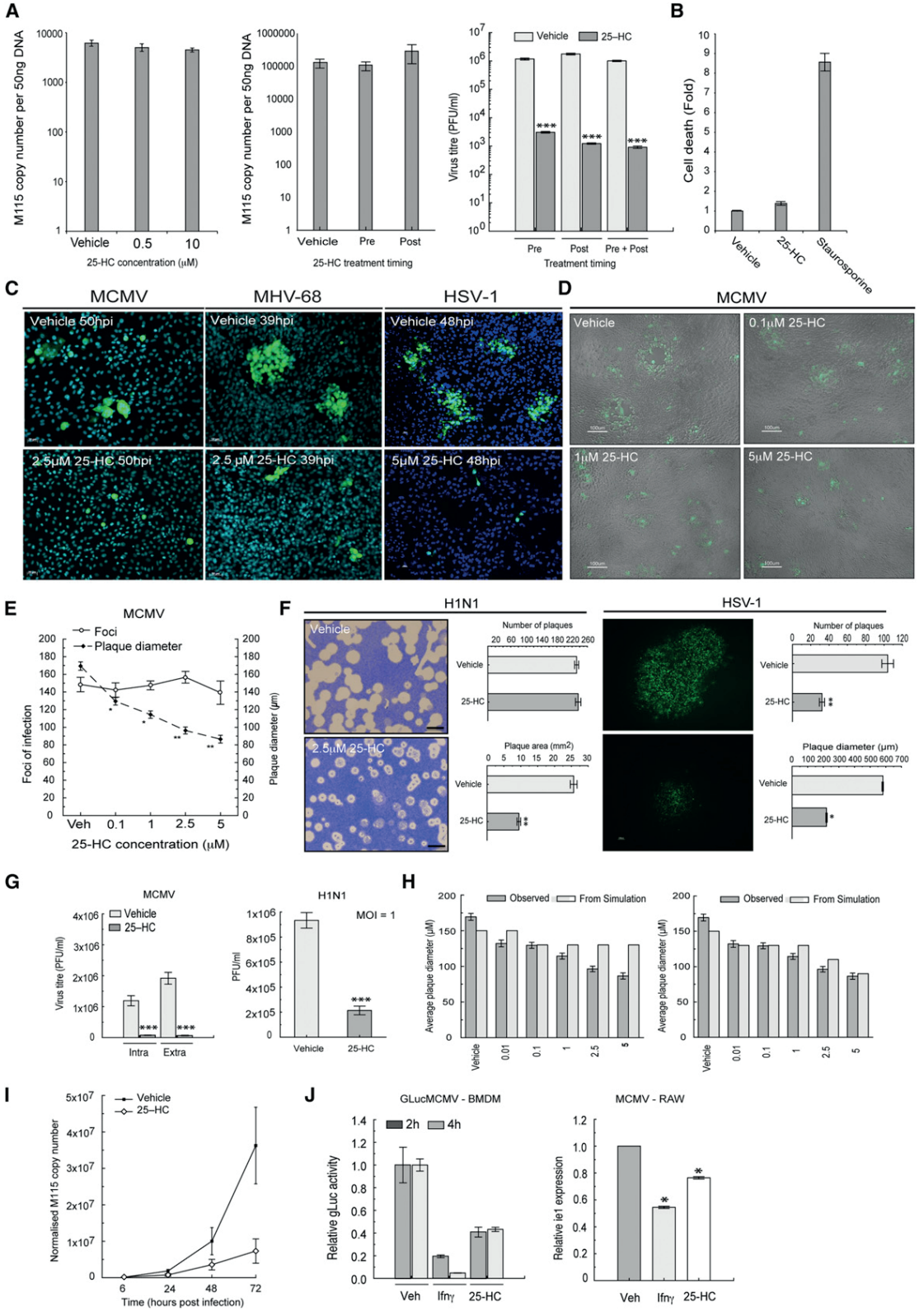

Figure 5. Analysis of 25HC Effects on Cell Death, Virus Entry and Cell-to-Cell Spread, See Also Figure S3 and Movie S1

(A) Left shows NIH 3T3 cells treated with 25HC in delipidized medium and MCMV infected (MOI = 2). Three hpi DNA levels were determined by qRT-PCR. Middle shows RAW 264.7 cells treated with 25HC (5 μM) pre- or postinfection with MCMV (MOI = 1) in normal medium. At 3 hpi, amounts of internalized viral DNA were

(legend continued on next page)

(Figure S2A), they failed to elicit an antiviral response and, therefore, we conclude that LXR activation is insufficient to affect viral inhibition of MCMV in both normal or lipid depleted media conditions (Figures 4G and 4H; Figures S2B and S2C).

25HC Antiviral Action Partially Involves the Mevalonate Branch, Blocking Postentry Viral Growth

A decrease in the Srebp2 target genes of the sterol pathway and especially the mevalonate-isoprenoid side branch is notable (in particular *Mvd* and *Fdps*) (Figures 4E and 4F). Mevalonate is a shared precursor of coenzyme Q, ubiquinone, dolichol, farnesyl, and geranylgeranyl pyrophosphates. The latter two isoprenoids are necessary for protein prenylation. Many viruses require prenylation of essential viral or host proteins (e.g., the large delta antigen of HDV or the pseudorabies virus tegument protein) (Bordier et al., 2003; Clase et al., 2003) or (e.g., host protein FBL2 for hepatitis C virus [HCV] or RhoA activation for RSV) (Ye et al., 2003) (Wang et al., 2005) (Gower and Graham, 2001). In the case of MCMV, we find, upon inhibition of the prenyltransferase branch by RNAi, that viral replication is selectively reduced upon knockdown of GGTase II but not GGTase I or farnesyltransferase (Figure 4J), confirming previous work defining the dependency of MCMV for the isoprenoid pathway (Blanc et al., 2011). In the present study, Rabggta and Rabggtb small interfering RNA (siRNA) reduced the abundance of their target transcript by around 60% (Figure S4F) and none of the above siRNA significantly reduced cell viability (Figure S4D). To investigate whether 25HC antiviral functions involve the mevalonate branch, we treated MCMV infected cells with nonsaturating inhibitory levels of 25HC (<1 μM) and coincubated with mevalonolactone (MEV), geranylgeraniol (GGOH), or Farnesol (FOH), and the amount of infectious virus determined. In these metabolic rescue experiments, viral growth was restored with MEV or GGOH but not FOH (Figure 4I). However, in the presence of saturating inhibitory concentrations of 25HC (>5 μM), viral growth is not recovered with MEV, GGOH, or FOH cotreatment (data not shown) indicating that under these conditions the isoprenoid-prenylation arm is not required. It is possible that other derivatives such as dolichol may be required. Altogether, these investigations are indicative that for MCMV, 25HC blocking of the mevalonate branch imparts a contributory role but is not absolutely essential. As expected, inhibitors of GGTase I (GGTT-2133) or farnesyltransferases (FTI-277) fail to inhibit MCMV, whereas psoromic acid (an inhibitor of GGTase II [Deraeve et al., 2012]) restricts viral growth (Figure 4K). None of these compounds significantly affected cell viability (Figure S2E).

We next investigated at what stage in infection 25HC blocks MCMV growth. The results shown in Figure 5A indicate that the level of internalized MCMV genomes is unaffected by 25HC. Furthermore, in plaque reduction assays the number of primary infectious foci is equivalent in the presence or absence of 25HC (Figure 5E). These results argue against viral entry as a primary mode for MCMV inhibition. In this connection, we also find that 25HC is highly effective at blocking (at 40 nM inhibitory concentration) VZV infection of MeWo cells (Figure 3E). This represents an infection model in which cell-free virus is not produced and the infection process is exclusively dependent on cell-cell spread. 25HC at high concentrations has been shown to promote apoptosis, a well-characterized antiviral mechanism, in a range of cell types including Mϕ (Rusiñol et al., 2004). Notably, however, as shown for NIH 3T3 cells (Figure 5B), 25HC at high antiviral concentrations (10 μM) fails to significantly induce cellular apoptosis in comparison with staurosporine. Again, we cannot rule out that other cell-virus systems may

determined by qRT-PCR. Right shows MEFs treated with 25HC (5 μM) 24 hr prior to and after infection with MCMV (MOI = 2.5) in delipidized media and infected virus titers determined by plaque assay 4 dpi. n = 4, with mean ± SEM. ***p ≤ 0.001.

(B) NIH 3T3 cells were treated with 10 μM 25HC or 10 μM staurosporine in normal media and cell death measured. Data are mean ± SEM for three replicates.

(C) Left shows images of NIH 3T3 cells with and without 25HC 2.5 μM infected with MCMV (MOI 0.01). Middle shows cells treated with 2.5 μM 25HC in normal media. Images of NIH 3T3 cells infected with MHV-68 39 hpi. Right shows HeLa cells infected with HSV-1 VP26-YFP (MOI = 3), treated with 25HC (20 μM) in normal medium and images taken 24 hpi.

(D) NIH 3T3 cells infected with MCMV (MOI = 0.005) and treated with 0.1, 1, or 5 μM 25HC in normal media. Images were taken at 72 hpi.

(E) $p53^{-/-}$ MEFs were infected with MCMV-GFP (MOI = 0.001) and overlaid in normal medium containing 2.5% agarose and 0.1, 1, 2.5, or 5 μM 25HC. Plaque diameter was measured 3 dpi. Data are mean 170 and 220 plaques counted ± SEM (three biological replicates). *p ≤ 0.05, **p ≤ 0.01.

(F) H1N1: Plaque reduction assay of Influenza A/WSN/33 (H1N1) virus infection of MDCK cells in the presence or absence of 25HC (2.5 μM) and a 0.5% agarose overlay. Forty-eight hpi, cells were stained with 0.1% toluidine blue and number and size of plaques determined. Left upper (vehicle) and lower (25HC) panels are representative images showing differences in plaque size and morphology. Right panels show mean number of plaques per well (upper) and mean plaque area (lower, mm^2) per well. HSV-1-eGFP (C12) infection of A549 cells pretreated with vehicle or 25HC (5 μM) with a 0.5% agarose overlay. Plaque numbers and diameters were determined 72 hpi. cell. Representative fluorescent microscopic images of plaques from vehicle- (top left) or 25HC- (bottom left) treated cells are shown. Plaque numbers (top right) and mean plaque diameter (bottom right) from HSV-1 infected cells are shown. n = 6, data are mean ± SEM. *p ≤ 0.05, **p ≤ 0.01.

(G) Left shows that NIH 3T3 cells were infected with MCMV (MOI = 2.5) in delipidized medium containing vehicle or 25HC (5 μM). Two dpi supernatants (extracellular virus) and intracellular virus quantitated by plaque assay. n = 4, mean ± SEM. ***p ≤ 0.001. Right shows MDCK cells infected with A/WSN/33 (H1N1) influenza virus (MOI = 1), serum-free medium containing vehicle, or 25HC (2.5μM), and 0.5% agarose was added to the monolayers. After 16 hpi, monolayers were fixed and stained. n = 4 mean ± SEM. ***p ≤ 0.001.

(H) Left shows plaque diameters observed in experiment and predicted by modeling when cell permissivity and viral growth both mediate 25HC antiviral effect. Right shows that plaque diameters observed in experiment and predicted by modeling when only cell permissivity contributes to the infectious transmission between cells in a dose-dependent manner.

(I) MEFs pretreated with 25HC (5 μM) for 24 hr, infected with MCMV (MOI = 0.3), and DNA levels quantitated at indicated times.

(J) Left shows that BMDM were pretreated with Ifn-γ (10 U/ml) or 25HC (5 μM) for 24 hr, infected with GLucMCMV and at 2 or 4 hpi and Gaussia luciferase activity measured using supernatants. n = 6 ± SEM. Right shows that RAW264.7 cells were pretreated for 24 hr with Ifn-γ (10 U/ml) or 25HC (2 μM), infected with MCMV (MOI = 2), in normal medium containing vehicle, IFN-γ (10 U/ml) or 25HC (2 μM) for 24 hr, relative abundance of the MCMV ie1 assayed by qRT-PCR. n = 3; mean ± SEM. *p ≤ 0.05.

employ a 25HC mediated apoptotic antiviral response. In this regard, we have found BMDM to be especially sensitive to 25HC concentrations above 2 μM.

We noted marked inhibitory effects on plaque development for all viruses investigated (Figure 5C–5G). Dose response analyses of MCMV plaque formation clearly indicated that the ability of the virus to spread decreased with increasing dose of 25HC (Figures 5C and 5D), while no statistical differences in numbers of infection foci in the presence or absence of 25HC were obtained (Figure 5E). In plaque reduction assays a significant dose-dependent difference in the diameter of the viral plaque was observed (Figure 5E). Similar results were also obtained from plaque reduction assays for influenza virus (Figure 5F). A simple mathematical model that best fits the experimental data is the one in which growth dominates over susceptibility to infection (Figure 5H; Figure S3F; Movie S1). In agreement, single hit growth analyses of MCMV and influenza infection show that 25HC effectively inhibits viral growth (Figure 5G) and for MCMV, 25HC inhibits yields of intracellular and secreted virus to the same extent (Figure 5G). However, in the case of HSV-1 we observed a significant difference in both plaque size and number of plaques (Figure 5F; Figure S3E) suggesting viral entry and growth can be affected and further indicating the multiple levels of control exerted by 25HC depending on the virus-host cell system.

In accordance with the above results we observed a reduction at the level of viral DNA replication by 25HC (Figure 5I). This is associated with reduced amounts of early (E1) and late (M115) gene expression in a 25HC dose-dependent manner strongly supporting a postentry stage inhibition of MCMV infection (Figure S3A). For MCMV Mϕ infection, IFNs mediate antiviral effects through inhibition of the major immediate-early promoter (MIEP) (Kropp et al., 2011). We also find that 25HC imparts, in a dose dependent manner, inhibition of the MIEP monitored by using either reporter virus assay or the endogenous *ie1* expression levels, resulting in approximately 50% inhibitory activity in comparison with Ifnγ treatment (Figure 5J; Figures S3B and S3C).

Interferon Stimulation of 25HC Production Involves Direct Binding of Stat1 to *Ch25h* Promoter

A central question regarding the role of 25HC in terms of innate immunity is how IFN signaling precisely regulates *Ch25h*. Thus, in our next experiments we sought to investigate in further detail the regulatory interferon dependence of the 25HC responses by using host and viral genetic knockouts in our macrophage-infection experiments. First we assessed whether the IFN-β plays a role in mediating the induction 25HC in infection. Figure 6A shows that greater than 80% of the induction response of *Ch25h* is lost in *Ifnb1*$^{-/-}$ Mϕ, whereas 100% of the response is eliminated in *Ifnar1*$^{-/-}$ Mϕ. Because all type I IFNs signal through the Ifnar1 receptor, these results indicate that upon infection of Mϕ, Ifn-β is the primary mediator, whereas other members of the type 1 interferon family serve a minor nonredundant role.

To determine whether a productive infection is required, we used a mutant virus (MCMVd*ie3*) that is fully proficient in infecting cells but fails to initiate viral gene expression. In the following experiments, infection of Mϕ with MCMVd*ie3* resulted in an equal response of *Ch25h* activation in comparison with the parental wild-type (WT) virus but with slightly delayed temporal kinetics (Figure 6B). In this case, and in comparison with *Ifnar1*$^{-/-}$-infected cells, Ifn-β dominates the response (Figure 6B). These results show that productive infection is not required; indicating that pattern recognition receptor activation by the viral particle is sufficient to activate the transcriptional induction of *Ch25h*.

In our Mϕ cultures, Ifn-γ is not expressed but, as shown in Figure 1, is a potent inducer of *Ch25h* activity. Figure 6C shows that infection or treatment with exogenous Ifn-β of *Ifnar1*$^{-/-}$ Mϕ abolishes the induced levels of 25HC, whereas exogenous Ifn-γ treatment does not. Because signal transducer and activator of transcription factor 1 (Stat1) is activated by Ifn-γ though its receptor Ifngr and Stat1 and Stat2 are activated by Ifn-β through its receptor Ifnar1, we next tested the ability of MCMV, Ifn-β and Ifn-γ to activate *Ch25h* mRNA levels in *Stat1*$^{-/-}$ cells. Figure 6D clearly shows that genetic elimination of Stat1 results in the marked loss of the ability of Mϕ to activate *Ch25h* upon infection or treatment with type 1 or type 2 IFNs.

To further investigate the kinetic transcriptional induction of *Ch25h*, we quantitatively determined the de novo synthesis of RNA using 4-thiouridine incorporation. A schematic of this procedure is shown in Figure S4A. In these experiments, between 60 and 90 min after treatment, de novo synthesis of the *Ch25h* transcript increased by approximately 30-fold in Ifn-γ treated cells relative to the mock sample (Figure 6E). To test whether signaling from Ifnar1 was necessary for the induction of *Ch25h* during viral infection, we next conducted de novo synthesis experiments in *Tyk2*$^{-/-}$ macrophage cells. The results shown in Figure 6F indicate that direct signaling by the receptor rather than an indirect or secondary mode of activation is crucial in virus-induced *Ch25h* synthesis and is consistent with the possibility of Stat1 involvement in this process. To explore this possibility further, we next conducted a microarray analysis of de novo transcription during the first 8 hr after IFN-γ stimulation of macrophages. An unbiased clustering analysis of temporal differential synthesis profiles identified a subset of 51 gene transcripts kinetically related to *Ch25h*, including Irf1 and Tap1, (Table S1; Figure 6G). Having demonstrated a notable increase in *Ch25h* transcript synthesis during the first 30 min after IFN-γ treatment, we sought to bioinformatically investigate promoter regions for common transcription factor binding sites. To this end, we applied a statistical analysis of transcription factor overrepresentation in transcripts increased by >2-fold during the first 30 min after IFN-γ treatment. An analysis of 109 transcripts identified (including *Ch25h*) (Table S2) revealed Stat1 as the only transcription factor identified with a combined *Z* score of >10 and Fisher score of <0.01 (values defined by empirical studies).

Because Stat1 is activated under all three conditions tested (MCMV infection, Ifn-β and Ifn-γ treatment) and multiple potential Stat1 binding sites are present upstream of *Ch25h* start site (Figures S4B and S4D). We sought to directly test these predictions using a chromatin immunoprecipitation (ChIP) of Stat1-bound DNA from BMDM treated with Ifn-γ for 1 hr (Figure 6I). The ChIP analysis of *Ch25h* promoter proximal sequences revealed an Ifn-γ-mediated recruitment of Stat1 to the predicted binding region of the *Ch25h* locus (Figure 6I). To extend this analysis, a ChIP-Seq analysis of histone modifications identified as markers of accessible and active chromatin regions, revealed

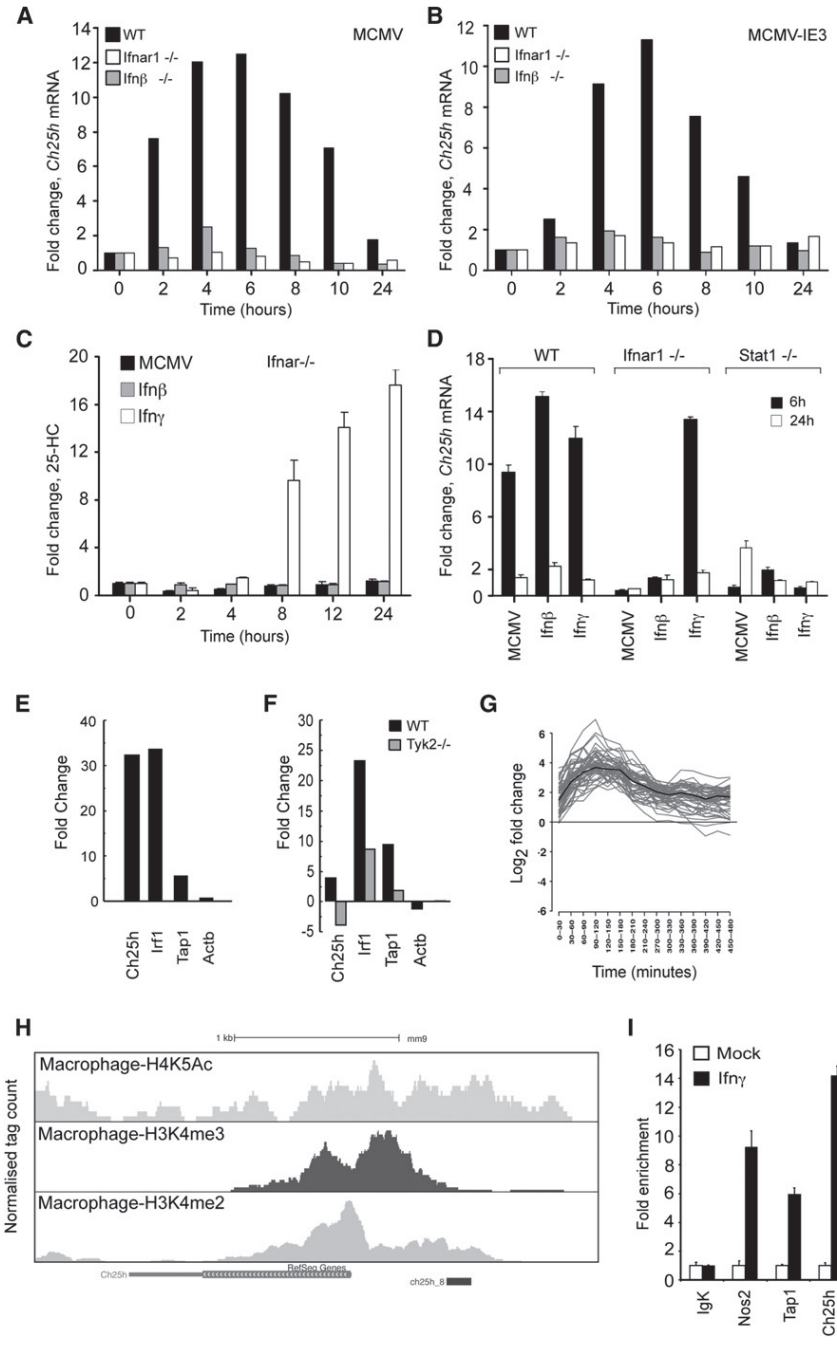

Figure 6. 25HC Synthesis Is Interferon-Dependent and Regulated by Stat1; See Also Figure S4 and Tables S1 and S2

(A and B) *Ch25h* gene expression (relative to mock infected cells) in WT, *Ifnb*$^{-/-}$ or *Ifnar1*$^{-/-}$ BMDM infected with MCMV or MCMVdIE3 (MOI = 1).

(C) Changes in intracellular 25HC in Ifnar1 KO BMDM following MCMV infection, Ifn-β (10 U/ml) or Ifn-γ (10 U/ml) stimulation for 24 hr. n = 3; data are mean ± SD.

(D) qRT-PCR analysis of *Ch25h* mRNA expression at 6 and 24 hpi with MCMV (MOI = 1) or treatment with Ifn-γ (10 U/ml) or Ifn-β (25 U/ml) in WT, *Ifnar1*$^{-/-}$ or *Stat1*$^{-/-}$ BMDM. n = 3, data are mean ± SD.

(E) Differential ntRNA synthesis between 60 and 90 min in Ifn-γ treated (F) or MCMV-infected BMDM (H) relative to mock were analyzed and fold-change values in treated or infected cells calculated relative to the control.

(G) WT BMDM treated with Ifn-γ (10 U/ml). Microarray analysis of newly transcribed RNA isolated from 16 successive 30 min windows after treatment.

(H) UCSC genome browser image is shown for *Ch25h* locus indicating Stat1 binding site (labeled ch25h_8) in promoter region. Normalized tag counts for H3K4me2-MNase ChIP-Seq, H4K5Ac-ChIP-Seq, and H3K4me3-ChIP-Seq are shown for untreated BMDM.

(I) ChIP analysis of Stat1 binding at *Igk* (negative control), *Tap1*, and *Nos2* (positive controls), and *Ch25h* loci (as indicated in Figure 5I) in mock- or Ifn-γ– (20 U/ml, 1 hr) treated BMDMs. Fold enrichment for each locus is the ratio of percentage input of Ifn-γ-treated versus mock-treated BMDMs. IgK (negative control) refers to genomic region lacking Stat1 enrichment. Data are representative of two independent experiments performed in duplicate.

that, in BMDM, the Stat1 binding occurs within a region characterized by these active signatures (Figure 6H). Collectively, these experiments show that *Ch25h* transcriptional activation is coupled to the interferon response through a direct molecular link with Stat1.

DISCUSSION

The innate immune response and the homeostatic pathways controlling cellular sterol levels are now known to regulate each other reciprocally (Castrillo et al., 2003; Kwak et al., 2000; Weitz-Schmidt et al., 2001). Our present findings demonstrate that Mϕ have evolved a program by which IFN is directly coupled to the regulation of 25HC. Although 25HC is a well-known negative feedback mediator of the sterol pathway, we present evidence that it can mediate, at multiple levels, antiviral cellular functions. We show that the mechanism for this coupling is through the direct recruitment of Stat1 to the promoter proximal region of the *Ch25h* gene. Strikingly, a comprehensive metabolome profiling of oxysterols shows that the classical activated Mϕ response is highly focused toward a single oxysterol, 25HC. We find that 25HC can impart antiviral cellular functions via an LXR-independent but Srebp-dependent subordinate mechanism, highlighting a previously unrecognized biological role for 25HC as part of the innate-immune response.

The subordinate involvement of the Srebp pathway for 25HC antiviral activity is based on the following: (1) In normal media, under conditions that reduce the cells reliance on the

Srebp-processing pathway, IC_{50} values obtained are far higher than the known IC_{50} for 25HC inhibition of Srebp processing. (2) An enantiomer of 25HC inhibits viral infection; however, this only occurs at concentrations above 1 μM. We infer from this a Srebp-independent mode of action. (3) The antiviral potency of 25HC viral is dramatically increased for most, but not all, infections under lipid-depleted conditions that favor Srebp processing. Under these conditions, IC_{50} values for 25HC approximate those that actively inhibit the Srebp-pathway. (4) Oxysterols known to target the Srebp-pathway can effectively inhibit viral growth in lipid-depleted conditions, whereas those that do not regulate Srebp fail to affect viral growth. Future studies will be required to further understand the contribution of the Srebp-dependent and independent pathways to 25HC-induced antiviral activity.

How IFN couples with the regulation of the sterol metabolic network is relevant for both innate and adaptive immunity. In recent years, several groups have defined new mechanistic links between the sterol metabolic network and innate (Blanc et al., 2011; Diczfalusy et al., 2009; Im et al., 2011; Liu et al., 2012; Yi et al., 2012) or adaptive (Bauman et al., 2009; Hannedouche et al., 2011) immune responses. Similar to IFN, 25HC is found to halt MCMV growth in Mϕ cells by impeding postentry viral gene expression. IFN is known to dramatically alter in BMDMs both an increase and decrease in abundance of prenylated proteins (Vestal et al., 1995). One potential pathway for blocking MCMV growth is through altering the mevalonate (isoprenoid) branch of the pathway. Our previous studies had indicated that coincubation of IFN treated infected cells with GGOH partially rescues the antiviral response (Blanc et al., 2011). It is noteworthy that many viruses require prenylation of either viral or host proteins for productive infection (Amet et al., 2008; Bordier et al., 2003; Clase et al., 2003; Gower and Graham, 2001; Wang et al., 2005; Ye et al., 2003). Whether 25HC affects protein prenylation remains to be determined; however, we note that a number of highly specific prenylation inhibitors have been shown to significantly inhibit viral multiplication in vitro and in vivo (Bordier et al., 2003; Glenn et al., 1992; Gower and Graham, 2001; Ye et al., 2003).

In summary, our study demonstrates a previously unrecognized biological role for 25HC as an effector of the early innate-interferon response capable of imparting antiviral intracellular functions. Stat1 binding the *Ch25h* promoter provides a critical molecular link between innate immune stimulation, infection, and the Mϕ secretion of a single oxysterol, 25HC.

EXPERIMENTAL PROCEDURES

Cell Propagation and Culture

BMDM were derived from femur and tibia isolated from C57BL/6 mice and grown in DMEM/F12 + GlutaMAX (Lonza, Vervier, Belgium) supplemented with 10% fetal bovine serum (FCS), 10% L929 conditioned medium (containing colony-stimulating factor Csf1) and Penicillin + Streptomycin. FACs assessed BMDMs for Mϕ cell surface markers, F480 and CD11b. All procedures were carried out under project and personal licences approved by the Secretary of State for the Home Office, under the United Kingdom's 1986 Animals (Scientific Procedures) Act and the Local Ethical Review Committee at Edinburgh University. All cultures are routinely tested for mycoplasma and endotoxin levels. Full details for these cultures and for MEFs and cell lines; NIH 3T3, RAW264.7, 199, MDCK, HeLa, MeWo and 293 cells are provided in the Supplemental Experimental Procedures.

Reporter Viruses and Viral Plaque Assays

Viral growth including plaque assays, reporter GFP, and luciferase assays for viral growth and gene expression measurements for WT MCMV, MCMV-GFP, GLuc-MCMV Murine Gammaherpesvirus 68 (MHV-68-GFP), VZV-GFP (vaccine strain Oka), HSV-1-eGFP (C12), A/WSN/33 (H1N1) influenza virus, Ad5-gfp, and Ad19a-gfp are described in Supplemental Experimental Procedures. Plaque reduction assays used an agarose overlay for MCMV, HSV, and Influenza virus infection. For MCMV and HSV, plaque numbers and dimensions were quantified using fluorescent microscopy of infection foci. Phase-contrast and fluorescence visualization of infected was performed using a Zeiss Axio Observer Z1 inverted microscope (Carl Zeiss, Germany). Microscope control and image capture were undertaken using Axiovision Software (Carl Zeiss, Germany). All images were captured and diameters quantified using ImageJ software.

Metabolic Profiling of Oxysterols

Details for the extraction of oxysterols and sterols are provided in Supplemental Experimental Procedures. The extracted oxysterol and sterol fractions were derivatized with Girard P reagent and analyzed by LC-MS(MS^n) on a LTQ-Orbitrap Velos. Mass spectra were recorded at high resolution in the Orbitrap analyzer, and MS^n spectra recorded simultaneously in the LTQ ion-trap. Quantification was performed by stable isotope dilution on reconstructed ion-chromatograms generated in the Orbitrap.

Microarray Analysis, RNA Labeling, and Isolation from BMDM Cultures

Incorporation of 4-thiouridine (Sigma) into newly-transcribed RNA including experiments of RNA time course microarray analysis of transcriptional changes in WT, $Ifnar^{-/-}$, and $Ifnb1^{-/-}$ BMDM following MCMV infection and quantitative RT-PCR using taqman primer probe sets (from Applied Biosystems) or for viral transcripts see Supplemental Experimental Procedures. Time course microarray analysis data are compliant with the National Centre for Biotechnology Information Gene Expression Omnibus (GEO) under SuperSeries accession number GSE42505 (SubSeries numbers GSE42503, GSE42504) (GEO, http://www.ncbi.nlm.nih.gov/geo/).

Statistical Analysis of Transcription Factor Binding Site Overrepresentation

Entrez gene ID's for 164 transcripts with a fold change of >2-fold in the Ifn-γ-treated BMDM samples between 0 and 30 min were imported into the oPOSSUM software tool (http://www.cisreg.ca/cgi-bin/oPOSSUM/opossum) and analyzed as described in Supplemental Experimental Procedures.

Isolation and Quantification of Viral Genome Copy Number by Using qPCR

For DNA extraction, cells were extensively washed thrice 3 hr postinfection and total genomic DNA isolated and genome copy number normalized to input DNA or to gapdh using quantitative procedures described in Supplemental Experimental Procedures.

Oxysterol Screening against MCMV, HSV-1, MHV-68, VZV, Influenza A, and Adenovirus

For these experiments, respective host cell systems were conducted in black 96-well plates using media conditions and oxysterol treatment as described in the figure legends and Supplemental Experimental Procedures. The IC_{50} values were calculated as the concentration at 50% viral inhibition. Cell viability and toxicity assays were determined using the CellTiter Blue (CTB, Promega) reagent.

Metabolite Treatment of Cells

Murine embryo fibroblasts were infected with MCMV (MOI = 0.01). After adsorption, cells were washed 5 times with normal medium (DMEM, 10% FCS, L-Glutamine and Penicillin/Streptomycin). After washing, normal medium containing vehicle (Ethanol) or 25HC (1 μM) ± Geranylgeraniol (GGOH, 20 μM) (Sigma G3278) or Mevalonolactone (Mev, 20μM) (Sigma M4667), Farnesol (FOH, 20 μM) (Sigma F203) or Squalene (Sqle, 20 μM) (Sigma S3026) was added to the infected wells. After 4 days, supernatants were collected and MCMV titer calculated by plaque assay.

Computational Prediction of Stat1 Binding Sites in the Ch25h Promoter

To analyze and predict potential Stat1 binding sites in the promoter of Human and Mouse *Ch25h* genes, we used the open source software Toucan. In brief, 1Kb 5′ *cis*-regulatory regions upstream of the transcriptional start sites of human (ENSG00000138135) or mouse (ENSMUSG00000050370) *Ch25h* were imported into Toucan. Predicted transcription factor binding sites were then identified in these sequences using the MotifLocator algorithm. Position Weight Matrices for this analysis were derived from the TransFac database V7.0 (public) and the background model used was either mouse or human DBTSS promoters depending on input sequence. A default stringency threshold of 0.9 was used for all predictions.

Chromatin Immunoprecipitation (ChIP)

For ChIP of Stat1, 6×10^7 Mϕ were used per ChIP, as detailed in the Supplemental Experimental Procedures, including the analysis of ChIP-Seq data for UCSC Browser image of Ch25h locus.

SUPPLEMENTAL INFORMATION

Supplemental Information includes four figures, two tables, Supplemental Experimental Procedures, and one movie and can be found with this article online at http://dx.doi.org/10.1016/j.immuni.2012.11.004.

ACKNOWLEDGMENTS

This work was supported by the Wellcome Trust (WT066784), the BBSRC and EPSRC (SynthSys BB/D019621/1), the University of Edinburgh Alumni Fund, and reagent support from RNAi Global Initiative to P.G.; BBSRC studentships to P.L. and A.M.; BHF studentship (FS/05/022) to M.B.; SNRF award (CRPNo. 2007-04), BRCS (R-183-000-211-305) and NMRC (R-183-000-224-213) to M.R.W.; BBSRC (BB/C5157712, BB/C5113561, BB/I0017351) to W.J.G. and (BB/H0010181) to Y.W.; Spanish Ministry of Science and Innovation (SAF 2011-25155) to A.A.; NIH grant (HL67773) to D.F.C. We are grateful to David Russell for LY295427 and LY306039, Birgit Strobl and Matthias Müller for *Ifnar*$^{-/-}$ and *Stat1*$^{-/-}$ Mϕ, Sam Pattle for help with viral infections, and Daniel S. Ory for advice.

Received: June 26, 2012
Accepted: November 6, 2012
Published: December 27, 2012

REFERENCES

Adams, C.M., Reitz, J., De Brabander, J.K., Feramisco, J.D., Li, L., Brown, M.S., and Goldstein, J.L. (2004). Cholesterol and 25-hydroxycholesterol inhibit activation of SREBPs by different mechanisms, both involving SCAP and Insigs. J. Biol. Chem. *279*, 52772–52780.

Amet, T., Nonaka, M., Dewan, M.Z., Saitoh, Y., Qi, X., Ichinose, S., Yamamoto, N., and Yamaoka, S. (2008). Statin-induced inhibition of HIV-1 release from latently infected U1 cells reveals a critical role for protein prenylation in HIV-1 replication. Microbes Infect. *10*, 471–480.

Bauman, D.R., Bitmansour, A.D., McDonald, J.G., Thompson, B.M., Liang, G., and Russell, D.W. (2009). 25-Hydroxycholesterol secreted by macrophages in response to Toll-like receptor activation suppresses immunoglobulin A production. Proc. Natl. Acad. Sci. USA *106*, 16764–16769.

Blanc, M., Hsieh, W.Y., Robertson, K.A., Watterson, S., Shui, G., Lacaze, P., Khondoker, M., Dickinson, P., Sing, G., Rodríguez-Martín, S., et al. (2011). Host defense against viral infection involves interferon mediated down-regulation of sterol biosynthesis. PLoS Biol. *9*, e1000598.

Bordier, B.B., Ohkanda, J., Liu, P., Lee, S.Y., Salazar, F.H., Marion, P.L., Ohashi, K., Meuse, L., Kay, M.A., Casey, J.L., et al. (2003). In vivo antiviral efficacy of prenylation inhibitors against hepatitis delta virus. J. Clin. Invest. *112*, 407–414.

Castrillo, A., Joseph, S.B., Vaidya, S.A., Haberland, M., Fogelman, A.M., Cheng, G., and Tontonoz, P. (2003). Crosstalk between LXR and toll-like receptor signaling mediates bacterial and viral antagonism of cholesterol metabolism. Mol. Cell *12*, 805–816.

Clark, P.J., Thompson, A.J., Vock, D.M., Kratz, L.E., Tolun, A.A., Muir, A.J., McHutchison, J.G., Subramanian, M., Millington, D.M., Kelley, R.I., and Patel, K. (2012). Hepatitis C virus selectively perturbs the distal cholesterol synthesis pathway in a genotype-specific manner. Hepatology *56*, 49–56.

Clase, A.C., Lyman, M.G., del Rio, T., Randall, J.A., Calton, C.M., Enquist, L.W., and Banfield, B.W. (2003). The pseudorabies virus Us2 protein, a virion tegument component, is prenylated in infected cells. J. Virol. *77*, 12285–12298.

Contreras, F.X., Ernst, A.M., Haberkant, P., Björkholm, P., Lindahl, E., Gönen, B., Tischer, C., Elofsson, A., von Heijne, G., Thiele, C., et al. (2012). Molecular recognition of a single sphingolipid species by a protein's transmembrane domain. Nature *481*, 525–529.

del Real, G., Jiménez-Baranda, S., Mira, E., Lacalle, R.A., Lucas, P., Gómez-Moutón, C., Alegret, M., Peña, J.M., Rodríguez-Zapata, M., Alvarez-Mon, M., et al. (2004). Statins inhibit HIV-1 infection by down-regulating Rho activity. J. Exp. Med. *200*, 541–547.

Deraeve, C., Guo, Z., Bon, R.S., Blankenfeldt, W., DiLucrezia, R., Wolf, A., Menninger, S., Stigter, E.A., Wetzel, S., Choidas, A., et al. (2012). Psoromic acid is a selective and covalent Rab-prenylation inhibitor targeting autoinhibited RabGGTase. J. Am. Chem. Soc. *134*, 7384–7391.

Diczfalusy, U., Olofsson, K.E., Carlsson, A.M., Gong, M., Golenbock, D.T., Rooyackers, O., Fläring, U., and Björkbacka, H. (2009). Marked upregulation of cholesterol 25-hydroxylase expression by lipopolysaccharide. J. Lipid Res. *50*, 2258–2264.

Espenshade, P.J., and Hughes, A.L. (2007). Regulation of sterol synthesis in eukaryotes. Annu. Rev. Genet. *41*, 401–427.

Glenn, J.S., Watson, J.A., Havel, C.M., and White, J.M. (1992). Identification of a prenylation site in delta virus large antigen. Science *256*, 1331–1333.

Gong, Y., Lee, J.N., Lee, P.C., Goldstein, J.L., Brown, M.S., and Ye, J. (2006). Sterol-regulated ubiquitination and degradation of Insig-1 creates a convergent mechanism for feedback control of cholesterol synthesis and uptake. Cell Metab. *3*, 15–24.

Gower, T.L., and Graham, B.S. (2001). Antiviral activity of lovastatin against respiratory syncytial virus in vivo and in vitro. Antimicrob. Agents Chemother. *45*, 1231–1237.

Hannedouche, S., Zhang, J., Yi, T., Shen, W., Nguyen, D., Pereira, J.P., Guerini, D., Baumgarten, B.U., Roggo, S., Wen, B., et al. (2011). Oxysterols direct immune cell migration via EBI2. Nature *475*, 524–527.

Horton, J.D., Goldstein, J.L., and Brown, M.S. (2002). SREBPs: activators of the complete program of cholesterol and fatty acid synthesis in the liver. J. Clin. Invest. *109*, 1125–1131.

Im, S.S., Yousef, L., Blaschitz, C., Liu, J.Z., Edwards, R.A., Young, S.G., Raffatellu, M., and Osborne, T.F. (2011). Linking lipid metabolism to the innate immune response in macrophages through sterol regulatory element binding protein-1a. Cell Metab. *13*, 540–549.

Janowski, B.A., Shan, B., and Russell, D.W. (2001). The hypocholesterolemic agent LY295427 reverses suppression of sterol regulatory element-binding protein processing mediated by oxysterols. J. Biol. Chem. *276*, 45408–45416.

Kropp, K.A., Robertson, K.A., Sing, G., Rodriguez-Martin, S., Blanc, M., Lacaze, P., Hassim, M.F., Khondoker, M.R., Busche, A., Dickinson, P., et al. (2011). Reversible inhibition of murine cytomegalovirus replication by gamma interferon (IFN-γ) in primary macrophages involves a primed type I IFN-signaling subnetwork for full establishment of an immediate-early antiviral state. J. Virol. *85*, 10286–10299.

Kwak, B., Mulhaupt, F., Myit, S., and Mach, F. (2000). Statins as a newly recognized type of immunomodulator. Nat. Med. *6*, 1399–1402.

Liu, C., Yang, X.V., Wu, J., Kuei, C., Mani, N.S., Zhang, L., Yu, J., Sutton, S.W., Qin, N., Banie, H., et al. (2011). Oxysterols direct B-cell migration through EBI2. Nature *475*, 519–523.

Liu, S.Y., Sanchez, D.J., Aliyari, R., Lu, S., and Cheng, G. (2012). Systematic identification of type I and type II interferon-induced antiviral factors. Proc. Natl. Acad. Sci. USA *109*, 4239–4244.

Munger, J., Bennett, B.D., Parikh, A., Feng, X.J., McArdle, J., Rabitz, H.A., Shenk, T., and Rabinowitz, J.D. (2008). Systems-level metabolic flux profiling identifies fatty acid synthesis as a target for antiviral therapy. Nat. Biotechnol. *26*, 1179–1186.

O'Neill, L.A., and Bowie, A.G. (2010). Sensing and signaling in antiviral innate immunity. Curr. Biol. *20*, R328–R333.

Park, K., and Scott, A.L. (2010). Cholesterol 25-hydroxylase production by dendritic cells and macrophages is regulated by type I interferons. J. Leukoc. Biol. *88*, 1081–1087.

Peña, J., and Harris, E. (2012). Early dengue virus protein synthesis induces extensive rearrangement of the endoplasmic reticulum independent of the UPR and SREBP-2 pathway. PLoS ONE *7*, e38202.

Potena, L., Frascaroli, G., Grigioni, F., Lazzarotto, T., Magnani, G., Tomasi, L., Coccolo, F., Gabrielli, L., Magelli, C., Landini, M.P., and Branzi, A. (2004). Hydroxymethyl-glutaryl coenzyme a reductase inhibition limits cytomegalovirus infection in human endothelial cells. Circulation *109*, 532–536.

Radhakrishnan, A., Ikeda, Y., Kwon, H.J., Brown, M.S., and Goldstein, J.L. (2007). Sterol-regulated transport of SREBPs from endoplasmic reticulum to Golgi: oxysterols block transport by binding to Insig. Proc. Natl. Acad. Sci. USA *104*, 6511–6518.

Rodwell, V.W., Nordstrom, J.L., and Mitschelen, J.J. (1976). Regulation of HMG-CoA reductase. Adv. Lipid Res. *14*, 1–74.

Rusiñol, A.E., Thewke, D., Liu, J., Freeman, N., Panini, S.R., and Sinensky, M.S. (2004). AKT/protein kinase B regulation of BCL family members during oxysterol-induced apoptosis. J. Biol. Chem. *279*, 1392–1399.

Song, B.L., Javitt, N.B., and DeBose-Boyd, R.A. (2005). Insig-mediated degradation of HMG CoA reductase stimulated by lanosterol, an intermediate in the synthesis of cholesterol. Cell Metab. *1*, 179–189.

Spencer, C.M., Schafer, X.L., Moorman, N.J., and Munger, J. (2011). Human cytomegalovirus induces the activity and expression of acetyl-coenzyme A carboxylase, a fatty acid biosynthetic enzyme whose inhibition attenuates viral replication. J. Virol. *85*, 5814–5824.

Sun, L.P., Seemann, J., Goldstein, J.L., and Brown, M.S. (2007). Sterol-regulated transport of SREBPs from endoplasmic reticulum to Golgi: Insig renders sorting signal in Scap inaccessible to COPII proteins. Proc. Natl. Acad. Sci. USA *104*, 6519–6526.

Taylor, H.E., Linde, M.E., Khatua, A.K., Popik, W., and Hildreth, J.E. (2011). Sterol regulatory element-binding protein 2 couples HIV-1 transcription to cholesterol homeostasis and T cell activation. J. Virol. *85*, 7699–7709.

Vestal, D.J., Maki, R.A., and Buss, J.E. (1995). Induction of a prenylated 65-kd protein in macrophages by interferon or lipopolysaccharide. J. Leukoc. Biol. *58*, 607–615.

Wang, C., Gale, M., Jr., Keller, B.C., Huang, H., Brown, M.S., Goldstein, J.L., and Ye, J. (2005). Identification of FBL2 as a geranylgeranylated cellular protein required for hepatitis C virus RNA replication. Mol. Cell *18*, 425–434.

Watterson, S., Guerriero, M.L., Blanc, M., Mazein, A., Loewe, L., Robertson, K.A., Gibbs, H., Shui, G., Wenk, M.R., Hillston, J., and Ghazal, P. (2012). A model of flux regulation in the cholesterol biosynthesis pathway: Immune mediated graduated flux reduction versus statin-like led stepped flux reduction. Biochimie. Published online June 1, 2012. http://dx.doi.org/10.1016/j.biochi.2012.05.024.

Weitz-Schmidt, G., Welzenbach, K., Brinkmann, V., Kamata, T., Kallen, J., Bruns, C., Cottens, S., Takada, Y., and Hommel, U. (2001). Statins selectively inhibit leukocyte function antigen-1 by binding to a novel regulatory integrin site. Nat. Med. *7*, 687–692.

Yabe, D., Brown, M.S., and Goldstein, J.L. (2002). Insig-2, a second endoplasmic reticulum protein that binds SCAP and blocks export of sterol regulatory element-binding proteins. Proc. Natl. Acad. Sci. USA *99*, 12753–12758.

Ye, J., Wang, C., Sumpter, R., Jr., Brown, M.S., Goldstein, J.L., and Gale, M., Jr. (2003). Disruption of hepatitis C virus RNA replication through inhibition of host protein geranylgeranylation. Proc. Natl. Acad. Sci. USA *100*, 15865–15870.

Yi, T., Wang, X., Kelly, L.M., An, J., Xu, Y., Sailer, A.W., Gustafsson, J.A., Russell, D.W., and Cyster, J.G. (2012). Oxysterol gradient generation by lymphoid stromal cells guides activated B cell movement during humoral responses. Immunity *37*, 535–548.

Yu, Y., Maguire, T.G., and Alwine, J.C. (2012). Human cytomegalovirus infection induces adipocyte-like lipogenesis through activation of sterol regulatory element binding protein 1. J. Virol. *86*, 2942–2949.

Chapter 4

Investigation of redundant antiviral pathways in MCMV replication

4.1 Introduction

The sterol biosynthesis pathway encompasses sequential enzymatic reactions, starting with acetyl-CoA and leading to the production of cholesterol (Figure 1.2). The work of Schoenheimer and Rittenberg first studied the synthesis of cholesterol molecules. Injecting chicken embryos (which do not synthesize cholesterol) with heavy water (D_2O) did not lead to the formation of deuterium cholesterol, whereas feeding mice with heavy water led to the accumulation of deuterium cholesterol (Schoenheimer and Rittenberg, 1935). Further kinetic analysis revealed that the incorporation of deuterium into cholesterol in rat's liver was a slow process in comparison with fatty acid synthesis. These findings suggested that cholesterol is synthesized through coupling of a number of small molecules. During a search for a replacement for acetate, a carbon source for *Lactobacillus acidophilus*, the work of Wright and Folks led to the successful isolation of mevalonic acid (mevalonate), the product of HMGCR (Wright et al., 1956). Further biochemical studies showed the process of converting mevalonate to squalene, which involves the formation of sterol intermediates including isopentenyl pyrophosphate (IPP) (Agranoff et al., 1960), dimethylallyl pyrophosphate (DMAPP) (Goodman and Popjak, 1960), geranyl pyrophosphate (GPP) (Nandi and Porter, 1964), and farnesyl pyrophosphate (FPP) (Popjak and Goodman, 1961). With the aforementioned studies by Bloch, Kandustch and Russell (see Chapter 1), these secondary metabolites form the fundamental building blocks of cholesterol, oxysterols, and other steroid hormones.

Prior to the successful purification of the enzyme β-hydroxy-β-methylglutaryl-CoA (now known as 3-hydroxy-3-methylglutaryl-CoA, HMGCR (Higgins et al., 1971)), several lines of evidence pointed to the homeostatic nature of cholesterol regulation. In particular, experimentation in dogs, cats, and rabbits by Gould and colleagues demonstrated that cholesterol levels in these animal tissues were maintained in a state of dynamic equilibrium: rates of cholesterol synthesis and absorption responded quickly to changes in diet (Gould et al., 1953). Moreover, a landmark study by Siperstein and Fagan showed that the conversion rate of acetate-2-^{14}C to mevalonate or cholesterol is repressed in rat hepatocytes in response to increasing concentration of mevalonic acid (Siperstein and Fagan, 1966). The first direct evidence showing feedback regulation of cholesterol biosynthesis came from studies of HMGCR. After cholesterol feeding, the increase in rat liver cholesterol concentration was accompanied by a decrease in the rate of cholesterol synthesis. The decline in cholesterol synthesis measured in liver microsomes was closely paralleled to the decline in HMGCR activity (Shapiro and Rodwell, 1971). Remarkably, the activity of HMGCR in the liver exhibited a diurnal variation that was dependent on feeding cycles (Dugan et al., 1972; Shapiro and Rodwell, 1971). This oscillating behaviour was completely abolished with treatments of cycloheximide or puromycin (both of which block protein synthesis) (Dugan et al., 1972; Edwards and Gould, 1972; Higgins et al., 1971). These studies indicated that HMGCR is regulated at the level of protein synthesis, and appeared to be the sole regulatory site between acetyl-CoA and cholesterol (Shapiro and Rodwell, 1971).

Although the above experiments showed a correlation between HMGCR and cholesterol synthesis, it was noted that there were two lag periods: the first lag period occurs between the time of feeding and the reduction in HMGCR activity. The second lag period occurs between the reduction in HMGCR activity and the declining rate of cholesterol synthesis (Dugan et al., 1972; Higgins and Rudney, 1973). These observations suggested that additional enzymes on the pathway might also vary diurnally due to cholesterol feeding, and that cholesterol feeding seemed to have two effects: the immediate inhibition of enzymatic activities (e.g. post-translational

inhibition or degradation), and the subsequent inhibition of enzyme synthesis, possibly through transcriptional control (now known as the SREBP2 pathway) (Higgins and Rudney, 1973). Indeed, an earlier work published by Gould and Swyryd had already demonstrated the potential feedback regulation of the cholesterol pathway (Gould and Swyryd, 1966). In these time-series experiments, rats were first put on a long-term (30 - 640 days) cholesterol feeding diet, and subsequently sacrificed to obtain liver extracts. The ability of liver homogenates to synthesize cholesterol from acetate (feeds into HMGCR), mevalonate (Mev) (feeds into MVK), farnesyl diphosphate (FPP) (feeds into FDFT1), squalene (SQ) (feeds into SQLE), and the interconversion between mevalonate to FPP were assessed (see Figure 4.1). Initial observations revealed that the maximum synthesis capacity of cholesterol from mevalonate was far greater than from acetate, indicating that the conversion of HMG-CoA to mevalonate (by the enzyme HMGCR) might be the rate-limiting step. Significantly, cholesterol-fed animals showed decreased rates of conversion from mevalonate to FPP, whereas the rate of synthesis of cholesterol from squalene remained unaffected. Sites of inhibition of cholesterol synthesis were also detected before mevalonate, between mevalonate and FPP, and between FPP and squalene (Figure 4.1).

The possibility of feedback inhibition beyond mevalonate raises the question of whether these inhibition sites actually exist and their mechanism of action. On one level, the work of Brown and Goldstein already showed that the transcription of sterol biosynthesis genes are under the control of SREBP2, and that SREBP2 itself is regulated by sterol (Horton et al., 2003). However, transcriptional control alone could not explain specific sites of inhibition identified by Gould and the above HMGCR studies, indicating that additional post-transcriptional feedback control must be present. Enzyme kinetic studies using purified human MVK, PVMK, and MVD revealed that the activity of MVK could be competitively inhibited (listed from the strongest inhibitory effect) by geranylgeranyl-diphosphate (GGPP, C_{20}), farnesyl-diphosphate (FPP, C_{15}), geranyl-diphosphate (GPP, C_{10}), isopentenyl-diphosphate (IPP, C_5), 3,3-dimethylallyl-diphosphate (DMAPP, C_5), farnesol (C_{15}), and dolichol-phosphate (DP, $C_{80\text{-}100}$) (Dorsey and Porter, 1968; Hinson et al., 1997;

Tanaka et al., 1990). Conversely, mevalonate-diphosphate, geraniol, and dolichol were not inhibitory toward MVK. Using 6-fluoromevalonate (Fmev), a compound that blocks the conversion of mevalonate-phosphate to IPP (an inhibitor of MVD), Cuthbert and Lipsky showed that the accumulation of mevalonate phosphate in malignant T, B and myeloid cell lines, and PBMC led to proliferation inhibition (as measured by DNA synthesis) (Cuthbert and Lipsky, 1991, 1990). The magnitude of inhibition in different Fmev treated cell types was correlated with the activity of HMGCR. In addition, Fmev mediated inhibition was prevented by either co-treating cells with lovastatin (which blocks HMGCR, reducing mevalonate synthesis), or supplementing with high quantities of LDL (which also inhibits HMGCR through SREBP2). These results indicated that mevalonate/mevalonate-phosphate derivative could act as a source of both positive and negative regulatory influence on targets that are yet to be identified.

At the junction of the mevalonate-isoprenoid arm, farnesyl pyrophosphate synthase (FDPS) catalyses the head-to-tail condensation of DMAPP with an additional IPP to produce farnesyl diphosphate (FPP) (Thulasiram and Poulter, 2006). FPP has been shown to inhibit MVK activity (see above), and its natural derivative farnesol (FOH) was also shown to accelerate the degradation of HMGCR in CHO and SSD cells (using ≥20μM of FOH) (Meigs and Simoni, 1997; Roseman, 1996). Furthermore, increasing FPP concentration in reticulocytes led to a decrease in the rate of IPP synthesis. However, this decrease was accompanied by an accumulation of IPP and DMAPP in the cytosol, indicating that FPP could also inhibit its own synthesis (Lutz et al., 1992). Similar to FPP, GGPP is another isoprenoid that exhibits feedback regulation on the mevalonate arm. GGPP is synthesized through condensation of FPP with IPP. This process is catalysed by the enzyme GGPS1 (Sagami et al., 1993). Comparable to FPP, treatments of reticulocytes with GGPP also led to repression of MVK activity (see above) and IPP synthesis (Lutz et al., 1992). However, treatment of GGPP had no effect on FPP synthesis. Moreover, geranylgeraniol (GGOH), the natural derivative of GGPP, was also shown to enhance under a combination of 25-HC (2.5μM) and cholesterol (2.5μM) for mediating HMGCR degradation in SV-589 cells (using ≥10μM of GGOH) (Sever et al., 2003). Collectively, these findings

suggested isoprenoids act as negative feedback signals to the pathway, possibly through competitive inhibition, or by promoting protein degradation.

The last inhibitory site (Figure 4.1, I_3) identified by Gould and Swyryd was the synthesis of squalene from FPP. The two-step reaction is catalysed by the squalene synthase (farnesyl-diphosphate farnesyltransferase, FDFT1). These reactions are the first committed steps in cholesterol biosynthesis. In the first step, FDFT1 catalyses the condensation of two FPP (C_{15}) molecules to form presqualene diphosphate (SQPP, C_{30}) (Tansey and Shechter, 2001). In the second step, the presqualene is reduced at the expense of NADPH to produce squalene (Blagg et al., 2002; Radisky and Poulter, 2000). The requirement of NADPH during the synthesis of squalene from SQPP was first demonstrated by Sasiak and Rilling using semi-purified yeast squalene synthase (Sasiak and Rilling, 1988). *In vitro* synthesis of squalene could not proceed without inputs of NADPH, and the low energy NADP subsequently acted as a non-competitive inhibitor for FDFT1 (Sasiak and Rilling, 1988). Interestingly, the ratio of SQPP to squalene synthesized from FPP by FDFT1 was approximately 6:1, indicating that the intermediates could accumulate in the cytosol (Kuswik-Rabiega and Rilling, 1987; Sasiak and Rilling, 1988). Whether SQPP can act as a feedback signal on the pathway is yet to be determined.

Mammalian innate immunity against foreign pathogens involves the secretion of soluble protein factors by pathogen-sensing cells. Cytokines, such as interferon, provide both autocrine and paracrine signalling to non-infected cells to inform pathogen challenge. The activation of interferon-stimulated genes (ISGs) (Ablasser et al., 2013) leads to the remodelling of the intracellular environment, thus providing resistance to viral infection (Wagner and Levy, 1960). Our previous study showed that the host sterol biosynthesis pathway is downregulated by interferon as an antiviral response (Blanc and Hsieh, 2011). In Chapters 2 and 3, I showed that lipophilic statins and 25-HC elicit broad antiviral effects. The antiviral effects of these sterol mediators were lipid condition dependent. Yet, little is known about how lipid condition affects viral growth and the underlying mechanisms. Moreover, it is worth noting that the activities of interferon have considerable overlap with many of the activities of statins

(Neuhaus et al., 2005), in particular, at lowering cholesterol. Whether statins, interferon, 25-HC, and antiviral drugs such as ganciclovir have overlapping antiviral mechanisms remains to be examined. Here, the aim of this chapter was to examine redundant and non-redundant controls of the sterol biosynthesis pathway in regulating viral replication. In particular, experiments were conducted to explore multilayer inhibitory effects of statin, 25-HC, and interferon on MCMV replication. Results presented in this chapter further support the development of selectively combinatorial targeting host pathways as an efficacious anti-infective strategy.

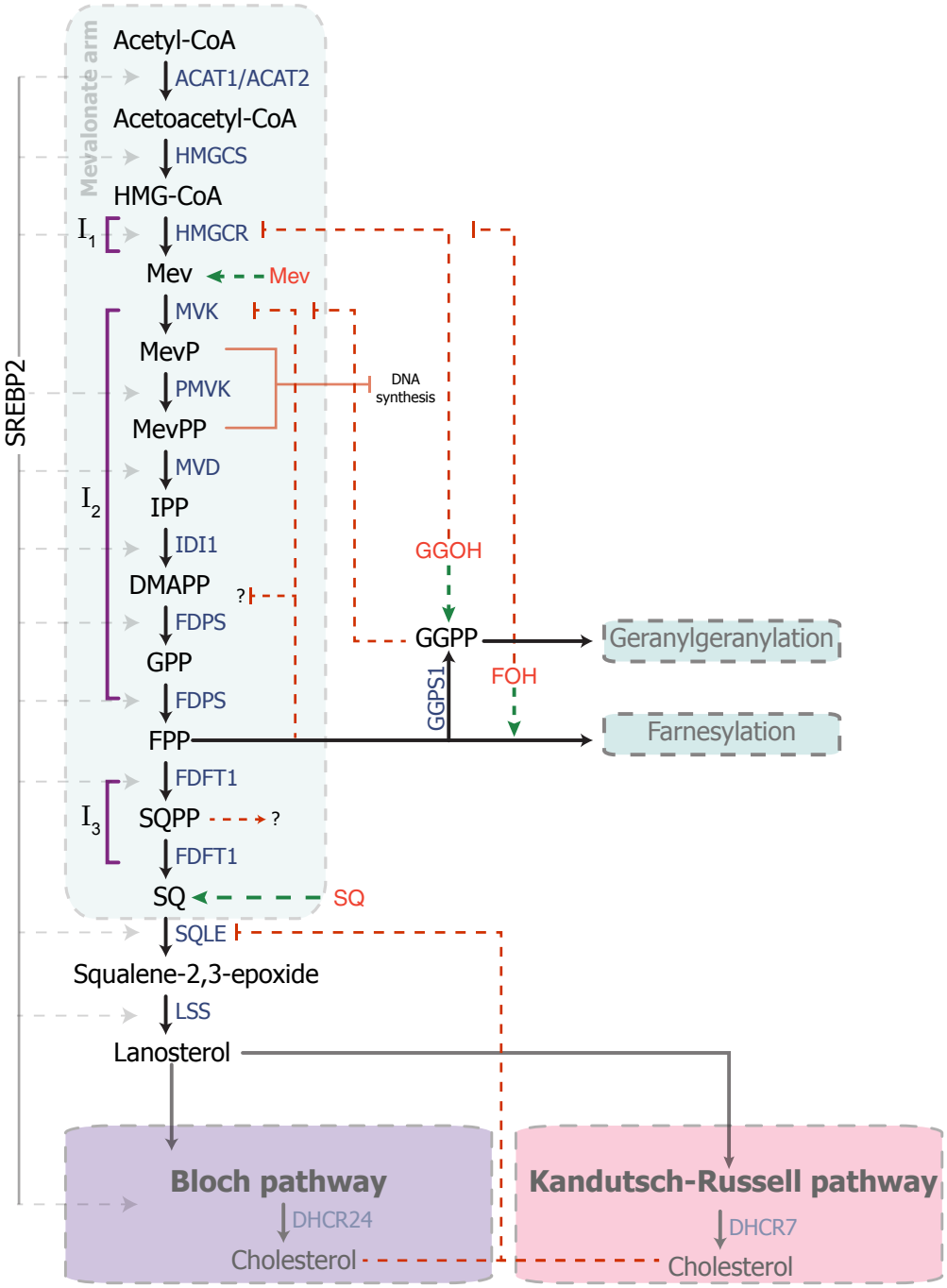

Figure 4.1 Potential non-SREBP2 mediated feedback regulation of the sterol biosynthesis pathway.

Transcriptional control of SREBP2 on the sterol biosynthesis is shown on the left-hand side of the figure. The right-hand side of the figure is a simplified illustration of the feedback mechanisms proposed by Gould and others. I1, I2, and I3, were inhibitory points on the mevalonate arm initially identified by Gould by measuring the conversion rate of sterol intermediates to cholesterol in long-term cholesterol feeding mice. Subsequent enzymatic studies have found that both GGPP, and FPP are competitive inhibitors of the enzyme MVK, and induce degradation of HMGCR. In addition, evidence suggests that the synthesis of FPP is self-regulated (represented by the accumulation of IPP and DMAPP), however the exact mechanism is unknown. Inhibition of MVD by 6-fluromevalonate causes the accumulation of MevP and MevPP, which act as inhibitory signals for DNA synthesis in lymphocytes. Secondary metabolites used in this chapter are labelled red: Mev = mevalonolactone, SQ = squalene, FOH = farnesol, GGOH = geranylgeraniol.

4.2 Results

4.2.1 Viral replication is affected by changes in lipid conditions

In Chapter 3 experiments, treatment of NIH-3T3 fibroblasts with 25-HC in the delipidated media led to a noticeable increase in potency in the IC_{50} of 25-HC against MCMV in comparison with the lipidated media (1.83μM ➔ 0.31μM). These studies implicated that lipid conditions may play a role in influencing the antiviral action of 25-HC. As a first step to examine the effects of lipid condition on viral replication, NIH-3T3 fibroblasts were first infected with MCMV-GFP, and then cultured in media supplemented with either lipidated or delipidated serum. The progression of infection was monitored over time by fluorescent viral reporter assay or by viral growth curves. Figure 4.2A shows that the replication of MCMV in the delipidated media had a lower growth rate (represented by the GFP intensity) and particle yield (shown Figure S4.1) in comparison with the lipidated media.

Because cells can alter their growth rate in response to changes in media condition, it is likely that the reduction in viral replication in the delipidated media was the result of reduction in cellular growth. The growth rate of cells can be directly measured through cell counting over time using a haemocytometer. A more convenient method is to use a cell-line expressing a reporter construct, where changes in the reporter expression reflect the division rate (growth) of the cell. To examine the effects of serum condition on cellular growth, NIH-3T3 fibroblasts stably expressing a GFP tagged histone H2B, NIH-3T3-H2B-GFP, were used (Gibbs et al., 2013). In these experiments, NIH-3T3-H2B-GFP cells were grown in either lipidated or delipidated media, and the growth of cells was monitored by measuring the fluorescent intensity. Figure 4.2B shows that cells grown in the delipidated media (grey and blue lines) had a lower growth rate than the lipidated serum (black and red lines). Thus, the slower growth rate of the cell in the delipidated media could not be ruled out in explaining the deficiencies in MCMV replication.

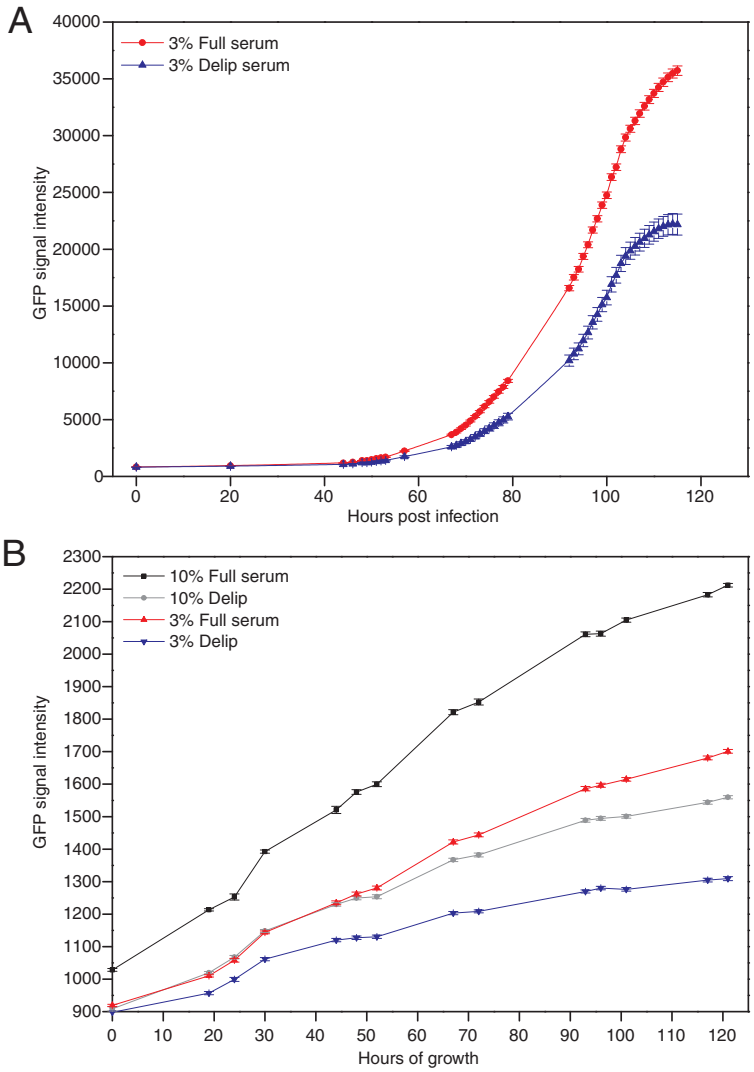

Figure 4.2 Changes in media serum condition affects MCMV replication.
(A) Virus replication was monitored as a function of kinetic GFP fluorescence. NIH-3T3 fibroblasts were seeded at a seeding density of $3x10^4$ cells/well in black 96-well plates in normal media. The next day, cells were infected with MCMV-GFP (MOI = 0.016) for 1 hr. After absorption, the viral inoculum was removed and cells were incubated with DMEM supplemented with either 10%, 3% normal media, or 3% delipidised media. Data are mean of two experiments (4 replicates per experiment) ± SEM. (B) NIH-3T3-H2B-GFP were seeded at a seeding density of $1x10^4$ cells/well in 96-well plates. The next day, cells were incubated in 185µl of phenol red-free media supplemented with different serum types as indicated. Growth of the cells was monitored by the increasing in fluorescent intensity. Data are the mean of two experiments (32 biological replicates) ± SEM.

4.2.2 Treatments of sterol intermediates stimulate MCMV replication but have no effects on cellular growth

The above experiments suggested that the replication of MCMV was altered in response to changes in lipid content. This result is consistent with the reduced growth of NIH-3T3-H2B-GFP in the delipidated media, indicating that cellular responses to sterol depletion were partly responsible for the observed reduction in viral replication. However, the work by Goldstein et al., 1983 showed that the method of producing delipidated serum required the use of multistep ultracentrifugation, charcoal filtering, NaCl solution dialysis, and thrombin reconstitution. This method is effective at removing cholesterol, but also removes other hormones, cytokines, fatty acids, and growth factors from the serum. Thus, the effects of delipidated serum on both viral replication and cell proliferation could involve a combination of both “sterol dependent”, and “sterol independent” effects. Due to product information confidentiality, the exact formulation of the delipidated serum and its method of synthesis are unknown. To demonstrate sterol dependent and independent mechanisms, and to determine whether rejuvenating the sterol biosynthesis pathway in a lipid-depleted condition can recover MCMV replication deficiency, a series of metabolic rescue experiments were performed. In these experiments, NIH-3T3 fibroblasts were first infected with MCMV-GFP, then cultured in either lipidated or delipidated media supplemented with mevalonate, squalene, farnesol, or geranylgeraniol at various concentrations. The progression of viral replication was determined by measuring the fluorescent readouts. Treatments with mevalonate and geranylgeraniol increased MCMV replication in both lipidated and delipidated media (Figure 4.3A), whereas squalene and farnesol did not (see Figure S4.2 – S4.6 for the complete metabolite dose-viral growth curves). Due to technical difficulties, treatment with cholesterol was not examined. The increase in MCMV replication was independent of cell growth, as the proliferation of NIH-3T3-H2B-GFP remained unchanged in the presence or absence of sterol metabolites (Figure 4.3B). Moreover, the addition of mevalonate and geranylgeraniol in the delipidated media only provided partial recovery to the MCMV growth (Figure S4.2, S4.6). Altogether, these studies agree with previous chapter findings that increasing the metabolite flow towards the geranylgeraniol arm,

rather than stimulating cell proliferation, has beneficial effects on viral replication. However, it was also observed that the addition of mevalonate (Figure S4.2A vs. B) or geranylgeraniol (S4.6A vs. B) could not fully restore the growth deficiencies of MCMV in the delipidated media, .

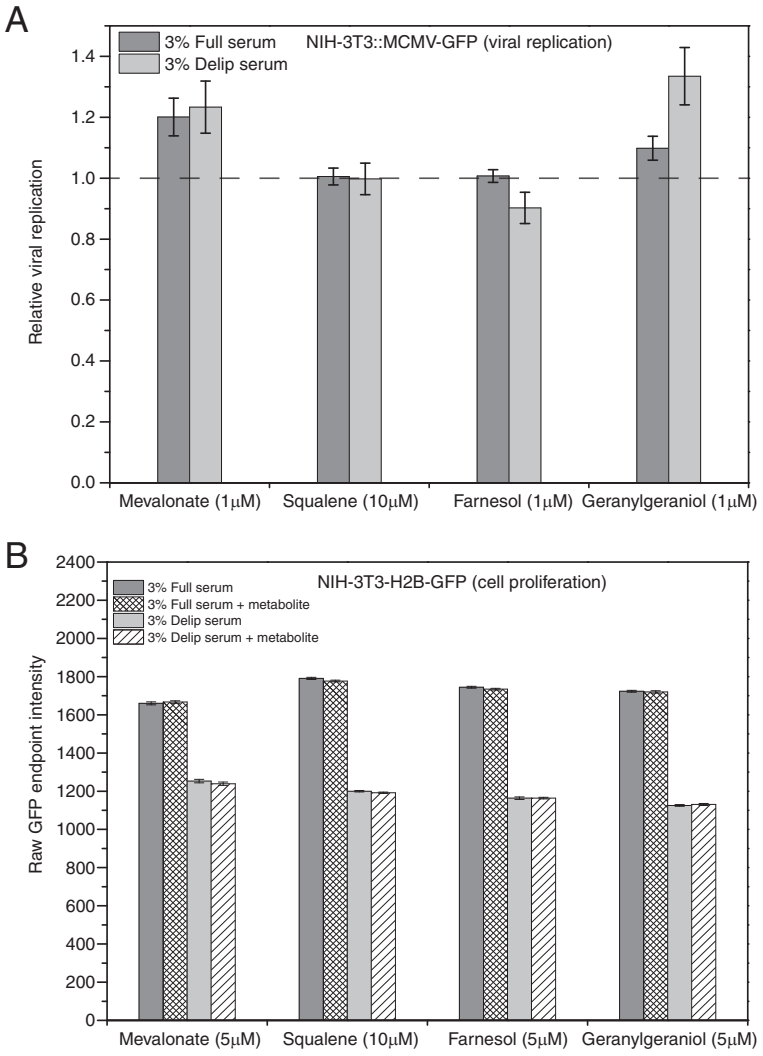

Figure 4.3 The effects of sterol metabolites on MCMV replication and cell growth in different serum conditions.

(A) NIH-3T3 fibroblasts (2x10^4 cells/well) were seeded in 96-well plates for 24 hr. The next day, cells were infected with MCMV-GFP (MOI = 0.016) for 1 hr. Following the removal of viral inoculum, cells were incubated in 3% lipidated (full) or 3% delipidated (delip) media supplemented with mevalonate (1μM), squalene (10μM), farnesol (1μM) or geranylgeraniol (1μM). Relative viral replication was calculated and normalized to vehicle treated cells using the endpoint GFP intensity at 120 hpi. The graph represents two experiments (one performed by Saikou Y Bah in conjunction) with 4 replicates each ± SEM. (B) NIH-3T3-H2B-GFP were seeded at a seeding density of 1x10^4 cells/well in 96-well plates. The next day, cells were incubated in 185μl of phenol red-free media supplemented with different serum types ± sterol metabolites as indicated. Growth of the cells was monitored by their fluorescent intensity. Raw GFP endpoint intensity at 123 hr have been plotted. Data are the mean of two experiments (32 biological replicates) ± SEM.

4.2.3 Identification of SREBP2 dependent genes and cellular response to changes in lipid condition

In order to explain the mechanistic differences between sterol-depleted and -replete conditions, subsequent experiments focused on understanding of the sterol biosynthesis pathway at the transcriptional level. Transcriptional activation of the cholesterol biosynthesis genes is mediated by SREBP2 in response to sterol depletion (see Chapter 2). The work by Horton et al., 2003 using conditional *Srebf2* knockout mice (complete SREBP knockout is embryonic lethal) have shown that nearly all cholesterol biosynthesis genes in the liver are under the regulation control of SREBP2. However, whether the same type of regulation exists in NIH-3T3 fibroblasts is yet to be determined. To identify which genes on the cholesterol biosynthesis pathway are under the transcriptional controls of SREBP2, NIH-3T3 fibroblasts were transfected with either control *RISC free* siRNA or siRNA targeting *Srebf2* for 48 hr. Relative abundance of mRNA transcripts between treatments was assayed by qRT-PCR (see Experimental procedure 7.6.1 for probe efficiency). It was noted that the probe for *Tm7sf2* fell below the efficiency threshold (<90%), and thus was excluded from all the qPCR assays. In this regard, Figure 4.4A shows that knockdown of *Srebf2* by 70% led to a decrease in gene expressions in most of the enzymes on the pathway, with the exception of *Acat1*, *Hmgcl*, *Ggps1*, and *Dhdds* (DHDDS is responsible for the synthesis of dolichol). This finding was consistent with studies showing that the expressions of *Hmgcr* (Sato, Miyamoto et al. 1999), *Fdps* (Ericsson et al., 1996), and *Sqle* (Guan et al., 1995) were mediated by SREBP2. In addition, *Insig1*, the feedback inhibitor of SREBP2 translocation, was also downregulated in response to *Srebf2* knockdown. This finding was consistent with previous publications, showing that *Insig1* was one of the SREBP-responsive genes, whereas *Insig2* was not (Chatterjee et al., 2009; Kamisuki et al., 2011). Based on the knockdown assay, it was concluded that most of the sterol biosynthesis genes on the pathway are transcriptionally regulated by SREBP2.

Oxysterols, such as 25-HC, also supress sterol biosynthesis through the inhibition of SREBP2 proteolytic activation. Thus, the effects of 25-HC on the sterol biosynthesis pathway would be anticipated to be similar to the effects of *Srebf2*

knockdown. To directly test whether treatment with 25-HC led to the downregulation of the sterol biosynthesis pathway, NIH-3T3 fibroblasts were treated with vehicle or 25-HC (2.5μM) for 24 hr. The relative abundance of mRNA transcripts between treatments was assayed by qRT-PCR. Figure 4.4B shows that treatment with 25-HC also led to the suppression of the pathway. The inhibitory effects of 25-HC were strongly correlated with the knockdown of *Srebf2* (Figure 4.4C, Pearson's r = 0.84). This finding demonstrates that the suppression of sterol biosynthesis by 25-HC is achieved through a SREBP2 mediated mechanism.

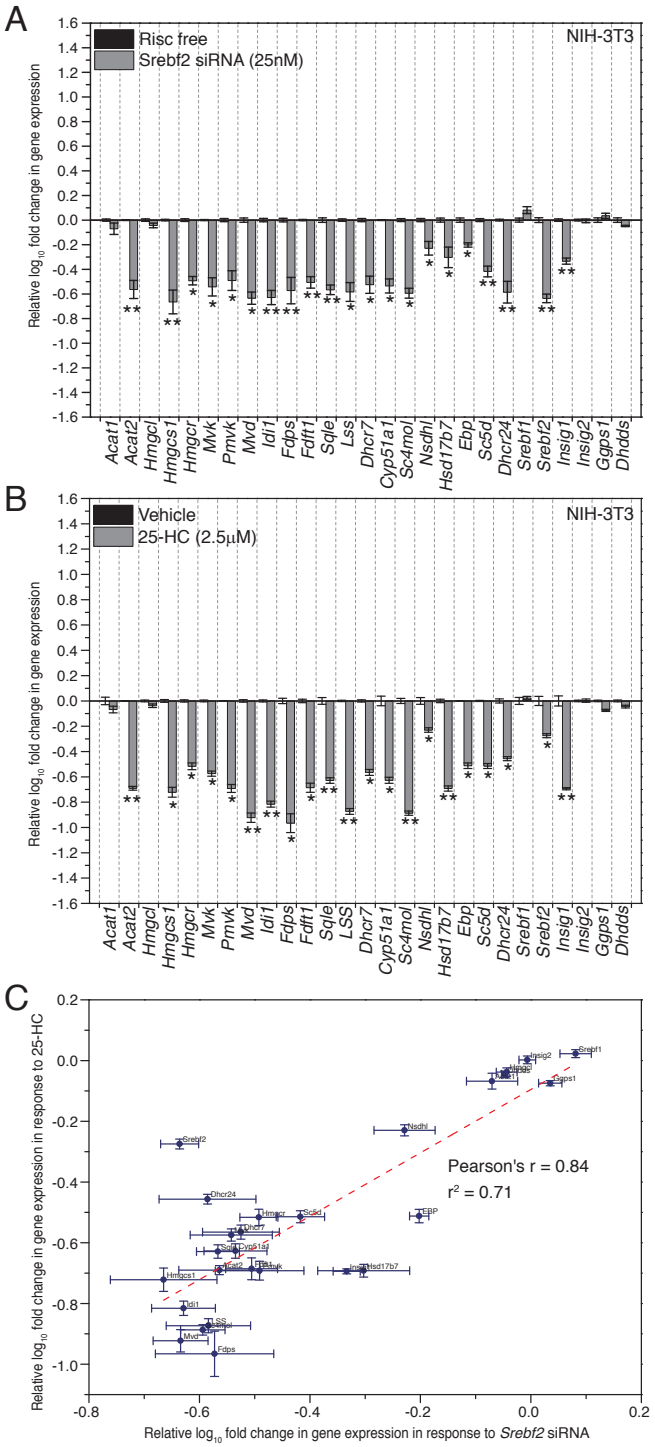

Figure 4.4 The effects of *Srebf2* knockdown and 25-HC treatments on sterol biosynthesis gene expressions.

(A) NIH-3T3 fibroblasts ($1.5x10^5$ cells/well) were transfected with On-target plus siRNAs targeting *Srebf2* in 24-well plates for 48 hr. (Transfection was done by Dr. Kevin Robertson) Relative abundance of the specific siRNA targeted gene transcript with respect to *Risc free* transfected sample was assayed by qRT-PCR using 30ng of RNA. Data are the mean of 6 biological replicates ± SEM. (B) NIH-3T3 fibroblasts ($2x10^4$ cells/well) were seeded in 96-well plates for 24 hr. The next day, cells were incubated in 10% normal media supplemented with 2.5μM of 25-HC for 24 hr. Relative abundance of the specific siRNA targeted gene transcript with respect to the 10% normal media sample was assayed by qRT-PCR using 30ng of RNA. Data are the mean of 3 biological replicates ± SEM. *$p \leq 0.05$, **$p \leq 0.01$ (C) Agreement between sterol biosynthesis gene expressions in response to *Srebf2* siRNA (x-axis) and 25-HC (y-axis). The calculated Pearson's r is 0.84 between the two conditions and the coefficient of determination (r^2) is 0.71.

To examine the differences in gene expressions in cells grown under lipidated and delipidated conditions, NIH-3T3 fibroblasts were cultured in media supplemented with lipidated or delipidated serum for 24 hr. Gene expression of the pathway was quantified by qRT-PCR. Marked differences between the two conditions were observed across the mevalonate-isoprenoid arm, with *Idi1*, *Fdps*, *Dhdds*, and *Ggps1* downregulated in the sterol-depleted condition (Figure 4.5A). This result indicates that under sterol-depleted condition, there is likely to be a reduction in the pathway activity of isoprenoid synthesis. In addition, treatment of NIH-3T3 fibroblasts with 25-HC (2.5μM) in the delipidated media further suppresses the entire sterol biosynthesis pathway (Figure 4.5B). When comparing the pathway response to 25-HC under lipidated (Figure 4.4B) and delipidated (Figure 4.5B) conditions, it was found that although the behaviour of the pathway to the treatments was similar, but the magnitude of downregulation was different. Together, these findings showed that there is a heightened sensitivity of cells to 25-HC under a sterol-depleted state, and that sterol-depletion also negatively influences the side branch of the pathway.

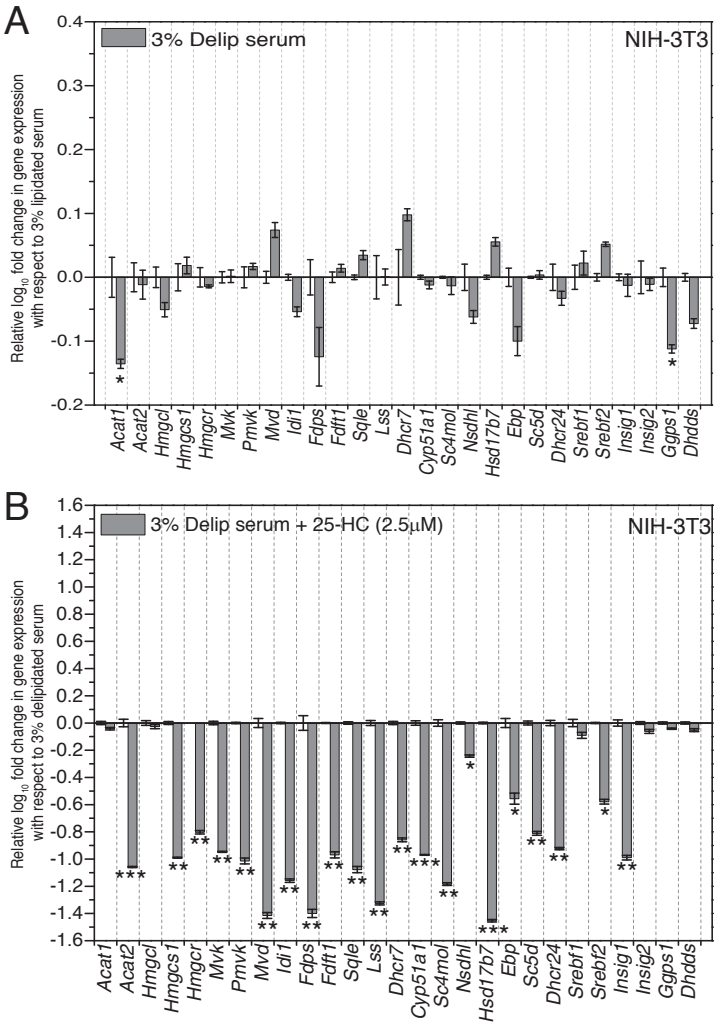

Figure 4.5 Effects of changing serum conditions on sterol biosynthesis gene expressions.
(A) NIH-3T3 fibroblasts (3x10^5 cells/well) were seeded in 6-well plates for 24 hr. The next day, cells were incubated in 3% normal (full) or 3% delipidated (delip) media for 24 hr. Relative abundance of the specific siRNA targeted gene transcript with respect to the 3% normal media sample was assayed by qRT-PCR using 30ng of RNA. Data are the mean of 3 biological replicates ± SEM. (B) NIH-3T3 fibroblasts (2x10^4 cells/well) were seeded in 96-well plates for 24 hr. The next day, cells were incubated in 3% delipidated media supplemented with 2.5μM of 25-HC for 24 hr. Relative abundance of the specific siRNA targeted gene transcript with respect to the vehicle treated sample was assayed by qRT-PCR using 30ng of RNA. Data are the mean of 3 biological replicates ± SEM. *p ≤ 0.05, **p ≤ 0.01, ***p ≤ 0.001

4.2.4 Differential feedback response to sterol biosynthesis inhibition by 25-HC and statin in BMDM

The previous chapters showed that the inhibition of sterol biosynthesis by statin or 25-HC is antiviral. Statin inhibits the production of mevalonate by competitively inhibiting the enzyme HMGCR. In contrast, 25-HC inhibits sterol biosynthesis through the inhibition of SBRPB2 activation (Figure 4.4B), and possibly, accelerated degradation of HMGCR (Sever et al., 2003). Several lines of evidence indicated that the inhibition of HMGCR triggers a robust homeostatic feedback response in tumour cells (Clendening and Penn, 2012) and *in vivo* (Pocathikorn et al., 2010). This was the result of SREBP2 activation in response to intracellular cholesterol depletion, thereby causing the activation of the sterol biosynthesis pathway. To compare and contrast the role of sterol feedback responses in statin and 25-HC mediated antiviral activity, BMDM were treated with either 25-HC (2.5μM) or mevastatin (2.5μM) for 24 hr. Gene expression of the sterol biosynthesis pathway were quantified by qRT-PCR. Figure 4.6A shows that treatment with 25-HC resulted in the downregulation of the pathway in BMDM. The expression profile of the pathway was similar to that of 25-HC treated or *Srebf2* knockdown fibroblasts. In contrast, BMDM treated with mevastatin showed an increase in the pathway activity (Figure 4.6B). Importantly, the expression *Fdps*, the key enzyme in the synthesis of isoprenoids was downregulated in both treatments. Collectively, these experiments demonstrated that although both statin and 25-HC suppress isoprenoid synthesis through the downregulation of *Fdps*, 25-HC contains additional inhibitory effects on the pathway by blocking the feedback response.

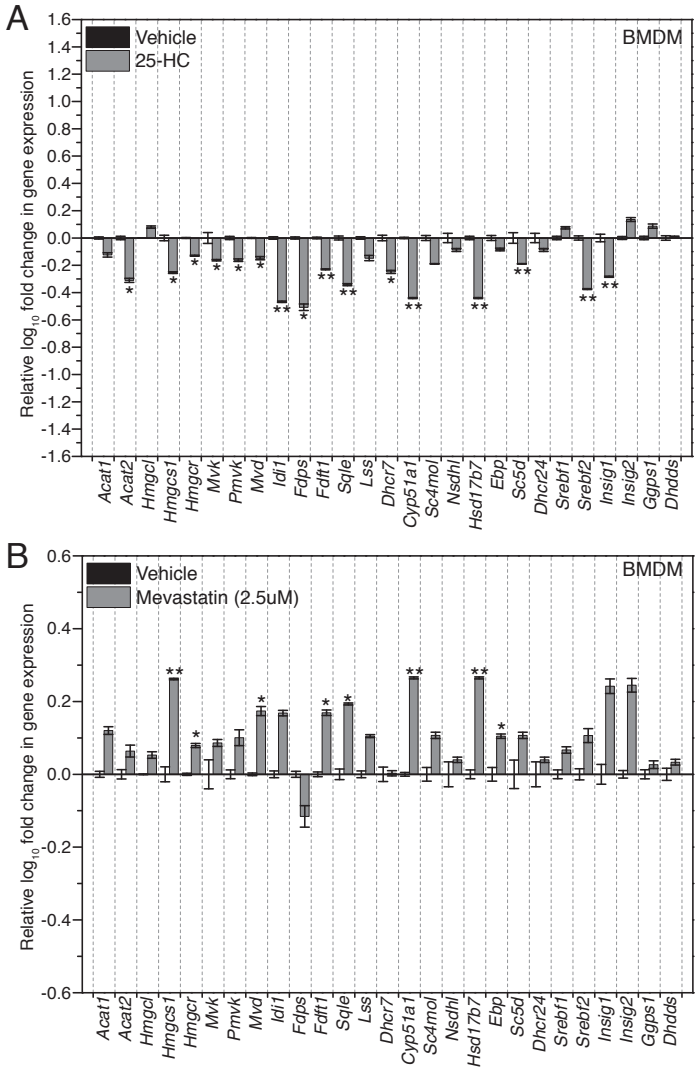

Figure 4.6 Effects of 25-HC and mevastatin on sterol biosynthesis gene expressions in BMDM. BMDM ($1x10^6$ cells/well) were seeded in 6-well plates for 24 hr. The next day, cells were incubated in 10% normal media supplemented with 2.5μM of (A) 25-HC, or (B) mevastatin for 24 hr. Relative abundance of the specific siRNA targeted gene transcript with respect to the vehicle treated sample was assayed by qRT-PCR using 30ng of RNA. Data are the mean of 3 biological replicates ± SEM. *$p \leq 0.05$, **$p \leq 0.01$

4.2.5 Analysis of drug combination reveals common and facilitated antiviral modes of action and potential interaction profiles

When two drugs target the same pathway, their combination would produce the same effect at different magnitudes in comparison with the effects of the individual drug. A drug combination is considered pharmacodynamically synergistic, or additive, if the effect of the combination is greater or equal to the effect of the individual component (Jia et al., 2009). Conversely, a drug combination is considered antagonistic when the two compounds interfere with each other, reducing the overall therapeutic effect. Two drugs that possess antiviral capacity may function in modulating the same pathway, in redundant pathways or in parallel pathways that are essential for viral replication (Hays, 2011). Thus, the interaction profile of the two drugs depends on their mechanism of action, as well as their designated targets. To explore the possible synergistic effects between mevastatin, 25-HC and IFN, a series of pharmacological combination experiments were performed. As a control experiment to test for the expected synergistic antiviral profile due to targeting different pathways, 25-HC and ganciclovir (Cymevene), a clinically approved anti-CMV drug, were used. Ganciclovir is a synthetic analogue of 2′-deoxy-guanosine that acts as a competitive inhibitor of deoxyguanosine triphosphate (dGTP) to the CMV DNA polymerase. In these experiments, pMEFs were first infected with MCMV-GFP, and subsequently treated with 25-HC, ganciclovir, or ganciclovir in the presence of 25-HC (0.01μM). Figure 4.7A shows that the addition of 25-HC at a non-antiviral concentration reduced the IC_{50} of ganciclovir from 0.76μM to 0.37μM. This provides an anticipated base-line response of a synergistic antiviral profile through targeting independent pathways that are required for MCMV replication.

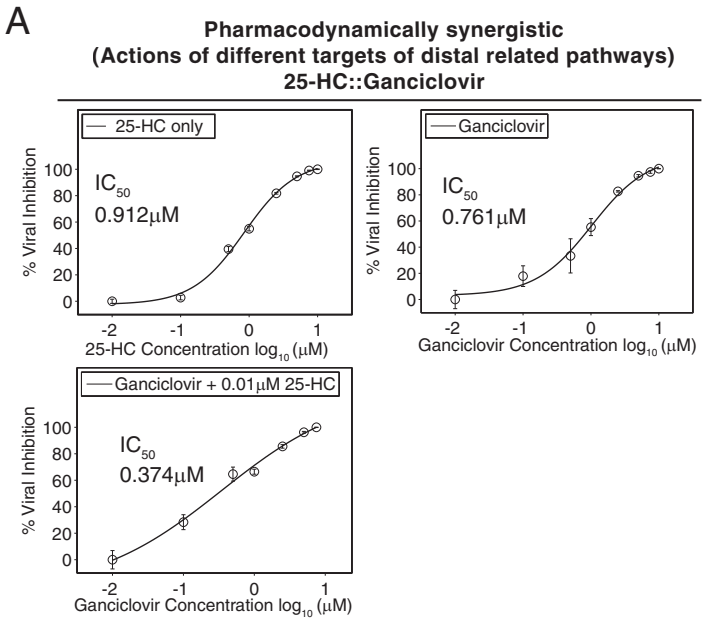

Figure 4.7 Synergistic antiviral effects of 25-HC and ganciclovir.
(A) pMEFs ($3x10^4$ cells/well) were seeded in 96-well plates for 24 hr. The next day, cells were first infected with MCMV-GFP (MOI = 0.1) for 1 hr. After absorption, the viral inoculum was removed and cells were washed once with 100μl of DMEM. Following the wash, cells were incubated in 10% normal media supplemented with an increasing concentration of 25-HC or ganciclovir alone, or a combination of 25-HC and ganciclovir as indicated. Replication slopes over the linear phase were calculated and normalized to vehicle treated cells, and the mean replication slope from independent experiments calculated. The IC_{50} concentration of ganciclovir was calculated as described in the Experimental procedure. Data are mean ± SEM for two experiments (4 replicates per experiment).

In Chapter 3, it was shown that *Ch25h* is one of the ISGs. Further investigation by Blanc and Hsieh et al., 2013 showed that the transcription of *Ch25h* is STAT1 dependent, as *Ch25h* is not activated in $STAT1^{-/-}$ BMDM. To examine the combinatorial effects of IFN and 25-HC, pMEFs were pre-treated with a combination of IFNγ and 25-HC for 24 hr, followed by infection with MCMV-GFP and drug retreatment. Figure 4.8A shows that the addition of IFNγ below the IC_{50} (<8U/ml) had minor effects on the IC_{50} of 25-HC (0.91μM ➔ 0.80μM). This interaction profile was different from the ganciclovir result, suggesting that the antiviral effects of IFN and 25-HC are not synergistic, but instead indicating possible overlapping mechanisms. However, a slight reduction in the IC_{50} of 25-HC was also observed when cells were co-treated with a higher dose of IFN (25U/ml). This result suggests that IFN provides additional enhancement to the effects of 25-HC, likely through other antiviral mechanisms outside the activity of 25-HC.

To further elucidate the interaction profile between a pharmacological compound, statin, and components of IFN mediated sterol immunity, similar combinatorial studies were subsequently performed. In the next set of experiments, pMEFs were pre-treated with a combination of mevastatin and IFNγ or 25-HC for 24 hr, followed by infection with MCMV-GFP and retreatment. Figure 4.9A shows that the addition of 25-HC below 2.5μM reduced the IC_{50} of mevastatin (5.2μM ➔ 0.78μM). However, further increase in the concentration of 25-HC above 2.5μM did not improve the efficacy of mevastatin. Similar results were also observed between the combination of mevastatin and IFNγ (Figure 4.9B). Co-treatment of IFNγ below the IC_{50} with mevastatin generated enhanced antiviral effect, while no further enhancement was observed when the concentration of IFNγ reached above the IC_{50}. Together, these two studies illustrated that the combination of mevastatin and IFNγ or 25-HC is mildly synergistic. Furthermore, it is likely that IFNγ and 25-HC facilitate the antiviral action of mevastatin.

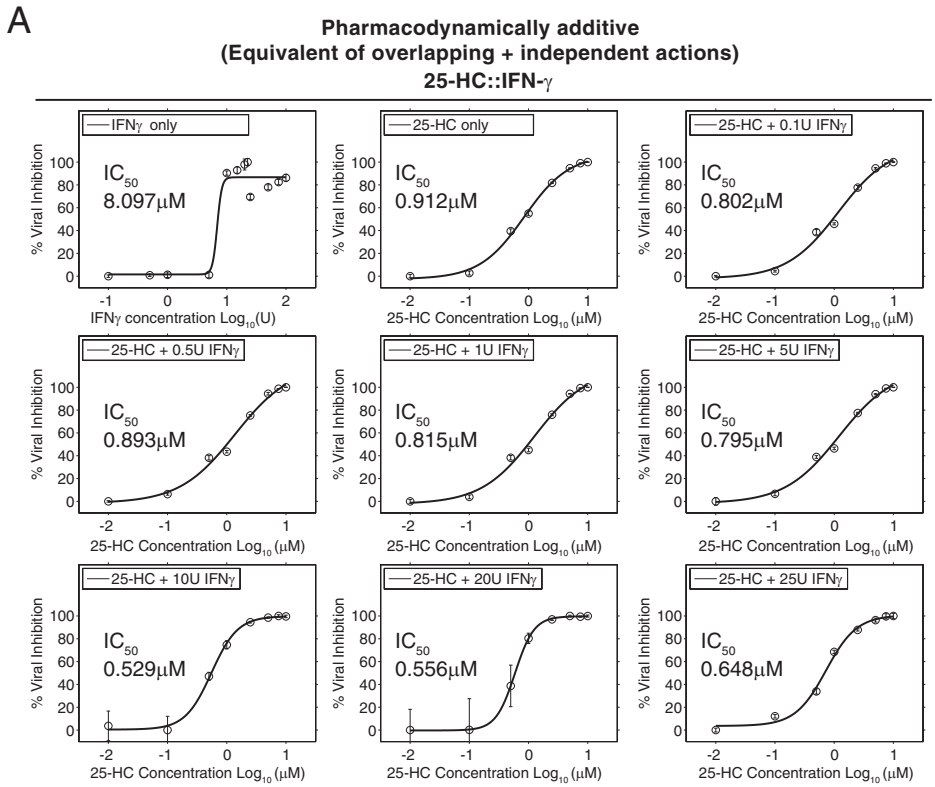

Figure 4.8 The combination of 25-HC and IFN has an additive effect on viral growth.
(A) pMEFs ($3x10^4$ cells/well) were seeded in 96-well plates for 24 hr. The next day, cells were pre-treated with vehicle, IFNγ alone, or a combination of IFNγ and 25-HC at an increasing concentration as indicated for 24 hr. The next day, cells were infected with MCMV-GFP (MOI = 0.1) for 1 hr. After absorption, the viral inoculum was removed and cells were washed once with 100μl of DMEM. Following the wash, cells were incubated in 10% normal media supplemented with the identical treatment. Replication slopes over the linear phase were calculated and normalized to vehicle treated cells (e.g. no interferon or 25-HC wells), and the mean replication slope from independent experiments calculated. The IC_{50} concentration of 25-HC was calculated as described in the Experimental procedure. Data are mean ± SEM for two experiments (4 replicates per experiment). 25-HC alone at 10μM results in 97% inhibition in MCMV replication, while IFNγ alone at the highest concentration of 25U/ml yields 55% MCMV inhibition. Combining 25-HC and IFNγ at the highgest concentration yields 98% viral inhibition.

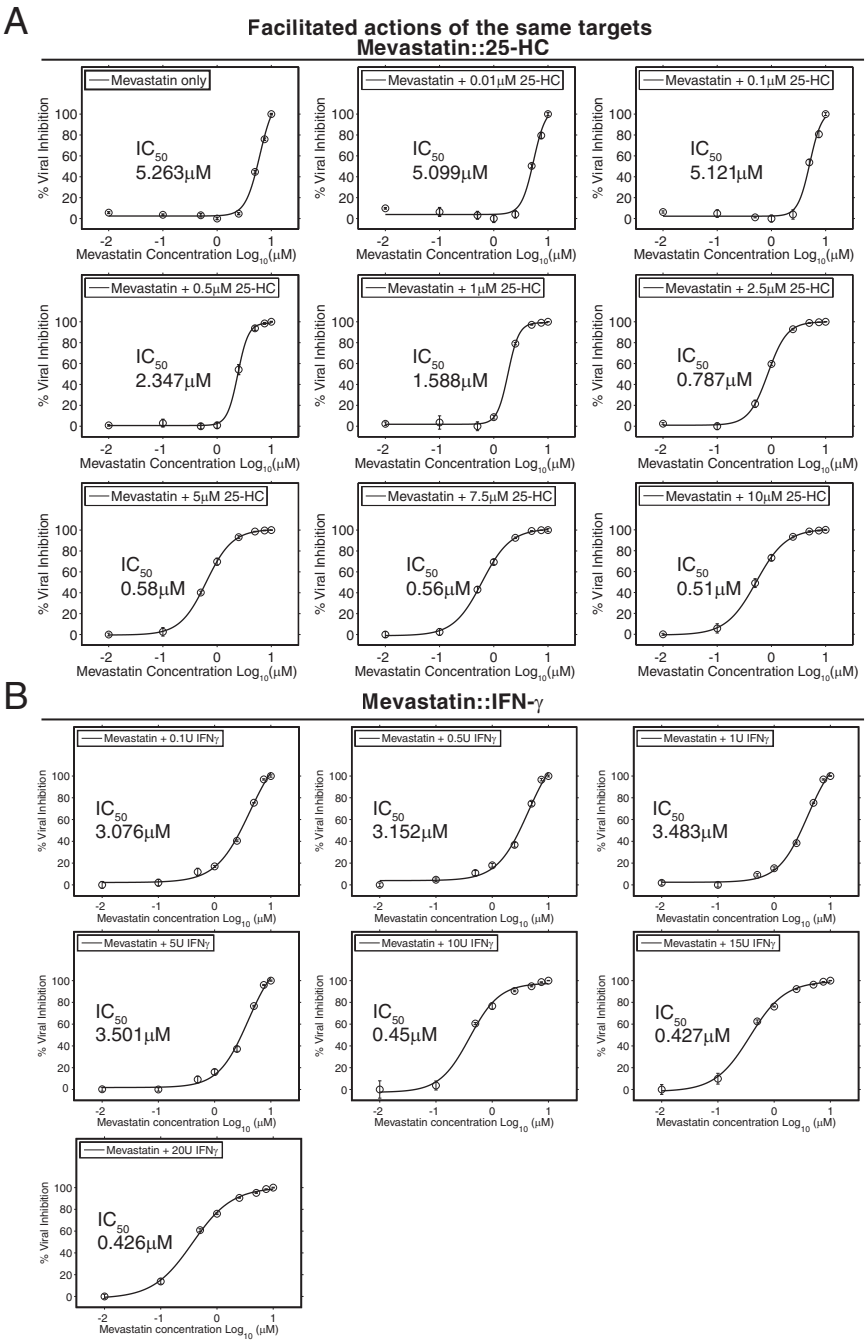

Figure 4.9 The combination of mevastatin and 25-HC/IFN has mild synergistic antiviral effects. (A) pMEFs ($3x10^4$ cells/well) were seeded in 96-well plates for 24 hr. The next day, cells were pre-treated with vehicle, mevastatin alone, or a combination of mevastatin and 25-HC at an increasing concentration as indicated for 24 hr. The next day, cells were infected with MCMV-GFP (MOI = 0.1) for 1 hr. After absorption, the viral inoculum was removed and cells were washed once with 100μl of DMEM. Following the wash, cells were incubated in 10% normal media supplemented with the identical treatment. Replication slopes over the linear phase were calculated and normalized to vehicle treated cells (e.g. no interferon, 25-HC, or mevastatin wells), and the mean replication slope from independent experiments calculated. The IC_{50} concentration of mevastatin was calculated as described in the Experimental procedure. Data are mean ± SEM for two experiments (4 replicates per experiment). 25-HC alone at 10μM results in 97% inhibition in MCMV replication, while statin alone 10μM results in 80% MCMV replication. Combining 25-HC and mevastatin at the highgest concentration yields 99% viral inhibition. (B) pMEFs ($3x10^4$ cells/well) were seeded in 96-well plates for 24 hr. The next day, cells were pre-treated with vehicle, IFNγ alone, or a combination of IFNγ and mevastatin at an increasing concentration as indicated for 24 hr. The next day, cells were infected with MCMV-GFP (MOI = 0.1) for 1 hr. After absorption, the viral inoculum was removed and cells were washed once with 100μl of DMEM. Following the wash, cells were incubated in 10% normal media supplemented with the identical treatment. Replication

slopes over the linear phase were calculated and normalized to vehicle treated cells, and the mean replication slope from independent experiments calculated. The IC_{50} concentration of mevastatin was calculated as described in the Experimental procedure. Data are mean ± SEM for 2 experiments (4 replicates per experiment). Mevastatin alone at 10μM results in 80% MCMV replication. while IFNγ alone at the highest concentration of 20U/ml yields 49% MCMV inhibition. Combining IFNγ and mevastatin at the highgest concentration yields 98% viral inhibition.

4.2.6 Non-redundant siRNA knockdown of the sterol biosynthesis pathway under lipidated and delipidated conditions reveals additional antiviral targets of interest

In Chapter 2, siRNA knockdown of selected targets on the sterol biosynthesis pathway provided evidence for the importance of the mevalonate-isoprenoid arm in the replication of MCMV (Figure 2.2A). However, results from Figure 4.2 and 4.5A show that changing lipid conditions altered the transcriptional activity of the sterol biosynthesis pathway, as well as the rate of MCMV replication. Thus, it is possible that additional enzymes on the pathway could play a role in modulating MCMV replication under different serum conditions. To identify additional targets of interest, a non-redundant siRNA knockdown screening was performed. This screening was done using pMEFs instead of NIH-3T3 fibroblasts to reduce technical complications associated with siRNA knockdown and viral infection under a sterol-depleted condition in NIH-3T3 fibroblasts. In these experiments, pMEFs were first transfected with siRNA targeting individual enzymes on the sterol biosynthesis pathway for 48 hr, followed by MCMV-GFP infection. Figure 4.10B shows that at 48 hr post-transfection, none of the transfected siRNAs exhibit significant cell toxicity. In agreement with my previous findings, Figure 4.10A shows that knockdown of genes leading to the mevalonate-isoprenoid arm of the sterol biosynthesis pathway led to a significant decrease in MCMV replication. This inhibition was further enhanced in sterol-depleted condition. In contrast to the screening results from NIH-3T3 fibroblasts, siRNA knockdown in pMEFs of both *Idi1* and *Ggps1* that are important for the synthesis of IPP (the precursor of isoprenoids) and geranylgernayl, respectively, showed significant antiviral effect.Silencing *Fdps* only displayed significant antiviral effect under a sterol-depleted condition. This finding highlights the potential differences in the regulation of sterol biosynthesis between different cell types.

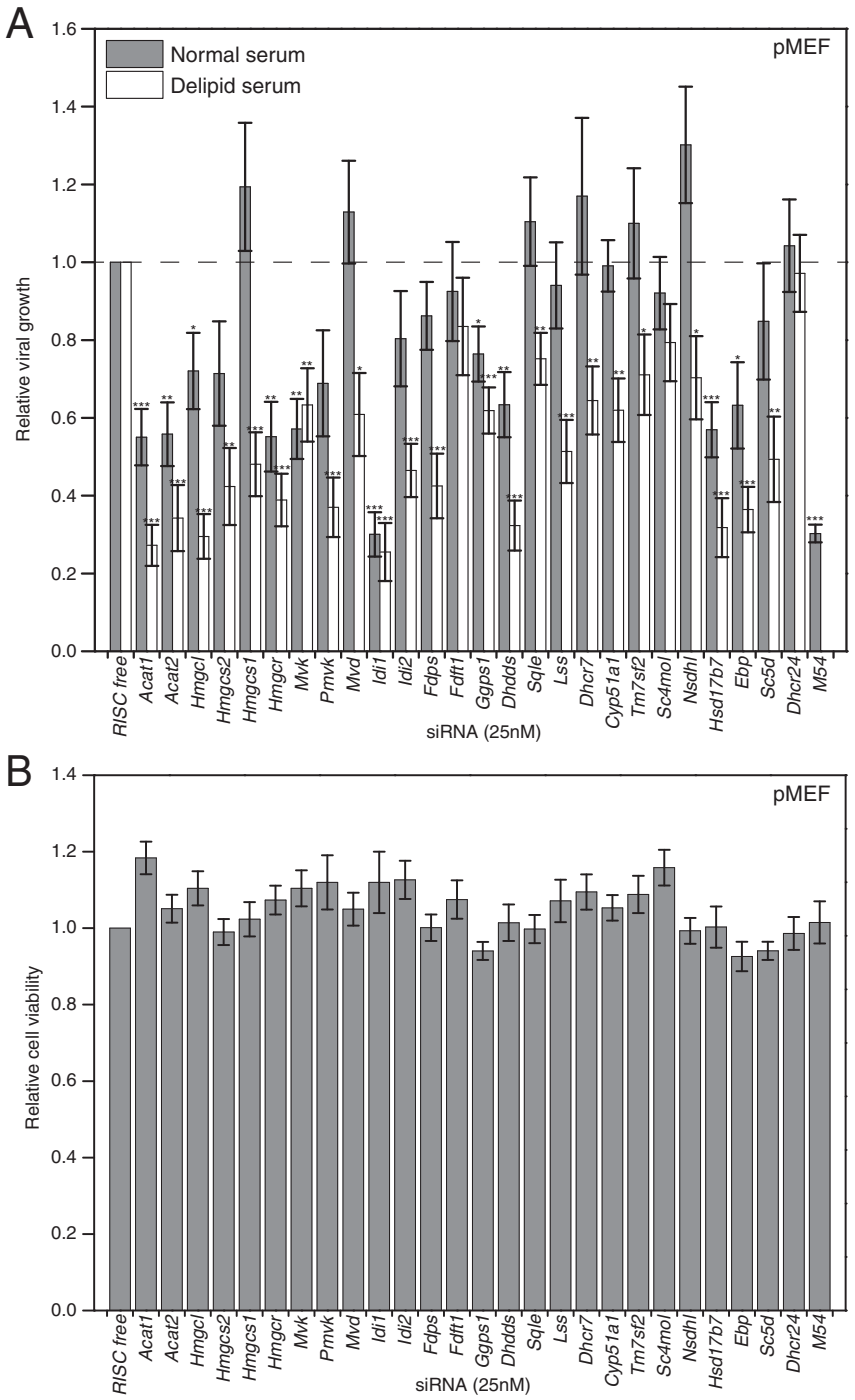

Figure 4.10 Non-redundant siRNA knockdown of sterol biosynthesis pathway on MCMV replication under different serum condition.

(A) pMEFs ($1.5x10^4$ cells/well) were transfected in 96-well plates with On-target plus siRNAs as indicated for 48 hr then infected with MCMV-GFP (MOI = 0.1) for 1 hr. After the removal of viral inoculum, cells were incubated in either 10% normal, or 3% delipidated media. *Risc free* was used as a transfection control, while *M54* specifically targets MCMV polymerase. The level of infection was determined by measuring the increase in GFP fluorescence (slope) during the linear-phase of viral growth. The graph represents the relative level of infection compared to *Risc free* transfected and data are the mean of 8 biological replicates ± SEM. $*p \leq 0.05$, $**p \leq 0.01$, $***p \leq 0.001$. (B) pMEFs ($1.5x10^4$ cells/well) were transfected with On-target plus siRNAs as indicated in 96-well plates for 48 hr then the cell viability was measured using CellTiter-Blue. Relative cell viability was calculated by normalizing to the *RISC free* transfected samples, and data are the mean of 4 biological replicates ± SEM.

In the Bloch-Kandutsch pathway, siRNA knockdown of *Sqle, Lss, Dhcr7, Cyp51a1, Tm7sf2,* and *Nsdhl* in lipidated media had no inhibitory effect on MCMV replication. However, under sterol-depleted condition, knockdown of these genes also led to significant viral inhibition. This result suggests that under a lipid-depleted condition, there is a potential dependency of MCMV replication on the product of these enzymes. In contrast with these findings, silencing of *Hsd17b7* or *Ebp* in either sterol-deplete or replete conditions showed significant viral inhibition. Furthermore, siRNA knockdown of *Dhcr24*, which catalyses the last step of cholesterol synthesis had no effects on viral replication regardless of lipid conditions. This is in agreement with Chapter 1 studies, and the metabolic rescue assay (Figure 4.3), showing that cholesterol itself is not a primary factor in regulating viral replication. Collectively, these findings provided further evidence of the importance of the mevalonate-isoprenoid arm, but also hinted at a previous uncharacterized role of the distal pathways in supporting MCMV replication.

4.3 Discussion

This chapter has explored the feedback response of the sterol biosynthesis pathway under different lipid conditions. Data presented in this chapter demonstrates how feedback mechanisms of the sterol pathway have significant impacts on viral replication. Further combinatorial studies of statin, interferon, and 25-HC revealed different antiviral modes of action, highlighting the potential of multicomponent antiviral therapies.

4.3.1 Sterol dependent and independent effects on viral replication

In chapter 3, the antiviral activity of 25-HC in lipid-replete condition was found to occur at a concentration higher than the concentration that is required to inhibit SREBP2 activation. In parallel, the work of Radhakrishnan et al., 2008 showed that the processing of SREBP2 is restricted under a sterol-replete condition. Collectively, this suggests that the antiviral effect of 25-HC is independent of SREBP2 in a sterol-replete condition. Conversely, the antiviral action of 25-HC was significantly enhanced in cells grown in the delipidated media, whereas the sterol-depleted condition favours the processing of SREBP2. This suggests that under a delipidated condition, the antiviral effect of 25-HC is likely mediated through multiple processes involving SREBP2 dependent and independent mechanisms. To directly compare the progression of MCMV replication under the two lipid conditions, the concentration of lipidated serum used in the experiments was adjusted to 3% (v/v). Results demonstrated that sterol depletion had a clear effect on both the replication rate and particle yield of the virus.

When comparing growth curves between MCMV-GFP and NIH-3T3-GFP-H2B, it was noted that the growth of the virus followed an exponential trajectory, while the growth of the cell was relatively linear (Figure 4.2). Thus, the doubling time of the virus is independent of the cell cycle, indicating that the reduction in cellular growth cannot explain the growth deficiency of the virus in sterol depleted media. This finding is in agreement with other studies showing that HCMV IE1-72 or IE2-86 proteins promote cell cycle arrest to facilitate viral replication (Noris et al., 2002; Sinclair et al., 2000).

Transcriptional profiling of the pathway revealed that there was a downregulation of the mevalonate-isoprenoid arm, including genes *Idi1*, *Fdps*, and *Ggps1.* These enzymes are critical in catalyzing the sequential steps in the synthesis of geranylgeranyl, a key metabolite involved in the process of protein prenylation. The deficiencies in MCMV replication due to a reduction in the synthesis of geranylgeranyl were subsequently demonstrated in metabolic rescue experiments. The growth of MCMV in the delipidated serum could be rescued with the addition of mevalonate and geranylgeraniol. This finding contrasted with results showing that the addition of farnesol or squalene had no effect on viral replication. Together, these studies indicate that there is a clear dependency of MCMV replication on geranylgeranyl, and that farnesyl metabolism or cholesterol synthesis are not responsible for the growth deficiencies of MCMV in a sterol-depleted condition.

Gene expression profiling of both NIH-3T3 fibroblasts and BMDM treated with 25-HC provided potential mechanistic explanations to the previous metabolic rescue experiment of 25-HC (Figure 3.9A and B). In those two experiments, the antiviral effect of 25-HC was reversed with the addition of mevalonate and geranylgeraniol. However, this only occured when the concentration of 25-HC was below its IC_{50}. In the current study, treatment with 25-HC led to a systematic downregulation of the sterol biosynthesis pathway. The effects of 25-HC on the pathway are different from mevastatin. Statin inhibits isoprenoid synthesis through the inhibition of a single enzyme (HMGCR) rather than the pathway. As a result, the addition of mevalonate or geranylgeraniol can be subsequently metabolized by the downstream enzymes to reverse viral inhibition. However, treatments with 25-HC caused transcriptional suppression of the entire sterol pathway. This effect is likely to restrict the activity of the mevalonate-isoprenoid arm, preventing the metabolism of these sterol intermediates. Based on this reasoning, in the delipidated media, the enhanced antiviral effect of 25-HC is likely to be a combination of both the inhibition of SREBP2 activation and the intrinsic downregulation of the mevalonate arm as the result of sterol depletion.

Although treatments with either mevastatin or 25-HC in BMDM led to the downregulation of *Fdps*, it was noted that mevastatin also induced the expression

of the pathway. This was due to the feedback response of SREBP2 in responses to cholesterol depletion (Clendening et al., 2010). The increase in overall pathway activity might stimulate viral replication. Indeed, it was observed that treatment of MCMV-GFP infected pMEF and NIH-3T3 fibroblasts with nanomolar concentration (10 ~ 25nM) of mevastatin led to an increase (but not statistically significant) in viral replication. Whether this feedback response could actually increase MCMV particle yield requires further investigation.

Despite the importance of geranylgeranyl in boosting MCMV replication under a sterol-depleted condition, it was noted that under a sterol-depleted condition, neither mevalonate nor geranylgeranyl could fully rescue viral replication. This observation is supported by the NIH-3T3-H2B-GFP results, showing that the growth of cells was not rescued with the addition of sterol metabolites. Thus, these two studies suggest that the extended effect of sterol depletion is beyond the sterol biosynthesis pathway and that those other pathways such as fatty acid synthesis and glucose metabolism could play a role in MCMV replication.

4.3.2 Combinatorial effects of statin, 25-HC, IFN, and ganciclovir and their respective antiviral modes of action

In the previous two chapters, treatments of statin and 25-HC showed significant MCMV inhibitory effects. The synthesis of 25-HC is interferon dependent, indicating that upon pathogen challenges, both interferon and 25-HC will be present at sites of infection. The review by Jia et al., 2009 provided excellent definitions of different types of pharmacological interactions and their respective interaction profile. Thus, the interpretation of the antiviral mode of action between these components was based on the work of Jia et al., 2009.

The antiviral effect of ganciclovir was strongly enhanced (marked by the shift in the IC_{50}) in the presence of a non-antiviral concentration of 25-HC. On the one hand, 25-HC achieves an antiviral affect through the suppression of the sterol biosynthesis pathway and the downregulation of MCMV immediate early gene. On the other hand, ganciclovir is a competitive inhibitor of deoxyguanosine triphosphate (dGTP) to the CMV DNA polymerase. These two components inhibit two independent pathways

involved in the life cycle of MCMV. Thus, the strong synergistic combinations between 25-HC and Ganciclovir showed the effect of unrelated pathways in inhibiting viral growth. This effect was similar to the combinatorial effect of ampicillin (inhibitor of cell-wall synthesis), and daptomycin (disruption of bacterial membrane synthesis) on vancomycin-resistant enterococci (Rand and Houck, 2004). This concept is illustrated in Figure 4.11A showing that 25-HC and ganciclovir inhibit two independent pathways (**AB** and **KL** respectively) resulting in a synergistic antiviral effect.

The addition of sub-IC_{50} IFNγ had no effects on the antiviral activity of 25-HC. This indicates that, in the primary fibroblasts, there are likely to be overlapping actions between two components. This effect is similar to the combination of amnestic agents, propfol and sevoflurane, which both perturb the activity of gamma-aminobutyric acid receptor α (GABAα) (Harris et al., 2006). However, increasing concentrations of IFNγ above the IC_{50} enhanced the antiviral effect of 25-HC. This result indicates that IFNγ elicits additional antiviral effects at a higher concentration that is independent of 25-HC. This effect is similar to the combination of anti-bacterial drugs, azithromycin and imipenem, inhibitors of bacterial protein translation and penicillin-binding proteins. At a saturating concentration, azithromycin complements the activity of imipenem by inhibiting the translation of penicillin-binding proteins (Ono et al., 2005). Collectively, these results suggest that 25-HC and IFN have an additive effect on viral growth, indicating common and independent pathway targets. This concept is illustrated in 4.11B, showing the pathway inference on the possible antiviral mode of IFNγ and 25-HC. In this scenario, pathway **A** is critical for viral replication. In the partial redundancy model, a combination of 25-HC and IFNγ is effective at inhibiting viral replication. The transcription of *Ch25h* depends on IFN/STAT1 signalling, and thus, in an *Ifn*$^{-/-}$ or *Stat1*$^{-/-}$ background, the production of 25-HC is inhibited. Conversely, the production of IFN is independent of 25-HC, such that in a *Ch25h*$^{-/-}$ background, IFN is still effective at inhibiting viral replication through the inhibition of pathway **A** via other mechanisms.

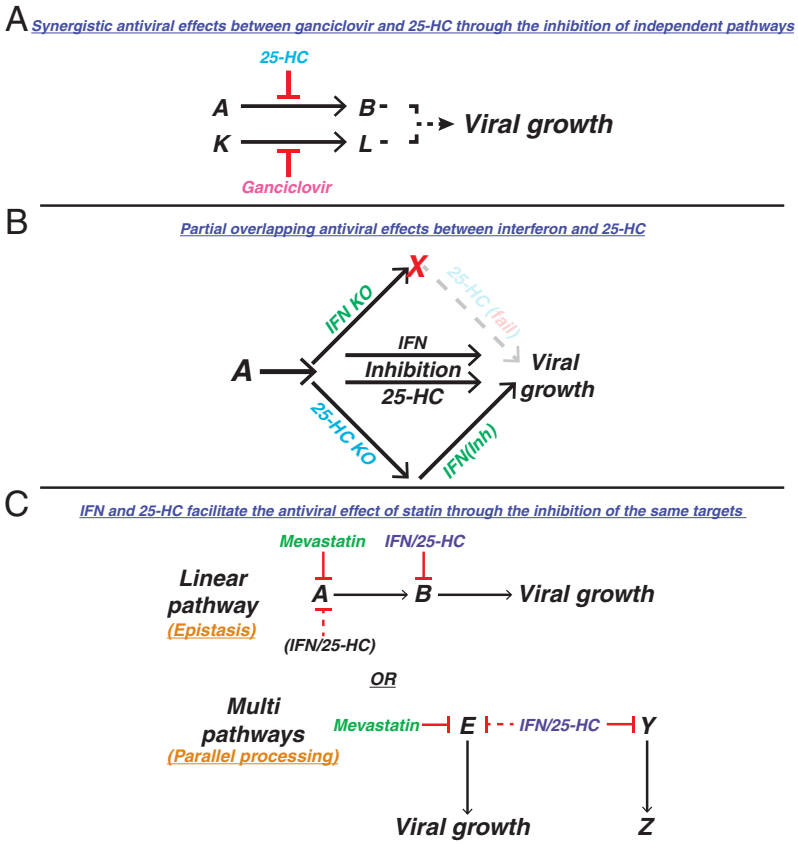

Figure 4.11 Pathway inference on the possible antiviral mode of action between IFN, 25-HC, mevastatin, and ganciclovir.

(A) Interaction profile between 25-HC and ganciclovir. 25-HC inhibits the sterol biosynthesis pathway, leading to an antiviral state. Ganciclovir is an inhibitor of the CMV polymerase. Co-treatment of both components led to significant synergistic antiviral effects. (B) Interaction profile between 25-HC and IFNγ. In this model, IFN stimulates the synthesis of 25-HC. In the presence or absence of *Ch25h*, IFN can still achieve an antiviral state via other mechanisms. However, in the absence of IFN/STAT1 signalling, the synthesis of 25-HC is inhibited. Thus, 25-HC cannot elicit a normal antiviral effect through the suppression of the sterol biosynthesis pathway. (C) Interaction profile between mevastatin and 25-HC/IFN. In this combination, both linear pathways (Epistasis) and multi pathways (parallel processing) models can co-exist. In both models, mevastatin inhibits viral replication by suppressing the mevalonate-isoprenoid arm, while 25-HC/IFN could also block the same pathway at a threshold concentration. In addition, 25-HC/IFN also provides additional antiviral effects through other mechanisms.

The combination of mevastatin with either 25-HC or IFNγ showed similar interaction profiles. Mevastatin functions as an inhibitor of the sterol biosynthesis pathway, whereas IFNγ elicits 25-HC in the suppression of the sterol biosynthesis pathway. Notably, the addition of sub-IC_{50} 25-HC or IFNγ provided enhancement to the antiviral activity of mevastatin. This suggests that both 25-HC and IFNγ facilitate mevastatin in the suppression of the sterol biosynthesis pathway. Furthermore, when the concentration of IFNγ or 25-HC exceeds their respective IC_{50}, the antiviral effects of mevastatin are dominated by the effects of IFNγ or 25-HC, resulting in no additional shifts in the IC_{50} of the statin. Collectively, these results showed mildly synergistic

antiviral action between statin and 25-HC or IFN on viral growth, indicating a facilitated action of a common pathway. This concept is illustrated in Figure 4.11C. This pathway inference scenario has two possible models. In the linear model (epistasis), enzyme **A** and **B** catalyse two sequential steps of a single pathway that is involved in the replication of the virus. Enzyme **A** is inhibited by mevastatin, while enzyme **B** is inhibited by either IFNγ or 25-HC. When the concentration of IFNγ or 25-HC is above a certain threshold, IFNγ or 25-HC can also provide additional inhibitory effect on enzyme **A**. This further enhances the antiviral capacity of mevastatin. In the multi pathway model (parallel processing), enzyme **E** is important for viral replication, whereas pathway **YZ** is not. Mevastatin inhibits enzyme **E**, resulting in an antiviral state. Pathway **YZ** is inhibited by IFNγ or 25-HC; however, this has no effect on viral replication. Similar to the linear model, when the addition of IFNγ or 25-HC is above a certain concentration, IFNγ or 25-HC can also provide additional inhibitory effects on enzyme **E**, thereby further enhancing the antiviral capacity of mevastatin.

4.3.3 Potential importance of the Bloch-Kandutsch pathways in MCMV replication

The non-redundant siRNA knockdown of the sterol biosynthesis pathway in pMEFs showed similar and contrasting results in comparison with the knockdown experiment performed in Chapter 2. This data could be further strengthened with the validation of knockdown efficiency. In agreement with the NIH-3T3 fibroblasts results, siRNA knockdown of the mevalonate-isoprenoid arm of the sterol biosynthesis pathway showed significant antiviral effect. This effect was further enhanced under sterol-depletion. This indicates that under a sterol-depleted condition, there is a clear dependency of MCMV on SREBP2 mediated transcriptional activation of the pathway. siRNA knockdown of *Idi1* in pMEFs showed significant inhibition on MCMV replication. This is in contrast with the data in NIH-3T3 fibroblasts, showing that silencing of *Fdps* but not *Idi1* led to significant antiviral effects. *Idi1* catalyses the isomerization of IPP to DMAPP. This reaction removes the C3-C4 double bond of IPP, while creating the C2-C3 double bond for DMAPP (Zhou et al., 2013). Currently, little is known about the extended function of IDI1 in humans or mice to explain the contrasting siRNA results between NIH-3T3 fibroblasts and pMEFs. The review published by Berthelot et al., 2012 compiled the enzymatic activity (V_{max}) of IDI1 across 31 different species, including plants, prokaryotes, and other eukaryotes. Results indicated that the V_{max} of IDI1 across species could range from 0.004 to 3000 mmol/mg/min. This implicates that it is possible that the activity of IDI1 is significantly higher in NIH-3T3 fibroblasts than in pMEFs, in which the reduction expression of *Idi1* by siRNA in NIH-3T3 fibroblasts had minimal effects on the production of DMAPP. This also suggests that in some cell types, the production of isoprenoid is limited by the enzyme FDPS, rather than IDI1. This is demonstrated in the work of Tanaka et al., 2014 showing that the accumulation of IPP in HeLa and Vγ9Vδ2 T cells significantly dependent on the inhibition of FDPS rather than IDI1. In addition to the difference in the enzymatic activity, *in vivo* work by Nemoto et al., 2013 also showed that *Idi1* is differentially expressed in Wistar-Kyoto (WKY) rats (a normotensive control strain), and Stroke-Prone Spontaneously Hypertensive Rats (SPSHR). The reduction in the sterol biosynthesis activity in SPSHR rats has been suggested to modulate the response of SPSHR rats to high cholesterol feeding and hypertension. Future studies will re-examine how the

mevalonate-isoprenoid arm is differentially regulated across different cell types.

In addition to *Idi1*, siRNA knockdown of *Sqle*, *Dhcr7*, *Cyp51a1*, *Tm7sf2*, and *Sc5d* in the delipidated media showed significant MCMV inhibition. This indicates that the distal branch of the sterol biosynthesis arm might play a role in regulating viral replication. However, the metabolic rescue experiments shown in Figure 4.3A and B revealed that supplementing squalene in the delipidated media had no effects on MCMV replication or cell growth. This outcome suggests that under a sterol-depleted condition, these enzymes could play an indirect role in supporting viral replication, possibly through the production of other secondary metabolites. In contrast with the above enzymes, silencing *Ebp* or *Hsd17b7* in both lipidated and delipidated serum showed significant antiviral activity, with a higher sensitivity occurring in delipidated serum. This phenotype was different from other enzymes on the pathway, indicating that the antiviral effects of silencing these two enzymes involved at least two possible mechanisms: the accumulation of the sterol precursors and the viral dependencies on the metabolites of the enzyme. HSD17B7 (17β hydroxysteroid dehydrogenase) is involved in the conversion of both estrone to estradiol and zymosterone to zymosterol, and is essential for the proper development of mouse embryos (Jokela et al., 2010). Furthermore, mutations in *Ebp* (emopamil binding protein) in human leads to Conradi-Hünermann-Happle syndrome (CHH). CHH is an X-linked dominant chondrodysplasia punctate that is characterized by stippled epiphyses (deformity of long bones), cataracts, alopecia (hair loss) and skin lesions, including ichthyosis (dry, thickened, scaly or flaky skin) (Shirahama et al., 2003). Importantly, as the result of EBP deficiencies, CHH patients suffer from accumulation of (9)-cholestenol and 8-dehydrocholesterol (8DHC) in plasma and tissue (Cañueto et al., 2014; Kolb-Mäurer et al., 2008). Currently, there is no evidence indicating whether estrone, zymosterone, (9)-cholestenol, or 8-dehydrocholesterol (8DHC) is antiviral. Future studies are needed to address the role of these sterol pre-cursors and the importance of the distal arm of the sterol biosynthesis pathway.

In summary, results presented in this chapter provide a new understanding of how the host sterol-feedback responses alter MCMV replication. Further siRNA screening has provided evidence to the potential importance of the distal arm of the sterol biosynthesis pathway on MCMV replication. Drug combinatorial studies between IFN, statin, and 25-HC reveal critical pathway connections to viral replication, and identify potential treatments with an increased therapeutic efficacy.

4.4 References

Ablasser, A., Schmid-Burgk, J.L., Hemmerling, I., Horvath, G.L., Schmidt, T., Latz, E., and Hornung, V. (2013). Cell intrinsic immunity spreads to bystander cells via the intercellular transfer of cGAMP. Nature 503, 530–534.

Agranoff, B.W., Eggerer, H., Henning, U., and Lynen, F. (1960). ARTICLE : Biosynthesis of Terpenes : VII . of Terpenes.

Berthelot, K., Estevez, Y., Deffieux, A., and Peruch, F. (2012). Isopentenyl diphosphate isomerase: A checkpoint to isoprenoid biosynthesis. Biochimie 94, 1621–1634.

Blagg, B.S.J., Jarstfer, M.B., Rogers, D.H., and Poulter, C.D. (2002). Recombinant squalene synthase. A mechanism for the rearrangement of presqualene diphosphate to squalene. J. Am. Chem. Soc. 124, 8846–8853.

Blanc, M., Hsieh, W.Y., Robertson, K.A., Watterson, S., Shui, G., Lacaze, P., Khondoker, M., Dickinson, P., Sing, G., Rodriguez-Martin, S., et al. (2011). Host defense against viral infection involves interferon mediated down-regulation of sterol biosynthesis. PLoS Biol 9, e1000598.

Blanc, M., Hsieh, W.Y.Y., Robertson, K.A. a, Kropp, K.A. a, Forster, T., Shui, G., Lacaze, P., Watterson, S., Griffiths, S.J.J., Spann, N.J.J., et al. (2013). The transcription factor STAT-1 couples macrophage synthesis of 25-hydroxycholesterol to the interferon antiviral response. Immunity 38, 106–118.

Cañueto, J., Girós, M., and González-Sarmiento, R. (2014). The role of the abnormalities in the distal pathway of cholesterol biosynthesis in the Conradi-Hünermann-Happle syndrome. Biochim. Biophys. Acta 1841, 336–344.

Chatterjee, S., Szustakowski, J.D., Nanguneri, N.R., Mickanin, C., Labow, M. a, Nohturfft, A., Dev, K.K., and Sivasankaran, R. (2009). Identification of novel genes and pathways regulating SREBP transcriptional activity. PLoS One 4, e5197.

Clendening, J.W., and Penn, L.Z. (2012). Targeting tumor cell metabolism with statins. Oncogene 31, 4967–4978.

Clendening, J.W., Pandyra, A., Boutros, P.C., El Ghamrasni, S., Khosravi, F., Trentin, G. a, Martirosyan, A., Hakem, A., Hakem, R., Jurisica, I., et al. (2010). Dysregulation of the mevalonate pathway promotes transformation. Proc. Natl. Acad. Sci. U. S. A. 107, 15051–15056.

Cuthbert, J. a, and Lipsky, P.E. (1991). Negative regulation of cell proliferation by mevalonate or one of the mevalonate phosphates. J. Biol. Chem. 266, 17966–17971.

Cuthbert, J., and Lipsky, P. (1990). Inhibition by 6-fluoromevalonate demonstrates that mevalonate or one of the mevalonate phosphates is necessary for lymphocyte proliferation. J. Biol. Chem. 265, 18568–18575.

Dorsey, J., and Porter, J. (1968). The inhibition of mevalonic kinase by geranyl and farnesyl pyrophosphates. J. Biol. Chem.

Dugan, R.E., Slakey, L.L., Briedis, A. V, and Porter, J.W. (1972). Factors affecting the diurnal variation in the level of -hydroxy--methylglutaryl coenzyme A reductase and cholesterol-synthesizing activity in rat liver. Arch. Biochem. Biophys. 152, 21–27.

Edwards, P., and Gould, R. (1972). Turnover rate of hepatic 3-hydroxy-3-methylglutaryl coenzyme A reductase as determined by use of cycloheximide. J. Biol. Chem. 247, 1520–1524.

Ericsson, J., Jackson, S.M., and Edwards, P.A. (1996). Synergistic binding of sterol regulatory element-binding protein and NF-Y to the farnesyl diphosphate synthase promoter is critical for sterol-regulated expression of the gene. J Biol Chem 271, 24359–24364.

Gibbs, H.C., Sing, G., González Armas, J.C., Campbell, C.J., Ghazal, P., and Yeh, A.T. (2013). Time-lapse ultrashort pulse microscopy of infection in three-dimensional versus two-dimensional culture environments reveals enhanced extra-chromosomal virus replication compartment formation. J. Biomed. Opt. 18, 031111.

Goldstein, J.L., Basu, S.K., and Brown, M.S. (1983). Receptor-mediated endocytosis of low-density lipoprotein in cultured cells. Methods Enzymol. 98, 241–260.

Goodman, D.S., and Popjak, G. (1960). Studies on the biosynthesis of cholesterol. XII. Synthesis of allyl pyrophosphates from mevalonate and their conversion into squalene with liver enzymes. J. Lipid Res. 1, 286–300.

Gould, R.G., and Swyryd, E. a (1966). Sites of control of hepatic cholesterol biosynthesis. J. Lipid Res. 7, 698–707.

Gould, R.G., Taylor, C.B., Hagerman, J.S., Warner, I., and Cambell, D.J. (1953). Cholesterol metabolism. I. Effect of dietary cholesterol on the synthesis of cholesterol in dog tissue in vitro. J. Biol. Chem. 201, 519–528.

Guan, G., Jiang, G., Koch, R.L., and Shechter, I. (1995). Molecular cloning and functional analysis of the promoter of the human squalene synthase gene. J Biol Chem 270, 21958–21965.

Harris, R.S., Lazar, O., Johansen, J.W., and Sebel, P.S. (2006). Interaction of propofol and sevoflurane on loss of consciousness and movement to skin incision during general anesthesia. Anesthesiology 104, 1170–1175.

Hays, J.B. (2011). New analytical methods for genetic dissection of biological responses to DNA lesions. DNA Repair (Amst). 10, 526–535.

Higgins, M., and Rudney, H. (1973). Regulation of rat liver beta-hydroxy-beta-methylglutaryl-CoA reductase activity by cholesterol. Nat. New Biol. 246, 60–61.

Higgins, M., Kawachi, T., and Rudney, H. (1971). The mechanism of the diurnal variation of hepatic HMG-CoA reductase activity in the rat. Biochem. Biophys. Res. … 45, 138–144.

Hinson, D.D., Chambliss, K.L., Toth, M.J., Tanaka, R.D., and Gibson, K.M. (1997). Post-translational regulation of mevalonate kinase by intermediates of the cholesterol and nonsterol isoprene biosynthetic pathways. J. Lipid Res. 38, 2216–2223.

Horton, J.D., Shah, N.A., Warrington, J.A., Anderson, N.N., Park, S.W., Brown, M.S., and Goldstein, J.L. (2003). Combined analysis of oligonucleotide microarray data from transgenic and knockout mice identifies direct SREBP target genes. Proc Natl Acad Sci U S A 100, 12027–12032.

Jia, J., Zhu, F., Ma, X., Cao, Z., Cao, Z.W., Li, Y., Li, Y.X., and Chen, Y.Z. (2009). Mechanisms of drug combinations: interaction and network perspectives. Nat. Rev. Drug Discov. 8, 111–128.

Jokela, H., Rantakari, P., Lamminen, T., Strauss, L., Ola, R., Mutka, A.-L., Gylling, H., Miettinen, T., Pakarinen, P., Sainio, K., et al. (2010). Hydroxysteroid (17beta) dehydrogenase 7 activity is essential for fetal de novo cholesterol synthesis and for neuroectodermal survival and cardiovascular differentiation in early mouse embryos. Endocrinology 151, 1884–1892.

Kamisuki, S., Shirakawa, T., Kugimiya, A., Abu-Elheiga, L., Choo, H.-Y.P., Yamada, K., Shimogawa, H., Wakil, S.J., and Uesugi, M. (2011). Synthesis and evaluation of diarylthiazole derivatives that inhibit activation of sterol regulatory element-binding proteins. J. Med. Chem. 54, 4923–4927.

Kolb-Mäurer, A., Grzeschik, K.-H., Haas, D., Bröcker, E.-B., and Hamm, H. (2008). Conradi-Hünermann-Happle syndrome (X-linked dominant chondrodysplasia punctata) confirmed by plasma sterol and mutation analysis. Acta Derm. Venereol. 88, 47–51.

Kuswik-Rabiega, G., and Rilling, H.C. (1987). Squalene synthetase. Solubilization and partial purification of squalene synthetase, copurification of presqualene pyrophosphate and squalene synthetase activities. J. Biol. Chem. 262, 1505–1509.

Lutz, R.J., McLain, T.M., and Sinensky, M. (1992). Feedback inhibition of polyisoprenyl pyrophosphate synthesis from mevalonate in vitro. Implications for protein prenylation. J. Biol. Chem. 267, 7983–7986.

Meigs, T.E., and Simoni, R.D. (1997). Farnesol as a regulator of HMG-CoA reductase degradation: characterization and role of farnesyl pyrophosphatase. Arch. Biochem. Biophys. 345, 1–9.

Nandi, D., and Porter, J. (1964). The enzymatic synthesis of geranyl geranyl pyrophosphate by enzymes of carrot root and pig liver. Arch. Biochem. Biophys. 105, 7–19.

Nemoto, K., Ikeda, A., Ito, S., Miyata, M., Yoshida, C., and Degawa, M. (2013). Comparison of constitutive gene expression levels of hepatic cholesterol biosynthetic enzymes between Wistar-Kyoto and stroke-prone spontaneously hypertensive rats. Biol. Pharm. Bull. 36, 1216–1220.

Neuhaus, O., Stüve, O., Archelos, J.J., and Hartung, H.-P. (2005). Putative mechanisms of action of statins in multiple sclerosis--comparison to interferon-beta and glatiramer acetate. J. Neurol. Sci. 233, 173–177.

Noris, E., Zannetti, C., Demurtas, A., Andrea, M. De, Gariglio, M., Noris, E., Zannetti, C., Demurtas, A., Sinclair, J., Andrea, M. De, et al. (2002). Cell Cycle Arrest by Human Cytomegalovirus 86-kDa IE2 Protein Resembles Premature Senescence Cell Cycle Arrest by Human Cytomegalovirus 86-kDa IE2 Protein Resembles Premature Senescence.

Ono, S., Muratani, T., and Matsumoto, T. (2005). Mechanisms of Resistance to Imipenem and Ampicillin in Enterococcus faecalis Mechanisms of Resistance to Imipenem and Ampicillin in Enterococcus faecalis. 49.

Pocathikorn, A., Taylor, R.R., and Mamotte, C.D.S. (2010). Atorvastatin increases expression of low-density lipoprotein receptor mRNA in human circulating mononuclear cells. Clin. Exp. Pharmacol. Physiol. 37, 471–476.

Popjak, G., and Goodman, D. (1961). Mechanism of squalene biosynthesis from mevalonate and farnesyl pyrophosphate. Biochem. … 4, 138–142.

Radhakrishnan, A., Goldstein, J.L., McDonald, J.G., and Brown, M.S. (2008). Switch-like control of SREBP-2 transport triggered by small changes in ER cholesterol: a delicate balance. Cell Metab. 8, 512–521.

Radisky, E.S., and Poulter, C.D. (2000). Squalene synthase: steady-state, pre-steady-state, and isotope-trapping studies. Biochemistry 39, 1748–1760.

Rand, K.H., and Houck, H. (2004). Daptomycin synergy with rifampicin and ampicillin against vancomycin-resistant enterococci. J. Antimicrob. Chemother. 53, 530–532.

Roseman, D.S. (1996). Regulation of 3-Hydroxy-3-methylglutaryl-Coenzyme A Reductase Degradation by the Nonsterol Mevalonate Metabolite Farnesol in Vivo. J. Biol. Chem. 271, 7916–7922.

Sagami, H., Korenaga, T., and Ogura, K. (1993). Geranylgeranyl diphosphate synthase catalyzing the single condensation between isopentenyl diphosphate and farnesyl diphosphate. J. Biochem. 114, 118–121.

Sasiak, K., and Rilling, H.C. (1988). Purification to homogeneity and some properties of squalene synthetase. Arch. Biochem. Biophys. 260, 622–627.

Schoenheimer, R., and Rittenberg, D. (1935). Deuterium as an Indicator in the Study of Intermediary Metabolism. I. J. Biol. Chem. 82, 156–157.

Sever, N., Song, B.-L., Yabe, D., Goldstein, J.L., Brown, M.S., and DeBose-Boyd, R. a (2003). Insig-dependent ubiquitination and degradation of mammalian 3-hydroxy-3-methylglutaryl-CoA reductase stimulated by sterols and geranylgeraniol. J. Biol. Chem. 278, 52479–52490.

Shapiro, D.J., and Rodwell, V.W. (1971). Regulation of hepatic 3-hydroxy-3-methylglutaryl coenzyme A reductase and cholesterol synthesis. J. Biol. Chem. 246, 3210–3216.

Shirahama, S., Miyahara, A., Kitoh, H., Honda, A., Kawase, A., Yamada, K., Mabuchi, A., Kura, H., Yokoyama, Y., Tsutsumi, M., et al. (2003). Skewed X-chromosome inactivation causes intra-familial phenotypic variation of an EBP mutation in a family with X-linked dominant chondrodysplasia punctata. Hum. Genet. 112, 78–83.

Sinclair, J., Baillie, J., Bryant, L., and Caswell, R. (2000). Human cytomegalovirus mediates cell cycle progression through G(1) into early S phase in terminally differentiated cells. J. Gen. Virol. 81, 1553–1565.

Siperstein, M., and Fagan, V. (1966). Feedback control of mevalonate synthesis by dietary cholesterol. J. Biol. Chem. 241, 602–609.

Tanaka, R.D., Schafer, B.L., Lee, L.Y., Freudenberger, J.S., and Mosley, S.T. (1990). Purification and regulation of mevalonate kinase from rat liver. J. Biol. Chem. 265, 2391–2398.

Tansey, T.R., and Shechter, I. (2001). Squalene synthase: structure and regulation. Prog. Nucleic Acid Res. Mol. Biol. 65, 157–195.

Thulasiram, H. V, and Poulter, C.D. (2006). Farnesyl diphosphate synthase: the art of compromise between substrate selectivity and stereoselectivity. J. Am. Chem. Soc. 128, 15819–15823.

Wagner, R., and Levy, A. (1960). Interferon as a chemical intermediary in viral interference. Ann. New York Acad. … 88, 1308–1318.

Wang, H., Sarikonda, G., Puan, K.-J., Tanaka, Y., Feng, J., Giner, J.-L., Cao, R., Mönkkönen, J., Oldfield, E., and Morita, C.T. (2011). Indirect stimulation of human Vγ2Vδ2 T cells through alterations in isoprenoid metabolism. J. Immunol. 187, 5099–5113.

Wright, L.D., Cresson, E.L., Skeggs, H.R., MacRae, G.D.E., Hoffman, C.H., Wolf, D.E., and Folkers, K. (1956). Isolation of a New Acetate-replacing Factor. J. Am. Chem. Soc. 78, 5273–5275.

Zhou, C., Li, Z., Wiberley-Bradford, A.E., Weise, S.E., and Sharkey, T.D. (2013). Isopentenyl diphosphate and dimethylallyl diphosphate/isopentenyl diphosphate ratio measured with recombinant isopentenyl diphosphate isomerase and isoprene synthase. Anal. Biochem. 440, 130–136.

4.5 Supporting information

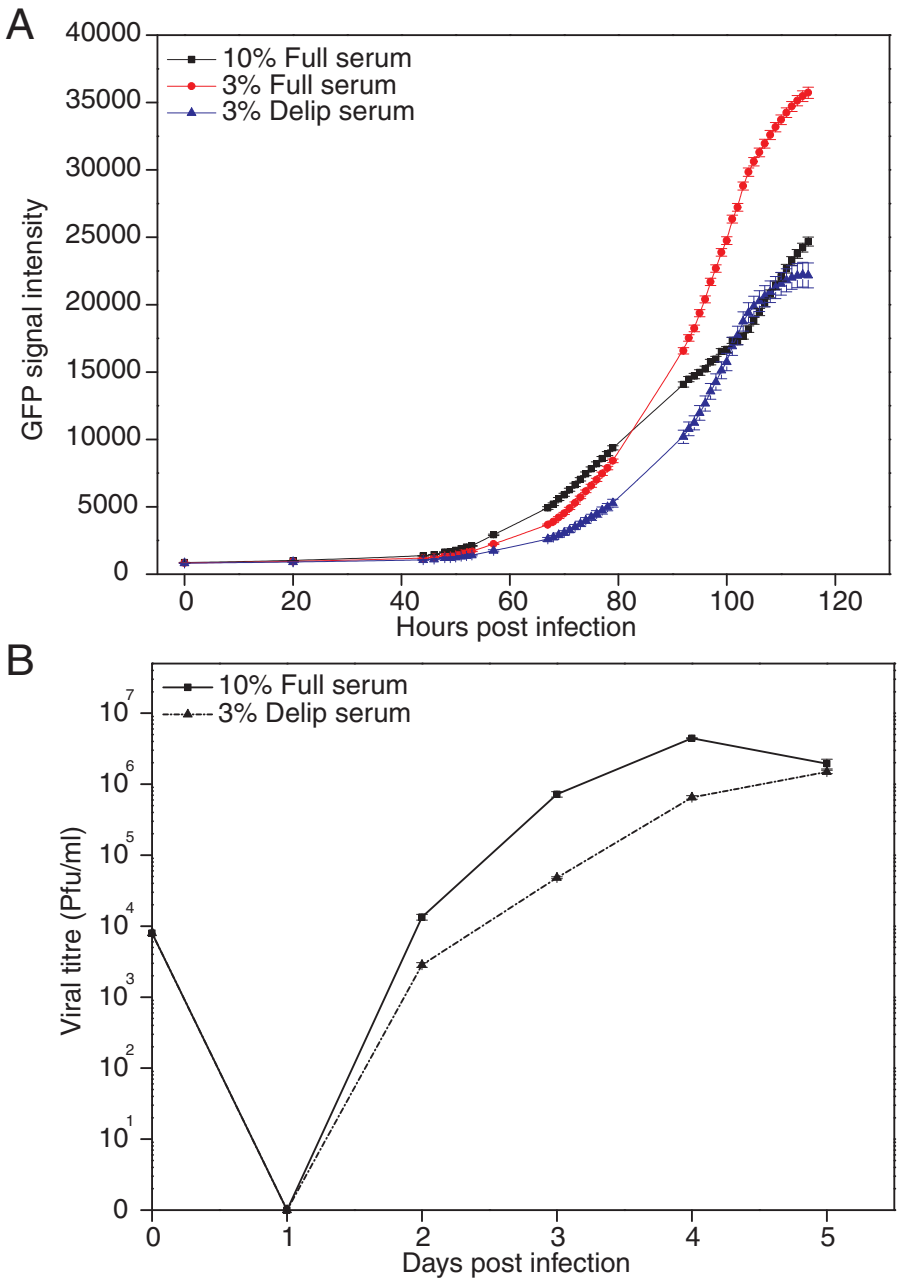

Figure S4.1 Changes in media serum condition affects MCMV replication.
(A) Virus replication was monitored as a function of kinetic GFP fluorescence. NIH-3T3 fibroblasts were seeded at a seeding density of $3x10^4$ cells/well in black 96-well plates in normal media. The next day, cells were infected with MCMV-GFP (MOI = 0.016) for 1 hr. After absorption, the viral inoculum was removed and cells were incubated with DMEM supplemented with either 10%, 3% normal media, or 3% delipidised media. Data are the mean of two experiments (4 replicates per experiment) ± SEM. (B) NIH-3T3 fibroblasts were seeded at a seeding density of $8x10^5$ cells/well in 6-well plates. The next day, cells were infected with MCMV-C3X (MOI = 0.05). After adsorption, cells were washed 5 times with blank medium (DMEM only). After washing, cells were cultured in 10% normal or 3% delipidised media. Supernatants were collected every day and the virus titre was quantitated by plaque assay. Data are the mean of 3 biological replicates ± SEM.

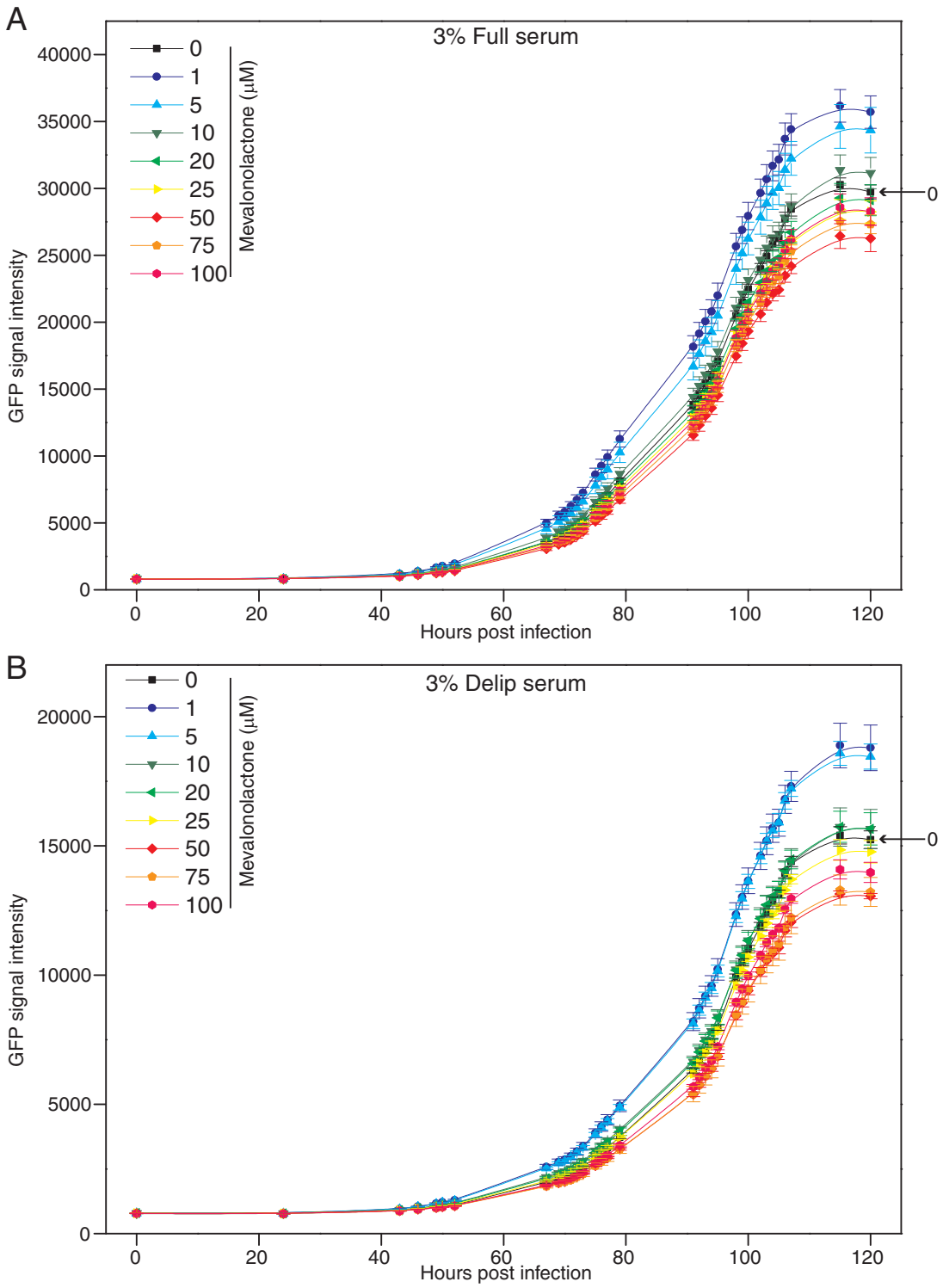
A
3% Full serum
Mevalonolactone (μM)
0
1
5
10
20
25
50
75
100
GFP signal intensity
Hours post infection
0
B
3% Delip serum
Mevalonolactone (μM)
0
1
5
10
20
25
50
75
100
GFP signal intensity
Hours post infection
0

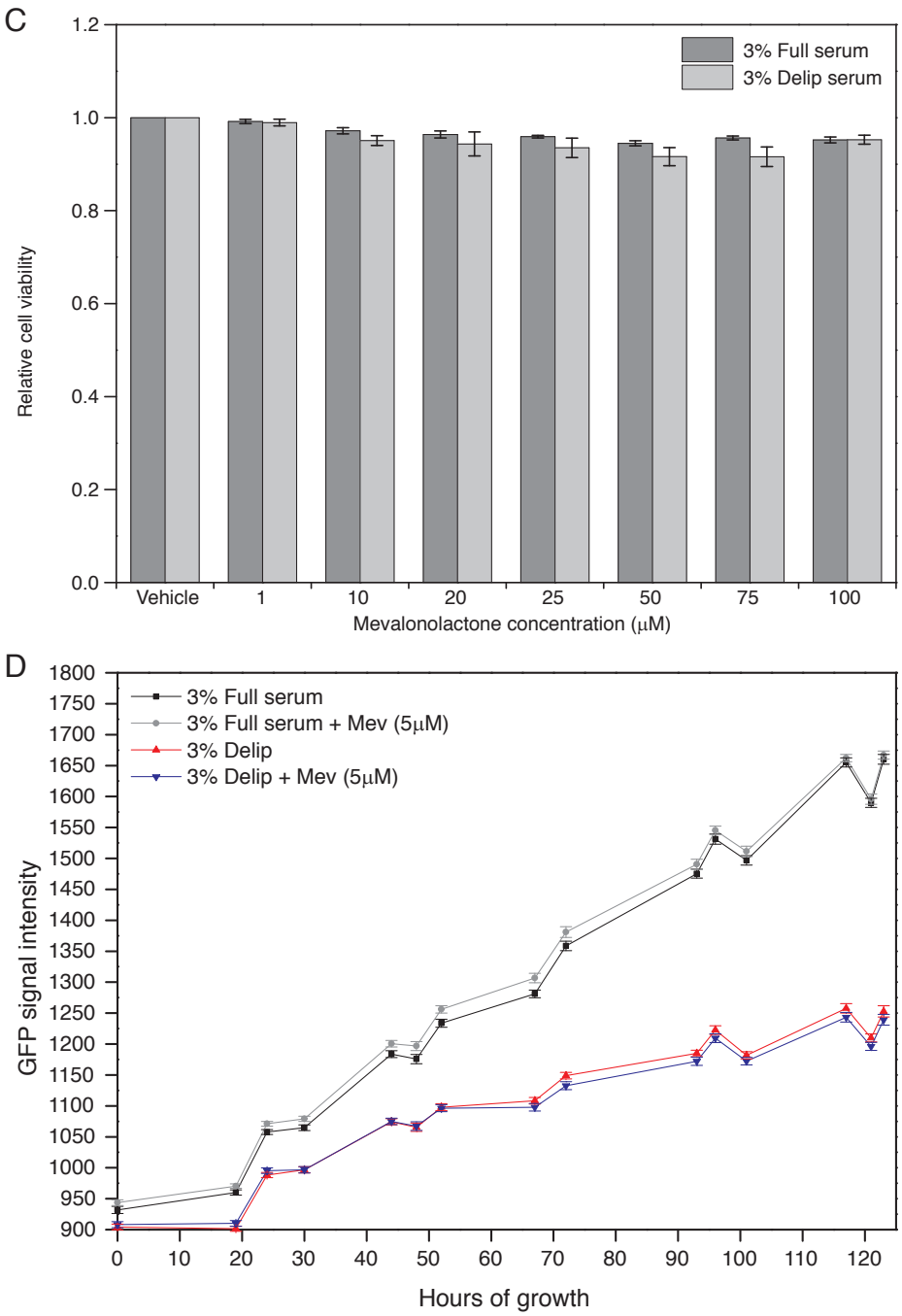

Figure S4.2 The effects of mevalonate on MCMV replication and cell growth in different serum conditions.

NIH-3T3 fibroblasts (2x10^4 cells/well) were seeded in 96-well plates for 24 hr. The next day, cells were infected with MCMV-GFP (MOI = 0.016) for 1 hr. Following the removal of viral inoculum, cells were incubated in (A) 3% normal (full) or (B) 3% delipidised (delip) media supplemented with mevalonolactone at an increasing concentration. The level of infection was determined and plotted by the increase in GFP fluorescence over time. The graph represents 2 experiments (one performed by Saikou Y Bah in conjunction) with 4 replicates each ± SEM. (C) NIH-3T3 fibroblasts (2x10^4 cells/well) were treated with mevalonolactone at an increasing concentration in either 3% normal or 3% delipidised media and the cell viability was measured 48 hr post-treatment using CellTiter-Blue. Relative cell viability was calculated by normalizing to the vehicle treated samples and data are the mean of 16 biological replicates ± SEM. (D) NIH-3T3-H2B-GFP were seeded at a seeding density of 1x10^4 cells/well in 96-well plates. The next day, cells were incubated in 185μl of phenol red-free media supplemented with 3% normal or 3% delipidised serum ± mevalonate as indicated. Growth of the cells was monitored by their fluorescent intensity. Data are the mean of 2 experiments (32 biological replicates) ± SEM.

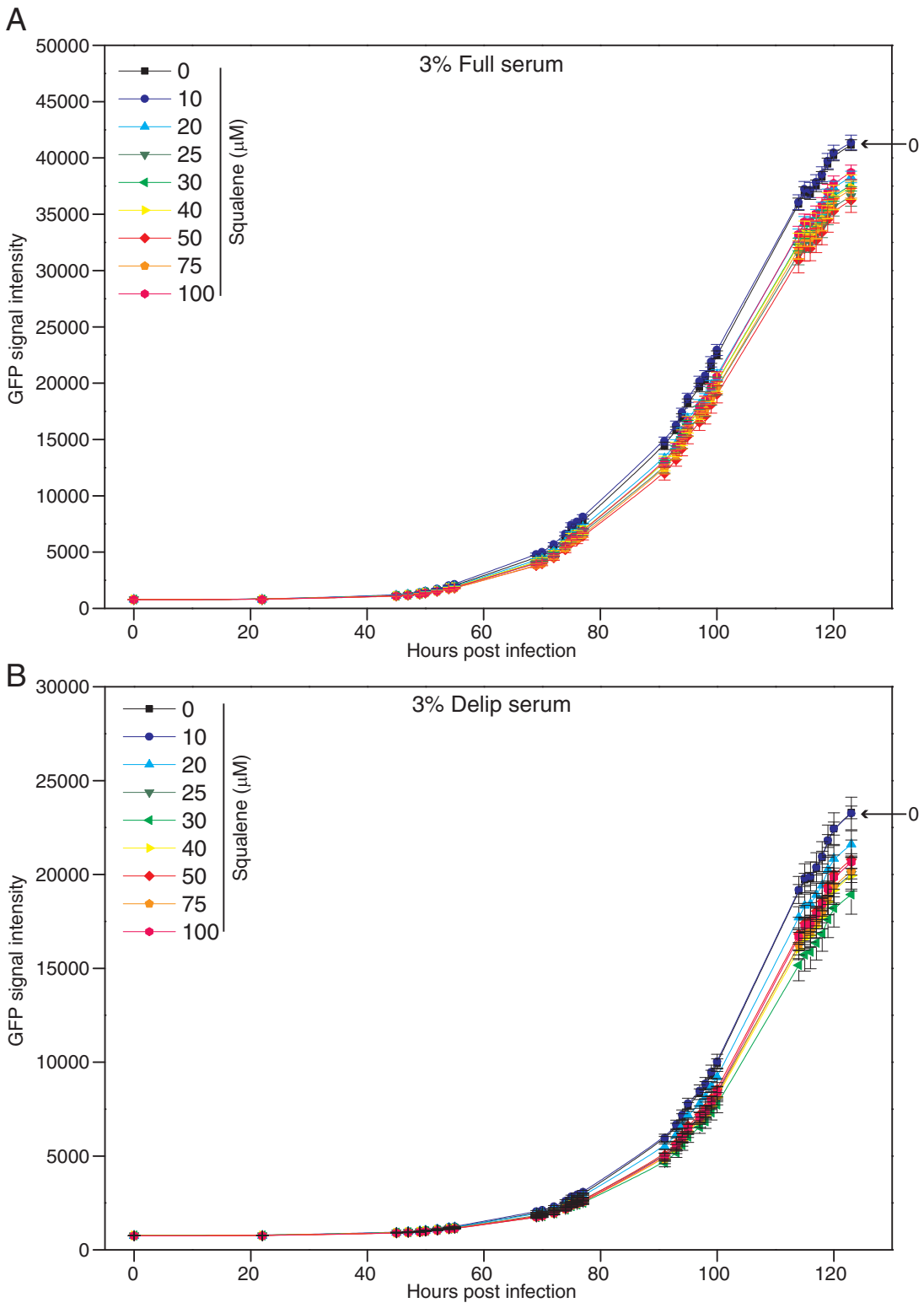
A
3% Full serum
Squalene (μM)
0
10
20
25
30
40
50
75
100
GFP signal intensity
Hours post infection
0
B
3% Delip serum
Squalene (μM)
0
10
20
25
30
40
50
75
100
GFP signal intensity
Hours post infection
0

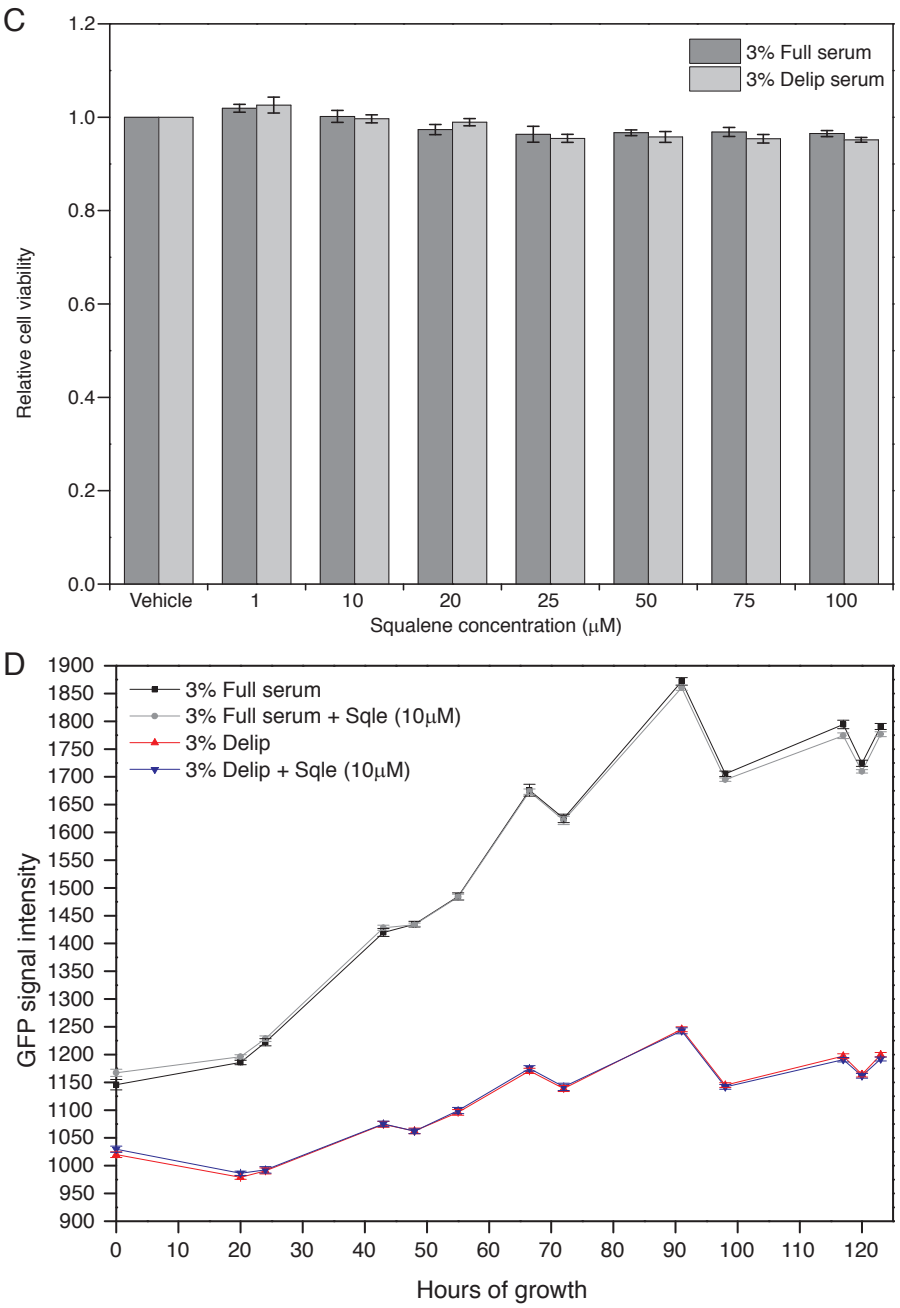

Figure S4.3 The effects of squalene on MCMV replication in different serum conditions.
NIH-3T3 fibroblasts (2x10^4 cells/well) were seeded in 96-well plates for 24 hr. The next day, cells were infected with MCMV-GFP (MOI = 0.016) for 1 hr. Following the removal of viral inoculum, cells were incubated in (A) 3% normal (full) or (B) 3% delipidised (delip) media supplemented with squalene at an increasing concentration. The level of infection was determined and plotted by the increase in GFP fluorescence over time. The graph represents two experiments (one performed by Saikou Y Bah in conjunction) with 4 replicates each ± SEM. (C) NIH-3T3 fibroblasts (2x10^4 cells/well) were treated with squalene at an increasing concentration in either 3% normal or 3% delipidised media and the cell viability was measured 48 hr post-treatment using CellTiter-Blue. Relative cell viability was calculated by normalizing to the vehicle treated samples and data are the mean of 16 biological replicates ± SEM. (D) NIH-3T3-H2B-GFP were seeded at a seeding density of 1x10^4 cells/well in 96-well plates. The next day, cells were incubated in 185μl of phenol red-free media supplemented with 3% normal or 3% delipidised serum ± squalene as indicated. Growth of the cells was monitored by their fluorescent intensity. Data are the mean of two experiments (32 biological replicates) ± SEM.

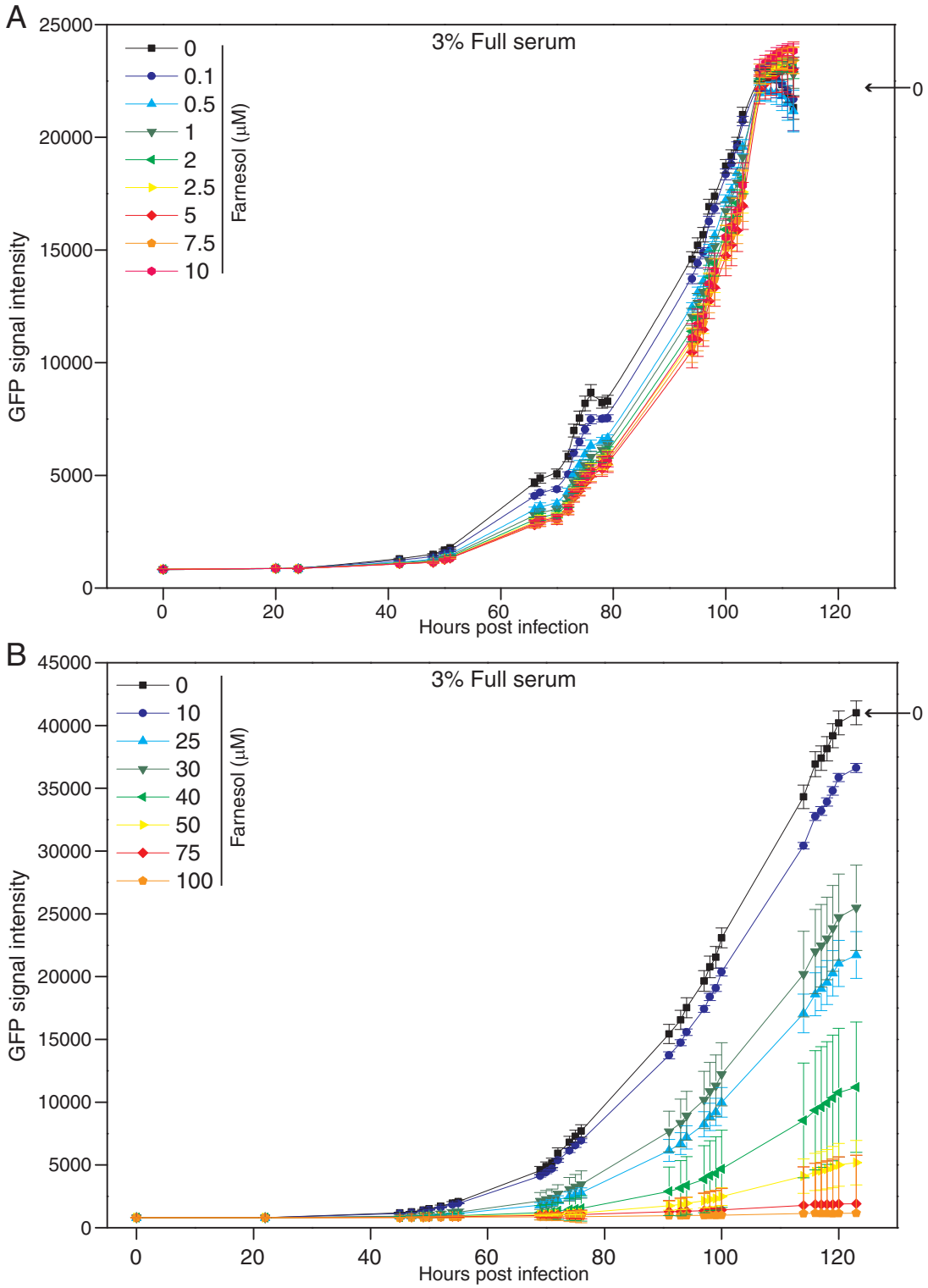
A
3% Full serum
Farnesol (μM)
0
0.1
0.5
1
2
2.5
5
7.5
10
GFP signal intensity
Hours post infection
0
B
3% Full serum
Farnesol (μM)
0
10
25
30
40
50
75
100
GFP signal intensity
Hours post infection
0

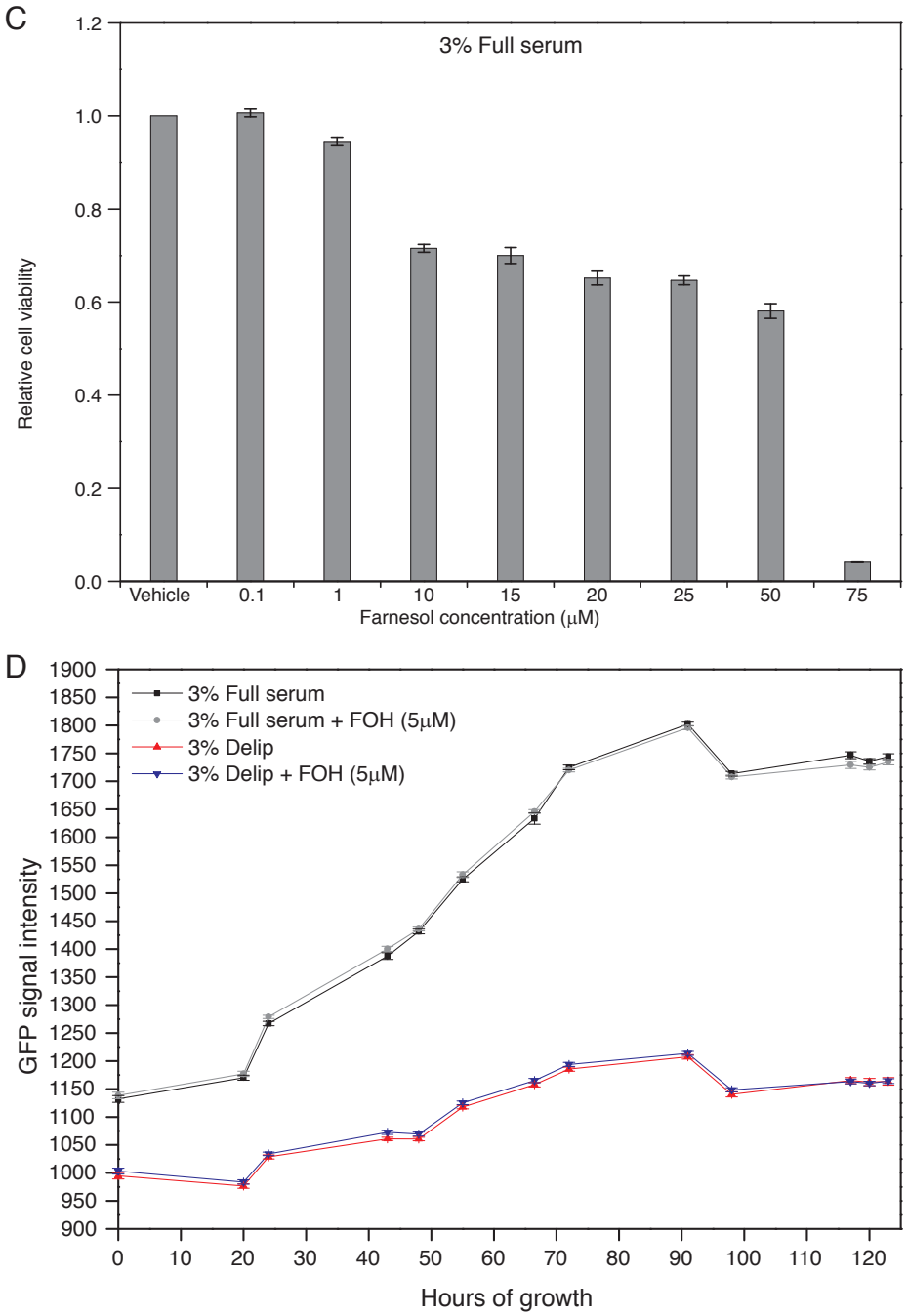

Figure S4.4 The effects of farnesol on MCMV replication in full serum conditions.
(A and B) NIH-3T3 fibroblasts ($2x10^4$ cells/well) were seeded in 96-well plates for 24 hr. The next day, cells were infected with MCMV-GFP (MOI = 0.016) for 1 hr. Following the removal of viral inoculum, cells were incubated in 3% normal media supplemented with farnesol at an increasing concentration. The level of infection was determined and plotted by the increase in GFP fluorescence over time. The graph represents 2 experiments (one performed by Saikou Y Bah in conjunction) with 4 replicates each ± SEM. (C) NIH-3T3 fibroblasts ($2x10^4$ cells/well) were treated with farnesol at an increasing concentration in 3% normal media and the cell viability was measured 48 hr post-treatment using CellTiter-Blue. Relative cell viability was calculated by normalizing to the vehicle treated samples and data are the mean of 16 biological replicates ± SEM. (D) NIH-3T3-H2B-GFP were seeded at a seeding density of $1x10^4$ cells/well in 96-well plates. The next day, cells were incubated in 185μl of phenol red-free media supplemented with 3% normal or 3% delipidised serum ± farnesol as indicated. Growth of the cells was monitored by their fluorescent intensity. Data are the mean of two experiments (32 biological replicates) ± SEM.

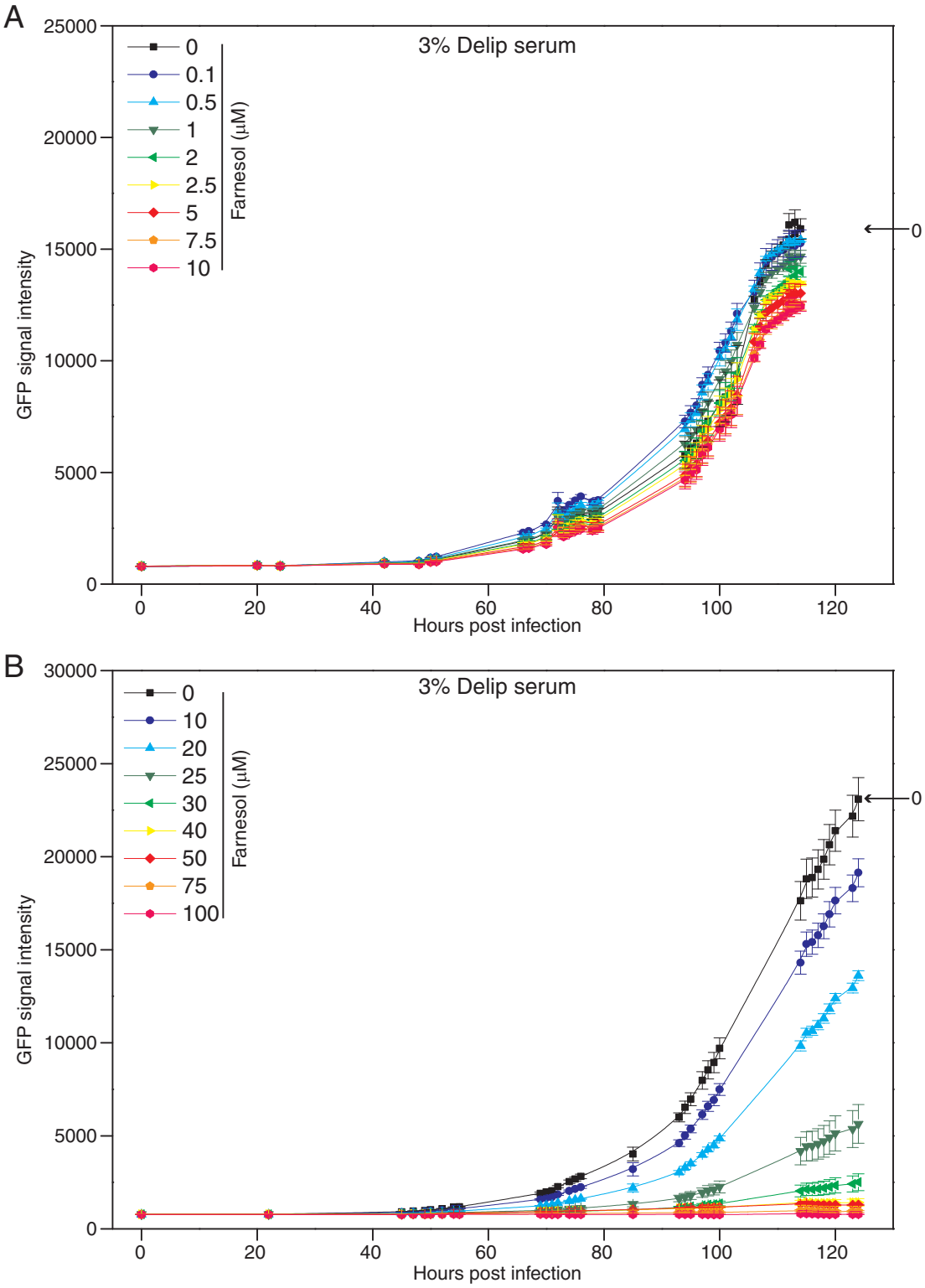
A
3% Delip serum
Farnesol (μM)
0
0.1
0.5
1
2
2.5
5
7.5
10
GFP signal intensity
Hours post infection
0
B
3% Delip serum
Farnesol (μM)
0
10
20
25
30
40
50
75
100
GFP signal intensity
Hours post infection
0

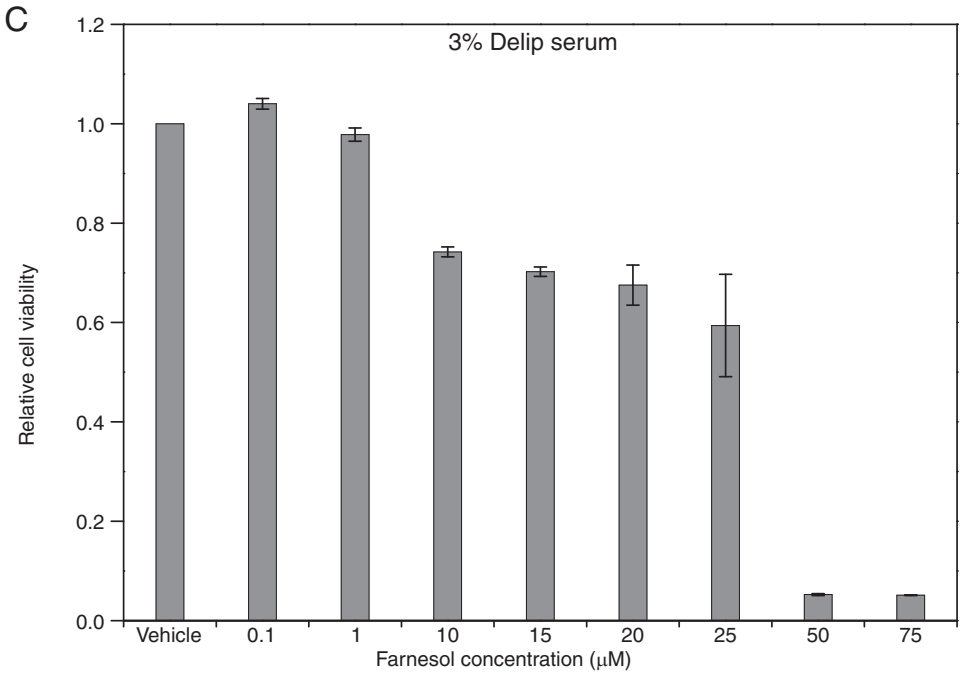

Figure S4.5 The effects of farnesol on MCMV replication in delipidised serum conditions.
(A and B) NIH-3T3 fibroblasts ($2x10^4$ cells/well) were seeded in 96-well plates for 24 hr. The next day, cells were infected with MCMV-GFP (MOI = 0.016) for 1 hr. Following the removal of viral inoculum, cells were incubated in 3% delipidised media supplemented with farnesol at an increasing concentration. The level of infection was determined and plotted by the increase in GFP fluorescence over time. The graph represents two experiments (one performed by Saikou Y Bah in conjunction) with 4 replicates each ± SEM. (C) NIH-3T3 fibroblasts ($2x10^4$ cells/well) were treated with farnesol at an increasing concentration in 3% delipidised media and the cell viability was measured 48 hr post-treatment using CellTiter-Blue. Relative cell viability was calculated by normalizing to the vehicle treated samples and data are the mean of 16 biological replicates ± SEM.

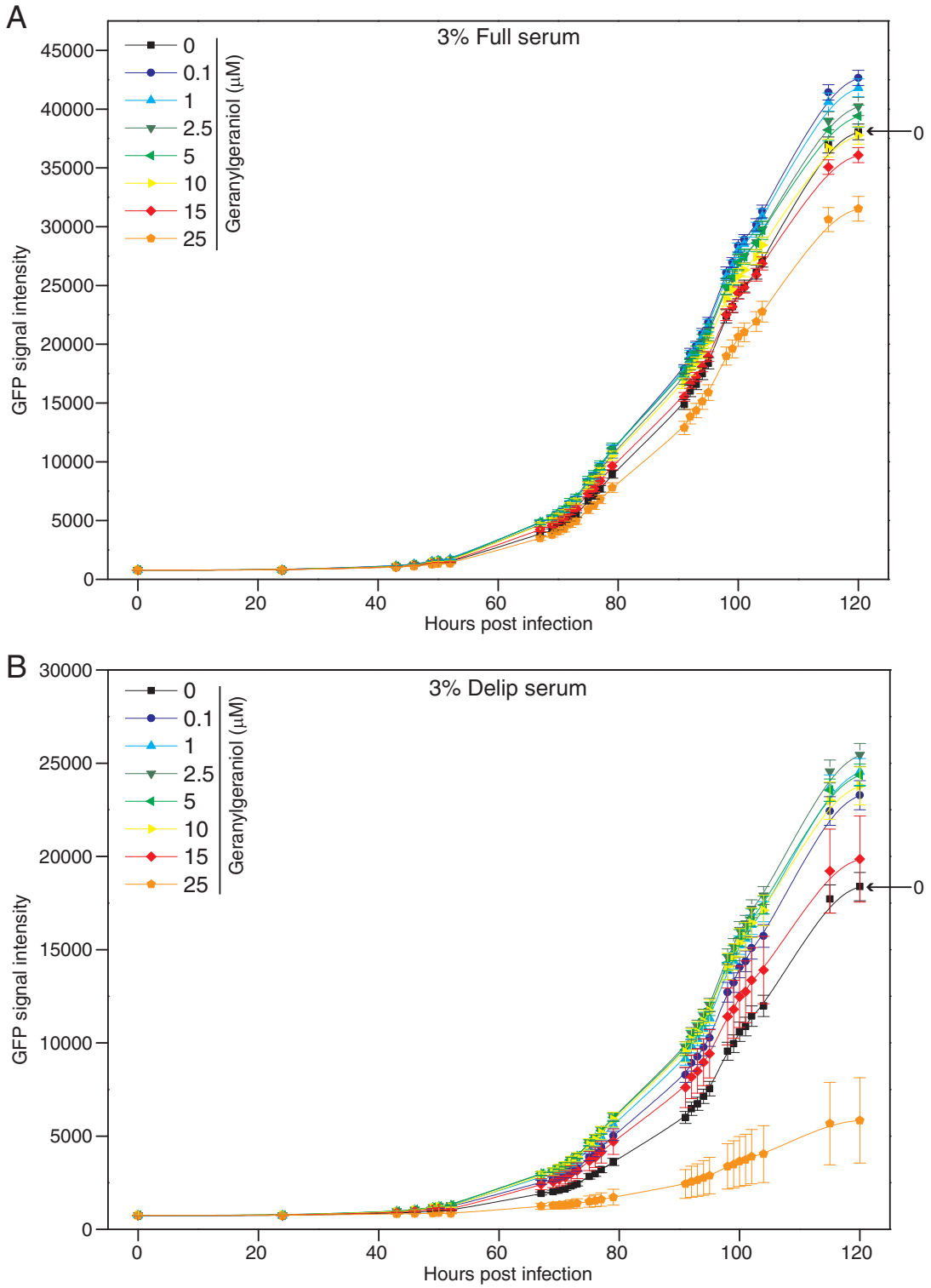
A
3% Full serum
Geranylgeraniol (μM)
0
0.1
1
2.5
5
10
15
25
GFP signal intensity
Hours post infection
0
B
3% Delip serum
Geranylgeraniol (μM)
0
0.1
1
2.5
5
10
15
25
GFP signal intensity
Hours post infection
0

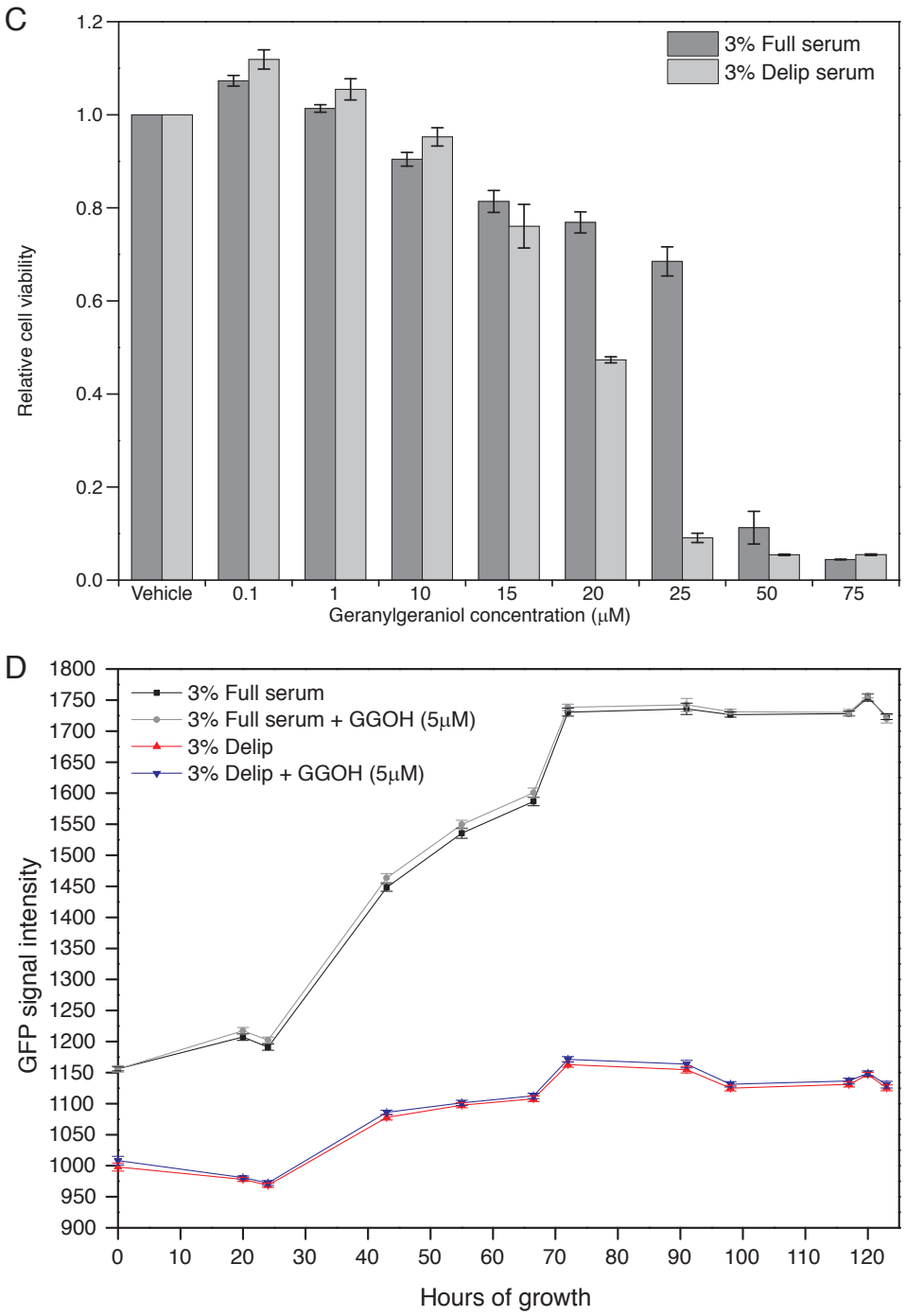

Figure S4.6 The effects of geranylgeraniol on MCMV replication in different serum conditions. NIH-3T3 fibroblasts (2x10^4 cells/well) were seeded in 96-well plates for 24 hr. The next day, cells were infected with MCMV-GFP (MOI = 0.016) for 1 hr. Following the removal of viral inoculum, cells were incubated in (A) 3% normal (full) or (B) 3% delipidised (delip) serum supplemented with geranylgeraniol at an increasing concentration. The level of infection was determined and plotted by the increase in GFP fluorescence over time. The graph represents two experiments (one performed by Saikou Y Bah in conjunction) with 4 replicates each ± SEM. (C) NIH-3T3 fibroblasts (2x10^4 cells/well) were treated with geranylgeraniol at an increasing concentration in either 3% normal or 3% delipidised media and the cell viability was measured 48 hr post-treatment using CellTiter-Blue. Relative cell viability was calculated by normalizing to the vehicle treated samples and data are the mean of 16 biological replicates ± SEM. (D) NIH-3T3-H2B-GFP were seeded at a seeding density of 1x10^4 cells/well in 96-well plates. The next day, cells were incubated in 185μl of phenol red-free media supplemented with 3% normal or 3% delipidised serum ± geranylgeraniol as indicated. Growth of the cells was monitored by their fluorescent intensity. Data are the mean of two experiments (32 biological replicates) ± SEM.

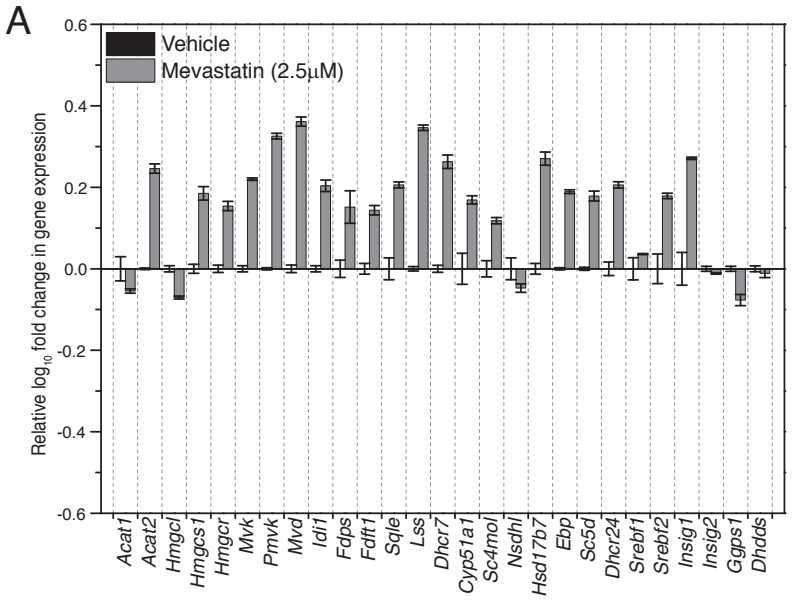

Figure S4.7 Effects of mevastatin on sterol biosynthesis gene expressions in NIH-3T3 fibroblasts. NIH-3T3 fibroblasts ($8x10^5$ cells/well) were seeded in 6-well plates for 24 hr. The next day, cells were incubated in 10% normal media supplemented with 2.5μM of mevastatin for 24 hr. Relative abundance of specific sterol biosynthesis gene transcripts between treated and vehicle treated samples were assayed by qRT-PCR using 30ng of RNA. Data are the mean of 3 biological replicates ± SEM.

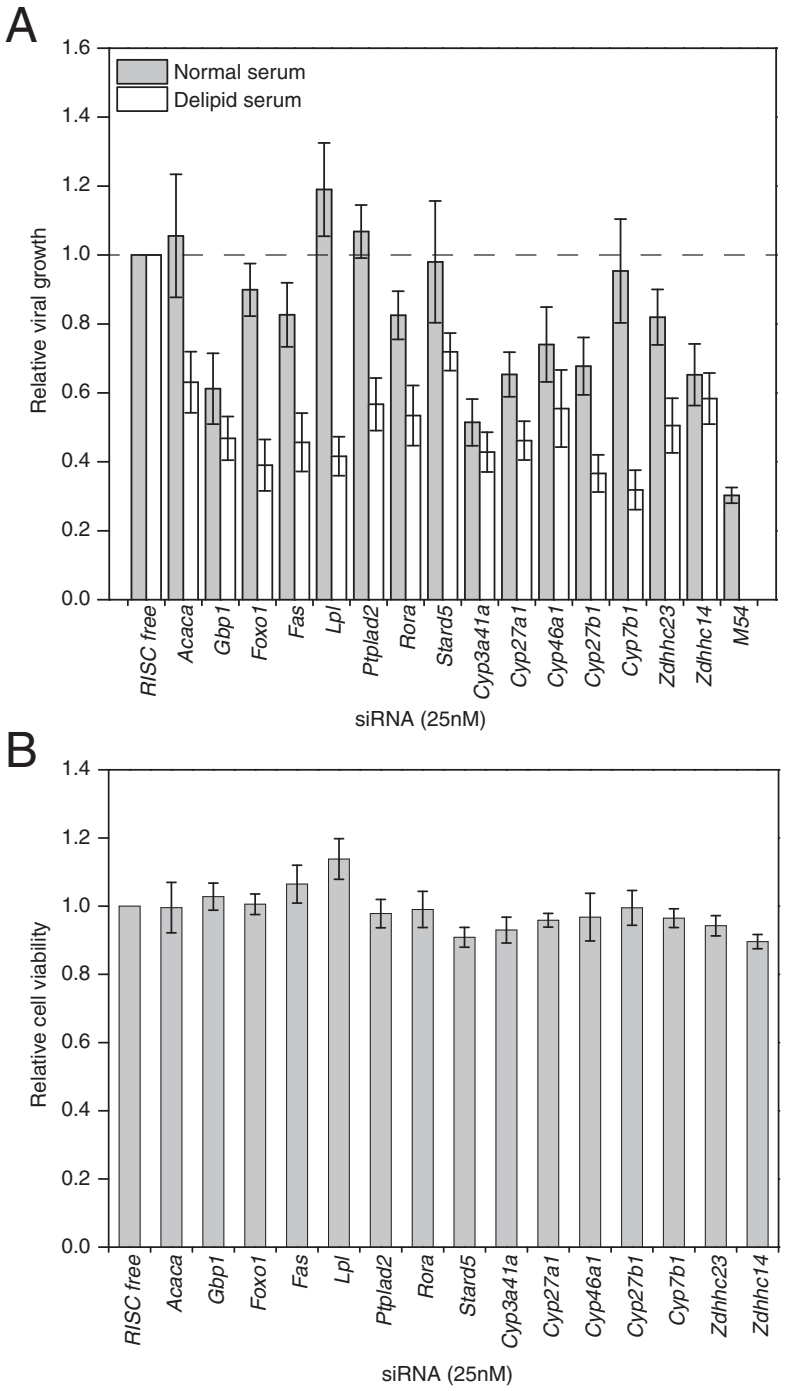

Figure S4.8 siRNA knockdown of selective fatty acid and cholesterol biosynthesis regulatory genes on MCMV replication under different serum conditions.

(A) pMEFs ($1.5x10^4$ cells/well) were transfected in 96-well plates with On-target plus siRNAs as indicated for 48 hr then infected with MCMV-GFP (MOI = 0.1) for 1 hr. After the removal of viral inoculum, cells were incubated in either 10% normal, or 3% delipidised media. *RISC free* was used as a transfection control, while *M54* specifically targets MCMV polymerase. The level of infection was determined by measuring the increase in GFP fluorescence (slope) during the linear-phase of viral growth. The graph represents the relative level of infection compared to *RISC free* transfected and data are the mean of 9 biological replicates ± SEM. (B) pMEFs ($1.5x10^4$ cells/well) were transfected with On-target plus siRNAs as indicated in 96-well plates for 48 hr then the cell viability was measured using CellTiter-Blue. Relative cell viability was calculated by normalizing to the *RISC free* transfected samples and data are the mean of 4 biological replicates ± SEM.

Publications associated with Chapter 4

Rodríguez-Martín S, Kropp KA, Wilhelmi V, Lisnic VJ, **Hsieh WY**, Blanc M, Livingston A, Busche A, Tekotte H, Messerle M, Auer M, Fraser I, Jonjic S, Angulo A, Reddehase MJ, Ghazal P. Ablation of the regulatory IE1 protein of murine cytomegalovirus alters in vivo pro-inflammatory TNF-alpha production during acute infection. PLoS Pathog. 2012;8(8):e1002901.

Kropp KA, **Hsieh WY**, Isern E, Forster T, Krause E, Brune W, Angulo A, Ghazal P. A Temporal Gate for Viral Enhancers to Co-opt Toll-Like-Receptor Transcriptional Activation Pathways upon Acute Infection. PLoS Pathog. 2015 Apr 9;11(4):e1004737.

OPEN ACCESS Freely available online

PLOS | PATHOGENS

Ablation of the Regulatory IE1 Protein of Murine Cytomegalovirus Alters *In Vivo* Pro-inflammatory TNF-alpha Production during Acute Infection

Sara Rodríguez-Martín[1☯], Kai Alexander Kropp[1☯], Vanessa Wilhelmi[2], Vanda Juranic Lisnic[3], Wei Yuan Hsieh[1], Mathieu Blanc[1], Andrew Livingston[1], Andreas Busche[4], Hille Tekotte[5], Martin Messerle[4], Manfred Auer[6], Iain Fraser[7], Stipan Jonjic[3], Ana Angulo[8], Matthias J. Reddehase[2], Peter Ghazal[1]*

1 Division of Pathway Medicine and Centre for Infectious Diseases, University of Edinburgh, Edinburgh, United Kingdom, **2** Institute for Virology, University Medical Center of the Johannes Gutenberg University, Mainz, Germany, **3** Department of Histology and Embryology/Center for Proteomics, Faculty of Medicine, University of Rijeka, Rijeka, Croatia, **4** Department of Virology, Hannover Medical School, Hannover, Germany, **5** Wellcome Trust Centre for Cell Biology, University of Edinburgh, Edinburgh, United Kingdom, **6** University of Edinburgh, School of Biological Sciences (CSE) and School of Biomedical Sciences (CMVM), Edinburgh, United Kingdom, **7** Laboratory of Systems Biology, National Institution of Allergy and Infectious Disease, National Institutes of Health, Bethesda, Maryland, United States of America, **8** Institut d'Investigacions Biomediques August Pi i Sunyer, Barcelona, Spain

Abstract

Little is known about the role of viral genes in modulating host cytokine responses. Here we report a new functional role of the viral encoded IE1 protein of the murine cytomegalovirus in sculpting the inflammatory response in an acute infection. In time course experiments of infected primary macrophages (MΦs) measuring cytokine production levels, genetic ablation of the immediate-early 1 (*ie1*) gene results in a significant increase in TNFα production. Intracellular staining for cytokine production and viral early gene expression shows that TNFα production is highly associated with the productively infected MΦ population of cells. The *ie1*- dependent phenotype of enhanced MΦ TNFα production occurs at both protein and RNA levels. Noticeably, we show in a series of *in vivo* infection experiments that in multiple organs the presence of *ie1* potently inhibits the pro-inflammatory cytokine response. From these experiments, levels of TNFα, and to a lesser extent IFNβ, but not the anti-inflammatory cytokine IL10, are moderated in the presence of *ie1*. The *ie1*- mediated inhibition of TNFα production has a similar quantitative phenotype profile in infection of susceptible (BALB/c) and resistant (C57BL/6) mouse strains as well as in a severe immuno-ablative model of infection. *In vitro* experiments with infected macrophages reveal that deletion of *ie1* results in increased sensitivity of viral replication to TNFα inhibition. However, *in vivo* infection studies show that genetic ablation of TNFα or TNFRp55 receptor is not sufficient to rescue the restricted replication phenotype of the *ie1* mutant virus. These results provide, for the first time, evidence for a role of IE1 as a regulator of the pro-inflammatory response and demonstrate a specific pathogen gene capable of moderating the host production of TNFα *in vivo*.

Citation: Rodríguez-Martín S, Kropp KA, Wilhelmi V, Lisnic VJ, Hsieh WY, et al. (2012) Ablation of the Regulatory IE1 Protein of Murine Cytomegalovirus Alters *In Vivo* Pro-inflammatory TNF-alpha Production during Acute Infection. PLoS Pathog 8(8): e1002901. doi:10.1371/journal.ppat.1002901

Editor: William J. Britt, University of Alabama at Birmingham, United States of America

Received February 7, 2012; **Accepted** July 27, 2012; **Published** August 30, 2012

This is an open-access article, free of all copyright, and may be freely reproduced, distributed, transmitted, modified, built upon, or otherwise used by anyone for any lawful purpose. The work is made available under the Creative Commons CC0 public domain dedication.

Funding: This work was supported by: The Wellcome Trust (WT066784/Z/02/Z), and the BBSRC/EPSRC to SynthSys, a Centre for Integrative Systems Biology (CISB) reference BB/D019621/1 to PG. Deutsche Forschungsgemeinschaft, research fellowship KR-3890/1-1 to KK. BBSRC studentship, and University of Edinburgh Principal's Fellowship to SRM. The work of HT was supported by grants from the Wellcome Trust and the European Research Council (233457-SCG) to Mike Tyers. Deutsche Forschungsgemeinschaft, SFB 587, individual project A13 to MM. Deutsche Forschungsgemeinschaft, SFB 490, individual projects E2 and E4 to VW and MJR. Ministerio de Ciencia e Innovacion (SAF2008-00382 and SAF2011-25155) to AA. SULSA (Scottish Universities Life Sciences Alliance) to MA. Helmholtz Society through collaborative research program VISTRIE to SJ. British Heart Foundation reference FS/05/022 and University of Edinburgh Alumni Fund to MB. IF is funded by National Institutes of Health. The funders had no role in study design, data collection and analysis, decision to publish, or preparation of the manuscript.

Competing Interests: The authors have declared that no competing interests exist.

* E-mail: p.ghazal@ed.ac.uk

☯ These authors contributed equally to this work.

Introduction

The β-herpesvirus human cytomegalovirus (HCMV) is a species-specific virus and a clinically important pathogen that can establish both acute and latent infections. The murine counterpart (MCMV) provides a useful model for studying CMV natural infection in its natural host. CMV has a dsDNA genome that is sequentially expressed in a hierarchical cascade, immediate early (IE), early (E) and late (L) [1]. The MCMV IE1 protein has been implicated in the transcriptional activation of viral early genes in combination with the IE3 protein [2] as well as in the expression of cellular genes [3–5]. The IE1-induced activation of gene expression is not completely understood, although the ability of IE1 to interact with chromatin through histones [6,7] might be one mode of action responsible for its transactivating functions.

The ability of MCMV IE1 protein to activate cellular gene expression has been documented for genes involved in immune signalling pathways, DNA metabolism and cell cycle control [3,4,8,9]. Recently, a single point mutation in MCMV IE1 has been shown to disrupt its capacity of trans-activating cellular genes ribonucleotide reductase and thymidylate synthase, involved in

Author Summary

The suppression of the production rather than the blockage of action of the potent inflammatory mediator TNFα is a particular hallmark of anti-TNFα mechanisms associated with microbial and parasitic infections. Whether this mode of counter-regulation is an important feature of infection by viruses is not clear. Also, it remains to be determined whether a specific pathogen gene in the context of an infection *in vivo* is capable of modulating levels of TNFα production. In this study we disclose a virus-mediated moderation of TNFα production, dependent on the *ie1* gene of murine cytomegalovirus (MCMV). The *ie1* gene product IE1 is a well-characterized nuclear protein capable of altering levels of host and viral gene expression although its biological role in the context of a natural infection is to date unknown. We provide evidence showing that *ie1* is associated with a moderated pro-inflammatory cytokine response, in particular with TNFα production. Further, we show that the viral moderation of this cytokine is not only readily apparent *in vitro* but also in the natural host. The identification of a viral gene responsible for this mode of regulation *in vivo* may have therapeutic potential in the future in both anti-viral and anti-inflammatory strategies.

nucleotide metabolism [10]. IE1 is also a potent disruptor of promyelocytic leukemia gene product (PML) oncogenic domains (PODs/ND10) [11,12], which have been implicated in intrinsic cell immunity to infection [13–15]. *In vitro*, an IE1-deleted MCMV grows with the same efficiency as wild type MCMV in different cell types [11]. However, this mutant is severely attenuated in immune competent BALB/c mice as well as in SCID mice lacking the adaptive immune control, and shows a reduced doubling time in various organs of BALB/c mice after hematoablative treatment [10,11]. On the basis of these studies we have previously speculated about a putative role of IE1 in interfering with some early intrinsic or innate immune mechanism [11], involving pro-inflammatory cytokine production or signalling. In this context, the homologous HCMV IE1 protein has recently been reported to counteract the type I interferon response by targeting principally STAT2 [16]. Moreover, in the case of HCMV, there are an increasing number of studies pointing to IE1 promoting a nuclear environment conducive for viral expression by modulating epigenetic regulation of the viral major immediate early promoter (MIEP). In these studies, ND10 associated-proteins, in particular hDaxx, have been shown to be repressors of the MIEP [17]. In this scenario, the dispersion of ND10s by the IE1 protein at early time of infection is thought to increase MIEP transcription efficiency indicating a potential role of ND10s as part of an antiviral defence mechanism inactivated by IE1 [12]. However, it is important to note that in the absence of the *ie1* gene HCMV, unlike MCMV or rat CMV [18], displays growth impairment under conditions of low multiplicity of infection (MOI) on primary fibroblasts [19,20]. The growth phenotype of the HCMV *ie1*-deficient strains adds an additional level of complication that can be avoided by utilising a rodent CMV model. Overall, while the mode of action of IE1 has been extensively studied in different species of CMV, the functional relationship of this protein in the regulation of host-virus interaction pathways, especially in a more biologically relevant context such as in infection of MΦ or at a whole organism level, remains unknown to date.

Macrophages (MΦs) play a central role in CMV infection with regard to viral dissemination, replication and establishment of latency [21,22]. At the host response level, MΦs constitute one of the principal effectors of innate immunity. Upon activation, MΦs produce a number of pro-inflammatory cytokines such as TNFα, IL1, IL6, IFNα/β and IL12, which are reported to be key mediators of the response against MCMV [23–25]. Of these pro-inflammatory cytokines, TNFα represents a key player in innate immunity. It is produced in response to a wide range of pathogens and is a hallmark of inflammatory diseases. One of the main activities of this pro-inflammatory cytokine is to provide protection against pathogen invasion. It is therefore not too surprising that there exist a number of pathogens which have developed several mechanisms to inhibit or modulate different stages of the TNFα action, ranging from the blockage of TNFα binding to the receptor to inhibition of specific TNFα-induced responses, such as gene expression or caspase activation [26–28]. To date, both human and mouse CMV have been reported to block TNFα-mediated gene activation by interfering with cell signalling and TNFα receptor expression [29–31]. Others have shown that HCMV inhibits TNFα-induced caspase-dependent apoptosis by encoding viral inhibitors [32]. It has also been shown that MCMV blocks caspase-independent apoptosis by direct binding and degradation of receptor-interacting protein RIP1 by the viral M45 protein [33,34].

Despite the several known viral strategies to modulate TNFα-induced responses, there are only a few examples in the literature of viruses that interfere with TNFα production [35,36]. In contrast, numerous studies have shown that bacteria and parasites almost exclusively interfere with TNFα by blocking its production, specifically targeting p38 MAPK, JNK and NF-κB signalling pathways involved in the activation of the cytokine production. For instance, *Yersinia* outer protein (Yop) J has been reported to bind to members of the MAPK family and IκB kinase β, and interfere with the MAPK and NF-κB signal transduction responsible for activating TNFα production (reviewed in [37]). In addition, *Yersinia pestis* was reported to also block TNFα production in MΦs by inhibition of MAPK activation by the antigenic proteins Low calcium response V (LcrV) and Yop B [38]. Also in monocytes/MΦs, *Salmonella* SptP protein reduces TNFα production by blocking the Raf/MAPK signalling pathway [39] and *Escherichia coli* K1 protein specifically targets NF-κB for inhibition of the pro-inflammatory response [40]. Whether any of the described cell-culture characterised viral or microbial pathogen-mediated suppression of TNFα production also occurs *in vivo* in an intact physiological system is not known.

We report *in vivo and in vitro* studies disclosing a previously unrecognized biological role of MCMV in moderating the production of pro-inflammatory cytokines, in particular TNFα involving an IE1 dependent mechanism, detectable at the protein and transcriptional level, in both immune intact strains of mice and in a severe immune-ablative model of infection. While the loss of *ie1* results in increased sensitivity of viral replication in macrophages to TNFα inhibition, *in vivo* the ablation of TNFα is insufficient to rescue the replication phenotype.

Results

A comparison of MCMV and MCMVdie1 infection in primary BMMΦ

MΦs are a key cellular population for MCMV infection. Furthermore, replication of MCMV in primary bone marrow-derived macrophages (BMMΦ) reflects more closely the *in vivo* phenotype than the replication in fibroblasts [21]. Accordingly, our first experiments sought to characterize the level of infection of MCMVdie1 and parental and revertant MCMV strains in this

particular cell population. Therefore, bone marrow (BM) cells were isolated from 10–12 week-old male BALB/c mice for selection of BMMΦ during 7 days of maturation in cell culture before use in infection studies. The $F4/80^{+}CD11b^{+}$ phenotype of the BMMΦ was confirmed by flow cytometry analysis prior to infection (Figure S1). First, we determined the virion DNA:PFU ratios for wild-type (referred to as MCMV in this manuscript), *ie1* deficient (MCMVdie1) and revertant-virus (MCMVrev) infection stocks as reported in previous studies [10,41]. Figure 1A shows that MCMVdie1 develops a similar number of genome equivalents per PFU in comparison with MCMV or MCMVrev. Furthermore, Western blot analysis determining the level of expression of the MCMV early protein E1 24-hrs after infection of BMMΦ further indicated a similar level of early stage-infection of MCMVdie1 and control viruses (Figure 1B). For later stages of infection, the viral growth was determined by standard plaque assays in a single-hit viral growth analysis in the fibroblast cell line NIH-3T3 as well as in BMMΦ (Figure 1C and D, respectively). As expected the results in Figure 1C show that in fibroblasts MCMVdie1 had no defective growth in these cells [11]. However, infection of BMMΦ (Figure 1D) results in a small but significant difference in the growth of MCMVdie1 in comparison with MCMV and MCMVrev. This macrophage phenotype for MCMVdie1 infection is reflective of its *in vivo* phenotype [10,11] and raises the question of whether this might be due to a possible macrophage-specific pro-inflammatory cytokine response.

Modulation of BMMΦ cytokine response upon MCMV and MCMVdie1 infection

On the basis of the attenuated growth phenotype of *ie1* null mutant in infection of mice deficient in adaptive immunity (SCID mice), we have previously speculated about a role for IE1 in countering intrinsic or innate cell immunity [11]. As indicated above, infected macrophages characteristically produce a vigorous and varied pro-inflammatory cytokine response, in particular TNFα and are therefore in contrast to other cells, such as NIH 3T3 fibroblast cells that are restricted in their repertoire of cytokine expression. Since *ie1* is known to influence gene expression, it is plausible that IE1 can affect cytokine gene expression in monocyte/MΦ cells. Thus, to directly test the possibility of IE1 protein modulating the cytokine response in infected BMMΦ, we first investigated pro-inflammatory cytokine production after infection of BMMΦ. In these experiments, levels of several cytokines were measured at early times post infection prior to any new infectious virus production. BMMΦ were either mock infected or infected with MCMVdie1 and MCMV at an MOI of 1. Supernatants were harvested at 10 hpi and flow cytometry-based Cytometric Bead Array (CBA) was performed for IFNγ, IL10, IL12p70 and TNFα. As seen from Figure 2A none of the infections differentially altered IFNγ, IL10 or IL12p70 production. However, the TNFα production was only mildly induced by MCMV, but in contrast, MCMVdie1-infected BMMΦs showed a markedly pronounced TNFα response

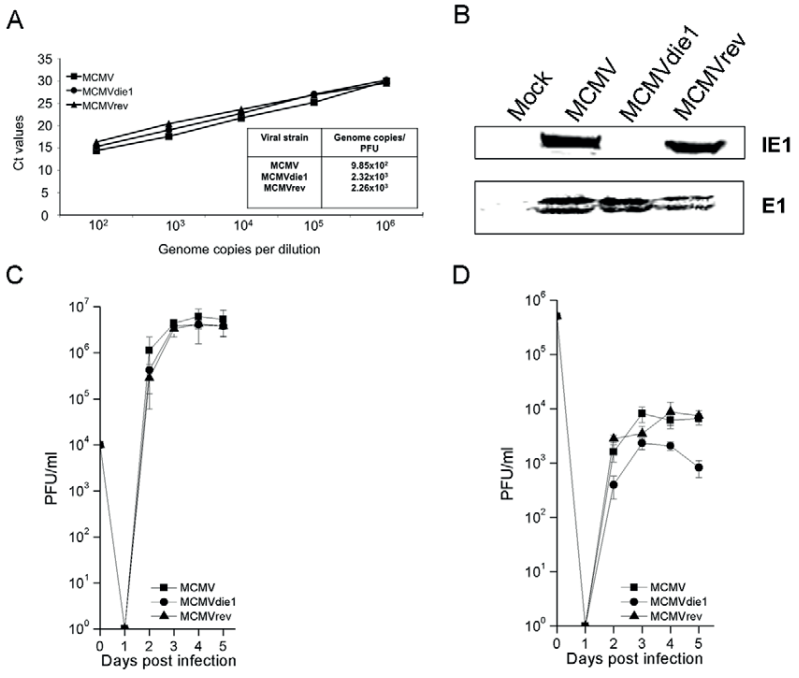

Figure 1. Comparison of MCMV, MCMVdie1 and MCMVrev. (A) Genome copy number-to-PFU ratios of MCMV, MCMVdie1 and MCMVrev stocks. Viral DNA was extracted from 200 µl of viral stock from each strain and the number of genome copies per ml was measured by qPCR and related to infectivity measured as PFU by virus plaque assay. (B) Western blot shows equal infection of BMMΦ. Total protein was extracted at 24 hpi and Western blot was carried out to assess the expression of both IE1 and E1 viral proteins, showing that cells were equally infected. (C) (D) Growth of MCMV, MCMVdie1 and MCMVrev in NIH-3T3 and BMMΦ cells. Cells were infected with the different viruses at an MOI of 1. At indicated times cellular supernatant from infected NIH3T3 cells (C) and intracellular and extracellular virus from infected BMMΦ (D) were harvested and titrated by standard plaque assays in MEFs. Shown are the median values of 2 independent experiments (n = 3, each experiment) along with SD.
doi:10.1371/journal.ppat.1002901.g001

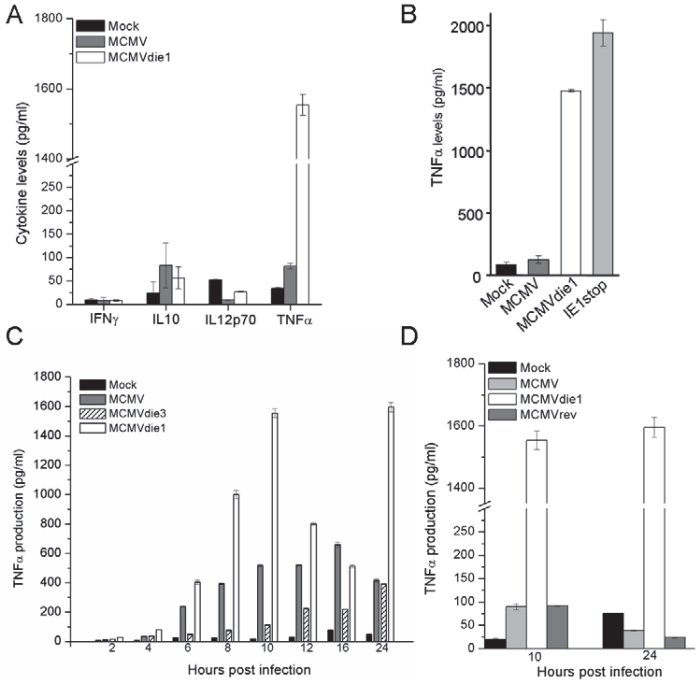

Figure 2. Cytokine production in infected MΦs. (A) Cells were mock-infected or infected with either MCMV or MCMVdie1 (MOI 1). IFNγ, IL10, IL12p70 and TNFα levels from cellular supernatants at 10 hpi were measured by flow cytometry-based CBA. (B) TNFα production after infection of RAW 264.7 macrophages. Cells were either mock-infected or infected with MCMV, MCMVdie1 or the MCMV IE1stop mutant (MOI 1). TNFα levels from the supernatants were determined by ELISA at 10 hpi. (C) TNFα production after infection of BMMΦ with MCMV, MCMVdie1 or MCMVdie3. Cytokine levels from cellular supernatants were measured by flow cytometry based CBA for 12 h time course, 16 and 24 hpi. (D) TNFα production from mock-infected BMMΦ or MCMV-, MCMVdie1- or MCMVrev-infected cells after 10 and 24 h. Cytokine levels were measured by ELISA. Experiments were done in triplicate and tested in duplicates. Bars show mean values with SE.
doi:10.1371/journal.ppat.1002901.g002

producing a >15-fold higher amount when compared to the levels seen for MCMV-infected cells. It is worth noting that the response can vary due to batch variability in primary macrophages cultures and viral stocks. Nevertheless, similar results have been consistently obtained from multiple independent BMMΦ preparations using different viral stocks.

Furthermore, after infection of a MΦ cell line (RAW 264.7 cells) with MCMVdie1 or another *ie1*-mutant (IE1stop), an approximately 15- to 20-fold higher production of TNFα is also observed in comparison with MCMV (Figure 2B). In the case of the IE1stop mutant the IE1 open reading frame is selectively interrupted, without genetically resecting any further sequences, strongly suggesting that the IE1 protein is responsible for the suppression of the TNFα production and not any other viral protein, that might potentially originate from a the MCMV major IE region.

To further characterise the modulation of TNFα by IE1 during infection we investigated the kinetics of TNFα production. In the following experiments BMMΦ were mock-infected or infected with either MCMVdie1, MCMV or an *ie3* defective MCMV (MCMVdie3) [42] during a 24 h time course. MCMVdie3 is completely defective for viral replication, with viral gene and protein expression essentially restricted to the IE1 and IE2 proteins [41] and thus serves as an excellent comparator for the loss of *ie1* in the MCMVdie1 mutant. Figure 2C shows that after MCMV infection BMMΦ produced detectable levels of TNFα from 4 h onward, until 24 h when it started to decrease. In agreement with the preceding experiment, MCMVdie1 generally induced higher levels of TNFα. Again, the levels of induction found in cellular supernatants from MCMVdie1-infected BMMΦ were higher than those induced by MCMV. It is noteworthy that MCMV does not completely inhibit TNFα production and this may reflect a level of leakiness derived from a pool of low IE1 expressivity of infected cells. Alternatively it could be that low levels of TNFα may be advantageous. In this time course experiment MCMVdie3 moderates the TNFα response with delayed kinetics to the MCMV and MCMVdie1 reaching similar levels as the MCMV by 24 h post-infection (Figure 2C). The observation that MCMVdie3 develops lower levels of TNFα than wild-type MCMV may reflect the importance of an active viral gene transcription that produces double-stranded viral transcripts to induce a full TNFα response. This possibility is consistent with studies showing the role of the cytoplasmic detector for viral RNA RIG-I in inducing and sustaining a TNFα response to infection with a DNA-virus [43]. In such a scenario we would anticipate to see MCMV infection developing higher levels of TNFα than the MCMVdie3. Thus, while an on-going infection is required to trigger a full TNFα response these results appear to indicate that mutation of the *ie1* gene is strongly associated with increased production of the cytokine.

To further evaluate whether the altered production of TNFα after infection with MCMVdie1 is due to the loss of *ie1* gene function and not an accidental second site mutation in the recombinant virus, a revertant virus of MCMVdie1 was also tested. In these experiments BMMΦ were either mock-infected or infected with MCMV, MCMVdie1 and MCMVrev. Supernatants were used to test the levels of TNFα after 10 and 24 hpi. As shown in Figure 2D significant production of the cytokine was found only after infection with MCMVdie1 at both time points, whereas comparably low levels of TNFα were found after infection with MCMV and MCMVrev.

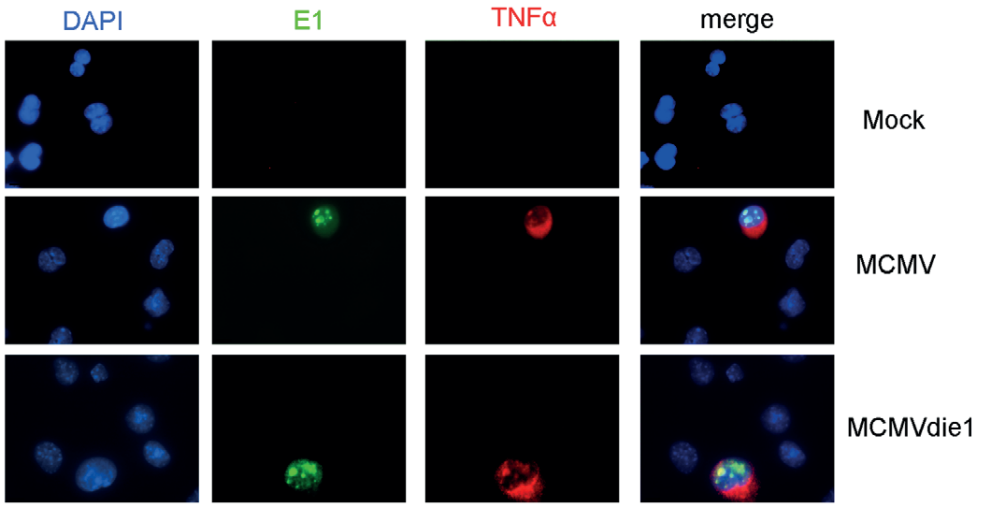

Figure 3. In situ staining of TNFα in viral-infected macrophages. RAW264.7 macrophages were infected with MCMV or MCMVdie1 at an MOI of 1 for 24 h. Cells were fixed with 4% paraformaldehyde and double staining was performed for TNFα and MCMV E1 protein. DNA was counterstained with DAPI.
doi:10.1371/journal.ppat.1002901.g003

Overall, the viral deletion mutant experiments indicate that the MCMV *ie1* gene plays a previously undisclosed role in moderating the production of a key pro-inflammatory cytokine, namely TNFα, in infected BMMΦ.

TNFα production is altered in infected cells and not bystander cells

In our next experiments we sought to determine whether the production of TNFα is specifically associated with the productively infected cells, or bystander cells or both. For these studies immunofluorescence staining monitored the intracellular production of TNFα while staining for viral early E1 antigen simultaneously monitored infection. RAW 264.7 cells were mock-infected or infected with MCMV or MCMVdie1. After 24 hpi, double labelling was performed for MCMV E1 protein and TNFα. As shown in Figure 3, production of TNFα was only detectable in cells that also expressed the E1 protein. LPS was used as a positive control to trigger TNFα production independent of viral infection showing that all cells were competent for TNFα production (Figure S2). These experiments directly show that induced TNFα production is almost exclusively associated with infected cells and not by neighbouring bystander cells.

These observations raise the possibility that IE1 might play a direct role in moderating the TNFα response in infected macrophages. To explore this possibility and to test whether IE1 alone is capable of moderating TNFα gene expression independent of the infection process, we next used transient transfection assays. To quantify the TNFα promoter activity we constructed a reporter plasmid, pTNF-gLuc, containing the *gaussia* luciferase reporter gene [44,45] under the control of the murine TNFα promoter/enhancer (position −670 to +1) element. We first assessed the activity of the pTNF-gLuc using the cell line Bam25 [42] that stably expresses the viral IE-genes. For these experiments Bam25 or NIH3T3 cells were transfected with pTNF-gLuc together with the vector pGL3 (Promega) for normalisation of the reporter gene expression measurements. As the infection process results in activation of Toll-like-receptor (TLR) signalling, triggering the expression of pro-inflammatory cytokines, including TNFα [46], we sought to ensure TLR activation in the absence of infection by treating transfected cells with bacterial lipopolysaccharide (LPS). LPS is a known potent inducer for TNFα gene expression [47–50]. The transfected cells were incubated for 24 h, culture medium was changed and subsequently stimulated with 100 ng/ml LPS for 4 h. As a control for inhibition of the LPS induced TNFα expression, control cultures were pre-treated with 300 nM Trichostatin A (TSA), an established inhibitor of the TNFα response, for 2 h prior to the LPS stimulation. As shown in Figure 4A, LPS can further induce the normalised reporter gene expression in transfected NIH3T3 cells, while the pre-treatment with TSA inhibits this induction. In contrast to this, LPS stimulation does not induce higher expression levels of *gaussia* luciferase in the Bam25 cell line. These experiments indicate that the expression of the viral IE-genes results in reduced capacity of LPS-induced TNFα activation.

Since the Bam25 cells also express IE3 and IE2 proteins in addition to IE1, we next sought to test if IE1 expression alone is sufficient to restrict LPS-induced reporter gene expression in MΦs. However, transfection of primary MΦs has a low efficiency and therefore we used RAW G9 cells for these experiments. RAW G9 cells were co-transfected with 125 ng of an IE1-expression plasmid, or as a negative control the pcR3.1 cloning vector (Invitrogen), and pGL3 for normalisation. After 48 h incubation medium was changed and cells stimulated with 10 ng/ml and 100 ng/ml LPS respectively. The results shown in Figure 4B reveal that transfection with 125 ng IE1 plasmid was sufficient to block stimulation with both, low and high doses of LPS. These experiments support the suggestion that IE1 alone is sufficient to block LPS induced reporter gene expression.

IE1 deficient MCMV infection exhibits increased levels of *tnf* gene expression

We next asked whether the absence of IE1 in the context of an infection of BMMΦ also has an effect on TNFα expression at the RNA level. Cells were mock infected or infected at an MOI of 1 with MCMVdie1, MCMV or MCMVrev and harvested for total RNA extraction after 10 hpi. Total RNA was used in quantitative (q)RT-PCR to measure relative *tnf* transcript levels. Data was normalized against *gapdh* levels and the levels of *tnf* from MCMV-

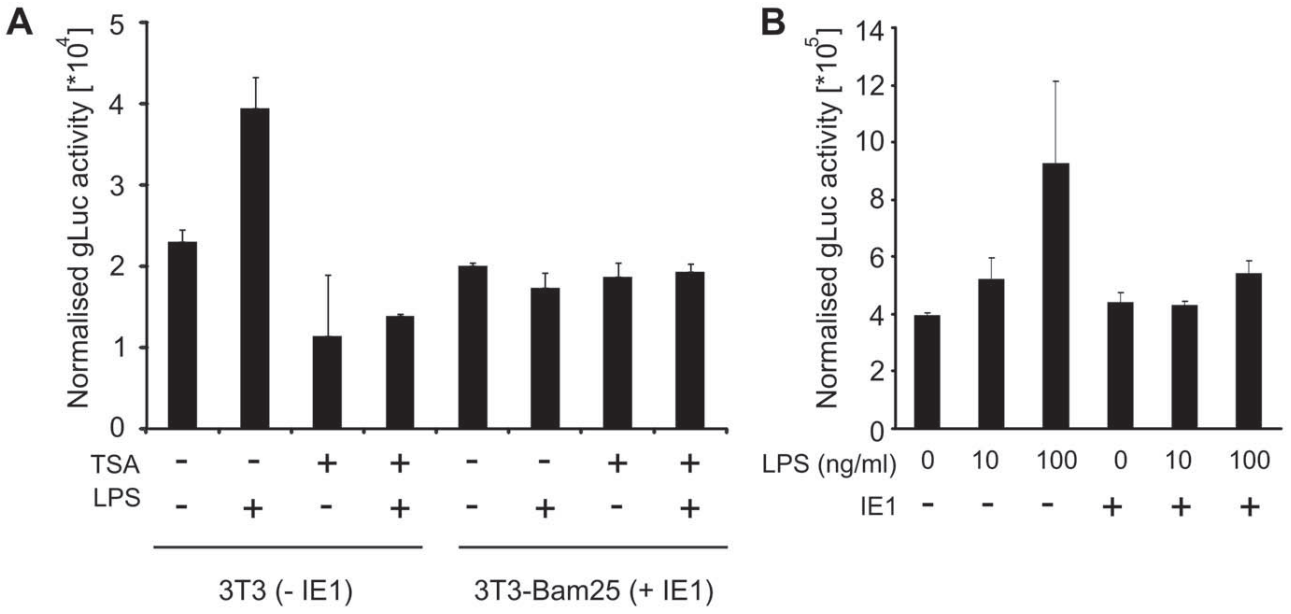

Figure 4. IE1 expression can moderate induced TNFα promoter activity. (A) NIH3T3 cells (−IE1) or Bam25 cells (+IE1) were transfected with 50 ng pTNF-gLuc expression plasmid or pcR3.1 as a negative control. For transfection control 50 ng of pGL3 were co-transfected in all cultures. 24 h post transfection cells were treated for 2 h with 300 nM TSA in PBS or a comparable dilution of DMSO (vehicle) and then LPS (100 ng/ml) stimulated. GLuc activity was measured and normalised to firefly activity per well. Bars show averages (n = 2) of a representative experiment (Error bars = SE). (B) RAW cells were transfected with 125 ng of IE1 expression plasmid pp89UC and 50 ng pGL3 for normalisation. 48 h after transfection cells were stimulated with LPS and normalised gLuc activity was determined. Bars show averages (n = 6) with SE.
doi:10.1371/journal.ppat.1002901.g004

infected cells were used as a calibrator. Figure 5 shows relative levels of *tnf* transcripts. When compared to the mock-infected samples, MCMV infection induced expression of *tnf* RNA ($p<0.05$). However, TNFα mRNA levels in the absence of IE1 protein in MCMVdie1-infected BMMΦ were 2.5-fold higher than those seen for the parental and revertant MCMVs ($p<0.01$). MCMVrev induction of *tnf* expression was similar to that induced by MCMV. We conclude from these experiments that the viral-induced TNFα production is reduced by MCMV in an IE1-dependent manner in the context of infected MΦs.

Investigation of IκBα, JNK and p38 kinase signalling in the course of infection

TNFα transcription is induced by different stimuli in a cell-type dependent manner [28,51–54]. The key signalling molecules, NFκB, JNK and p38 MAPK are a common set of targets by which microbial and fungal pathogens inhibit TNFα production [28,37,38,40]. However, in quantitative Western blot experiments involving infection of BMMΦs with MCMV, MCMVdie1 or MCMVrev analysis of IκBα, p38 and JNK proteins and their phosphorylated forms (Figure 6A) reveals that at 10 hpi there are no significant differences between the three different viruses tested (for quantification see Figure S7). All three viruses induce activation of both p38 and JNK kinases but not IκBα. The absence of IE1 upon infection did not result in a differential change in the level of IκBα or in the expression or phosphorylation levels of the tested kinases at 10 h post infection. It is possible that the time point analysed is too late to detect any quantitative differences and that they may be temporally masked by a range of cross-talking signalling events during the infection process.

While lack of activation of NFκB by MCMV is consistent with our previous studies it is possible that its activation is only detectable at IE times of infection. For the purpose of exploring whether differences in the activation of NFκB may be observable at more immediate early times we have used a stably transfected cell line, RAW G9 cells [55], to visualise the activation of NFκB. These cells express the NFκB subunit p65 as a GFP fusion protein. In rested cells the NFκB complex is distributed throughout the cytoplasm, producing a weak and diffuse GFP signal in the cells (Figure S4, mock treated sample). After LPS stimulation NFκB is activated and translocates to the nucleus, leading to an enrichment of GFP in the nucleus. The translocation of p65-GFP to the nucleus from the cytoplasm consequently develops a visibly concentrated nuclear GFP signal. We therefore infected RAW G9 cells for 45 min and observe enrichment in nuclear fluorescent cells for LPS but not for MCMV and MCMVdie1 infected samples (Figure S4). Quantification of the level of cytoplasmic and nuclear fluorescence indicates similar levels for MCMV and MCMVdie1. This indicates that MCMV and MCMVdie1 are equally restrictive for NFκB signalling during the IE1-phase of infection.

As noted in the previous section the expression of IE1 in the transient transfection reporter assays appears to have a similar inhibitory effect on the LPS-induced activity of the TNFα-promoter as the HDAC inhibitor TSA (Figure 4A). The mechanism for the TSA-mediated inhibition of TNFα activation is known to work through inhibiting p38 phosphorylation in RAW 264.7 cells [56]. Therefore we sought to test if IE1 in the transient transfection assay can interfere with the phosphorylation of p38 after LPS stimulation. RAW cells were either left untreated or were transfected with pp89UC or pEYFP-C2, an YFP expressing control vector. 48 h after transfection cells were stimulated with LPS for 15 min and pp38 levels were analysed by quantitative western blot analysis (Figure S7). Figure 6B shows, as expected, that treatment of mock-transfected cells with LPS leads to an increase in p38 phosphorylation. Notably, transfection with the

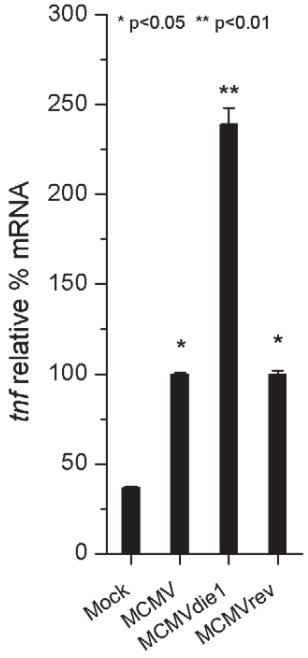

Figure 5. *tnf* gene expression in infected-BMMΦ. Total RNA was extracted at 10 h after mock infection or MCMV, MCMVdie1 and MCMVrev infection of BMMΦ. Quantitative RT-PCR was performed for relative expression levels of *tnf* mRNA in these cells. Shown are relative levels of *tnf* gene expression, which have been normalized against the *gapdh* gene expression and calibrated against MCMV induced-gene expression. SE bars are also shown (n = 3). Significance of differences in mRNA levels in MCMV and MCMVrev infected cells compared to mock infected cells was $p<0.05$ (*) and for comparison between MCMVdie1 and MCMV or mock $p<0.01$ (**), respectively (Student's *t*-test).
doi:10.1371/journal.ppat.1002901.g005

IE1 plasmid (pp89UC) led to a high level of p38 phosphorylation that could not be further increased by subsequent LPS stimulation. In our system, the inability of LPS to induce higher levels of pp38 in IE1-expressing cells is not due to an exhaustion of the p38 pool, since transfection with the YFP control plasmid led to ~1.4-fold higher signal for pp38 than the transfection with pp89UC (Figure S7). These experiments therefore indicate that IE1 might impart the ability to restrict the phosphorylation of p38.

We next sought to extend this observation to the infection system at IE-times of infection. We compared the induction of p38 phosphorylation by LPS (15 min) in infected RAW cells at 4 and 10 hpi in comparison to mock-infected samples. As shown in Figure 6B the treatment of control cultures with LPS induces the phosphorylation of p38. In contrast to this the virus infected samples showed a slightly weaker signal for pp38 than the mock infected samples at 4 hpi, indicating that the virus might be capable to moderate the phosphorylation of p38. MCMVdie1, however, showed no increased phosphorylation over the MCMV infection for both the non-stimulated and the LPS stimulated samples. Normalisation of the pp38 signal to the levels of p38 protein revealed that there was no detectable difference in levels of pp38 in the LPS stimulated samples (Figure S7). In accordance to this we found no increase in levels of phosphorylated p38 at 10 hpi. Under these experimental conditions quantification of the western blot and normalisation to p38 abundance actually revealed that treatment of MCMVdie1 infected cells induced slightly less pp38 compared to MCMV infected samples (Figure S7). To also check for differences in phosphorylation of JNK we subsequently determined the levels of pJNK on the same membranes and found that MCMV and MCMVdie1 induced the same level of pJNK signal as stimulation with LPS (Figure S7).

Altogether these experiments provide evidence against a mechanism involving IE1 inhibition of p38, NFκB or JNK signalling for the induction of TNFα in the context of an infected macrophage.

Role of IE1 in moderating TNFα transcript levels *in vivo* in the immune compromised host model of CMV disease

While modulation of TNFα by a wide range of pathogens has been extensively studied in cell-culture (reviewed in [28]), it remains to be determined whether such modulation occurs *in vivo*. Accordingly, biological significance of cell culture-based observations should be treated with some caution. Thus, to directly determine the physiological significance played by IE1 in moderating TNFα, we next studied the role of MCMV IE1 protein *in vivo*. As suggested above for BMMΦs in cell culture, IE1 modulates TNFα expression already at the transcript level. We therefore tested if this applies also to TNFα transcription in host organs relevant to CMV pathogenesis. The experiment was performed in immune compromised, γ-irradiated BALB/c mice, an established model for lethal, multiple-organ CMV disease [57]. In this model it was demonstrated previously [10] that wild type MCMV replicates in the liver with a doubling time of ~19 h, whereas MCMVdie1 was found to be growth-attenuated with a doubling time extended to ~34 h. Likewise, MCMVdie1 was found to be growth-attenuated also in spleen and lungs [10]. As suggested above for BMMΦs in cell culture, IE1 modulates TNFα expression. We therefore tested if this applies also to TNFα in the liver by quantitating steady-state levels of *tnf* transcripts with qRT-PCR. As seen in Figure 7A, TNFα gene expression in both infected groups is detectable above the baseline defined by uninfected liver tissue. At first glance, one might conclude that the TNFα gene expression level is modestly higher in MCMV-infected livers compared to MCMVdie1. For correctly interpreting the gene expression data, however, one must consider the different viral burden in tissue due to the growth-attenuation of the *ie1*-deletion mutant [10]. To account for this problem, we normalized TNFα gene expression to the number of viral E1 transcripts determined by qRT-PCR (Figure 7B). As shown in Figure 1 expression levels of E1 were comparable in the infected BMMΦs in the *in vitro* system. However, in the more complex *in vivo* system it is unclear at which level this impairment is manifest in the viral replication cycle. To exclude that an impaired E- or L-gene expression could influence our normalisation strategy for the qRT-PCR, we sought to use a method for normalisation that is independent of transcript levels in infected cells. To normalise for the different levels of infection in the sampled organs we therefore directly measured the number of infected cells by *in situ* immunostaining for the late major capsid protein (MCP, M86) (Figure 7C). Regardless of which normalization strategy was used, the normalised expression level of TNFα was found to be ~10-fold higher in MCMVdie1-infected livers than in MCMV infected organs. For comparison, normalized gene expression levels of the cytokines IFNβ and IL10 were measured in order to further probe the role of IE1 in regulating the innate cytokine response. Interestingly, infection with the *ie1*-deletion mutant also induced significantly higher amounts of IFNβ transcripts (Figure 7B and C) as compared to MCMV. In accordance with the IL-10 expression in BMMΦs (Figure 2A), IL10 transcription in the liver was induced by the infection (Figure 7A) but was not significantly influenced by IE1 (Figure 7B and C). Altogether, TNFα, and to some degree also IFNβ, are suppressed on the transcript level in an

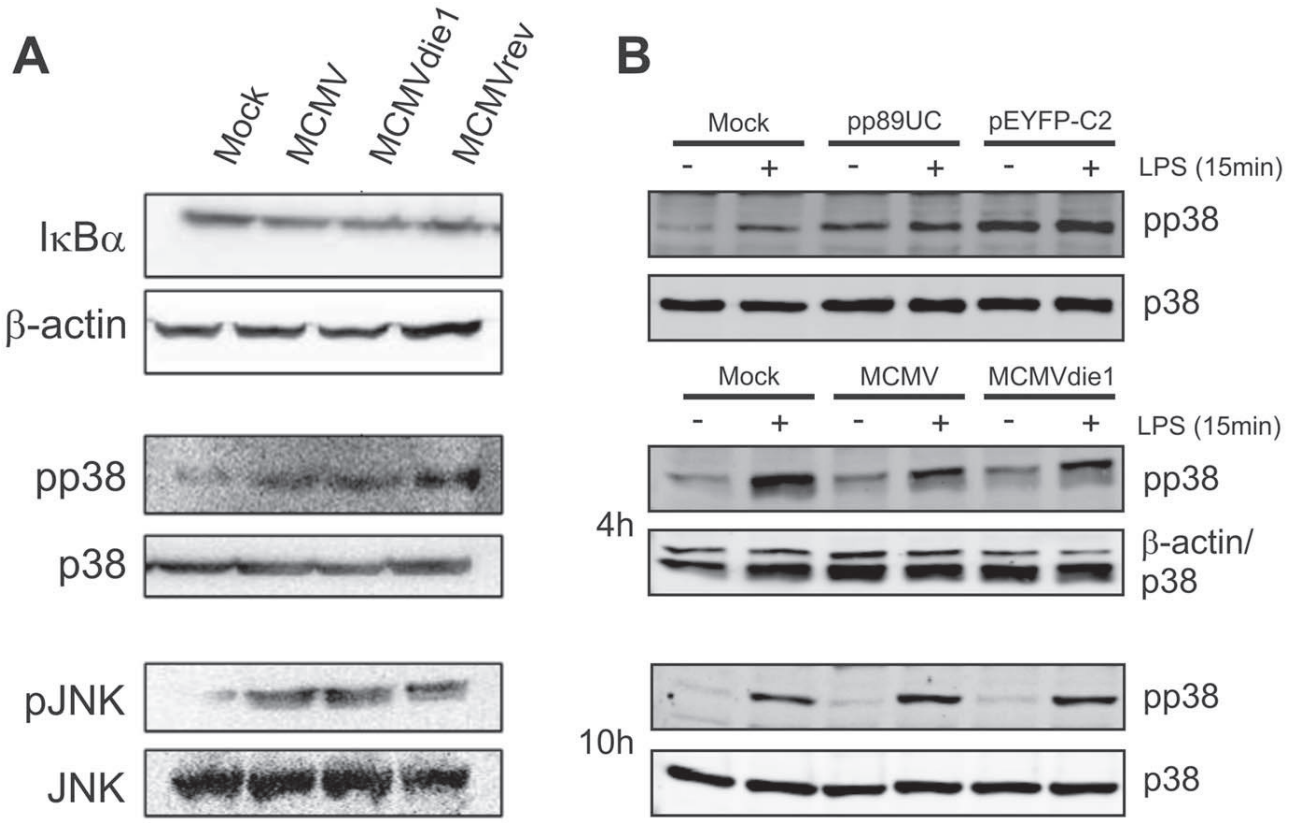

Figure 6. Investigation of IE1-mediated NF-κB, p38 or JNK activation. BMMΦs were mock infected or infected at an MOI of 1 with MCMV, MCMVdie1 or MCMVrev (n = 3). (A) Western blots for IκBα and the activated forms of the p38 and JNK kinases are shown. (B) Western Blots with transfected and infected RAW cells after LPS stimulation. RAW cells were transfected with IE1 expression plasmid pp89UC or a control vector (pEYFP-C2) and stimulated with 10 ng/ml LPS for 15 min or infected (MOI 1) and stimulated at 4 and 10 hpi, respectively.
doi:10.1371/journal.ppat.1002901.g006

ie1-dependent manner *in vivo* at a relevant organ site of CMV disease.

MCMV IE1 modulation of TNFα protein levels *in vivo*

We next determined if transcriptional control by IE1 also translates into TNFα protein levels in host tissues. In a first set of *in vivo* experiments, groups of 4 to 5 BALB/c and C57BL/6 immune competent mice were infected by the i.p. route, with the viral mutant and control strains. Viral yields and TNFα levels were determined at day 4 p.i. for selected organs. As seen in Figure 8 A and C, MCMVdie1 showed the expected attenuated phenotype in both mouse strains when compared to MCMV and MCMVrev [11]. Viral titres in spleen, liver, heart and lung from infected BALB/c mice were 6-, 12-, 21- and 35-fold reduced, respectively. The attenuation was even more dramatic in kidneys where the MCMVdie1 titres were reduced by a factor of >100. In C57BL/6, as in BALB/c mice, both MCMV and MCMVrev exhibited comparable replication (Figure 8C). MCMVdie1 titres were significantly reduced in all organs examined with a 10-fold reduction in spleen and liver and over 100-fold reduction in kidneys. From this data we conclude that the attenuation shown by MCMVdie1 is not mouse strain-dependent, since in BALB/c, C57BL/6 and also in the 129 strain (data not shown) as well as in γ-irradiated mice [10], the *ie1*-deletion mutant MCMVdie1 is not able to replicate as efficiently as MCMV or MCMVrev.

As described above for the RNA expression studies, MCMV induces TNFα production in an acute infection [58–60], and it is understood that TNFα levels positively correlate with the level of infection [59–61]. In agreement with these previous studies we also observed a positive correlation between TNFα protein levels and infectivity per gram of tissue in kidneys and heart (Figure S3). On this basis, TNFα was quantified and cytokine levels were calibrated against viral titres in those samples where infectious virus was detectable. Accordingly, normalized TNFα levels are shown in Figure 8B and D. At day 4 p.i., MCMVdie1 induces by an order of magnitude higher levels of TNFα than those detected for MCMVrev in all organs tested except in the spleen of both BALB/c (C), and C57BL/6 mice, and liver of C57BL/6 mice (D).

Taken together, these results support a role of IE1 in moderating the production of TNFα *in vivo*.

Because of the attenuated phenotype of the *ie1*-deletion mutant, the virus titres per gram of tissue differ significantly between infected groups. It is therefore possible that an IE1 expressing virus is simply able to replicate more efficiently and consequently will block TNFα production by alternative mechanisms. We therefore sought to establish an equivalent level of infection (PFU per gram of tissue) by adjusting the initial infectious dose of the inoculums and determining TNFα production. In the following experiments, immune competent BALB/c mice were infected with 3×10^5 PFU of MCMV or 3×10^6 PFU of MCMVdie1, and both viral titres and the absolute TNFα response were compared in different organs at days 4 and 7 post-infection. Under such conditions, viral titres of MCMV and of the *ie1*-deletion mutant were found to be comparable in all organs (Figure 9, left panels), except in the

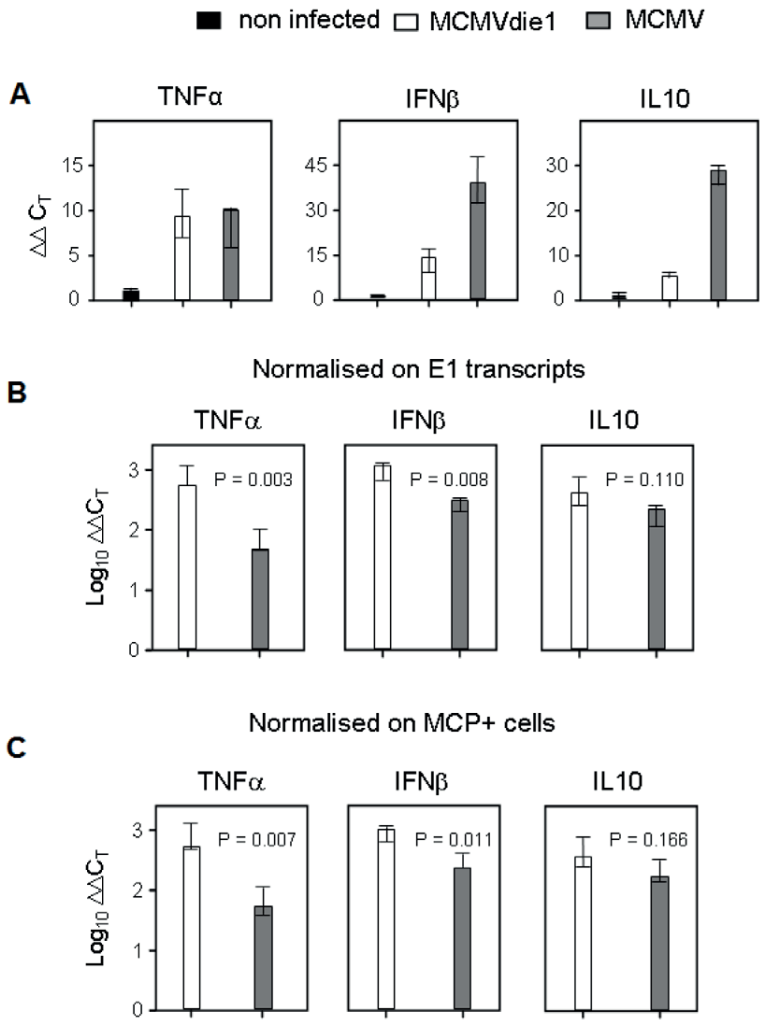

Figure 7. In situ activation of cellular genes TNFα, IFNβ and IL10 during infection of the liver. Immune compromised female BALB/c mice (n = 3 per group) were infected with 1×10^5 PFU of MCMV or MCMVdie1 or not infected, i.e. uninfected but immune compromised mice to take into account that a 6.5 Gy total-body γ-irradiation by itself slightly stimulates the expression of the genes under investigation. The analysis was performed 10 days after infection. (A) Expression levels ($\Delta\Delta C_T$ values) relative to β-actin transcripts. (B, C) Normalisation of the relative expression levels of TNFα, IFNβ, and IL10 to the numbers of E1 transcripts per 500 ng of total RNA (B) or to the numbers of infected MCP^+ cells per representative 10-mm^2 areas of liver tissue sections (C) in order to take account of differences in tissue infection density. Throughout, bars represent median values for three mice per experimental group. Variance bars indicate the range. P values for significance are indicated for group comparisons of interest (unpaired *t*-test, two-sided, performed with log-transformed data).
doi:10.1371/journal.ppat.1002901.g007

kidneys (Figure 9C) at day 4 p.i. In comparison to day 4 p.i. the observed reduction in titres by day 7 p.i, is indicative of the clearance of the virus from these various organs. TNFα levels after infection were measured in the different organs from viral-infected and mock-infected mice (right panels). Results show that MCMV induced TNFα production after 4 days of infection in all organs tested, except in the heart (Figure 9D). Importantly, there was also a marked increase in the levels of TNFα between MCMV and MCMVdie1. In general, the mutant virus induced statistically higher levels of TNFα in spleen, liver and kidney after 4 days of infection; however, there was no difference in the heart (Figure 9D). At one week of infection, viral clearance of both MCMV and MCMVdie1 has mostly taken place in all organs tested with the levels of TNFα having returned to mock levels except for a residual higher level in the spleen for the MCMV infection (Figure 9A). Strikingly, and in stark contrast to the MCMV infection, TNFα levels remained elevated in MCMVdie1 infected animals.

Altogether these results show that the production of TNFα can be significantly moderated by an *ie1*-dependent mechanism in an acute *in vivo* infection by MCMV.

TNFα is sufficient to inhibit MCMVdie1 *in vitro* but is not essential for inhibition *in vivo*

It has been shown by others that despite the protective effects of TNFα pre-treatment *in vitro* an *in vivo* pre-treatment does not increase survival rates of MCMV infected mice [62]. We therefore first sought to determine the effect of TNFα on MCMV and MCVMdie1 replication in macrophages *in vitro*. Differentiated macrophage cultures were pre-treated with 1 U/ml or 10 U/ml recombinant mouse TNFα (Endogen, PIERCE; 10 μg/ml corre-

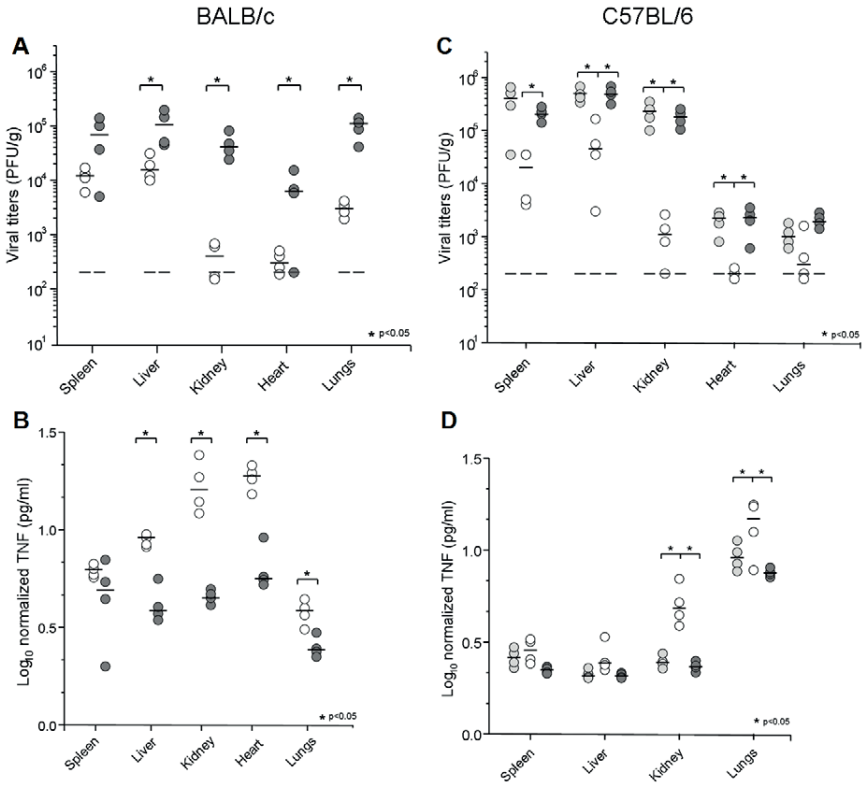

Figure 8. Growth of MCMV, MCMVdie1 and MCMVrev and TNFα production in different organs from infected mice. BALB/c (A, B) or C57BL/6 mice (C, D) were infected with 3×10^6 PFU or 2×10^6 PFU, respectively, by the i.p. route. Groups of mice (4 to 5 mice per group) were inoculated with the specified dose of parental MCMV (light grey circles), MCMVdie1 (open circles) or MCMVrev (dark grey circles). On day 4 post infection mice were killed and the indicated organs were harvested, weighted, and sonicated as a 10% (wt/vol) tissue homogenate in DMEM. (A and C). Viral titres were determined by standard plaque assay on MEFs. Dashed lines show limit of detection. Dark horizontal marks show median values. (B and D). Ratios between TNFα levels and PFU in different organs at day 4 after infection are shown in a log scale. Statistically significant differences in viral titres and TNFα levels between MCMVrev or MCMV and MCMVdie1 are indicated by an asterisk ($p<0.05$).
doi:10.1371/journal.ppat.1002901.g008

sponded to 10^5 U/ml) for 24 h prior to infection and viral replication monitored by plaque assay at day 3 p.i. As expected Figure 10A shows that pre-treatment with TNFα *in vitro* reduces viral titres of MCMV. Notably TNFα has a much stronger effect on the titres of MCMVdie1, which are reduced to the limit of detection, indicating that MCMVdie1 is more susceptible to TNFα control compared to MCMV *in vitro*.

We next sought to determine the contribution of TNFα in controlling viral replication *in vivo* by using mouse strains deficient either in TNFα expression ($TNF^{-/-}$) or TNFα signalling ($TNFRp55^{-/-}$). For these investigations groups of mice were infected with either MCMVdie1 or MCMVrev as indicated in Figure 10B and viral titres were measured in organs at day 4 p.i. to investigate if abrogation of TNFα expression or signalling could enhance or rescue the replication of MCMVdie1. In both tested mutant mouse strains the impairment of TNFα expression ($TNF^{-/-}$) or TNF signalling ($TNFR^{-/-}$) did not rescue impaired replication of the MCMVdie1 in the livers, spleens or other organs analysed (see Figure S5). To complement this experiment and to control for side effects of the genetic ablation of TNFα we also analysed the effects of antibody-mediated depletion of TNFα in vivo. Mice were infected with equal doses of MCMVdie1 and MCMVrev and anti-TNFα antibodies were injected at day 0 and 2 p.i. As shown in Figure S6 at 4 dpi no significant differences between the MCMV and MCMVdie1 viruses could be detected in all analysed organs.

Together these results show that while TNFα is sufficient to inhibit MCMVdie1 *in vitro* it is not essential for inhibition *in vivo* and may indicate that in the more complex *in vivo* setting other host factors can complement for the loss of TNFα function.

Discussion

In this study we have presented evidence revealing that a viral gene, *ie1*, of MCMV is involved in altering the pro-inflammatory cytokine response, in particular TNFα production *in vitro* and *in vivo*. Our results not only identify a new and previously undisclosed functional role for IE1 in moderating the inflammatory response to infection, but also show for the first time the association of a specific pathogen-encoded gene to restrict TNFα protein and RNA production *in vivo* in the context of a natural infection.

Several pathogens have been shown to modulate TNFα-induced response by a wide range of different mechanisms. For instance, direct interaction with TNFα has been reported for the M-T2 protein of the Myxoma virus avoiding TNFα-TNFR interaction [63]. African swine fever virus also targets TNFα-induced gene expression in infected-MΦs by a mechanism involving the viral protein A238L [64]. Inhibition of TNF receptor has also been shown for Adenovirus and Poliovirus [65,66]. Moreover, HCMV and MCMV have also been shown to down modulate TNF receptor expression [29–31], blocking TNFα-induced gene expression in infected cells. However, there are only

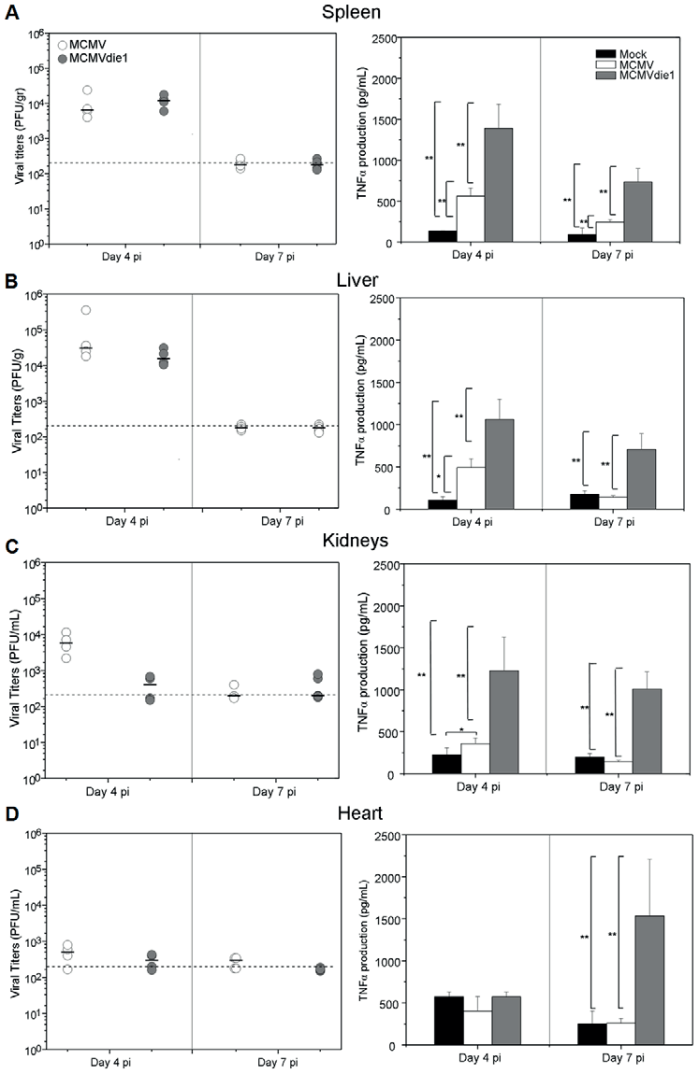

Figure 9. Growth of MCMV and MCMVdie1 and TNFα levels in different organs of infected BALB/c mice. Groups of BALB/c mice (4 mice per group) were inoculated with either 3×10^5 or 3×10^6 PFU of parental MCMV or MCMVdie1, respectively. On day 4 and 7 post infection mice were killed and spleens, livers, kidneys and hearts (A, B, C and D, respectively) were harvested, weighted, and sonicated as a 10% (wt/vol) tissue homogenates in DMEM. **Left panels.** Viral titres were determined by standard plaque assay on MEFs. Grey lines show limit of detection. Black horizontal marks show median values. **Right panels.** Levels of TNFα in different organs of infected BALB/c mice. At indicated times organs were harvested, weighted and homogenated as a 10% (wt/v). TNFα levels were determined by ELISA from the homogenates. Mock infected mice were also included as a negative control. No significant differences were found in production of infectious virus between infections, except in kidneys at 4 dpi. Statistically significant differences in TNFα levels are shown as * = $p<0.05$ or ** = $p<0.01$.
doi:10.1371/journal.ppat.1002901.g009

a few examples in the literature of viral proteins that interfere with TNFα production [36]. From the literature it can be seen that targeting the production of TNFα is a common feature in microbial infections, as seen for *Salmonella*, *Yersinia* and *E. coli* [37–40]. All known mechanisms by which microbial pathogens alter the TNFα production involve targeting p38 MAPK and JNK kinases and/or NF-κB activation (reviewed in [28]). Here, we demonstrate that the viral IE1 protein of MCMV moderates TNFα production in infected BMMΦs. Moreover, although the exact mechanism by which IE1 exerts its effect on TNFα production remains open, our experiments studying the contribution of key signalling molecules p38 MAPK, and JNK, as well as NF-κB, suggest that IE1-induced modulation of TNFα production does not involve altering the function of these signalling proteins. Although, we do not exclude that the phosphorylation of JNK or other phosphatases is also influenced by other viral factors and therefore effects of IE1 deletion on phosphorylation of these signalling factors could be masked.

Comparison of TNFα levels between MCMV and the MCMVdie3 mutant virus showed that MCMVdie3 infection produces much lower levels of TNFα compared to MCMV infection until 24 hpi. This indicates the importance of viral gene transcription for inducing and sustaining a full scale TNFα response. This observation is in good accordance with evidence showing that RIG-I mediated detection of Myxoma virus transcripts in human macrophages is necessary to induce a full TNFα response [45]. Furthermore we show that MCMV does not completely inhibit TNFα production. It has been demonstrated

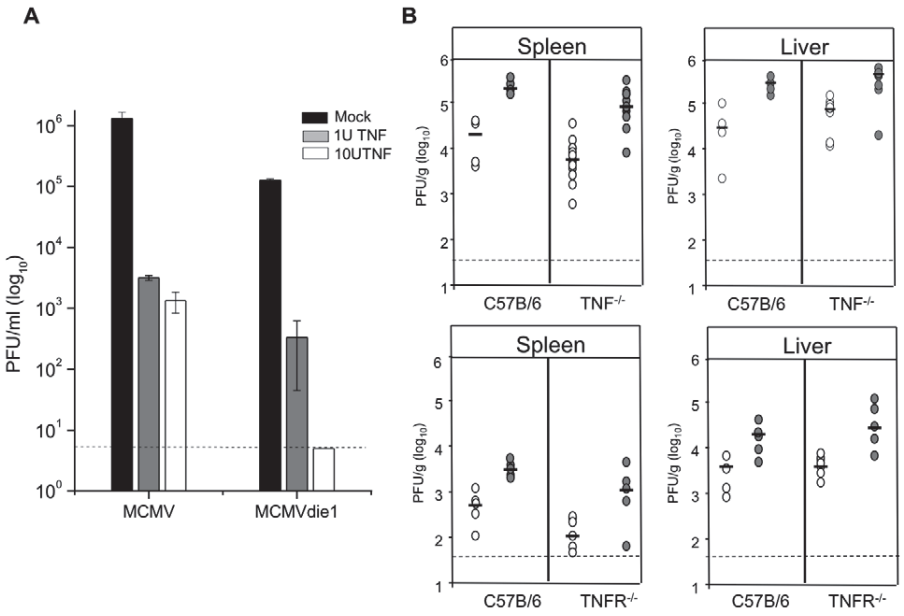

Figure 10. TNFα blocks viral replication *in vitro* but is not essential *in vivo*. (A) BMMΦs were pre-treated for 24 h with TNFα as indicated and subsequently infected with either MCMV or MCMVdie1 (MOI 1). Total virus was measured by plaque assay at day 3 p.i. and dashed line indicates limit of detection with bars showing averages (n = 3) with SE. (B) Organs from infected C57B/6, TNFα$^{-/-}$ or TNFRp55$^{-/-}$ mice (2×10^6 PFU i.p.) were harvested at 4 d p.i. and homogenated for analysis with standard plaque assay (MCMV = grey circles; MCMVdie1 = open circles). Titres were normalised per sample weight, black lines indicate median values and dashed line represents limit of detection.
doi:10.1371/journal.ppat.1002901.g010

that CMV can reduce the effects of TNFα by down-regulation of the TNFα receptor during infection [29] and thereby increasing tolerance to extra-cellular TNFα levels. A major factor determining permissiveness of cells of the myeloid-monocytic lineage for infection with CMV is the state of maturation ([67] and references therein) and it has been demonstrated that TNFα also facilitates maturation of macrophages [68]. In addition TNFα can be pro-viral by initiating infection through signalling to the MIE enhancer. Taken together this indicates that low levels of TNFα may well be tolerated by CMV and could under certain conditions also have a pro-viral effect. Thus it may not be to the best advantage for CMV to completely abrogate TNFα production.

IE1 has been described to have a very general effect on gene transcription levels including more genes than are controlled by p38 signalling directly and is better known for its intra-nuclear activities including the disruption of ND10 bodies [15,69]. In the case of HCMV, the ability of IE1 to disrupt ND10 bodies has been correlated with the disruption of an intrinsic defence mechanism involving nuclear repressor proteins, such as hDaxx and histone deacetylases (HDACs), to inhibit viral immediate-early gene expression [17]. In case of MCMV, a direct interaction of IE1 with Daxx and HDAC2 has been demonstrated [12] in good accordance with the general induction of transcription caused by IE1 [9], probably involving de-repression of chromatin. It has been demonstrated that expression of TNFα is partially regulated by chromatin re-modelling and that treatment with TLR ligands such as LPS initiates de-repression of chromatin in macrophages [47,48]. Therefore it is possible that the influence of IE1 on HDAC function could interfere with TNFα expression by disrupting the de-repression or maintaining repressive chromatin associated with the TNFα promoter. It remains to be determined how IE1 precisely inhibits TNFα expression while also potentially inducing a de-repression of chromatin.

It is noteworthy that Trichostatin A (TSA), which we used as a control reagent to block LPS induced TNFα gene expression [56], is also an inhibitor of HDACs and therefore leads to a general de-repression of chromatin, while it is capable of inhibiting TNFα expression [50,56]. This presents parallels between TSA and IE1 and allows speculating that these molecules work potentially through a similar mechanism. A known mechanism for the effect of TSA on TNFα is mediated through the p38-inhibtor MAPK phosphatase-1 (MKP-1). In this case the stability of the interaction of MKP-1 with its target molecule, p38 MAPK, is regulated by the acetylation of the interaction site, which is negatively regulated by HDACs. Treatment with the HDAC inhibitor TSA increases the level of the acetylated form of MKP-1 and thereby links the inhibitory function of MKP-1 on the p38 signalling pathway to HDAC activity [56]. In accordance with this it has been furthermore demonstrated that LPS stimulation activates HDAC-3 [50] and is also known to induce expression of HDAC members in BMMΦs [70]. This would negatively regulate MKP-1 activity, increasing p38 signalling and therefore TNFα expression. Since it is established that IE1 interacts and inhibits HDAC activity [12] it raises the question if IE1, at least partially, could function through this mechanism.

In this scenario we would anticipate increased pp38 levels in MCMVdie1-infected cells. However, we do not detect any increase in pp38 levels in MCMVdie1 infected cells compared to MCMV in the first 10 hpi and thus strongly indicating that IE1 does not interfere with p38 phosphorylation in the context of infection. Although notably, studies have shown that changes in acetylation of proteins can take up to 9–11 h to occur in the case of histones [71]. This might indicate that IE1-mediated changes on MKP-1 acetylation become apparent at later stages of the infection and could therefore have a role in the late phase of replication, complementing other viral factors interfering with

TNFα action, such as M45 [29,31]. A more thorough investigation of MKP-1 and its effects on MCMV replication and induction of TNFα will be necessary to clarify if IE1 inhibits p38 signalling.

However, it is also noteworthy that the immune-modulatory cytokine IL10 is induced upon infection by MCMV in MΦs and *in vivo* and since IL10 is known to function as an anti-inflammatory mediator, it is possible that a host IL10 autocrine loop might be involved in modulating TNFα. While we cannot exclude the possibility for IL10 involvement in TNFα suppression we failed to detect any significant difference in expression of IL10 between MCMV with and without *ie1* indicating that the mechanism for TNFα moderation does not involve regulation of IL10.

While many pathogens have been shown to counter-regulate TNFα production in cell culture, in particular in MΦs, little or no information is available to indicate whether this mode of regulation also occurs in an *in vivo* system. Our investigations show that the viral gene, *ie1*, in the context of a natural infection contributes to a significant moderation of TNFα production in multiple organs *in vivo*. TNFα levels, relative to the amount of detected virus, in selected organs were significantly higher in animals infected with MCMVdie1 than in animals infected with MCMV or MCMVrev, and this was consistently observed in several genetic backgrounds and in different infection models. This is quite striking, as we would anticipate a significantly reduced inflammatory response to be associated with the severely attenuated *in vivo* growth by MCMVdie1. *In vivo* we observed a relatively enhanced production of the pro-inflammatory cytokines TNFα and IFNß but not for the anti-inflammatory cytokine, IL10, with MCMVdie1 infection. Because of the attenuated phenotype of the *ie1*-deletion mutant, the virus titres per gram of tissue differ significantly between infected groups. It is therefore possible that an IE1 expressing virus simply is able to replicate more efficiently *in vivo* and consequently blocks TNF production through alternative methods. While we have not investigated in the present study other similarly attenuated viruses in their ability to develop an elevated pro-inflammatory cytokine response, we have evaluated TNFα production levels in the context of establishing an equivalent level of infection per organ between the *ie1* deficient and wild-type strains. These studies clearly indicate that even in the presence of comparable levels of infection, MCMVdie1 induces significantly higher levels of TNFα. Those levels were sustained for at least 1 week after infection, whereas wild-type MCMV-induced TNFα production had returned to the mock-infected levels by 7 days p.i. The results of our investigation provide the first demonstration of a counter-regulatory role encoded by the *ie1* gene in moderating the TNFα cytokine production in the context of a natural infection *in vivo*. In accordance with the attenuated *in vivo* phenotype of MCMVdie1 we could demonstrate a higher sensitivity of MCMVdie1 replication *in vitro* compared to MCMV but neither genomic deletion of the TNFα gene, the TNFα receptor gene or in vivo depletion of TNFα by administration of anti-TNFα antibodies could rescue the attenuated MCMVdie1 phenotype, indicating that other anti-viral host factors complement the loss of TNFα function. In accordance to this we find a slight but significant increase in IFNb1 expression in infected organs.

In summary, we identify a new biological role for the *ie1* gene of MCMV involving the regulation of pro-inflammatory cytokines, especially TNFα production, in both *in vitro* and *in vivo* infections. This suggests a novel viral counter-immune strategy preventing a robust inflammatory response during an infection. Our findings demonstrate that IE1, in addition to blocking intrinsic cell defences, also acts as a virulence factor contributing to viral modulation of the inflammatory response. This new role of *ie1* may also have therapeutic anti-viral and anti-inflammatory applications in the future. In this regard, our results provide the first evidence of a viral strategy capable of suppressing pro-inflammatory TNFα production *in vivo* mediated by a pathogen-encoded gene.

Materials and Methods

Ethics statement

All procedures involving animals and their care were approved by the Ethics Committee of the University of Barcelona (Spain) and were conducted in compliance with institutional guidelines, as well as with catalan (Generalitat de Catalunya decree 214/1997, DOGC 2450) laws and policies. In the United Kingdom experiments were approved by the University of Edinburgh Animal Procedures and Ethics Committee and were performed under licence from the United Kingdom Home Office under the Animals (Scientific Procedures) Act 1986. In Germany, mice were bred and housed under specified pathogen-free conditions in the Central Laboratory Animal Facility of the Johannes Gutenberg-University, Mainz. Animal experiments were approved according to German federal law under permission number 177-07-04/051-62. In Croatia all animals were bred and housed at the Breeding Facility of the Faculty of Medicine, University of Rijeka. Experiments were approved by the Ethics Committee of the University of Rijeka and were performed in accordance with the Croatian Law for Protection of Laboratory Animals (matched with EU legislation (DIRECTIVE 2010/63/EU OF THE EUROPEAN PARLIAMENT AND OF THE COUNCIL of 22 September 2010 on the protection of animals used for scientific purposes).

Cells and viruses

The murine fibroblast cell line NIH3T3 cells (ATCC CRL1658) and the macrophage cell line RAW 264.7 (ATCC TIB-71) were obtained from the American Type Culture Collection (Manassas, VA). Primary murine embryonic fibroblasts (MEFs) were prepared from embryos of pregnant BALB/c mice on day 16 of gestation. RAW G9 cell line was constructed as described previously [55] and expresses a p65-GFP fusion protein under transcriptional control of the native p65-promoter. NIH3T3, were cultured in Dulbecco's modified Eagle's medium (DMEM) supplemented with 10% calf serum (CS) and RAW 264.7, RAW G9 and MEFs were cultured in Dulbecco's modified Eagle's medium (DMEM) supplemented 10% fetal CS (FCS). All cell media also contained 2 mM glutamine and 100 U of penicillin/streptomycin per ml. The *ie1*-deficient mutant (MCMVdie1) and corresponding revertant virus were described in [11]. The IE1stop mutant carries a stop codon at the 5′-end of exon 4 of the MCMV *ie1* gene preventing the synthesis of the pp89 IE1 protein. Briefly, two successive PCR rounds were performed using the primer pairs IE1_stop_fw1 (5′-GCAATCTTACAGGACAACAGAACGCTCTACACTGGAGGATGACGACGATAAGTAGGG-3′) and IE1_stop_rv1 (5′-TACAAACCACTCTTATATTCCAGTGTAGAGCGTTCTGTTGCAACCAATTAACCAATTCTGATTAG-3′), and IE1_stop_fw2 (5′-GATTGATAGTTCTGTTTTATCATGAGGTGTGCAATCTTACAGGACAACAGAACGCTCTACACTGGA-3′) and IE1_stop_rv2 (5′-CTGTCTTTCATATTCACCCACACAGAACACTTGAGTTATACAAACCACTCTTATATTCCAGTGTAGAGCG-3′), respectively, to amplify a kanamycin resistance marker, followed by recombination in *E. coli* using the MCMV BAC pSM3fr [72] and applying the *en passant* mutagenesis procedure as described in [73] The parental BAC-derived MCMV strain MW97.01 ([72], named MCMV in this study) and the recombinant MCMVs were propagated on NIH3T3 cells. Cells were grown to 70%–80% confluency and

infected at an MOI of 0.01 with MCMV, MCMVdie1 and MCMVrev in DMEM supplemented with 2% CS. When cultures reached cytopathic effect, supernatants were harvested and kept at −70°C after clearing cellular debris. Viral titres were determined by standard plaque assays on MEFs. Bone marrow derived macrophages (BMMΦ) were prepared from 10–12 week-old male BALB/c mice as described previously [74]. Femur lavages were plated out at 5×10^5 or 8×10^5 cells per well (24- and 6-well plates, respectively) and left for maturation for 7 days in DMEM:F-12 containing 10% FCS, 10% L929 conditioned media as a source of macrophage colony stimulating factor [75], and 100 U of penicillin/streptomycin per ml.

Expression plasmids

Plasmid pp89UC codes for the MCMV IE1 protein pp89, carrying the insert of plasmid pIE 100/1 [2] in the pUC19 vector. IE1 expression is under control of its native MCMV major immediate early enhancer/promoter. Plasmid pEYFP-C2 was produced by transferring the EYFP ORF from pEYFP-C1 (BD Biosciences Clonetech) into the pEGFP-C2 vector (BD Biosciences Clonetech), replacing the EGFP ORF using endonucleases AgeI and BsrGI. The expression plasmid pTNF-gLuc was produced by replacing the MCMV enhancer/promoter in the plasmid pmCherryP2AGLucKanR [76] with the TNFα enhancer/promoter (−670 to +1). To do so the TNF enhancer/promoter was synthesised by MWG/Operon including restriction sites for KpnI and BglII, used for the cloning procedure.

Lipofection

To transfect cultured cells with expression plasmids we used the Lipofect LTX reagent (Invitrogen). IE1 or TNF-reporter plasmids were mixed with the firefly vector pGL3 (Promega) for internal control of transfection efficiency. To ensure that all cultures were exposed to the same amounts of DNA during transfection, mixtures of plasmids were adjusted to the same total amount of DNA within one experiment with the cloning vector pCR3.1 (Invitrogen). For transfection cell line specific protocols provided by Invitrogen were used (detailed protocols available at: www.invitrogen.com/transfections) and adjusted to the respective culture size as described in the NIH3T3 specific protocol.

Luciferase reporter assays

Gaussia luciferase assays were carried out as described previously [76], with the exception that plain DMEM medium was used to produce coelenterazine working solution. Substrate (50 µl) was mixed with 50 µl culture supernatant and measured with a POLARstar plate reader (BMG Labtech, UK). To measure firefly luciferase activity we used the Luciferase Assay System (Promega) as described in the manual. In short, cells were lysed for 15 min on a rocking platform and 15 µl lysate were subsequently transferred into a black/white plate and mixed with 30 µl substrate for measuring luminescence in the POLARstar plate reader. To stimulate luciferase expression, cells were washed 1× in growth medium and then stimulated with LPS (10 or 100 ng/ml in growth medium, as indicated) for 4 h before reporter gene activity in the culture supernatant was measured.

Characterization of BMMΦ by flow cytometry

Maturation of BMMΦ cells was tested by flow cytometry analysis for the expression of murine proteins specific for mature macrophages. Analyses were performed for F4/80 (Caltag Laboratories, UK) and CD11b (eBiosciences, UK) using a FACScan or FACSCalibur instrument.

BMMΦ infection

Cells were infected with the different viruses at an MOI of 1, unless specified otherwise. After 1 h of adsorption, cells were washed in PBS and incubated in fresh DMEM:F12 supplemented with 10% FCS, 10% L929, and 100 U of penicillin/streptomycin per ml.

Mouse infections

8 weeks-old male BALB/c and C57BL/6 mice were obtained from Charles Rivers Lab (Barcelona, Spain and Edinburgh, UK, respectively), C57/Bl6 $TNF^{-/-}$ mice were obtained from B&K Universal (UK). Experiments with C57/Bl6 $TNFRp55^{-/-}$ mice [77] were conducted in the University of Rijeka. Animals were housed at the animal facilities (University of Barcelona, University of Rijeka or Edinburgh University) under pathogen-free conditions. Mice were intraperitoneally inoculated with 3×10^5 or $2–3\times10^6$ PFU of tissue culture-derived MCMV recombinants. At designated times mice were sacrificed and spleen, liver, kidneys, heart and lungs were removed, weighted and harvested as a 10% (wt/v) homogenate. Part of the tissue homogenate was sonicated and viral titres were determined on MEF by standard plaque assay. When infectious virus could not be detected in a particular organ, a titre corresponding to the limit of detection of the assay was assigned to that particular organ in order to calculate the median values.

For *in vivo* analysis of TNFα transcription levels, female BALB/c mice were immune depleted and infected essentially as described in greater detail previously [78]. In brief, hematoablative conditioning of 8- to 9-week-old female mice was achieved by total-body γ-irradiation with a single dose of 6.5 Gy. Intraplantar infection at the left hind footpad was performed ~2 h later with 10^5 PFU of either BAC-cloned virus MCMV wild-type [72] or MCMVdie1 [11].

TNFα levels

Cytokine levels were determined from cell culture supernatants by flow cytometry (BD Cytometric Bead Array, BD Biosciences) and from tissue homogenates by ELISA (mouse TNF-α/TNFSF1A DuoSet ELISA Development kit, R&D Systems Europe Ltd.) following manufacturer's instructions. TNFα concentration was determined by reading the absorbance at 450 nm in a POLARstar OPTIMA Multifunction Microplate Reader (BMG LabTech, UK).

Immunofluorescence

50 µl of suspension containing 10^4 cells were added onto each dot of a Teflon coated microdot slide. Cells were incubated at 37°C for 24 h. After infection and treatment, cells were fixed with 4% paraformaldehyde for 10 min and permeabilized in 0.5% Triton X-100 for 3 min. After blocking for 1 h with 20% FCS, cells were stained with primary antibody Croma103 (provided by S. Jonjic) and TNFα (Santa Cruz, SC-1351) and secondary antibody Alexa Fluor 488 rabbit anti-mouse IgG and Alexa FluorAR 594 donkey anti-goat IgG (both from Invitrogen, CA), respectively.

Nuclear translocation assay

RAW G9 cells (5×10^3 per well) were seeded in glass bottom optical 384 well plates. After 24 h cells were stimulated with 10 ng/ml LPS or infected with virus in 20 µl. Subsequently cells were fixed with 4% PFA for 30 min (RT), quenched in 50 mM NH_4Cl solution for 5 min and permeabilised with 0.5% Triton X-100 for 3 min. Cell nuclei were counterstained with DAPI. For

analysis pictures were taken on an OPERA system (PerkinElmer, USA) with 40× magnification and for GFP nuclear translocation assay the corresponding standard script of the Acapella (v2.3) analysis software was used.

Total RNA extraction from BMMΦ

RNA from BMMΦ cells in 6-well plates was extracted by adding 200 µl Trizol reagent (Invitrogen, CA) and incubating for 5 min. Samples were then transferred to a 1.5 ml microfuge tube and 40 µl chloroform were added. Samples were incubated at room temperature for 15 min before being centrifuged (13,000 rpm, 4°C, 5 min). The upper aqueous layer was removed and 0.1 volumes 3 M NaOAc, 2.5 volumes EtOH were added. Samples were incubated (−20°C, 60 min) and then centrifuged (13,000 rpm, 4°C, 30 min). Supernatant was removed and the pellets washed in 200 µl 70% (v/v) ethanol and centrifuged as before. RNA pellets were then resuspended in 50 µl RNAse-free H2O. RNA quantity and quality was assayed by measuring the A260 and the A260/A280 ratio respectively using a Nanodrop ND-1000 (Nanodrop Technologies, DE).

Isolation of total RNA from liver tissue

RNA was isolated as described in detail previously [10] from whole livers shock-frozen in liquid nitrogen.

qRT-PCR

For each sample, 2× Taqman PCR mix (Applied Biosystems; CA) was mixed with 40 U of Superscript III (Invitrogen, CA). 4 µl total RNA was then added and each sample split into two reactions. A Taqman primer/probe set (Applied Biosystems, CA) for the gene of interest was then added to one reaction at the recommended concentration while a Taqman primer/probe set for GAPDH mRNA was added to the other reaction. Samples were then run on a MX1000P quantitative PCR thermal cycler (Stratagene, CA). Samples were first heated to 50°C for 30 minutes then heated to 95°C for 10 minutes. Samples were then subjected to 40 cycles under Taqman standard conditions. Stratagene MXPro software was used to analyse the data.

Quantification of transcripts

Quantification of β-actin and E1 transcripts was performed with homemade primers and probes as described previously, yielding amplicons of 88 bp [10] and 200 bp [79], respectively.

Quantification of IFNβ, IL10 and TNFα transcripts was done with custom-made TaqMan Gene Expression Assays.

(i) **IFNβ transcripts.** TaqMan Gene Expression Assay (catalog no. Mm00439546-s1; Applied Biosystems). Amplicon length: 61 bp.

(ii) **IL10 transcripts.** TaqMan Gene Expression Assay (catalog no. Mm00439614-m1; Applied Biosystems). Amplicon length: 79 bp.

(iii) **TNFα transcripts.** TaqMan Gene Expression Assay (catalog no. Mm00443258-m1; Applied Biosystems). Amplicon length: 81 bp.

Reactions were performed in a total volume of 20 µl, including 4 µl of 5 X QIAGEN OneStep RT-PCR buffer, 1 µl of QIAGEN OneStep RT-PCR enzyme mix, 668 µM of each dNTP, 1.5 mM additional $MgCl_2$, 0.132 µM 5-carboxy-X-rhodamine as passive reference, and 0.6 µM of each β-actin primer and 0.26 µM of β-actin probe, or 1 µl of the corresponding 20× TaqMan Gene Expression Assay Mix (in the case of IFNβ, IL10, and TNFα). Reverse transcription was performed at 50°C for 30 min. The cycle protocol for cDNA amplification started with an activation step at 95°C for 15 min, followed by 40 cycles of denaturation for 15 sec at 95°C and a combined primer annealing/extension step for 1 min at 60°C during which data collection was performed. The efficiencies of the RT-PCRs were >90% throughout. Relative quantifications were made with the comparative C_T (cycle threshold) method as described previously [10,79].

Quantification of viral genomes

Number of viral genomes was determined by measuring copy numbers of the viral M115 gene as described previously [41].

Quantification of infected cells in liver tissue

Immunohistochemical staining of major capsid protein (MCP; M86) present within inclusion bodies in the nuclei of infected cells was performed in liver tissue sections as described previously [10].

Western blot

Whole lysate was extracted from non-infected and infected-BMMΦ using Beadlyte® Cell Signalling Lysis Buffer (Milipore, UK), following manufacturer's instructions. BMMΦs were cultured for 7 days in 6-well plates at a seeding density of 10^6 cells/well. Prior to infection, cells were serum starved for 24 h. After infection cells were washed with ice-cold TBS and lysed in lysis buffer, containing Complete Miniprotease Inhibitor (Roche, UK) and Phosphatase Inhibitor Cocktail I and II (both from Sigma, UK). Protein concentration was determined using the MicroBCA protein assay (Pierce, UK), following manufacturer's instructions. Equal amounts of protein were mixed with 2× Laemmli Sample Buffer, containing 10% of DTT and loaded onto a 10% SDS-PAGE gels. Proteins were transferred to a PVDF membrane which was then probed with anti-phosphor-p38, anti p38, anti-phosphor-JNK, anti JNK (Cell Signaling, UK), and anti IκBα (Sigma, UK) and incubated with HRP-conjugated anti mouse or rabbit IgG (Cell Signalling, UK). Proteins were detected with ECL Plus Western Blotting Detection Reagents (Amersham Biosciences, UK) using VersaDoc imaging system 4000. Densitometric analysis of the blots was performed by Quantity One software 4.5.0. For pp38 MAPK and IE1 expression plasmid experiments, RAW 264.7 cells were washed with PBS and resuspended in whole-cell lysis buffer (50 mM Tris-HCl, pH 7.5, 100 mM NaCl, 1% NP40, protease inhibitors, and phosphatase inhibitors), and cell lysates were centrifuged at 4°C for 10 min and the collected supernatants were stored at −20°C. Protein concentration was measured by Pierce BCA assay (Thermo Scientific). For Western blotting, proteins were separated by 10% SDS-PAGE, transferred to Immobilon-FL membranes (Millipore), and probed with rabbit anti-p38α (Santa Cruz, sc-27578, 1:2000), mouse anti-pp38 MAPK (Cell signalling, 9216L, 1:1000), and rabbit anti-β-actin (Cell Signalling, 4970, 1:2500) diluted in PBST (0.1% Tween20). For secondary anti-rabbit IR-680 (Invitrogen, A21109, 1:10,000), IR-800 anti-mouse (Thermo Fisher Scientific, 35571, 1:10,000), antibodies were diluted in PBST (0.1% Tween20). For visualization, the Odyssey protocol (LI-COR) was followed. The fluorescence was quantified using ImageJ (ver. 1.45s).

Statistical analysis

Statistical analysis was performed in MATLAB (2007, The MathWorks, Inc). Viral titres and cytokine levels from *in vivo* experiments were compared by using Mann-Whitney U test. Analysis from *in vitro* experiments was compared by Student's t-test.

Normalisation procedure

For data normalisation, values of respective control (e.g. firefly activity) for each sample were expressed relative to the average of the control in the respective experiment. This normalisation factor was then used to correct the corresponding measured value in the assay (e.g. gLuc activity).

Gene accession numbers

(Entrez Gene ID) TNFa (Tnf, 21926), TNFR (Tnfrsf1a, 21937), p38 (Mapk14, 26416), NFκB-p65 (Rela, 19697), JNK (Mapk8, 26419), Ifnb1 (15977), IL10 (16153), CD11b (Itgam, 16409), F4/80 (Emr1, 13733), Ifng (15978), MKP-1 (Dusp1, 19252), IL12A (3592)

Supporting Information

Figure S1 Characterization of BMMΦ by flow cytometry. Maturation of day 7 BMMΦ assessed by staining for the specific expression of murine MΦ cell surface proteins F4/80 and CD11b. **A.** FACS dot blot showing the gating forward scatter (FSC) and side scatter (SSC). (B) This panel shows the population of $F4/80^{+}CD11b^{+}$ MΦ (93.1%). Histograms for F4/80 (C) and CD11b (D) staining are also shown.
(TIF)

Figure S2 Positive activation of MΦ after LPS stimulation. As a control for normal activation of cells, RAW264.7 macrophages were stimulated with LPS for 6 h. Cells were then fixed with 4% paraformaldehyde and staining was performed for TNFα. Cytokine production was compared to mocked-stimulated cells. DNA was counterstained with DAPI.
(TIF)

Figure S3 Correlation between TNFα levels and infectious virus in heart and kidney after 4 days of MCMVrev infection. Pearson's correlation coefficient shows a significant correlation between the levels of cytokine produced and PFU per gram of tissue in kidneys (A) and heart (B) from MCMVrev-infected BALB/c mice for 4 days.
(TIFF)

Figure S4 Infection with MCMV and MCMVdie1 suppresses NFκB activation and translocation to the nucleus. (A) RAW G9 cells, stably expressing a NFκB(p65)-GFP fusion protein, were infected or LPS treated and 45 min after the first contact with virions cells were fixed in 4% PFA, counterstained with DAPI and GFP translocation was monitored with an OPERA system (PerkinElmer). (B) Quantification of cytoplasmic and nuclear GFP fluorescence in treated cells. OPERA Acapella analysis software was used to quantify fluorescence in treated cells in 3 different snapshots of 4 wells per respective treatment. A standard fluorescence translocation script from the Acapella software ("NFkB Cytoplasm to Nuclei Translocation Assay") with standard settings was used for quantification of nuclear NFκB translocation. Bars represent averages of normalised fluorescence with SE.
(TIF)

Figure S5 Viral replication in organs of $TNF^{-/-}$ and $TNFR^{-/-}$ mice. Organs from infected C57B/6, $TNF\alpha^{-/-}$ (A) or Balb/c $TNFRp55^{-/-}$ (B) mice (2×10^{6} PFU i.p.) were harvested at 4 dpi and homogenated for analysis with standard plaque assay (MCMV = grey circles; MCMVdie1 = open circles). Titres were normalised per sample weight, black lines indicate median values and dashed line represents limit of detection.
(TIFF)

Figure S6 Viral replication in organs of Bl6 mice treated with 100 ug of anti-TNFα antibody (IP) at day 0 and day 2 p.i. Organs from infected mice (3×10^{5} PFU i.p.) were harvested at 4 dpi and homogenated for analysis with standard plaque assay. Black lines indicate median values and dashed line represents limit of detection.
(TIF)

Figure S7 Quantification of LiCor western blot images for detection of p38/pp38 and pJNK. Average of quantification (n = 3) of one representative experiment is shown, error bars represent SE of quantification. MCMVdie1 is abbreviated as die1 in this figure. (A) Quantification of pp38/p38 levels and normalised signal intensity in plasmid transfected RAW cells after LPS stimulation. (B) Quantification of pp38/p38 and pJNK levels and normalised signal intensity in infected RAW cells at 10 hpi after LPS stimulation. (C) Quantification of pp38/p38 levels and normalised signal intensity infected RAW cells at 4 hpi after LPS stimulation. (D) Densitometric quantification of IκBα, pp38 and pJNK levels at 10 hpi.
(TIF)

Figure S8 Characterisation of fluorochrome conjugated primary anti-TNF antibody by flow cytometric analysis. BMMΦs were stimulated with indicated concentration of LPS and stained with anti-TNF antibody or isotype control antibody. Fluorescence was analysed using a FACScan instrument.
(TIF)

Acknowledgments

We thank all the members of the Division of Pathway Medicine and Sarah Howie. We also thank Montse Gustems for her advice on the animal work and Chris Benedict for reading this manuscript. We want to thank Mike Tyers for kindly providing access to the OPERA facilities.

Author Contributions

Conceived and designed the experiments: SRM KAK AL VW VJL MA SJ MJR AA PG. Performed the experiments: SRM KAK WYH AL VW VJL MB HT AB. Analyzed the data: AA MM SJ MJR PG. Contributed reagents/materials/analysis tools: IF. Wrote the paper: SRM KAK VW MJR PG.

References

1. Keil GM, Ebeling-Keil A, Koszinowski UH (1984) Temporal regulation of murine cytomegalovirus transcription and mapping of viral RNA synthesized at immediate early times after infection. J Virol 50: 784–795.
2. Messerle M, Buhler B, Keil GM, Koszinowski UH (1992) Structural organization, expression, and functional characterization of the murine cytomegalovirus immediate-early gene 3. J Virol 66: 27–36.
3. Gribaudo G, Riera L, Lembo D, De Andrea M, Gariglio M, et al. (2000) Murine cytomegalovirus stimulates cellular thymidylate synthase gene expression in quiescent cells and requires the enzyme for replication. J Virol 74: 4979–4987.
4. Lembo D, Gribaudo G, Hofer A, Riera L, Cornaglia M, et al. (2000) Expression of an altered ribonucleotide reductase activity associated with the replication of murine cytomegalovirus in quiescent fibroblasts. J Virol 74: 11557–11565.
5. Schickedanz J, Philipson L, Ansorge W, Pepperkok R, Klein R, et al. (1988) The 89,000-Mr murine cytomegalovirus immediate-early protein stimulates c-fos expression and cellular DNA synthesis. J Virol 62: 3341–3347.
6. Munch K, Keil GM, Messerle M, Koszinowski UH (1988) Interaction of the 89K murine cytomegalovirus immediate-early protein with core histones. Virology 163: 405–412.

7. Munch K, Messerle M, Plachter B, Koszinowski UH (1992) An acidic region of the 89K murine cytomegalovirus immediate early protein interacts with DNA. J Gen Virol 73 (Pt 3): 499–506.
8. Gribaudo G, Ravaglia S, Guandalini L, Cavallo R, Gariglio M, et al. (1996) The murine cytomegalovirus immediate-early 1 protein stimulates NF-kappa B activity by transactivating the NF-kappa B p105/p50 promoter. Virus Res 45: 15–27.
9. Koszinowski UH, Keil GM, Volkmer H, Fibi MR, Ebeling-Keil A, et al. (1986) The 89,000-Mr murine cytomegalovirus immediate-early protein activates gene transcription. J Virol 58: 59–66.
10. Wilhelmi V, Simon CO, Podlech J, Bohm V, Daubner T, et al. (2008) Transactivation of cellular genes involved in nucleotide metabolism by the regulatory IE1 protein of murine cytomegalovirus is not critical for viral replicative fitness in quiescent cells and host tissues. J Virol 82: 9900–9916.
11. Ghazal P, Visser AE, Gustems M, Garcia R, Borst EM, et al. (2005) Elimination of ie1 significantly attenuates murine cytomegalovirus virulence but does not alter replicative capacity in cell culture. J Virol 79: 7182–7194.
12. Tang Q, Maul GG (2003) Mouse cytomegalovirus immediate-early protein 1 binds with host cell repressors to relieve suppressive effects on viral transcription and replication during lytic infection. J Virol 77: 1357–1367.
13. Gongora R, Stephan RP, Zhang Z, Cooper MD (2001) An essential role for Daxx in the inhibition of B lymphopoiesis by type I interferons. Immunity 14: 727–737.
14. Grotzinger T, Sternsdorf T, Jensen K, Will H (1996) Interferon-modulated expression of genes encoding the nuclear-dot-associated proteins Sp100 and promyelocytic leukemia protein (PML). Eur J Biochem 238: 554–560.
15. Cosme-Cruz R, Martinez FP, Perez KJ, Tang Q (2011) H2B homology region of major immediate-early protein 1 is essential for murine cytomegalovirus to disrupt nuclear domain 10, but is not important for viral replication in cell culture. J Gen Virol 92: 2006–2019.
16. Paulus C, Krauss S, Nevels M (2006) A human cytomegalovirus antagonist of type I IFN-dependent signal transducer and activator of transcription signaling. Proc Natl Acad Sci U S A 103: 3840–3845.
17. Tavalai N, Papior P, Rechter S, Stamminger T (2008) Nuclear domain 10 components promyelocytic leukemia protein and hDaxx independently contribute to an intrinsic antiviral defense against human cytomegalovirus infection. J Virol 82: 126–137.
18. Sandford GR, Schumacher U, Ettinger J, Brune W, Hayward GS, et al. (2010) Deletion of the rat cytomegalovirus immediate-early 1 gene results in a virus capable of establishing latency, but with lower levels of acute virus replication and latency that compromise reactivation efficiency. J Gen Virol 91: 616–621.
19. Greaves RF, Mocarski ES (1998) Defective growth correlates with reduced accumulation of a viral DNA replication protein after low-multiplicity infection by a human cytomegalovirus ie1 mutant. J Virol 72: 366–379.
20. Mocarski ES, Kemble GW, Lyle JM, Greaves RF (1996) A deletion mutant in the human cytomegalovirus gene encoding IE1(491aa) is replication defective due to a failure in autoregulation. Proc Natl Acad Sci U S A 93: 11321–11326.
21. Hanson LK, Slater JS, Karabekian Z, Virgin HWt, Biron CA, et al. (1999) Replication of murine cytomegalovirus in differentiated macrophages as a determinant of viral pathogenesis. J Virol 73: 5970–5980.
22. Stoddart CA, Cardin RD, Boname JM, Manning WC, Abenes GB, et al. (1994) Peripheral blood mononuclear phagocytes mediate dissemination of murine cytomegalovirus. J Virol 68: 6243–6253.
23. Orange JS, Biron CA (1996) Characterization of early IL-12, IFN-alphabeta, and TNF effects on antiviral state and NK cell responses during murine cytomegalovirus infection. J Immunol 156: 4746–4756.
24. Orange JS, Wang B, Terhorst C, Biron CA (1995) Requirement for natural killer cell-produced interferon gamma in defense against murine cytomegalovirus infection and enhancement of this defense pathway by interleukin 12 administration. J Exp Med 182: 1045–1056.
25. Randolph-Habecker J, Iwata M, Geballe AP, Jarrahian S, Torok-Storb B (2002) Interleukin-1-mediated inhibition of cytomegalovirus replication is due to increased IFN-beta production. J Interferon Cytokine Res 22: 765–772.
26. Benedict CA, Banks TA, Senderowicz L, Ko M, Britt WJ, et al. (2001) Lymphotoxins and cytomegalovirus cooperatively induce interferon-beta, establishing host-virus detente. Immunity 15: 617–626.
27. Herbein G, O'Brien WA (2000) Tumor necrosis factor (TNF)-alpha and TNF receptors in viral pathogenesis. Proc Soc Exp Biol Med 223: 241–257.
28. Rahman MM, McFadden G (2006) Modulation of tumor necrosis factor by microbial pathogens. PLoS Pathog 2: e4.
29. Baillie J, Sahlender DA, Sinclair JH (2003) Human cytomegalovirus infection inhibits tumor necrosis factor alpha (TNF-alpha) signaling by targeting the 55-kilodalton TNF-alpha receptor. J Virol 77: 7007–7016.
30. Montag C, Wagner J, Gruska I, Hagemeier C (2006) Human cytomegalovirus blocks tumor necrosis factor alpha- and interleukin-1beta-mediated NF-kappaB signaling. J Virol 80: 11686–11698.
31. Popkin DL, Virgin HWt (2003) Murine cytomegalovirus infection inhibits tumor necrosis factor alpha responses in primary macrophages. J Virol 77: 10125–10130.
32. Skaletskaya A, Bartle LM, Chittenden T, McCormick AL, Mocarski ES, et al. (2001) A cytomegalovirus-encoded inhibitor of apoptosis that suppresses caspase-8 activation. Proc Natl Acad Sci U S A 98: 7829–7834.
33. Mack C, Sickmann A, Lembo D, Brune W (2008) Inhibition of proinflammatory and innate immune signaling pathways by a cytomegalovirus RIP1-interacting protein. Proc Natl Acad Sci U S A 105: 3094–3099.
34. Upton JW, Kaiser WJ, Mocarski ES (2008) Cytomegalovirus M45 cell death suppression requires receptor-interacting protein (RIP) homotypic interaction motif (RHIM)-dependent interaction with RIP1. J Biol Chem 283: 16966–16970.
35. D'Addario M, Ahmad A, Morgan A, Menezes J (2000) Binding of the Epstein-Barr virus major envelope glycoprotein gp350 results in the upregulation of the TNF-alpha gene expression in monocytic cells via NF-kappaB involving PKC, PI3-K and tyrosine kinases. J Mol Biol 298: 765–778.
36. Gosselin J, Flamand L, D'Addario M, Hiscott J, Stefanescu I, et al. (1992) Modulatory effects of Epstein-Barr, herpes simplex, and human herpes-6 viral infections and coinfections on cytokine synthesis. A comparative study. J Immunol 149: 181–187.
37. Navarro L, Alto NM, Dixon JE (2005) Functions of the Yersinia effector proteins in inhibiting host immune responses. Curr Opin Microbiol 8: 21–27.
38. Sodhi A, Sharma RK, Batra HV (2005) Yersinia rLcrV and rYopB inhibits the activation of murine peritoneal macrophages in vitro. Immunol Lett 99: 146–152.
39. Lin SL, Le TX, Cowen DS (2003) SptP, a Salmonella typhimurium type III-secreted protein, inhibits the mitogen-activated protein kinase pathway by inhibiting Raf activation. Cell Microbiol 5: 267–275.
40. Selvaraj SK, Prasadarao NV (2005) Escherichia coli K1 inhibits proinflammatory cytokine induction in monocytes by preventing NF-kappaB activation. J Leukoc Biol 78: 544–554.
41. Lacaze P, Forster T, Ross A, Kerr LE, Salvo-Chirnside E, et al. (2011) Temporal profiling of the coding and noncoding murine cytomegalovirus transcriptomes. J Virol 85: 6065–6076.
42. Angulo A, Ghazal P, Messerle M (2000) The major immediate-early gene ie3 of mouse cytomegalovirus is essential for viral growth. J Virol 74: 11129–11136.
43. Wang F, Gao X, Barrett JW, Shao Q, Bartee E, et al. (2008) RIG-I mediates the co-induction of tumor necrosis factor and type I interferon elicited by myxoma virus in primary human macrophages. PLoS Pathog 4: e1000099.
44. Verhaegent M, Christopoulos TK (2002) Recombinant Gaussia luciferase. Overexpression, purification, and analytical application of a bioluminescent reporter for DNA hybridization. Anal Chem 74: 4378–4385.
45. Wurdinger T, Badr C, Pike L, de Kleine R, Weissleder R, et al. (2008) A secreted luciferase for ex vivo monitoring of in vivo processes. Nat Methods 5: 171–173.
46. Beutler B, Jiang Z, Georgel P, Crozat K, Croker B, et al. (2006) Genetic analysis of host resistance: Toll-like receptor signaling and immunity at large. Annu Rev Immunol 24: 353–389.
47. Falvo JV, Tsytsykova AV, Goldfeld AE (2010) Transcriptional control of the TNF gene. Curr Dir Autoimmun 11: 27–60.
48. Jesus Iglesias M, Reilly SJ, Emanuelsson O, Sennblad B, Pirmoradian Najafabadi M, et al. (2012) Combined chromatin and expression analysis reveals specific regulatory mechanisms within cytokine genes in the macrophage early immune response. PLoS One 7: e32306.
49. Lu YC, Yeh WC, Ohashi PS (2008) LPS/TLR4 signal transduction pathway. Cytokine 42: 145–151.
50. Zhu H, Shan L, Schiller PW, Mai A, Peng T (2010) Histone deacetylase-3 activation promotes tumor necrosis factor-alpha (TNF-alpha) expression in cardiomyocytes during lipopolysaccharide stimulation. J Biol Chem 285: 9429–9436.
51. Kuprash DV, Udalova IA, Turetskaya RL, Kwiatkowski D, Rice NR, et al. (1999) Similarities and differences between human and murine TNF promoters in their response to lipopolysaccharide. J Immunol 162: 4045–4052.
52. Rutault K, Hazzalin CA, Mahadevan LC (2001) Combinations of ERK and p38 MAPK inhibitors ablate tumor necrosis factor-alpha (TNF-alpha) mRNA induction. Evidence for selective destabilization of TNF-alpha transcripts. J Biol Chem 276: 6666–6674.
53. Tsai EY, Falvo JV, Tsytsykova AV, Barczak AK, Reimold AM, et al. (2000) A lipopolysaccharide-specific enhancer complex involving Ets, Elk-1, Sp1, and CREB binding protein and p300 is recruited to the tumor necrosis factor alpha promoter in vivo. Mol Cell Biol 20: 6084–6094.
54. Zhu W, Downey JS, Gu J, Di Padova F, Gram H, et al. (2000) Regulation of TNF expression by multiple mitogen-activated protein kinase pathways. J Immunol 164: 6349–6358.
55. Wall EA, Zavzavadjian JR, Chang MS, Randhawa B, Zhu X, et al. (2009) Suppression of LPS-induced TNF-alpha production in macrophages by cAMP is mediated by PKA-AKAP95-p105. Sci Signal 2: ra28.
56. Cao W, Bao C, Padalko E, Lowenstein CJ (2008) Acetylation of mitogen-activated protein kinase phosphatase-1 inhibits Toll-like receptor signaling. J Exp Med 205: 1491–1503.
57. Reddehase MJ, Weiland F, Munch K, Jonjic S, Luske A, et al. (1985) Interstitial murine cytomegalovirus pneumonia after irradiation: characterization of cells that limit viral replication during established infection of the lungs. J Virol 55: 264–273.
58. Lenzo JC, Mansfield JP, Sivamoorthy S, Cull VS, James CM (2003) Cytokine expression in murine cytomegalovirus-induced myocarditis: modulation with interferon-alpha therapy. Cell Immunol 223: 77–86.
59. Tang-Feldman YJ, Wojtowicz A, Lochhead GR, Hale MA, Li Y, et al. (2006) Use of quantitative real-time PCR (qRT-PCR) to measure cytokine transcription

and viral load in murine cytomegalovirus infection. J Virol Methods 131: 122–129.
60. Trgovcich J, Stimac D, Polic B, Krmpotic A, Pernjak-Pugel E, et al. (2000) Immune responses and cytokine induction in the development of severe hepatitis during acute infections with murine cytomegalovirus. Arch Virol 145: 2601–2618.
61. Yerkovich ST, Olver SD, Lenzo JC, Peacock CD, Price P (1997) The roles of tumour necrosis factor-alpha, interleukin-1 and interleukin-12 in murine cytomegalovirus infection. Immunology 91: 45–52.
62. van der Meer JW, Rubin RH, Pasternack M, Medearis DN, Lynch P, et al. (1989) The in vivo and in vitro effects of interleukin-1 and tumor necrosis factor on murine cytomegalovirus infection. Biotherapy 1: 227–231.
63. McFadden G, Schreiber M, Sedger L (1997) Myxoma T2 protein as a model for poxvirus TNF receptor homologs. J Neuroimmunol 72: 119–126.
64. Granja AG, Nogal ML, Hurtado C, Del Aguila C, Carrascosa AL, et al. (2006) The viral protein A238L inhibits TNF-alpha expression through a CBP/p300 transcriptional coactivators pathway. J Immunol 176: 451–462.
65. Fessler SP, Chin YR, Horwitz MS (2004) Inhibition of tumor necrosis factor (TNF) signal transduction by the adenovirus group C RID complex involves downregulation of surface levels of TNF receptor 1. J Virol 78: 13113–13121.
66. Neznanov N, Kondratova A, Chumakov KM, Angres B, Zhumabayeva B, et al. (2001) Poliovirus protein 3A inhibits tumor necrosis factor (TNF)-induced apoptosis by eliminating the TNF receptor from the cell surface. J Virol 75: 10409–10420.
67. Reddehase MJ (2006) Cytomegaloviruses : molecular biology and immunology. Wymondham: Caister Academic. xxvii, 619 p.
68. Witsell AL, Schook LB (1992) Tumor necrosis factor alpha is an autocrine growth regulator during macrophage differentiation. Proc Natl Acad Sci U S A 89: 4754–4758.
69. Cosme-Cruz R, Puerta Martinez F, Perez KJ, Tang Q (2011) H2B homology region of major immediate-early (MIE) protein 1 (IE1) is essential for murine cytomegalovirus to disrupt nuclear domain 10 (ND10), but not important for viral replication in cell culture. J Gen Virol 92 (Pt 9): 2006–19.
70. Aung HT, Schroder K, Himes SR, Brion K, van Zuylen W, et al. (2006) LPS regulates proinflammatory gene expression in macrophages by altering histone deacetylase expression. Faseb J 20: 1315–1327.
71. Shankaranarayanan P, Chaitidis P, Kuhn H, Nigam S (2001) Acetylation by histone acetyltransferase CREB-binding protein/p300 of STAT6 is required for transcriptional activation of the 15-lipoxygenase-1 gene. J Biol Chem 276: 42753–42760.
72. Wagner M, Jonjic S, Koszinowski UH, Messerle M (1999) Systematic excision of vector sequences from the BAC-cloned herpesvirus genome during virus reconstitution. J Virol 73: 7056–7060.
73. Tischer BK, von Einem J, Kaufer B, Osterrieder N (2006) Two-step red-mediated recombination for versatile high-efficiency markerless DNA manipulation in Escherichia coli. Biotechniques 40: 191–197.
74. Lucas M, Stuart LM, Savill J, Lacy-Hulbert A (2003) Apoptotic cells and innate immune stimuli combine to regulate macrophage cytokine secretion. J Immunol 171: 2610–2615.
75. Martinat C, Mena I, Brahic M (2002) Theiler's virus infection of primary cultures of bone marrow-derived monocytes/macrophages. J Virol 76: 12823–12833.
76. Kropp KA, Robertson KA, Sing G, Rodriguez-Martin S, Blanc M, et al. (2011) Reversible inhibition of murine cytomegalovirus replication by gamma interferon (IFN-gamma) in primary macrophages involves a primed type I IFN-signaling subnetwork for full establishment of an immediate-early antiviral state. J Virol 85: 10286–10299.
77. Markotic A, Lumen R, Marusic A, Jonjic S, Muthing J (1999) Ganglioside expression in tissues of mice lacking the tumor necrosis factor receptor 1. Carbohydr Res 321: 75–87.
78. Podlech J, Holtappels R, Grzimek NKA, Reddehase MJ (2002) Animal Models: murine cytomegalovirus. In: Kaufman SHE, Kabelitz D, editor. Methods in Microbiology. second ed. London and San Diego. pp. 493–525.
79. Livak KJ, Schmittgen TD (2001) Analysis of relative gene expression data using real-time quantitative PCR and the 2(−Delta Delta C(T)) Method. Methods 25: 402–408.

PLOS | PATHOGENS

RESEARCH ARTICLE

A Temporal Gate for Viral Enhancers to Co-opt Toll-Like-Receptor Transcriptional Activation Pathways upon Acute Infection

Kai A. Kropp[1¤]*, Wei Yuan Hsieh[1], Elena Isern[2], Thorsten Forster[1], Eva Krause[3], Wolfram Brune[3], Ana Angulo[2], Peter Ghazal[1,4]*

1 Division of Pathway Medicine, Edinburgh Infectious Diseases, University of Edinburgh, Edinburgh, United Kingdom, **2** Institut d'Investigacions Biomèdiques August Pi i Sunyer, University of Barcelona, Barcelona, Spain, **3** Heinrich Pette Institute, Leibniz Institute for Experimental Virology, Hamburg, Germany, **4** SynthSys, University of Edinburgh, The King's Buildings, Edinburgh, United Kingdom

¤ Current address: Department of Virology, Hanover Medical School, Hanover, Germany
* Kropp.Kai@mh-hannover.de (KAK); P.Ghazal@ed.ac.uk (PG)

CrossMark
click for updates

OPEN ACCESS

Citation: Kropp KA, Hsieh WY, Isern E, Forster T, Krause E, Brune W, et al. (2015) A Temporal Gate for Viral Enhancers to Co-opt Toll-Like-Receptor Transcriptional Activation Pathways upon Acute Infection. PLoS Pathog 11(4): e1004737. doi:10.1371/journal.ppat.1004737

Editor: Ren Sun, University of California, Los Angeles, UNITED STATES

Received: February 26, 2014

Accepted: February 9, 2015

Published: April 9, 2015

Copyright: © 2015 Kropp et al. This is an open access article distributed under the terms of the Creative Commons Attribution License, which permits unrestricted use, distribution, and reproduction in any medium, provided the original author and source are credited.

Funding: This work was supported by: The Wellcome Trust (WT066784/Z/02/Z), the BBSRC/EPSRC to SynthSys, a Centre for Integrative Systems Biology (CISB) reference BB/D019621/1 and reagent support from RNAi Global Initiative to PG. WYH was supported by a University of Edinburgh College Studentship. KAK was supported by the Deutsche Forschungsgemeinschaft (DFG) with a research fellowship (KR-3890/1-1) and an Innovation Initiative Grant (GR000943) from the University of Edinburgh Development Trust. AA was supported by the Ministerio de Ciencia e Innovacion

Abstract

Viral engagement with macrophages activates Toll-Like-Receptors (TLRs) and viruses must contend with the ensuing inflammatory responses to successfully complete their replication cycle. To date, known counter-strategies involve the use of viral-encoded proteins that often employ mimicry mechanisms to block or redirect the host response to benefit the virus. Whether viral regulatory DNA sequences provide an opportunistic strategy by which viral enhancer elements functionally mimic innate immune enhancers is unknown. Here we find that host innate immune genes and the prototypical viral enhancer of cytomegalovirus (CMV) have comparable expression kinetics, and positively respond to common TLR agonists. In macrophages but not fibroblasts we show that activation of NFκB at immediate-early times of infection is independent of virion-associated protein, M45. We find upon virus infection or transfection of viral genomic DNA the TLR-agonist treatment results in significant enhancement of the virus transcription-replication cycle. In macrophage time-course infection experiments we demonstrate that TLR-agonist stimulation of the viral enhancer and replication cycle is strictly delimited by a temporal gate with a determined half-maximal time for enhancer-activation of 6 h; after which TLR-activation blocks the viral transcription-replication cycle. By performing a systematic siRNA screen of 149 innate immune regulatory factors we identify not only anticipated anti-viral and pro-viral contributions but also new factors involved in the CMV transcription-replication cycle. We identify a central convergent NFκB-SP1-RXR-IRF axis downstream of TLR-signalling. Activation of the RXR component potentiated direct and indirect TLR-induced activation of CMV transcription-replication cycle; whereas chromatin binding experiments using wild-type and enhancer-deletion virus revealed IRF3 and 5 as new pro-viral host transcription factor interactions with the CMV enhancer in macrophages. In a series of pharmacologic, siRNA and genetic loss-of-function experiments we determined that signalling mediated by the TLR-adaptor protein MyD88 plays a vital role for governing the inflammatory activation of the CMV enhancer in macrophages. Downstream TLR-regulated transcription factor binding motif disruption for NFκB,

(SAF2008-00382 and SAF2011-25155). The funders had no role in study design, data collection and analysis, decision to publish, or preparation of the manuscript.

Competing Interests: The authors have declared that no competing interests exist.

AP1 and CREB/ATF in the CMV enhancer demonstrated the requirement of these inflammatory signal-regulated elements in driving viral gene expression and growth in cells as well as in primary infection of neonatal mice. Thus, this study shows that the prototypical CMV enhancer, in a restricted time-gated manner, co-opts through DNA regulatory mimicry elements, innate-immune transcription factors to drive viral expression and replication in the face of on-going pro-inflammatory antiviral responses in vitro and in vivo and; suggests an unexpected role for inflammation in promoting acute infection and has important future implications for regulating latency.

Author Summary

Here we discover how inflammatory signalling may unintentionally promote infection, as a result of viruses evolving DNA sequences, known as enhancers, which act as a bait to prey on the infected cell transcription factors induced by inflammation. The major inflammatory transcription factors activated are part of the TLR-signalling pathway. We find the prototypical viral enhancer of cytomegalovirus can be paradoxically boosted by activation of inflammatory "anti-viral" TLR-signalling independent of viral structural proteins. This leads to an increase in viral gene expression and replication in cell-culture and upon infection of mice. We identify an axis of inflammatory transcription factors, acting downstream of TLR-signalling but upstream of interferon inhibition. Mechanistically, the central TLR-adapter protein MyD88 is shown to play a critical role in promoting viral enhancer activity in the first 6h of infection. The co-option of TLR-signalling exceeds the usage of NFκB, and we identify IRF3 and 5 as newly found viral-enhancer interacting inflammatory transcription factors. Taken together this study reveals how virus enhancers, employ a path of least resistance by directly harnessing within a short temporal window, the activation of anti-viral signalling in macrophages to drive viral gene expression and replication to an extent that has not been recognised before.

Introduction

Infection by pathogens is detected by the host innate immune system through interaction of Pathogen-Associated Molecular Patterns (PAMPs) using a range of extra and intra-cellular host Pathogen-Recognitions-Receptors (PRRs) [1–3]. The major group of PRRs is represented by the family of Toll-Like-Receptors (TLRs) that detect a range of PAMPs and are located either at the cell surface, e.g. TLR2 and TLR4, or in endosomes, e.g. TLR3, 7 and 9 [3–5]. Binding of the corresponding ligands to these receptors leads to the activation of downstream signalling factors and TLR-receptors are dependent on the adaptor molecule MyD88, with exception of TLR3 and 4. TLR3 signals exclusively through the adaptor TRIF and TLR4 is the only TLR that can utilise both signalling pathways [3,6]. The activity of the TLR-signalling pathway triggers the expression of type I interferons and other antiviral factors that aid to control infections [7–9].

Cytomegalovirus (CMV) is recognised by the innate immune system using a diverse set of PRRs [1,10,11]. At the cell surface a direct interaction between the viral glycoproteins and TLR2 has been reported for human CMV (HCMV) [12,13] and also for the related human Herpesvirus 1 (HSV1) [14]. Other TLRs that play a role in resistance to CMV infection are TLR3 and TLR9. Homozygotic knockout animals for *Tlr2*, *Tlr3* or *Tlr9* are highly susceptible for CMV infection and show increased mortality rates [15,16]. Other types of PRRs have also

been implicated to contribute to the detection of CMV infection. The cytoplasmic DNA sensors DAI (ZBP-1) [17] and AIM2 [18] have been shown to detect CMV. The interaction of viruses at the cell surface (TLR2), or intracellular recognition of viral genomes (by DAI, AIM2, TLR9) and virion packaged RNA (through RIG-I, TLR3, TLR7) [19] results in triggering anti-viral responses through the signal activation of downstream inflammatory transcription factors (TFs). Depending on the infected cell type, these signal regulated TFs include NFκB, AP1, CREB/ATF, IRF3 or IRF7 which govern the expression of pro-inflammatory and anti-viral host factors and effector molecules.

Virus genomes encode a number of proteins, termed evasins that help to evade and subvert the host immune response to the infection [20–23], many of which target molecules of the adaptive immune response. Some evasins, however, inhibit the innate immune response to infection, in particular the production of IFN. For example the *UL83* gene product pp65 [24,25] and the IE86 protein (IE2) of HCMV and the Ie1 protein of MCMV have been reported to moderate production of pro-inflammatory cytokines [26,27]. Human CMV has also been shown to disrupt functionality of the interferon stimulated gene factor 3 (ISGF3), reducing IFNα production [28] and very recently the early gene UL26 has also been described to antagonise NFκB activation [29].

Two well-characterised inhibitors of innate immune signalling in murine CMV (MCMV) infection are the proteins M27 and M45. M27 and its HCMV homologue UL27 are efficient inhibitors of Type I and Type II IFN signalling through interaction and degradation of STAT2 and interference with tyrosine phosphorylation [30–32], therefore interfering with downstream autocrine and paracrine effects of TLR activation with the exception of plasmocytoid dendritic cells [33]. On the other hand, expression of M45 during the early phase of the infection cycle has been demonstrated to block NFκB activation, therefore interfering directly with PRR signalling pathways [34]. The mechanism of action for M45 is based on interaction with RIP1/3 and NEMO, proteins involved in the signalling cascade controlling the degradation of the inhibitor of NFκB, Ikbα [34,35]. However, *de novo* expression of both inhibitors M27 [30–32] and M45 [36] is necessary for their inhibitory activity and takes place during the early phase of the infection cycle. Of these proteins only M45 has been detected in virions [37]. Recently and unexpectedly the viral particle associated M45 protein has been shown to promote the activation of NFκB in fibroblasts during the immediate early (IE) phase of infection [36]. However, the functional relevance of this to infection is not clear at present. This poses the question if other mechanisms are in place to ensure sufficient viral gene expression despite the activation of anti-viral signalling events during the IE-phase of the CMV transcription-replication cycle.

IE-gene expression is under control of a potent enhancer that plays a critical role in determining success of a productive CMV infection [38–42]. *In vivo* the loss of the complete enhancer results in greater than a 3-log reduction in viral load and fails in exponential growth [31, 34]. Indeed, the human CMV genome has been long established to contain one of the strongest known enhancers as part of its major immediate early promoter (MIEP) with a 650 bp core that binds multiple transcription factors and which governs expression of the viral IE-genes [43–45]. While this region is functionally present in all CMV genomes the enhancer sequences are not conserved but instead share many of the same regulatory TF binding elements [41]. In particular all CMV enhancer regions contain a large number of highly redundant signal-regulated transcription factor binding sites, such as those interacting with NFκB, AP1 and CREB/ATF, factors that can be also activated by the TLR signalling pathways, [5,41,46,47]. This overlap combined with the combinatorial flexibility of the enhancer TF interactions indicates a potential for CMV to utilise the activation of anti-viral signalling pathways in the host cell. It has been reported that TLR9 stimulation plays both positive and negative roles in

HCMV infection [48] and that TLR4 and TLR9 activation can increase gene expression from a human CMV enhancer expression plasmid [46]. It is thus conceivable that the CMV enhancer might advantageously co-opt the triggered TLR-signalling pathway and therefore efficiently initiate its transcription-replication-cycle before the host-cell could produce any anti-viral effector molecules [47]. The basis of this concept has been discussed before [49] however, previous models have focused mainly on the role of NFκB, placing hijacking of NFκB signalling at the centre of the co-opting strategy. Notably, for both HCMV and MCMV it has been shown that NFκB is not essential for wild-type virus to drive its gene expression and only becomes crucial when other TF binding sites are impaired [50,51]. This poses the question whether the CMV viral enhancer has evolved a functional role in effectively co-opting multiple redundant immune signal-regulated TFs for initiating a productive transcription-replication cycle.

Hence, the underlying hypothesis for the present study is that inflammatory signalling at immediate-early times may promote viral infection through viral enhancer sequences. We report our first experimental tests to refute this hypothesis by systematically investigating the requirements and mechanisms for innate immune regulation of the CMV enhancer, in particular upon infection of macrophages and upon *in vivo* infection. We use a combination of RNAi library screens with host and viral genetics to delineate the TF network controlling the enhancer. Our findings reveal an integrated inflammatory TF-network consisting of IRF5, SP1, RXR and NFκB pathways with signal activation strongly dependent on MyD88 that is delimited by a specific temporal window for activation. These results support the hypothesis and further advance the concept of viral enhancer mimicry of innate immune promoters as an immune evasion strategy.

Results

Host innate immune genes and viral IE-gene expression have comparable expression kinetics and respond to common inflammatory activators

We first sought to examine whether viral IE-genes show similar expression kinetics to host innate immune genes upon infection of macrophages and test if they react to common stimuli. For these experiments we compared the expression kinetics of the host innate immune genes *Ifnb1*, *Il6* and *Tnf* with the viral major IE-gene *M123* (*Ie1*) by relative qPCR. As expected infection of bone marrow derived macrophage (BMDM) cells from C57/BL6 mice with MCMV triggered expression of the host pro-inflammatory cytokines IFNβ, IL6 and TNF (Fig. 1A). Notably, the overall kinetics of the viral *Ie1* gene and the host factors are similar, with a rapid induction of gene expression within the first 2 h post infection (hpi). To more extensively examine the induction of host innate immune genes we performed a microarray clustering analysis of expression levels in BMDMs after MCMV infection (Fig. 1B). For this study we used a set of well-known innate immune genes and TLR signalling components. This analysis revealed genes with expression profiles similar to the *Ie1* expression profile shown in Fig. 1A, with a rapid induction within 2–4 hpi (Fig. 1B, left panel). Exceptions of this pattern were *Il10*, *Tlr4*, *Tlr7* and *Tlr9*. *Il10*, *Tlr7* and 9 were induced with delayed kinetics and reaching peak expression levels by 6 h or later. In contrast, *Tlr4* seemed to have a high level of steady state expression in the mock sample and was down regulated after infection. To determine whether these changes in gene expression can be, at least partially, triggered by TLR activation alone, we further analysed the same set of genes in BMDMs stimulated with Poly IC, which activates TLR3 signalling (Fig. 1B, right panel). The stimulation with Poly IC recapitulates the observed pattern triggered by CMV infection with the exception of TLR4 expression. The down regulation of TLR4 observed in the infected sample was strongly delayed after Poly IC challenge. This

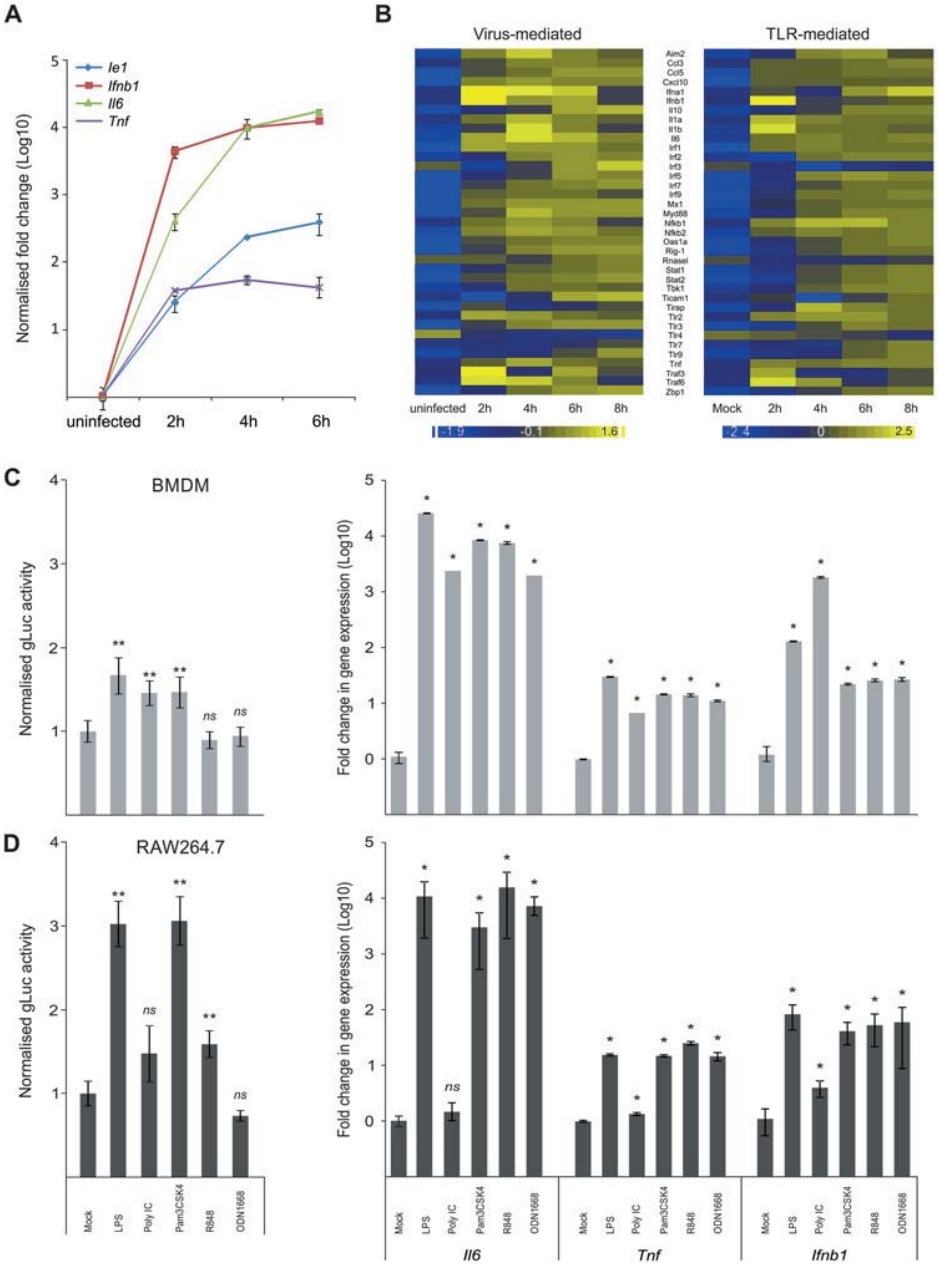

Fig 1. Host innate-immune response genes and viral IE-gene expression have comparable kinetics and are activated by common factors. A) Induction of gene expression for the host *Tnf*, *Ifnb1* an *IL6* genes and the viral *Ie1* gene were measured by qPCR (n = 4) after infection with MCMV. *IL6* and *Ie1* were not expressed in uninfected sample, so Ct of 36 was set as arbitrary comparison point. B) Heat maps of Microarray data for representative innate immune genes after infection with MCMV (left panel) or stimulation with Poly IC (right panel) showing comparable kinetics of gene induction after stimulation for most of the genes. Gene expression was normalised per gene to average expression levels and colour scale indicates fold change over average expression. C) Left panel: BMDMs (n = 50) were incubated with TLR-agonists for TLR4 (LPS), TLR3 (Poly IC), TLR2 (Pam3CSK4), TLR7 (R848) and TLR9 (ODN1668) for 15 min prior to infection with MCMV-gLuc to stimulate TLR signalling (for x-axis categories see Fig 1D). IE-gene expression was measured at 2 hpi by determining gLuc activity. Asterisks depict statistical significant changes identified by Wilcoxon two-sample test (* = p-value $\leq$ 0.05, ** = p-values $\leq$ 0.01, ns = not significant). Right panel: Induction of *Il6*, *Tnf* and *Ifnb1* expression in BMDMs after stimulation (4h) with the TLR-agonists (for x-axis categories see Fig 1D) used in this study with average fold changes over mock (n = 4) measured by relative qPCR. Asterisks depict statistical significant changes identified by Wilcoxon two-sample test (* = p-value $\leq$ 0.05). D) Left panel: Raw264.7

(n = 18) were incubated with TLR agonists and infected with MCMV-gLuc as described for Fig 1C. IE-gene expression was measured at 2 hpi by determining gLuc activity. Asterisks depict statistical significant changes identified by Welch two-sample t-test (* = p-value $\leq$ 0.05, ** = p-values $\leq$ 0.01, ns = not significant). Right panel: Induction of host cytokines *Il6*, *Tnf* and *Ifnb1* in RAW264.7 (n = 4) cells was measured as described for Fig 1C. Asterisks depict statistical significant changes identified by Wilcoxon two-sample test (* = p-value $\leq$ 0.05, ns = not significant).

doi:10.1371/journal.ppat.1004737.g001

might reflect the synergistic effect of parallel activation of several PAMPs by the infection process, which could explain the more pronounced down regulation in the infected versus the single stimulus by Poly IC.

Since HCMV-enhancer-driven reporter plasmids have been shown to positively respond to LPS and CpG [46], we tested if the viral IE-gene expression responds to stimulation of TLR signalling in the context of the viral infection. For these experiments RAW264.7 and primary BMDMs were pre-stimulated for 15 min with ligands for TLR4, TLR3, TLR2, TLR7 and TLR9 to stimulate the TFs activated by TLR signalling. These cells were subsequently infected with a gaussia luciferase [52,53] reporter virus (MCMV-gLuc) to quantitatively measure in the context of infection the activity of enhancer. This recombinant virus (S1 Fig for structure and mutagenesis strategy) has had the dispensable *m128* (*Ie2*) gene [54–56] replaced by a reporter cassette expressing a *gaussia luciferase* (*gluc*) reporter under direct control of the murine CMV enhancer. Levels and kinetics of *gluc* and *Ie1* expression in this reporter mutant are comparable as demonstrated by qPCR measurement (S2 Fig). Subsequent to TLR stimulation the cells were infected and 2 hpi the activity of the secreted gLuc reporter was measured in the cell culture supernatant (uninfected background for BMDMs was determined as 370.28 RLU with SEM = 4.81, n = 35 independent biological experiments; uninfected background for RAW264.7 was 82 RLU with SEM = 1.44, n = 32). As shown in Fig. 1C (left panel) and Fig. 1D (left panel), both cell systems showed a significant increase in reporter gene expression for specific TLR ligands (pre-normalised average of RLU for mock in BMDMs = $3.23x10^4$ RLU with min = $1.26x10^3$ and max = $1.69x10^5$, n = 50; not normalised average mock for RAW264.7 = 4.04x102 RLU with min = $9.6x10^1$ and max = $9.39x10^2$ RLU, n = 18). Notably, there are differences between the monocytic cell line RAW264.7 and the primary BMDMs in the measured levels of gene expression, for TLR4, TLR2 and TLR7 ligands LPS, Pam3CSK4 and R848, respectively. In these cases the RAW264.7 cells show a stronger response to the respective ligands, which is most likely related to differences in expression levels of their respective TLR repertoire. We therefore compared the expression levels of selected TLRs between BMDMs and RAW264.7 cells and found all of the assessed TLRs had increased expression levels in the RAW264.7 cells (S3 Fig). We furthermore could find no significant changes in uptake of viral genomes after TLR ligand treatment in BMDMs (S4 A and B Fig), indicating that the observed increase in gLuc activity is due to increased gene expression. To check if the used TLR ligands are biologically active and can induce host innate immune gene expression, we measured induction of *Ifnb1*, *Il6* and *Tnf* in primary BMDMs and RAW264.7 by the same TLR ligands (Fig. 1C and Fig. 1D, right panels). Notably, Poly IC was ineffective in activating gene expression in RAW264.7 cells in contrast to BMDMs. This might be due to differences in uptake of Poly IC since TLR3 is mainly localised in endosomes and its subcellular location is cell type dependent [57–60]. Taken together these data clearly show that inflammatory stimuli that induce expression of innate immune genes also enhance viral IE-gene expression in the analysed cell systems.

Altogether we conclude that the CMV enhancer is activated with similar kinetics to innate immune genes in the context of infection and is positively responsive to inflammatory TLR-signalling.

A temporal gate for TLR-triggered signalling to boost viral enhancer activity and replication

Our results so far indicate that stimulation of TLR signalling close to the time point of infection is sufficient to increase viral enhancer activity. While this concurs with work that demonstrated a stimulation of human CMV reporter-plasmids after LPS/CpG treatment, it is in contrast to the well-established observation that activation of TLR signalling is necessary for resistance to pathogens such as CMV [15]. As shown in Fig. 2A, long term pre-treatment (24 h) of BMDMs with all TLR ligands used in this study significantly inhibits MCMV as expected. The inhibitory effects of the TLR-ligands are most likely due to the induced expression of anti-viral effectors such as IFNβ (compare with Fig. 1C and 1D) that subsequently establish an anti-viral state through autocrine and paracrine effects [61–63].

For the anti-viral effector molecule IFNγ we have shown previously [64], that it has a half maximum pre-treatment time (ET_{50}) of 1.5 h to impart 50% inhibition of CMV enhancer activity in BMDMs. Since production of IFNs in naive cells needs to be induced first, this indicated that there should be a lag in the system between first contact with the virus and production of IFNs. In agreement, we have previously found that upon infection of BMDMs, IFNβ secreted protein levels peak by 6 hpi [64]. This lag predicts a possible temporal gate that would be open for a period no more than 7 hours for MCMV to establish infection before anti-viral effectors fully inhibit the virus.

Therefore we sought to determine if the anti- and pro-viral effects we observed are dependent on a time window and if so to define the boundaries of this potential temporal gate by comparing different pre-treatment times ranging from 0–24 h. When we tested pre-treatment times with ligands for TLR2, TLR4 and TLR9 ranging from parallel treatment (0 min) to 60 min pre-treatment, we found that all conditions were pro-viral, showing that there seems to be no measurable lower limit for the temporal gate (Fig. 2B). To establish the upper limit of the temporal gate we tested pre-treatment times ranging from 1–24 h. Fig. 2C shows that the effects of TLR ligands for TLR2, TLR4 and TLR9 changed over time from anti-viral to pro-viral with decreasing pre-treatment times. Matching the observations shown in Fig. 2A, the TLR ligands showed different levels of anti-viral activity with 24 h pre-treatment, with TLR2 showing only weak anti-viral activity and becoming pro-viral from 6 h or less. The more highly potent anti-viral states induced by TLR4 and TLR9 agonists, required shorter pre-treatment times to establish resistance to infection. To more precisely quantify the temporal window we determined the half maximal time for pro-viral enhancer stimulation by computing the ET_{50} for the TLR agonists. We fitted a regression function to the linear phase of the response (Fig. 2D) and estimated the ET_{50} values as -5 h 15 min for TLR4 and -6 h 9 min for TLR9, respectively.

Therefore, these experiments revealed the existence of a temporal gate in which CMV IE-gene expression can co-opt TLR signalling to its advantage, within the first 6 h of infection.

We next sought to investigate if the observed boost in enhancer activity conveyed a benefit for viral production. We assessed effects of TLR signalling on viral replication by quantifying replication of the viral genome and the production of infectious particles. To measure viral genome replication we used absolute quantification of viral genome copies by qPCR in infected BMDMs at 24 hpi, a time point at which the first round of replication is completed [65]. Detection of the host gene *Gapdh* was used to correct for potential variation in the amount of input material and values were furthermore normalised to the copy numbers of the mock sample (average genome copy number without normalisation was $1.73x10^5$ with min = $3.28x10^3$ copies and max = $2.5x10^5$ copies). Fig. 2E shows that 15 min pre-treatment with all tested TLR ligands significantly increased viral genome replication compared to the mock control. We then tested the impact of TLR activation on the production of infectious viral particles by standard plaque

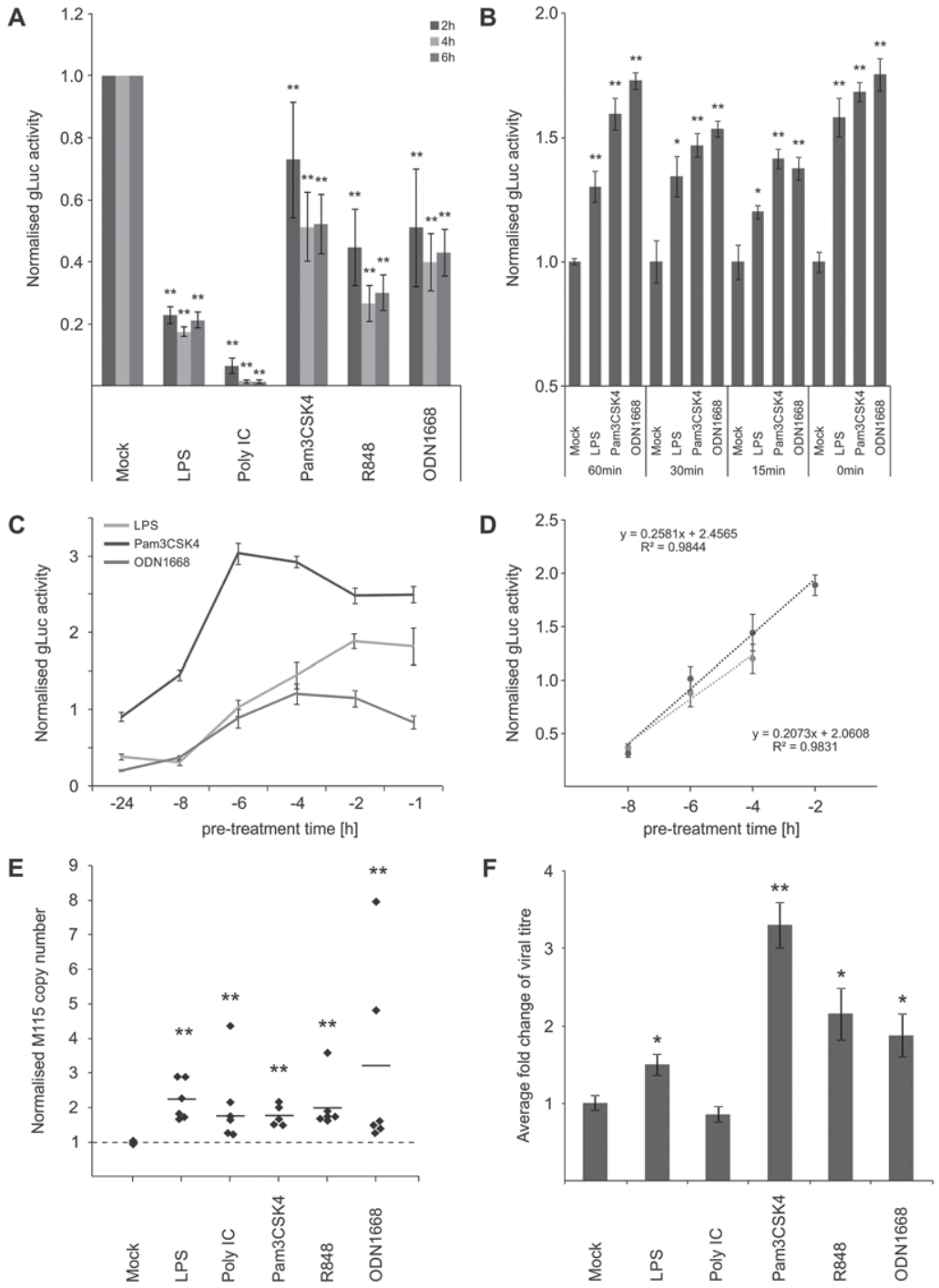

Fig 2. IE temporal gate for TLR-triggered signalling to boost IE-gene expression and viral replication. A) Inhibitory effects of long-term pre-treatment with TLR ligands. BMDMs were incubated for 24 h with indicated TLR ligands and subsequently infected (MCMV-gLuc). Reporter activity was measured at indicated time point p.i. Bars represent mean of normalised activity from n = 64 with error bars showing SEM and asterisks indicating statistical significant changes identified by Wilcoxon two-sample test (* = p-value $\leq$ 0.05, ** = p-values $\leq$ 0.01, ns = not significant). B) and C) IE-Time kinetic experiments of TLR-agonist pre-treatment and its effect on MIEP activity. BMDMs were pre-treated for indicated time points and infected with MCMV-gLuc (MOI 0.2). Reporter activity in culture SN was measured at 3 hpi (B, n = 6) or 4 hpi (C, n = 8). Averages of cultures are shown with SEM, normalised to mock activity and asterisks indicate statistical significant changes identified by Welch two-sample t-test (* = p-value $\leq$ 0.05, ** = p-values $\leq$ 0.01). D) Linear phases of time-effect curves for TLR4 (black circles) and TLR9 (grey circles) agonists were estimated from plots in Fig 2C. Linear trend-lines were fitted to the respective

data points (average with SEM) and were used to determine ET50 values (TLR4 = -5.25 h; TLR9 = -6.15 h). E) Quantification of viral genomes in infected BMDMs (MCMV-gLuc) shows increased numbers of genomes for all used TLR-agonists. Genome copy numbers were absolutely quantified, corrected by *Gapdh* as cellular control and then normalised to copy numbers from mock-treated samples. Dotted line indicates level in mock samples and thick solid black lines mark the average of the treatment groups (n = 6). Asterisks indicate statistical significant changes over the mock group identified by Wilcoxon two-sample test (** = p-value≤0.01). F) Measurement of viral replication in BMDMs by plaque assay (MCMV-gLuc). Supernatant from n = 6 infected BMDM cultures were harvested at day 3 p.i. and assayed for infectious viral particles on *Stat1*$^{-/-}$ MEFs. Plaque numbers were normalised to average of mock samples (2.8x10^3 PFU/ml) and asterisks indicate statistical significant changes over mock identified by Welch two-sample t-test (* = p-value≤0.05; ** = p-value≤0.01).

doi:10.1371/journal.ppat.1004737.g002

assay. To reduce interference of IFNs produced by the infected experimental BMDM cultures and to increase sensitivity we used *Stat1*$^{-/-}$ MEFs for the plaque assay. As shown in Fig. 2F all treatments, except for Poly IC, significantly increased the production of viral particles in the culture at 3 days post infection. While quantitative variation in IE gene expression is observed for the different ligands, the levels of boosted IE-gene expression and viral genome replication do not completely reflect the detected increase in viral particle production in the plaque assay. Although we do not fully understand this variation it is most likely due to the downstream anti-viral factors and their effects elicited by the respective TLR signalling pathways (compare to Fig. 1 and Fig. 2A).

Nevertheless these data demonstrate that TLR activation can boost at IE-times of infection both viral gene expression and subsequent replication and supports the notion that CMV enhancer might co-opt activity of innate immune signalling to its own advantage.

A direct effect of TLR-signalling on CMV enhancer activity

Comparison of TFs known to bind the HCMV enhancer with TFs activated by TLR signalling show that several factors are shared, including NFκB, AP1 and ATF [41,66–68]. To analyse the importance of these TFs in our system we used a set of chimaeric viral recombinants in which the human CMV wild-type and mutant enhancers replace the native murine CMV enhancer [38,69]. We analysed the effects of TLR activation on *Ie1* gene expression in the chimaeric virus carrying the wild-type human CMV enhancer (hMCMV) and compared this with a triple knockout mutant (hMCMV-Δ3) in which all enhancer binding motifs for NFκB, AP1 and ATF have been rendered non-functional by point mutations. As can be seen in Fig. 3 the disruption of the binding motifs significantly reduced the expression of *Ie1* after TLR stimulation, demonstrating that the observed effects are in part due to direct activation by NFκB, AP1 and/or ATF. However, we note that the mutation of all NFκB, AP1 and ATF binding sites could not completely abolish the boost of viral *Ie1* gene expression by TLR activation. Stimulation of TLR4 (p-value≤0.05), TLR3 (p-value≤0.01) and, with a trend, TLR2 (p-value = 0.099) was still able to boost viral gene expression. This result indicates that additional host factors must also be involved in the stimulation of CMV enhancer activity by TLR signalling.

It is possible that a viral tegument protein rather than indirect TLR signalling could lead to activation of TFs. A very recent publication showed that the viral protein M45, which is delivered into cells initially by viral particles, is a potent activator of NFκB signalling at IE times despite its role as an inhibitor of NFκB at early and late times of infection [36]. However, these studies were limited to fibroblasts and found no necessity for M45 to activate viral IE-gene expression. To assess whether M45 or other tegument proteins are involved in the observed TLR-mediated effects on IE-gene expression, we first examined the effect of TLR stimulation on genomic MCMV-gLuc DNA transfected into primary MEFs. After the transfection cells were visually checked for successful transfection by assessing if individual fluorescent cells were present in the cultures. Subsequently, half of the transfected cultures were treated with LPS to

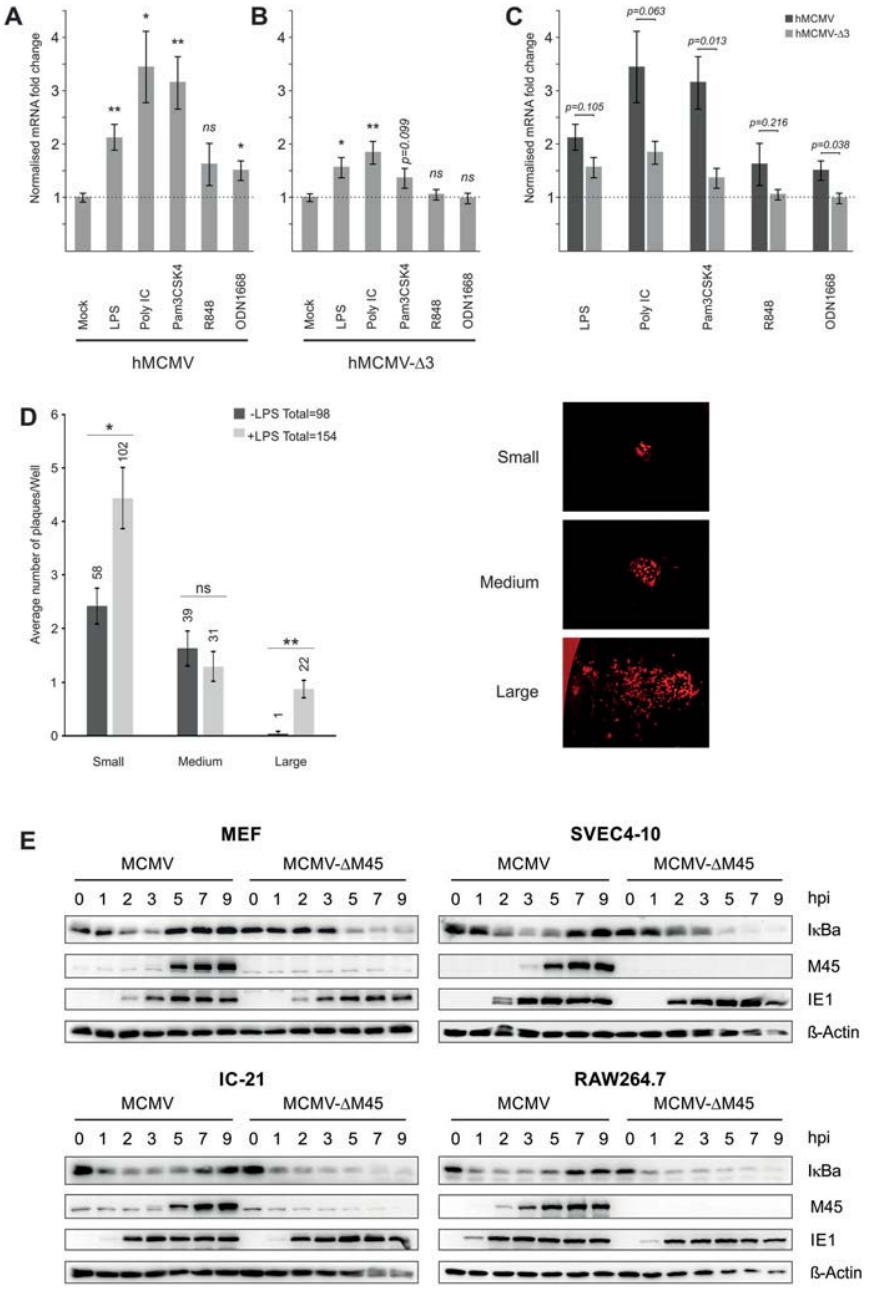

Fig 3. Effects of TLR-agonists go beyond NFκB activity and are independent of tegument proteins. Comparison of 6 biological replicates measuring *Ie1*-gene expression of chimaeric MCMV recombinant viruses carrying either a human CMV enhancer (hMCMV) (A) or a human CMV-NFκB/AP1/ATF-motif-disrupted-enhancer (hMCMV-Δ3) (B) after stimulation with indicated TLR-agonists in BMDMs by qPCR. Expression was normalised to *Gapdh* and is shown relative to mock treated samples and asterisks indicate statistical significant changes over mock for each group as identified by Welch two-sample t-test (* = p-value≤0.05; ** = p-value≤0.01, ns = not significant). C) Statistical comparison (two-sample Welch's t-test) of differences in fold changes between hMCMV and hMCMV-Δ3 viruses for each TLR-agonist (n = 6). D) TLR stimulation acts independent of delivered tegument proteins. Primary MEF cultures were transfected with MCMV-gLUC DNA (16 h) and subsequently either mock (n = 24) or LPS (n = 24) stimulated. At 6 days post stimulus viral plaque production was quantified and plaques were classified into small, medium and large categories (representative plaques for the categories are shown). Bars depict average plaque numbers (indicated above each bar) with SEM. Statistical significance of observed differences between treatments is indicated by asterisks (Mann Whitney U Test, * = p-value≤0.05; ** = p-value≤0.01; ns = not significant). E)

In monocytes NFκB activation and IE1 protein levels are not dependent on M45. Representative western blots detecting proteins IκBa, M45, IE1 and b-Actin in primary MEFs, SVEC4-10 endothelial cells, IC-21 and RAW264.7 macrophage cells infected with either MCMV or MCMV-ΔM45 virus (MOI of 10 $TCID_{50}$/cell). Cells were lysed at the indicated times post-infection, and protein levels determined by immunoblotting.

doi:10.1371/journal.ppat.1004737.g003

trigger TLR signalling. Over the first 8h we checked repeatedly for changes in expression of the reporter gene *gLuc* and found that from 4h post treatment a shift in in a number of independent LPS treated cultures to higher reporter expression was detectable. To determine if this initial boost of gene expression translated into increased viral replication, we assessed the number of plaques and the size of plaques at 6 days post treatment (Fig. 3D). This analysis showed that the group of LPS treated cultures produced more viral plaques in total and had statistically significant higher numbers of plaques in the small and large categories. It is noteworthy that large plaques were mainly present in the LPS treated group. This experiment demonstrates that an initial boost through TLR stimulation can translate into an enhancement of the transcription-replication cycle from viral genomic DNA. This observation further supports the notion that the observed effects are not absolutely dependent on viral tegument proteins.

Since it has been recently demonstrated that in NIH3T3 fibroblasts the activation of NFκB immediately after infection is strictly dependent on M45 [36], we next assessed the role of this tegument protein in the macrophage system using a ΔM45 recombinant virus. A comparison of protein levels in MEFs infected with wild type and mutant virus confirmed the phenotype published for NIH3T3 cells. In MCMV infected MEFs a rapid degradation of the inhibitor of NFκB (IκBa) could be observed that was blocked at later times (≥5 hpi) when *de novo* synthesised M45 became visible (Fig. 3E, top left panel). In MEFs infected with the MCMV-ΔM45 virus the degradation of IκBa only became detectable at 5 hpi. In contrast to this, rapid degradation of IκBa was observed in the SVEC4-10 endothelial cell line and in the macrophage cell lines IC-21 and RAW264.7 after infection with both, the MCMV and MCMV-ΔM45 viruses (Fig. 3E, top right and lower panels). This demonstrates that, in contrast to fibroblast cells, NFκB activation at IE-times in infected endothelial and macrophages is not dependent on M45. Overall, the loss of M45 did not overtly impact on IE1 protein levels in any of the tested systems. In separate experiments we also find the M45 MCMV mutant was still responsive to TLR activation in macrophages by stimulation with TLR2 agonist (S5 B Fig).

We conclude from these experiments a direct involvement of the enhancer elements in mediating responsiveness to TLR-signalling and while not mutually exclusive from the possible contribution of viral particle associated proteins, is shown to be independent of the virion-delivered M45 protein.

Loss-of-function screen for enhancer activity identifies an integrative network of immune activated transcription factors linking retinoid receptor activation and TLR stimulation

To explore more fully the TF network required for enhancer activation, we used a library of small interfering RNAs (siRNAs) for targeted knock-down of immune signalling components and TFs that are either known to bind the CMV enhancer or to be activated by TLR signalling and a range of positive and negative control genes (targeting in total 149 host factors, complete list of targets are shown in S1 Table). We transiently transfected primary MEFs with targeted SMARTpools (Dharmacon, Lifetechnologies) and subsequently infected them with the gLuc-reporter virus (MCMV-gLuc) to monitor exclusively enhancer activity at 6 hpi (25nM siRNA screens). Fig. 4A shows the summarised results of 4 independent, normalised gLuc screens that

passed the quality control filter (detectable expression of the reporter in the mock transfected samples and knock-down by several positive control siRNAs, e.g. targeting either the reporter *gLuc* or TFs known to be important for CMV enhancer activation, e.g. *Sp1* [68,70]). Due to a high level of redundancy in the CMV enhancer overall inhibitory effects of the knockdowns rarely reach more than two-fold, even with the positive controls. We therefore ranked the siRNA knockdowns relative to the maximal achieved knockdown by the *gLuc* targeting positive control siRNA (Ranked list of all genes see S1 Table, for corresponding knock-down data see S2 Table). For analysis we set cut-offs representing different ranks of our 149 targeted host factors. We used three levels of stringency to sort our target list; the high stringency group (>75% of maximal knock-down effect) consisted of the top 25 candidate genes, the medium stringency group (>50%) included the top 63 genes and the low stringency group (>25%) included the top 101 gene candidates.

To investigate whether the hits from the screen were dispersed over a range of different interaction networks or were limited to a discrete network of biochemical/molecular interactions we undertook a network analysis of the high stringency group of 25 candidates with the STRING web tool. This approach determines edge connectivity of the hits based on known and predicted molecular interactions [71]. The results of this analysis shown in Fig. 4B, reveal that most of the target genes of the >75%-group could be mapped to a principal network with the TLR-adaptor protein MyD88 at its centre (confidence of interaction is indicated by thickness of connecting edges, asterisks next to network node indicates statistical significant knock-down) and a link to an RXR network. We found that a substantial part of our statistically significant hits could be mapped to the TLR immune response pathway (top hit in GO term enrichment test was "activation of innate immune response" with $p\text{-value} \leq 7.609 \times 10^{-9}$) with associated innate immune factors, such as TLR7, IRAK1/4, MyD88, IRF5 and also RIG-I (Ddx58), and AIM2. This functional network was connected to the NFκB subunit RelA as was to be expected but also included the TFs, SP1, ETS1, Nfyb, Nfyc and RXRA. The presence of RXRA, ETS1 and SP1 in the list of significant hits affecting viral enhancer activity was not surprising, since interactions with the CMV enhancer for SP1 [70], the ETS-family (ELK1 [72], ETS-2 [73]) and RXRA [41,74–76] have been described in the literature. In support, Fig. 4C shows the normalised average gLuc activity of all members of the RXR network, the IRF family and the TLR signalling components for comparison. Notably, the factors IRF5, AIM2, RIG-I, Nfyb and Nfyc have not been previously implicated in mediating activation of CMV gene expression.

An analysis of the medium and low stringency factors with the topology inferred by the STRING software tool showed a highly integrated network, comprising TLR signalling components linked to the RXR network (see S6 and S7 Figs).

Statistical meta-analysis of an extended series of independent screens for viral growth and enhancer activity identifies divergent and a convergent NFκB-SP1-RXR-IRF transcription factor axis

We next sought to assess whether transcription factor requirements are convergent or divergent for viral growth and enhancer activity. Due to the inherent redundancy of TF requirement for enhancer activity we, therefore, conducted a large number (up to n = 24) of systematic independent siRNA screens for the 149 TFs. For these screens we used a GFP-expressing reporter virus (MCMV-GFP) to monitor viral replication at 72 hpi and MCMV-gLuc to monitor enhancer activity at 6 hpi. By applying a robust statistical meta-analysis we aimed to increase the statistical power and identify the most consistent siRNA effects on the results of all screens over all experimental conditions. Fig. 5 shows the medians of each siRNA over all screens from

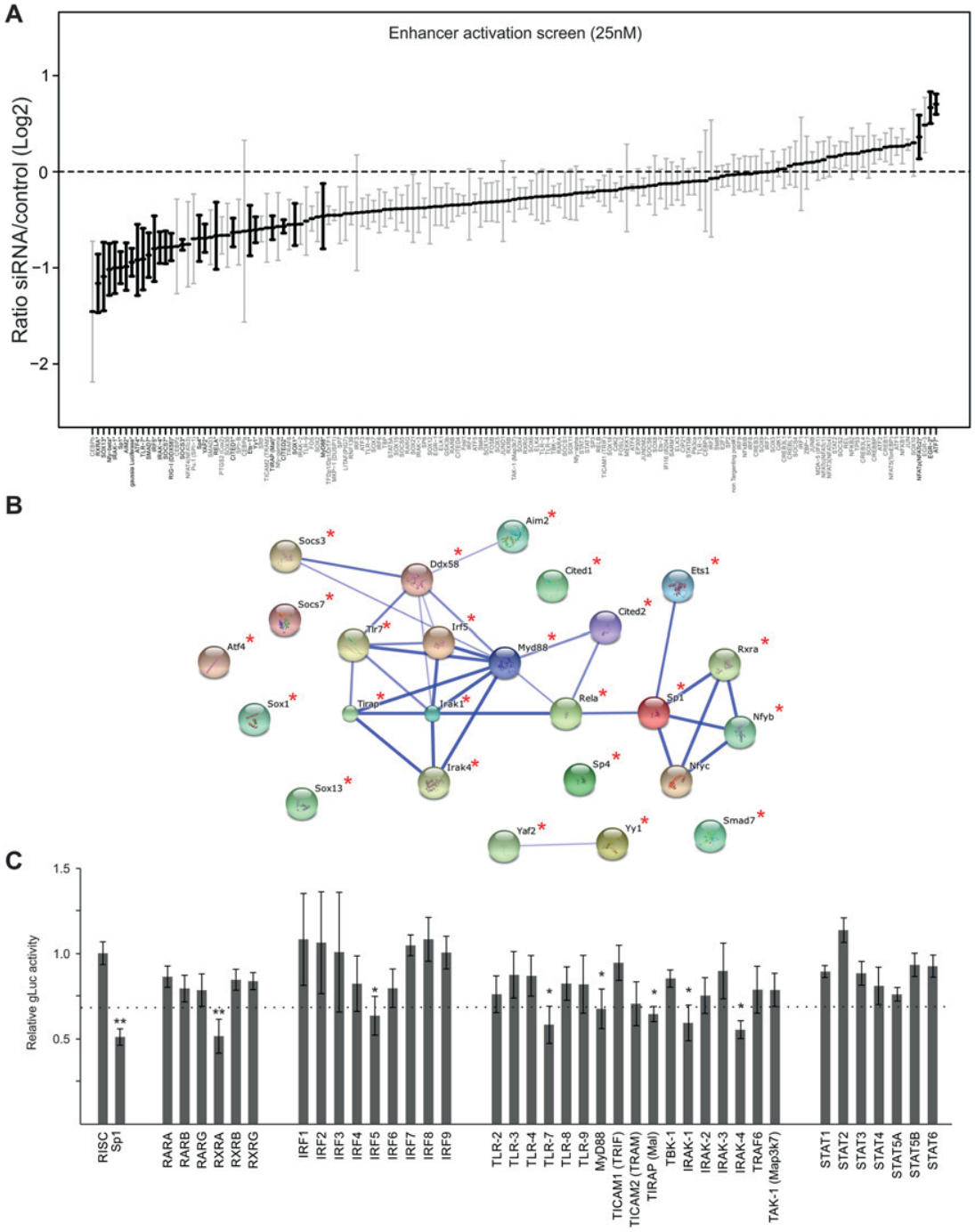

Fig 4. Small interfering RNA screens identifies TLR-signalling network. A) GLuc activity data from all 25nM siRNA screens (n = 4). Reporter activity shown is normalised to RISCfree control siRNA. Black circles and bold gene name indicate statistically significant effects for corresponding gene knockdown (Wilcoxon test; p-value≤0.05). B) STRING network of the candidate genes that showed >75% maximal knockdown effect compared to controls in all 25nM siRNA screens (n = 4). Asterisks indicate statistical significant knockdown (p-value≤0.05). Corresponding data is shown in S2 Table. C) GLuc activity data for the RXR-network, the IRF family and the TLR network, from all 25nM siRNA screens (n = 4). Reporter activity shown is normalised to RISCfree control siRNA. *Sp1* siRNA knockdown show maximally achieved inhibition and asterisks indicate statistical significant knockdowns (Wilcoxon test; * = p-value≤0.05; ** = p-value≤0.01) and dotted line depicts 75% maximal knockdown cut-off used to identify candidates for STRING network.

doi:10.1371/journal.ppat.1004737.g004

all experimental conditions with those highlighted in bold being significantly different from the infected controls (number of screens per siRNA up to n = 24, see figure legend). The upper panel of Fig. 5 shows replication efficiency at 72 hpi, while the lower panel shows enhancer activity at 6 hpi (see also S3 Table). This analysis allowed for statistically stringent assessment of viral replication and enhancer activation screens and revealed, as expected from the literature, components of the TLR signalling pathway, such as TAK1, TBK1 and IRF2 that have a statistically significant anti-viral effect when measuring replication.

In contrast and in concordance with the temporal gate model for immune activation we also find many of the TLR signalling components, such as TLR9, IRAK2, IRAK4 and IRF3, IRF4, IRF5 and IRF6 to have a pro-viral effect shown in the lower panel of Fig. 5. For significant hits and overlap between the two screens see Table 1. Assessing the overlap between the two approaches, we find several genes that significantly reduced enhancer activation as well as viral replication, namely ELK1, FOSB, IRF4, IRF5, IRF6, RELA, RXRA, Sp1, SP6, SP7, SRF and YY1. Notably, IRF5, RELA, RXRA, SP1 and YY1 were also part of the network identified in the initial enhancer activation screen (Fig. 4). Taken together these targets indicate that discrete innate immune signalling plays an important role in activating the viral enhancer.

Overall this data implies that the TLR-activated host factors NFκB (RelA), SP1, RXR and members of the IRF family play a central role in activating the enhancer in infection and that these factors may form a functional network. Thus, the TLR signalling pathway might be necessary for normal IE-gene expression levels in infections with the potential for cooperation with the retinoic-acid signalling pathway.

Retinoic acid pre-treatment cooperatively increases the effects of TLR-ligands on viral enhancer activity

The above-described screens identified RXRA as part of the integrated TLR-network affecting viral IE-gene expression. While retinoic acid receptors have been shown to bind to and regulate human and murine CMV enhancer activity [74,77], it is known that retinoic acid receptors can also positively influence TLR expression [78,79]. To functionally test the effects of retinoids in our system, we pre-treated BMDMs with the RAR/RXR ligand [80] *9-cis*-retinoic acid (*9-cis*-RA) for 24 h prior to TLR-pre-treatment. As shown in Fig. 6A, we find that the *9-cis*-RA pre-treatment triggers an increased sensitivity of our cells to the effects of TLR pre-treatment. The ratios of gLuc activity between *9-cis*-RA-treated and vehicle-treated samples show that RA has a broadly positive effect on the system, since all TLR treatments, independent of the ligand, showed ratios significantly larger than 1 (Fig. 6B). This suggests that the viral enhancer may also directly benefit from RA stimulation. As can be seen in Fig. 6C, we monitored gLuc expression in vehicle and *9-cis*-RA treated BMDMs over a time course and observed that the *9-cis*-RA treatment increases IE-gene expression for up to 72 hpi in absence of any prior TLR ligand treatment.

The direct effects of RA on viral gene expression are mediated through multiple high affinity retinoic acid receptor binding sites (RA Response Elements, RAREs) that have been previously characterised for both the HCMV and MCMV enhancers and shown to influence IE-gene expression [74–76]. To analyse if the *9-cis*-RA treatment has a direct effect we used a chimaeric murine CMV mutant similar to those described above, in which all RAREs in the human CMV enhancer have been disrupted by point mutations (hMCMV-ΔRARE) and measured *Ie1* expression by qPCR. We found reduced levels of *Ie1* expression with the hMCMV-ΔRARE mutant compared to the parental hMCMV virus (S8 Fig). Fig. 6D shows that disruption of all RAREs in the viral enhancer still allows TLR-ligands to stimulate IE-gene expression after pre-treatment with the vehicle or 9-*cis*-RA but the additional boost observed with the MCMV virus

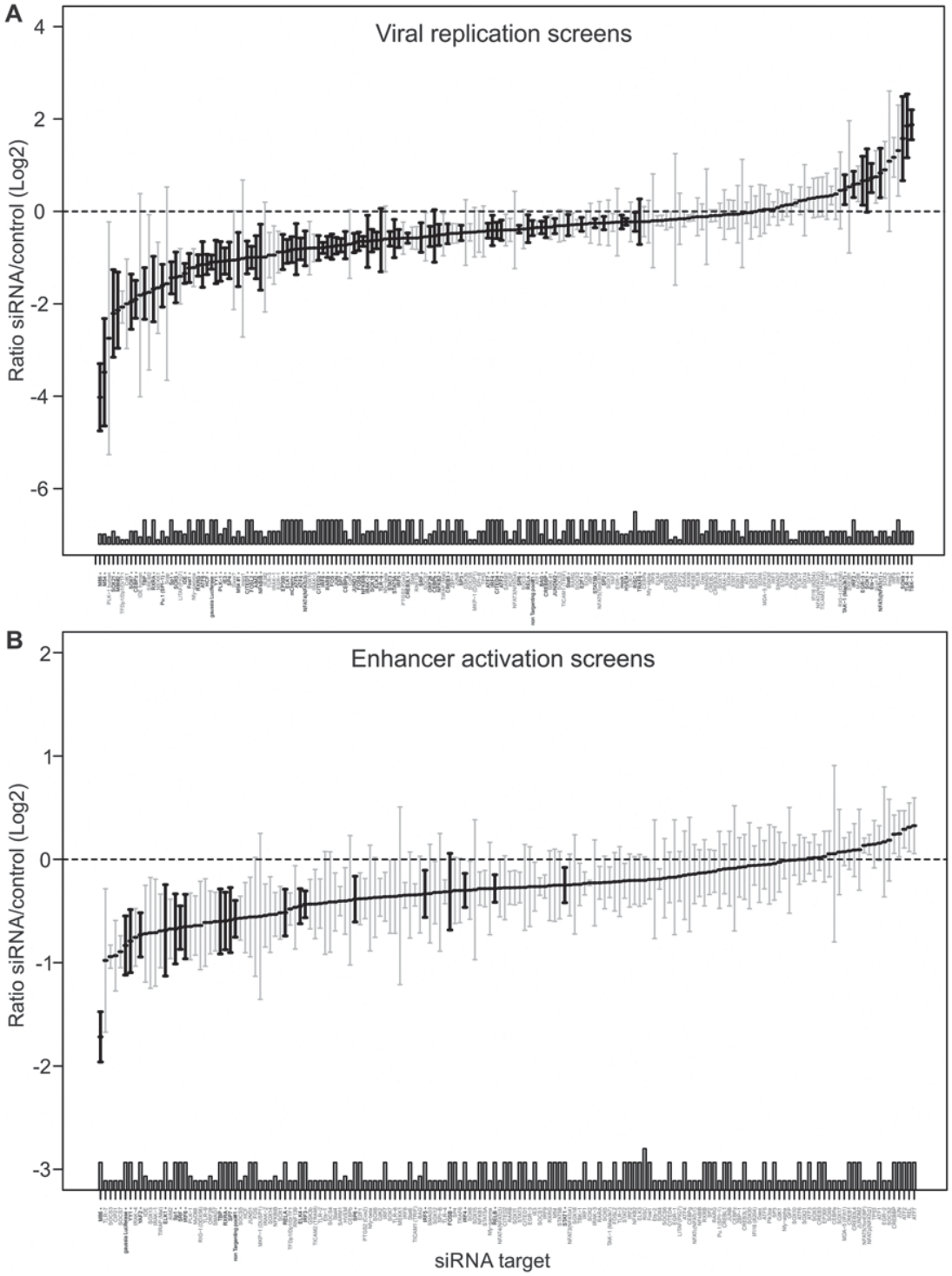

Fig 5. Summary of all Loss-of-function siRNA screening data. Ordered lists with all values for siRNA targets on x-axis available in S3 Table. A) Viral replication: Median (and bootstrapped standard error of median) of fold change (y-axis) between siRNA and infected controls, measured by GFP activity across all screens (MCMV-GFP). The numbers of independent screens for a particular siRNA is available in bars (on x-axis) and are n = 4, 6, 8, 10, 12, 18 or 24. Data points highlighted in bold are significantly different (by Wilcoxon Signed Rank test) from a zero fold change, i.e. infected controls. B) IE-gene expression: Median (and bootstrapped standard error of median) of fold change (y-axis) between siRNA and infected controls, measured by gLuc activity (MCMV-GFP) across all screens (n is 3, 4, 7 or 10), symbols as described in (A).

doi:10.1371/journal.ppat.1004737.g005

Table 1. Comparison of significant siRNA hits for viral replication and enhancer activation from statistical meta-analysis.

Viral replication siRNA target	effect of knock-down on virus	Viral replication siRNA target	effect of knock-down on virus	Enhancer activation siRNA target	effect of knock-down on virus
AIM2	-	RARB	-	ELK1*	-
ATF2	-	RELA*	-	ELK4	-
ATF4	-	RXRA*	-	FOSB*	-
ATF5	-	RXRG	-	IRF3	-
ATF6	-	SOX1	+	IRF4*	-
ATF7	-	SOX18	-	IRF5*	-
CEBPb	-	SOX21	-	IRF6*	-
CEBPg	-	SOX5	-	RELA*	-
CEBPz	-	SOX7	-	RELB	-
CITED1	-	SOX9	+	RXRA*	-
CITED2	-	Sp1*	-	Sp1*	-
CITED4	-	SP2	-	SP6*	-
CREB3	-	SP3	-	SP7*	-
CREB3L1	-	SP4	-	SRF*	-
CREBBP	-	SP6*	-	STAT1	-
EGR-3	+	SP7*	-	YAF2	-
ELK1*	-	SRF*	-	YY1*	-
ELK3	-	STAT3	-		
Ets-2	+	STAT5A	-		
FOS	-	STAT5B	-		
FOSB*	-	Stat6	-		
Fosl1	-	TAK-1	+		
FOSL2	-	TBK-1	+		
IRAK-2	-	TLR-4	+		
IRF2	+	TLR-9	-		
IRF4*	-	TRAF6	-		
IRF5*	-	YY1*	-		
IRF6*	-				
JUN	-				
JUND1	-				
JUNDM2	-				
NFAT4	-				
NFATc	+				
NFKB2	-				
NFKBIB	-				
NFkBIB	-				
Pu.1	-				

* = indicates siRNA hit overlaps between both screen types

doi:10.1371/journal.ppat.1004737.t001

(Fig. 6C) is lost with the hMCMV-ΔRARE mutant infection. These findings suggest that the RAREs are not necessary for TLR activation of the enhancer but are required for cooperative activation. In agreement, the ratios of *Ie1* mRNA expression between *9-cis*-RA and vehicle treated samples were not statistically significantly >1 after infection with the mutant virus (Fig. 6E), and thus demonstrate that the RAREs in the viral enhancer contribute to the

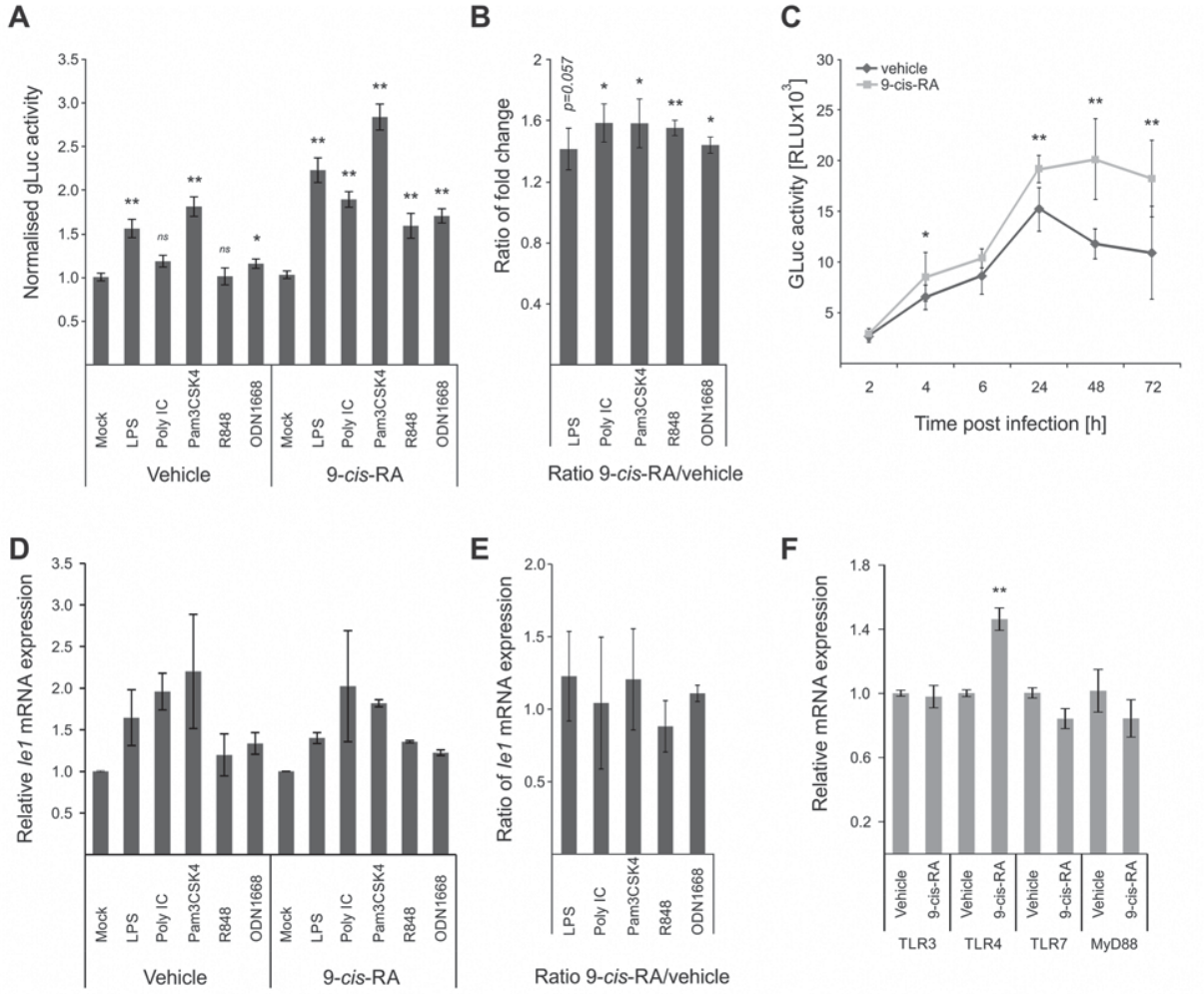

Fig 6. Retinoic acid pre-treatment increases effect of TLR ligands on IE-gene expression. A) Characterisation of the effects of 9-*cis* RA pre-treatment of BMDMs prior to TLR stimulation. Cells were pre-treated for 24 h before TLR stimulation and infection (MCMV-gLuc). Gluc activity was measured at 2 hpi and is shown relative to mock treated samples. Average of n = 32 with SEM is shown and asterisks indicate statistical significant changes over mock for each group (Wilcoxon test; * = p-value≤0.05; ** = p-value≤0.01, ns = not significant). B) Ratios of gLuc activities in 9-*cis* treated cultures over vehicle treated controls derived from data shown in panel A. Bars show averages of 4 independent experiments with SEM and asterisks indicate means that are statistical significant different from 1 as tested by a one-sample t-test versus a constant (* = p-value≤0.05; ** = p-value≤0.01). C) Time kinetic of gLuc activity in BMDMs after 9-*cis*-RA treatment without further TLR stimulation. BMDMs were pre-treated for 24 h with 9-*cis*-RA or vehicle and subsequently infected (MCMV-gLuc) and gLuc activity was measured at indicated time points. Data points represent averages (n = 8) with SEM. Asterisks indicate statistical significant differences between vehicle and 9-*cis*-RA treated cultures for each time point (Wilcoxon test; * = p-value≤0.05; ** = p-value≤0.01). D) Deletion of RA response elements (RARE) on the viral genome leads to a loss of the increased sensitivity for TLR stimulation triggered by 9-*cis*-RA. BMDMs were pre-treated with 9-*cis*-RA or vehicle before infection with a chimaeric hMCMV-ΔRARE mutant. At 4 hpi RNA was isolated and analysed by qPCR for *Ie1* expression (n = 2). E) Average of *Ie1* expression ratios of 9-*cis*-RA treated BMDMs over vehicle treated samples derived from data shown in panel D. F) 9-*cis*-RA treatment effects on expression on TLR signalling components. Expression of TLR 3, 4 and 7 and MyD88 were measured in RAW264.7 after 9-*cis*-RA treatment (n = 7, mean with SEM is shown). Asterisks indicate statistical differences in expression over vehicle (two sample Welch t-test; ** = p-value≤0.01).

doi:10.1371/journal.ppat.1004737.g006

enhanced sensitivity for TLR stimulation after RA treatment. However, the involvement of the enhancer RAREs is not mutually exclusive from an additional contribution involving an increase in TLR expression triggered by RA that has been implicated in other cell systems [79]. However, in experiments that measured *Myd88* and TLR expression in BMDMs after vehicle or 9-*cis*-RA treatment (Fig. 6F) we could only find a significant change in TLR4 alone, which

may explain the TLR4 synergistic effect in the presence of 9-*cis*-RA but not the general increase found for the other TLR-agonists.

Taken together we conclude that *9-cis*-RA can cooperatively enhance viral enhancer activity with TLR-signalling.

A MyD88-dependent pathway contributes to CMV enhancer activity

Our data show that all tested TLR ligands can boost viral enhancer activity and replication and consistent with this our functional network analysis identified MyD88 as a key hub. Therefore to further test and validate the results of the transient siRNA knockdowns in MEFs in our experimental BMDM system, we next treated BMDMs with a MyD88-inhibitor peptide at increasing concentrations before infection (Fig. 7A). These experiments showed that reporter gene activity was significantly inhibited in a dose dependent manner by the MyD88-inhibitor peptide but not by a scrambled control peptide. These results further corroborate the siRNA loss of function screens.

To unequivocally test the role of TLR-signalling and to establish the maximal impact of MyD88 on viral enhancer activity we next used BMDMs from genetic knockout animals (*Myd88*$^{-/-}$). Firstly, we characterised uptake of viral genomes for WT and *Myd88*$^{-/-}$ BMDMs by qPCR of intracellular viral genomes to eliminate the possibility that differential uptake causes differences in IE-gene expression (Fig. 7B) and found no reduction in the uptake of viral genomes in *Myd88*$^{-/-}$ cells. We next sought to confirm our results from the transient siRNA and peptide mediated inhibition in the genetic knockout system by infecting WT and *Myd88*$^{-/-}$ BMDMs with the gLuc reporter virus and measuring the reporter activity at 6 hpi. As shown in Fig. 7C (left panel) the loss of *Myd88* leads to a statistically significant (~70%) reduction of reporter activity. We also find a statistically significant reduction in endogenous *Ie1* gene expression levels as measured by qPCR under the same experimental conditions (Fig. 7C, right panel), excluding that this effect is an artefact of the reporter system. These experiments indicate that MyD88 is necessary for developing full levels of viral enhancer-activation upon infection.

Following this we further sought to determine how and to what extent the innate immune enhanced stimulation was specific and TLR-mediated. We compared the effects of a MyD88-dependent and MyD88-independent TLR ligand in WT and *Myd88*$^{-/-}$ BMDMs. As expected, stimulation of TLR3 by Poly IC significantly enhances viral IE-gene expression in both cell systems, while TLR2 activation by Pam3CSK4 increased viral IE-expression only in the WT but not in the MyD88-deficient cells (Fig. 7D).

Loss of MyD88 co-ordinately affects expression levels of both, viral and host innate immune gene expression

Our results indicate that the host innate immune genes and the viral enhancer are governed by common factors and react to common stimuli. The observation that MyD88 is central and is a shared signalling factor regulating viral and host gene expression, suggests that the loss of MyD88 would impact on the host innate immune genes in a similar way as on the viral IE gene expression. To compare the impact of MyD88 on host and viral gene expression directly, we measured the expression kinetics of *Tnf*, *Il6* and *Ifnb1* with the viral *Ie1* gene in the context of the infection of *Myd88*$^{-/-}$ and WT BMDMs. Fig. 7E shows the comparison for each of the tested genes between the cell systems. The expression levels of viral and host genes are reduced in *Myd88*$^{-/-}$ cells compared to levels in WT cells. This data further supports the notion that induction of viral and host gene expression are governed by common host factors and that their expression is largely, but not exclusively, governed by a MyD88-dependent signalling pathway. It

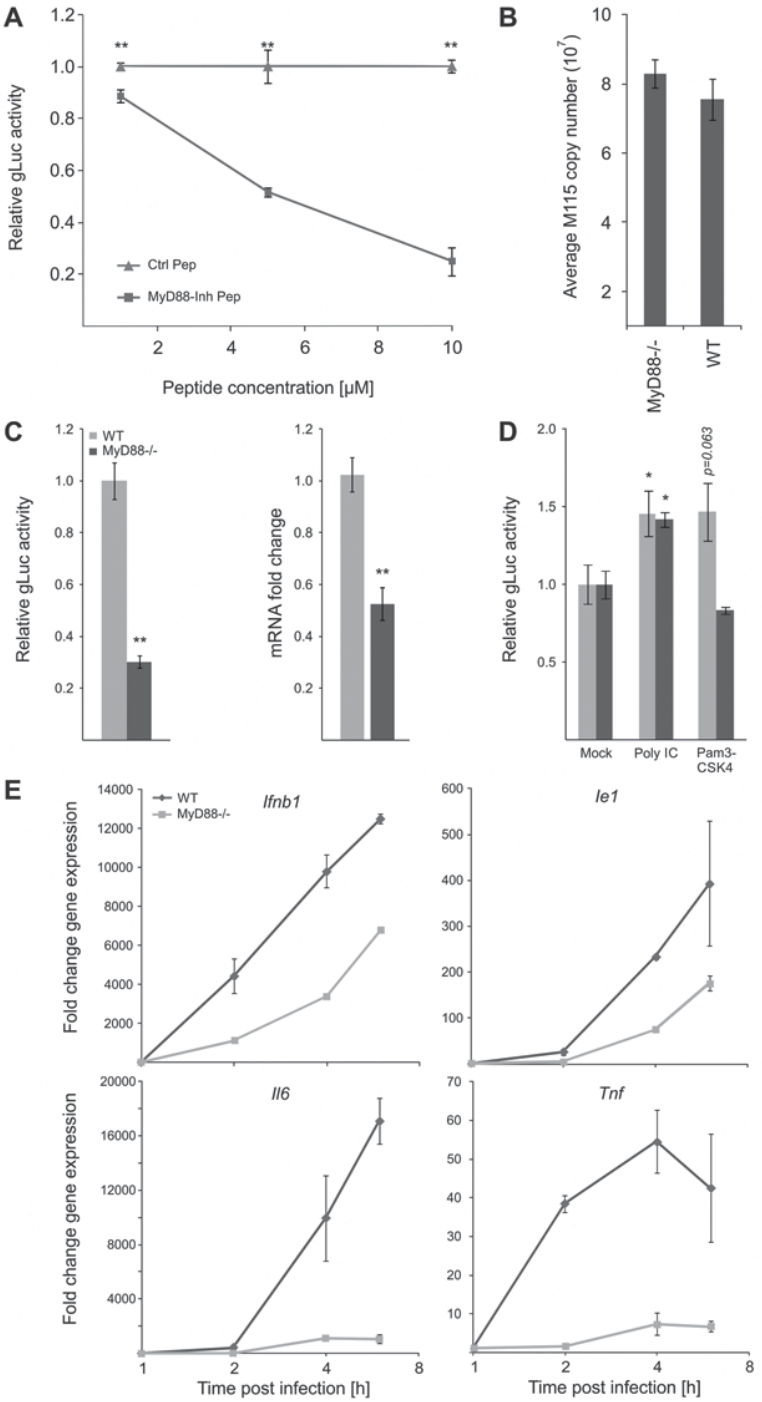

Fig 7. MyD88 governs MIEP activity. A) MyD88-specific inhibitor peptide reduces reporter gene expression compared to control peptide. MyD88 activity was inhibited in BMDMs by increasing concentration of a specific peptide inhibitor (MyD88-Inh Pep) prior to infection (MCMV-gLuc). Gluc activity was determined at 4 hpi and compared to the effects of a non-inhibiting control peptide (Ctrl Pep). Averages of normalised gLuc activity are shown (n = 6, with SEM). Asterisks indicate statistical differences in expression over vehicle (two sample Welch t-test; ** = p-value$\leq$0.01). B) Loss of MyD88-signalling does not inhibit uptake of viral genomes. BMDMs from WT or *Myd88*$^{-/-}$ mice were infected with MCMV-gLuc and the number of intracellular viral genomes was determined at 6 hpi by absolute qPCR (n = 3). C) BMDMs from genetic knockout mice show lower MIEP activity. WT and *Myd88*$^{-/-}$ BMDMs were infected with MCMV-gLuc and reporter gene

activity (left panel) and *Ie1* mRNA expression (right panel) was measured. Averages of normalised values f are shown with n = 15 (error bars show SEM) for gLuc activity and n = 7 for measurement of *Ie1* expression. Asterisks indicate statistical differences in expression over vehicle (Wilcoxon test; ** = p-value≤0.01). D) Induction of MIEP activity by TLR-agonists works through MYD88-dependent and—independent signalling. Stimulation with Poly IC (TLR3, MyD88-independent) is still capable to increase MIEP activity in *Myd88*$^{-/-}$ BMDMs while TLR2 stimulation (Pam3CSK4, MyD88-dependent) cannot increase MIEP activity in *Myd88*$^{-/-}$ cells. Averages of normalised gLuc activity are shown (n = 8, error bars show SEM) with asterisks indicating statistical differences over mock (Wilcoxon test; * = p-value≤0.05). E) Loss of Myd88 signalling reduces levels of viral Ie1 gene and host cytokine mRNA levels. Relative qPCR measurement of fold changes in expression levels for *Tnf*, *Il6*, *Ifnb1* and *Ie1* in WT and *Myd88*$^{-/-}$ BMDMs after infection (MCMV-gLuc). RNA was harvested at indicated time points from two infected cultures and measured in duplicates (n = 2). Expression levels were normalised to *Gapdh* and fold changes are relative to mock levels. *Il6* and *Ie1* did not show expression in mock samples so an arbitrary Ct value of 36 was chosen as reference point.

doi:10.1371/journal.ppat.1004737.g007

furthermore indicates that MyD88-dependent TLR signalling is necessary to achieve normal levels of IE-gene expression within the first 6 h post infection and shows that the boost in viral enhancer activity can be triggered by both, MyD88-dependent and -independent TLR signalling.

Requirement of immune-activated transcription factor binding to the enhancer for viral gene expression and growth

We next sought to characterise the role of key immune TLR-activated TFs for the virus and their contribution to viral replication. While we used Myd88$^{-/-}$ macrophages to test for the effects on IE-gene expression, the impaired production of anti-viral cytokines, such as IFNβ and TNFα (see Fig. 7E) in this system would also influence viral replication and thus mask the effects of impaired TLR-signalling. Therefore, in an attempt to avoid this issue and to test directly the role of immune activated TFs, we analysed the IE-gene expression and *in vitro* and *in vivo* replication of the hMCMV-Δ3 mutant, which lacks the binding motifs for the major inflammatory TLR-activated transcription factors NFκB, AP1 and ATF that are known to bind the CMV enhancer. While we do not exclude the activation of these TFs by other signalling pathways, infection of NIH3T3 fibroblasts that are known to be insensitive to TLR agonists [81] with a M45 deletion mutant shows no activation of NFκB [36]. The *Ie1* expression in hMCMV-Δ3 mutant (Fig. 8A) reflected the effects we observed in the Myd88$^{-/-}$ system (Fig. 7C, right panel), with a significant drop in *Ie1* expression compared to the hMCMV virus. To evaluate whether the enhancer point mutations affect viral growth we infected primary MEFs, the epithelial cell line C127I, RAW264.7 or primary BMDMs with the hMCMV and hMCMV-Δ3 viruses and measured production of viral progeny over 6 days (Fig. 8B). Notably, reduced levels of viral replication were detectable in multiple cells types. We next tested viral fitness of the two viruses *in vivo*. For these experiments neonatal BALB/c mice were intraperitoneally infected with either of the viruses and viral replication was monitored in the spleen, lungs, kidney and liver at day 4 and day 7 (Fig. 8C). In all tested organs and at both time points we found statistically significant reduction of infectious virus levels for the hMCMV-Δ3 mutant, indicating impaired viral fitness during an acute primary infection. Thus, while these experiments clearly show that the loss of the important immune regulated TFs NFκB, AP1 and ATF of the viral enhancer impacts on subsequent viral replication, *in vitro* and *in vivo*, we do not exclude contributions by other immune pathways, including possible activation by tegument proteins.

The IRF TF-network: New candidates for TLR-induced host factors driving CMV-enhancer activity

The main target of the TLR-MyD88 signalling axis besides NFκB, is the family of IRF transcription factors. In our screening experiment we identified IRF5 as a member of the high

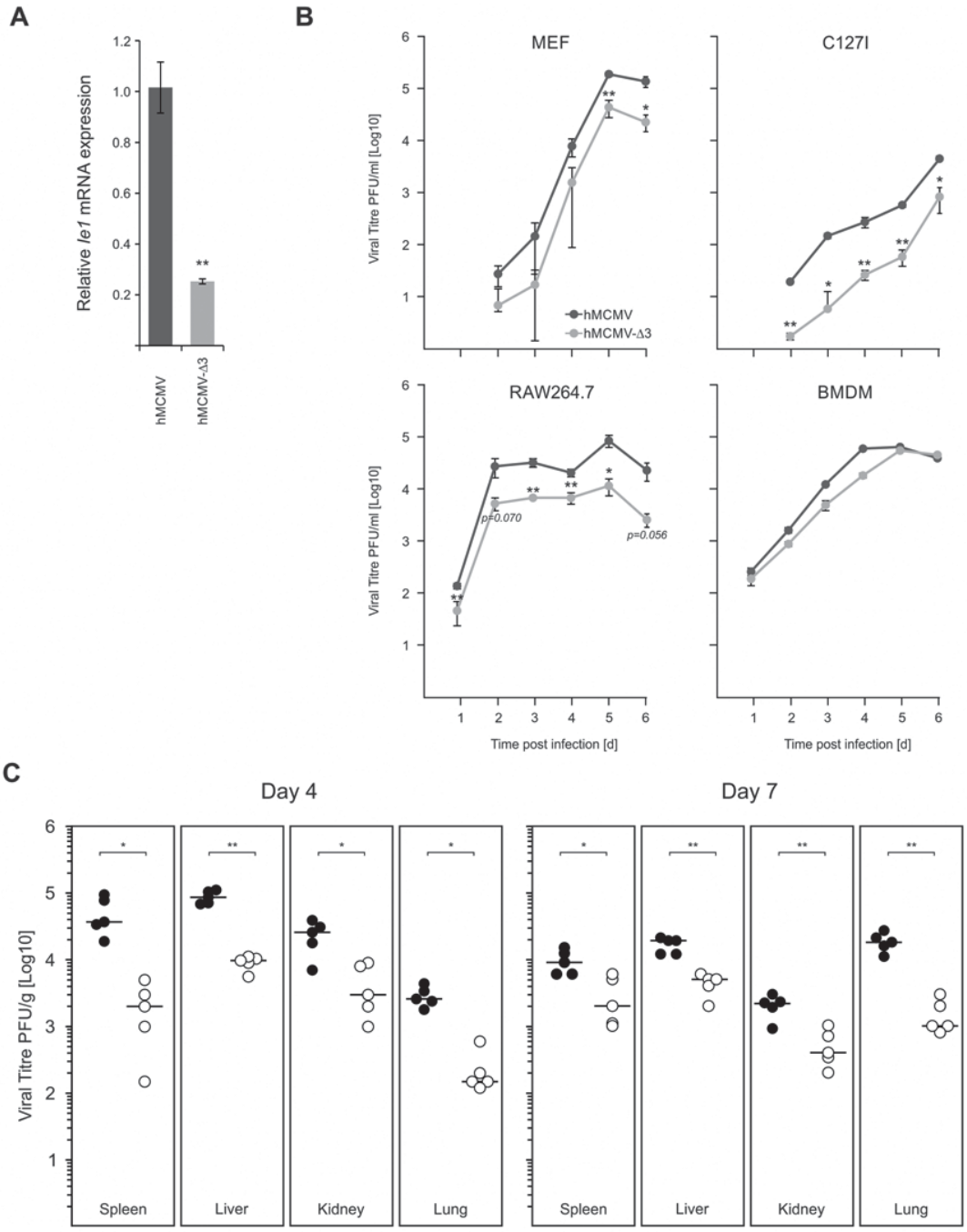

Fig 8. Loss of TLR-activated transcription factor binding motifs has impacts on viral replication and fitness. A) Comparison of viral IE-gene expression in hMCMV and hMCMV-Δ3 infected BMDMs (n = 4). Asterisks show statistical significant changes (two-sample Welch t-test; ** = p-value≤0.01). B) Comparison of in vitro replication of hMCMV and hMCMV-Δ3 virus in different cell types. Primary MEFs (MOI 0.025, n = 3), C127I (MOI = 0.025, n = 3), RAW264.7 (MOI 0.1, n = 3) or BMDMs (MOI = 2) were infected with either of the viruses and viral replication was measured by plaque assay at indicated time points on NIH3T3-Bam25 complementing cell line. Graphs show averages and error bars depict SEM. Asterisks show statistical significant changes (two-sample Welch t-test; * = p-value≤0.05, ** = p-value≤0.01). C) Comparison of viral fitness in neonate BALB/c mice. 3-day-old BALB/c females (n = 5) were i.p. inoculated with 5x104 PFU with either virus and sacrificed at indicated times post infection for plaque assay. Viral titres normalised per gram of tissue are shown (black circles = hMCMV; open circles = hMCMV-Δ3), with black bars showing median of groups. Asterisks indicate statistical significant differences between the two infected groups for each organ (two-sample Welch t-test; * = p-value≤0.05; ** = p-value≤0.01).

doi:10.1371/journal.ppat.1004737.g008

stringency pro-viral network connected to the MyD88-dependent TLR pathway (Fig. 4 and 5A). A comparison of all IRFs in our siRNA screens showed that loss of the factors IRF4, IRF5 and IRF6 reduced gLuc activity and of these candidates, IRF5 knockdown had the most significant and strongest effect (Fig. 5B). This was an unexpected observation since IRFs are usually associated with driving the expression of type I interferons and other cellular defence factors such as NO after viral infection [7,82–85]. Furthermore, the HCMV tegument protein pp65 has been indicated to inhibit IRF3 activation after HCMV infection [24,25]. Firstly, to verify the efficiency of our siRNA knockdown approach, we measured relative expression levels for the IRFs in the context of infection and found that the siRNA treatment was sufficient to completely abrogate the up-regulation of IRFs 3, 5 and 7 and partially abrogate the induction of *Irf1* (S9 A Fig).

Next we asked whether these factors could interact with the CMV enhancer, therefore we analysed the human CMV and murine CMV enhancer sequences for potential IRF binding sites. We used the JASPAR binding motif database [86] to scan the viral enhancer sequences and were able to identify two potential IRF binding sites in the murine CMV enhancer and five potential binding sites in the human CMV enhancer (Fig. 9A). The level of sequence identity, with the IRF consensus binding motif (5'-AANNGAAA-3'), was relatively low with ~70% for both tested CMV enhancers. Work on *Irf5* has been focused so far on lymphoid immune cells such as B-cells and DCs [87–89] and therefore we asked whether *Irf5* is expressed in MEFs and in monocytes (RAW264.7) and if the *Irf5* expression in these cell systems is inducible by infection with MCMV. This experiment shows that we could detect *Irf5* expression in MEFs and that the expression could be further induced by MCMV infection. In the monocytic cell line RAW264.7 we could also detect higher levels of *Irf5* mRNA after infection, although the effect of the infection was lower than in MEFs (Fig. 9B, compare with S9 B Fig). However, we found that the RAW264.7 samples produced lower Ct values in the qPCR assay than the MEF samples, indicating that RAW264.7 cells have higher base levels of *Irf5* expression (average Ct 28.18 vs Ct 22.82, respectively). The expression data shown in Fig. 1B clearly indicates that *Irf5* expression is also inducible in BMDMs. These experiments demonstrate that *Irf5* is expressed in MEFs, BMDMs and RAW264.7 cells and that expression can be further induced in all our experimental systems by infection. It is therefore conceivable that IRFs might play a role in the direct activation of viral IE-gene expression.

To directly test whether the IRF sites in the MCMV enhancer interact with their cognate factors in the context of infection we performed a chromatin immunoprecipitation (ChIP) experiment firstly under low stringency conditions (S10 A Fig) using antibodies against IRFs 1, 3, 5 and 7 to pull down DNA-IRF complexes formed in infected RAW264.7 cells after 24 hpi. Since it is well established that NFκB has several binding sites in the CMV enhancer, we used an antibody specific for the p65 (RelA) subunit of NFκB as a positive control and also included a polymerase II subunit (Pol II) specific antibody to pull down transcriptionally active complexes. As a positive control of the pull-down we checked, if the Pol II antibody was able to enrich the host gene *ActB* over the unspecific IgG background control. When we used a primer pair spanning the TATA-box of the viral *Ie1* gene to detect enrichment of viral sequences, we could detect different levels of enrichment with the Pol II (~1.5x) and IRF3 (~2.1x), IRF5 (~1.2x) and p65 (~5.7x) antibodies over IgG. While similar results were obtained in an independent experiment, we cannot rule out the possibility that IRF1 or 7 may also interact with the enhancer region.

To further independently test the specificity of the interactions for IRF3 and 5 we next used a two-tier approach. First, we increased the stringency conditions in the experiment to further reduce unspecific background in the IgG sample. As shown in Fig. 9C the higher stringency conditions did not abolish but further enhanced the enrichment with the antibodies for Pol II

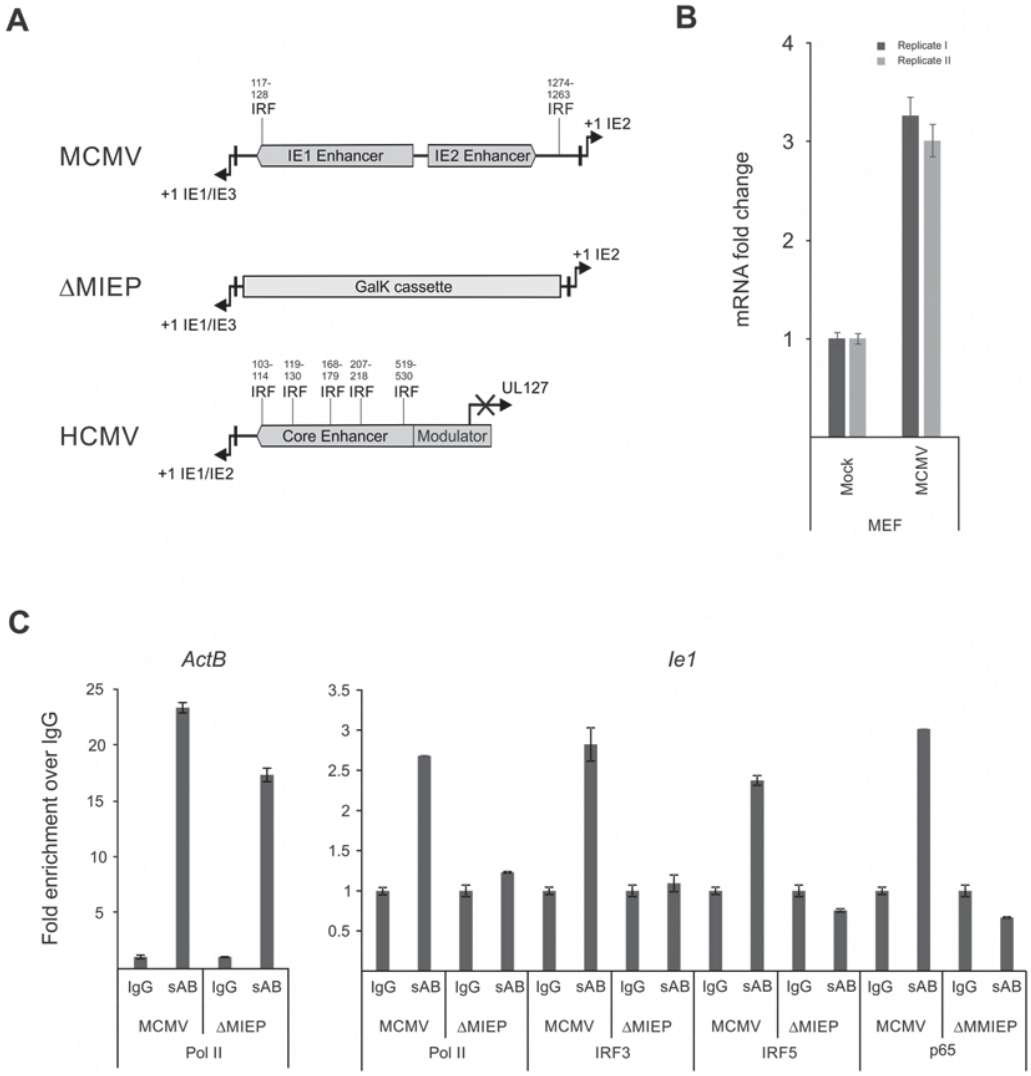

Fig 9. Family of IRF proteins represents new candidates for driving IE-gene expression. A) Sequence analysis of murine and human CMV enhancer regions shows potential IRF binding motifs with (~70% identity with canonical motif) at indicated bp positions (from +1 position of *Ie1/3* and *Ie1/2* respectively). Structure of the MIEP region in the MCMV-ΔMIEP recombinant is shown for comparison. B) *Irf5* is expressed in MEF cells. Relative qPCR data for *Irf5* expression, with mock-treated cells as calibrator. Cells were infected with MCMV for 6h before isolation of total RNA (n = 2) for qPCR. Samples were measured in technical replicates (n = 3, SEM). C) Representative ChIP experiment in infected RAW264.7 cells (MCMV, MOI 0.5, 24 hpi) with IgG as unspecific control and antibodies specific (sAB) for IRF3, IRF5, NFκB (p65) and RNA-polymerase II (Pol II), detecting the *ActB* and the viral MCMV enhancer (*Ie1*) by SYBRgreen qPCR measured in duplicates. Fold enrichment over IgG is shown and specificity was controlled by infection with the enhancer deletion mutant (ΔMIEP).

doi:10.1371/journal.ppat.1004737.g009

(~2.6x), p65 (~3x) and IRF3 (~2.8x) and IRF5 (~2.4x) over IgG for the viral sample. The enrichment of IRF3 and 5 was consistently observed in other independent experiments (S10 B Fig). As a functional positive control for the antibodies, we also measured enrichment of the established inflammatory and IRF-controlled genes *Cxcl10* and *Ifnb1* and we could detect enrichment with Pol II (~9x), IRF3 (~2x) and p65 (~3x) antibodies for *Cxcl10* but only minor enrichment for Pol II (~2x) and IRF3/p65 (~1.2x) for *Ifnb1*. Second, as an additional control for the specificity of the pull-downs, we used a mutant virus lacking the enhancer sequence (MCMV-ΔMIEP) to assess if a loss of the binding sites in the MIEP region of the viral genome

also leads to a loss of the enrichment in the ChIP experiment (Fig. 9C). The level of enrichment for the *ActB* control gene in the MCMV-ΔMIEP sample was lower than in the wild-type MCMV infection but overall similar. The pull-down with the Pol II control antibody produced a smaller enrichment of the viral MIEP sequence with the MCMV-ΔMIEP sample than in the MCMV infected sample, which corresponds well with the overall drop in gene expression in a MCMV-ΔMIEP recombinant [42]. When we compared the enrichment of viral MIEP sequence for the IRF5 or p65-binding antibodies we could not detect any enrichment (level less than IgG control), while we detected a minimal increase in the IRF3 sample. These data show that the observed enrichment was reproducible and specific, since loss of TF binding sites abolishes the interaction of the host factors with the viral sequence and therefore the enrichment in the ChIP experiment. Further studies will be required to more precisely define the role of IRFs in the regulation of the enhancer.

Taken together these data highlight the IRF protein family as representing a new group of host factors that target the MIEP within the first hours of infection. These factors are directly driven by TLR signalling and are involved in driving the expression of important anti-viral factors. Hence these results provide a direct molecular link outside NFκB for the co-option of the TLR signalling pathway and TF network by CMV and suggest a new strategy for CMV to stay ahead of the anti-viral response.

Discussion

The initial interactions between host and pathogen trigger PRR-signalling that lead to the production of inflammatory antiviral cytokines and innate immune effector molecules, such as type I interferons [2,90]. Activation of these inflammatory signalling pathways is therefore generally considered to be detrimental for the pathogen. To ensure successful initiation of viral gene expression and replication in the case of DNA nuclear viruses two main strategies are employed: 1) inhibition of the host signalling molecules and TFs to prevent initialisation of an anti-viral state or 2) co-opting the activated signalling molecules to ensure a rapid initiation of viral gene expression to stay ahead of the production of antiviral factors [91]. Of the central TFs activated by canonical TLR signalling pathways [47, 90], NFκB, AP1 and CREB/ATF are known to bind and regulate a wide range of viral enhancer/promoter sequences [47]. NFκB is a central inflammatory transcription factor that controls expression of innate immune genes [2,3,83,92] and is hijacked by several viruses (as reviewed in [93]). It has been shown that TLR8-mediated activation of NFκB is necessary for replication of HIV1 [94] and the human CMV and murine CMV [50,51,95–97]. However, when we assessed the contribution of these factors to the observed effects of TLR stimulation we found that the pro-viral effects were markedly reduced but not completely abolished. Therefore other TLR-activated TFs had to be involved in the observed phenotype. We used a siRNA screening approach to systematically investigate host factors. This loss-of-function screen indicated that the overlap in shared TFs is considerably more extensive than so far recognised, identifying novel potential interactions with host factors including several IRFs. In addition, knockdown of a SOX gene reduced viral gene expression. We initially included this gene family as a negative control since SOX genes are mainly associated with developmental genes [98,99]. However, a subsequent bioinformatics analysis [86] of the MCMV enhancer showed several potential binding sites for SOX proteins. Also notable is the presence of YY1 as a hit in this screen since YY1 so far is associated with inhibition of human CMV [100]. Furthermore, knockdown of STATs did not show an anti-viral effect in our system [101]. We also found retinoic acid receptor RAR-RXR to be part of the integrated TF network. While retinoids are known to directly regulate human and murine CMV enhancer activity [74,77], our results suggest both direct binding of RARE motifs on the viral

genome and possible indirect mechanisms including changes in TLR expression through retinoic acid [78,79] and possible alteration of NFκB binding kinetics to the viral enhancer [102].

We identified IRFs 4, 5 and 6 as potential novel pro-viral host factors. IRF4 is a lymphocyte specific factor [103] and the IRF6 gene is largely uncharacterised except for an association with van-der-Woude-syndrome [104]. We therefore focused on IRF5 as it also showed the strongest effects in our functional experiments. Since the first study characterising IRF5 [85] it has been associated with systemic lupus erythematosus [105] and plays an important role in controlling type I IFN expression [58,85,89]. It is a central component of the TLR7 signalling pathway [106] but also part of TLR3, 4 and 9 signalling and is therefore target of MyD88 and TRIF/TBK1-dependent TLR signalling [58]. Notably, in some cell systems IRF5 is directly activated by TRAF6, therefore forming a signalling bypass around the highly controlled and modulated NFκB pathway [87,107,108]. As a result of its role in controlling the IFN anti-viral response, IRF5 is blocked by Newcastle Disease Virus [109] and Epstein-Barr Virus [110]. Considering that we observed the knock-down of *Irf5* to have a strong effect in the enhancer screen, we tested if the CMV enhancer is capable of directly interacting with the activated IRF proteins by ChIP. We observed interactions of IRFs 3 and 5 with the viral enhancers that have not been previously documented, however other IRFs have been reported to interact with enhancers of HPV-16 [111], HBV [112] and HIV-1 [113]. Notably, it has recently been shown that IRF3, IRF5 and IRF7 co-ordinately regulate type I interferon production downstream of RIG-I [114], of which retinoic-acid induced gene-1 (RIG-I) and IRF3 and IRF5 are statistical significant hits in our enhancer activation screen, implying that other PRR signalling pathways might contribute to the initial activation of the viral enhancer. Further studies will be required to more fully characterise the IRF family interactions with the CMV enhancer. Nonetheless, the engagement of IRFs appears to be a general feature for a wide range of viral enhancers. However, in contrast to these other studies we delineate the time restricted dependency on TLR signalling that is exploited to the advantage of the virus.

Concordant with inflammatory signalling promoting infection, we observed comparable expression kinetics for the immune genes *Il6*, *Ifnb1* and *Tnf* in comparison with the viral gene *Ie1* with microarray experiments extending this finding to a larger class of known innate immune genes, although not all of the identified genes belong to the immediate early immune response class. These results indicate that the similarity in the expression kinetics of the host immediate response genes and the viral IE-genes is likely based on the same inflammatory mechanisms. This notion is further supported by the experiments in the genetic knockout system for the signalling adapter *Myd88* that equally affected cellular and viral gene expression.

While long term stimulation of TLR signalling is associated with inhibition of viral gene expression and replication, we found that short-term stimulation of the TLR signalling pathway, just prior to infection, can actually boost viral IE-gene expression. This indicates the existence of a temporal gate in which CMV can exploit TLR signalling before it initiates anti-viral effects (illustrated in Fig. 10). We have previously characterised the involvement of Type I interferon inhibition of the CMV enhancer in our macrophage system with IFNβ protein levels peaking by 6 hpi in BMDMs [64]. In the present study we define a temporal gate for TLRs 4 and 9, as being open for murine CMV to co-opt TLR-signalling with a positive effect within $\leq$ 6 hpi and a negative effect for >6 hpi, which correlates well with known timing of TLR signalling and the induction of TLR controlled gene expression in various systems [115–117] and the induction of ISGs by HCMV [118]. This indicates that a *naiive* macrophage needs optimally 6 h to establish a full anti-viral state after activation of TLR signalling.

We find that the TLR ligands had differential effects. In the BMDM system, only ligands for TLR2, TLR3 and TLR4 triggered an increase of IE-gene expression. In support of this finding it has been described before for human CMV that glycoprotein B on the viral particle surface can

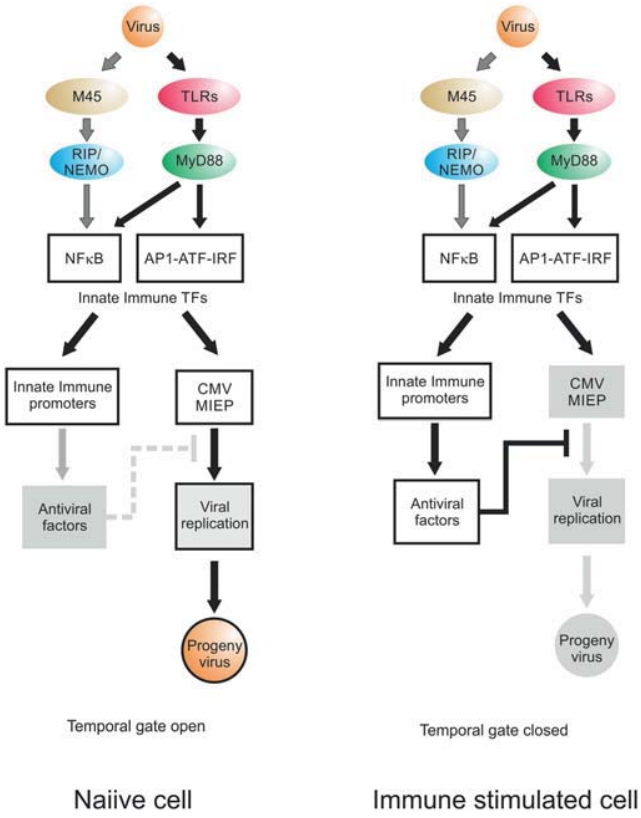

Fig 10. Temporal gate model. Virion delivered M45 and PRR signalling activate NFκB and other TFs downstream of TLRs, leading to transcription of innate immune effectors and viral IE-gene expression. Temporal gate open: In a *naiive* cell, viral infection triggers innate immune effector expression but at the same time drives viral gene expression. By the time host innate immune effectors are produced and can act on the viral IE-gene expression and replication, the virus already has progressed through this checkpoint of replication, produced viral inhibitors of innate immune signalling such as UL26, M27 or M45 and, using this lag-phase, escapes host control. Temporal gate closed: In a non-*naiive*, immune stimulated cell, the anti-viral effectors are already active at the point of infection and directly inhibit viral IE-gene expression. The viral gene expression cannot effectively progress beyond the IE-phase and the viral infection is controlled; the temporal gate is therefore closed.

doi:10.1371/journal.ppat.1004737.g010

bind to TLR2 and that the interaction with this receptor is sufficient to activate NFκB and to induce production of pro-inflammatory cytokines [12,13,92,119]. This interaction is conserved within Herpesviruses, since the gB protein of HSV1 can also interact with TLR2 and activates NFκB, via a MyD88/TRAF6 dependent signalling pathway [14,120]. This indicates that the gB-TLR2 interaction might be the result of evolutionary selective pressure, since this interaction has the most beneficial impact on CMV replication with the longest determined temporal gate, the weakest inhibition and the largest boost in progeny virus production.

Besides triggering of host PRR-signalling pathways by CMV leading to the activation of NFκB it has been recently demonstrated that the viral protein M45 mediates NFκB activation immediately after infection in NIH3T3 fibroblasts [36]. This finding is in contrast to the NFκB inhibitory function M45 has during the early and late phase of the infection at >5 hpi [34–36]. Notably, in macrophages and endothelial cells M45 is not essential for NFκB activation and IE1 protein levels. TLR agonist mediated stimulation of *Ie1* expression was not impaired in cells infected with M45 negative virions, showing that both ways of activating NFκB operate independently.

Taken together, our data show for the first time a direct dependency of the CMV enhancers on MyD88-dependent TLR-signalling to ensure the maximum expression of the essential IE-genes. We identified IRF3 and IRF5 as novel pro-viral factors within a specific temporal gate which shows that CMV is not limited to exploiting NFκB and that many innate immune TFs could contribute to viral IE-gene expression. This strategy allows the CMV expression program to stay ahead of the anti-viral state in the infected cell. We therefore propose a model (schematically shown in Fig. 10) incorporating a temporal component for infection of *naiive* cells, in which a CMV virion exploits the TLR response through the downstream transcription factors NFκB, AP1, CREB/ATF and IRFs, additionally to and independent from the activation of NFκB by virion delivered M45. These activated TFs then facilitate rapid viral IE-gene expression initiating the viral replication cycle before the cell can express any anti-viral effector molecules. By the time the cellular anti-viral factors (e.g. IFNβ) start to inhibit the viral IE-gene expression, the viral replication already progressed through this checkpoint, expresses viral modulators of signalling and the virus escapes host control. This is likely to be a common mechanism for a wide range of DNA viruses including retroviral enhancers such as those of HIV [47]. Since the exact composition of the activated TFs downstream of the TLR signalling pathway differs dependent on cell type, functional mimicry of a combination of host innate immune enhancers by viral enhancers in general would provide flexibility to harness activation of different innate immune related TFs in the context of different cell systems.

Materials and Methods

Cell preparation and culture

Primary mouse embryonic fibroblasts (MEFs) were prepared from C57/BL6 embryos at gestational age day 10–14 as described in [121]. Immortalized murine embryonic fibroblasts (MEF) used in the western blot experiments were provided by Edward Mocarski (Emory University, Atlanta, GA). MEFs were cultivated in MEM (Lonza) (+ 2 mM L-glutamine, 100 U Penicillin/Streptomycin (Pen/Strep) and 10% Fetal calf serum (FCS, Lonza) for 3 passages before being used for any experimental procedure. Bone marrow derived macrophages (BMDMs) were prepared from bone marrow of C57/BL6 mice and differentiated in DMEM F-12 GlutaMAX (Lonza) (+Pen/Strep, 10% L929 conditioned medium (contains Csf1) and 10% FCS) for 7 days. Efficiency of differentiation medium was analysed by FACS, testing for surface markers C11b and F480. MyD88$^{-/-}$ BMDMs were prepared from MyD88$^{-/-}$ homozygous knock-out animals [122] on C57/BL6 background, provided by the MacDonald group in the Institute of Immunology & Infection Research, University of Edinburgh, UK. C57BL/6 (BL6) mice were purchased from Charles River Laboratories (Kent, United Kingdom) and maintained under specific pathogen-free conditions at the University of Edinburgh. BALB/cOlaHsd mice were obtained from Harlan (Netherlands) and housed in the vivarium (University of Barcelona). All procedures were carried out under project and personal licences approved by the Secretary of State for the Home Office, under the United Kingdom's 1986 Animals (Scientific procedures) Act and the Local Ethical Review Committee at Edinburgh University and by the Ethics Committee (protocol number CEEA 308/12) of the University of Barcelona (Spain) and were conducted in compliance with institutional guidelines as well as with national (Generalitat de Catalunya decree 214/1997, DOGC 2450) and international (Guide for the Care and Use of Laboratory Animals, National Institutes of Health, 85–23, 1985) laws and policies. All cultures are routinely tested for mycoplasma and endotoxin levels.

IC-21 macrophages ATCC TIB-186), RAW264.7 (ATCC TIB-71), RAW264.7 for the western blot experiments (ATCC CRL-2278), C127I (ATCC CRL-1616) and NIH3T3 (ATCC CRL-1658) cells were obtained from the American Type Culture Collection (Manassas, VA)

and were cultivated in DMEM (Lonza) supplemented with 100 U Pen/strep and 2 mM L-glutamine and either 10% FCS (RAW264.7 and C127I cells) or 10% CS (NIH 3T3 cells). All cells were cultivated under standard tissue culture conditions. The Institute of Animal Breeding and Genetics, Department provided STAT1-/- fibroblasts for Biomedical Sciences, University of Veterinary Medicine Vienna, Austria.

Viral strains and infection procedures

Viral infections, growth procedures and plaque assays were carried out as described in [121,123]. In short, to infect cells volume of culture medium was reduced depending on the culture size and viral particles were added, pre-diluted in growth medium, to an MOI of 0.1 if not stated differently, followed by incubation for 1 h at 37°C for adsorption of viral particles. Cells were subsequently washed briefly 1x in medium after adsorption. To produce viral stocks NIH3T3 cells were infected at low MOI with a viral seed stock and subsequently infectious viral particles were harvested at day 4 for further concentration and titred by plaque assay.

Virus reconstituted from the bacterial artificial chromosome (BAC) pSM3fr was used as wild type MCMV [124]. The fluorescent MCMV-GFP reporter virus used for viral replication assay [125] has been described before. In this study we used a previously described viral mutant [36] lacking the entire M45 open reading frame (ORF) that was generated by *en passant* mutagenesis, here named MCMV-ΔM45. The viral gLuc-mutant MCMV-gLuc was constructed by homologous recombination [126] with a bacterial artificial chromosome (BAC) carrying the viral genome [124,127]. The mutation strategy is summarised in S1 Fig. In short, the reporter cassette containing the bicistronic ORF for the Gaussia luciferase (*gLuc*) and GFP genes and the kanamycin resistance gene was constructed by splice-PCR [128], including homologous sequences at the 5' and 3' ends to enable the replacement of the non-essential *Ie2* gene in the BAC by homologous recombination. The GFP gene was amplified using primers GFP-HOMO-FOR1: 5'-GACGGACCGCGGCTCGATACGACCCTATCTACGTTAACGA-**ATGGTGAGCAAGGGCGAGGA**-3' and GFP-P2A-REV3: 5'-CGGCCTGCTTCAG-GAGGCTGAAGTTCGTGGCTCCCGAGCC-**CTTGTACAGCTCGTCCATGC**-3' with viral DNA from strain MCMV-GFP as a template (bold stretches indicate primer sequence complementary to template sequence). The *gLuc* reporter gene and the kanamycin reporter gene were amplified using the primers P2A-FOR: 5'-CTCGGGAGCCACGAAC-3' and GLUC-HOMO-REV2: 5'-GAATAAAACCTCTTTATTTATTGATTAAAAACCATGACAT-**CGCCAAGC-TAAGCTTGGATC**-3' with the plasmid mCMV-mcherry-gLuc-kanamycin-puc19 [64] as a template. The two products of these reactions were then spliced together by using them as primers/template in the first 5 cycles in a splicing PCR [128]. After the first 5 cycles primers GFP-HOMO-FOR1 and GLUC-HOMO-REV2 were then added to the reaction for further 30 cycles to amplify the full-length cassette. The final product contained therefore 40bp stretches of sequence homologies to the viral BAC, allowing for targeted replacement of the viral *Ie2* gene by homologous recombination.

For construction of the enhancerless MCMV-ΔMIEP reporter virus, the viral enhancer sequence was replaced from transcription start of the *Ie1* gene to the transcription start point of the *Ie2* gene with the galactose kinase (GalK) ORF, allowing for selection by carbon source [129]. The GalK ORF was amplified using primers GALK-BAC-FOR: 5'-CGCCTCTTATACC-CACGTAGAACGCAGCTCAGCCAATA-**CCTGTTGACAATTAATCATCGG**-3' and GALK-BAC-REV: 5'-GCTTTTATATGGTTAACTCCGCCCGTTTTATGACTAGAAC-**TCAGCACTGTCCTGCTCCTT**-3' with the plasmid pGalK as a template molecule. Restriction digests with BamHI and EcoRI and PCR assessed successful recombination and integrity of the BAC and viral genome. The mutant MCMV-gLuc was reconstituted by transfection of

NIH3T3 cells with isolated BAC DNA and infectious particles were harvested and further propagated. For the MCMV-ΔMIEP virus the complementary cell line NIH3T3-Bam25 was used to allow for reconstitution and propagation of this growth deficient viral mutant as described before [54,125].

For the generation of hMCMV-ΔRARE and hMCMV-Δ3 mutants, the hMCMV-ES.RARE BAC and hMCMV-ESNFkB/Ap1/ATF BAC, respectively, were constructed by the two-step mutagenesis procedure as described in [50] using the MCMV pSM3fr BAC [124] and the shuttle plasmid pST76-AsacB.MIEP.RARE for the construction the hMCMV-ES.RARE BAC, and the MCMV enhancerless C3XdE [39] and the shuttle plasmid pST-ES.NFkB/Ap1/ATF for the construction of hMCMV-ESNFkB/Ap1/ATF BAC. Vector pST76-AsacB.MIEP.RARE carries the four RAR/RXR binding sites [76] present in the 613-bp HCMV enhancer region (from nt -52 to nt -667) disrupted by site directed mutagenesis. pST-ES.NFkB/Ap1/ATF contains the two AP-1 [69], the four NF-kB [50], and the five ATF/CREB binding sites within the 613-bp HCMV enhancer abolished by site directed mutagenesis (S5 Table). ATF/CREB binding sites disrupted in pST-ES.NFkB/Ap1/ATF were located at enhancer positions from -464 to -457, from -410 to -403, from -328 to -321, from -142 to -135, and from -66 to -59. The resulting BACs were transfected in NIH3T3 cells. Progeny virus obtained from the transfections were amplified, subjected to three rounds of plaque purification, and used for the preparation of viral stocks. The integrity of the viruses generated was confirmed by restriction enzyme analysis, and enhancer regions were sequenced.

Viral growth assays in neonate BALB/c mice

Three-day-old female BALB/cOlaHsd mice were inoculated intraperitoneally (i.p.) with 5x 10^4 PFU of tissue culture-propagated hMCMV or hMCMV-Δ3. At designated times after infection, mice were sacrificed, and specific organs were removed and harvested as a 10% (weight/volume) tissue homogenate. Tissue homogenates were sonicated and centrifuged, and viral titers from the supernatants were determined by standard plaque assays, including centrifugal enhancement of infectivity on MEFs.

TLR ligand pre-treatment

For stimulation of TLR-signalling, cells were incubated with 5 ng/ml LPS from *E.coli* 0111:B4 (Sigmal-Aldrich, L2630), 10 μg/ml Poly IC (Invivogen, Tlrl-pic), 100 nM Pam3CSK4 (Imgenex, Img2201), 100 nM R848 (Alexis, ALX-420-038-M005) or 100 nM ODN1668 (Invivogen, tlrl-1668) in cell culture medium for indicated pre-treatment times. After pre-treatment, cells were carefully washed with medium 1x and subsequently used for infections or other experiments.

9-*cis* pre-treatment

For pre-treatment with 9-*cis* retinoic acid (9-*cis* RA, Sigma-Aldrich UK) cells were incubated with 1 μM 9-*cis* RA for 24h before being used in subsequent experiments. Stock solution was 1 mM in DMSO and 9-*cis* RA working solution was prepared with medium immediately before use. 9-*cis* RA stock solutions was handled under reduced light conditions and stored at -80°C under Argon gas. A DMSO solution as a vehicle control was used with the corresponding dilution.

BAC-DNA transfection

MEFs were seeded in 48-well plates to reach ~90% confluency on the day of transfection. For transfection (per well) 250ng of BAC DNA and 0.75ul JET-PEI (PolyplusTransfection, Illkirch,

France) were used as described in supplier's instructions. DNA-transfection complexes were dripped onto cells and system was left for recovery o/n (16h) before experiments.

Viral entry assay

To measure entry of viral particles, BMDMs were seeded ($1x10^5$ cells/well) in 24 wells. The next day, cells were infected with MCMV (MOI = 0.5) for 1 hr. After adsorption, cells were washed 3x with medium, trypsinised for 5 min and scraped off the culture plates for lysis and DNA isolation. Viral genomes were measured by absolute qPCR of viral ORF M115. To establish effectiveness of Trypsin treatment, cells were infected as described above and subsequently either washed A) 4 times with PBS, or B) 1 time with PBS, tyrpsinised for 1 min, then washed twice with PBS, or C) 1 time with PBS, washed with citric acid buffer (40mM citric acid, 10mM KCL, 135mM NaCl) for 1 min, then washed twice with PBS. DNA was extracted using the Qiagen Qiaamp mini kit (51304) protocol and the copy number of the virus was determined by measuring M115.

Microarray data analysis

For Affymetrix Mouse Gene 1.0 ST Microarray analysis, data from study [130] was processed using the PARTEK software Package. In short, expression data was RMA normalised (quantile normalisation) and subsequently normalised per gene to average signal intensity over the time course (mean = 0.0, SD = 1.0). We then sorted the expression profiles for all genes by their similarity to a generated profile displayed by the genes in Fig. 1 A. The profile used showed no expression in the mock, rapid induction of expression within 2 h, a peak expression between 4 and 6 h and a drop in expression levels at 8 h. Gene expression profiles were sorted by similarity to this profile using a Bayesian statistical clustering function, identifying a large number of immune related genes in the cluster with the highest similarity including the selected 37 known innate immune genes used in this study.

Small molecule inhibitors

Gene knockdown by siRNAs. For transient siRNA mediated gene knock-down of host cells primary MEFs were reverse transfected with Dharmacon SMARTpools (Life Technologies) as described in manufacturers manual. In short, siRNAs were plated (final concentration of 25 nM or 2.5 nM) in siRNA buffer into 96-well tissue culture plates (Black plates clear bottom, Costar), and were then mixed with Dharmafect 1 transfection reagent (0.4% final concentration) diluted in OPTIMEM (Invitrogen). After incubation for 20 min at RT to allow formation of transfection complexes a cell suspension ($2x10^4$ cells/well) in antibiotic free medium was added. Cells were then incubated for 48 h after transfection to allow for protein depletion before being infected with either the GLuc-MCMV or the GFP-MCMV reporter viruses to assess IE-gene expression or viral replication respectively. Short interfering RNA duplexes designed to target the gLuc reporter (TCAAAGAAATGGAAGCCAA), the viral DNA polymerase M54 (AGAAAGACGACCTGAGCTA) or the viral major capsid protein M86 (CGACGGAGCTGCTGCCTAA) were designed using the Dharmacon siRNA design centre software and used as positive controls for gene knock-down and viral inhibition.

MyD88-inhibitory peptide. For transient inhibition of MyD88 protein function a 26aa (RQIKIWFQNRRMKWKK-RDVLPGTCVNS-NH2) inhibitory peptide (Pepinh-MYD) was used (Invivogen, tlrl-piMYD). The first domain of the peptide is a sequence that allows it to translocate through the cell membrane and the second domain (underlined in above sequence) binds and blocks the function of the TIR domain. As a control a peptide with a translocation sequence followed by a non-interacting domain was used (RQIKIWFQNRRMKWKK-SLHGRGDPMEAFII-NH2). For

inhibition of MyD88 activity, BMDMs were pre-treated with increasing amounts (1–50 μM) of the inhibitor or the control peptide for 6 h before using them for subsequent experiments.

Gaussia luciferase enzyme assay

The gaussia luciferase enzyme reporter assays were performed as described elsewhere [64]. In short, cells were infected with the reporter virus at MOI 0.1 if not stated differently (adsorption for 1h at 37°C) and then washed 2x with medium. Infected cells were then incubated for indicated time windows and complete culture supernatant was then repeatedly harvested. After each sampling time point cells were re-fed with fresh medium and further incubated as indicated in the respective experiments. To measure enzyme activity, 50μl of sample were mixed with 50μl fresh substrate working solution (20nM native coelenterazine in PBS + 5M NaCl) and light emission was measured using a POLARstar plate reader (BMG Labtech, Germany).

Immunoblotting

Viral titers were determined using the median tissue culture infective dose ($TCID_{50}$) method [131]. Infections were carried out with centrifugal enhancement (1,000 × g, 30 min). For infection kinetics, cells were grown in 12-well dishes, infected at an MOI of 10 $TCID_{50}$/cell, lysed in SDS-PAGE sample buffer, and subjected to SDS-PAGE and immunoblotting.

Antibodies. Monoclonal antibodies against M45 (M45.01 mAb, provided by Stipan Jonjic, University of Rijeka), IE1 (Chroma101; provided by Stipan Jonjic) and β-Actin (AC-74; Sigma) and polyclonal antibodies against IκBα (C-21; Santa Cruz) and M45 [132] (provided by David Lembo, University of Turin, Turin, Italy) were used.

Chromatin Immunoprecipitation (ChIP)

To analyse DNA-protein interactions RAW264.7 cells or primary MEFs, cells were infected at MOI 0.5 for 24 h before cells were used for chromatin immune-precipitation as described before [133,134]. In short, cells were fixed in 1% formaldehyde for 10 min (stopped with 0.125 M Glycine) and directly used for sonication of chromatin. Sonicated chromatin was aliquoted and stored at -80°C until used for pull-downs. For the immune-precipitation a mix of magnetic beads coated with protein A and G (Dynalbeads, Invitrogen) were coupled to 5μg primary antibody (per pull-down) and were used with 100 μg of chromatin o/n at 4°C to precipitate DNA-protein complexes. For low stringency runs, the precipitated complexes were washed 4x for 3 min at 4°C on a rotator with LiCl buffer (250mM) and 2x with Tris-EDTA (TE) to remove unbound chromatin. For high stringency washes, protocol was adjusted, considering procedures described in [135]. Complexes were pre-cleared by incubating them with uncoupled protein A/G Dynalbeads on a rotor for 1 h at 4°C before performing the immune-precipitation. For high stringency washes complexes were incubated 4x for 10 min at 4°C with LiCl buffer (500mM) and 2x with TE before reversing crosslinking and elution from beads. Used antibodies for ChIP experiments: IgG (Sant-Cruz, rabbit IgG sc-2027), Pol II (Abcam, 8WG RNAPII: Covance RNA Polymerase II 8WG16 Monoclonal- MMS-126R), NFκB (p65, AbCam, Ab7970), IRF1 (Bethyl, Rabbit A303-376A), IRF3 (Bethyl, Rabbit A303-383A, IRF5 (Bethyl, Rabbit A303-386A), IRF7 (Abcam, ab62505).

Eluted DNA was cleaned up using a Qiaquick PCR purification kit (Qiagen, 28104) and genes of interest were detected by qPCR using a Quanta PerfeCTa Sybrgreen Mix (95073) and primers detecting either ActB as a control gene or the CMV *Ie1* transcription start site (Enh1_L 5'-CGCCTCTTATACCCACGTAGA-3'; Enh1_R 5'-CACGTCAATGGGAAGTGAAA-3') with a relative standard curve produced from input DNA. To detect DNA of the ΔMIEP mutant the primers Enh1_L and dEnh_gLuc_R (5'-CTGCCTCCTGGGTTTAGTT-3')

were used. Quantities were measured relative to input DNA and enrichment of target sequences was calculated relative to the signal in the unspecific IgG-antibody pull-downs.

Quantitative real-time PCR

To measure relative gene expression from total cellular RNA we used FAM-labelled AB gene assays for host genes (Tnfa: Mm00443260_g1, *IL6*: Mm99999064_m1, Ifnb1: Mm00439546_s1) in duplex with a VIC-labelled GAPDH assay (Mm99999915_g1) for normalisation and the Quanta TOUGH-mix (Quanta, 95123) ready-to-use qPCR master mix. For detection of the viral *Ie1* gene expression we used a custom probe and primers described previously [136]. Expression levels were measured with a Stratagene Mx3000P qPCR machine (Agilent) and fold changes were determined by the ΔΔCt method using the MxPro software package.

For absolute quantification of viral genomes in infected cells or in culture supernatant, DNA was isolated using the Qiaamp mini kit (Qiagen, 51304) and subsequently used in absolute quantification by quantitative PCR. To quantify viral genomes we used a custom gene assay from AB (1166810B8) specifically designed to detect the viral M115 gene. A standard curve of a linearized plasmid carrying the M115 gene was used for absolute quantification as described previously [54,137].

Statistical meta-analysis

Meta-analysis of siRNA screens was performed to combine the results of multiple independent screens under similar biological conditions. Meta-analysis was applied separately for siRNA screens conducted with a GFP readout and for siRNA screens with a gLuc readout. The GFP data set comprises a total of 24 studies, where a study is defined as an independently performed siRNA screen on a 96-well plate containing multiple knockdown and control replicates. The gLuc data set comprises 10 studies. The number of within-study replicate knockdowns and controls (i.e. wells) differs from study to study and is detailed in S4 Table. For each study (screen on plate), the average fold change between each siRNA knock-down and the infected control was calculated, with average computed on the Log_2 scale and the fold change computed as difference = mean (siRNA)-mean (infected control). The robustness of the fold change estimates will depend on the presence and number of replicate measurements as shown in S4 Table. The fold change estimates are considered as the per study effect sizes. For each siRNA, these effect sizes are then combined across studies by an un-weighted median, and the standard error of this median estimated through b = 1000 bootstrap samples of the data for a given siRNA. For each siRNA, the significance of this median fold change is then tested by a two-sided location test (Wilcoxon Signed Rank Test) against the underlying Null hypothesis that the distribution of the fold change values is symmetrical around zero. The statistical power for each analysis will depend on the number of studies a given siRNA has been measured in (not all siRNAs are present in all screens). For the GFP set the overall n for siRNAs is 4, 6, 8, 10, 12, 18 or 24. For the gLuc overall n is 3, 4, 7 or 10. For each siRNA, the corresponding n is indicated in Fig. 5 by vertical bars along the x-axis. With results intended as an interest filter for further validation, p-values were not adjusted for multiple testing on these 184 siRNAs simultaneously. Differences in replicate number per study and number of studies available per siRNA suggest limited reliability of the meta-analysis outcomes and are therefore used as an interest filter in conjunction with corroborating evidence from subsequent validation experiments.

Statistical analysis

Inference testing for each experiment is applied in all cases where the number of independent biological replicates is 3 or higher. This consists of assessing underlying data distributions (Shapiro-Wilks test [138]), removing any objectively extreme outlier observations (Grubbs' test [139]) and subsequent retesting for the remaining data distribution. In experiments where no observation groups deviate from a normal distribution, 2-sample (or 1-sample where the comparison is to a constant value) Welch t tests were used to compare experiment groups. In experiments where one or more observation groups significantly deviate from a normal distribution, the non-parametric equivalent (Wilcoxon Rank Sum Test) was used to compare experiment groups. Note that all experiment figures show arithmetic means and standard errors of means, irrespective of the statistical test being parametric or non-parametric. The type of test performed and associated groups sizes are stated in each figure legend. All statistical analyses were performed with R [140].

STRING pathway analysis

For detection of networks in the screening data we used the STRING [71] online tool (v9.05, http://string-db.org). Hits were sorted by % of maximum knockdown effect (gLuc control siRNA = 100%) and cut-off levels of 25%, 50% and 75% of maximum effect were applied. List of gene names were then imported into STRING and identity of the factors manually checked. String association networks were built using standard settings (confidence networks) with thickness of edges representing confidence in direct interaction between network nodes. Enrichment function provided was then used to test for enrichment of GO terms (GO biological processes, using standard settings).

Supporting Information

S1 Fig. Mutagenesis strategy for construction of the MCMV-gLuc reporter virus (ΔIE2-GFP-gLuc-MCMV). The GFP gene and the gLuc expression cassette were amplified (PCR I) and fused together by splicing PCR (PCR II). The product containing a Kanamycin resistance gene was subsequently used to replace the *Ie2* gene in the viral BACmid pSM3fr, producing a virus in which the reporter genes are under direct transcriptional control by the viral major IE-enhancer/promoter (MIEP).
(TIF)

S2 Fig. Comparison of viral IE-gene and reporter gene expression during MCMV-gLuc infection. Expression kinetics of the viral *Ie1* gene and the *gLuc* reporter gene were compared by SYBRgreen qPCR detecting the respective mRNAs. Primary MEFs and BMDMs were infected (MCMV-gLuc) and RNA was isolated at indicated time points post infection (uninfected, 2, 4, 6 and 24 hpi). The *Ie1* and *gLuc* reporter genes are not detectable in the uninfected sample; therefore an arbitrary Ct value of 36 was set as a reference point.
(TIF)

S3 Fig. Differences in TLR expression between BMDM and RAW264.7. Expression levels of TLR3, TLR4 and TLR7 were compared between BMDMs (n = 3) and RAW264.7 cells (n = 2) by relative quantitative PCR.
(TIF)

S4 Fig. Effects of TLR ligands on viral entry. A) BMDMs were pre-treated with indicated TLR ligands for 15 min and subsequently infected (MCMV-gLuc). After adsorption cells were washed with medium and incubated for 6 h. At 6 hpi cells of three cultures were washed 3x

with medium, trypsinised for 5 min and scraped off the culture plates for lysis and DNA isolation. Numbers of intra-cellular viral genomes were measured by absolute qPCR (n = 3, SE). B) Comparison of effectiveness of treatment to remove extracellular virus. BMDMs (n = 4) were infected (MOI 0.5) as described in S4 A Fig and either washed with PBS alone or additionally treated with either trypsin or citric acid to remove extracellular virus. DNA was subsequently isolated and M115 copies measured by qPCR.
(TIF)

S5 Fig. TLR-agonists boost *Ie1* expression independent of tegument. A) RAW264.7 cells (24-well) were either mock treated or incubated with Pam3CSK4 (15 min) and subsequently infected with MCMV-ΔM45 (MOI = 1). *Ie1* expression was measured at 4 hpi (n = 3, mean fold change shown with SEM).
(TIF)

S6 Fig. String network for siRNA targets >50% of max. knock-down. The list of all target genes that were identified in the siRNA screen to have >50% of the maximum knockdown effect (medium stringency) was used to produce an interaction network using the STRING online tool.
(TIF)

S7 Fig. String network for siRNA targets >25% of max. knock-down. The list of all target genes that were identified in the siRNA screen to have >25% of the maximum knockdown effect (low stringency) was used to produce an interaction network using the STRING online tool.
(TIF)

S8 Fig. Comparison of Ie1 levels between hMCMV and hMCMV-ΔRARE. BMDMs were infected (MOI = 1) with either hMCMV or hMCMV-ΔRARE and total RNA was harvested 4h p.i. and *Ie1* levels were measured by qPCR (n = 2).
(TIF)

S9 Fig. Functional test of siRNA knockdown for IRFs and inducibility of IRF5 expression. A) MEFs were transfected either with control siRNA (RISC) or siRNAs targeting IRFs 1, 3, 5 or 7. Cells were subsequently infected with MCMV-gLuc and expression levels of IRF mRNAs were measured by relative qPCR and normalised to mock expression levels. B) IRF5 expression is inducible in RAW264.7 cells. IRF5 expression was measured by relative qPCR in infected cells (MCMV-gLuc) relative to mock samples.
(TIF)

S10 Fig. ChIP experiments. A) RAW264.7 cells were infected with MCMV (MOI 0.5, 24 hpi) and used for ChIP analysis, using antibodies for IRFs 1, 3, 5 and 7 for pull-downs in comparison to unspecific IgG. Pull-downs for NFκB and Pol II were used as positive controls. Enrichment of host gene (*ActB*) or viral gene (*Ie1*) sequences was detected by SYBR-green qPCR. B) Summary of all ChIP experiments (n = 3) irrespective of experimental conditions for sAB IRF3, IRF5, p65 and Pol ll. Data points show fold enrichment over IgG control for individual experiments.
(TIF)

S1 Table. Ranked lists of siRNA targets. List of siRNA targets sorted by their relative knockdown efficiency used to produce the STRING network graphs with the corresponding accession numbers. The three groups of stringency levels are indicated correspondingly.
(PDF)

S2 Table. Relative gLuc activities and knock-down effects. Relative gLuc-activities for all siRNA targets and controls relative to the RISCfree control siRNA and the corresponding percentage of their knockdown effects relative to the maximum effect of the *gaussia luciferase* control siRNA.
(PDF)

S3 Table. Ranked median activities of all siRNA targets for gLuc and GFP reporter assays. Ranked lists of all siRNA targets for GFP and gLuc reporter assays (compare to Fig. 5).
(PDF)

S4 Table. Distribution of Replicates per siRNA screen. List of replicates distribution per siRNA screen used for statistical Meta-analysis.
(PDF)

S5 Table. Sequence and position of NFκB/AP1/ATF binding motifs and point mutations. Positions of binding motifs in the human CMV enhancer are given relative to transcription start site of *Ie1*. Point mutations are shown and where applicable introduced endonuclease restriction sites are indicated by name of the enzyme.
(PDF)

Acknowledgments

We thank Paul Lacaze for providing microarray data and Paul Dickinson and Kostas Kostamanis for their support with analysing the microarray data. We would like to especially thank Andrew MacDonald and Lauren Webb for providing access to *Myd88*$^{-/-}$ mice and their help with the preparation of primary *Myd88*$^{-/-}$ BMDMs and Birgit Strobl for providing access to Stat1$^{-/-}$ MEFs. We thank Martin Messerle for help with the construction of the CMV recombinants and Eva Borst for support with BAC transfection experiments.

Author Contributions

Conceived and designed the experiments: KAK WB AA PG. Performed the experiments: KAK WYH EK. Analyzed the data: KAK TF AA PG. Wrote the paper: PG KAK.

References

1. Beutler B, Eidenschenk C, Crozat K, Imler JL, Takeuchi O, et al. (2007) Genetic analysis of resistance to viral infection. Nat Rev Immunol 7: 753–766. PMID: 17893693
2. Kumar H, Kawai T, Akira S (2011) Pathogen Recognition by the Innate Immune System. International Reviews of Immunology: Informa Clin Med. pp. 16–34.
3. Takeuchi O, Akira S (2010) Pattern recognition receptors and inflammation. Cell 140: 805–820. doi: 10.1016/j.cell.2010.01.022 PMID: 20303872
4. Kawai T, Akira S (2006) TLR signaling. Cell Death Differ 13: 816–825. PMID: 16410796
5. Kawai T, Akira S (2006) Innate immune recognition of viral infection. Nat Immunol 7: 131–137. PMID: 16424890
6. Hoebe K, Du X, Georgel P, Janssen E, Tabeta K, et al. (2003) Identification of Lps2 as a key transducer of MyD88-independent TIR signalling. Nature 424: 743–748. PMID: 12872135
7. Honda K, Takaoka A, Taniguchi T (2006) Type I interferon [corrected] gene induction by the interferon regulatory factor family of transcription factors. Immunity 25: 349–360. PMID: 16979567
8. Takaoka A, Yanai H (2006) Interferon signalling network in innate defence. Cell Microbiol 8: 907–922. PMID: 16681834
9. Yurochko AD, Huang ES (1999) Human cytomegalovirus binding to human monocytes induces immunoregulatory gene expression. J Immunol 162: 4806–4816. PMID: 10202024

10. Takeuchi O, Akira S (2007) Recognition of viruses by innate immunity. Immunol Rev 220: 214–224. PMID: 17979849
11. Barbalat R, Lau L, Locksley RM, Barton GM (2009) Toll-like receptor 2 on inflammatory monocytes induces type I interferon in response to viral but not bacterial ligands. Nat Immunol 10: 1200–1207. doi: 10.1038/ni.1792 PMID: 19801985
12. Compton T, Kurt-Jones EA, Boehme KW, Belko J, Latz E, et al. (2003) Human cytomegalovirus activates inflammatory cytokine responses via CD14 and Toll-like receptor 2. J Virol 77: 4588–4596. PMID: 12663765
13. Boehme KW, Guerrero M, Compton T (2006) Human cytomegalovirus envelope glycoproteins B and H are necessary for TLR2 activation in permissive cells. J Immunol 177: 7094–7102. PMID: 17082626
14. Leoni V, Gianni T, Salvioli S, Campadelli-Fiume G (2012) Herpes Simplex Virus Glycoproteins gH/gL and gB Bind Toll-Like Receptor 2, and Soluble gH/gL Is Sufficient To Activate NFκB. J Virol 86: 6555–6562. doi: 10.1128/JVI.00295-12 PMID: 22496225
15. Tabeta K, Georgel P, Janssen E, Du X, Hoebe K, et al. (2004) Toll-like receptors 9 and 3 as essential components of innate immune defense against mouse cytomegalovirus infection. Proc Natl Acad Sci USA 101: 3516–3521. PMID: 14993594
16. Szomolanyi-Tsuda E, Liang X, Welsh RM, Kurt-Jones EA, Finberg RW (2006) Role for TLR2 in NK cell-mediated control of murine cytomegalovirus in vivo. J Virol 80: 4286–4291. PMID: 16611887
17. DeFilippis VR, Alvarado D, Sali T, Rothenburg S, Fruh K (2010) Human cytomegalovirus induces the interferon response via the DNA sensor ZBP1. J Virol 84: 585–598. doi: 10.1128/JVI.01748-09 PMID: 19846511
18. Rathinam VA, Jiang Z, Waggoner SN, Sharma S, Cole LE, et al. (2010) The AIM2 inflammasome is essential for host defense against cytosolic bacteria and DNA viruses. Nat Immunol 11: 395–402. doi: 10.1038/ni.1864 PMID: 20351692
19. Bresnahan WA, Shenk T (2000) A Subset of Viral Transcripts Packaged Within Human Cytomegalovirus Particles. Science. pp. 2373–2376. PMID: 10875924
20. Vandevenne P, Sadzot-Delvaux C, Piette J (2010) Innate immune response and viral interference strategies developed by human herpesviruses. Biochem Pharmacol 80: 1955–1972. doi: 10.1016/j.bcp.2010.07.001 PMID: 20620129
21. Babic M, Krmpotic A, Jonjic S (2011) All is fair in virus-host interactions: NK cells and cytomegalovirus. Trends Mol Med 17: 677–685. doi: 10.1016/j.molmed.2011.07.003 PMID: 21852192
22. Jackson SE, Mason GM, Wills MR (2011) Human cytomegalovirus immunity and immune evasion. Virus Res 157: 151–160. doi: 10.1016/j.virusres.2010.10.031 PMID: 21056604
23. Lemmermann NA, Fink A, Podlech J, Ebert S, Wilhelmi V, et al. (2012) Murine cytomegalovirus immune evasion proteins operative in the MHC class I pathway of antigen processing and presentation: state of knowledge, revisions, and questions. Med Microbiol Immunol 201: 497–512. doi: 10.1007/s00430-012-0257-y PMID: 22961127
24. Browne EP, Shenk T (2003) Human cytomegalovirus UL83-coded pp65 virion protein inhibits antiviral gene expression in infected cells. Proc Natl Acad Sci U S A 100: 11439–11444. PMID: 12972646
25. Abate DA, Watanabe S, Mocarski ES (2004) Major Human Cytomegalovirus Structural Protein pp65 (ppUL83) Prevents Interferon Response Factor 3 Activation in the Interferon Response. J Virol 78: 10995–11006. PMID: 15452220
26. Taylor RT, Bresnahan WA (2005) Human cytomegalovirus immediate-early 2 gene expression blocks virus-induced beta interferon production. J Virol 79: 3873–3877. PMID: 15731283
27. Taylor RT, Bresnahan WA (2006) Human cytomegalovirus immediate-early 2 protein IE86 blocks virus-induced chemokine expression. J Virol 80: 920–928. PMID: 16378994
28. Miller DM, Zhang Y, Rahill BM, Waldman WJ, Sedmak DD (1999) Human Cytomegalovirus Inhibits IFN-α-Stimulated Antiviral and Immunoregulatory Responses by Blocking Multiple Levels of IFN-α Signal Transduction. J Immunol 162: 6107–6113. PMID: 10229853
29. Mathers C, Schafer X, Martinez-Sobrido L, Munger J (2014) The Human Cytomegalovirus UL26 Protein Antagonizes NF-kappaB Activation. J Virol 88: 14289–14300. doi: 10.1128/JVI.02552-14 PMID: 25275128
30. Le VT, Trilling M, Wilborn M, Hengel H, Zimmermann A (2008) Human cytomegalovirus interferes with signal transducer and activator of transcription (STAT) 2 protein stability and tyrosine phosphorylation. J Gen Virol 89: 2416–2426. doi: 10.1099/vir.0.2008/001669-0 PMID: 18796709
31. Le VT, Trilling M, Zimmermann A, Hengel H (2008) Mouse cytomegalovirus inhibits beta interferon (IFN-beta) gene expression and controls activation pathways of the IFN-beta enhanceosome. J Gen Virol 89: 1131–1141. doi: 10.1099/vir.0.83538-0 PMID: 18420790

32. Zimmermann A, Trilling M, Wagner M, Wilborn M, Bubic I, et al. (2005) A cytomegaloviral protein reveals a dual role for STAT2 in IFN-γ signaling and antiviral responses. J Ex Med 201: 1543–1553. PMID: 15883169

33. Doring M, Lessin I, Frenz T, Spanier J, Kessler A, et al. (2014) M27 expressed by cytomegalovirus counteracts effective type I interferon induction of myeloid cells but not of plasmacytoid dendritic cells. J Virol 88: 13638–13650. doi: 10.1128/JVI.00216-14 PMID: 25231302

34. Fliss PM, Jowers TP, Brinkmann MM, Holstermann B, Mack C, et al. (2012) Viral mediated redirection of NEMO/IKKgamma to autophagosomes curtails the inflammatory cascade. PLoS Pathog 8: e1002517. doi: 10.1371/journal.ppat.1002517 PMID: 22319449

35. Mack C, Sickmann A, Lembo D, Brune W (2008) Inhibition of proinflammatory and innate immune signaling pathways by a cytomegalovirus RIP1-interacting protein. Proc Natl Acad Sci U S A 105: 3094–3099. doi: 10.1073/pnas.0800168105 PMID: 18287053

36. Krause E, de Graaf M, Fliss PM, Dolken L, Brune W (2014) Murine cytomegalovirus virion-associated protein M45 mediates rapid NF-kappaB activation after infection. J Virol 88: 9963–9975. doi: 10.1128/JVI.00684-14 PMID: 24942588

37. Varnum SM, Streblow DN, Monroe ME, Smith P, Auberry KJ, et al. (2004) Identification of proteins in human cytomegalovirus (HCMV) particles: the HCMV proteome. J Virol 78: 10960–10966. PMID: 15452216

38. Angulo A, Messerle M, Koszinowski UH, Ghazal P (1998) Enhancer requirement for murine cytomegalovirus growth and genetic complementation by the human cytomegalovirus enhancer. J Virol 72: 8502–8509. PMID: 9765387

39. Ghazal P, Messerle M, Osborn K, Angulo A (2003) An essential role of the enhancer for murine cytomegalovirus in vivo growth and pathogenesis. J Virol 77: 3217–3228. PMID: 12584345

40. Meier JL, Stinski MF (2006) Major Immediate-Early Enhancer and its Geneproducts. In: Reddehase MJ, Lemmermann N, editors. Cytomegaloviruses: Molecular Biology and Immunity. 1 ed. Wymondham, Norfolk United Kingdom: Caister Academic Press. pp. 151–166.

41. Stinski MF, Isomura H (2008) Role of the cytomegalovirus major immediate early enhancer in acute infection and reactivation from latency. Med Microbiol Immunol 197: 223–231. PMID: 18097687

42. Podlech J, Pintea R, Kropp KA, Fink A, Lemmermann NAW, et al. (2010) Enhancerless Cytomegalovirus Is Capable of Establishing a Low-Level Maintenance Infection in Severely Immunodeficient Host Tissues but Fails in Exponential Growth. J Virol 84: 6254–6261. doi: 10.1128/JVI.00419-10 PMID: 20375164

43. Boshart M, Weber F, Jahn G, Dorsch-Hasler K, Fleckenstein B, et al. (1985) A very strong enhancer is located upstream of an immediate early gene of human cytomegalovirus. Cell 41: 521–530. PMID: 2985280

44. Dorsch-Häsler K, Keil GM, Weber F, Jasin M, Schaffner W, et al. (1985) A long and complex enhancer activates transcription of the gene coding for the highly abundant immediate early mRNA in murine cytomegalovirus. Proc Natl Acad Sci USA. pp. 8325–8329. PMID: 3001696

45. Ghazal P, Lubon H, Fleckenstein B, Hennighausen L (1987) Binding of transcription factors and creation of a large nucleoprotein complex on the human cytomegalovirus enhancer. Proc Natl Acad Sci U S A 84: 3658–3662. PMID: 3035545

46. Lee Y, Sohn WJ, Kim DS, Kwon HJ (2004) NF-KB and c-Jun-dependent regulation of human cytomegalovirus immediate-early gene enhancer/promoter in response to lipopolysaccharide and bacterial CpG-oligodeoxynucleotides in macrophage cell line RAW 264.7. Eur J Biochem 271: 1094–1105. PMID: 15009188

47. Kropp KA, Angulo A, Ghazal P (2014) Viral enhancer mimicry of host innate-immune promoters. PLoS Pathog 10: e1003804. doi: 10.1371/journal.ppat.1003804 PMID: 24516378

48. Iversen AC, Steinkjer B, Nilsen N, Bohnhorst J, Moen SH, et al. (2009) A proviral role for CpG in cytomegalovirus infection. J Immunol 182: 5672–5681. doi: 10.4049/jimmunol.0801268 PMID: 19380814

49. Mocarski ES (2002) Virus self-improvement through inflammation: No pain, no gain. Proc Natl Acad Sci USA 99: 3362–3364. PMID: 11904398

50. Benedict CA, Angulo A, Patterson G, Ha SW, Huang H, et al. (2004) Neutrality of the canonical NF-kappa B-dependent pathway for human and murine cytomegalovirus transcription and replication in vitro. J Virol 78: 741–750. PMID: 14694106

51. Gustems M, Borst E, Benedict CA, Perez C, Messerle M, et al. (2006) Regulation of the transcription and replication cycle of human cytomegalovirus is insensitive to genetic elimination of the cognate NF-kappa B binding sites in the enhancer. J Virol 80: 9899–9904. PMID: 16973595

52. Verhaegen M, Christopoulos TK (2002) Recombinant Gaussia luciferase. Overexpression, purification, and analytical application of a bioluminescent reporter for DNA hybridization. Anal Chem 74: 4378–4385. PMID: 12236345

53. Wurdinger T, Badr C, Pike L, de Kleine R, Weissleder R, et al. (2008) A secreted luciferase for ex vivo monitoring of in vivo processes. Nat Methods 5: 171–173. doi: 10.1038/nmeth.1177 PMID: 18204457

54. Lacaze P, Forster T, Ross A, Kerr LE, Salvo-Chirnside E, et al. (2011) Temporal profiling of the coding and noncoding murine cytomegalovirus transcriptomes. J Virol 85: 6065–6076. doi: 10.1128/JVI.02341-10 PMID: 21471238

55. Busche A, Angulo A, Kay-Jackson P, Ghazal P, Messerle M (2008) Phenotypes of major immediate-early gene mutants of mouse cytomegalovirus. Med Microbiol Immunol 197: 233–240. doi: 10.1007/s00430-008-0076-3 PMID: 18239940

56. Messerle M, Keil GM, Koszinowski UH (1991) Structure and expression of murine cytomegalovirus immediate-early gene 2. J Virol 65: 1638–1643. PMID: 1847480

57. Matsumoto M, Funami K, Tanabe M, Oshiumi H, Shingai M, et al. (2003) Subcellular localization of Toll-like receptor 3 in human dendritic cells. J Immunol 171: 3154–3162. PMID: 12960343

58. Paun A, Reinert JT, Jiang Z, Medin C, Balkhi MY, et al. (2008) Functional characterization of murine interferon regulatory factor 5 (IRF-5) and its role in the innate antiviral response. J Biol Chem 283: 14295–14308. doi: 10.1074/jbc.M800501200 PMID: 18332133

59. Vercammen E, Staal J, Beyaert R (2008) Sensing of viral infection and activation of innate immunity by toll-like receptor 3. Clin Microbiol Rev 21: 13–25. doi: 10.1128/CMR.00022-07 PMID: 18202435

60. Pohar J, Pirher N, Bencina M, Mancek-Keber M, Jerala R (2013) The role of UNC93B1 protein in surface localization of TLR3 receptor and in cell priming to nucleic acid agonists. J Biol Chem 288: 442–454. doi: 10.1074/jbc.M112.413922 PMID: 23166319

61. Gribaudo G, Ravaglia S, Caliendo A, Cavallo R, Gariglio M, et al. (1993) Interferons inhibit onset of murine cytomegalovirus immediate-early gene transcription. Virology 197: 303–311. PMID: 8212566

62. Landolfo S, Gribaudo G, Angeretti A, Gariglio M (1995) Mechanisms of viral inhibition by interferons. Pharmacol Ther 65: 415–442. PMID: 7544016

63. Dag F, Dolken L, Holzki J, Drabig A, Weingartner A, et al. (2014) Reversible silencing of cytomegalovirus genomes by type I interferon governs virus latency. PLoS Pathog 10: e1003962. doi: 10.1371/journal.ppat.1003962 PMID: 24586165

64. Kropp KA, Robertson KA, Sing G, Rodriguez-Martin S, Blanc M, et al. (2011) Reversible Inhibition of Murine Cytomegalovirus Replication by Gamma Interferon (IFN-γ) in Primary Macrophages Involves a Primed Type I IFN-Signaling Subnetwork for Full Establishment of an Immediate-Early Antiviral State. J Virol 85: 10286–10299. doi: 10.1128/JVI.00373-11 PMID: 21775459

65. Mocarski ESJ, Shenk T, Pass RF (2007) Cytomegaloviruses. In: Knipe DM, Howley PM, editors. Fields Virology. 5 ed. Philadelphia: Lippincott Williams & Wilkins. pp. 2701–2772. PMID: 18002552

66. Chang YN, Crawford S, Stall J, Rawlins DR, Jeang KT, et al. (1990) The palindromic series I repeats in the simian cytomegalovirus major immediate-early promoter behave as both strong basal enhancers and cyclic AMP response elements. J Virol 64: 264–277. PMID: 2152815

67. Keller MJ, Wu AW, Andrews JI, McGonagill PW, Tibesar EE, et al. (2007) Reversal of human cytomegalovirus major immediate-early enhancer/promoter silencing in quiescently infected cells via the cyclic AMP signaling pathway. J Virol 81: 6669–6681. PMID: 17301150

68. Lashmit P, Wang SH, Li HM, Isomura H, Stinski MF (2009) The CREB Site in the Proximal Enhancer Is Critical for Cooperative Interaction with the Other Transcription Factor Binding Sites To Enhance Transcription of the Major Intermediate-Early Genes in Human Cytomegalovirus-Infected Cells. J Virol 83: 8893–8904. doi: 10.1128/JVI.02239-08 PMID: 19553322

69. Isern E, Gustems M, Messerle M, Borst E, Ghazal P, et al. (2011) The Activator Protein 1 Binding Motifs within the Human Cytomegalovirus Major Immediate-Early Enhancer Are Functionally Redundant and Act in a Cooperative Manner with the NF-kappa B Sites during Acute Infection. J Virol 85: 1732–1746. doi: 10.1128/JVI.01713-10 PMID: 21106746

70. Isomura H, Stinski MF, Kudoh A, Daikoku T, Shirata N, et al. (2005) Two Sp1/Sp3 binding sites in the major immediate-early proximal enhancer of human cytomegalovirus have a significant role in viral replication. J Virol 79: 9597–9607. PMID: 16014922

71. Franceschini A, Szklarczyk D, Frankild S, Kuhn M, Simonovic M, et al. (2013) STRING v9.1: protein-protein interaction networks, with increased coverage and integration. Nucleic Acids Res 41: D808–815. doi: 10.1093/nar/gks1094 PMID: 23203871

72. Chan YJ, Chiou CJ, Huang Q, Hayward GS (1996) Synergistic interactions between overlapping binding sites for the serum response factor and ELK-1 proteins mediate both basal enhancement and phorbol ester responsiveness of primate cytomegalovirus major immediate-early promoters in monocyte and T-lymphocyte cell types. J Virol 70: 8590–8605. PMID: 8970984

73. Wright E, Bain M, Teague L, Murphy J, Sinclair J (2005) Ets-2 repressor factor recruits histone deacetylase to silence human cytomegalovirus immediate-early gene expression in non-permissive cells. J Gen Virol 86: 535–544. PMID: 15722512

74. Angulo A, Ghazal P (1995) Regulation of human cytomegalovirus by retinoic acid. Scandinavian journal of infectious diseases Supplementum 99: 113–115. PMID: 8668933

75. Angulo A, Suto C, Boehm MF, Heyman RA, Ghazal P (1995) Retinoid activation of retinoic acid receptors but not of retinoid X receptors promotes cellular differentiation and replication of human cytomegalovirus in embryonal cells. J Virol 69: 3831–3837. PMID: 7745731

76. Angulo A, Suto C, Heyman RA, Ghazal P (1996) Characterization of the sequences of the human cytomegalovirus enhancer that mediate differential regulation by natural and synthetic retinoids. Mol Endocrinol 10: 781–793. PMID: 8813719

77. Angulo A, Chandraratna RA, LeBlanc JF, Ghazal P (1998) Ligand induction of retinoic acid receptors alters an acute infection by murine cytomegalovirus. J Virol 72: 4589–4600. PMID: 9573222

78. Liu PT, Krutzik SR, Kim J, Modlin RL (2005) Cutting edge: all-trans retinoic acid down-regulates TLR2 expression and function. J Immunol 174: 2467–2470. PMID: 15728448

79. Bernardo AR, Cosgaya JM, Aranda A, Jimenez-Lara AM (2013) Synergy between RA and TLR3 promotes type I IFN-dependent apoptosis through upregulation of TRAIL pathway in breast cancer cells. Cell Death & Disease 4: e479.

80. Sussman F, de Lera AR (2005) Ligand recognition by RAR and RXR receptors: binding and selectivity. J Med Chem 48: 6212–6219. PMID: 16190748

81. Burger-Kentischer A, Abele IS, Finkelmeier D, Wiesmuller KH, Rupp S (2010) A new cell-based innate immune receptor assay for the examination of receptor activity, ligand specificity, signalling pathways and the detection of pyrogens. J Immunol Methods 358: 93–103. doi: 10.1016/j.jim.2010.03.020 PMID: 20385141

82. Hiscott J (2007) Triggering the innate antiviral response through IRF-3 activation. J Biol Chem 282: 15325–15329. PMID: 17395583

83. Honda K, Yanai H, Takaoka A, Taniguchi T (2005) Regulation of the type I IFN induction: a current view. Int Immunol 17: 1367–1378. PMID: 16214811

84. Kamijo R, Harada H, Matsuyama T, Bosland M, Gerecitano J, et al. (1994) Requirement for Transcription Factor Irf-1 in No Synthase Induction in Macrophages. Science 263: 1612–1615. PMID: 7510419

85. Barnes BJ, Moore PA, Pitha PM (2001) Virus-specific activation of a novel interferon regulatory factor, IRF-5, results in the induction of distinct interferon alpha genes. J Biol Chem 276: 23382–23390. PMID: 11303025

86. Bryne JC, Valen E, Tang MH, Marstrand T, Winther O, et al. (2008) JASPAR, the open access database of transcription factor-binding profiles: new content and tools in the 2008 update. Nucleic Acids Res 36: D102–106. PMID: 18006571

87. Takaoka A, Yanai H, Kondo S, Duncan G, Negishi H, et al. (2005) Integral role of IRF-5 in the gene induction programme activated by Toll-like receptors. Nature 434: 243–249. PMID: 15665823

88. Yasuda K, Richez C, Maciaszek JW, Agrawal N, Akira S, et al. (2007) Murine Dendritic Cell Type I IFN Production Induced by Human IgG-RNA Immune Complexes Is IFN Regulatory Factor (IRF)5 and IRF7 Dependent and Is Required for IL-6 Production. J Immunol 178: 6876–6885. PMID: 17513736

89. Barnes BJ, Richards J, Mancl M, Hanash S, Beretta L, et al. (2004) Global and distinct targets of IRF-5 and IRF-7 during innate response to viral infection. J Biol Chem 279: 45194–45207. PMID: 15308637

90. O'Neill LA, Golenbock D, Bowie AG (2013) The history of Toll-like receptors—redefining innate immunity. Nat Rev Immunol 13: 453–460. doi: 10.1038/nri3446 PMID: 23681101

91. Amsler L, Verweij MC, DeFilippis VR (2013) The tiers and dimensions of evasion of the type I interferon response by human cytomegalovirus. J Mol Biol 425: 4857–4871. doi: 10.1016/j.jmb.2013.08.023 PMID: 24013068

92. Boehme KW, Compton T (2006) Virus Entry and Activation of Innate Immunity. In: Reddehase MJ, Lemmermann N, editors. Cytomegaloviruses: Molecular Biology and Immunity. 1 ed. Norfolk, UK: Caister Academic Press. pp. 111–130.

93. Santoro MG, Rossi A, Amici C (2003) NF-kappaB and virus infection: who controls whom. EMBO J 22: 2552–2560. PMID: 12773372

94. Gringhuis SI, van der Vlist M, van den Berg LM, den Dunnen J, Litjens M, et al. (2010) HIV-1 exploits innate signaling by TLR8 and DC-SIGN for productive infection of dendritic cells. Nat Immunol 11: 419–426. doi: 10.1038/ni.1858 PMID: 20364151

95. DeMeritt IB, Milford LE, Yurochko AD (2004) Activation of the NF-kappa B pathway in human cytomegalovirus-infected cells is necessary for efficient transactivation of the major immediate-early promoter. J Virol 78: 4498–4507. PMID: 15078930

96. DeMeritt IB, Podduturi JP, Tilley AM, Nogalski MT, Yurochko AD (2006) Prolonged activation of NF-kappaB by human cytomegalovirus promotes efficient viral replication and late gene expression. Virology 346: 15–31. PMID: 16303162

97. Caposio P, Luganini A, Bronzini M, Landolfo S, Gribaudo G (2010) The Elk-1 and Serum Response Factor Binding Sites in the Major Immediate-Early Promoter of Human Cytomegalovirus Are Required for Efficient Viral Replication in Quiescent Cells and Compensate for Inactivation of the NF-κB Sites in Proliferating Cells. J Virol 84: 4481–4493. doi: 10.1128/JVI.02141-09 PMID: 20147408

98. Pevny LH, LovellBadge R (1997) Sox genes find their feet. Current Opinion in Genetics & Development 7: 338–344.

99. Jiang T, Hou CC, She ZY, Yang WX (2013) The SOX gene family: function and regulation in testis determination and male fertility maintenance. Mol Biol Rep 40: 2187–2194. doi: 10.1007/s11033-012-2279-3 PMID: 23184044

100. Liu R, Baillie J, Sissons JGP, Sinclair JH (1994) The transcription factor YY1 binds to negative regulatory elements in the human cytomegalovirus major immediate early enhancer/promoter and mediates repression in nonpermissive cells. Nucleic Acids Research 22: 2453–2459. PMID: 8041605

101. Netterwald J, Yang S, Wang W, Ghanny S, Cody M, et al. (2005) Two gamma interferon-activated site-like elements in the human cytomegalovirus major immediate-early promoter/enhancer are important for viral replication. J Virol 79: 5035–5046. PMID: 15795289

102. de Martin R (1996) Synergistic Activation of Interleukin-8 Gene Transcription by All-trans-retinoic Acid and Tumor Necrosis Factor-alpha Involves the Transcription Factor NF-kappa B. J Biol Chem 271: 26954–26961. PMID: 8900181

103. Grossman A, Mittrucker HW, Nicholl J, Suzuki A, Chung S, et al. (1996) Cloning of human lymphocyte-specific interferon regulatory factor (hLSIRF/hIRF4) and mapping of the gene to 6p23-p25. Genomics 37: 229–233. PMID: 8921401

104. Kondo S, Schutte BC, Richardson RJ, Bjork BC, Knight AS, et al. (2002) Mutations in IRF6 cause Van der Woude and popliteal pterygium syndromes. Nat Genet 32: 285–289. PMID: 12219090

105. Xu WD, Pan HF, Xu Y, Ye DQ (2013) Interferon regulatory factor 5 and autoimmune lupus. Expert Rev Mol Med 15: e6. doi: 10.1017/erm.2013.7 PMID: 23883595

106. Schoenemeyer A, Barnes BJ, Mancl ME, Latz E, Goutagny N, et al. (2005) The interferon regulatory factor, IRF5, is a central mediator of toll-like receptor 7 signaling. J Biol Chem 280: 17005–17012. PMID: 15695821

107. Kawai T, Akira S (2010) The role of pattern-recognition receptors in innate immunity: update on Toll-like receptors. Nat Immunol 11: 373–384. doi: 10.1038/ni.1863 PMID: 20404851

108. Akira S, Uematsu S, Takeuchi O (2006) Pathogen recognition and innate immunity. Cell 124: 783–801. PMID: 16497588

109. Barro M, Patton JT (2007) Rotavirus NSP1 inhibits expression of type I interferon by antagonizing the function of interferon regulatory factors IRF3, IRF5, and IRF7. J Virol 81: 4473–4481. PMID: 17301153

110. Martin HJ, Lee JM, Walls D, Hayward SD (2007) Manipulation of the toll-like receptor 7 signaling pathway by Epstein-Barr virus. J Virol 81: 9748–9758. PMID: 17609264

111. Arany I, Grattendick KJ, Whitehead WE, Ember IA, Tyring SK (2003) A functional interferon regulatory factor-1 (IRF-1)-binding site in the upstream regulatory region (URR) of human papillomavirus type 16. Virology 310: 280–286. PMID: 12781715

112. Alcantara FF, Tang H, McLachlan A (2002) Functional characterization of the interferon regulatory element in the enhancer 1 region of the hepatitis B virus genome. Nucleic Acids Res 30: 2068–2075. PMID: 11972347

113. Sgarbanti M, Remoli AL, Marsili G, Ridolfi B, Borsetti A, et al. (2008) IRF-1 is required for full NF-kappaB transcriptional activity at the human immunodeficiency virus type 1 long terminal repeat enhancer. J Virol 82: 3632–3641. doi: 10.1128/JVI.00599-07 PMID: 18216101

114. Lazear HM, Lancaster A, Wilkins C, Suthar MS, Huang A, et al. (2013) IRF-3, IRF-5, and IRF-7 coordinately regulate the type I IFN response in myeloid dendritic cells downstream of MAVS signaling. PLoS Pathog 9: e1003118. doi: 10.1371/journal.ppat.1003118 PMID: 23300459

115. Ramsey SA, Klemm SL, Zak DE, Kennedy KA, Thorsson V, et al. (2008) Uncovering a macrophage transcriptional program by integrating evidence from motif scanning and expression dynamics. PLoS Comput Biol 4: e1000021. doi: 10.1371/journal.pcbi.1000021 PMID: 18369420

116. Suet Ting Tan R, Lin B, Liu Q, Tucker-Kellogg L, Ho B, et al. (2013) The synergy in cytokine production through MyD88-TRIF pathways is co-ordinated with ERK phosphorylation in macrophages. Immunol Cell Biol 91: 377–387. doi: 10.1038/icb.2013.13 PMID: 23567895

117. Kobayashi K, Inohara N, Hernandez LD, Galan JE, Nunez G, et al. (2002) RICK/Rip2/CARDIAK mediates signalling for receptors of the innate and adaptive immune systems. Nature 416: 194–199. PMID: 11894098

118. Simmen KA, Singh J, Luukkonen BG, Lopper M, Bittner A, et al. (2001) Global modulation of cellular transcription by human cytomegalovirus is initiated by viral glycoprotein B. Proc Natl Acad Sci U S A 98: 7140–7145. PMID: 11390970

119. Boyle KA, Pietropaolo RL, Compton T (1999) Engagement of the cellular receptor for glycoprotein B of human cytomegalovirus activates the interferon-responsive pathway. Mol Cell Biol 19: 3607–3613. PMID: 10207084

120. Cai M, Li M, Wang K, Wang S, Lu Q, et al. (2013) The herpes simplex virus 1-encoded envelope glycoprotein B activates NF-kappaB through the Toll-like receptor 2 and MyD88/TRAF6-dependent signaling pathway. PLoS One 8: e54586. doi: 10.1371/journal.pone.0054586 PMID: 23382920

121. Lemmermann NAW, Podlech J, Seckert CK, Kropp KA, Grzimek NKA, et al. (2010) CD8 T-Cell Immunotherapy of Cytomegalovirus Disease in the Murine Model. In: Stefan DKa, editor. Immunology of Infection. Volume 37 ed: Academic Press. pp. 369–420.

122. Adachi O, Kawai T, Takeda K, Matsumoto M, Tsutsui H, et al. (1998) Targeted disruption of the MyD88 gene results in loss of IL-1- and IL-18-mediated function. Immunity 9: 143–150. PMID: 9697844

123. Podlech J, Holtappels R, Grzimek NKA, Reddehase MJ (2002) Animal models: Murine cytomegalovirus. Method Microbiol 32: 493–525.

124. Wagner M, Jonjic S, Koszinowski UH, Messerle M (1999) Systematic excision of vector sequences from the BAC-cloned herpesvirus genome during virus reconstitution. J Virol 73: 7056–7060. PMID: 10400809

125. Angulo A, Ghazal P, Messerle M (2000) The major immediate-early gene ie3 of mouse cytomegalovirus is essential for viral growth. J Virol 74: 11129–11136. PMID: 11070009

126. Lee EC, Yu D, Martinez de Velasco J, Tessarollo L, Swing DA, et al. (2001) A highly efficient Escherichia coli-based chromosome engineering system adapted for recombinogenic targeting and subcloning of BAC DNA. Genomics 73: 56–65. PMID: 11352566

127. Messerle M, Crnkovic I, Hammerschmidt W, Ziegler H, Koszinowski UH (1997) Cloning and mutagenesis of a herpesvirus genome as an infectious bacterial artificial chromosome. Proc Natl Acad Sci USA 94: 14759–14763. PMID: 9405686

128. Heckman KL, Pease LR (2007) Gene splicing and mutagenesis by PCR-driven overlap extension. Nature protocols 2: 924–932. PMID: 17446874

129. Warming S, Costantino N (2005) Simple and highly efficient BAC recombineering using galK selection. Nucleic Acids Research 33: 1–12. PMID: 15640442

130. Lacaze PA (2011) Systems analysis of the dynamic macrophage response to productive and non-productive murine cytomegalovirus infection [Doctoral]. Edinburgh: University of Edinburgh.

131. Mahy BW, Kangro HO (1996) Virology methods manual: Academic Press London, UK.

132. Lembo D, Donalisio M, Hofer A, Cornaglia M, Brune W, et al. (2004) The Ribonucleotide Reductase R1 Homolog of Murine Cytomegalovirus Is Not a Functional Enzyme Subunit but Is Required for Pathogenesis. J Virol 78: 4278–4288. PMID: 15047841

133. Johnson DS, Mortazavi A, Myers RM, Wold B (2007) Genome-wide mapping of in vivo protein-DNA interactions. Science 316: 1497–1502. PMID: 17540862

134. Pradeepa MM, Sutherland HG, Ule J, Grimes GR, Bickmore WA (2012) Psip1/Ledgf p52 binds methylated histone H3K36 and splicing factors and contributes to the regulation of alternative splicing. PLoS Genet 8: e1002717. doi: 10.1371/journal.pgen.1002717 PMID: 22615581

135. Carey MF, Peterson CL, Smale ST (2009) Chromatin immunoprecipitation (ChIP). Cold Spring Harb Protoc 2009: pdb prot5279. doi: 10.1101/pdb.prot5279 PMID: 20147264

136. Simon CO, Kuhnapfel B, Reddehase MJ, Grzimek NKA (2007) Murine cytomegalovirus major immediate-early enhancer region operating as a genetic switch in bidirectional gene pair transcription. J Virol 81: 7805–7810. PMID: 17494084

137. Simon CO, Seckert CK, Dreis D, Reddehase MJ, Grzimek NK (2005) Role for tumor necrosis factor alpha in murine cytomegalovirus transcriptional reactivation in latently infected lungs. J Virol 79: 326–340. PMID: 15596827

138. Royston J (1982) An extension of Shapiro and Wilk's W test for normality to large samples. Applied Statistics 31: 115–124.

139. Grubbs FE (1950) Sample Criteria for Testing Outlying Observations. Ann Math Stat 21: 27–58.

140. Team RC (2014) R: A Language and Environment for Statistical Computing [Internet]. 2013.

Chapter 5

Investigation of the dependency of MCMV replication on the prenylation branch of the mevalonate pathway

5.1 Introduction

Prenylation is the attachment of a hydrophobic 15-carbon (farnesyl) or a 20-carbon (geranylgeranyl) isoprenoid moiety to one or more cysteines located at the C terminus of a protein (Figure 5.1A). Isoprenoids are secondary metabolites of the sterol biosynthesis pathway. The consensus of the prenylation sequence contains the CAAX motif, where A is an aliphatic amino acid residue (Ile, Val, Leu, Ala, and Pro), and the X amino acid determines the type of prenylation (X = Ala, Ser, Cys, Met or Gln leads to farnesylation, and Leu or Phe for geranylgeranylation) (Nantais et al., 1996; Vestal et al., 1995). Protein farnesylation is carried out by a single enzyme, farnesyltransferase (FTase), whereas geranylgeranylation is carried out by protein geranylgeranyltransferase type I (GGTase1) and by geranylgeranyltransferase type II (GGTase2, also known as RabGGTase) for the Rab proteins (Lerner et al., 1997).

Prenylation controls the signalling activation of several cellular proteins. Attachment of isoprenoid moieties increases protein hydrophobicity, allowing prenylated proteins to be inserted into lipid rafts and to exert their biological functions. Examples of prenylated proteins include the small GTPase Ras superfamily (Ras, Rad, Rap, Rab, Ran, Rho, Rheb, Rit, and Arf) that are involved in specific aspects of cell physiology, such as cell adhesion (Rap) and proliferation (Ras). Central to membrane trafficking is a family of Ras-like GTPases termed RabGTPases (Rabs).

Similar to other Ras-like GTPases, RabGTPases contain the common core G domain, which provides essential GTPase and nucleotide exchange activity (Stenmark, 2009). In mammals, more than 60 members of RabGTPases have been identified (Fukuda, 2003, 2008). These Rab proteins can be further classified into several subgroups based on their phylogeny and function. For example, Rab8, -10 and -14 are localized to the trans-Golgi network (TGN) that regulates the trafficking of newly synthesized glucose transporter isoform 4 (GLUT4) from the TGN to the cell surface (Chen et al., 2012; Reed et al., 2013; Sun et al., 2010), whereas Rab3, -26, -27, and -37 are involved in the exocytosis of cargos to the extracellular space (Figure 5.3) (Hutagalung and Novick, 2011).

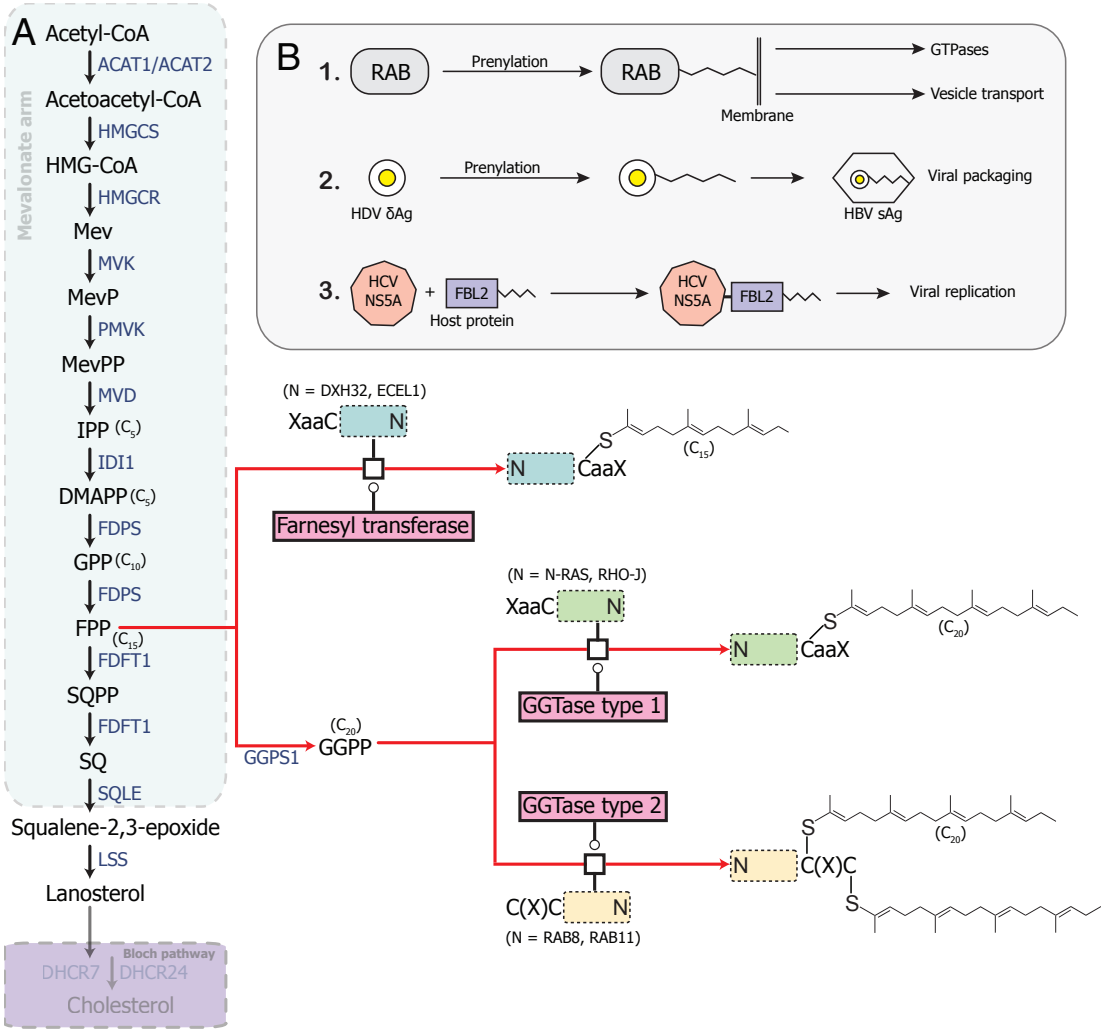

Figure 5.1 Overview of the protein prenylation pathway.
Protein prenylation involves the addition of farnesyl (C_{15}) or geranylgeranyl (C_{20}) moieties to a CAAX motif at the C terminus of proteins. Farnesyl and geranylgeranyl are derived from the cholesterol biosynthesis and are also involved in dolichol and ubiquinone synthesis. Protein farnesylation is carried by the farnesyl transferase, while geranylgeranylation is carried out by geranylgeranylation transferase. Geranylgeranyl transferase type II is specific to RabGTPases. In addition to the CAAX motif, RabGTPases can also contain -XXXCC, -XXCXC, -XXCCX, -XCCXX, or –CCXXX motifs that can be targeted by the transferase. (B) The function of protein prenylation: 1) The newly synthesized RabGTPase is prenylated by the GGTase II then inserted into the membrane of specific organelles, where it mediates the vesicular transport of the cargo. In the replication cycle of pathogens, 2) hepatitis D δ antigen is farnesylated by the FTase, allowing the antigen to be packaged into the hepatitis B surface antigen (Bordier et al., 2003). C) The translocation of hepatitis C non-structural 5A protein (NS5A) to the site of viral replication requires the geranylgeranylation of the host protein FBL2 by GGTase I (Wang et al., 2005).

Rab proteins cycle within specific cellular compartments. The newly synthesized Rab protein first associates with Rab escort protein (REP), which directs it to the Rab geranylgeranyl transferase (RabGGT, also known as GGTase2) (Figure 5.2A) (Fukuda, 2008). In a two-step reaction, geranylgeranyl lipid groups are attached to the CAAX boxes of the Rab protein (Figure 5.3B) (Pylypenko et al., 2003). This differs from other proteins that are subjected to type I geranylgeranylation or farnesylation, as prenylations in Rabs by RabGGTase are strictly REP dependent (Goody et al., 2005). During the next step, the prenylated RabGTPase subsequently binds to the GDP dissociation inhibitor (GDI), prompting the displacement of REP (Figure 5.2C) (Beranger et al., 1994). The binding of Rab to GDI also conceals Rab's prenyl tails, as well as the GTPase activity, allowing translocation of the Rab-GDI complex to the target membrane (e.g. Golgi, ER). A GDI displacement factor (GDF) releases the Rab from GDI, allowing the insertion of Rab into the target membrane (Dirac-Svejstrup et al., 1997). A guanine nucleotide exchange factor (GEF) subsequently catalyzes the exchange of GDP for GTP to activate Rab (Figure 5.2D) (Kim et al., 1995). The assembly of the Rab protein, the cargo, and other accessory proteins, such as V-SNARE (Soluble NSF Attachment Protein Receptor (Fasshauer et al., 1998)), form the transport vesicle, which leads to vesicle trafficking (Figure 5.2E). The GTP-bound Rab interacts with an effector protein that mediates membrane traffic, resulting in the docking, fusion of the vesicle, and the delivery of the cargo (Figure 5.2F). The Rab protein can then interact with its associated GTPase-activating protein (GAP) that catalyzes the hydrolysis of GTP to GDP (Figure 5.2G). The GDP bound Rab is then removed by GDI and translocated back to the target membrane in preparation for the next cycle (Figure 5.2H) (Goody et al., 2005).

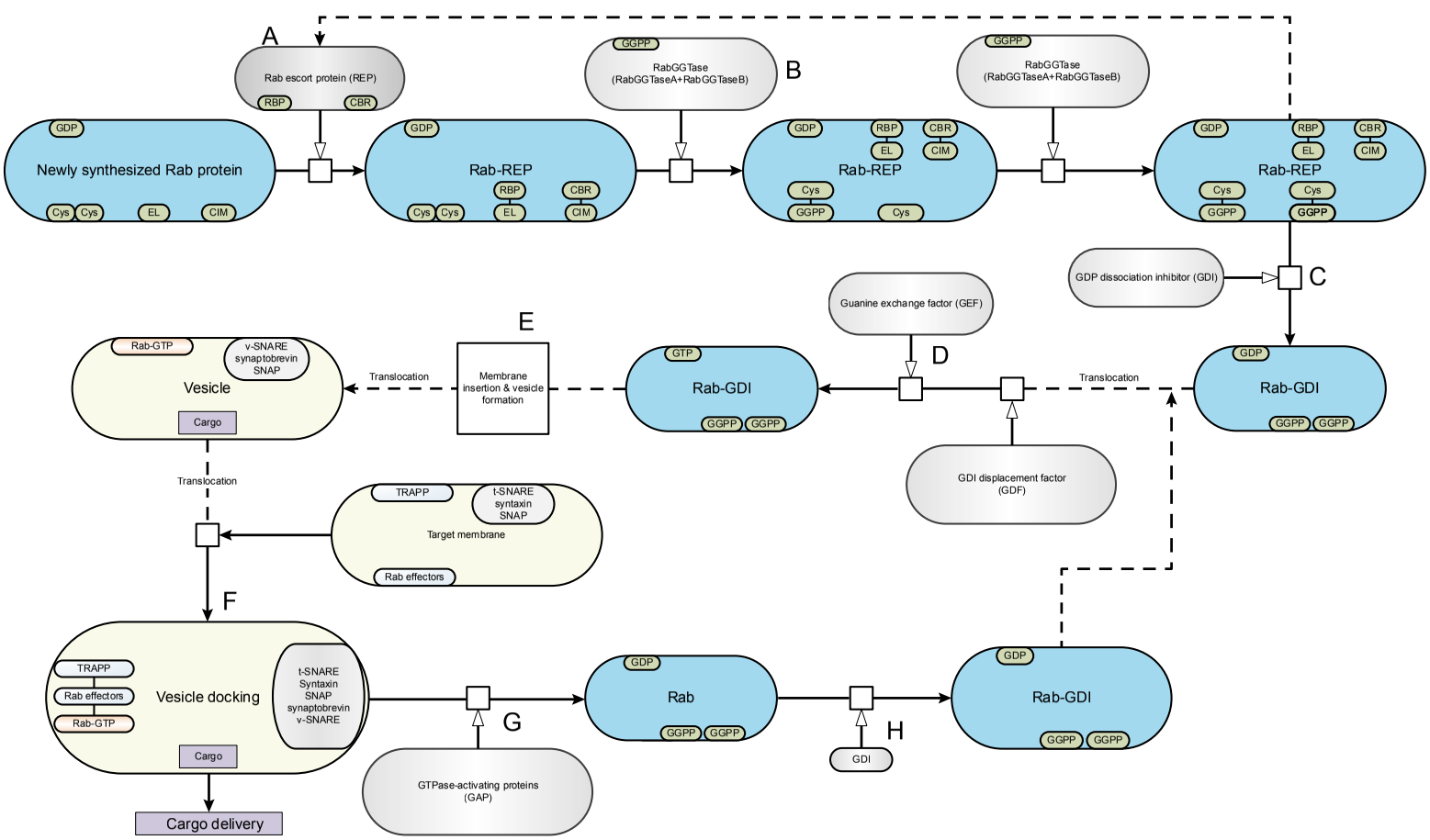

Figure 5.2 Overview of the RabGTPase cycle and vesicular transport.
The newly synthesized Rab protein first associates with Rab escort protein (REP). REP directs the Rab protein to Rab geranylgeranyl transferase (RabGGTase) to receive its prenyl tails (GGPP). The prenylated Rab protein is then bound by GDP dissociation inhibitor, which delivers that Rab to the target membrane. Throughout this process, the Rab is GDP bound. A GDI displacement factor (GDF) removes GDI, and a guanine exchange factor (GDF) catalyzes exchange of GDP to GTP, activating the Rab. The GTP-bound Rab interacts with cargo and the v-SNARE complex, forming the vesicle. The Rab then interacts with effector proteins that promote vesicle docking and fusion, delivering the cargo. The Rab then interacts with its associated GTPase activating protein (GAP) that hydrolyzes GTP to GDP, thus inactivating the RAB. The Rab is then removed from the membrane by GDI and translocates back to the target membrane.

The RabGTPase cycle is critical for regulating the traffic and exchange of molecules between particular organelles, thus differentiating them from other Ras-like GTPases. Perturbation in the Rab cycle can result in a variety of disease states. Mutations in the human REP-1 gene (REP) lead to choroideremia, an X-linked disease characterized by the progressive degeneration of the choroid, resulting in night blindness, view restrictions, and eventual blindness (Seabra et al., 1993). The mutation REP leads to the accumulation of unprenylated Rab27a, resulting in loss of function (Seabra et al., 1995). GDI1 mutations in humans lead to X-linked nonspecific mental retardation, with symptoms similar to mice carrying *Gdi1* gene deletions (defects in short-term memory and social interaction patterns) (D'Adamo et al., 1998). Accumulation of membrane bound Rab4 and -5 were observed in mouse brains carrying *Gdi1* deletions (D'Adamo et al., 2002). Moreover, mutations in Rab3GAP regulatory and catalytic subunits lead to Warburg Micro and Martsolf syndromes, autosomal recessive diseases characterized by ongenital cataracts (clouding of the lens of the eye), microphthalmia (small eyes), postnatal microcephaly (small head), and developmental delay (Aligianis et al., 2005, 2006). Loss of function in *RabggtA* in gunmetal (gm) mice displayed a decrease in Rab prenylation and platelet synthesis (Seabra et al., 2002). This resulted in prolonged bleeding, thrombocytopenia (persistent decrease in the number of blood platelets), and reductions in platelet granule content, which is phenotypically similar to patients with Hermansky-Pudlak syndrome (Bonifacino, 2004; Di Pietro and Dell'Angelica, 2005).

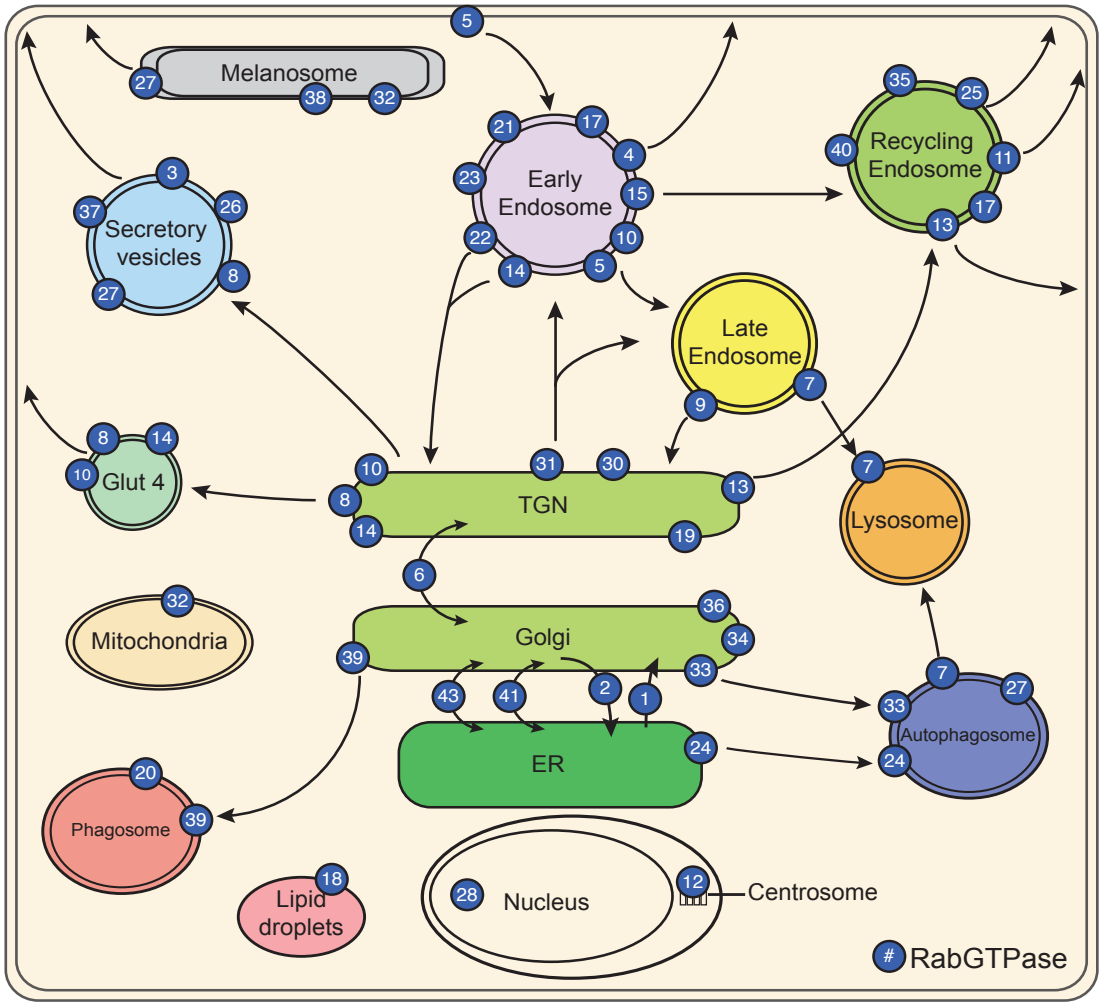

Figure 5.3 The intracellular localization of Rabs.
A simplified pathway showing the intracellular localization and associated vesicle transport pathways of RabGTPases, adopted and modified from Hutagalung and Novick, 2011 with permission. Rab1 regulates ER to Golgi trafficking, while Rab18 is involved in the formation of Lipid droplets. Rab6 transits between Golgi and the trans Golgi network (TGN). Rab11, -13, and -17 are involved in recycling of cargo from recycling endosomes to the plasma membrane. Several secretory vesicles and granules use Rab3, -26, -27, and -37 to exocytose their cargo. Rab27 is well-studied in melanosome transport.

In addition to several autosomal-recessive diseases related to the disruption of the Rab cycle, recent studies have implicated the involvement of Rabs in several neurological and infectious diseases. In Parkinson's disease (PD), Rab3a, -5, and -8 have been shown to interact with mutant α-Synucleins (α-syn), but not with the wild-type control α-syn (Dalfo et al., 2004). Missense point mutations in α-syn can result in the formation of protein aggregates (known as the Lewy bodies) in neurons, the hallmark pathological feature of PD (Gasser, 2009). Subsequent animal models have shown that the disruption of ER-Golgi trafficking by α-syn is reversible with the overexpression of Rab3a and -8a (Dalfo et al., 2004). Mutations in Rab23

have been identified as a causative agent of Carpenter syndrome, an autosomal recessive disorder marked by defects of the skull, face, fingers, toes, and also by mental retardation (Jenkins et al., 2007). Rab23 acts as a negative regulator of sonic hedgehog (shh) signalling during dorsal-ventral axis formation of the neural tube. Rab23 mutants fail to suppress shh signalling, thus inhibiting formation of ventral cells of the spinal cord (Eggenschwiler et al., 2001). In the context of infectious diseases, multiple Rabs and their effectors have been identified as targets by infectious microorganisms for entry, replication, egress and immune invasion. Studies have shown that *Salmonella enterica* and *Chlamydia pneumonia* avoid lysosome degradation by inhibiting the recruitment of Rab5, -7, and -9 (Harrison et al., 2004; Meresse et al., 1999; Rzomp et al., 2003). Similarly, *Legionella pneumophila* (Lozach et al., 2010) was shown to express SidM/DrrA, a bifunctional enzyme which acts as both a GDF and a GEF for Rab1 (Machner and Isberg, 2007). The activity of SidM/DrrA allows the recruitment of Rab1 and the formation of vacuolar-like compartments in which *Legionella* resides (Machner and Isberg, 2006). Recent studies of several RNA viruses, including HCV, Bunyavirus, and Hantavirus, implicated endosomal Rabs (Rab5a,-6b, -7a, and -11) are involved in viral entry and replication (Coller et al., 2009; Rowe et al., 2008).

In previous chapters, treatments with either statins (Figure 2.7) or 25-HC (Figure 3.8) led to significant reductions in plaque expansion. In addition, statin was also shown to inhibition RAP1A prenylation (Figure 2.10). Furthermore, in our previous publication, Blanc and Hsieh et al., 2013, we showed that 25-HC is also highly effective at blocking varicella zoster virus (VZV) infection in MeWo cells. This represents an infection model in which cell-free viruses are not produced and the infection process is exclusively dependent on cell-cell spread (Kramer and Enquist, 2013). Together, these observations argue that the inhibition of viral spread by the statins and 25-HC is a part of the antiviral mechanisms. Given the importance of RabGTPases in regulating various aspects of vesicular transport and pathogen propagation, I hypothesize that there is a specific dependency of MCMV replication on one or more substrates of the type 2 GGTase. Specifically, this chapter aims to identify all the prenylation

targets of the type 2 GGTase and to determine whether these targets are important for MCMV replication. In this present study, I first showed that chemical inhibition of RabGGTase is antiviral against MCMV replication. Subsequent bioinformatics analysis was applied to identify protein targets in human, mouse, and the MCMV proteome that are substrates of protein prenylation. Systematic small interference RNA screening showed that silencing of *Rab6a*, *-11a*, *-11b*, *-26*, *-37*, and *-32* significantly inhibits MCMV replication. Furthermore, silencing of specific Rab effectors corresponding to the above RabGTPases also showed significant MCMV growth inhibition. Together, these results demonstrated the MCMV dependency of host vesicular transport complex for viral replication and egress.

5.2 Results

5.2.1 Inhibition of GGTase2 by psoromic acid is antiviral against MCMV

In chapter 2 (Figure 2.2A), silencing of *Rabggta* and *Rabggtb* by siRNA led to significant inhibition on MCMV replication. To complement this study, chemical inhibition of GGTase2 was first performed to examine whether inhibition of prenyltransferase activity affects MCMV replication. Deraeve et al., 2012 identified psoromic acid as a selective inhibitor of GGTase2. The crystal structure of GGTase2 and psoromic acid revealed that psoromic acid binds to the α-subunit (encoded by *Rabggta*) of the transferase and prevents its interaction with the geranylgeranyl moiety. In these experiments, MEFs were pretreated with psoromic acid at an increasing concentration for 24 hr, followed by infection with MCMV-GFP. As controls, additional MEFs were also pre-treated with IFNγ (100U/ml) or 25-HC (10μM) to demonstrate the expected antiviral profile. Figure 5.4A shows that treatment with psoromic acid led to significant MCMV-GFP growth inhibition as measured by fluorescent readouts. In Chapter 4, it was shown that MCMV replication was reduced in a delipidated environment (Figure 4.2 and S4.1). This was partially due to reduction in the availability of the isoprenoids (Figure 4.3B, S4.2, and S4.5). To examine whether the antiviral effects of psoromic acid can be enhanced in a delipidated condition, vehicle or psoromic acid (25μM) pretreated pMEFs were first infected with MCMV-C3X and incubated in either normal or delipidated media containing the identical treatments. Supernatant at 4 dpi were collected, and the viral titre was determined by plaque assay. Cells treated with psoromic acid led to a significant reduction in viral particle formation (Figure 5.4B). The antiviral effect was further enhanced in the delipidated condition (1 log → 2 log decrease). These results support my previous findings, showing that there is a significant dependency of MCMV replication on the host type II geranylgeranyl transferase and geranylgeranyl secondary metabolites.

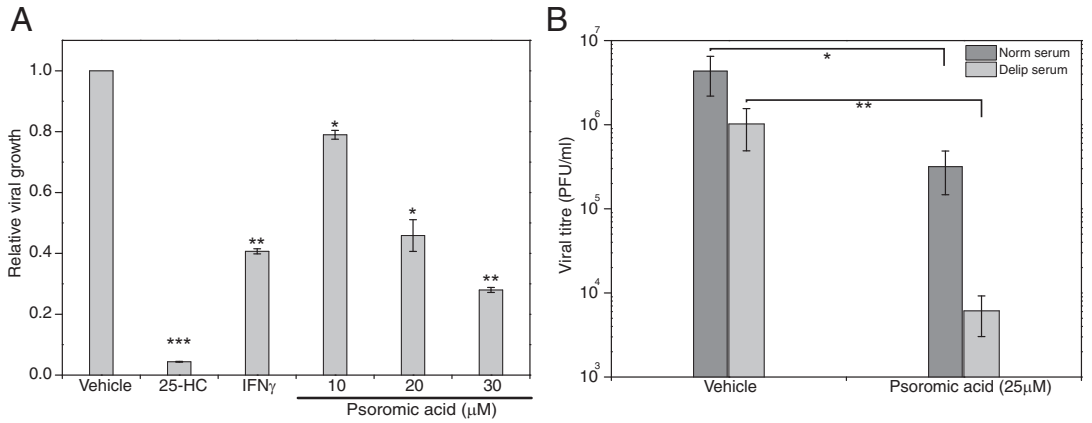

Figure 5.4 Inhibition of geranylgeranyl transferase type 2 (RabGGTase) by psoromic acid is antiviral.

(A) MEFs were seeded in 96 well plates at $3x10^4$ cells/well. The next day, cells were treated with 25-HC (10μM), IFNγ (100U/ml), or psoromic acid (10-30μM) for 24 hr. The next day, cells were infected with MCMV-GFP (MOI = 0.05). After adsorption, infection inoculum was removed and cells were cultured in media containing the exact same treatment. The level of infection was determined by measuring the increase in GFP fluorescence (slope) during the linear-phase of viral growth. n = 6, mean ± SEM. *p<0.05, **p<0.01, ***p<0.001 (B) MEFs were seeded in 6 well plates at $8x10^5$ cells/well. The next day, cells were pre-treated with psoromic acid (25μM) for 48 hr. Cells were then infected with MCMV-C3X (MOI = 0.1). After adsorption, cells were washed 5 times with normal medium. After washing, cells were cultured in normal or delipidated medium containing vehicle or psoromic acid (25μM) as indicated. Four dpi supernatants were collected and virus titre was quantitated by plaque assay as described in Experimental procedures. Data are the mean of 3 biological replicates ± SEM. *p<0.05, **p<0.01

5.2.2 Bioinformatics prediction of prenyltransferases targets

In order to associate the dependency of protein prenylation with viral replication, we first conducted bioinformatics analysis to identify protein targets within the human and the MCMV proteome that are substrates for the three prenyltransferases. This analysis was performed in collaboration with Frank Eisenhaber's group at the A*STAR Singapore (bioinformatics institute). Using an in-house algorithm that screens protein peptides containing the CAAX motifs, scanning of the MCMV proteome did not reveal any prenylation targets. We thus next directed the analysis on the human targets. A total of 290 proteins were predicted to be prenylated (Table S5.1). Figure 5.5 shows the distribution of prenylation targets among the three prenyltransferases, including their substrate protein overlaps. A large population of proteins was FT specific, while the nature of the target appeared disperse. Among the 53 GGT2 specific targets identified, 51 were RabGTPases. It is worth knowing that Rab8a, -8b and -18 were substrates of all three transferases, while Rab40a, -40c, -25, and -23 were shared between FT and GGT2 (Figure 5.5, Table S5.1).

To specifically identify GGTase2 substrates in mouse, an additional analysis was performed on the mouse proteome. 59 mouse protein targets were identified as being GGTase2 specific (Table S5.2), of which, 55 proteins belong to the RabGTPase family.

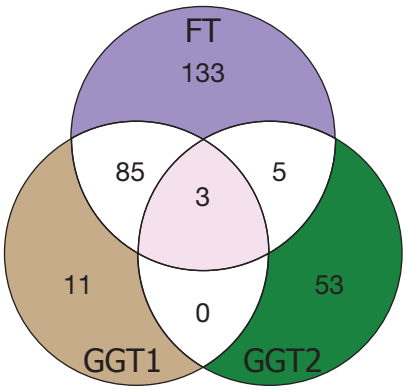

Figure 5.5 Distribution of predicted prenylation targets among the three prenyltransferases.
A total of 290 proteins from the human proteome were identified as predicted substrates among the three transferases based on the work of Maurer-Stroh et al., 2007. The complete list is presented in Table S5.1. The same algorithm was used to identify all of the GGT2 targets in the mouse genome, with the list supplemented in Table S5.2.

5.2.3 Systematic unbiased loss-of-function screening of GGT2 targets on MCMV replication

To explore more fully the RabGTPase transport network required for MCMV replication, I used a library of siRNAs for targeted knockdown of all known RabGTPases in the mouse genome (list of the target genes in Table S5.2). In these experiments, NIH-3T3 fibroblasts were transiently transfected with siRNAs. As controls, additional cells were transfected with *RISC free* or *M54* siRNAs for their expected profiles. Figure 5.6B shows that none of the RabGTPase siRNAs exhibit cell toxicity in comparison with *RISC free* transfected controls. Cells were infected with MCMV-GFP (MOI = 0.05), and the progression of the infection was monitored by changes in fluorescent intensity. Figure 5.6A shows the summarized results of four independent, normalized screens from proviral to antiviral. siRNA knockdown of *Rab17*, *-21*, *-40c*, *-5a*, *-5c*, *-34*, and *-39* showed significant increase in MCMV replication, while knockdown of *Rab11a*, *-11b*, *26*, *32*, *37*, and *-6a* significantly inhibits viral replication.

As the objective of this chapter was to identify specific virus dependent host factors (e.g. pro-viral factors), subsequent experiments were focused on these proviral RabGTPases. Subsequent hit verification secondary screening was performed

following the primary screening. Hit verification involves deconvoluting the pooled siRNA used in the primary screen by testing the individual siRNAs that target the genes of interest. Deconvolution is an important step in ruling out off-target effects that may be observed in siRNA library experiments. A minimum of 2 out of 4 siRNAs must demonstrate similar effects for the primary screen to be valid. In the deconvolution experiments, NIH-3T3 were first transfected with 4 single individual siRNAs targeting *Rabggtb*, *Rab6a*, *-11a*, *-11b*, *-26*, *-37*, and *-32*, followed by MCMV-GFP infection. Figure 5.7 shows that all four individual siRNA targeting *Rab6a*, *-11a*, *-11b*, *-26*, and *-37* led to significant antiviral effects, while only 3 out of 4 siRNAs targeting *Rab32* were antiviral. Although only 2 siRNAs targeting *Rabggtb* showed significant antiviral effects, this result was consistent with the inhibitory effects of psoromic acid. It is noted that this data can further be strengthen with the knockdown efficiency of these RabGTPases.

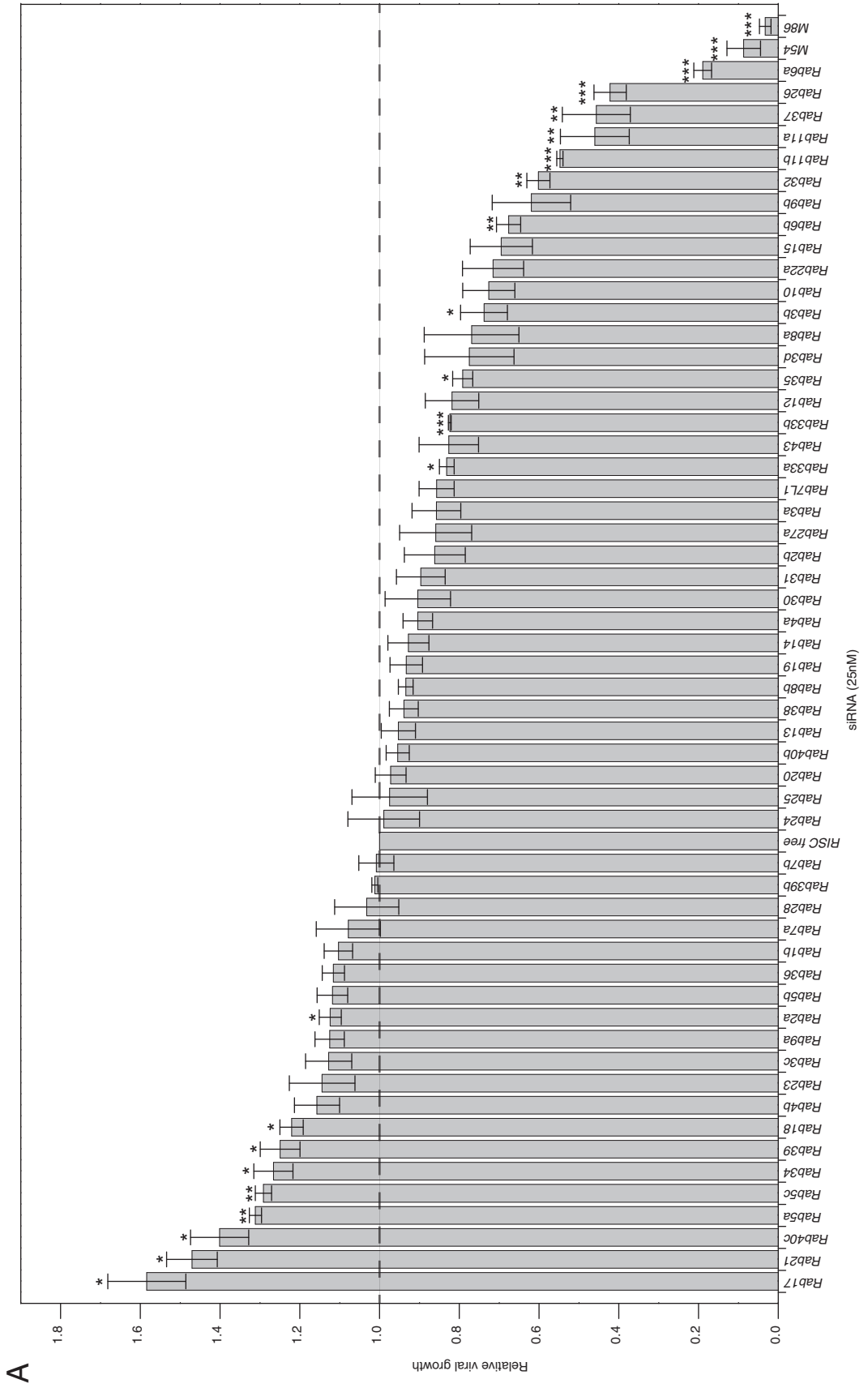
A
Relative viral growth
0.0
0.2
0.4
0.6
0.8
1.0
1.2
1.4
1.6
1.8
siRNA (25nM)
Rab17
Rab21
Rab40c
Rab5a
Rab5c
Rab34
Rab39
Rab18
Rab4b
Rab23
Rab3c
Rab9a
Rab2a
Rab5b
Rab36
Rab1b
Rab7a
Rab28
Rab39b
Rab7b
RISC free
Rab24
Rab25
Rab20
Rab40b
Rab13
Rab38
Rab6b
Rab19
Rab14
Rab4a
Rab30
Rab31
Rab2b
Rab27a
Rab3a
Rab7L1
Rab33a
Rab43
Rab33b
Rab12
Rab35
Rab3d
Rab8a
Rab3b
Rab10
Rab22a
Rab15
Rab6b
Rab9b
Rab32
Rab11b
Rab11a
Rab37
Rab26
Rab6a
M54
M86

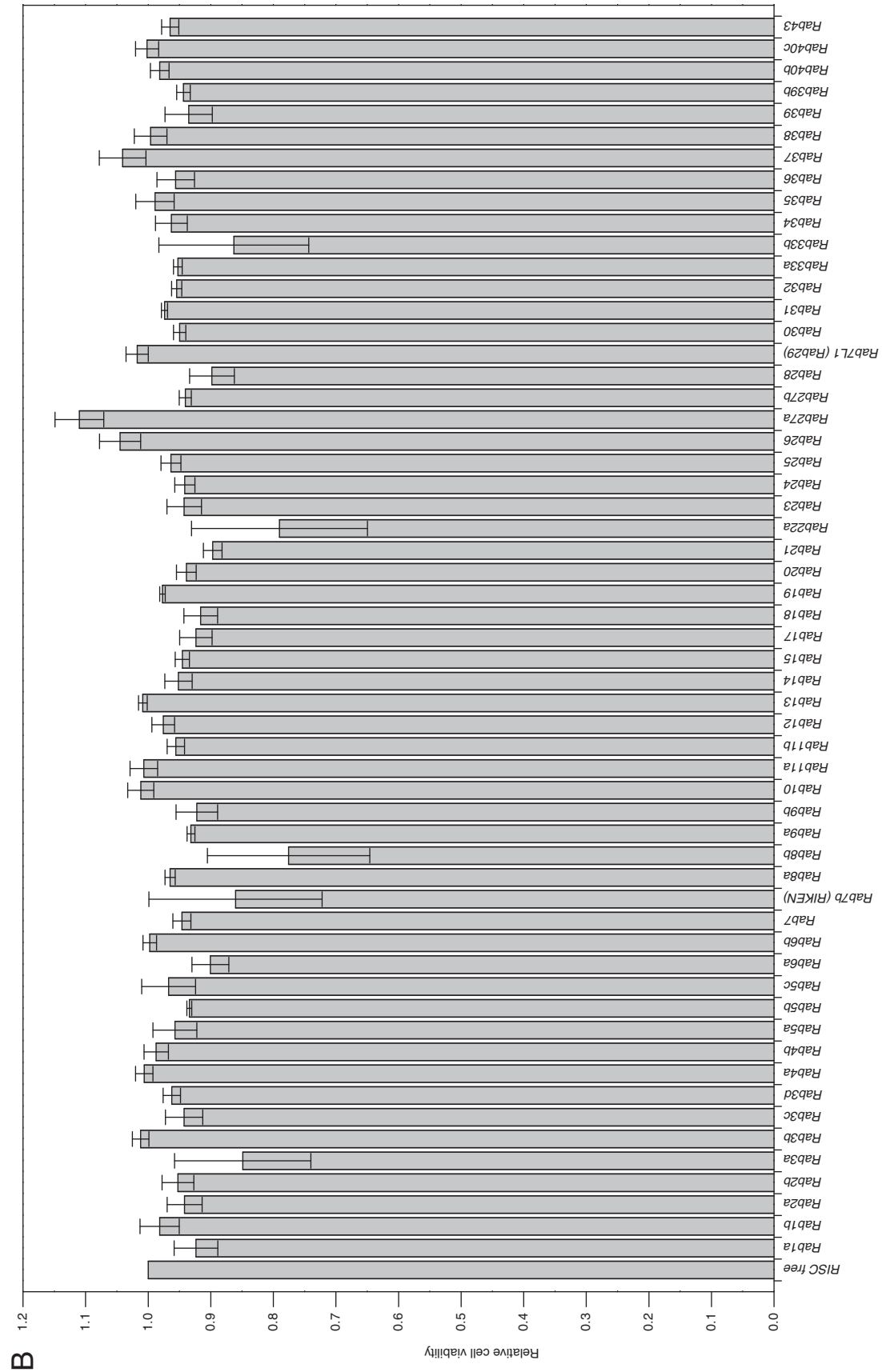
B
Relative cell viability
0.0
0.1
0.2
0.3
0.4
0.5
0.6
0.7
0.8
0.9
1.0
1.1
1.2
RISC free
Rab1a
Rab1b
Rab2a
Rab2b
Rab3a
Rab3b
Rab3c
Rab3d
Rab4a
Rab4b
Rab5a
Rab5b
Rab5c
Rab6a
Rab6b
Rab7
Rab7b (RIKEN)
Rab8a
Rab8b
Rab9a
Rab9b
Rab10
Rab11a
Rab11b
Rab12
Rab13
Rab14
Rab15
Rab17
Rab18
Rab19
Rab20
Rab21
Rab22a
Rab23
Rab24
Rab25
Rab26
Rab27a
Rab27b
Rab28
Rab7L1 (Rab29)
Rab30
Rab31
Rab32
Rab33a
Rab33b
Rab34
Rab35
Rab36
Rab37
Rab38
Rab39
Rab39b
Rab40b
Rab40c
Rab43

Figure 5.6 Small interfering RNA screen identifies the dependency of MCMV on RabGTPases.
(A) NIH-3T3 fibroblasts (1.5x10^4 cells/well) were transfected in 96-well plates with On-target plus siRNAs as indicated for 48 hr then infected with MCMV-GFP (MOI = 0.05). *RISC free* was used as a transfection control, while *M54* specifically targets MCMV polymerase. *M86* was another siRNA targeting MCMV capsid. The level of infection was determined by measuring the increase in GFP fluorescence (slope) during the linear-phase of viral growth. The graph represents the relative level of infection compared to *RISC free* transfected and data are the mean of 6 biological replicates ± SEM. *p<0.05, **p<0.01, ***p<0.001 (B) NIH-3T3 fibroblasts (1.5x10^4 cells/well) were transfected with On-target plus siRNAs as indicated in 96-well plates for 48 hr then the cell viability was measured using CellTiter-Blue as described in Experimental procedure 7.4.2. Relative cell viability was calculated by normalizing to the *RISC free* transfected samples and data are the mean of 6 biological replicates ± SEM.

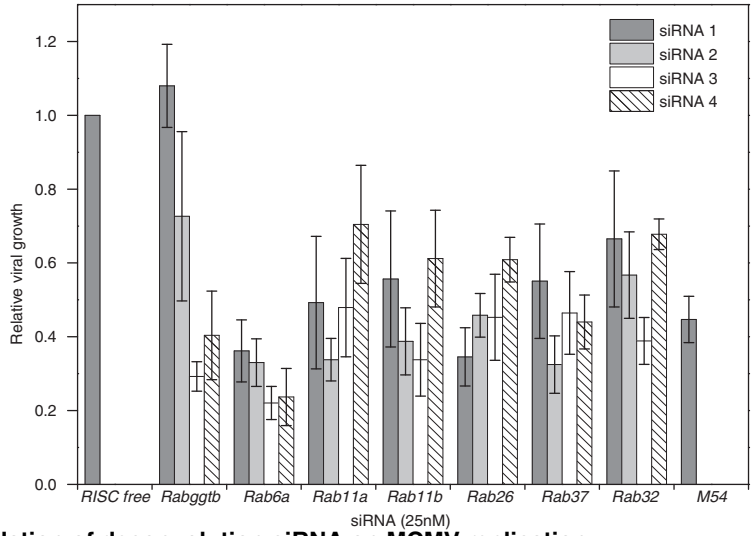

Figure 5.7 Validation of deconvolution siRNA on MCMV replication.
NIH-3T3 fibroblasts (1.5x10^4 cells/well) were transfected in 96-well plates with On-target plus deconvolution siRNAs as indicated for 48 hr then infected with MCMV-GFP (MOI = 0.05). *RISC free* was used as a transfection control, while *M54* specifically targets MCMV polymerase. The graph represents the relative level of infection compared to *RISC free* transfected and data are the mean of 6 biological replicates ± SEM.

5.2.4 Effects of siRNA knockdown of selected RabGTPase effectors on MCMV replication

Rab effectors play many essential roles in the process of vesicular transport, including formation of vesicles, guiding vesicle movement through tethering, as well as the process of uncoating. Previous works reviewed by Hutagalung and Novick, 2011 and others have uncovered many interactions between the GTPases and their effectors, and their functional roles. For example, the work of Lombardi et al., 1993 showed that Rab9 regulates membrane trafficking between the late endosome and the trans-Golgi network (TGN) (Figure 5.3). Rab9 and its effector TIP47 are required for the transport of mannose 6-phosphate receptors (MPRs) between the endosome and the Golgi complex (Carroll et al., 2001). The interactions between TIP47 and MPRs, and then Rab9 ensures that only endosome-bound

MRPs (rather than other compartment-bound) are packaged into the vesicle. In the aspects of cargo trafficking, Rab11a in MDCK and HeLa cells interacts with myosin Vb through its effector Rab11-FIP2 (Rab11 family interacting protein) (Hales et al., 2002). This interaction provides a mechanism for plasma membrane recycling in both polarized and non-polarized cells.

Based on the above RabGTPase screening results, effector proteins of Rab6a, -11a, -11b, -26, and -37 were first identified through literature reviews (see Figure 5.8A for effector names). Rab6a was shown to interact with R6IP1 (Rab6-interacting protein 1, (Miserey-Lenkei et al., 2007)), COG6 (Conserved Oligomeric Golgi 6, (Smith et al., 2010)), Rab6KIFL (Rab6-binding kinesin, (Hill et al., 2000)), and BICD1/2 (Bicaudal-D1/2, (Matanis et al., 2002)). Rab11a and -11b were shown to interact with Rab11-FIP1/2/4 (Rab11 family interacting protein 1, 2, and 4, (Baetz and Goldenring, 2013)). Rab32 was shown to interact with effectors VARP (VPS9-ankyrin-repeat protein, (Tamura et al., 2009)), and PKA (cAMP-dependent protein kinase, (Alto et al., 2002)). Both Rab26 and -37 shared identical affinity to the effector Rims1 but not Rims2 (Regulating synaptic membrane exocytosis, (Fukuda, 2003)).

To identify which effector proteins are important for MCMV replication, MEFs were transfected with siRNAs targeting Rab effectors, as indicated in Figure 5.8A, for 48 hr, then infected with MCMV-GFP. Figure 5.8B shows that none of the siRNAs are cytotoxic. Silencing *Bicd1* (effector of Rab6a), *Rab11-fip1/4* (effector of Rab11a/b), *Varp* (effector of Rab32), and *Rims1* (effector of Rab26/37) showed significant antiviral effects. In agreement with RabGTPase screening (Figure 5.6A), siRNA knockdown of *Rims2* and Rab3in (effectors for Rab3a/b/c/d) had no effect on MCMV replication.

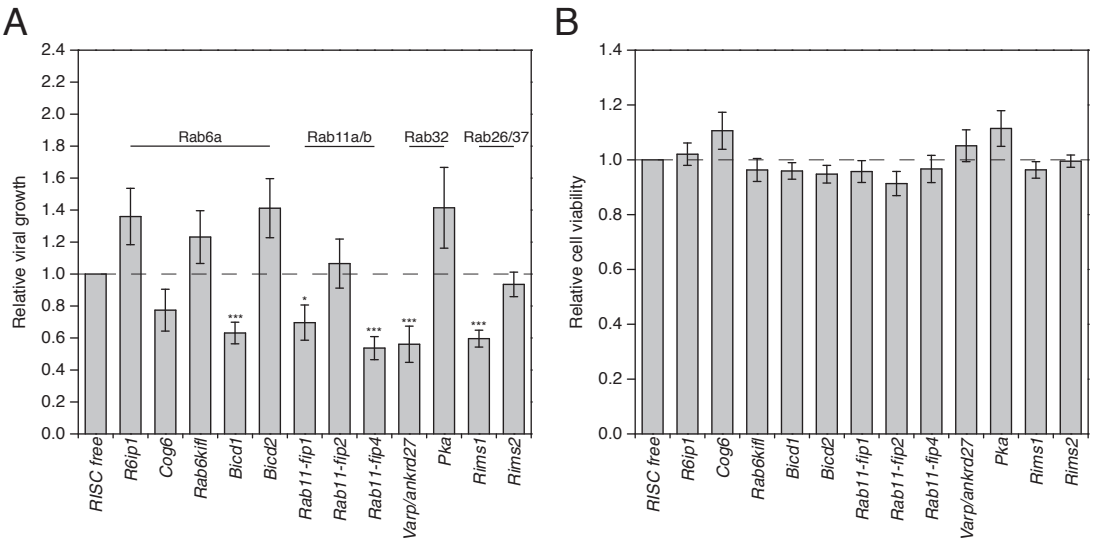

Figure 5.8 Validation of deconvolution siRNA on MCMV replication.
NIH-3T3 fibroblasts (1.5x10^4 cells/well) were transfected in 96-well plates with On-target plus deconvolution siRNAs as indicated for 48 hr then infected with MCMV-GFP (MOI = 0.05). *RISC free* was used as a transfection control, while *M54* specifically targets MCMV polymerase. The graph represents the relative level of infection compared to *RISC free* transfected and data are the mean of 6 biological replicates ± SEM.

5.3 Discussion

In this current study, I utilized a combination of literature review, bioinformatics analysis and experiments to explore the relationships between protein prenylation and viral replication. Bioinformatics analysis revealed that the majority of the RabGTPases are specific to geranylgeranyl transferase II. Importantly, inhibition of GGTase2 activity by psoromic acid showed significant antiviral effects. Subsequent siRNA screening showed that the knockdown of *Rab6a*, *-11a*, *-11b*, *-26*, *-37*, and *-32*, negatively affects viral growth.

5.3.1 Identification of prenylation targets

In an effort to correlate the dependency of viral replication on host factor prenylation, I first adopted an *in silico* approach to identify prenylation targets within the human proteome. A total of 290 predicted targets were identified. A large proportion of proteins were shared by both FT and GGT1, mainly because FT can also prenylate substrates with a terminal leucine (Maurer-Stroh et al., 2007). While the clustering of Rab GTPases with the geranylgeranyl transferase II was not surprising (due to the requirement of Rab-REP complex), it is interesting that there is an overlap of transferases for several Rab proteins (Rab8 can be prenylated by FT, GGT1, and GGT2, and Rab23, -25. -40a, and -40c are targets of FT and GGT2) (Table S5.1). Rab8 prenylation state ambiguity has been demonstrated *in vitro* (Wilson et al., 1998), while the others have not. It has to be mentioned that this analysis represents only the capacity of a given substrate to be modified when presented to the prenyltransferase. The activity, binding affinity, substrate concentration, and the availability of FT, GGT1, and GGT2 in the cellular context ultimately determine the type of prenylation for a given substrate. Furthermore, such analysis is dependent on the quality of the protein database. In contrast to the human and mouse proteome, the MCMV proteome remains relatively incomplete. Despite its limitation, this technique provides a tentative global view on protein prenylation in the human proteome and provides the basis for subsequent siRNA screening.

Although the prediction from the human proteome was sufficient to justify the subsequent siRNA screen, it was noted that not all human RabGTPases are conserved in the mouse proteome. Indeed, analyses revealed that Rab40a, -40al, and -43 are not found in mice. Due to limited publications currently available, it is unknown whether these RabGTPases would affect the overall vesicular transport network between the two species.

5.3.2 siRNA knockdown of RabGTPases

As the virus did not contain any predicted prenylation targets, an siRNA knockdown assay was conducted to explore the dependency of host prenylated factors on viral replication. Viral growth is determined using a strain of MCMV expressing GFP (controlled by HCMV major immediate early promoter (MIEP)). Changes in GFP intensity during the linear phase of viral replication determine the growth rate (slope) of the virus. Silencing of an antiviral factor enhances the replication of the virus. Conversely, silencing of a pro-viral factor inhibits viral proliferation. Unbiased siRNA screening identified 6 RabGTPases that are important for MCMV replication. These GTPases were further validated in a secondary screening using deconvolution siRNAs to demonstrate siRNA specificity. In addition, silencing specific Rab effectors corresponding to the 6 RabGTPases also showed significant MCMV inhibition. Coupled with the psoromic acid data, this work supports the hypothesis that the replication of MCMV depends on specific host RabGTPases that are the substrates of type II prenyltransferase.

In these experiments, knockdown of Rab26 and -37 and the effector Rims1 showed antiviral effects. Rab26 was first identified in rat pancreatic zymogen granules and shared amino acid similarity with Rab3a (Wagner et al., 1995). Further investigation indicated that Rab26 was also expressed in parotid gland acinar cells and localized to mature secretory granules (Yoshie et al., 2000). The localization of Rab26 is similar to the Rab3 and -8 families, and thus is classified as part of the regulated secretory pathway (Yoshie et al., 2000). In contrast to the constitutive secretory pathway that is ubiquitously present in various cell types (such as fibroblasts (Peranen et al., 1996)), the regulated secretory pathway is only present in excytotic, endocrine and exocrine cells,

and in neurons (Ozawa and Takata, 1995; Yoshie et al., 2000). Indeed, transcription profiling of BMDM (MITCH24) failed to show the presence of Rab26, suggesting that Rab26 might not be expressed in BMDM or NIH-3T3 fibroblasts. This finding is an apparent contradiction to the siRNA screening data. However, in the context of viral infection, HCMV has been shown to induce gene expression of Rab27a, -32, and -38 (Hertel and Mocarski, 2004), while expression of Rab26 during MCMV infection remains to be investigated. Overexpression of Rab26 (see Figure S5.2 for Rab26 plasmid construct) can be used to explore the role of Rab26 in MCMV replication.

Currently, little is known about the functional aspect of Rab26. In rat parotid acinar cells, Rab26 has been shown to participate in amylase secretion, in a cAMP dependent, Ca^{2+} independent manner (Nashida et al., 2006). Treatment with isoproterenol (a non-selective β-adrenergic agonist) activates the β-adrenergic receptor, leading to the activation of downstream cAMP-dependent kinases, resulting in a high level of amylase release. This release can be inhibited using anti-Rab26 antibodies. Because regulated exocytosis is dependent on an increase in intracellular Ca^{2+}, which triggers vesicle fusion (Rickman et al., 2006), it is possible that Rab26 is involved in the process of exocytosis but not in the release of the vesicle. In the context of herpesvirus egress, after the fusion of virion with the cell membrane (see Figure 1.5 for the life cycle of CMV), most enveloped virus particles are found attached to the outer surface of the plasma membrane, rather than being released from the cell (Johnson and Baines, 2011). This observation supports the role of Rab26 as a viral exocytosis facilitator (and not involved in viral release). In order to show this, immunostaining of FLAG-tagged Rab26 (Figure S5.2 for construct reference) and MCMV glycoprotein would determine whether Rab26 co-localizes with the MCMV particle. Furthermore, if cellular exocytosis machinery is indeed necessary for MCMV egress, treatment with *Botulinum* toxin (which degrades SNAP-25) would be expected to inhibit any exocytosis, preventing viral egress.

Another pro-viral target identified in this study was Rab37. Rab37 shares 73% amino acid sequence similarity with Rab26, especially at the C terminus. Studies indicated Rab37 is localized only in the dense core secretory granules of

mast cell lines (Masuda et al., 2000; Tsuboi and Fukuda, 2006). However, it was also shown that Rab37 can localize to insulin secretory granules (Brunner et al., 2007). It is hypothesized that Rab37 may function in regulating vesicle translocation and attachment to the plasma membrane, and does not participate in the fusion of the vesicle. Based on the expression pattern of Rab26 and -37, it is possible that these two RabGTPases only participate in viral egress in a limited number of cell types, where they compensate for the function of other secretory Rabs.

It has been suggested that herpesviruses alter TGN trafficking during the late stage of infection. Both HSV gB and the cellular TGN marker (TGN46) were redistributed to the plasma membrane, indicating the blockage of reverse transport from endosome to TGN (Figure 1.5 for reference) (Wisner and Johnson, 2004). This blockage would promote the forward transport of the virion to the cell surface. Furthermore, activation of myosin Va has been shown to promote viral secretion; however, no direct evidence of this interaction has been found (Roberts and Baines, 2010). The Rab GTPases and Rab effectors have been shown to regulate myosin Va activity (Fukuda, 2003; Seabra and Coudrier, 2004); thus, it is possible that the herpesvirus utilizes the secretory Rabs to facilitate its transport.

Surprisingly, targeting Rab27a (Figure 5.6A) failed to show significant inhibition on MCMV growth as in contrast to the effects on HCMV (Fraile-Ramos et al., 2010). It is possible that considerable divergence between MCMV and HCMV resulted in such difference (McGeoch et al., 1995), as MCMV and HCMV share only 42.5% genome sequence identity and only 78 ORFs showed significant amino acid similarity (Varnum et al., 2004). Differences between the MCMV and the HCMV proteome can result in the recruitment of different cellular factors during the replication process. Additionally, cell type variation between the experimental settings can also generate different findings. MeOW (cell line), melan-α (primary), and ashen-3 (primary) that are used in the Rab27a experiments are either immortalized or primary melanocytes enriched with Rab27a. In contrast, NIH-3T3 fibroblasts lacks melanosome, and therefore it is reasonable to suggest that either Rab27a is not expressed in NIH-3T3 fibroblasts, or does not participate in its normal function.

An unexpected RabGTPase identified through the siRNA screening was the combination of Rab32 and its effector Varp. Molecular cloning of human Rab32 revealed that Rab32 was expressed in various human melanoma cell lines and platelets (Bao and Faris, 2002). Likewise, murine Rab32 exhibits a ubiquitous expression pattern in various organs, including the spleen, lung, liver, kidney, as well as various cell types including melanocytes, platelets, mast cells, and NIH-3T3 fibroblasts (Cohen-Solal et al., 2003). Initial functional characterization has shown that Rab32 functions as an A-kinase anchoring protein (AKAP) that recruits the cAMP-dependent protein kinase (PKA) to the mitochondria (Alto et al., 2002). PKA regulates mitochondria ATP synthesis through the phosphorylation of mitochondrial proteins (Acin-Perez et al., 2009). Overexpression of a Rab32 GTP binding–deficient mutant (Figure 5.2D) in Cos7 cells (monkey kidney tissue) causes the condensation of mitochondria at the microtubule organizing centre, leading to mitochondrial collapse (Alto et al., 2002). Rab32 and its effector Varp were first identified to be involved in the transport of a melanogenic enzyme TYRP1 (pigment synthesis) in melanosomes (Tamura et al., 2009). siRNA silencing of Rab32 in Rab38-deficient background mice enhanced the melanosome biogenesis defect (Bultema and Di Pietro, 2013; Wasmeier et al., 2006). Importantly, Rab32 deficient cells showed accelerated lysosomal targeted degradation of Tyrp1, indicating that Rab32-Varp regulates the post-TGN sorting of Tryp1 to the melanosome, rather than lysosome. Interestingly, *in vivo* experiments showed that Rab32 in mouse brain microglia was induced upon LPS injection, suggesting that Rab32 might participate in the early inflammation process (Liang et al., 2012). However, the exact involvement is unknown. In addition, Rab32 was also shown to be incorporated into *Legionella pneumophila*-containing vacuoles (LCV) in macrophages as a part of the replication complex (Hoffmann et al., 2013). Depletion of Rab32 inhibits the accumulation of *Legionella* SidC protein, a multifunctional protein for modulating host vesicular trafficking, in LCV (Gazdag et al., 2014; Hoffmann et al., 2013). This effectively interferes with the replication of *Legionella*. In this current study, siRNA knockdown of Rab32 and Varp significantly inhibits MCMV replication, indicating that there is a dependency of Rab32-Varp trafficking complex during the replication cycle of the

virus. Despite the evidence, the precise role of Rab32-Varp in MCMV infection remains to be elucidated. One possibility is that the MCMV virion recruits Rab32-Varp to ensure correct TGN-endosome trafficking and prevents targeted lysosomal degradation. It is also possible that MCMV requires the trafficking of specific host or viral factors during the assembly of the virion. Interestingly, my siRNA screening also showed that silencing Rab21 led to a significant increase in MCMV replication. This is an agreement with Hoffmann et al., 2013, showing that depletion of Rab21 also enhances *Legionella* replication. Rab21 is involved in the maturation of macropinosome prior to the fusion with lysomsome. In addition, prior to the discovery of Rab32, Varp was initially characterized as the guanine nucleotide exchange factor (GEF) (see Figure 5.2C for Rab cycle reference) for Rab21(Zhang et al., 2006). It is possible that Rab21 and -32 are mutual competitors for Varp, such that silencing Rab21 promotes the association between Rab32 and Varp. Silencing Rab21 could also prevent the uptake of MCMV particles into macropinosomes and subsequent lysosomal degradation.

In agreement with the work of Krzyzaniak et al., 2009, my results showed that there is a dependency of HCMV replication on Rab11a and its effector FIP4 (Rab11-Fip4). In particular, HCMV glycoprotein M (UL100), a part of the gM/gN complex, was directly shown to interact with FIP4 using both chemical and microscopy assays. HCMV gM first binds to FIP4 and recruits Rab11a to facilitate the transport from TGN to the endosomal recycling compartment. The accumulation of gM/gN complex and other viral glycoproteins in the endosomal recycling compartment leads to the formation of the assembly complex (AC), where the final stage of viral assembly and maturation takes place (Sanchez et al., 2000). Mutations in Rab11a or shRNA silencing of FIP inhibits HCMV assembly and subsequent particle formation (Krzyzaniak et al., 2009). In this chapter, siRNA knockdown of either Rab11a or FIP4 also led to significant MCMV replication inhibition, suggesting that Rab11a-FIP4 might also play a similar role in sorting viral proteins. In addition to Rab11a and FIP4, my results also indicated that Rab11b and FIP1 (Rab11-FIP1) were involved in the replication of MCMV. Similar to FIP4, FIP1 has been shown as an effector for both Rab11a and -11b (Hales et al., 2001). However, whether Rab11b and FIP1 form a

vesicular transport complex with a specific viral protein is yet to be determined.

Surprisingly, recent work published by Hook et al., 2014 showed that HCMV encodes three micro RNAs, miR UL112-1, US5-1, and US5-2, that specifically target Rab5c and -11a. Rab5c and -11a were both shown to be important for the secretion of antiviral cytokines, IL-6 and TNF-α. miRs transfected HEK-293T cells showed significant reduction of Rab5c and -11a at the protein level. Furthermore, overexpression of miRs led to a significant decrease in the secretion of IL-6 and TNF-α in LPS stimulated THP-1. Mutation of HCMV miRNAs results in reduced virus yield and reduction in plaque size. Microscopy results indicated that silencing of Rab5c and -11a are required for the disruption of Golgi and the endosomal recycling complex, and the formation of the CMV assembly complex. In agreement with the work of Hook et al., 2014, my results also suggest that silencing Rab5c provides a significant enhancement for MCMV replication. Indeed, murine Rab5c was involved in the secretion of IL-6 in J774E macrophages (Bhattacharya et al., 2006). However, whether MCMV encodes these miRs for silencing Rab5c and inhibition of cytokine secretion requires further experimentation. With regards to Rab11a, results from Hook et al., 2014 initially seemed contradictory to the work of Krzyzaniak et al., 2009 and my results. However, further examination of the results and data from Nelson's group (personal communication) suggested that silencing of Rab11a is temporarily required for the condensation and reorganization of the Golgi, TGN, and endosomes into the assembly complex adjacent to the nucleus. Upon the transcription attenuation of miRs, Rab11a is subsequently resynthesized and utilized for sorting viral proteins to the newly formed assembly complex. This is evident by the observation that the protein expression of Rab11a was never completely diminished during HCMV infection (maximum 40~50% reduction, recovers at 72 hpi). Thus, the results from Hook et al., 2014 do not contradict my findings. Currently, it is unclear whether MCMV replication requires the formation of an assembly complex and the precise role of Rab11a. Further microscopy experiments are needed to address these questions.

Among the 53 RabGTPases screened in this chapter, silencing Rab6a showed the strongest inhibition of MCMV replication. Rab6a and the effector Drosophila

Bicaudal-D 1 and 2 (BicD1/2) are involved in dynein-mediated microtubule transport, as well as in COPI-independent Golgi-endoplasmic reticulum (ER) transport (Matanis et al., 2002). Importantly, Rab6a-BicD1 specifically mediates the membrane traffic from the Golgi apparatus towards the endoplasmic reticulum (ER). Functional characterization of the BicD2 structure revealed that BicD2 binds to its cargo via the C-terminal domain, forming the vesicle, while the N-terminal domain interacts with the dynein-dynactin complex for the movement of the vesicle (Hoogenraad et al., 2001). The importance of dynein-dynactin mediated trafficking in the replication of pathogens was highlighted experimentally using *Chlamydia trachomatis*. Chlamydiae are obligate intracellular bacteria that consist of two distinct developmental cycles. The infectious elementary body (EB) give rise to primary infection of susceptible hosts through physical attachment. In the second phase, the EB resides within a membrane bound vacuole, known as the inclusion (reticulate body), where the replication of the bacteria takes place (Grieshaber et al., 2003; Kerr et al., 2005). The work of Moorhead et al., 2007 first showed that Rab6a and BicD1are recruited to *Chlamydia trachomatis* serovar L2 inclusions in HeLa cells within 18 hr of infection. Importantly, the recruitment of Rab6a was guanine nucleotide-dependent, since GTPase-deficient Rab6a mutant failed to localize to the inclusion. Furthermore, unpublished results from Moorhead et al., 2007 indicated that Rab6a is not recruited to chloramphenicol treated EB-containing vacuoles. Collectively, these findings suggest that only the active GTP-bound Rab6a is recruited to the replication vacuoles, possibly through chlamydial proteins expressed only during intracellular growth. In the case of *Chlamydia trachomatis* serovar L2, this recruitment is achieved through the interactions between Rab6a and BicD1. However, the exact role of Rab6a-BicD1 in the replication of *Chlamydia trachomatis* remains to be elucidated.

The importance of Rab6a-BicD1 in CMV replication came from the study of the HCMV tegument protein pp150 (ppUL32). In HCMV infected primary human foreskin fibroblast (HFF), pp150 accumulates in the assembly compartment, which co-localizes with other tegument proteins, including pp28 and pp65, and envelope glycoproteins gB, gH, and gM/gN (Indran et al., 2010; Krzyzaniak et al., 2009). Mutations in the

pp150 carboxyl-terminal led to a significant reduction in secondary viral spread (AuCoin et al., 2006). Fluorescent microscopy and complementation experiment using pp150 expression plasmids revealed that the reduction in viral spread of the ΔUL32 HCMV mutant is independent of defects of DNA synthesis, nuclear egress, and viral gene expression. Nevertheless, infection of HFF with ΔUL32 HCMV led to abnormal accumulation of gB in the assembly complex. Based on these observations, it was postulated that pp150 is responsible for the final maturation of the virion. Site-directed mutagenesis showed that pp150 directly interacts with the C-terminal domain of BicD1 for localization to the assembly complex, and that silencing BicD1 with shRNA inhibits HCMV replication (Indran et al., 2010). Further experimentation by Indran and Britt, 2011 showed that the formation of Rab6a-BicD1-pp150 vesicular complex is necessary for the translocation of newly synthesized pp150 to the assembly complex. Overexpression of truncated BicD1 or dominant-negative Rab6a negatively affects viral yield. Collectively, these findings suggest that Rab6a-BicD1 plays an essential role in directing trafficking of viral tegument protein to the sites of viral assembly.

5.3.3 Integrating the role of RabGTPases with the assembly and egress of HCMV and MCMV

While this chapter primarily focuses on the role of RabGTPases in the replication of MCMV, a detailed understanding of the assembly process of MCMV is currently lacking. Therefore, the following discussion aims to integrate my findings with recent studies on the egress of HCMV.

During the course of HCMV replication, a hallmark of infected cells is an enlarged, kidney-shaped nucleus wrapping around a perinuclear body, termed the assembly compartment (AC) (Alwine, 2012). The work of Das, Vasanji, & Pellett, 2007 using HCMV infected HFF first showed that the AC was comprised of two distinctive layers, an inner early endosome layer (identified using the marker EEA1), and an outer Golgi layer (using the marker mannosidase 2) (see Figure 6.2**A**). Interestingly, Rab5, a traditional marker for the early endosome, was absent in the AC. This observation was consistent with the study of Hook et al., 2014, showing that Rab5 was targeted by

HCMV miR-UL112-1 for proteasome degradation (Figure 6.2**C**). A more recent study by Subhendu Das & Pellett, 2011 using an expanded list of organelle markers provided further understanding to the structure of the AC. In these microscopy experiments, the early endosome was found to be at the centre of the AC (using the marker EEA1). The presence of EEA1 was also accompanied by two recycling endosome markers, TfR, and Rab11a. Furthermore, the outer Golgi layer of the AC was further dissected into a cis-Golgi (using GM-130) and a trans- (using mannosidase 2 and p230) layer. From these data, a diagrammatic representation of the AC model was proposed in Figure 6.2**A** showing a cylindrical-spherical AC composed of many organelle-specific vesicles.

More recently, additional components of the vesicular transport system have been shown to be involved in the assembly of HCMV. As discussed above, Rab6a is involved in the transport of pp150 to the AC via the effector BicD1 (Indran et al., 2010), while trafficking of HCMV gM to the AC requires Rab11 and the effector FIP4 (Krzyzaniak et al., 2009). Additionally, SNAP23 (Cepeda and Fraile-Ramos, 2011) and syntaxin 3 (Liu et al., 2011), which are part of the SNARE complex responsible for the docking and the fusion of the vesicle, were shown to play important roles for the egress of the virion (Figure 6.2**B**). Collectively, these investigations illustrate how host vesicles contribute to the final stages of HCMV assembly and envelopment.

In addition to the formation of the AC, HCMV also induces chaperone BiP (also known as glucose-regulated protein 78 (GRP78)) for the stabilization of the AC (Buchkovich et al., 2008) (Figure 6.2**C**). Depletion of BiP by shRNA, or by BiP-specific SubAB subtilase cytotoxin causes the deterioration of the AC and inhibits the production of infectious virions (Buchkovich et al., 2008, 2009). BiP/GRP78 has been shown to be an important mediator of ER stress and the unfolded protein response (UPR). In mammalian cells, UPR is initiated by three ER transmembrane proteins: Inositol Requiring 1 (IRE1), PKR-like ER kinase (PERK), and Activating Transcription Factor 6 (ATF6) (Oslowski and Urano, 2011). Under normal conditions, IRE1, PERK and ATF-6 are bound by BiP, preventing the activation of signalling pathways (Bertolotti et al., 2000; Sommer and Jarosch, 2002). Upon ER stress, BiP disassociates

from these factors, resulting in their activation. Activation of IRE1 leads to the splicing of X-box binding protein 1 (XBP-1) mRNA, which, upon translation, acts as a transcription factor activating UPR target genes (Oslowski and Urano, 2011). PEAK activation leads to the phosphorylation of eukaryotic initiation factor 2 (eIF2α). Phosphorylated eIF2α prevents the assembly of the ribosomal initiation complexes, leading to mRNA translational attenuation. ATF6 is synthesized as a membrane-bound transcription factor. Upon ER stress, ATF6 is released by BiP and translocated from ER to Golgi, where ATF6 is cleaved by S1P and S2P, the same enzymes that process SREBP2 in response to sterol depletion (Ye et al., 2000). However, different from SREBP2, the cleavage process is SCAP independent. The processed ATF6 is subsequently translocated to the nucleus, where it binds to UPR genes containing ER stress response element (ERSE), activating gene transcription (Shen and Prywes, 2005). Collectively, the activation of these stress sensors leads to protein translation attenuation, as well as transcriptional activation of UPR genes involved in protein folding, processing, degradation, and cellular apoptosis (Oslowski and Urano, 2011). In HCMV infected cells, the level of BiP is significantly elevated as a result of increasing BiP transcription by HCMV IE72 (IE1) and IE86 (IE2). In addition, HCMV also enhances BiP mRNA translation through the BiP IRES (Buchkovich et al., 2010). Thus, the induction of BiP by HCMV is likely to serve two purposes: providing stabilization to the HCMV AC, while acting as a repressor for ER stress.

During the process of viral egress, progeny viruses are released from cells by lysis or membrane budding. Several viruses, including HIV (Van Engelenburg et al., 2014; von Schwedler et al., 2003), Ebola (Silvestri et al., 2007), and HCV (Ariumi et al., 2011) utilize the ESCRT (endosomal sorting complex required for transport) machinery for the release of the virion. The core ESCRT machinery consists of five protein complexes (ESCRT-0, -I, II, -III, and VPS4-VTA1) (von Schwedler et al., 2003). Vacuolar protein sorting-4 (VPS4) is a critical ATPase that acts as the final step in the release of ESCRT complexes from membranes (Stuchell-Brereton et al., 2007). The assembly of the ESCRT complex begins when the cargo interacts with one of several ESCRT-associated proteins, such as TSG101 (tumour susceptibility gene-101), or ALIX

(apoptosis linked gene-2 interacting protein X). This event triggers the formation of the ESCRT-I complex, and the further recruitment of the ESCRT-II complex. The formation of ESCRT-II permits the subsequent establishment of the ESCRT-III complex. The ESCRT-III complex is the most important ESCRT component because it directly mediates the cleavage of the vesicle from the cell membrane (Wollert et al., 2009). In Saccharomyces cerevisiae, the ESCRT-III complex is assembled in a specific order, with VPS20 (CHMP6), SNF7 (CHMP4A, B, C), VPS24 (CHMP3), and VPS2 (CHMP2A, B) first forming the essential unit, while nonessential units, including VPS60 (CHMP5) and DID2 (CHMP1A, B), are subsequently added to the complex (reviewed in Wollert et al., 2009). During the budding process of HIV, the HIV-1 Gag p6 protein recruits the ESCRT-I via an L-domain. This interaction is mediated by conserved amino acid motifs (PTAP, PPXY, and YXXL) of the L-domain with components of the ESCRT complex (Van Engelenburg et al., 2014; Morita et al., 2011). Gag p6 also directly interacts with ALIX, resulting in the recruitment of CHMP4 subunits and the activation of the ESCRT-III complex (Wollert et al., 2009). In the Ebola virus, the matrix protein VP40 recruits TSG101, resulting in the assembly of the ESCRT-I complex, and the subsequent activation of the ESCRT pathway (Silvestri et al., 2007). Importantly, from these studies, silencing of CHMP4 or VPS4 led to significant viral inhibition. In herpes virus, overexpression of dominant-negative TSG101 or ALIX had no effects on HSV-1 virion production and release, whereas dominant-negative ESCRT-III proteins significantly inhibited viral replication (Pawliczek and Crump, 2009). This suggests that different from HIV and Ebola virus, HSV-1 could directly recruit the ESCRT-III complex without complex –II and –I. The importance of ESCRT-VPS4 was further demonstrated showing the incorporation of CHMP2B, CHMP6, and VPS4 as part of the HSV-1 matured particle.

In contrast to the HSV-1 studies, the work of Fraile-Ramos et al., 2007 first showed that siRNA knockdown of Tsg101, Alix, or Vps4 in RPE1 cells (human retinal pigmented epithelial) had no effects on the replication of HCMV-AD169. This result indicates that the egress of HCMV is ESCRT independent. However, the work of Tandon, AuCoin, & Mocarski, 2009 showed that overexpression of dominant-negative

CHMP1A (the ESCRT-III complex) or VPS4 in HFFs significantly inhibits HCMV-Towne replication, while overexpression of dominant-negative TGS101 or ALIX did not. This finding implicates that similar to HSV-1, HCMV can directly recruit the ESCRT-III complex for egress, and that ESCRT-VPS4 plays an important role in the replication cycle of the virus. It was argued that due to the defective expression of UL131, HCMV-AD169 was incapable of efficient entry and replication in RPE1 (Detrick et al., 1996). Thus, Tandon, AuCoin, & Mocarski, 2009 indicated that the experimental design from Fraile-Ramos et al., 2007 was flawed. The importance of ESCRT-III-VPS4 in the egress of HCMV was further shown in independent microscopy experiments showing that both CHMP1A and VPS4 are co-localized to the HCMV AC (Das and Pellett, 2011). Despite the disagreement between studies, the ESCRT pathway is likely to be one of the important egress routes of the virus. These findings are illustrated in Figure 6.2**D**. Currently, there is no information regarding the formation of the AC in MCMV. The utilization of microscopy to examine the composition of MCMV AC will be one of the important steps in clarifying the assembly process of MCMV.

Previous studies in HCMV showed that Rab6a is required for the trafficking of HCMV pp150 (UL32) via BicD1. Mutation of tegument protein pp150 inhibits the spreading of the virus (AuCoin et al., 2006b). In my results, silencing of Rab6a or BicD1 also showed significant inhibition on MCMV replication. Currently, the cargo for Rab6a is unknown. It is possible that the translocation of MCMV M32 also requires Rab6a and BicD1. Although both UL32 and M32 share the same nomenclature, MCMV M32 only shares 27% amino acid identity, and 44% DNA sequence similarity to HCMV UL32. Thus, it is possible that the functions of the two genes are completely different. This is evident in the study by AuCoin et al., 2006, showing that murine CMV M32 failed to complement the growth defect of HCMV-ΔUL32, while African green monkey CMV UL32 homolog rescued the virus. This is consistent with the considerable divergence between human and murine cytomegalovirus. The difference between HCMV UL32 and MCMV M32 also suggests that how the virus interacts with the ESCRT machinery might be different. As mentioned above, the recruitment of the ESCRT-I complex depends on the interaction between an L-domain containing protein and the ESCRT

adaptor proteins, such as Tsg101 and ALIX. In HCMV, one of the two L-domain containing viral proteins is M32 (the other being pUL56, a nonstructural protein). However, the work of Tandon et al., 2009 showed that the recruitment of the ESCRT-III complex by HCMV is independent of Tsg101, M32 L-domain, and ESCRT-I. In contrast, my results showed that silencing of Tsg101 significantly inhibits MCMV replication (Figure S5.1). This argues that unlike HCMV, the recruitment of the ESCRT-III complex by MCMV requires the initial formation of complex –I, possibly through the interaction between TSG101 and MCMV M32. In addition, disruption of the murine ESCRT-III complex (via silencing Chmp4b) also led to significant inhibition in MCMV replication (Figure S5.1). Though there are differences between how MCMV and HCMV interact with the host transport machinery, my preliminary results support a common route of egress between the two viruses.

In summary, results presented in this chapter demonstrate the dependency of MCMV replication on components of the cellular vesicular transport pathway. These findings argue for important new functions of RabGTPases in the intracellular localization and accumulation of CMV proteins during virus assembly.

5.4 References

Acin-Perez, R., Salazar, E., Kamenetsky, M., Buck, J., Levin, L.R., and Manfredi, G. (2009). Cyclic AMP produced inside mitochondria regulates oxidative phosphorylation. Cell Metab. 9, 265–276.

Aligianis, I.A., Johnson, C.A., Gissen, P., Chen, D., Hampshire, D., Hoffmann, K., Maina, E.N., Morgan, N. V, Tee, L., Morton, J., et al. (2005). Mutations of the catalytic subunit of RAB3GAP cause Warburg Micro syndrome. Nat. Genet. 37, 221–223.

Aligianis, I.A., Morgan, N. V, Mione, M., Johnson, C.A., Rosser, E., Hennekam, R.C., Adams, G., Trembath, R.C., Pilz, D.T., Stoodley, N., et al. (2006). Mutation in Rab3 GTPase-activating protein (RAB3GAP) noncatalytic subunit in a kindred with Martsolf syndrome. Am. J. Hum. Genet. 78, 702–707.

Alto, N.M., Soderling, J., and Scott, J.D. (2002). Rab32 is an A-kinase anchoring protein and participates in mitochondrial dynamics. J. Cell Biol. 158, 659–668.

Alwine, J. (2012). The human cytomegalovirus assembly compartment: A masterpiece of viral manipulation of cellular processes that facilitates assembly and egress. PLoS Pathog. 8, 1–4.

Ariumi, Y., Kuroki, M., Maki, M., Ikeda, M., Dansako, H., Wakita, T., and Kato, N. (2011). The ESCRT system is required for hepatitis C virus production. PLoS One 6, e14517.

AuCoin, D.P., Smith, G.B., Meiering, C.D., and Mocarski, E.S. (2006a). Betaherpesvirus-conserved cytomegalovirus tegument protein ppUL32 (pp150) controls cytoplasmic events during virion maturation. J. Virol. 80, 8199–8210.

AuCoin, D.P., Smith, G.B., Meiering, C.D., and Mocarski, E.S. (2006b). Betaherpesvirus-conserved cytomegalovirus tegument protein ppUL32 (pp150) controls cytoplasmic events during virion maturation. J. Virol. 80, 8199–8210.

Baetz, N.W., and Goldenring, J.R. (2013). Rab11-family interacting proteins define spatially and temporally distinct regions within the dynamic Rab11a-dependent recycling system. Mol. Biol. Cell 24, 643–658.

Bao, X., and Faris, A. (2002). Molecular cloning, bacterial expression and properties of Rab31and Rab32. Eur. J. … 269, 259–271.

Beranger, F., Cadwallader, K., Porfiri, E., Powers, S., Evans, T., de Gunzburg, J., and Hancock, J.F. (1994). Determination of structural requirements for the interaction of Rab6 with RabGDI and Rab geranylgeranyltransferase. J. Biol. Chem. 269, 13637–13643.

Bertolotti, a, Zhang, Y., Hendershot, L.M., Harding, H.P., and Ron, D. (2000). Dynamic interaction of BiP and ER stress transducers in the unfolded-protein response. Nat. Cell Biol. 2, 326–332.

Bhattacharya, M., Ojha, N., Solanki, S., Mukhopadhyay, C.K., Madan, R., Patel, N., Krishnamurthy, G., Kumar, S., Basu, S.K., and Mukhopadhyay, A. (2006). IL-6 and IL-12 specifically regulate the expression of Rab5 and Rab7 via distinct signaling pathways. EMBO J. 25, 2878–2888.

Blanc, M., Hsieh, W.Y.Y., Robertson, K.A. a, Kropp, K.A. a, Forster, T., Shui, G., Lacaze, P., Watterson, S., Griffiths, S.J.J., Spann, N.J.J., et al. (2013). The transcription factor STAT-1 couples macrophage synthesis of 25-hydroxycholesterol to the interferon antiviral response. Immunity 38, 106–118.

Bonifacino, J.S. (2004). Insights into the biogenesis of lysosome-related organelles from the study of the Hermansky-Pudlak syndrome. Ann. N. Y. Acad. Sci. 1038, 103–114.

Bordier, B.B., Ohkanda, J., Liu, P., Lee, S., Salazar, F.H., Marion, P.L., Ohashi, K., Meuse, L., Kay, M.A., Casey, J.L., et al. (2003). In vivo antiviral efficacy of prenylation inhibitors. Pharmacia 112, 407–414.

Brunner, Y., Coute, Y., Iezzi, M., Foti, M., Fukuda, M., Hochstrasser, D.F., Wollheim, C.B., and Sanchez, J.C. (2007). Proteomics analysis of insulin secretory granules. Mol. Cell. Proteomics 6, 1007–1017.

Buchkovich, N.J., Maguire, T.G., Yu, Y., Paton, A.W., Paton, J.C., and Alwine, J.C. (2008). Human cytomegalovirus specifically controls the levels of the endoplasmic reticulum chaperone BiP/GRP78, which is required for virion assembly. J. Virol. 82, 31–39.

Buchkovich, N.J., Maguire, T.G., Paton, A.W., Paton, J.C., and Alwine, J.C. (2009). The endoplasmic reticulum chaperone BiP/GRP78 is important in the structure and function of the human cytomegalovirus assembly compartment. J. Virol. 83, 11421–11428.

Buchkovich, N.J., Yu, Y., Pierciey, F.J., and Alwine, J.C. (2010). Human cytomegalovirus induces the endoplasmic reticulum chaperone

BiP through increased transcription and activation of translation by using the BiP internal ribosome entry site. J. Virol. 84, 11479–11486.

Bultema, J.J., and Di Pietro, S.M. (2013). Cell type-specific Rab32 and Rab38 cooperate with the ubiquitous lysosome biogenesis machinery to synthesize specialized lysosome-related organelles. Small GTPases 4, 16–21.

Carroll, K.S., Hanna, J., Simon, I., Krise, J., Barbero, P., and Pfeffer, S.R. (2001). Role of Rab9 GTPase in facilitating receptor recruitment by TIP47. Science 292, 1373–1376.

Cepeda, V., and Fraile-Ramos, A. (2011). A role for the SNARE protein syntaxin 3 in human cytomegalovirus morphogenesis. Cell. Microbiol. 13, 846–858.

Chen, Y., Wang, Y., Zhang, J., Deng, Y., Jiang, L., Song, E., Wu, X.S., Hammer, J. a, Xu, T., and Lippincott-Schwartz, J. (2012). Rab10 and myosin-Va mediate insulin-stimulated GLUT4 storage vesicle translocation in adipocytes. J. Cell Biol. 198, 545–560.

Cohen-Solal, K. a., Sood, R., Marin, Y., Crespo-Carbone, S.M., Sinsimer, D., Martino, J.J., Robbins, C., Makalowska, I., Trent, J., and Chen, S. (2003). Identification and characterization of mouse Rab32 by mRNA and protein expression analysis. Biochim. Biophys. Acta - Proteins Proteomics 1651, 68–75.

Coller, K.E., Berger, K.L., Heaton, N.S., Cooper, J.D., Yoon, R., and Randall, G. (2009). RNA interference and single particle tracking analysis of hepatitis C virus endocytosis. PLoS Pathog 5, e1000702.

D'Adamo, P., Menegon, A., Lo Nigro, C., Grasso, M., Gulisano, M., Tamanini, F., Bienvenu, T., Gedeon, A.K., Oostra, B., Wu, S.K., et al. (1998). Mutations in GDI1 are responsible for X-linked non-specific mental retardation. Nat. Genet. 19, 134–139.

D'Adamo, P., Welzl, H., Papadimitriou, S., Raffaele di Barletta, M., Tiveron, C., Tatangelo, L., Pozzi, L., Chapman, P.F., Knevett, S.G., Ramsay, M.F., et al. (2002). Deletion of the mental retardation gene Gdi1 impairs associative memory and alters social behavior in mice. Hum. Mol. Genet. 11, 2567–2580.

Dalfo, E., Gomez-Isla, T., Rosa, J.L., Nieto Bodelon, M., Cuadrado Tejedor, M., Barrachina, M., Ambrosio, S., and Ferrer, I. (2004). Abnormal alpha-synuclein interactions with Rab proteins in alpha-synuclein A30P transgenic mice. J. Neuropathol. Exp. Neurol. 63, 302–313.

Das, S., and Pellett, P.E. (2011). Spatial relationships between markers for secretory and endosomal machinery in human cytomegalovirus-infected cells versus those in uninfected cells. J. Virol. 85, 5864–5879.

Das, S., Vasanji, A., and Pellett, P.E. (2007). Three-dimensional structure of the human cytomegalovirus cytoplasmic virion assembly complex includes a reoriented secretory apparatus. J. Virol. 81, 11861–11869.

Deraeve, C., Guo, Z., Bon, R.S., Blankenfeldt, W., DiLucrezia, R., Wolf, A., Menninger, S., Stigter, E.A., Wetzel, S., Choidas, A., et al. (2012). Psoromic acid is a selective and covalent Rab-prenylation inhibitor targeting autoinhibited RabGGTase. J. Am. Chem. Soc. 134, 7384–7391.

Detrick, B., Rhame, J., Wang, Y., Nagineni, C.N., and Hooks, J.J. (1996). Cytomegalovirus replication in human retinal pigment epithelial cells. Altered expression of viral early proteins. Invest. Ophthalmol. Vis. Sci. 37, 814–825.

Dirac-Svejstrup, A.B., Sumizawa, T., and Pfeffer, S.R. (1997). Identification of a GDI displacement factor that releases endosomal Rab GTPases from Rab-GDI. EMBO J. 16, 465–472.

Eggenschwiler, J.T., Espinoza, E., and Anderson, K. V (2001). Rab23 is an essential negative regulator of the mouse Sonic hedgehog signalling pathway. Nature 412, 194–198.

Van Engelenburg, S.B., Shtengel, G., Sengupta, P., Waki, K., Jarnik, M., Ablan, S.D., Freed, E.O., Hess, H.F., and Lippincott-Schwartz, J. (2014). Distribution of ESCRT machinery at HIV assembly sites reveals virus scaffolding of ESCRT subunits. Science 343, 653–656.

Fasshauer, D., Sutton, R.B., Brunger, A.T., and Jahn, R. (1998). Conserved structural features of the synaptic fusion complex: SNARE proteins reclassified as Q- and R-SNAREs. Proc. Natl. Acad. Sci. U. S. A. 95, 15781–15786.

Fraile-Ramos, A., Pelchen-Matthews, A., Risco, C., Rejas, M.T., Emery, V.C., Hassan-Walker, A.F., Esteban, M., and Marsh, M. (2007). The ESCRT machinery is not required for human cytomegalovirus envelopment. Cell. Microbiol. 9, 2955–2967.

Fraile-Ramos, A., Cepeda, V., Elstak, E., and van der Sluijs, P. (2010). Rab27a is required for human cytomegalovirus assembly. PLoS One 5, e15318.

Fukuda, M. (2003). Distinct Rab binding specificity of Rim1, Rim2, rabphilin, and Noc2. Identification of a critical determinant of Rab3A/Rab27A recognition by Rim2. J Biol Chem 278, 15373–15380.

Fukuda, M. (2008). Regulation of secretory vesicle traffic by Rab small GTPases. Cell Mol Life Sci 65, 2801–2813.

Gasser, T. (2009). Molecular pathogenesis of Parkinson disease: insights from genetic studies. Expert Rev. Mol. Med. 11, e22.

Gazdag, E.M., Schöbel, S., Shkumatov, A. V, Goody, R.S., and Itzen, A. (2014). The structure of the N-terminal domain of the Legionella protein SidC. J. Struct. Biol. 186, 188–194.

Goody, R.S., Rak, A., and Alexandrov, K. (2005). The structural and mechanistic basis for recycling of Rab proteins between membrane compartments. Cell. Mol. Life Sci. 62, 1657–1670.

Grieshaber, S.S., Grieshaber, N. a, and Hackstadt, T. (2003). Chlamydia trachomatis uses host cell dynein to traffic to the microtubule-organizing center in a p50 dynamitin-independent process. J. Cell Sci. 116, 3793–3802.

Hales, C.M., Griner, R., Hobdy-Henderson, K.C., Dorn, M.C., Hardy, D., Kumar, R., Navarre, J., Chan, E.K., Lapierre, L. a, and Goldenring, J.R. (2001). Identification and characterization of a family of Rab11-interacting proteins. J. Biol. Chem. 276, 39067–39075.

Hales, C.M., Vaerman, J.-P., and Goldenring, J.R. (2002). Rab11 family interacting protein 2 associates with Myosin Vb and regulates plasma membrane recycling. J. Biol. Chem. 277, 50415–50421.

Harrison, R.E., Brumell, J.H., Khandani, A., Bucci, C., Scott, C.C., Jiang, X., Finlay, B.B., and Grinstein, S. (2004). Salmonella impairs RILP recruitment to Rab7 during maturation of invasion vacuoles. Mol. Biol. Cell 15, 3146–3154.

Hertel, L., and Mocarski, E.S. (2004). Global Analysis of Host Cell Gene Expression Late during Cytomegalovirus Infection Reveals Extensive Dysregulation of Cell Cycle Gene Expression and Induction of Pseudomitosis Independent of US28 Function Global Analysis of Host Cell Gene Expression Late .

Hill, E., Clarke, M., and Barr, F. a (2000). The Rab6-binding kinesin, Rab6-KIFL, is required for cytokinesis. EMBO J. 19, 5711–5719.

Hoffmann, C., Finsel, I., Otto, A., Pfaffinger, G., Rothmeier, E., Hecker, M., Becher, D., and Hilbi, H. (2013). Functional analysis of novel Rab GTPases identified in the proteome of purified Legionella-containing vacuoles from macrophages. Cell. Microbiol.

Hoogenraad, C.C., Akhmanova, a, Howell, S. a, Dortland, B.R., De Zeeuw, C.I., Willemsen, R., Visser, P., Grosveld, F., and Galjart, N. (2001). Mammalian Golgi-associated Bicaudal-D2 functions in the dynein-dynactin pathway by interacting with these complexes. EMBO J. 20, 4041–4054.

Hook, L.M., Grey, F., Grabski, R., Tirabassi, R., Doyle, T., Hancock, M., Landais, I., Jeng, S., McWeeney, S., Britt, W., et al. (2014). Cytomegalovirus miRNAs Target Secretory Pathway Genes to Facilitate Formation of the Virion Assembly Compartment and Reduce Cytokine Secretion. Cell Host Microbe 15, 363–373.

Hutagalung, A.H., and Novick, P.J. (2011). Role of Rab GTPases in membrane traffic and cell physiology. Physiol Rev 91, 119–149.

Indran, S. V, and Britt, W.J. (2011). A role for the small GTPase Rab6 in assembly of human cytomegalovirus. J. Virol. 85, 5213–5219.

Indran, S. V, Ballestas, M.E., and Britt, W.J. (2010). Bicaudal D1-dependent trafficking of human cytomegalovirus tegument protein pp150 in virus-infected cells. J. Virol. 84, 3162–3177.

Jenkins, D., Seelow, D., Jehee, F.S., Perlyn, C.A., Alonso, L.G., Bueno, D.F., Donnai, D., Josifova, D., Mathijssen, I.M., Morton, J.E., et al. (2007). RAB23 mutations in Carpenter syndrome imply an unexpected role for hedgehog signaling in cranial-suture development and obesity. Am. J. Hum. Genet. 80, 1162–1170.

Johnson, D.C., and Baines, J.D. (2011). Herpesviruses remodel host membranes for virus egress. Nat. Rev. Microbiol. 9, 382–394.

Kerr, K., Entrican, G., McKeever, D., and Longbottom, D. (2005). Immunopathology of Chlamydophila abortus infection in sheep and mice. Res. Vet. Sci. 78, 1–7.

Kim, S., McKay, R.R., Miller, K., and Shortridge, R.D. (1995). Multiple subtypes of phospholipase C are encoded by the norpA gene of Drosophila melanogaster. J. Biol. Chem. 270, 14376–14382.

Kramer, T., and Enquist, L.W. (2013). Directional spread of alphaherpesviruses in the nervous system. Viruses 5, 678–707.

Krzyzaniak, M. a, Mach, M., and Britt, W.J. (2009). HCMV-encoded glycoprotein M (UL100) interacts with Rab11 effector protein FIP4. Traffic 10, 1439–1457.

Lerner, E.C., Zhang, T.T., Knowles, D.B., Qian, Y., Hamilton, A.D., and Sebti, S.M. (1997). Inhibition of the prenylation of K-Ras, but not H- or N-Ras, is highly resistant to CAAX peptidomimetics and requires both a farnesyltransferase and a geranylgeranyltransferase I

inhibitor in human tumor cell lines. Oncogene 15, 1283–1288.

Liang, Y., Lin, S., Zou, L., Zhou, H., Zhang, J., Su, B., and Wan, Y. (2012). Expression profiling of Rab GTPases reveals the involvement of Rab20 and Rab32 in acute brain inflammation in mice. Neurosci. Lett. 527, 110–114.

Liu, S.T.H., Sharon-Friling, R., Ivanova, P., Milne, S.B., Myers, D.S., Rabinowitz, J.D., Brown, H.A., and Shenk, T. (2011). Synaptic vesicle-like lipidome of human cytomegalovirus virions reveals a role for SNARE machinery in virion egress. Proc. Natl. Acad. Sci. U. S. A. 108, 12869–12874.

Lombardi, D., Soldati, T., Riederer, M. a, Goda, Y., Zerial, M., and Pfeffer, S.R. (1993). Rab9 functions in transport between late endosomes and the trans Golgi network. EMBO J. 12, 677–682.

Lozach, P.Y., Mancini, R., Bitto, D., Meier, R., Oestereich, L., Overby, A.K., Pettersson, R.F., and Helenius, A. (2010). Entry of bunyaviruses into mammalian cells. Cell Host Microbe 7, 488–499.

Machner, M.P., and Isberg, R.R. (2006). Targeting of host Rab GTPase function by the intravacuolar pathogen Legionella pneumophila. Dev. Cell 11, 47–56.

Machner, M.P., and Isberg, R.R. (2007). A bifunctional bacterial protein links GDI displacement to Rab1 activation. Science (80-.). 318, 974–977.

Masuda, E.S., Luo, Y., Young, C., Shen, M., Rossi, A.B., Huang, B.C., Yu, S., Bennett, M.K., Payan, D.G., and Scheller, R.H. (2000). Rab37 is a novel mast cell specific GTPase localized to secretory granules. FEBS Lett. 470, 61–64.

Matanis, T., Akhmanova, A., Wulf, P., Del Nery, E., Weide, T., Stepanova, T., Galjart, N., Grosveld, F., Goud, B., De Zeeuw, C.I., et al. (2002). Bicaudal-D regulates COPI-independent Golgi-ER transport by recruiting the dynein-dynactin motor complex. Nat. Cell Biol. 4, 986–992.

Maurer-Stroh, S., Koranda, M., Benetka, W., Schneider, G., Sirota, F.L., and Eisenhaber, F. (2007). Towards complete sets of farnesylated and geranylgeranylated proteins. PLoS Comput. Biol. 3, e66.

McGeoch, D.J., Cook, S., Dolan, A., Jamieson, F.E., and Telford, E.A. (1995). Molecular phylogeny and evolutionary timescale for the family of mammalian herpesviruses. J Mol Biol 247, 443–458.

Meresse, S., Steele-Mortimer, O., Finlay, B.B., and Gorvel, J.P. (1999). The rab7 GTPase controls the maturation of Salmonella typhimurium-containing vacuoles in HeLa cells. EMBO J. 18, 4394–4403.

Miserey-Lenkei, S., Waharte, F., Boulet, A., Cuif, M.-H., Tenza, D., El Marjou, A., Raposo, G., Salamero, J., Héliot, L., Goud, B., et al. (2007). Rab6-interacting protein 1 links Rab6 and Rab11 function. Traffic 8, 1385–1403.

Moorhead, a R., Rzomp, K. a, and Scidmore, M. a (2007). The Rab6 effector Bicaudal D1 associates with Chlamydia trachomatis inclusions in a biovar-specific manner. Infect. Immun. 75, 781–791.

Morita, E., Sandrin, V., McCullough, J., Katsuyama, A., Baci Hamilton, I., and Sundquist, W.I. (2011). ESCRT-III protein requirements for HIV-1 budding. Cell Host Microbe 9, 235–242.

Nantais, D.E., Schwemmle, M., Stickney, J.T., Vestal, D.J., and Buss, J.E. (1996). Prenylation of an interferon-gamma-induced GTP-binding protein: the human guanylate binding protein, huGBP1. J Leukoc Biol 60, 423–431.

Nashida, T., Imai, A., and Shimomura, H. (2006). Relation of Rab26 to the amylase release from rat parotid acinar cells. Arch. Oral Biol. 51, 89–95.

Oslowski, C.M., and Urano, F. (2011). Measuring ER stress and the unfolded protein response using mammalian tissue culture system. (Elsevier Inc.).

Ozawa, H., and Takata, K. (1995). The granin family--its role in sorting and secretory granule formation. Cell Struct. Funct. 20, 415–420.

Pawliczek, T., and Crump, C.M. (2009). Herpes simplex virus type 1 production requires a functional ESCRT-III complex but is independent of TSG101 and ALIX expression. J. Virol. 83, 11254–11264.

Peranen, J., Auvinen, P., Virta, H., Wepf, R., and Simons, K. (1996). Rab8 promotes polarized membrane transport through reorganization of actin and microtubules in fibroblasts. J. Cell Biol. 135, 153–167.

Di Pietro, S.M., and Dell'Angelica, E.C. (2005). The cell biology of Hermansky-Pudlak syndrome: recent advances. Traffic 6, 525–533.

Pylypenko, O., Rak, A., Reents, R., Niculae, A., Sidorovitch, V., Cioaca, M.D., Bessolitsyna, E., Thoma, N.H., Waldmann, H., Schlichting, I., et al. (2003). Structure of Rab escort protein-1 in complex with Rab geranylgeranyltransferase. Mol. Cell 11, 483–494.

Reed, S.E., Hodgson, L.R., Song, S., May, M.T., Kelly, E.E., McCaffrey, M.W., Mastick, C.C., Verkade, P., and Tavaré, J.M. (2013). A role for Rab14 in the endocytic trafficking of GLUT4 in 3T3-L1 adipocytes. J. Cell Sci. 126, 1931–1941.

Rickman, C., Jimenez, J.L., Graham, M.E., Archer, D.A., Soloviev, M., Burgoyne, R.D., and Davletov, B. (2006). Conserved prefusion protein assembly in regulated exocytosis. Mol. Biol. Cell 17, 283–294.

Roberts, K.L., and Baines, J.D. (2010). Myosin Va enhances secretion of herpes simplex virus 1 virions and cell surface expression of viral glycoproteins. J. Virol. 84, 9889–9896.

Rowe, R.K., Suszko, J.W., and Pekosz, A. (2008). Roles for the recycling endosome, Rab8, and Rab11 in hantavirus release from epithelial cells. Virology 382, 239–249.

Rzomp, K.A., Scholtes, L.D., Briggs, B.J., Whittaker, G.R., and Scidmore, M.A. (2003). Rab GTPases are recruited to chlamydial inclusions in both a species-dependent and species-independent manner. Infect. Immun. 71, 5855–5870.

Sanchez, V., Greis, K.D., Sztul, E., and Britt, W.J. (2000). Accumulation of virion tegument and envelope proteins in a stable cytoplasmic compartment during human cytomegalovirus replication: characterization of a potential site of virus assembly. J. Virol. 74, 975–986.

Von Schwedler, U.K., Stuchell, M., Müller, B., Ward, D.M., Chung, H.-Y., Morita, E., Wang, H.E., Davis, T., He, G.-P., Cimbora, D.M., et al. (2003). The protein network of HIV budding. Cell 114, 701–713.

Seabra, M.C., and Coudrier, E. (2004). Rab GTPases and myosin motors in organelle motility. Traffic 5, 393–399.

Seabra, M.C., Brown, M.S., and Goldstein, J.L. (1993). Retinal degeneration in choroideremia: deficiency of rab geranylgeranyl transferase. Science (80-.). 259, 377–381.

Seabra, M.C., Ho, Y.K., and Anant, J.S. (1995). Deficient geranylgeranylation of Ram/Rab27 in choroideremia. J. Biol. Chem. 270, 24420–24427.

Seabra, M.C., Mules, E.H., and Hume, A.N. (2002). Rab GTPases, intracellular traffic and disease. Trends Mol. Med. 8, 23–30.

Shen, J., and Prywes, R. (2005). ER stress signaling by regulated proteolysis of ATF6. Methods 35, 382–389.

Silvestri, L.S., Ruthel, G., Kallstrom, G., Warfield, K.L., Swenson, D.L., Nelle, T., Iversen, P.L., Bavari, S., and Aman, M.J. (2007). Involvement of vacuolar protein sorting pathway in Ebola virus release independent of TSG101 interaction. J. Infect. Dis. 196 Suppl , S264–70.

Smith, R.D., Willett, R., Kudlyk, T., Pokrovskaya, I., Adrienne, W., Paton, J.C., and Lupashin, V. V (2010). retrograde trafficking pathway that is exploited by SubAB toxin. 10, 1502–1517.

Sommer, T., and Jarosch, E. (2002). BiP binding keeps ATF6 at bay. Dev. Cell 3, 1–2.

Stenmark, H. (2009). Rab GTPases as coordinators of vesicle traffic. Nat Rev Mol Cell Biol 10, 513–525.

Stuchell-Brereton, M.D., Skalicky, J.J., Kieffer, C., Karren, M.A., Ghaffarian, S., and Sundquist, W.I. (2007). ESCRT-III recognition by VPS4 ATPases. Nature 449, 740–744.

Sun, Y., Bilan, P.J., Liu, Z., and Klip, A. (2010). Rab8A and Rab13 are activated by insulin and regulate GLUT4 translocation in muscle cells. Proc. Natl. Acad. Sci. U. S. A. 107, 19909–19914.

Tamura, K., Ohbayashi, N., Maruta, Y., Kanno, E., Itoh, T., and Fukuda, M. (2009). Varp is a novel Rab32/38-binding protein that regulates Tyrp1 trafficking in melanocytes. Mol. Biol. Cell 20, 2900–2908.

Tandon, R., AuCoin, D.P., and Mocarski, E.S. (2009). Human cytomegalovirus exploits ESCRT machinery in the process of virion maturation. J. Virol. 83, 10797–10807.

Tsuboi, T., and Fukuda, M. (2006). Rab3A and Rab27A cooperatively regulate the docking step of dense-core vesicle exocytosis in PC12 cells. J. Cell Sci. 119, 2196–2203.

Varnum, S.M., Streblow, D.N., Monroe, M.E., Smith, P., Auberry, K.J., Pasa-Tolic, L., Wang, D., Camp 2nd, D.G., Rodland, K., Wiley, S., et al. (2004). Identification of proteins in human cytomegalovirus (HCMV) particles: the HCMV proteome. J. Virol. 78, 10960–10966.

Vestal, D.J., Maki, R.A., and Buss, J.E. (1995). Induction of a prenylated 65-kd protein in macrophages by interferon or lipopolysaccharide. J Leukoc Biol 58, 607–615.

Wagner, A.C., Strowski, M.Z., Goke, B., and Williams, J.A. (1995). Molecular cloning of a new member of the Rab protein family, Rab 26, from rat pancreas. Biochem. Biophys. Res. Commun. 207, 950–956.

Wang, C., Gale Jr., M., Keller, B.C., Huang, H., Brown, M.S., Goldstein, J.L., and Ye, J. (2005). Identification of FBL2 as a geranylgeranylated cellular protein required for hepatitis C virus RNA replication. Mol Cell 18, 425–434.

Wasmeier, C., Romao, M., Plowright, L., Bennett, D.C., Raposo, G., and Seabra, M.C. (2006). Rab38 and Rab32 control post-Golgi trafficking of melanogenic enzymes. J. Cell Biol. 175, 271–281.

Wilson, A.L., Erdman, R.A., Castellano, F., and Maltese, W.A. (1998). Prenylation of Rab8 GTPase by type I and type II geranylgeranyl transferases. Biochem. J. 333 (Pt 3, 497–504.

Wisner, T.W., and Johnson, D.C. (2004). Redistribution of cellular and herpes simplex virus proteins from the trans-golgi network to cell junctions without enveloped capsids. J. Virol. 78, 11519–11535.

Wollert, T., Yang, D., Ren, X., Lee, H.H., Im, Y.J., and Hurley, J.H. (2009). The ESCRT machinery at a glance. J. Cell Sci. 122, 2163–2166.

Ye, J., Rawson, R.B., Komuro, R., Chen, X., Dave, U.P., Prywes, R., Brown, M.S., and Goldstein, J.L. (2000). of Membrane-Bound ATF6 by the Same Proteases that Process SREBPs. 6, 1355–1364.

Yoshie, S., Imai, A., Nashida, T., and Shimomura, H. (2000). Expression, characterization, and localization of Rab26, a low molecular weight GTP-binding protein, in the rat parotid gland. Histochem. Cell Biol. 113, 259–263.

Zhang, X., He, X., Fu, X.-Y., and Chang, Z. (2006). Varp is a Rab21 guanine nucleotide exchange factor and regulates endosome dynamics. J. Cell Sci. 119, 1053–1062.

5.5 Supporting information

Table S5.1 Bioinformatics prediction of all prenylation targets in human identified in Maurer-Stroh et al., 2007

No.	Gene name	Prenylation type	Description
1	Lrrfip1	FT	GC-binding factor 2, TAR RNA-interacting protein
2	Inpp5a	FT	Type I inositol-1,4,5 trisphosphate 5-phosphatase
3	Phkb	FT	Isoform 2
4	Nap1l1	FT	Nucleosome assembly protein 1-like 1
5	Dnaja4	FT	DNAJA4 protein; possibly protein folding
6	Pex7	FT	Peroxisomal biogenesis factor 7; N terminus (1..113) is identical to PEX7_HUMAN, O00628; but C teminus differs !!
7	Loc116437	FT	Putative uncharacterized protein DKFZp434L2430
8	Ptp4a1	FT	Protein-tyrosine phosphatase 4a1;2 isoforms ?, C-termini identical
9	Ip6k2	FT	Inositol hexakisphosphate kinase 2,new isoform ?
10	C9orf169	FT	UPF0574 protein C9orf169
11	Tfdp2	FT	Transcription factor Dp-2, seq. is part of TFDP2_HUMAN, Q14188 (pos 88..292) but not the C-terminus ?? fragment or isoform
12	Zfand2b	FT	AN1-type zinc finger protein 2B
13	PARF, c9orf86	FT	Putative GTP-binding protein Parf; seq. differs in the C-terminus from PARF_HUMAN, Q3YEC7 !!
14	Prickle4	FT	Prickle-like protein 4, isoform 3
15	Usp32	FT	Ubiquitin carboxyl-terminal hydrolase 32
16	Ttc24	FT	Tetratricopeptide repeat protein 24
17	Wdtc1	FT	WD and tetratricopeptide repeats protein 1
18	Nap1l4	FT	Nucleosome assembly protein 1-like 4, new isoform or wrong ?? C-terminus differs from NP1L4_HUMAN, Q99733
19	Rhoh	FT	Rho-related GTP-binding protein RhoH
20	Rap2c	FT	Ras-related protein Rap-2c
21	Rhoq	FT	Rho-related GTP-binding protein RhoQ
22	Prickle2	FT	Prickle-like protein 2
23	Rab28	FT	Ras-related protein Rab-28
24	Pde6a	FT	Rod cGMP-specific 3',5'-cyclic phosphodiesterase subunit alpha
25	Eras	FT	GTPase ERas
26	Hras	FT	GTPase HRas
27	Pde6c	FT	Cone cGMP-specific 3',5'-cyclic phosphodiesterase subunit alpha'
28	Prickle1	FT	Prickle-like protein 1
29	Ptgir	FT	Prostacyclin receptor
30	Rap2a	FT	Ras-related protein Rap-2a
31	Ston1	FT	Stonin-1
32	Ppp1r16b	FT	Protein phosphatase 1 regulatory inhibitor subunit 16B
33	Syt14	FT	Synaptotagmin-14, isoform 2
34	Rasd2	FT	GTP-binding protein Rhes
35	Grk1	FT	Rhodopsin kinase
36	Oas1	FT	2'-5'-oligoadenylate synthase 1
37	Rasd1	FT	Dexamethasone-induced Ras-related protein 1
38	Gin1	FT	Gypsy retrotransposon integrase-like protein 1, isoform 3
39	Inpp5e	FT	72 kDa inositol polyphosphate 5-phosphatase, isoform 2
40	Gng11	FT	Guanine nucleotide-binding protein G(I)/G(S)/G(O) subunit gamma-11
41	Gngt1	FT	Guanine nucleotide-binding protein G(T) subunit gamma-T1
42	Haghl	FT	Hydroxyacylglutathione hydrolase-like protein, isoform 1

43	Gngt2	FT	Guanine nucleotide-binding protein G(I)/G(S)/G(O) subunit gamma-T2
44	Gpr109b	FT	G-protein coupled receptor 109B
45	Aspa	FT	Aspartoacylase
46	Ehbp1l1	FT	EH domain-binding protein 1-like protein 1
47	Cenpf	FT	Centromere protein F
48	Ehbp1	FT	EH domain-binding protein 1, isoform 3
49	C6orf204	FT	Coiled-coil domain-containing protein C6orf204, isoform 1
50	Casp14l	FT	Putative caspase-14-like protein
51	Atxn2l	FT	Ataxin-2-like protein, isoform 3
52	Ecel1	FT	Endothelin-converting enzyme-like 1, isoform 2
53	Crb3	FT	Crumbs protein homolog 3, isoform 2
54	Dcaf8l1	FT	DDB1- and CUL4-associated factor 8-like protein 1
55	Dqx1	FT	ATP-dependent RNA helicase DQX1, isoform 2
56	Dhx32	FT	Putative pre-mRNA-splicing factor ATP-dependent RNA helicase DHX32
57	Dpcd	FT	Protein DPCD
58	Dcaf8l2	FT	DDB1- and CUL4-associated factor 8-like protein 2
59	Cst6	FT	Cystatin-M
60	Bex4	FT	Protein BEX4
61	Ankdd1b	FT	Ankyrin repeat and death domain-containing protein 1B
62	Dnaja1	FT	DnaJ homolog subfamily A member 1
63	Lo 730167	FT	similar to protein tyrosine phosphatase 4a1 isoform1
64	Scamper	FT	sphingolipid Ca2+ release mediating protein of endoplasmic reticulum
65	Slc37a2	FT	Sugar phosphate exchanger 2, isoform 3
66	Ccdc99	FT	Protein Spindly, isoform 2
67	Kiaa1432	FT	RIC1 homolog (guanyl nucleotide exchange factor)
68	Asgr1	FT	Putative uncharacterized protein ASGR1
69	Zc3hav1	FT	Zinc finger CCCH-type antiviral protein 1, isoform 4
70	Lrrfip1	FT	GC-binding factor 2, TAR RNA-interacting protein
71	Inpp5a	FT	Type I inositol-1,4,5 trisphosphate 5-phosphatase
72	C1orf198	FT	C1orf198
73	Fam83f	FT	Protein FAM83F, isoform 2
74	-	FT	cDNA FLJ41508 fis, clone BRTHA2009846(gi:34529065)
75	Arrdc2	FT	Arrestin domain-containing protein 2, isoform 1
76	Cenpe	FT	Centromere-associated protein E, isoform 3
77	Dcaf8	FT	highly similar to Homo sapiens WD repeat domain 42A
78	C5orf45	FT	Putative uncharacterized protein C5orf45
79	Phkb	FT	Phosphorylase b kinase regulatory subunit beta,
80	Rab40b	FT	Ras-related protein Rab-40B
81	Irf5	FT	Interferon regulatory factor 5 variant 11
82	Lyzl1	FT	Lysozyme-like protein 1, isoform 1
83	Possibly new isoform of COL28A1	FT	Collagen alpha-1(XXVIII) chain, possibly serine-type endopeptidase inhibitor activity
84	Tmem134	FT	Transmembrane protein 134, isoform 3
85	C22orf30	FT	Uncharacterized protein C22orf30
86	Ccdc21	FT	Coiled-coil domain-containing protein 21, isoform 3
87	Gbp1	FT	interferon-induced guanylate binding protein 1
88	Nap1l1	FT	Nucleosome assembly protein 1-like 1
89	Inf2	FT	inverted formin-2 isoform 1
90	Ptp4a2	FT	Protein tyrosine phosphatase type IVA 2
91	Ulk3	FT	serine/threonine-protein kinase ULK3
92	Loc197350	FT	Putative caspase-14-like protein pseudogene??

93	Ap1s3	FT	AP-1 complex subunit sigma-3
94	Loc100288529	FT	hypothetical protein XP_002343035
95	C1orf58	FT	BRO1 domain-containing protein BROX
96	C3orf32	FT	Uncharacterized protein C3orf32
97	Prickle3	FT	Prickle-like protein 3
98	Pla2g4c	FT	Cytosolic phospholipase A2 gamma
99	Loc730167	FT	similar to protein tyrosine phosphatase 4a1 isoform 2
100	Loc100289624	FT	hypothetical protein XP_002343581
101	Tbc1d8b	FT	TBC1 domain family member 8B
102	St7	FT	Suppressor of tumorigenicity 7 protein
103	Stk11	FT	Serine/threonine-protein kinase 11
104	Spag11b	FT Different isoforms possible	Sperm-associated antigene 11B
105	Cyp27b1	FT Seq. doubtful	25-hydroxyvitamin D-1 alpha hydroxylase, mitochondrial
106	Ppt2	FT ??	Lysosomal thioesterase PPT2; inactive palmitoyl-protein thioesterase-2i
108	Ubap2	FT C-terminus ??	Putative uncharacterized protein UBAP2
109	Cotl1p2	FT fragment	Coactosin-like 1 pseudogene 2
110	Bcl11b	FT fragment	B-cell lymphoma/leukemia 11B
111	Mdh2	FT fragment	Malate dehydrogenase, mitochondrial
112	Fxr1	FT fragment	Fragile X mental retardation syndrome-related protein 2
113	Dcun1d2	FT fragment	DCN1-like protein 2
114	Arhgef7	FT fragment ??	rho guanine nucleotide exchange factor 7
115	TRAV12-3 fragment?	FT fragment??	T cell receptor alpha variable 12-3
116	??	FT fragment??	T cell receptor alpha variable 8 ??
117	Nup37	FT fragment??	pos 1..52 = N-terminus of NUP37_HUMAN, Q8NFH4
118	Abca7	FT fragment??	ATP-binding cassette sub-family A member 7
119	Gk	FT fragment??	Glycerol kinase
120	Iffo1	FT fragment??	Intermediate filament family orphan 1
121	Clta	FT fragment??	Clathrin light chain A
122	St8sia1	FT isoform or fragment??	Alpha-N-acetylneuraminide alpha-2,8-sialyltransferase
123	Cotl1p2	FT Seq. doubtful	Coactosin-like 1 pseudogene 2
124	Rpl24	FT Seq. doubtful	ribosomal protein L24 but different frame !!
125	Similar to OOSP1	FT Seq. doubtful	oocyte-secreted protein 1 homolog
126	Nalcn ??	FT Seq. doubtful	Voltage gated channel-like protein 1
127	Tmem200c ?	FT Seq. doubtful	??
128	Nwd1	FT, NACHT domain -> MHC transcription activation	NACHT and WD repeat domain-containing protein 1, isoform 1
129	Atxn10	FT, Ataxin-10 - C-terminus is different!	HUMEEP
130	Fam127a	FT, FAM127A seems to encode 2 proteins	CAAX box protein 1
131	Slc35b1?	FT, Seq. doubtful	UDP-galactose transporter-related protein 1
132	C3orf75	FT, sequence differs from CC075_HUMAN	UPF0405 protein C3orf75
133	Dpm2	FT, sequence differs from DPM2_HUMAN	dolichyl-phosphate mannosyltransferase polypeptide 2, regulatory subunit, transcript 2
1	Rpgr	FT, GGT1	X-linked retinitis pigmentosa GTPase regulator isoform 4, Isoform 1
2	Fbxl20	FT, GGT1	F-box/LRR-repeat protein 20, isoform 2

4	Cdc42	FT, GGT1	
5	Lmna	FT, GGT1	Lamin A/C
6	Chpf2	FT, GGT1	Chondroitin sulfate glucuronyltransferase; CHPF2_HUMAN, isoform 2
7	Rap1a	FT, GGT1	Ras-related protein Rap-1A
8	Rhob	FT, GGT1	Rho-related GTP-binding protein RhoB; Seq. is C-terminus of RHOB_HUMAN; P62745
9	Mras	FT, GGT1	Ras-related protein M-RasSeq. is C-terminus of RASM_HUMAN, O14807
10	Pde6b	FT, GGT1	Rod cGMP-specific 3',5'-cyclic phosphodiesterase subunit beta
11	Ykt6	FT, GGT1	Synaptobrevin homolog YKT6
12	C16orf45	FT, GGT1	Uncharacterized protein C16orf45
13	Rheb	FT, GGT1	GTP-binding protein Rheb
14	Rac2	FT, GGT1	Ras-related C3 botulinum toxin substrate 2
15	Rac1	FT, GGT1	Ras-related C3 botulinum toxin substrate 1
16	Slfnl1	FT, GGT1	Schlafen-like protein 1, isoform 1
17	Nras	FT, GGT1	GTPase NRas
18	Rhog	FT, GGT1	Rho-related GTP-binding protein RhoG
19	Ppp1r16a	FT, GGT1	Protein phosphatase 1 regulatory subunit 16A
20	Rasl10b	FT, GGT1	Ras-like protein family member 10B
21	Rhobtb3	FT, GGT1	Rho-related BTB domain-containing protein 3
22	Rap2b	FT, GGT1	Ras-related protein Rap-2b
23	Palm3	FT, GGT1	Paralemmin-3
24	Palm	FT, GGT1	Paralemmin
25	Rnd2	FT, GGT1	Rho-related GTP-binding protein RhoN
26	Rap1bl	FT, GGT1	Ras-related protein Rap-1b-like protein
27	Kras	FT, GGT1	GTPase KRas
28	Rasl10a	FT, GGT1	Ras-like protein family member 10A
29	Rnf208	FT, GGT1	RING finger protein 208
30	Rras	FT, GGT1	Ras-related protein R-Ras
31	Rac3	FT, GGT1	Ras-related C3 botulinum toxin substrate 3
32	Rnd1	FT, GGT1	Rho-related GTP-binding protein Rho6
33	Stx7	FT, GGT1	Syntaxin-7
34	Rhoc	FT, GGT1	Rho-related GTP-binding protein RhoC
35	Rala	FT, GGT1	Ras-related protein Ral-A
36	Rhof	FT, GGT1	Rho-related GTP-binding protein RhoF
37	Gng2	FT, GGT1	Guanine nucleotide-binding protein G(I)/G(S)/G(O) subunit gamma-2
38	Fam63b	FT, GGT1	Protein FAM63B, isoform 1
39	Lmnb1	FT, GGT1	Lamin-B1
40	Gng3	FT, GGT1	Guanine nucleotide-binding protein G(I)/G(S)/G(O) subunit gamma-3
41	Gng13	FT, GGT1	Guanine nucleotide-binding protein G(I)/G(S)/G(O) subunit gamma-13
42	Gstm4	FT, GGT1	Glutathione S-transferase Mu 4, isoform 2
43	Grk7	FT, GGT1	G protein-coupled receptor kinase 7
44	Gng12	FT, GGT1	Guanine nucleotide-binding protein G(I)/G(S)/G(O) subunit gamma-12
45	Camk1g	FT, GGT1	Calcium/calmodulin-dependent protein kinase type 1G, isoform 1
46	Hpse2	FT, GGT1	Heparanase-2, isoform 2
47	Gng4	FT, GGT1	Guanine nucleotide-binding protein G(I)/G(S)/G(O) subunit gamma-4
48	Fbxo10	FT, GGT1	F-box only protein 10
49	Gng7	FT, GGT1	Guanine nucleotide-binding protein G(I)/G(S)/G(O) subunit gamma-7
50	Gng8	FT, GGT1	Guanine nucleotide-binding protein G(I)/G(S)/G(O) subunit gamma-8
51	Nim1	FT, GGT1	Serine/threonine-protein kinase NIM1
52	Gbp5	FT, GGT1	Guanylate-binding protein 5
53	Cnp	FT, GGT1	2',3'-cyclic-nucleotide 3'-phosphodiesterase, isoform 2

54	Diras2	FT, GGT1	GTP-binding protein Di-Ras2
55	Diras1	FT, GGT1	GTP-binding protein Di-Ras1
56	Cplx3	FT, GGT1	Complexin-3
57	Dnajc25	FT, GGT1	DnaJ homolog subfamily C member 25, isoform 3
58	C10orf25	FT, GGT1	Uncharacterized protein C10orf25
59	Diras3	FT, GGT1	GTP-binding protein Di-Ras3
60	Cplx4	FT, GGT1	Complexin-4
61	Dnajb2	FT, GGT1	DnaJ homolog subfamily B member 2
62	Rpgr	FT, GGT1	X-linked retinitis pigmentosa GTPase regulator isoform 4, Isoform 1
63	Rhoj	FT, GGT1	Rho-related GTP-binding protein RhoJ, isoform 2
64	Lmnb2	FT, GGT1	lamin B2
65	Annotated as pseudogene	FT, GGT1	Cyclophilin A
66	Ptp4a3	FT, GGT1	protein tyrosine phosphatase type IVA, member 3, isoform 3
67	C17orf37	FT, GGT1	HBV X-transactivated gene 4 protein, annotation, no paper; breast carcinoma
68	Ralb	FT, GGT1	V-ral simian leukemia viral oncogene homolog B (ras- related; GTP binding protein)
69	Mpi	FT, GGT1	Mannose-6-phosphate isomerase, isoform 2
70	Fbxl20	FT, GGT1	F-box/LRR-repeat protein 20, isoform 2
71	Gng10	FT, GGT1	Guanine nucleotide-binding protein G(I)/G(S)/G(O) subunit gamma-10
72	Rhoa	FT, GGT1	Ras homolog gene family, member A
73	Tatdn1	FT, GGT1	Tat D DNase domain containing 1, putative deoxyribonuclease
74	Ubl3	FT, GGT1	Ubiquitin-like protein 3
75	Cdc42	FT, GGT1	Cell division control protein 42 homolog (GTP-binding)
76	Fbxl2	FT, GGT1	F-box/LRR-repeat protein 2
77	Rnd3	FT, GGT1	Rho family GTPase 3
78	Rap1b	FT, GGT1	Ras-related protein Rap-1b
79	Rras2	FT, GGT1	Ras-related protein R-Ras2
80	Palm2	FT, GGT1	Paralemmin-2
81	Pex19	FT, GGT1	Isoform 5 of Peroxisomal biogenesis factor 19
82	Fam63a	FT, GGT1	Protein FAM63A
83	Rnft2	FT, GGT1 Seq. is doubtful	Ring finger protein, transmembrane 2
84	Tfcp2	FT, GGT1 Construct does not contain the CP2 domain, C terminus different	Alpha-globin transcription factor
85	Idh3g	FT, GGT1 fragment	Isocitrate dehydrogenase 3 (NAD+) gamma isoform b variant
86	Syt14l	FT, GGT1 Seq. doubtful	Synaptotagmin-14-like protein?
1	Rab18	FT, GGT1, GGT2	RAB18 long isoform 1 Ras-related protein Rab-18
2	Rab8a	FT, GGT1, GGT2	Ras-related protein Rab-8A
3	Rab8b	FT, GGT1, GGT2	Ras-related protein Rab-8B
1	Rab40al	FT, GGT2	Ras-related protein Rab-40A-like
2	Rab40a	FT, GGT2	Ras-related protein Rab-40A
3	Rab25	FT, GGT2	Ras-related protein Rab-25
4	Rab23	FT, GGT2	Ras-related protein Rab-23
5	Rab40c	FT, GGT2	Ras-related protein Rab-40C
1	Sar1a	GGT1	GTP-binding protein SAR1a; N-terminus (1..116) is identical to SAR1A_HUMAN, Q9NR31; but C-teminus differs !!
2	Sult1a3	GGT1	Sulfotransferase 1A3/1A4, isoform 2
3	Sult1a4	GGT1	Sulfotransferase 1A3/1A4, isoform 2

4	Gbp2	GGT1	Interferon-induced guanylate-binding protein 2
5	Glyctk	GGT1 fragment	glycerate kinase
6	Krt13	GGT1 fragment	Keratin, type I cytoskeletal 13
7	Kpna1	GGT1 fragment or isoform??	Importin subunit alpha-1
8	Lmbr1l	GGT1 fragment??	Lipocalin-1-interacting membrane receptor
9	Pa2g4p3	GGT1 Seq. doubtful	proliferation-associated 2G4 pseudogene 3
10	Liph	GGT1, Seq. doubtful	Lipase member H
11	Cry1	GGT1, Seq. doubtful	Cryptochrome-1
1	Rab37	GGT2	RAB37; member RAS oncogene family
2	Rab4a	GGT2	Ras-related protein Rab-4A
3	Rab31	GGT2	Ras-related protein Rab-31
4	Efcab4b	GGT2	EF-hand calcium-binding domain-containing protein 4B, isoform 2
5	Rab2b	GGT2	Ras-related protein Rab-2B
6	Rab7a	GGT2	Ras-related protein Rab-7a
7	Rab5b	GGT2	Ras-related protein Rab-5B
8	Rab7l1	GGT2	Ras-related protein Rab-7L1
9	Rab5a	GGT2	Ras-related protein Rab-5A
10	Rab6b	GGT2	Ras-related protein Rab-6B
11	Rab24	GGT2	Ras-related protein Rab-24
12	Rab43l	GGT2	Putative Rab-43-like protein ENSP00000330714
13	Rasef	GGT2	Ras and EF-hand domain-containing protein, RAB45
14	Rab5c	GGT2	Ras-related protein Rab-5C
15	Rab26	GGT2	Ras-related protein Rab-26
16	Rab21	GGT2	Ras-related protein Rab-21
17	Rab4b	GGT2	Ras-related protein Rab-4B
18	Rab22a	GGT2	Ras-related protein Rab-22A
19	Rab3d	GGT2	Ras-related protein Rab-3D
20	Rab14	GGT2	Ras-related protein Rab-14
21	Rab36	GGT2	Ras-related protein Rab-36, isoform 2
22	Rab35	GGT2	Ras-related protein Rab-35
23	Rab33b	GGT2	Ras-related protein Rab-33B
24	Rab1c	GGT2	Putative Ras-related protein Rab-1C
25	Rab39	GGT2	Ras-related protein Rab-39A
26	Rab6a	GGT2	Ras-related protein Rab-6A
27	Rab27b	GGT2	Ras-related protein Rab-27B
28	Rab39b	GGT2	Ras-related protein Rab-39B
29	Rab9a	GGT2	Ras-related protein Rab-9A
30	Rab20	GGT2	Ras-related protein Rab-20
31	Rab3b	GGT2	Ras-related protein Rab-3B
32	Rab33a	GGT2	Ras-related protein Rab-33A
33	Rab30	GGT2	Ras-related protein Rab-30
34	Rab3c	GGT2	Ras-related protein Rab-3C
35	Rab17	GGT2	Ras-related protein Rab-17
36	Rab7b	GGT2	Ras-related protein Rab-7b
37	Rab32	GGT2	Ras-related protein Rab-32
38	Rab12	GGT2	Putative Ras-related protein Rab-12
39	Rab10	GGT2	Ras-related protein Rab-10
40	Rab9b	GGT2	Ras-related protein Rab-9B

41	Rab27a	GGT2	Ras-related protein Rab-27A
42	Rab15	GGT2	Ras-related protein Rab-15, isoform 1
43	Rab34	GGT2	Ras-related protein Rab-34
44	Rab11a	GGT2	Ras-related protein Rab-11A
45	Rab43	GGT2	Putative Rab-43-like protein
46	Rab2a	GGT2	Ras-related protein Rab-2A
47	Rab3a	GGT2	Ras-related protein Rab-3A
48	Rab1b	GGT2	Ras-related protein Rab-1B
49	Rab11b	GGT2	Ras-related protein Rab-11B
50	Rab19	GGT2	Ras-related protein Rab-19. isoform 2
51	Rab1a	GGT2	Ras-related protein Rab-1A
52	Rab41	GGT2	Ras-related protein Rab-41, isoform 2
53	Rab13	GGT2	Ras-related protein Rab-13

Table S5.2 Bioinformatics prediction of all GGT2 targets in mouse identified in Maurer-Stroh et al., 2007

No.	Protein Accession	Gene	Description	Human protein	siRNA screened
1	P62821	Rab1a	Ras-related protein Rab-1A	P62820	X
2	Q9D1G1	Rab1b	Ras-related protein Rab-1B	Q9H0U4	X
	-	Rab1c	Ras-related protein Rab-1C	Q92928	
3	P53994	Rab2a	Ras-related protein Rab-2A	P61019	x
4	P59279	Rab2b	Ras-related protein Rab-2B	Q8WUD1	x
5	P63011	Rab3a	Ras-related protein Rab-3A	P20336	x
6	Q9CZT8	Rab3b	Ras-related protein Rab-3B	P20337	x
7	P62823	Rab3c	Ras-related protein Rab-3C	Q96E17	x
8	P35276	Rab3d	Ras-related protein Rab-3D	O95716	x
9	P56371	Rab4a	Ras-related protein Rab-4A	P20338	x
10	Q91ZR1	Rab4b	Ras-related protein Rab-4B	P61018-1	x
11	Q9CQD1	Rab5a	Ras-related protein Rab-5A	P20339	x
12	P61021	Rab5b	Ras-related protein Rab-5B	P61020	x
13	P35278	Rab5c	Ras-related protein Rab-5C	P51148	x
14	P35279-1	Rab6a	Isoforms 1 and 2 of Ras-related protein Rab-6A	P20340-1	x
	P35279-2				
15	P61294	Rab6b	Ras-related protein Rab-6B	Q9NRW1	x
16	P51150	Rab7a	Ras-related protein Rab-7a	P51149	x
17	Q8VEA8-1	Rab7b	Isoforms 1 and 2 of Ras-related protein Rab-7b	Q96AH8	x/ also called Riken
	Q8VEA8-2				
18	Q91YQ1	Rab7l1	Ras-related protein Rab-7L1	O14966	x
19	P55258	Rab8a	Ras-related protein Rab-8A	P61006	x
20	P61028	Rab8b	Ras-related protein Rab-8B	Q92930	x
21	Q9R0M6	Rab9a	Ras-related protein Rab-9A	P51151	x
22	Q8BHH2	Rab9b	Ras-related protein Rab-9B	Q9NP90	x
23	P61027	Rab10	Ras-related protein Rab-10	P61026	x
24	P62492	Rab11a	Ras-related protein Rab-11A	P62491	x
25	P46638	Rab11b	Ras-related protein Rab-11B	Q15907	x
26	P35283	Rab12	Ras-related protein Rab-12	Q6IQ22	x

27	Q9DD03	Rab13	Ras-related protein Rab-13	P51153	x
28	Q91V41	Rab14	Ras-related protein Rab-14	P61106	x
29	Q8K386	Rab15	Ras-related protein Rab-15	P59190-1	x
30	P35292	Rab17	Ras-related protein Rab-17	Q9H0T7	x
31	P35293	Rab18	Ras-related protein Rab-18	Q9NP72	x
32	P35294	Rab19	Ras-related protein Rab-19	A4D1S5-2	x
33	P35295	Rab20	Ras-related protein Rab-20	Q9NX57	x
34	P35282	Rab21	Ras-related protein Rab-21	Q9UL25	x
35	P35285	Rab22a	Ras-related protein Rab-22A	Q9UL26	x
36	P35288	Rab23	Ras-related protein Rab-23	Q9ULC3	x
37	P35290	Rab24	Ras-related protein Rab-24	Q969Q5	x
38	Q9WTL2	Rab25	Ras-related protein Rab-25	P57735	x
39	Q504M8	Rab26	Ras-related protein Rab-26	Q9ULW5	x
40	Q9ERI2	Rab27a	Ras-related protein Rab-27A	P51159-2	x
41	Q99P58	Rab27b	Ras-related protein Rab-27B	O00194	x
42	Q923S9	Rab30	Ras-related protein Rab-30	Q15771	x
43	Q921E2	Rab31	Ras-related protein Rab-31	Q13636	x
44	Q9CZE3	Rab32	Ras-related protein Rab-32	Q13637	x
45	P97950	Rab33a	Ras-related protein Rab-33A	Q14088	x
46	O35963	Rab33b	Ras-related protein Rab-33B	Q9H082	x
47	Q64008	Rab34	Ras-related protein Rab-34	Q9BZG1	x
48	Q6PHN9	Rab35	Ras-related protein Rab-35	Q15286	x
49	Q8CAM5	Rab36	Ras-related protein Rab-36	O95755-2	x
50	Q9JKM7	Rab37	Ras-related protein Rab-37	Q8IWA7	x
51	Q8QZZ8	Rab38	Ras-related protein Rab-38	P57729	x
52	Q8BHD0	Rab39a	Ras-related protein Rab-39A	Q14964	x
53	Q8BHC1	Rab39b	Ras-related protein Rab-39B	Q96DA2	x
	-	Rab40a	Ras-related protein Rab-40A	Q8WXH6	
	-	Rab40al	Ras-related protein Rab-40A-like	P0C0E4	
54	Q8VHP8	Rab40b	Ras-related protein Rab-40B	Q12829	x
55	Q8VHQ4	Rab40c	Ras-related protein Rab-40C	Q96S21	x
	-	Rab41	Ras-related protein Rab-41	Q5JT25-2	
56	Q8CG50	Rab43	Ras-related protein Rab-43	Q86YS6	x
	-	Rab43l	Putative Rab-43-like protein	A6NDJ8	
57	Q8CB87	Rab44	Ras-related protein Rab-44	Q7Z6P3	
	-	Efcab4b	EF-hand calcium-binding do-main-containing protein 4B, isoform 2	Q9BSW2-2	
58	Q5RI75-1	Rasef	Ras and EF-hand domain-containing protein homolog	Q8IZ41-1	
	Q5RI75-2				

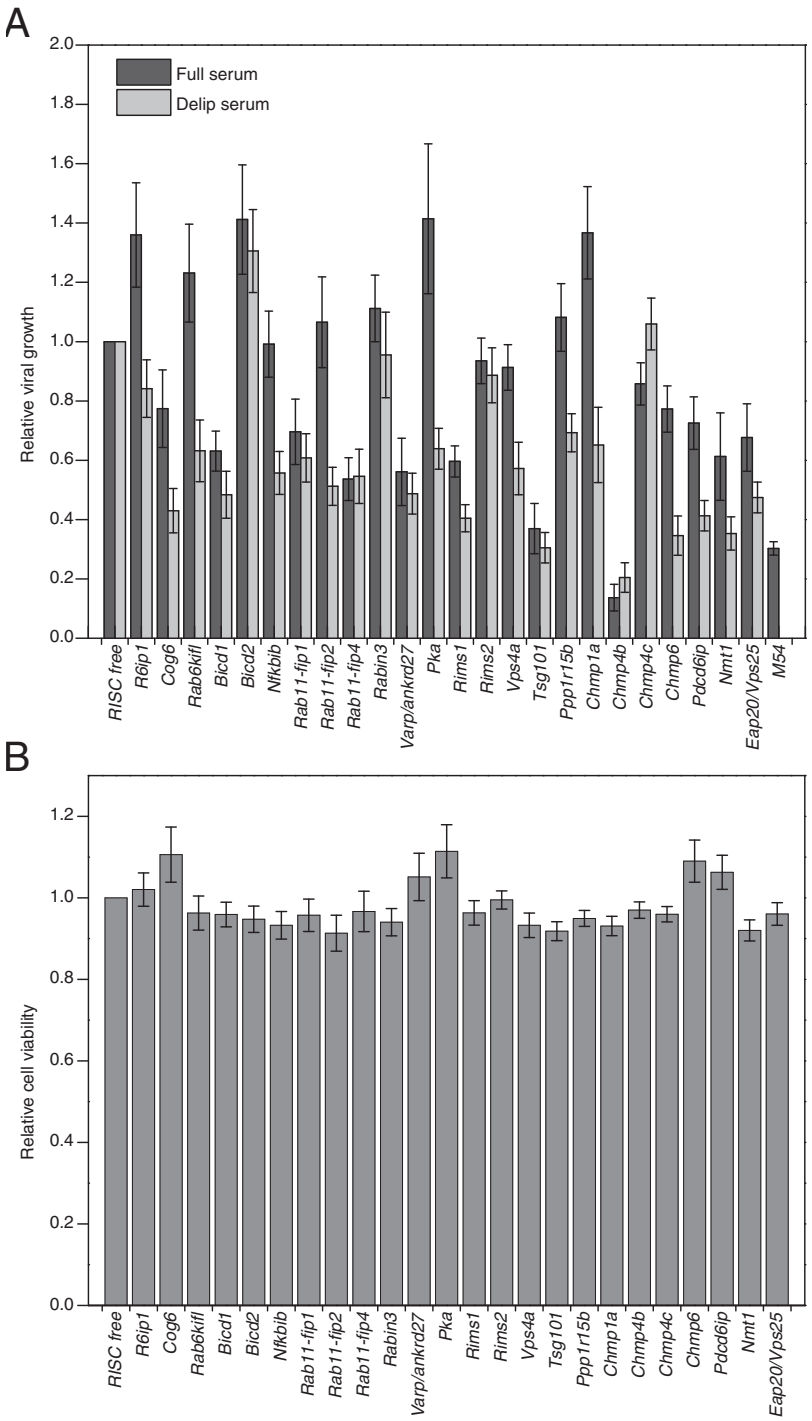

Figure S5.1 Effects on siRNA knockdown of selected RAB adaptor proteins and the ESCRT complex on MCMV replication under different serum conditions.

(A) pMEFs ($1.5x10^4$ cells/well) were transfected in 96-well plates with On-target plus siRNAs as indicated for 48 hr then infected with MCMV-GFP (MOI = 0.1) for 1 hr. After the removal of viral inoculum, cells were incubated in either 10% normal, or 3% delipidised media. *RISC free* was used as a transfection control, while *M54* specifically targets MCMV polymerase. The level of infection was determined by measuring the increase in GFP fluorescence (slope) during the linear-phase of viral growth. The graph represents the relative level of infection compared to *RISC free* transfected and data are the mean of 9 biological replicates ± SEM. (B) pMEFs ($1.5x10^4$ cells/well) were transfected with On-target plus siRNAs as indicated in 96-well plates for 48 hr then the cell viability was measured using CellTiter-Blue. Relative cell viability was calculated by normalizing to the *RISC free* transfected samples and data are the mean of 4 biological replicates ± SEM.

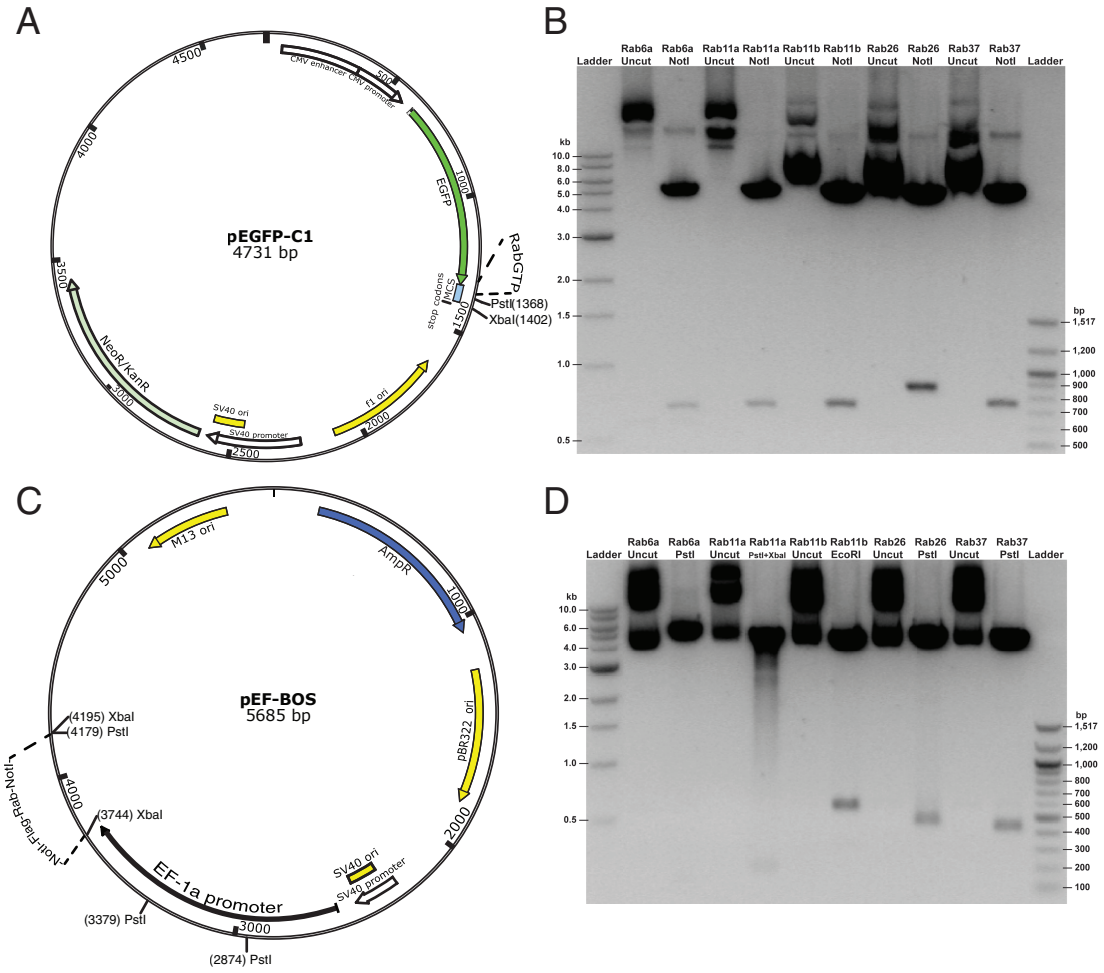

Figure S5.2 Restriction validation of RabGTPase expression vectors.
The plasmids containing a GFP tag or a Flag RabGTPases were a kind gift from Professor Mitsunori Fukuda at the Tohoku University, Japan. See personal communication letter with citation references at the end of the thesis.

Chapter 6

Conclusion: Converging innate-immune pathways with CMV replication and sterol metabolism

The central hypothesis of this thesis is that the antiviral effect of interferon is in part mediated by secondary sterol metabolites and the dependency of viral replication on the host mevalonate branch of the sterol biosynthesis pathway. This hypothesis is supported throughout the previous four chapters. Specifically, my findings address the question of how MCMV replication depends on the sterol biosynthesis pathway, and how the pathway is modulated by interferon as an antiviral response.

The importance of the sterol biosynthesis pathway to MCMV replication was demonstrated in Chapters 2 and 5. Results showed that the enzymatic step for the production of geranylgeranyl by the mevalonate-isoprenoid arm is essential for MCMV replication. Further investigation revealed that this was primarily due to the dependency of the virus on specific host geranylgeranylated RabGTPases. One of the mechanisms by which interferon modulates the sterol pathway is through the activation of CH25H, a cholesterol hydroxylase. CH25H converts cholesterol to 25-hydroxycholesterol (25-HC), an oxysterol that can act as a negative feedback regulator of SREBP2. Results presented in Chapters 3 and 4 showed that 25-HC elicits broad antiviral effects (including both MCMV and HCMV) through multiple mechanisms. These incorporate both sterol dependent and independent mechanisms, including suppression of the mevalonate-isoprenoid arm, and the inhibition of viral gene transcription. A diagrammatic representation of the main findings presented in this thesis is illustrated in Figure 6.1 (enclosed within a dashed magenta coloured box),

showing the coupling of statin and 25-HC to the antiviral effects or interferon. In this regard, whether 25-HC, interferon, and statins can directly alter RabGTPase prenylation *in vitro* and *in vivo* has not been demonstrated in the current study. This provides a direct linkage between sterol metabolic pathway and vesicular trafficking and will be the key focus of my future investigations.

This thesis has shown the importance of the sterol metabolic pathway in regulating innate immune response and viral replication. It has also revealed the important role of this pathway in viral trafficking and egress. As discussed in Chapter 5.3.3, there is emerging evidence suggesting that the process of cytomegalovirus assembly and egress is a complex and highly coordinated remodelling event. In Chapter 5, I showed that Rab6a, Rab26, Rab32, and Rab37 are important for the replication of MCMV. In addition, preliminary data has provided tentative evidence for the dependency of MCMV on the host ESCRT pathway. Although there are differences between how MCMV and HCMV utilized different components of the host transport machinery (see Chapter 5.3.3), my results support a common route of egress through the ESCRT pathway between the two viruses. Currently, there is very limited information regarding the late stage of MCMV replication, and whether MCMV, like HCMV, also requires the formation of an assembly complex for virion maturation. These aspects of the MCMV replication cycle will be examined through future imaging of infected macrophages and virus mutagenesis experiments.

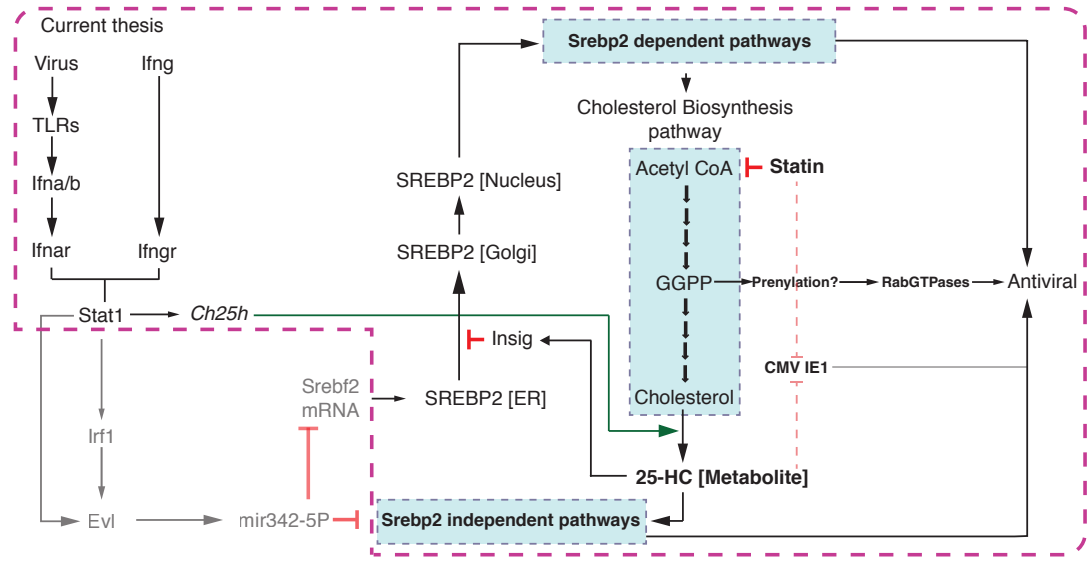

Figure 6.1 Summary of the main findings of the current study.
Viral entry or interferon stimulation trigger activation of STAT1 signalling cascade. Binding of STAT1 to the *Ch25h* promoter activates the transcription of CH25H, an oxysterol hydroxylase which converts cholesterol into 25-hydroxycholesterol (25-HC). Secreted 25-HC binds to Insig, which prevents the proteolytic activation of SREBP2. Inhibition of SREBP2 by 25-HC leads to the transcriptional silencing of the pathway, reducing the production of isoprenoids (GGPP) and the process of protein prenylation. The inhibition of isoprenoid synthesis can also be chemically inhibited using HMGCR inhibitor statin. 25-HC and statin exhibit additional antiviral properties through a SREBP2 independent mechanism by inhibiting CMV MIEP.

While CMV promotes the reorganization of organelles for the formation of the AC, detection of CMV by the host TLRs triggers interferon responses, leading to the synthesis and the secretion of 25-HC (Figure 6.1). 25-HC exhibits strong antiviral effects, partially through the suppression of CMV MIEP. Cytomegalovirus IE-gene expression is under the control of a potent enhancer (MIE) that plays a central role in the establishment of infection (Angulo et al., 2000; Kropp et al., 2011). Our recent work showed that TLR activation of immune signalling through MyD88-IRF-NF-κB pathways paradoxically provided activation and enhancement to the CMV MIEP in a temporal manner (Kropp and Hsieh, 2015). Removal of MIEP AP-1, NF-κB, and ATF binding sites led to crippling of MCMV *Ie1* activation and reduced viral replication. These results demonstrated that the cytomegalovirus enhancer is directly utilising the activation of an antiviral signalling pathway to drive viral IE gene expression. Given the importance of AP-1, NF-κB, and ATF in driving synthesis of pro-inflammatory cytokines (Chevrel et al., 2005; Fujisawa et al., 2011) and viral gene transcription, inhibition of these pathways would, thereby, provide both antiviral and anti-inflammatory effects. In Chapters 2 and 3, I showed that lipophilic statins and 25-HC significantly inhibit MCMV *Ie1*, while others have demonstrated the anti-inflammatory capability of statin

(Antonopoulos et al., 2012) and 25-HC (Reboldi et al., 2014) (see Chapter 3.3.5). Future studies will determine whether the antiviral and anti-inflammatory mechanisms of these two molecules involve perturbation of these transcription factors.

Whereas macrophages limit CMV replication through the secretion of interferon and 25-HC, CMV has evolved strategies to counter the immune system through the synthesis of immunoevasive proteins, known as evasins (Ameres et al., 2014). For example, HCMV pUL27 (MCMV pM27) inhibits STAT2 signalling by inhibiting STAT2 tyrosine phosphorylation (Le et al., 2008), whereas MCMV M45 rapidly stimulates the degradation NF-κB upon viral entry (Krause et al., 2014). Impairment of immune signalling pathways by CMV evasins prevents the activation of antiviral genes. Given the considerable coevolution between CMV and its host, it is likely that the virus would also encode specific evasins to counter the potent antiviral effect of 25-HC. HCMV US2 and US11 were first identified to interfere with $CD8^+$ T lymphocyte recognition through the downregulation of MHC of the infected cell. (Besold et al., 2009; Khan et al., 2005). Mechanistic studies have shown that both US2 and US11 can direct newly synthesized MHC I from ER to cytoplasm via direct and indirect interactions (Jones and Sun, 1997; Thilo et al., 2006; Wiertz et al., 1996). As a result, dislocated MHC molecules are degraded by ubiquitin-dependent proteasome complex (Han et al., 2013), allowing HCVM to escape from immune surveillance. While there is limited understanding of the extended function of US2 and US11, it is hypothesized that US2 and US11 could also direct CH25H and 25-HC for proteasome degradation, as part of mechanisms which the virus uses to evade the host immune response.

In summary, this thesis examines how the sterol biosynthesis pathway is utilized by the virus for replication, and by the innate immunity as a countermeasure to infection. In particular, production of isoprenoids by the mevalonate arm, and prenylated RabGTPases were shown to play key roles in the replication cycle of MCMV. Concurrently, interferon modulates this pathway through the secretion of 25-HC, leading to pathway downregulation and other antiviral mechanisms. These findings along with other studies discussed in this thesis are depicted in Figure 6.2, highlighting

the complex interactions and unknowns between CMV and the host metabolic network. Overall, my work demonstrates an important convergence between viral infection and innate immunity on a host metabolic pathway and raises new questions and hypotheses for future studies. The progress made in the current investigation has provided new mechanistic insights into the dependency of cytomegalovirus replication on the host cell trafficking pathways and lays the basis for further definition of this important aspect of host-viral interactions.

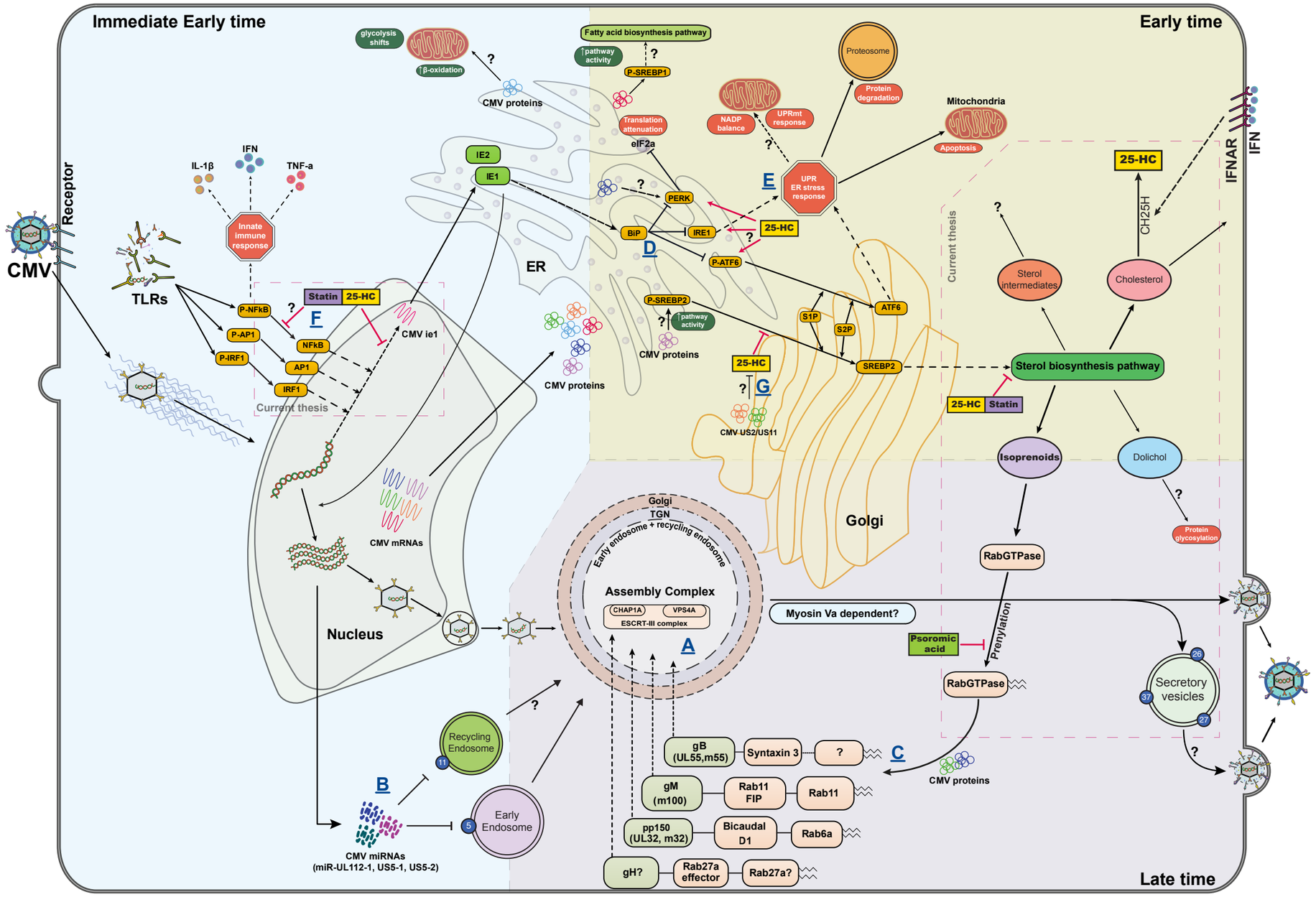

Figure 6.2 Converging innate-immune pathways with CMV replication and sterol metabolism.
This figure represents an updated version on the replication cycle of CMV and interferon mediated sterol immunity. The main findings of this thesis is indicated by the magenta dashed box, which contains the identical information as Figure 6.1. The rest of the figure were findings published in other studies and discussed throughout the entire thesis. (A) During the late stage of HCVM assembly, the virus induces the formation of an assembly complex (see Chapter 5.3.3). (B) The formation of the assembly complex is caused by the collapse of the endosomes due the effects of CMV miRNAs (see Chapter 5.3.2). (C) Trafficking of HCMV proteins to the assembly complex is mediated by prenylated RabGTPases. RabGTPases prenylation is depended on the production of geranylgeranyl from the mevalonate arm of the sterol biosynthesis pathway. This pathway can be inhibited by 25-hydoxcholesterol through a SREBP2 dependent mechanism or by targeting the enzyme HMGCR using statin. In addition, the process of prenylation can also be inhibited by using a GGTase II inhibitor, psoromic acid. (D) CMV IE1 protein stimulates the synthesis of BiP, which acts as a repressor for unfold protein response (UPR). (E) 25-HC, conversely, can induce UPR, leading to translation attenuation (see Chapter 3.3.5). (F) CMV IE transcription can be inhibited by statin and 25-HC as part of the antiviral mechanisms. However, it is unknown whether this process requires the perturbation of pro-inflammatory signalling. (G) Lastly, it is hypothesized that HCMV US2 and US11 could counter the antiviral effects of 25-HC by protosome degradation.

References

Ameres, S., Besold, K., Plachter, B., and Moosmann, A. (2014). CD8 T cell-evasive functions of human cytomegalovirus display pervasive MHC allele specificity, complementarity, and cooperativity. J. Immunol. *192*, 5894–5905.

Angulo, a, Ghazal, P., and Messerle, M. (2000). The major immediate-early gene ie3 of mouse cytomegalovirus is essential for viral growth. J. Virol. *74*, 11129–11136.

Antonopoulos, A.S., Margaritis, M., Lee, R., Channon, K., and Antoniades, C. (2012). Statins as anti-inflammatory agents in atherogenesis: molecular mechanisms and lessons from the recent clinical trials. Curr. Pharm. Des. *18*, 1519–1530.

Besold, K., Wills, M., and Plachter, B. (2009). Immune evasion proteins gpUS2 and gpUS11 of human cytomegalovirus incompletely protect infected cells from CD8 T cell recognition. Virology *391*, 5–19.

Chevrel, G., Granet, C., and Miossec, P. (2005). Contribution of tumour necrosis factor alpha and interleukin (IL) 1beta to IL6 production, NF-kappaB nuclear translocation, and class I MHC expression in muscle cells: in vitro regulation with specific cytokine inhibitors. Ann. Rheum. Dis. *64*, 1257–1262.

Fujisawa, T., Chang, M.M.-J., Velichko, S., Thai, P., Hung, L.-Y., Huang, F., Phuong, N., Chen, Y., and Wu, R. (2011). NF-κB mediates IL-1β- and IL-17A-induced MUC5B expression in airway epithelial cells. Am. J. Respir. Cell Mol. Biol. *45*, 246–252.

Han, J., Rho, S.B., Lee, J.Y., Bae, J., Park, S.H., Lee, S.J., Lee, S.Y., Ahn, C., Kim, J.Y., and Chun, T. (2013). Human cytomegalovirus (HCMV) US2 protein interacts with human CD1d (hCD1d) and down-regulates invariant NKT (iNKT) cell activity. Mol. Cells *36*, 455–464.

Jones, T.R., and Sun, L. (1997). Human cytomegalovirus US2 destabilizes major histocompatibility complex class I heavy chains. J. Virol. *71*, 2970–2979.

Khan, N., Bruton, R., Taylor, G.S., Cobbold, M., Jones, T.R., Rickinson, A.B., and Moss, P.A.H. (2005). Identification of cytomegalovirus-specific cytotoxic T lymphocytes in vitro is greatly enhanced by the use of recombinant virus lacking the US2 to US11 region or modified vaccinia virus Ankara expressing individual viral genes. J. Virol. *79*, 2869–2879.

Krause, E., de Graaf, M., Fliss, P.M., Dölken, L., and Brune, W. (2014). Murine Cytomegalovirus Virion-Associated Protein M45 Mediates Rapid NF-κB Activation after Infection. J. Virol. *88*, 9963–9975.

Kropp, K. a, Robertson, K. a, Sing, G., Rodriguez-Martin, S., Blanc, M., Lacaze, P., Hassim, M.F.B.N., Khondoker, M.R., Busche, A., Dickinson, P., et al. (2011). Reversible inhibition of murine cytomegalovirus replication by gamma interferon (IFN-γ) in primary macrophages involves a primed type I IFN-signaling subnetwork for full establishment of an immediate-early antiviral state. J. Virol. *85*, 10286–10299.

Kropp, K. a., Hsieh, W.Y., Isern, E., Forster, T., Krause, E., Brune, W., Angulo, A., and Ghazal, P. (2015). A Temporal Gate for Viral Enhancers to Co-opt Toll-Like-Receptor Transcriptional Activation Pathways upon Acute Infection. PLOS Pathog. 11, e1004737.

Le, V.T.K., Trilling, M., Wilborn, M., Hengel, H., and Zimmermann, A. (2008). Human cytomegalovirus interferes with signal transducer and activator of transcription (STAT) 2 protein stability and tyrosine phosphorylation. J. Gen. Virol. *89*, 2416–2426.

Reboldi, a., Dang, E. V., McDonald, J.G., Liang, G., Russell, D.W., and Cyster, J.G. (2014). 25-Hydroxycholesterol suppresses interleukin-1-driven inflammation downstream of type I interferon. Science (80-.). *345*, 679–684.

Thilo, C., Berglund, P., Applequist, S.E., Yewdell, J.W., Ljunggren, H.-G., and Achour, A. (2006). Dissection of the interaction of the human cytomegalovirus-derived US2 protein with major histocompatibility complex class I molecules: prominent role of a single arginine residue in human leukocyte antigen-A2. J. Biol. Chem. *281*, 8950–8957.

Wiertz, E.J., Jones, T.R., Sun, L., Bogyo, M., Geuze, H.J., and Ploegh, H.L. (1996). The human cytomegalovirus US11 gene product dislocates MHC class I heavy chains from the endoplasmic reticulum to the cytosol. Cell *84*, 769–779.

Chapter 7

Experimental procedures

7.1 Cell propagation and culture

BMDMs were derived from femur and tibia isolated from C57BL/6 mice and grown in DMEM/F12 + GlutaMAX (Lonza) supplemented with 10% (v/v) fetal bovine serum (FCS), 10% (v/v) L929 conditioned medium (containing colony-stimulating factor Csf1) and 50U/ml Penicillin + Streptomycin. FACs assessed BMDMs for MΦ cell surface markers, F480 and CD11b. All procedures were carried out under project and personal licences approved by the Secretary of State for the Home Office, under the United Kingdom's 1986 Animals (Scientific Procedures) Act and the Local Ethical Review Committee at The University of Edinburgh. All cultures are routinely tested for mycoplasma and endotoxin levels.

NIH-3T3 fibroblasts were obtained from LGC Standards and cultured in DMEM (Lonza) supplemented with 10% (v/v) bovine serum (CS), 2mM L-Glutamine and 50U/ml Penicillin + Streptomycin.

NIH-3T3-H2B-GFP was generated as described in Gibbs et al., 2013. Cells were cultured in DMEM (Lonza) supplemented with 10% (v/v) bovine serum (CS), 2mM L-Glutamine and 50U/ml Penicillin + Streptomycin.

Baby hamster kidney cells (BHK-21) were cultured in Eagle's minimum essential medium (EMEM) (Lonza) supplemented with 10% FCS, 2mM L-Glutamine and 50U/ml Penicillin + Streptomycin.

Mouse embryo fibroblasts (pMEFs) derived from the embryos of timed pregnant C57BL/6 mice on day 14-17 of gestation, were cultured in EMEM supplemented with 10% FCS, 2mM L-Glutamine and 50U/ml Penicillin + Streptomycin. MEFs were used at passage 3-4 post-isolation for experiments.

MRC-5 human lung fibroblasts were cultured in EMEM supplemented with 10% FCS, 2mM L-Glutamine and 50U/ml Penicillin + Streptomycin.

$p53^{-/-}$ MEF were cultured in DMEM supplemented with 10% FCS, 2mM L-Glutamine and 50U/ml Penicillin + Streptomycin.

In experiments where delipidated media is used, DMEM/EMEM was mixed with 3% (v/v) lipoprotein deficient fetal calf serum (Sigma, S5394), 2mM L-Glutamine and 50U/ml Penicillin + Streptomycin.

7.2 Chemical reagents

7.2.1 Sterol metabolites

Name	Supplier	Catalogue number	Stock concentration	Solvent	Storage
Mevalonic acid sodium salt	Sigma	41288	10mM	H_2O	-20° C
Mevalonolactone	Sigma	M4667	1M	EtOH	-20° C
Farnesol	Sigma	F203	100mM	EtOH	-20° C
Geranylgeraniol	Sigma	G3278	100mM	EtOH	-20° C
Squalene	Sigma	S3026	100mM	EtOH	-20° C

7.2.2 Statins

Name	Supplier	Catalogue number	Stock concentration	Solvent	Storage
Mevastatin	Sigma	M2537	10mM	DMSO	-80° C
Simvastatin	Sigma	S6196	10mM	EtOH	-80° C
Pravastatin	Sigma	P4498	10mM	EtOH	-80° C
Lovastatin	Millipore	438186	10mM	EtOH	-80° C
Fatostatin	Obtained from Timothy Osborne's lab.		10mM	DMSO	-80° C

Simvastatin and lovastatin required conversion to a sodium salt. This was achieved by dissolving each 25mg solid of statin in 625µl EtOH and adding 938µl of 0.1N NaOH solution. Each solution was heated at 50° C for 2 hr then brought to a pH of 7.2 using 0.1N HCl. Additional ethanol was added to create a 10mM stock solution. The structure of the 6 statins are shown below.

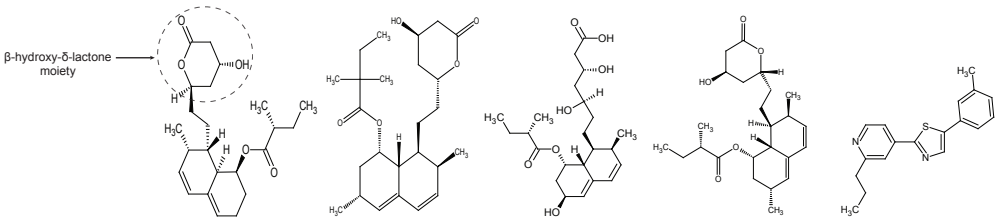

	Mevastatin	Simvastatin	Pravastatin	Lovastatin	Fatostatin
Trade Name	Not marketed	Zocor	Pravachol	Mevacor	Not marketed
Pharmacodynamics	HMGCR inhibitor	HMGCR inhibitor	HMGCR inhibitor	HMGCR inhibitor	SCAP inhibitor
Activation	None	NaOH	None	NaOH	None

7.2.3 Oxysterols and LXR ligands

Name	Supplier	Catalogue number	Stock concentration	Solvent	Storage
25-hydroxycholesterol	Avanti	700019	10mM	EtOH	-80° C under Ar gas
22(R)-hydroxycholesterol	Avanti	700058	10mM	EtOH	-80° C under Ar gas
GW3695	Sigma	G6295	10mM	DMSO	-20° C
T0901317	Tocris	2373	10mM	DMSO	-20° C

7.2.4 Prenylation inhibitors

Name	Supplier	Catalogue number	Stock concentration	Solvent	Storage
FTI-277	Millipore	344555	20mM	DMSO	-20° C
GGTI-2133	Sigma	G5294	20mM	DMSO	-20° C
Psoromic acid	Santa Cruz	SC363581	10mM	DMSO	-20° C

7.2.5 Cytokine and TLR ligands

Name	Supplier	Catalogue number	Working concentration	Solvent	Storage
Interferon-γ	Millipore	IF005	-	PBS	-80° C
LPS	Sigma	L3024	5ng/µl	PBS	-20° C
Poly I:C	Invivogen	Tlrl-pic	10µg/ml	PBS	-20° C
Pam3CSK4	Imgenex	Img2201	100nM	PBS	-20° C
R848	Alexis	ALX-420-038-M005	100nM	PBS	-20° C
ODN1668	Invivogen	Tlrl-1668	100nM	PBS	-20° C

7.3 Virology techniques

7.3.1 Reporter Viruses

The construction of the GFP-encoding Murine Cytomegalovirus (MCMV-GFP, originally named: pSM3fr-rev) used in this study was previously described in Angulo et al., 2000. The virus was propagated in mouse NIH-3T3 fibroblasts. The Gaussia luciferase (Gluc) reporter virus (Gluc-MCMV) was generated by site-specific homologous recombination as previously described and was obtained from M. Messerle at the University of Hanover (Kropp et al., 2011). The schematic representation of the wild type C3X virus and the two reporter viruses is shown below:

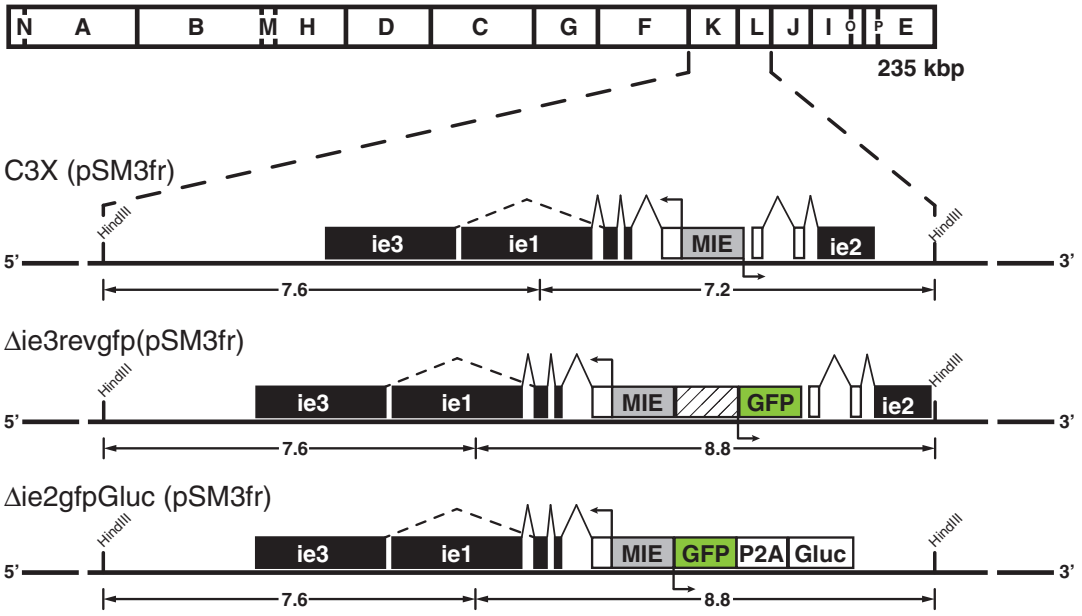

The construction of GFP-encoding Murine Gammaherpesvirus 68 (MHV-68-GFP, originally named: LHΔgfp) used in this thesis was previously described in Dutia, 2004. The virus was propagated in BHK-21.

The construction of GFP-encoding human cytomegalovirus (HCMV-AD169-GFP) used in this thesis was previously described in Marschall et al., 2000. The virus was propagated in human fetal lung fibroblast (MRC-5).

7.3.2 Determination of viral titre by plaque assay

The amount of infectious MCMV/MHV-68 present in the viral stock was quantified by plaque assay on $p53^{-/-}$ MEF monolayers in 48-well plates essentially as described by Gonzalez Armas and Spector (Gonzalez Armas, Morello et al., 1996). Briefly, cells were seeded at a density of $5x10^4$ cells/well. On the next day, viral stock was serially diluted (8 times, 10-fold dilution each time, starting from 1:1000) in DMEM supplemented with 10% FCS, 2mM L-Glutamine and 50U/ml Penicillin + Streptomycin. 110µl of each dilution stock was inoculated onto p53 monolayers, followed by 1 hr incubation at 37° C with agitation of the plate every 15 min. After absorption, fresh growth media containing 2.5% agarose (24ml media + 4ml agarose, 500µl/well) was added before the cells were grown for another 3 days. On day 4, the number of visible plaques per well were counted and multiplied by the respective dilution factor for that well. This number was readjusted based on the amount of viral stock that was added during dilution to obtain the final viral titre in plaque forming units/ml (PFU/ml).

Plaque assay plates can be fixed using 10% natural buffered formalin (pH 7.5). The formulation of the formalin is shown below:

Material	Catalogue number	Formulation
Sodium phosphate, monobasic	Sigma, S9638	4g
Sodium phosphate, dibasic	Sigma, S3264	6.5g
Formaldehyde, 37%	Sigma, 252549	100ml
Distilled water		900ml

The amount of infectious HCMV-AD169-GFP present in the viral stock was quantified by plaque assay on MRC-5 monolayers in 48-well plates. The experimental procedure is identical to the MCMV titre quantification with the exception of the cell type used. The number of GFP positive plaques was counted and the viral titre was represented as focus forming units/ml (FFU/ml).

7.3.3 Determination of intracellular and extracellular viral titre using single hit-kinetics

NIH-3T3 fibroblasts were seeded at a seeding density of $8x10^5$ cells/well in 6-plates. Following the pre-treatment, cells were infected with MCMV-C3X (MOI = 2.5) for 1 hr, followed by five washes with the blank media (DMEM + 2mM L-Glutamine and 50U/ml Penicillin + Streptomycin). Cells were then incubated with 2ml media supplemented with vehicle or treatments. 48 hpi, the supernatant (extracellular) was first collected. The monolayer was washed 3 times with PBS, and the cells were harvested into 1ml of media using a scraper (intracellular). Samples were immediately frozen using liquid nitrogen and stored in -80° C. Before performing the plaque assay, samples were subjected to 3 freeze-thaw cycles, first by defrost in a 37° C water bath, followed by vortexing for 30 sec, and freeze down again on dry ice. The viral titre was determined as previously described in 7.3.2.

7.3.4 Reporter virus screening

Virus replication was monitored as a function of GFP fluorescence hours post-infection (hpi). A general illustration of the infection procedure is shown on the next page, while specific experimental parameters, such as cell numbers, cell culture conditions, and treatments are specifically stated within the figure legends of each chapter. **1.** Cells were seeded in black 96-well plates for 24 hr. **2.** After the removal of media, cells were infected with GFP tagged viruses for 1 hr at 37° C. Followed by the removal of the viral inoculum, cells were incubated in growth media with the appropriate treatments. **3.** Virus replication was monitored as a function of GFP fluorescence hours post-infection (24-72 hr for MCMV, 19-48 hr for MHV-68, 65-100 hr for HCMV) using the POLARstar OPTIMA plate reader (BMG Labtech). **4.** Viral replication slopes over the linear phase were calculated and normalised to vehicle treated cells.

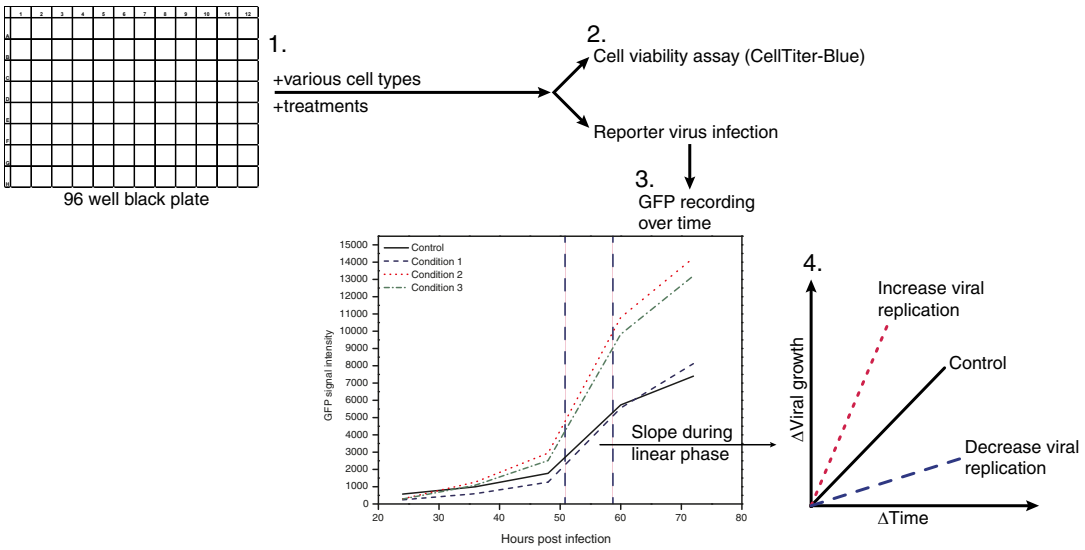

7.3.5 Transfection and siRNA knock-down assays

All siRNAs (SMARTpools-ON-TARGETplus modification) used in this thesis were purchased from Thermo Scientific. siRNAs were supplied at a concentration of 5nmol and diluted and aliquoted in 10μM amounts. To perform transfection in a 96-well with a siRNA final concentration of 25nM per well, 0.25μl of siRNA SMARTpool was first mixed with 9.75μl of Optimem (Invitrogen), while 0.4μl of Dharmafect 1 (Thermo Scientific) was mixed with 9.6μl Optimem. Following incubation for 5 min, the siRNA mix was added to the Dharmafect-1 (0.4%) mix and incubated for another 30 min. After incubation, $1.5x10^4$ NIH-3T3/pMEF cells in 80μl of DMEM 10% CS/FCS medium lacking antibiotics was added to the siRNA:Dharmafect-1 complexes. The final volume of siRNA + cell was 100μl per well. The amount of siRNA, cells, and Dharmafect-1 used can be scaled up proportionally (with respect to the well size) to accommodate the nature of the experiment.

When combining siRNA transfection with reporter virus screening, cells were first transfected with siRNA for 48 hr, then infected with MCMV-GFP. A simple illustration of the procedure is shown on the next page.

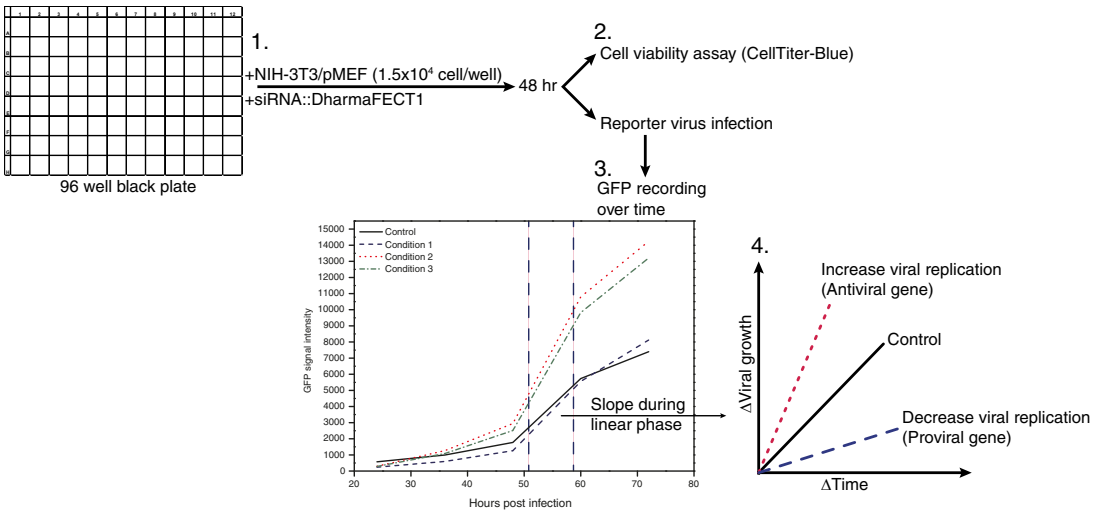

In all siRNA transfection experiments, siGENOME *RISC free* Control (*RISC free*) was used as a transfection control. This siRNA has been chemically modified and thus cannot uptake and be processed by the RISC complex. This is useful to isolate cellular effects specific to siRNA transfections. The level of infection was determined by measuring the increase in GFP fluorescence (slope) during the linear-phase of viral growth. The graph represents the relative level of infection compared to *RISC free* transfected and data.

7.3.6 Plaque reduction assay for statin and 25-HC

NIH-3T3 fibroblasts (for statin) or $p53^{-/-}$ MEF(for 25-HC) were seeded in 6-well plates ($5x10^5$ cells/well). After 24 hr, cells were infected with MCMV-GFP (MOI = 0.001-0.002), washed five times with media, and overlaid with medium containing 2.5% agarose and 0.1, 1, 2.5 or 5μM mevastatin or 25-HC (3ml/well). Foci of infection were counted 24hpi using a fluorescence microscope, a Zeiss Axio Observer Z1 inverted microscope (Carl Zeiss). Microscope control and image capture were undertaken using Axiovision Software (Carl Zeiss). All images were treated in an identical fashion and overlays were produced in Photoshop CS6 (Adobe). Plaque diameter was measured three days post infection (72 hpi). Thirty images per concentration of statin/25-HC were captured and diameters were quantified using ImageJ software.

7.3.7 Isolation and quantification of viral genome copy number using qPCR

Intracellular viral DNA was extracted with the QIAamp DNA extraction kit (Qiagen, 51304) by using the QIAcube running with the QIAamp blood and body fluid protocol (2009; available on Qiagen website) following manufacturer's instructions. Briefly, NIH-3T3 fibroblasts were seeded at a seeding density of $2x10^5$ cells/well in 24-well plates. The next day, cells were treated with mevastatin/25-HC for 24 hr. Cells were then infected with MCMV-C3X (MOI = 0.1) for 1 hr. After absorption, cells were washed three times with PBS. At 2 hpi, cells were collected by adding 200µl of PBS and scraped into 2ml collection tubes, followed by the viral genome extraction protocol. For the genome copy quantification, a custom qPCR assay was developed to measure the quantity of MCMV genomes in infected cell samples. Briefly, a reference DNA plasmid containing the MCMVm115 (gL) gene was constructed (a detailed protocol is described in Paul Lacaze's thesis, 2010). The concentration of purified DNA was determined using NanoDrop spectrophotometer (NanoDrop Technologies). The plasmid size (4167nt) and the DNA concentration were used together to calculate DNA copy number per µl in the purified plasmid stock. To perform qPCR, the purified MCMV M115 plasmid was first linearized by restriction digestion, followed by serial dilutions in RNase-free water (10^{-1} to 10^{-8}). The 82bp fragment from the M115 (gL) gene was amplified using a custom TaqMan gene expression assay (Applied Biosystems, 1166810B8) with primer sequences 5' GAGCTCAACGACGAGTTCCT 3' (forward) and 5' GCATCAGCGTCAGCAGAAC 3' (reverse). Samples were then subject to 50 cycles of amplification (including annealing and primer extension phase at 60° C for 60 seconds and a short denaturation at 95° C for 10 seconds). PerfeCta qPCR FastMIX II (Quanta) was used for all viral entry assays. The qPCR data from the MCMV M115 reference plasmid dilution series was used to generate a standard curve with cycle threshold (Ct) values plotted on the y-axis against the MCMV M155 copy number on the x-axis. At this stage Ct values derived from any sample could be inserted into the formula (as Y) to calculate copy number per µl compared to the reference plasmid. To control for variation in input material, data were normalised either to amount of input DNA or to abundance of Act-β (Applied Biosystems, Mm00607939_s1).

7.3.8 Comparison of methods for removing cell surface viral particles

In order to reduce the chance of bound but unentered viral particles interfering with the quantification of viral genome copies, several particle removal methods were tested. In these experiments, day 7 BMDM were seeded at a seeding density of $2x10^5$ cells/well in 24-well plate. The next day, cells were first infected with MCMV (MOI = 0.5) for 1.5 hr and then treated with the following methods prior to viral genome extractions:

Method 1	Method 2	Method 3
PBS wash 4x	PBS wash 2x, 1ml trypsin (1min), PBS wash 1x	PBS wash 2x, 1ml acid wash (pH 3.0) (40mM citric acid, 10mM KCL, 135mM NaCl in sterile H_2O) (1min), PBS wash 1x

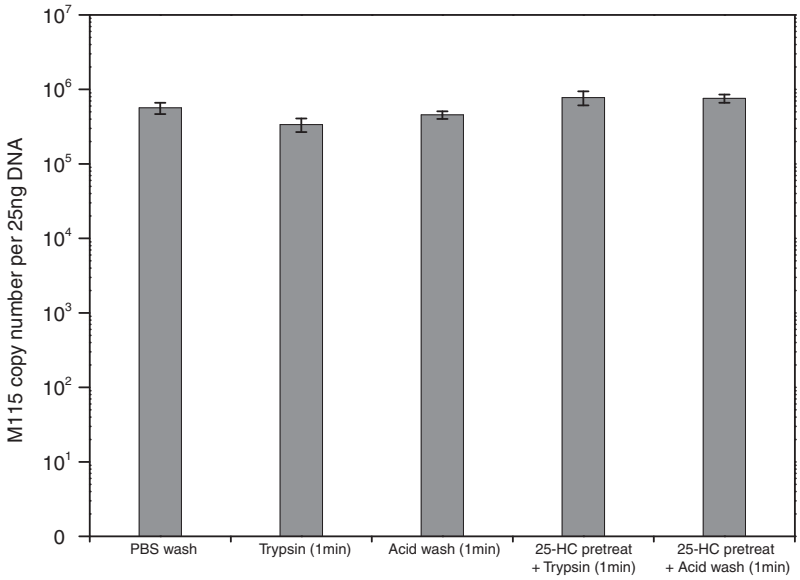

The above M115 quantification results showed that there was minimal or no difference between the three methods tested. PBS wash alone did not fully remove bound but unentered viral particles, but this difference was statistically insignificant. In the experiment in which cell types, such as NIH-3T3 fibroblasts, that cannot be washed with either trypsin or citric acid, extensive PBS washing was used. There was no difference between the trypsin and acid wash, hence that both methods are equally valid.

7.4 Molecular biology techniques

7.4.1 Gluc reporter assay

Gluc activity was measured using the native form of the Gluc substrate coelenterazine (Biosynth, C7001) as described previously (Kropp et al., 2011). The chemical reaction is shown below with the Gaussia luciferase encoded by the virus (see above for Gluc-MCVM) and is secreted into the media:

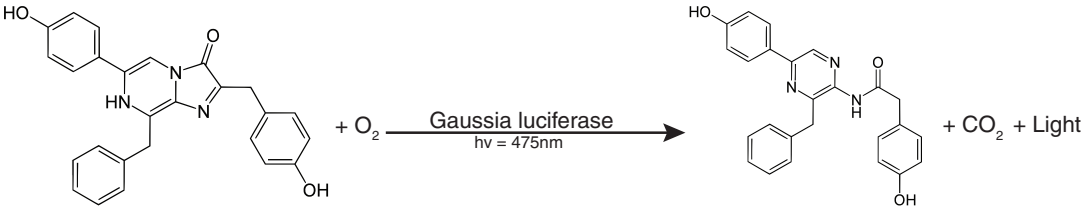

Coelenterazine was re-suspended in cold acidified (with 0.1M HCL) methanol to a stock concentration of 10mM. To make the coelenterazine substrate, 50µl of coelenterazine stock was mixed with 25ml of nitrogen purged PBS (supplemented with 5M of NaCl). The mixture was then incubated at room temperature in the dark for 30 min. The luciferase injector was first flushed once with 4ml of H_2O, followed by 4ml of EtOH, and again with 4ml of H_2O before primed with 800µl of substrate. 50µl of the sample media was transferred on to a 96-well black plate with opaque white bottom with 50µl of coelenterazine injected through the injector. Light signal was detected using an integration time of 10s.

7.4.2 Cell viability and apoptosis assay

Cell viability was determined using the CellTiter-Blue (Promega, G8080) reagent, and fluorescence was measured in a POLARstar OPTIMA plate reader. The principle of the CTB chemical reaction is shown below:

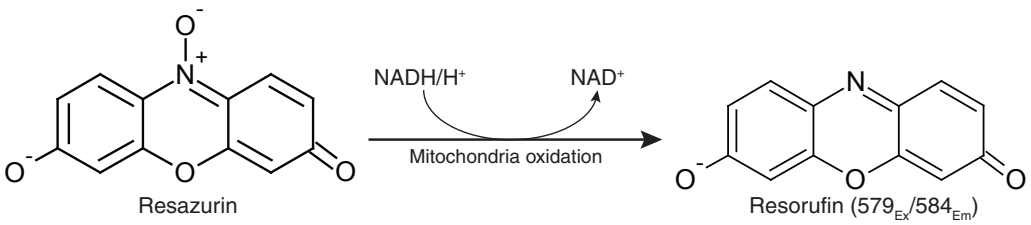

Briefly, 2ml of CTB was mixed with 10ml of media.120µl of the mixture (for a 96-well plate) was added into each well and incubated for 2 hr. Readings were normalised to viability of vehicle treated cells, and the mean cell viability was calculated over the replicates. Relative cell viability less than 70% (<0.7) between the treatment and the control is considered toxic.

For the measurement of apoptosis, Caspase-Glo 3/7 assay (Promega, G8091) was used. These assays measure capase (cysteine aspartic acid specific protease)-3 and -7 activities as an indicator of apoptosis. The chemical reaction describing the principle of Caspase-Glo 3/7 is shown below:

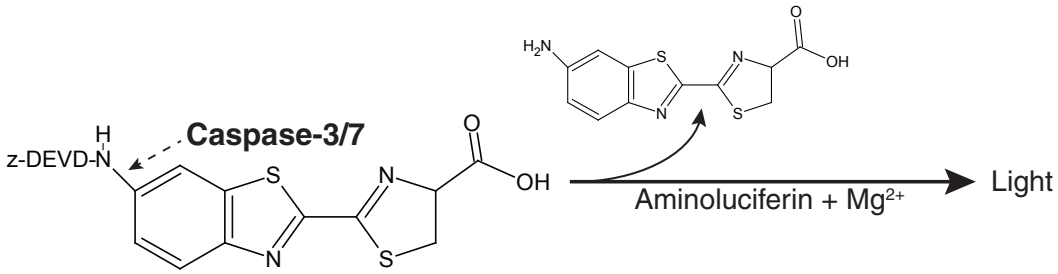

Briefly, cells were seeded in 96-well plate, followed by the treatments indicated in the figure legends. Staurosporine (0.1µM, Sigma, S6942), which induces apoptosis, was used as a positive control. At the end of the treatment, 100µl of supernatant from each well was transferred to a white bottom black 96-well assay plate. Mixing the Caspase-Glo substrate with the Caspase-Glo Buffer and 100µl of assay mix was then added into each well. The assay plate was incubated at room temperature for 2 hr. Caspase-3/7 activity was measured using a luminometer.

7.4.3 Duo luciferase reporter assay for the activation of LXR

phABCA1-LXR-Reporter and p-HA-LXRβ plasmids were obtained from Christopher K. Glass' lab. p-HA-LXRβ encodes the receptor LXRβ, while phABCA1-LXR-Reporter encodes Firefly luciferase under the control of the **ABCA1** promoter. The chemical reaction describing the principle of firefly luciferase is shown below:

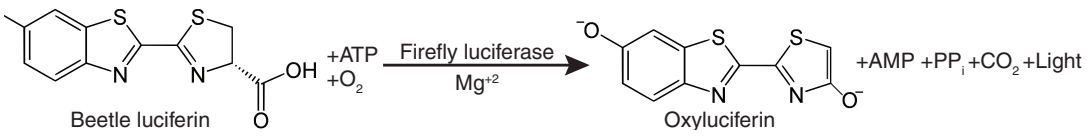

In these experiments, MEFs were seeded in 96-well plates at $1x10^4$ cells/well. Next day, cells were transfected with 25ng of p-HA-LXRβ, 15ng of pRL-TK (Promega), 50ng of phABCA1-LXR-Reporter or pGL3 empty vector using jetPRIME transfection reagent (Polyplus, 114) according to manufacturer's protocol. 4 hr post transfection, transfection medium was replaced with fresh media. The next day, cells were stimulated with either vehicle or GW3965 (1μM) or T0901317 (1μM) for 18 hr. Cells were then lysed by adding 60μl of 1X Passive Lysis Buffer (Promega, E1941) per well, followed by gentle shaking for 15 minutes at room temperature. Firefly reporter activity was assayed (30μl/well) using the Luciferase Assay System (Promega, E1501). For the transfection control, the Renilla reporter activity (25μl/well) was assayed using coelenterazine as described in Experimental procedure 7.4.1.

7.4.4 Testing the effects of solvents on viral replication and cell viability

To understand the general effects of chemical solvents ethanol (EtOH) and dimethyl sulfoxide (DMSO) that are used in pharmacological experiments, NIH-3T3 fibroblasts were first seeded in a seeding density of $2x10^4$ cells/well in 96-well plates. The next day, cells were treated with either EtOH or DMSO at an increasing concentration (0-5% v/v) for 48 hr. Cell viability was measured using CellTiter-Blue described above. The figure below shows that (A) EtOH or (C) DMSO above 0.5 volume percent concentration can cause cell toxicity regardless of serum lipid condition. To determine whether this toxicity can affect viral replication, NIH-3T3 fibroblasts were seeded in a seeding density of $2x10^4$ cells/well in 96-well plates and pre-treated with either EtOH or DMSO at an increasing concentration (0-5% v/v) for 24 hr. After the removal of media, cells were infected with MCMV-GFP (MOI = 0.1) for 1 hr. Cells were then incubated in growth media supplemented with the same concentration of DMSO/EtOH. Viral replication slopes over the linear phase were calculated and normalised to untreated treated cells. The panel below shows inhibition viral replication when cells are exposed to either (B) EtOH or (D) DMSO above 0.5% (v/v). To minimize the toxic effects of these solvents, all pharmacological experiments presented in this thesis contain solvent (either EtOH or DMSO) at a volume percentage concentration

below 0.1 (<0.1% v/v). In the case of generating a dose-response curve, all samples received the identical amount of solvent regardless the dosage of the drug.

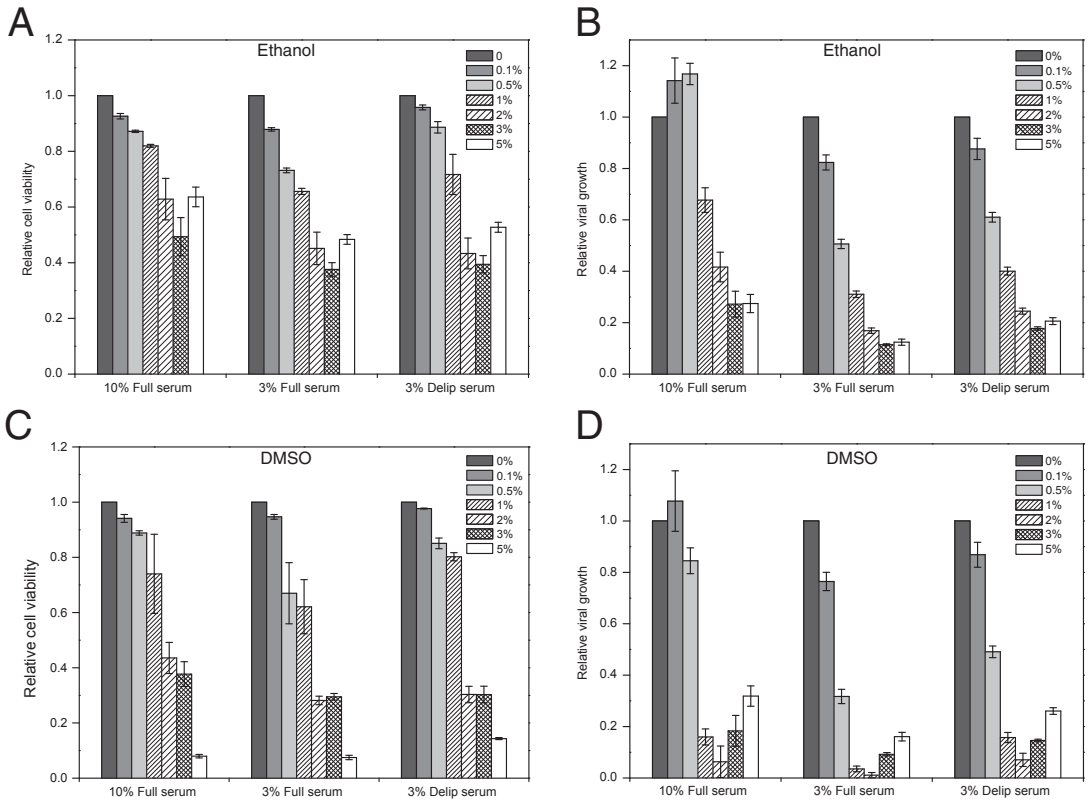

7.4.5 Statistical analysis and generating viral inhibition dose curves

Statistical analyses between the treatments and the control were performed in Microsoft Excel using the unpaired Student's *t* test (using the TDIST function). Statistical significance: *p<0.05, **p<0.01, ***p<0.001.

The scripts for performing IC_{50} calculations were written by Dr. Steven Watterson. Viral inhibition dose curves were calculated from biological and technical replicate data. Sigmoidal functions of the form $y=a/(b+e^{(-c(x-d))})+e$ were used throughout and curves fitted using the MATLAB curve fitting toolbox (MathWorks). For biological replicates, data was divided in each dose-response set by the control value to give a data set with values in the interval [0,1]. Each biological replicate had been obtained with a different set of metabolite concentrations. To facilitate comparison, we fitted a sigmoidal curve to each and sampled from these curves at intervals of half of an order of magnitude, calculating the mean and standard error. The resulting data points, curve and errors were then rescaled so that the viral inhibition extended from 0% to 100%.

For technical replicates, the viral inhibition values were averaged across the replicates and average values were scaled to span the interval [0%, 100%]. The standard error was calculated from the replicates and also rescaled. IC_{50} concentrations values were calculated as the point of 50% viral inhibition.

7.5 Proteomic techniques

7.5.1 Western blotting

Specific formulation of all buffers used in Western blotting are listed under this section. In brief, cells were washed with PBS and re-suspended in whole-cell lysis buffer (50mM Tris-HCl, pH 7.5, 100mM NaCl, 1% NP40 (Roche, 11754599001), protease inhibitors (Roche, 11836153001), and phosphatase inhibitors (Roche, 04906845001), and cell lysates were centrifuged at 4° C for 10 min and the collected supernatants were stored at –20° C. Protein concentration was measured by Pierce BCA assay (Thermo Scientific). For Western blotting, proteins were separated by SDS-PAGE, transferred to Immobilon-FL membranes, and probed with primary antibodies (see table below for specific antibody name, product number, and dilution factor). For secondary anti-goat IR-680 (Invitrogen, A21088, 1:10,000), IR-800 anti-mouse (Thermo Scientific, 35571, 1:10,000), or IR-800 anti-rabbit (Cell Signalling, 5151, 1:10,000), antibodies diluted in Odyssey blocking buffer (0.1% Tween20, 0.01% SDS) were used. For probing, visualization, and quantification, the Odyssey protocol (LI-COR) was followed.

Gel electrophoresis:

SDS-Page

Material	Catalogue number	Formulation
30% Acrylamide/Bis-acrylamide	Sigma, A3699	N/A
10% Ammonium persulfate (APS)	Sigma, A3678	1g APS in 10ml of H_2O
Tetramethylethylenediamine (TEMED)	Sigma, T9281	N/A
10% Sodium dodecyl sulphate (SDS)	Sigma, L4390	100g SDS in 1L of H_2O
1.5M Tris-base (pH 8.8)	Fisher Scientific, EC201-064-4	181g Tris-base in 1L of H_2O, adjust pH to 8.8
1M Tris-base (pH 6.8)	Fisher Scientific, EC201-064-4	120g Tris-base in 1L of H_2O, adjust pH to 6.8

Running buffer

10X Laemmli running buffer (Tris-Glycine), 1L

Material	Catalogue number	Formulation
Tris-base	Fisher Scientific, EC201-064-4	30.3g Tris-base
Glycine	Fisher Scientific, EC200-272-2	144.2g
Sodium dodecyl sulphate (SDS)	Sigma, L4390	10g

To make 1X running buffer → 100ml of 10X running buffer + 900ml of H_2O

Molecular weight marker

Material	Catalogue number	Formulation
SeeBlue Plus2 Pre-Stained Standard	Invitrogen, LC5925	10µl per well
PageRuler Plus Prestained Protein Ladder	Fermentas, SM1811	10µl per well

Other materials

Material	Catalogue number	Formulation
Isopropanol	N/A	N/A
Laemmli 2X Concentrate sample buffer	Sigma, S3401	N/A

Transfer:

For nitrocellulose membrane
Amersham Hybond ECL (GE Healthcare, RPN303D)
For PVDF membrane
Immobilon-FL transfer membrane (Millipore, ISEQ 00010)
Whatman Grade chromatography paper (Whatman, 3030917)
Methanol

10X Wet transfer buffer

Material	Catalogue number	Formulation
Tris-base	Fisher Scientific, EC201-064-4	30.3g
Glycine	Fisher Scientific, EC200-272-2	144g
10% SDS	N/A	25ml

To make 1X transfer buffer → 100ml of 10X transfer buffer + 200ml of methanol + 700ml of H_2O

10X Semi dry transfer buffer

Material	Catalogue number	Formulation
Tris-base	Fisher Scientific, EC201-064-4	58.2g
Glycine	Fisher Scientific, EC200-272-2	29.3g
Sodium dodecyl sulphate (SDS)	Sigma, L4390	3.7g

To make 1X transfer buffer → 100ml of 10X transfer buffer + 200ml of methanol + 700ml of H_2O

Blocking:

Odyssey Blocking Buffer (LI-COR, 927-4000)

Washing:

PBST (PBS + Tween 20), 1L

Material	Catalogue number	Formulation
PBS	Sigma, P4417	N/A
0.1% Tween 20 (Polyethylene glycol sorbitan monolaurate)	Sigma, P7949	N/A

To make 1L PBST → 5 PBS tablets + 1ml of Tween 20 + 1L of H_2O

TBST (PBS + Tween 20), 1L

Material	Catalogue number	Formulation
5M NaCl	Calbiochem, 567441	292.2g NaCl in 1L of H_2O
1M Tris-base (pH 7.5)	Fisher Scientific, EC201-064-4	121g Tris-base in 1L of H_2O, adjust pH to 7.5
0.1% Tween 20 (Polyethylene glycol sorbitan monolaurate)	Sigma, P7949	N/A

To make 1L PBST → 20ml of 5M NaCl + 10ml of 1M Tris-base (pH7.5) + 1ml of Tween 20 + 970ml of H_2O

Primary antibodies:

Antibody name	Catalogue number	Dilution factor
Rabbit anti-Rap1	SC-65	1:1000
Rabbit anti-Rap1A	SC-1482	1:500
Rabbit anti-β-actin	4967	1:2500

7.5.2 Extraction and measurement of intracellular cholesterol

NIH-3T3 fibroblasts were seeded at a seeding density of $6x10^5$ cells/well in 6-well plates. The next day, cells were treated with 2.5ml of DMEM containing mevastatin, simvastatin, or lovastatin at 2.5 or 7.5μM; pravastatin or fatostatin at 7.5μM; IFN-β at 100U/mL; IFN-γ at 100U/mL or vehicle. For the virus infected samples, cells were infected with MCMV (MOI = 1) for 1 hr, washed 3 times using media and incubated in 2.5ml of fresh media. For the delipidated samples, cells were cultured in 2.5ml of delipdized media. The plates were incubated for 24 hr before supernatant was removed and the identical treatment was repeated (except for the MCMV infected and delipidated samples). As a positive control for the removal of intracellular cholesterol, (2-Hydroxypropyl)-β-cyclodextrin (HPCD, Sigma, H107) was dissolved in media (1% w/v) and added to previously untreated wells 50 min before harvesting. 24 hr after the second treatment, cells were harvested by removing the media, washing once with ice-cold PBS and scraping the cells into collection tubes. The tubes were then centrifuged and the cell lysate pellet was re-suspended in 200μl of PBS and stored in -80° C.

20μl of lysate was then used for BCA to estimate the total protein concentrations in each sample for subsequent loading normalization calculation. For cholesterol extraction, 1:1 (v/v) ratio of methanol and chloroform solution was first prepared. 200μl of cell lysate was first mixed with 1.8ml of pure H_2O (total volume = 2ml) into a glass tube. 4.4ml of methanol:cholorform solution was then added into the lysate, followed by vortex until phases are mixed. The mixture was centrifuged at 2600 rpm (1360 rcf) for 10 min at 4° C. The bottom layer containing the cholesterol fraction was subsequently removed using a glass Pasteur pipette, transferred to glass tubes and dried at 37° C using N_2 leaving a pellet which was re-suspended in 500μl of ethanol. For the cholesterol measurement, Amplex Red Cholesterol Assay kit (Life technologies, A12216) was used. All reaction buffers are prepared according to manufacturer's

protocol. Briefly, 100µl of each sample was diluted in 100µl of reaction buffer provided. 50µl of each diluted samples were added to three wells of a 96-well black plate with opaque white bottom (three technical replicates). 50µl of the prepared reaction buffer was added to each well, and the plate was incubated at room temperature for 30 min. Fluorescence intensity from each well was measured in a fluorescence microplate reader using excitation in the range of 530–560 nm and emission detection at ~590nM. Signal intensity was first adjusted based on the protein concentration measured using BCA, and normalized to the vehicle treated sample.

7.6 Genomics techniques

7.6.1 Quantitative RT-PCR and probe efficiency testing

All probe-primer sets were purchased from either Applied Biosystems, Intergrated DNA Technologies (IDT), or Thermo Scientific. Only the probe-primers purchased from IDT contain sequence information and are listed under this section. Name and product number of the TaqMan primer-probe sets are listed in the subsequent tables. Quanta ToughMix (Quanta, 95123) 1-step qPCR master mix was used for all the qRT-PCR assays. For each sample, qRT-PCR was performed in 10µl volumes using 30ng of RNA in 96-well non-skirted, white PCR plates (Thermo Scientific, AB-0600/W) and flat PCR cap strips (Thermo Scientific, AB-0783). To measure relative gene expression from total cellular RNA, we used FAM-labelled gene assays for host genes in duplex with a VIC-labelled *Gapdh* assay (Mm99999915_g1) for normalisation. Every qRT-PCR performed in this thesis contain non-template controls (No RNA, water only) to ensure that there was no contamination. Depending on the probe set, the formulation for 1 reaction is listed below:

Simgleplex		Duplex with TaqMan probe		Duplex with IDT probe	
2X ToughMix	5µl	**2X ToughMix**	5µl	**2X ToughMix**	5µl
Probe-primer	0.5µl	**Probe-primer**	0.5µl	**Probe-primer**	1µl
-	-	**VIC-Gapdh**	0.17µl	**VIC-Gapdh**	0.17µl
RNA	2µl	**RNA**	2µl	**RNA**	2µl
H_2O	2.5µl	**H_2O**	2.33µl	**H_2O**	1.83µl
Total volume	10µl	**Total volume**	10µl	**Total volume**	10µl

Reverse transcription was undertaken for 10 minutes at 50° C. After which an incubation at 95° C for 1 minutes was used to activate the RNA polymerase. Samples were then subject to 37 cycles of amplification (including annealing and primer extension phase at 60° C for 60 seconds and a short denaturation at 95° C for 10 seconds). Expression levels were measured with a Stratagene Mx3000P qPCR machine (Agilent) and fold changes were determined by the ΔΔCt method normalized to *Gapdh* using the MxPro software package.

Gene names and primer sequences for the IDT probes	
ACAT1	
Item Name: Mm.PT.53a.16371877	
Name	**Sequence**
PrimeTime Primer 2	GCT CTC AGC TCT TAC ACC AG
PrimeTime Primer 1	TCT TCA TCT TCT TTC ACC ACC A
PrimeTime Probe	/56-FAM/CA AAC TTC C/Zen/C TGC GTC CCA CG/3IABkFQ/
ACAT2	
Item Name: Mm.PT.53a.9742054	
Name	**Sequence**
PrimeTime Primer 2	CCA ATT CCA GCC ATA AAG CAA G
PrimeTime Primer 1	CTT TAG CTA TTG CCG CAG AC
PrimeTime Probe	/56-FAM/AA CAG GTC A/Zen/A CAT CCT CCA GGG AC/3IABkFQ/
HMGCL	
Item Name: Mm.PT.53a.17723690	
Name	**Sequence**
PrimeTime Primer 2	CAT CAA CTA CCC AGT CCT GAC
PrimeTime Primer 1	GTG AAG AGC TCA GAC ACA GC
PrimeTime Probe	/56-FAM/CC GCA GCT A/Zen/C CGC TTC CTC AAA /3IABkFQ/
HMGCS1	
Item Name: Mm.PT.53a.29479770	
Name	**Sequence**
PrimeTime Primer 2	CTC CAT ACA GTG CTA CCT CAG
PrimeTime Primer 1	TGA GTG AAA GAT CAT GAA GCC A
PrimeTime Probe	/56-FAM/AC CGC TGC T/Zen/A TTC TGT CTA CCG C/3IABkFQ/
HMGCS2	
Item Name: Mm.PT.53a.13772562	
Name	**Sequence**
PrimeTime Primer 2	CAG CAG TGA CAA ACA GAA CAA C
PrimeTime Primer 1	GAG CCT TGT CTA CAT CCT TGT
PrimeTime Probe	/56-FAM/TT CCA GCT T/Zen/T AGA CCC CTG AAG GC/3IABkFQ/
HMGCR	
Item Name: Mm.PT.53a.31538611	
Name	**Sequence**
PrimeTime Primer 2	CAC ATT CAC TCT TGA CGC TCT
PrimeTime Primer 1	ACT GAC ATG CAG CCG AAG
PrimeTime Probe	/56-FAM/CA TGG TGC C/Zen/A ACT CCA ATC ACA AGG /3IABkFQ/
MVK	
Item Name: Mm.PT.53a.12677509	
Name	**Sequence**
PrimeTime Primer 2	GTG AGC GTC AAT TTA CCC AAC
PrimeTime Primer 1	TAC CGA GAC ATC ACC TTG C
PrimeTime Probe	/56-FAM/CC CAC ATC C/Zen/C ACA CCT GCT TAA TAC C/3IABkFQ/
PMVK	
Item Name: Mm.PT.53a.31894582	
Name	**Sequence**
PrimeTime Primer 2	GAG CAG ACT TGG AGG TAA CAT C
PrimeTime Primer 1	ACA GAT CAT GTC CCT CCG ATA

PrimeTime Probe	/56-FAM/TG TAG GTG C/Zen/T CGC ATC CAG AAG TC/3IABkFQ/
MVD	
Item Name: Mm.PT.53a.32103020	
Name	**Sequence**
PrimeTime Primer 2	GTC AAC ATC GCA GTT ATC AAG T
PrimeTime Primer 1	GTC CTC TGT GAA GTC CTT GC
PrimeTime Probe	/56-FAM/TG GTC GTT T/Zen/T TAG CTG GTC CTG GT/3IABkFQ/
IDI1	
Item Name: Mm.PT.53a.33221297	
Name	**Sequence**
PrimeTime Primer 2	ATT GGT GTG AAG CGA GCA
PrimeTime Primer 1	CAT CAG ATT GGG CCT TGT AGT
PrimeTime Probe	/56-FAM/AA GCC GAG T/Zen/T GGG AAT ACC CTT GG/3IABkFQ/
IDI2	
Item Name: Mm.PT.53a.29184625	
Name	**Sequence**
PrimeTime Primer 2	CAT TCA CTC CCA GGT TTC AGA
PrimeTime Primer 1	CAA TGA CAA TGC ACA TCT CCT C
PrimeTime Probe	/56-FAM/TG CCT GGA A/Zen/C ATA CCT CCT CTG AAG A/3IABkFQ/
FDPS	
Item Name: Mm.PT.53a.31961813	
Name	**Sequence**
PrimeTime Primer 2	GCA GAA TTT CAT CCA GCA CTT C
PrimeTime Primer 1	CCT AAG GCA TTG TAC TCT AGG AC
PrimeTime Probe	/56-FAM/CC TTC TCA G/Zen/T CAG CAC CTT GAC GAT /3IABkFQ/
FDFT1	
Item Name: Mm.PT.53a.12252682	
Name	**Sequence**
PrimeTime Primer 2	ACT TCC ACA CTT TCC TCT ATG AC
PrimeTime Primer 1	CTC AGC CAA ATT TCT AAA CTC CAG
PrimeTime Probe	/56-FAM/CT CCA GCA C/Zen/T TGT CGG TCC TTC T/3IABkFQ/
GGPS1	
Item Name: Mm.PT.53a.6692736	
Name	**Sequence**
PrimeTime Primer 2	GCA CTG CTA GTC TCG TAC C
PrimeTime Primer 1	GCT CTA GAA GAA TCC TCT CAG C
PrimeTime Probe	/56-FAM/TC ATC GTG G/Zen/A ACC GTC AGC TTT GAA /3IABkFQ/
DHDDS	
Item Name: Mm.PT.53a.15783930	
Name	**Sequence**
PrimeTime Primer 2	GCT TTG CAT ACA CAT CAC GTC
PrimeTime Primer 1	GCA CTT ATC GAG CAG AGA CTC
PrimeTime Probe	/56-FAM/TT CCA GCA G/Zen/A CCT TGT TCC ACG C/3IABkFQ/
SQLE	
Item Name: Mm.PT.53a.5713471	
Name	**Sequence**
PrimeTime Primer 2	TCT CTG CTT TGC CTC TTA TTG G
PrimeTime Primer 1	GCT CCT GTT AAT GTC GTT TCT G

PrimeTime Probe	/56-FAM/TC TTT TCT G/Zen/A TTC AGG TGA CTT GGC CC/3IABkFQ/
LSS	
Item Name: Mm.PT.53a.28640948	
Name	**Sequence**
PrimeTime Primer 2	GAG TAA CCT TTT ATG CCA AGC TG
PrimeTime Primer 1	GCA GAG AGA TGT GTG ATA TGT GA
PrimeTime Probe	/56-FAM/CC AGC CCA G/Zen/T GTC CAT CCT CAG /3IABkFQ/
DHCR7	
Item Name: Mm.PT.53a.16985491	
Name	**Sequence**
PrimeTime Primer 2	CTC ATT AAC CTG TCC TTC GCT
PrimeTime Primer 1	CAG ATG TCG ATG GTC TTC AGA T
PrimeTime Probe	/56-FAM/AA CAC GTA G/Zen/A TGG CCT GCA AGA CA/3IABkFQ/
CYP51	
Item Name: Mm.PT.53a.29021254	
Name	**Sequence**
PrimeTime Primer 2	GAC TTT AAT CCT GAC CGC TAC T
PrimeTime Primer 1	TCT CCA ACA CAA CGA TGA CG
PrimeTime Probe	/56-FAM/TG GCA CAT A/Zen/G GCA AAC TTC TCT CCT G/3IABkFQ/
TM7SF2	
Item Name: Mm.PT.53a.7536024	
Name	**Sequence**
PrimeTime Primer 2	ATA TTT CTG TGA GCT GAG ACC TG
PrimeTime Primer 1	CAT CAC CCA CAT ACA GCA ACT
PrimeTime Probe	/56-FAM/AG CCA TTG A/Zen/C CAG CCA CAT AGC C/3IABkFQ/
SC4MOL	
Item Name: Mm.PT.53a.9733563	
Name	**Sequence**
PrimeTime Primer 2	CAC AGA CTC CTT CAC CAC AA
PrimeTime Primer 1	ATG TGC GTA TTC TGC TTC GAT
PrimeTime Probe	/56-FAM/TC CAT CAC G/Zen/A GTT TCA GGC TCC ATT T/3IABkFQ/
NSDHL	
Item Name: Mm.PT.53a.9049868	
Name	**Sequence**
PrimeTime Primer 2	GTG TTC AGC CAG ACT TCT CT
PrimeTime Primer 1	TGG TTT CGT TTG CAA TCA ACT C
PrimeTime Probe	/56-FAM/AC TCA AAT G/Zen/A TCG ACC TCA GCT TGC A/3IABkFQ/
HSD17B7	
Item Name: Mm.PT.53a.16440852	
Name	**Sequence**
PrimeTime Primer 2	ACC GGA GTC TCT TAA TCC TCT
PrimeTime Primer 1	AGC AGT GTC TTC ATC TAT GTC C
PrimeTime Probe	/56-FAM/TT GGC CCG T/Zen/G ACG TAA TTA GTC CC/3IABkFQ/
EBP	
Item Name: Mm.PT.53a.9809050	
Name	**Sequence**
PrimeTime Primer 2	CTG GTT CTC TCT CTA CAA TGG C
PrimeTime Primer 1	GAC GAA GCT GTC ACT AAG GAT

PrimeTime Probe	/56-FAM/AG ACC AAG C/Zen/C TTC TTA TCC CAA CTC TG/3IABkFQ/
SC5D	
Item Name: Mm.PT.53a.11934042	
Name	**Sequence**
PrimeTime Primer 2	ACA GCA AAC TCT ACG ATG ACA T
PrimeTime Primer 1	CCC TAT GAA TCC AGT AGA TCA ACA
PrimeTime Probe	/56-FAM/AC GCT AAC C/Zen/A TGA GAT GAA TCC AGC C/3IABkFQ/
DHCR24	
Item Name: Mm.PT.53a.5182147	
Name	**Sequence**
PrimeTime Primer 2	CGC TCA TCT TCG ATA TCT ACT ACT
PrimeTime Primer 1	GTC TTA CTG CCC TGT TCC TT
PrimeTime Probe	/56-FAM/TT CCC GGA C/Zen/C TGT TTC TGG ATG TC/3IABkFQ/

Gene names and product number for the TaqMan probes

Gene Name	Product number	Fluorescent dye colour	Gene Name	Product number	Fluorescent dye colour
Hmgcs1	Mm00524111_m1	FAM	***Ch25h***	Mm00515486_s1	FAM
Hmgcr	Mm01282499_m1	FAM	***Ifnβ1***	Mm00439546_s1	FAM
Sqle	Mm00436772_m1	FAM	***Il-6***	Mm99999064_m1	FAM
Idi1	Mm00835417_m1	FAM	***Tnf-α***	Mm00443260_g1	FAM
Fdft1	Mm08819354_m1	FAM	***Srebf1***	Mm00550338_m1	FAM
RabggtA	Mm00490374_m1	FAM	***Srebf2***	Mm01306292_m1	FAM
RabggtB	Mm00599962_m1	FAM	***Insig1***	Mm00463389_m1	FAM
Pggt1b	Mm00553955_m1	FAM	***Insig2***	Mm00460121_m1	FAM
Act-β	Mm00607939_s1	FAM	***Gapdh***	Mm99999915_g1	VIC

MCMV *Ie1* gene expression was analysed by relative quantitative real-time PCR using TaqMan primers and probe combinations as described in Kropp et al., 2009 and Simon et al., 2007. Since the IDT probes have never been used in any of our previous studies, probe-primer efficiencies were calculated by generating standard curve plots of the log of starting template (2 fold serial dilution of the RNA, starting from 50ng) VS. PCR cycle number (see panel D below). A schematic representation on the analysis plot showing the standard curve of *Acat1* is shown on the next page.

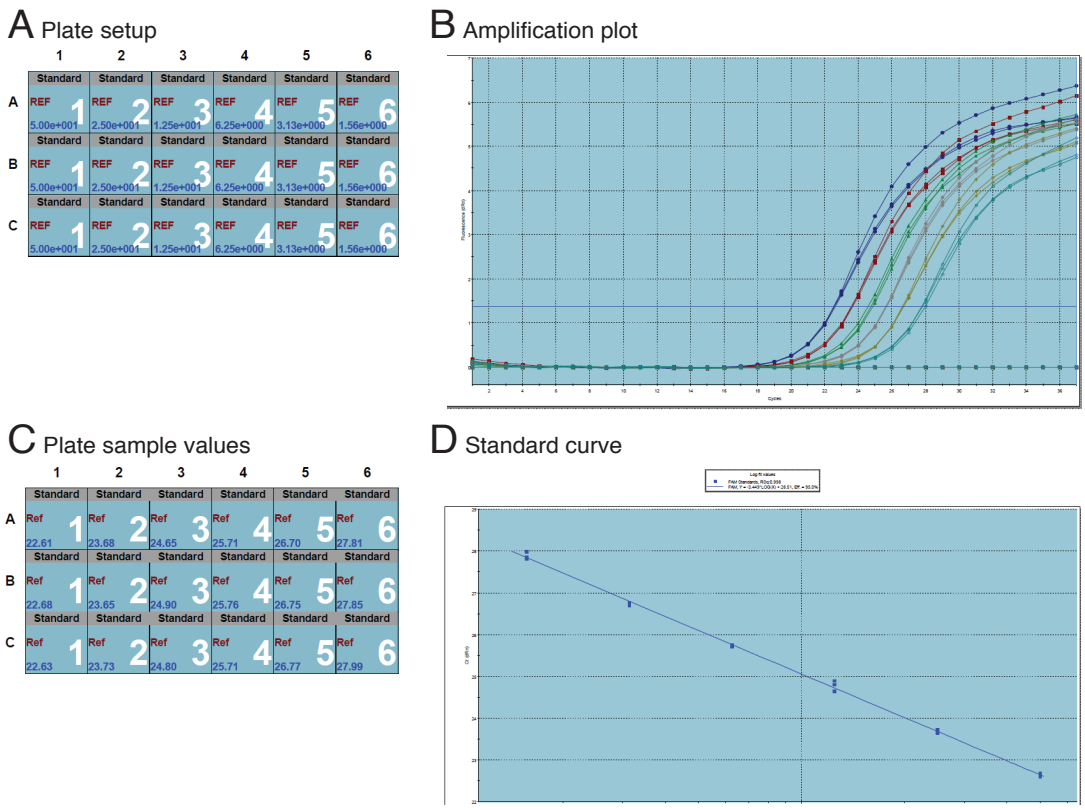

A linear fit with a slope between approximately -3.1 and -3.6, equivalent to a calculated 90–110% reaction efficiency is acceptable for relative quantification studies. The efficiency of the IDT probes tested using RNA from NIH-3T3 are listed below:

Gene	Probe efficiency (%)	Gene	Probe efficiency (%)	Gene	Probe efficiency (%)
Acat1	95	***Idi1***	98.5	***Cyp51***	98.7
Acat2	96.6	***Pdps***	93	***Tm7sf2***	87.7
Hmgcl	95.6	***Fdft1***	95.4	***Sc4mol***	95
Hmgcs1	96.4	***Lss***	93.3	***Nsdhl***	96.1
Hmgcr	94	***Dhdds***	97.4	***Hsd17b7***	92.8
Mvk	97.4	***Sqle***	93.4	***Ebp***	104.4
Pmvk	95.1	***Ggps1***	94.8	***Sc5d***	96.5
Mvd	97.8	***Dhcr7***	97	***Dhcr24***	97

Among the 26 probes, genes *Hmgcs2* and *Idi2* were shown not to be expressed in the two cell types tested (NIH-3T3, BMDM), while the probe for *Tm7sf2* fell below the efficiency threshold (<90%). Thus, these three genes are excluded from all subsequent gene expression studies.

7.7 References

Angulo, a, Ghazal, P., and Messerle, M. (2000). The major immediate-early gene ie3 of mouse cytomegalovirus is essential for viral growth. J. Virol. 74, 11129–11136.

Dutia, B.M. (2004). Identification of a region of the virus genome involved in murine gammaherpesvirus 68-induced splenic pathology. J. Gen. Virol. 85, 1393–1400.

Gibbs, H.C., Sing, G., González Armas, J.C., Campbell, C.J., Ghazal, P., and Yeh, A.T. (2013). Time-lapse ultrashort pulse microscopy of infection in three-dimensional versus two-dimensional culture environments reveals enhanced extra-chromosomal virus replication compartment formation. J. Biomed. Opt. 18, 031111.

Kropp, K. a, Simon, C.O., Fink, A., Renzaho, A., Kühnapfel, B., Podlech, J., Reddehase, M.J., and Grzimek, N.K. a (2009). Synergism between the components of the bipartite major immediate-early transcriptional enhancer of murine cytomegalovirus does not accelerate virus replication in cell culture and host tissues. J. Gen. Virol. 90, 2395–2401.

Kropp, K. a, Robertson, K. a, Sing, G., Rodriguez-Martin, S., Blanc, M., Lacaze, P., Hassim, M.F.B.N., Khondoker, M.R., Busche, A., Dickinson, P., et al. (2011). Reversible inhibition of murine cytomegalovirus replication by gamma interferon (IFN-γ) in primary macrophages involves a primed type I IFN-signaling subnetwork for full establishment of an immediate-early antiviral state. J. Virol. 85, 10286–10299.

Marschall, M., Freitag, M., Weiler, S., Sorg, G., and Stamminger, T. (2000). Recombinant green fluorescent protein-expressing human cytomegalovirus as a tool for screening antiviral agents. Antimicrob. Agents Chemother. 44, 1588–1597.

Simon, C.O., Kühnapfel, B., Reddehase, M.J., and Grzimek, N.K. a (2007). Murine cytomegalovirus major immediate-early enhancer region operating as a genetic switch in bidirectional gene pair transcription. J. Virol. 81, 7805–7810.

Conference posters

Statin protects against infection by targeting the prenylation branch of the sterol biosynthesis pathway

Wei Yuan Hsieh, Mathieu Blanc and Peter Ghazal

Division of Pathway Medicine. The Chancellor's Building, 49 Little France Crescent, Edinburgh, EH16 4SB, United Kingdom.

Introduction

Sterols play many important roles in physiology, including maintaining cell membrane integrity and are required for the production of vitamin D and hormones. In addition, the sterol biosynthesis pathway also produces several secondary metabolites, which are important for protein post-translational modifications and signaling. Recently, changes in sterol biosynthesis gene expressions have been observed during HCV[1] , HIV[2], and West Nile[3] virus infections, emphasizing the importance of sterol metabolism in viral replication. We previously showed sterol biosynthesis was down-regulated upon infection in bone marrow derived macrophages (BMDM) by type one interferon (IFN-I) as an antiviral response to murine cytomegalovirus (mCMV)[4]. Further investigation indicates that intermediates of the sterol biosynthesis are also effect by interferon. We thus are interested to explore whether these intermediates are involved in interferon's antiviral responses.

Conclusion

- The Prenylation branch of the cholesterol pathway plays an important role in viral replication.
- Statins are antiviral, but this effect can be reversed with the addition of geranylgeraniol, a prenylation branch specific secondary metabolite.
- Repeat administration of low doses of statin can elicit an antiviral effect.
- Statin treatments reduce viral release, preventing plaque formation.
- Statin can inhibit protein prenylation in NIH-3T3 and BMDM.

Hypothesis: Host interferon antiviral effect is in part due to the dependency of virus replication on sterol biosynthesis intermediate metabolites.

Results I: siRNA knock-down of mevalonate-isoprenoid branch of the sterol biosynthesis pathway is antiviral

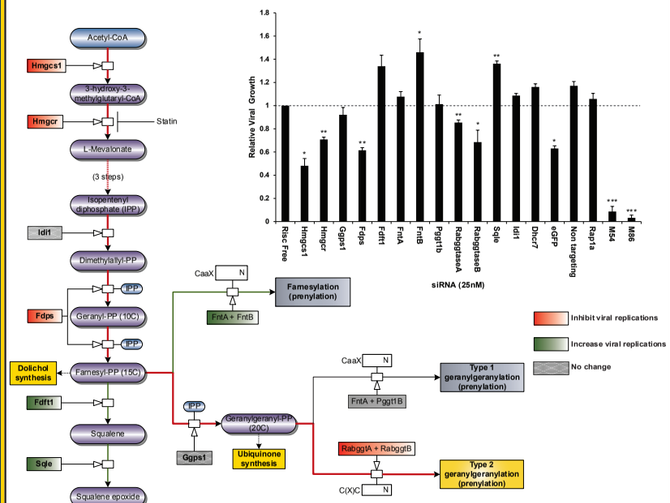

- Knockdown of Hmgcs and Fdps, upstream of the prenylation branch, inhibit viral replication.
- Knockdown of Sqle and Dhcr7 increased viral replication.
- Of the three prenyltransferases siRNA knockdowns, only geranylgeranyl transferase II knockdown showed inhibition of viral replication.

Results II: The antiviral effect of statin can be metabolically rescued with the addition of geranylgeraniol

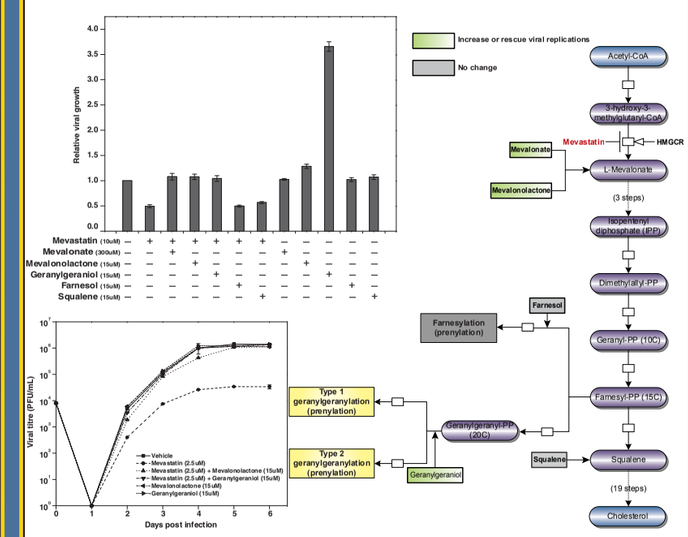

- Treatments with mevastatin led to decrease in both viral growth and viral load.
- The inhibition effect of mevastatin can be reversed with the addition of geranylgeraniol but not farnesol.
- Treatment wtih geranylgeraniol (GGOH) increased viral replication.

Results III: Statin treatments inhibits viral plaque expansion, while does not inhibit viral entry

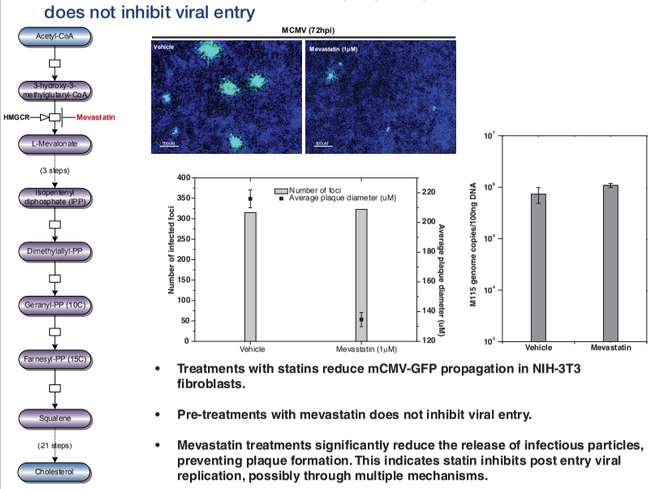

- Treatments with statins reduce mCMV-GFP propagation in NIH-3T3 fibroblasts.
- Pre-treatments with mevastatin does not inhibit viral entry.
- Mevastatin treatments significantly reduce the release of infectious particles, preventing plaque formation. This indicates statin inhibits post entry viral replication, possibly through multiple mechanisms.

Results IV: Statin treatments lead to the accumulation of unprenylated proteins in fibroblasts and macrophages

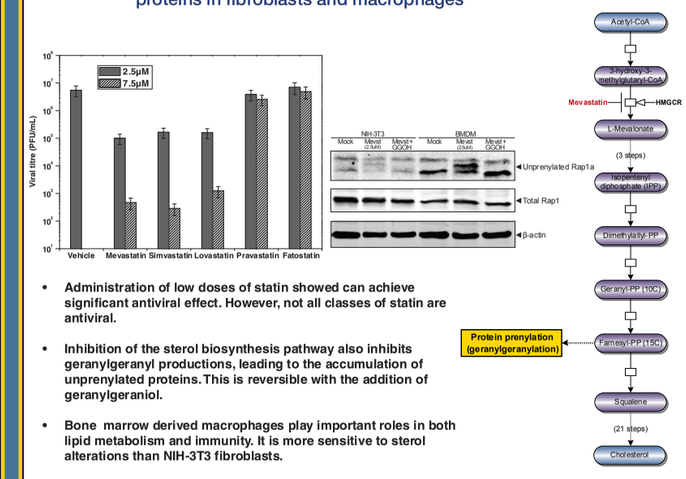

- Administration of low doses of statin showed can achieve significant antiviral effect. However, not all classes of statin are antiviral.
- Inhibition of the sterol biosynthesis pathway also inhibits geranylgeranyl productions, leading to the accumulation of unprenylated proteins. This is reversible with the addition of geranylgeraniol.
- Bone marrow derived macrophages play important roles in both lipid metabolism and immunity. It is more sensitive to sterol alterations than NIH-3T3 fibroblasts.

Future questions

- What are the host/viral targets of protein prenylation?
- Are these proteins pro/antiviral?
- Is alteration in protein prenylation a part of the innate response, or is it modulated by the pathogen?
- Does interferon have synergistic effect with statin treatments?
- Does interferon also alters protein prenylation?
- Does interferon also inhibits viral egress?

Contact information

Division of Pathway Medicine. The Chancellor's Building
49 Little France Crescent Edinburgh, EH16 4SB.
www.ed.ac.uk/schools-departments/pathway-medicine

Acknowledgements

I would like to thank Senthil Gandi, Kai Kropp, and Kevin Robertson for helping me with this poster.

Reference

1. Mankouri, J., P. R. Tedbury, et al. (2010). "Enhanced hepatitis C virus genome replication and lipid accumulation mediated by inhibition of AMP-activated protein kinase." Proceedings of the National Academy of Sciences of the United States of America 107(25): 11548-11554.
2. Zheng, Y. H., A. Plemenitas, et al. (2003). "Nef increases the synthesis of and transports cholesterol to lipid rafts and HIV-1 progeny virions." Proceedings of the National Academy of Sciences of the United States of America 100(14): 8460-8465.
3. Medigeshi, G. R., A. J. Hirsch, et al. (2008). "West Nile virus entry requires cholesterol-rich membrane microdomains and is independent of alphavbeta3 integrin." Journal of Virology 82(11): 5212-5219.
4. Blanc, M., W. Y. Hsieh, et al. (2011). "Host defense against viral infection involves interferon mediated down-regulation of sterol biosynthesis." PLoS Biol 9(3): e1001036.

Direct coupling of the 25-hydroxycholesterol sterol metabolic network to the interferon antiviral response

THE UNIVERSITY of EDINBURGH

Division of PATHWAY MEDICINE

Wei Yuan Hsieh, Mathieu Blanc, Kevin A. Robertson, Kai A. Kropp and Peter Ghazal

Division of Pathway Medicine, The Chancellor's Building, 49 Little France Crescent, Edinburgh, EH16 4SB, United Kingdom.

Recent studies suggest that the sterol metabolic network participates in the interferon (IFN) antiviral response. However, the molecular mechanisms linking IFN with the sterol network and the identity of sterol mediators remain unknown. Here, we report a cellular antiviral role for macrophage production of 25-hydroxycholesterol (cholest-5-en-3β,25-diol, 25-HC) as a component of the sterol metabolic network linked to the IFN response. Transcription profiling indicated one of the cholesterol hydroxylase genes, *Ch25h*, is rapidly activated in an IFN dependent manner. Further metabolome profiling of all naturally occurring oxysterols upon infection or IFN-stimulation revealed 25-HC as the only macrophage-synthesized and -secreted oxysterol.

We show that 25-HC can act at multiple levels as a potent paracrine inhibitor of viral infection for a broad range of viruses at sub-micromolar concentrations. Treatment of cells with 25-HC leads to significant reduction in viral production and retardation in plaque formation. Mechanistic studies revealed that 25-HC antiviral action partially involves the mevalonate branch of sterol biosynthesis pathway, blocking post entry viral growth, as well as suppression of viral immediate early (IE) gene transcription. Our studies describe a physiological role for 25-HC as a sterol-lipid effector of an innate immune pathway.

1. The sterol metabolic network leads to the production of cholesterol, isoprenoids, and oxysterols

- The sterol biosynthesis pathway starts with acetyl-coA, ends with the production of cholesterol and several secondary metabolites, including oxsterols and isoprenyloids.
- Evidence suggests that this pathway is modulated by interferon during infection as part of the antiviral response.

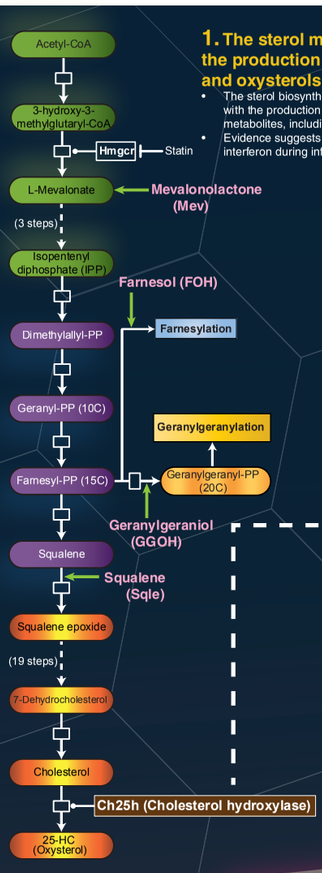

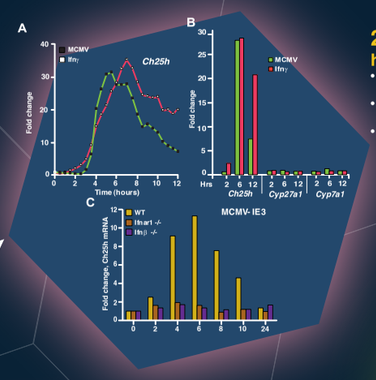

2. *Ch25h* is the only activated cholesterol hydroxylase upon interferon stimulation

- The activation of *Ch25h* peaked within 6h post infection/CMV stimulation.
- *Ch25h* is the only IFN inducible cholesterol hydroxylase gene.
- The activation of *Ch25h* is interferon dependent.

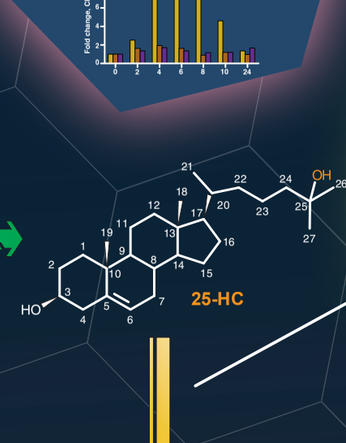

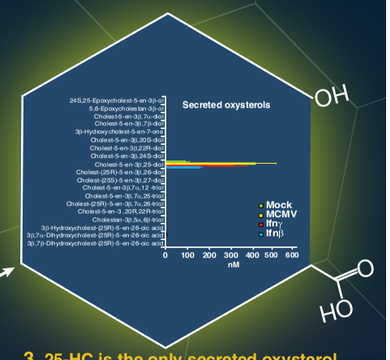

3. 25-HC is the only secreted oxysterol upon immune activation

- 25-HC is the only oxysterol detected upon infection or IFN stimulations.
- 25-HC is detectable both intracellular and extracellular (secreted).
- 10^6 macrophage is sufficient at secreting 25-HC at a detectable concentration.

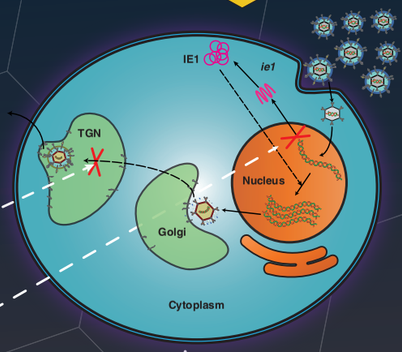

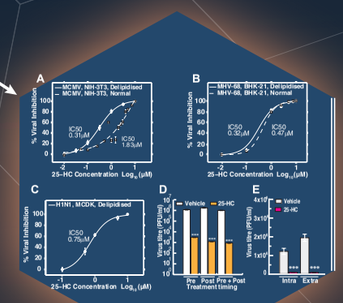

4. 25-HC shows broad antiviral activity

- Treatment with 25-HC is effective against CMV, infuenza, HSV1 and MHV-68 at submicromolar concentrations.
- 25-HC can elicit an antiviral effect post-infection, even at high MOI (2.5).
- Treatments with 25-HC lead to a decrease in intra and extracellular viral titre.

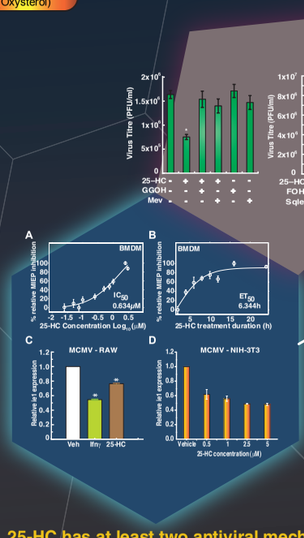

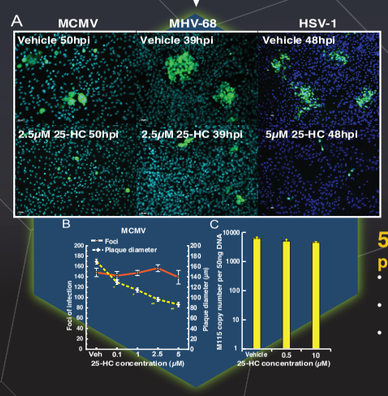

6. 25-HC has at least two antiviral mechanisms

- Treatment of 25-HC leads to a decrease in mCMV *ie1* gene expression.
- Suppression of *ie1* is conserved in primary macrophages and RAW cells.
- The antiviral effect of 25-HC can be reversed with the addition of mevalonate and geranylgeraniol, secondary metabolites of the sterol biosynthesis pathway.
- Metabolic rescue with farnesyl and squalene has no effect on the antiviral effect of 25-HC, suggesting the mevalonate-isoprenylation branch of the sterol pathway is important for viral replication.

5. 25-HC shows post-entry immune protection against infection

- Treatment with 25-HC leads to reductions in viral expansion, and viral plaque formation.
- The number of initial infected foci remain unchanged in the presence of 25-HC.
- Treatment with 25-HC does not alter the number of viral genomic copies entering the host cell, suggesting post-entry antiviral effect.

Future questions

- What is the natural receptor of 25-HC?
- Which part of the sterol biosynthesis pathway does 25-HC target?
- Do other oxysterols show antiviral effects?
- What is the active group of 25-HC?

Linked article

Blanc, M., Hsieh, W.Y., Robertson, K. A., Kropp, K. A., Forster, T., Shui, G., Lacaze, P., et al. (2013). The Transcription Factor STAT-1 Couples Macrophage Synthesis of 25-Hydroxycholesterol to the Interferon Antiviral Response. Immunity, 38(1), 106–118. doi:10.1016/j.immuni.2012.11.004

Contact information

Division of Pathway Medicine

www.ed.ac.uk/schools-departments/pathway-medicine

Author information: Wei Yuan Hsieh

e-mail: wayne.hsieh@ed.ac.uk, p.ghazal@ed.ac.uk

phone: +44(0)131242-6455

Acknowledgements

This work was supported by the Wellcome Trust, the BBSRC and EPSRC, the University of Edinburgh Alumni Fund, Spanish Ministry of Science and Innovation, and NIH. We are grateful to David Russell, William J Griffiths, Birgit Strobl and Matthias Müller, Sam Pattle, Daniel S. Ory, and Senthil Gandi for their contributions/advice to the project.

THE UNIVERSITY of EDINBURGH
School of Biomedical Sciences

Direct coupling of the host sterol metabolic network to the interferon antiviral response

Wei Yuan Hsieh, Mathieu Blanc, Kevin A. Robertson, Kai A. Kropp and Peter Ghazal

Division of Pathway Medicine, The Chancellor's Building, 49 Little France Crescent, Edinburgh, EH16 4SB, United Kingdom.

Sterols play many important roles in physiology, including maintaining cell membrane integrity, and are required for the production of vitamin D and hormones. Recent studies suggest that the sterol metabolism is involved in the interferon (IFN) antiviral response. However, the molecular mechanisms linking IFN with the sterol pathway and the identity of sterol mediators remain unknown. Using a clinically relevant model based on mouse cytomegalovirus (MCMV) infection of bone-marrow-derived macrophages (BMDM), the first work package **(WP) A** described here, uncovers a previously uncharacterized role of interferon in regulating the cholesterol pathway to protect against infection.

Subsequent **WP (B)** identifies a physiological role for macrophage produced oxysterol, called 25-hydroxycholesterol, as a sterol-lipid effector of the innate immunity. Additional gene expression analysis **(WP C)** of the sterol biosynthesis pathway under different stress conditions provides further insight into how the sterol pathway is homeostatically maintained. Lastly, pharmacological synergy studies **(WP D)** using combinations of chemical and biological compounds provide evidence to additive or synergistic antiviral drug combinations and their underlying mechanisms. Results presented here indicate the importance of interferon-sterol mediated antiviral effect and the potential development of multicomponent antiviral therapy.

WP A: The sterol metabolic network is moderated by the immune system upon viral infection and interferon stimulations

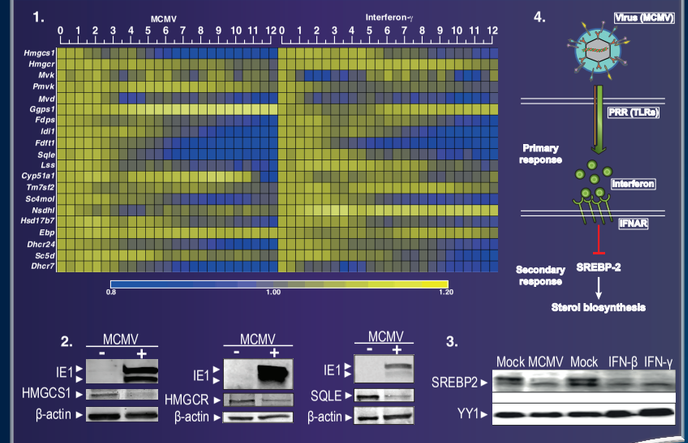

1. Microarray analysis revealed a selective and coordinated negative regulation of the complete sterol pathway in macrophage (BMDM, Mϕ) upon viral infection or treatment with interferon.
2. Suppression of the sterol biosysntheis gene is reflected on the protein level, leading to the decrease of intracellular cholesterol.
3. Levels of the active nuclear form of SREBP2, a key transcriptional regulator of sterol biosynthesis, are reduced upon infection or IFN treatment at both the protein and de novo transcription level.
4. Suppression of sterol biosynthesis is strictly interferon dependent.

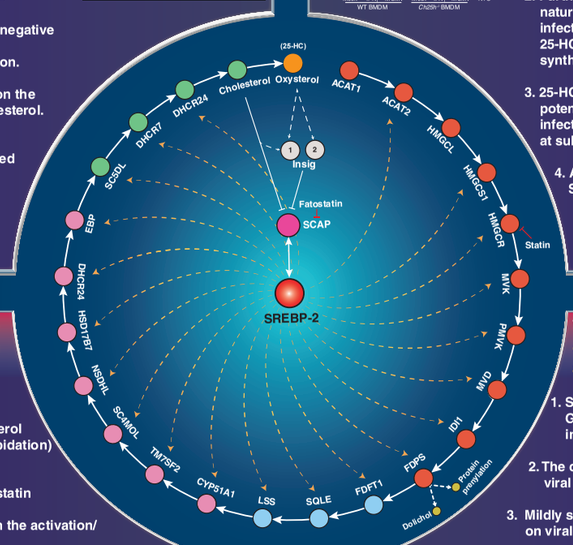

WP B: Production and secretion of 25-hydroxycholesterol is part of the host antiviral response upon interferon stimulations

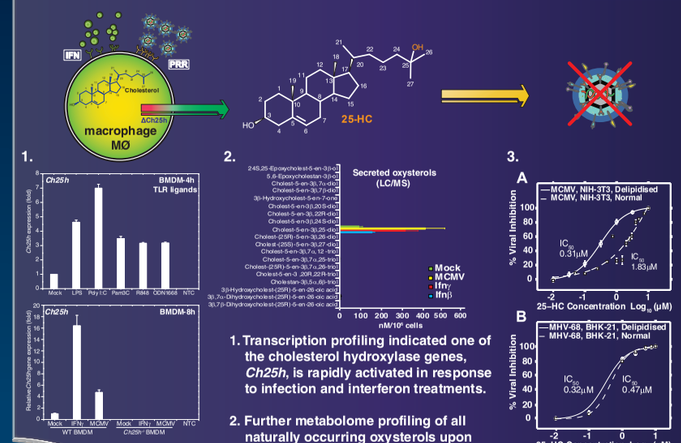

1. Transcription profiling indicated one of the cholesterol hydroxylase genes, *Ch25h*, is rapidly activated in response to infection and interferon treatments.
2. Further metabolome profiling of all naturally occurring oxysterols upon infection or IFN-stimulation revealed 25-HC as the only macrophage synthesized and secreted oxysterol.
3. 25-HC can act at multiple levels as a potent paracrine inhibitor of viral infection for a broad range of viruses at sub-micromolar concentrations.
4. Activation of *Ch25h* is strictly STAT1 dependent.

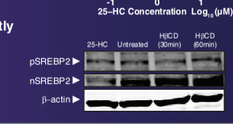

WP C: Monitoring the expression profile of the complete sterol pathway under different media and drug perturbations

1. Knocking down of SREBF-2 leads to the silencing of the sterol pathway. Altering lipid conditions (serum reduction or delipidation) induces sterol biosynthesis activation via SREBP-2.
2. Treatments of sterol biosynthesis inhibitors such as, mevastatin (targeting HMGCR), fatostatin (targeting SCAP), and 25-HC (targeting SREBP2) yield differential feedback responses in the activation/ suppression of the pathway.
3. Primary macrophages are more sensitive and responsive to sterol inhibitors than NIH-3T3 fibrobasts, highlighting the differences between the cell types.

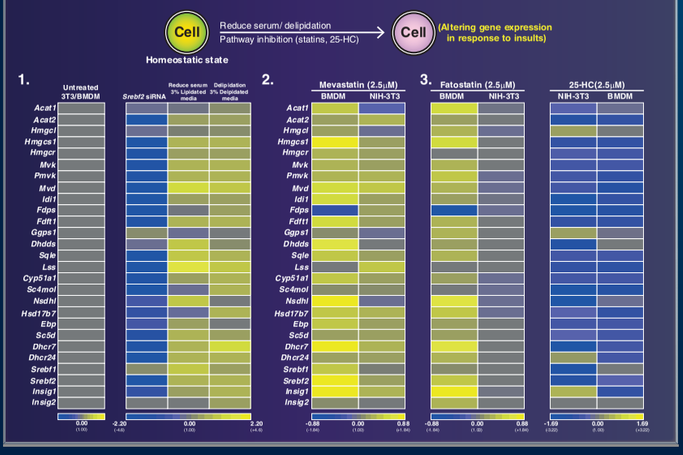

WP D: Analysis of drug combinations reveals common and facilitated antiviral modes of action and potential interaction profiles

1. Strongly synergistic combinations between 25-HC and Ganciclovir show the effect of unrelated pathway actions in inhibiting viral growth.
2. The combination of 25-HC and IFN have an additive effect on viral growth indicating common and independent pathway targets.
3. Mildly syngeristic antiviral action between statin and 25-HC or IFN on viral growth indicates a facilitated action of a common pathway.

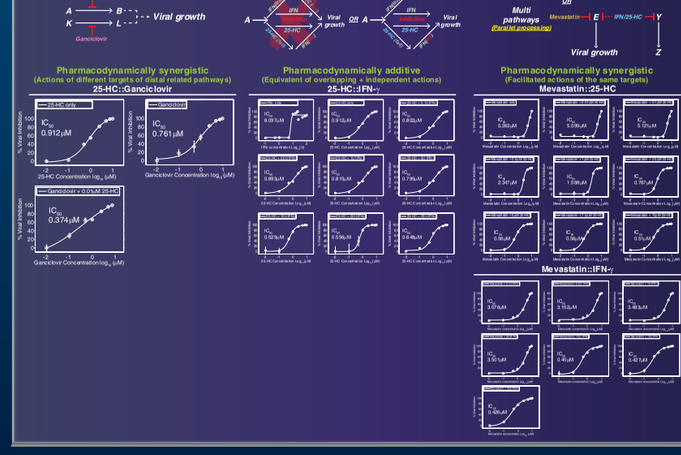

Future questions

- What is the natural receptor of 25-HC?
- Do other oxysterols show antiviral effects?
- What's the precise antiviral mechanism of 25-HC?

Linked articles

Blanc M, Hsieh WY, Robertson KA, Watterson S, Shui G, et al. (2011) Host Defense against Viral Infection Involves Interferon Mediated Down-Regulation of Sterol Biosynthesis. PLoS Biol 9(3): e1000598. doi:10.1371/journal.pbio.1000598

Blanc, M., Hsieh, W.Y., Robertson, K. A., Kropp, K. A., Forster, T., Shui, G., Lacaze, P., et al. (2013). The Transcription Factor STAT-1 Couples Macrophage Synthesis of 25-Hydroxycholesterol to the Interferon Antiviral Response. Immunity, 38(1), 106–118. doi:10.1016/j.immuni.2012.11.004

Contact information

Division of Pathway Medicine

www.ed.ac.uk/schools-departments/pathway-medicine

Author information: Wei Yuan Hsieh

e-mail: wayne.hsieh@ed.ac.uk, p.ghazal@ed.ac.uk

Acknowledgements

This work was supported by the Wellcome Trust, the BBSRC and EPSRC, the University of Edinburgh Alumni Fund, Spanish Ministry of Science and Innovation, and NIH.

We are grateful to David Russell, William J Griffiths' lab, Christopher K. Glass's lab, Timothy Osborne's lab, Birgit Strobl and Matthias Müller, Sam Pattle, Daniel S. Ory, Alan J. Ross, Senthil Gandi, and Elizabeth Vang for their contributions/advice to the project.

THE UNIVERSITY of EDINBURGH
School of Biomedical Sciences